AD_____

Award Number: W81XWH-04-1-0190

TITLE: Magnetic Resonance Spectroscopy: An Objective Technique for the Quantification of Prostate Cancer Pathologies

PRINCIPAL INVESTIGATOR: Leo L. Cheng, Ph.D.

CONTRACTING ORGANIZATION: Massachusetts General Hospital
Boston, MA 02114

REPORT DATE: February 2007

TYPE OF REPORT: Final

PREPARED FOR: U.S. Army Medical Research and Materiel Command
Fort Detrick, Maryland 21702-5012

DISTRIBUTION STATEMENT: (Check one)

x ☐ Approved for public release; distribution unlimited

☐ Distribution limited to U.S. Government agencies only; report contains proprietary information

REPORT DOCUMENTATION PAGE

Form Approved
OMB No. 0704-0188

1. REPORT DATE	2. REPORT TYPE	3. DATES COVERED
01-02-2007	Final	12 Jan 2004 – 11Jan 2007

4. TITLE AND SUBTITLE

Magnetic Resonance Spectroscopy: An Objective Technique for the Quantification of Prostate Cancer Pathologies

5a. CONTRACT NUMBER

5b. GRANT NUMBER
W81XWH-04-1-0190

5c. PROGRAM ELEMENT NUMBER

6. AUTHOR(S)

Leo L. Cheng, Ph.D.

5d. PROJECT NUMBER

5e. TASK NUMBER

5f. WORK UNIT NUMBER

7. PERFORMING ORGANIZATION NAME(S) AND ADDRESS(ES)

Massachusetts General Hospital
Boston, MA 02114

8. PERFORMING ORGANIZATION REPORT NUMBER

9. SPONSORING / MONITORING AGENCY NAME(S) AND ADDRESS(ES)
U.S. Army Medical Research and Materiel Command
Fort Detrick, Maryland 21702-5012

10. SPONSOR/MONITOR'S ACRONYM(S)

11. SPONSOR/MONITOR'S REPORT NUMBER(S)

12. DISTRIBUTION / AVAILABILITY STATEMENT
Approved for Public Release; Distribution Unlimited

13. SUPPLEMENTARY NOTES
Original contains colored plates: ALL DTCI reproductions will be in black and white

14. **ABSTRACT**
In the past year, the three years of the award, according to our proposed Statement of Work, we continued our efforts on the collection of specimens from prostate cancer patients, and spectroscopic and histopathological measurements of these samples for the construction of metabolic markers aimed at tumor diagnosis based on HRMAS 1HMR evaluation. Significant progresses have been achieved. Three peer-reviewed papers from the project have been published, and one new manuscript has been submitted. In addition, two peer-reviewed review articles and one book chapter are currently in pending for publication, and one patent application as the results of the direct funding support from this award. Furthermore, two NIH grants have been submitted as a direct result of researches supported by this award. These advancements will assist us to better understand tumor metabolism observed with MR spectroscopy, and contribute to better patient cares in the future.

15. SUBJECT TERMS
EX VIVO MAGNETIC RESONANCE SPECTROSCOPY, QUANTITATIVE PATHOLOGY CELLULAR METABOLIC MARKERS, PROSTATECTOMY

16. SECURITY CLASSIFICATION OF:			17. LIMITATION OF ABSTRACT	18. NUMBER OF PAGES	19a. NAME OF RESPONSIBLE PERSON
					USAMRMC
a. REPORT	b. ABSTRACT	c. THIS PAGE			19b. TELEPHONE NUMBER *(include area code)*
U	U	U	UU	234	

Standard Form 298 (Rev. 8-98)
Prescribed by ANSI Std. Z39.18

Table of Contents

INTRODUCTION:

In the past three years of the award, in accordance with our proposed time line in the Statement of Work, we finished the proposed Tasks 1, 2, and 3. We are still working on the some of the aspects proposed in Task 4: "Develop a Clinically Adaptable MRS Protocol," understandably due to the reality of research, in which the encounter is always more complicated than anticipation. However, the overall achievement of our completion of the proposed project can be summarized by hard numbers. In addition to the already published large numbers of peer-reviewed original papers, book chapters, review articles, and patent applications, one five-year NIH R01 has been award to us based on the data generated from this award. More importantly, based on the data gathered here, we have invented the concept of metabolomic imaging, which in addition to generating more NIH supports for our future research, will greatly impact the field of diagnostic radiology.

BODY:

Summary of Research Accomplishments

We will first summarize our achievements according to an overview of our proposed Statement of Work. At the end of the list of each sub-task, our related published references are given. .

STATEMENT OF WORK

Task 1 (Completed): Establish Procedures and Protocols.

A. Comparison of HRMAS 1HMRS spectra and degradation rates of fresh tissue specimen with those obtained from snap-frozen samples from the same cases. (Appendix **[2]**)
B. Preparation of detailed protocols for HRMAS 1HMRS examination and establishment of criteria for conducting homo- and heteronuclear correlation examinations. (Appendix **[1,4, 5]**)
C. Evaluation of histopathological integrity of specimen after HRMAS measurement by the primary project pathologist.
D. Establishment of detailed protocols for quantitative histopathology and computer-aided histopathological image analysis. (Appendix **[3]**)

Task 2: (Completed) Establish Correlations between MRS and Histopathology. (Specific Aim 1) (Appendix **[3,5]**)

A. Collection of prostate samples from i) 180-200 prostatectomies, "pseudo-biopsies" and "permanent section" will be performed on removed prostate, and ii) normal controls from autopsy subjects.
B. Performance of HRMAS 1HMRS analysis of i) tumor specimen, and ii) autopsy specimen.
C. Histopathological quantification of tissue specimens analyzed with MRS under Task 2B.

Task 3: (Completed) Determine Metabolite Markers for Prostate Cancer. (Specific Aim 2) (Appendices **[5,6]**)

A. Establishment of metabolite profiles for different prostate zones in normal controls. (Appendix **[5]**)
B. i). Performance of multivariate analysis on MRS data to identify metabolic markers that correlate with quantitative histopathology (from Task 2C), and with clinical data; (Appendix **[5]**)

ii). Evaluation of the sensitivity and specificity of metabolite markers for detecting the presence of cancer cells and predicting the quantity of each pathological component;
iii). Evaluation of the statistical significance of metabolite markers identified by samples from both pseudo-biopsy and permanent section; examination of the sensitivity and specificity of these markers for their ability to suggest the pathologic stage of prostate cancer by using only pseudo-biopsy samples.

C. Test of the sensitivity of these markers in reflecting the high disease occurrence among African-Americans; conclusion of findings and the clinical implications thereof, and the submission of final report.

Task 4: (Partially Completed) Develop a Clinically Adaptable MRS Protocol. (Specific Aim 3)

A. Identification of metabolite markers that can divide the Gleason score 5, 6(3+3) and 7(3+4) group into subgroups. (Appendices **[5, 6]**)

B. Preliminary evaluation and modification of the database markers (from Task 4A) in connection with the updated clinical information on patient outcome, and design of a clinical protocol that can be executed, objectively, by a technician without extensive training.

Details of our progress and achievements are summarized below.

Technical Development and Evaluation

Measurements of HRMAS spectra at reduced spinning rates[1, 4]. The accuracy of studies using HRMAS relies on maintaining tissue pathology; a potential source of tissue damage arises from HRMAS performed at a high spinning rate. When the rate is reduced, however, spinning sidebands (SSB) severely impede metabolite observation. We have studied slow HRMAS with various SSB suppression methodologies, including rotor-synchronized DANTE, rotor-synchronized WATERGATE, 1D-TOSS, and 2D-PASS sequences. Among these, we reported that the rotor-synchronized DANTE sequence at spinning rates of 600 and 700 Hz can be used for SSB suppression, particularly for those introduced by tissue water (Appendix **[4]**).

Recently, we further developed and published a novel scheme, (A+B-|A-B|), or Min(A, B), by using the smaller value of two water-suppressed spectra (A, B) of different low spinning rates to generate a sideband free spectrum. Compared with the above DANTE method, the Min(A, B) editing procedure can produce more accurate results**[4]**. Also reported in the publication were our results of using the intensity of the external rubber STD in the sample rotor. Using this STD, we were able to linearly correlate sample weights with the spectral intensity of [metabolites]/[STD], and the latter with the estimated metabolite concentration. We will use this simplified slow-spinning method, Min (A,B), in the proposed study (Appendix **[4]**).

Evaluation of Freeze-thawing Effect on Tissue Spectral Profiles[2]. Some researchers have speculated that improvement in the spectral resolution of intact tissue with HRMAS is due in part to freeze-thawing artifacts resulting from tissue storage. We analyzed 12 human prostate tissue specimens with the previously discussed DANTE method at HRMAS rates of 600 and 700 Hz. One sample from each specimen was measured fresh and another thawed, following 12-16 hours of freezing. In addition, we measured one sample from each specimen first fresh, then freeze-thawed. The spectral resolutions represented by line-widths and obtained from fresh and frozen samples were identical for most metabolites. Although metabolite intensities from fresh and freeze-thawed spectra

were not identical, the differences were less drastic than those reported in other studies (Appendix **[2]**).

Computer-aided Image Analysis (CAIA) on Prostate Tissue After Spectroscopy Analysis [3]. Our study, relying on 1:1 correlations between metabolic profiles and tissue pathologies, places a great demand on the accuracy of quantitative histopathology. Recently, we developed a CAIA protocol for H&E stained prostate tissues with the assistance of an Olympus BX41 Microscope Imaging System in conjunction with image analyzer MicroSuite™ (Soft Imaging System Corp., Lakewood, CO). **Figure 1** shows an example of the CAIA classification scheme performed on a cross-section of human prostate tissue containing both histo-benign and cancerous glands. Stroma, benign glandular epithelium (red), and benign glandular lumen (yellow) were particularly evident in (b). Image (c) shows the result of cancer cells and lumen, in blue and light blue, respectively.

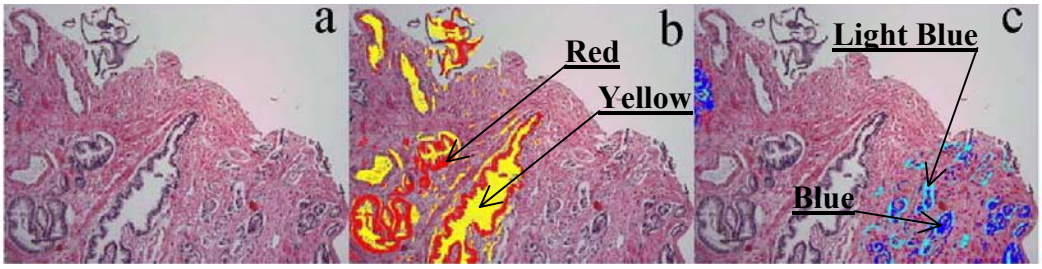

Figure 1. Identification of (b) histo-benign epithelial glands and lumens and (c) cancer glands and lumens with the CAIA protocol**[3]**.

With this protocol, we analyzed thirty-eight samples from 29 prostatectomy cases that had been evaluated with HRMAS 1HMRS. After spectroscopy analysis, samples were serial-sectioned, stained and visually assessed by pathologists. Cross-sections from these samples were then measured with the CAIA protocol. Results showed that human visual assessments overestimated the area percentages of tissue pathologies. Statistically significant correlations were found between both metabolites indicative of benign epithelium and those indicative of PCa and the CAIA quantitative results. CAIA based quantitative pathology proved to be more accurate than human visual assessment in establishing correlations useful for disease diagnosis between prostate pathology and metabolic concentrations (Appendix **[3]**).

^{31}P edited ^{1}H NMR Spectroscopy[6]. Choline and the related compounds phosphocholine (PC) and glycerophosphocholine (GPC) are linked to the development and progression of cancer. Current *in vivo* and tissue *ex vivo* magnetic resonance spectroscopy methods mostly center on measuring the total concentration of these metabolites and have difficulty differentiating between them. In this report we presented a new scheme that uses ^{31}P edited ^{1}H spectroscopy to quantify the concentrations of choline, PC, and GPC in biological samples. This method is particularly well-suited for analytical situations where the PC and GPC resonances are not sufficiently resolved and/or obscured by other metabolites, such as in *ex vivo* tissue studies (Appendix **[6]**).

Evaluation of Tissue Degradation at Different Temperatures. Metabolic decomposition ensues immediately following tissue excision. Thus, extrapolating the concentrations of metabolites before tissue excision is of great importance. To study this, degradation rates of various metabolites found in intact prostate tissue were analyzed by continuously recording prostate tissue HRMAS spectra for 18-48 hours at 4°C (n=6) and 37°C (n=3). These experiments were carried out on previously characterized specimens**[2]**. Examples of these metabolite degradation spectra are shown in **Figure 2;** measured changes in choline and citrate, at both temperatures, are shown in **Figure 3**. The

relationships in Figure 3 indicate that different prostate metabolites have different degradation rates at different temperatures, with changes in an hour being less than 2% (within the error margains of an NMR analysis) at 4°C. Tissue degradation curves may allow us to extrapolate the true metabolite concentration before tissue excision, if such a correction is necessary.

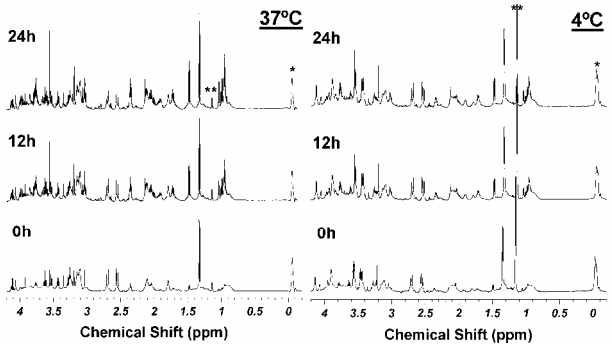

Figure 2. Intact prostate tissue HRMAS spectra measured at 4°C and 37°C at (0, 12, and 24) hours. * denotes an external rubber standard; ** indicates alcohol contaminations.

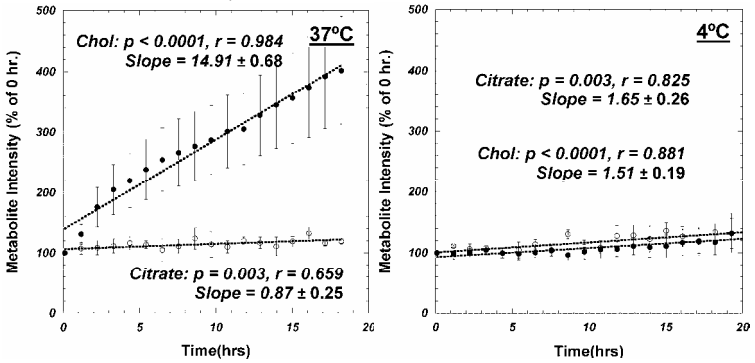

Figure 3. Comparisons of prostate metabolite degradation rates measured at 4°C and 37°C for choline and citrate.

Evaluation of Tissue Storage Duration on Prostate Metabolites [10]. Tissue storage at the –80ºC freezing condition is a common practice employed in biomedical research. The accepted assumption is that such a temperature condition halts biological and biochemical processes and preserves tissue molecular profiles for the duration of the storage. We tested this assumption on fifteen samples (from 11 cases) of previously characterized human prostate samples from our studies of freeze-thawing effects on tissue metabolites in July 2002**[10]**. These samples have been in storage under –80ºC for 32 months. After spectroscopy analysis, quantitative pathology evaluations also confirmed that the pathological compositions of the current samples were similar to those of the same specimens analyzed in 2002. In general, metabolic profiles do not show drastic alteration after storage, an example of such a comparison between metabolic spectra is given in **Figure 4**, where spectra (a) and (b) are the reproduction of Figure 1 in the freeze-thawing report**[10]**, while spectrum (c) was obtained in March 2005 from tissue samples of the same specimen that resulted in spectra (a) an (b) in July 2002. Quantitative analyses of the ratios over creatine for 12 metabolites suggest that the overall apparent increase, if confirmed, is less than 20% (**Figure 5**). Detailed comparisons are still in the process of analyses .

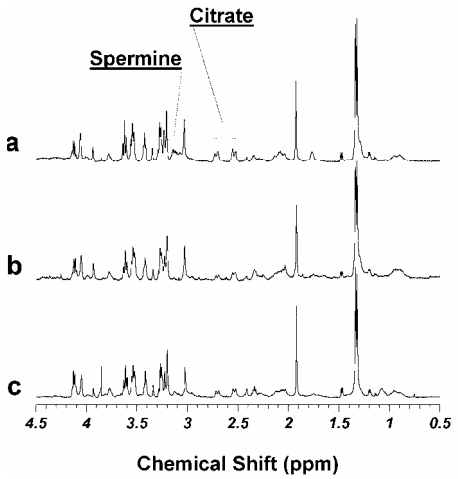

Figure 4. Comparison between metabolite spectra (a) and (b) reproduced from Fig. 1 in the publication of freeze-thawing studies in July 2002 **[10]**, and spectrum (c) obtained in March 2005 from samples of the same specimen that generated (a) and (b). No drastic changes in metabolite profiles are observed in association with tissue storage.

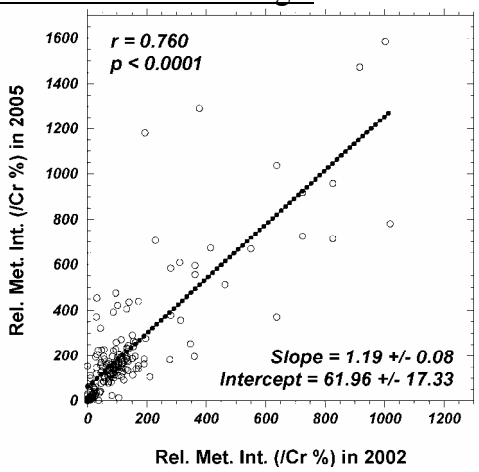

Figure 5. Quantitative analyses of 12 metabolites suggests that the overall apparent increases in metabolite ratios over creatine is less than 20%.

Studies of Prostate Cancer

Analysis of Prostate Metabolic Profiles with Principal Component Analysis [5]

Since the Urological Pathology Research Lab was approved by the MGH IRB to collect and distribute human prostate surgical specimens, we have incorporated more than 200 surgical cases (~470 specimens) into our study. From these specimens, we have measured ~300 samples with HRMAS 1HMRS, and finished quantitative pathology for 199 samples from 82 cases measured with the DANTE slow-spinning (600, 700 Hz) scheme**[5]**. Pathologies of each sample were also examined to record the percentages of each category including histo-benign epithelium, cancer, and stroma. The main conclusions of the study have been reported in Cancer Research**[5]**. Details of the study are presented below.

The 36 most intense resonance peaks/groups assigned to specific metabolites were subjected to Principal Component Analysis (PCA), and all components with eigenvalues greater than 0.5 (PC1 to PC15) were examined (**Table 1**), which included each eigenvalue as a percent of the total variability for the 36 standardized metabolite resonances, as well as the cumulative percent of variation represented by this and all previous PCs. It is clear from this table that 15 components can account

for more than 88% of variation for the 36 resonances. Linear regression analysis of the three measured pathology features vs. the PCs revealed that the 2nd and 13th/14th PCs are positively correlated with the fraction of histo-benign epithelium and cancer, respectively. The correlations (r) and their p-values (with 10 p values < 0.05) are listed in Table 1.

	EigenValue	Percent	CumPercent	Epithelium (r, p)		Cancer (r, p)		Stroma (r, p)	
PC1	9.7438	27.066	27.066	0.2322	0.0010	0.0438	0.5392	-0.2216	.00017
PC2	**5.9318**	**16.477**	43.543	**0.3813**	**<0.0001**	-0.0166	0.8163	**-0.3033**	**<0.0001**
PC3	2.9470	8.1861	51.729	0.0962	0.1767	0.0335	0.6380	-0.1023	0.1503
PC4	2.5294	7.0260	58.755	-0.0701	0.3255	-0.0913	0.1997	0.1204	0.0903
PC5	1.6851	4.6809	63.436	-0.0377	0.5968	-0.0843	0.2363	0.0889	0.2116
PC6	1.4127	3.9242	67.360	-0.0036	0.9602	0.095	0.1819	-0.0681	0.3393
PC7	1.3347	3.7075	71.068	-0.0203	0.7756	0.1368	0.0540	-0.077	0.2795
PC8	1.2062	3.3506	74.419	-0.1156	0.1039	0.0548	0.4424	0.0579	0.4169
PC9	1.0260	2.8501	77.269	0.057	0.4235	-0.2202	0.0018	0.1039	0.1442
PC10	0.85141	2.3650	79.634	-0.0355	0.6191	-0.1175	0.0984	0.1098	0.1226
PC11	0.78303	2.1751	81.809	-0.139	0.0503	-0.0034	0.9616	0.117	0.0998
PC12	0.71392	1.9831	83.792	-0.1536	0.0303	0.1022	0.1508	0.0567	0.4267
PC13	**0.67150**	**1.8653**	85.657	0.0652	0.3599	**0.1457**	**0.0401**	**-0.1537**	**0.0302**
PC14	**0.55362**	**1.5378**	87.195	-0.1302	0.0668	**-0.1597**	**0.0243**	**0.2169**	**0.0021**
PC15	0.50906	1.4141	88.609	0.063	0.3768	-0.0922	0.1954	0.0112	0.8751

Table 1. Results of PCA for the first 15 PCs on intensities of 36 resonances from 199 prostate tissue specimens. Percent: each eigenvalue as a percent of the total eigenvalue; CumPercent: the cumulative percent of variation represented by this and all the previous PCs. For histo-benign Epithelium, Cancer and Stroma columns: numbers are correlation r and p values.

The apparent difference in the correlations (0.38 and 0.15 for epithelium with PC2 and cancer with PC13/14, respectively) was a result of the relative sample sizes. Varying fractions of epithelium were observed in 174 samples, while cancer cells were detected for only 20/199 samples. This could also account for the difference between the two eigenvalues, of which PC2 (epithelium) represents 16.5% of the total variability, while PC13/14 (cancer) only 1.9%/1.5%. PC1 reflects mostly the total resonance intensities. The positive r (0.1457) value for PC13 indicates that the more cancer cells in a sample, the higher its PC13 value, while the negative r (-0.1597) value for PC14 suggests the opposite, i.e. the more cancer cells, the less its PC14 value. These observations also agree with existing knowledge, for instance, the loading factor for phosphocholine (PChol) in PC13 was a high positive number indicating above normal PChol contribution to PC13, while the same loading factor in PC14 was a significant negative number corresponding to the negative r value.

Prostate Zones and Metabolite Differences

Principal Component Analysis results can be used to analyze possible zone-related metabolite differences using one-way ANOVA evaluations of PC2 (epithelium) for samples from different zones. Among the 179 cancer-negative samples, 49 were from the central zone (CZ), 59 from the peripheral zone (PZ), and 55 from the transitional zone (TZ). In **Figure 6**, our results for PC2 show that there are measurable differences between TZ and CZ, as well as between TZ and PZ. No differences were detected between CZ and PZ. Furthermore, since PC2 was positively correlated with the vol% of histo-benign epithelium (Table 1), we tested and found that the zone-differentiating capability of PC2 seemed also to reflect the differences of epithelial content in the measured groups (**Figure 7)**.

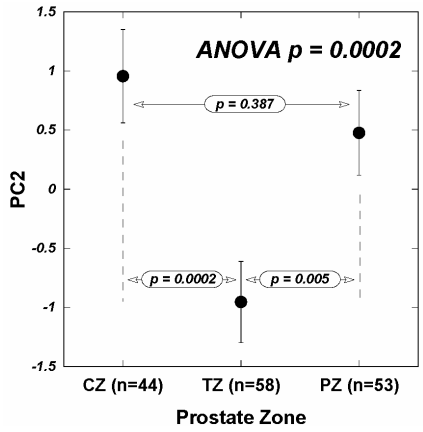

Figure 6. PC2 detects significant epithelium related differences between prostate zones: TZ vs. CZ, TZ vs. PZ.

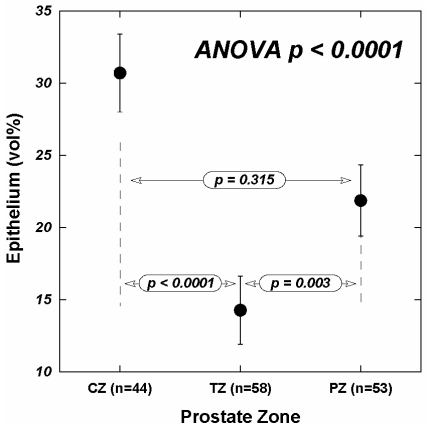

Figure 7. Epithelium differences among the measured samples of different prostate zone.

Identification of Cancer Containing Samples with Metabolic Profiles [5]

By examining the eigenvectors (i.e. the coefficients in the linear combinations of the original metabolites predicting each component) it was found that PC2 is associated with above average levels of inositols, spermine, creatine, and citrate, all of which are associated with epithelial cells; and PC13 is associated with above average levels of taurine, PC, choline, and lipids, and below average levels of inositols, citrate, and valine. These observations agree with common knowledge of tumor metabolism. The sensitivity of correlations between PCs and pathological features relies on the collective variation of all metabolites. Nevertheless, the sensitivities of the individual metabolites, depicted by their eigenvectors of PC13/14 as cancer-correlated, were tested with paired Student's t-tests for differentiating cancer from histo-benign tissues, obtained from the same 13 PCa patients. Results indicate that we can separate cancerous from histo- benign samples using a 2D projection of a 3D plot (**Figure 8,** copied from**[5]**) of PC13 vs. phosphocholine and choline. A ROC (receiver operating characteristic) curve obtained from these parameters revealed 98.2% overall accuracy, shown in **Figure 9** (copied from**[5]**). In addition, a linear correlation between patient serum PSA levels and PC2 was also identified and tested to be epithelial vol% independent **[5]**.

We expect that, by analyzing new cases according to this proposal, the number of cancer positive cases will greatly increase as a result of the standardization of tissue collection procedures. With a greater proportion of cancer positive samples, we expect our results to show that the relative eigenvalue of the PC for cancer increases (i.e. an earlier PC than 13 or 14), and we expect to gain additional knowledge of the metabolites associated with cancer. In addition, with more cancer

samples, we will be able to perform CANCOR analysis that will lead to the construction of ROC curves to establish a threshold value for PCa metabolic profiles in detection of cancer.

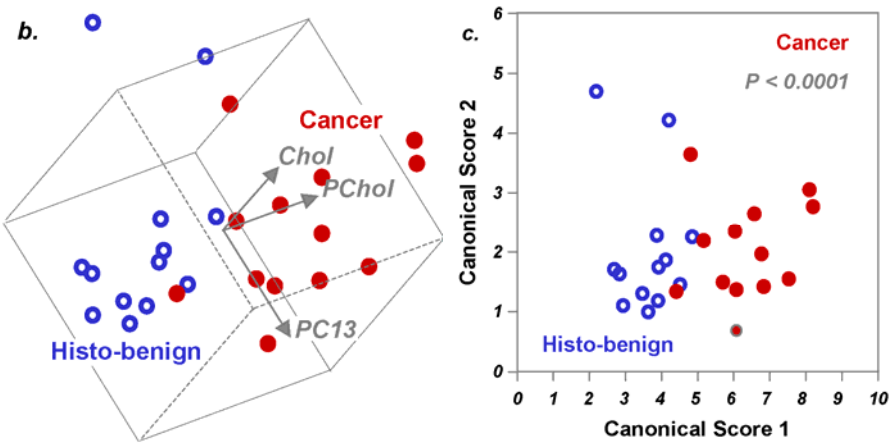

Figure 8. (**b**) 3D plot of Principal Component 13 (PC13 correlates linearly with vol% of cancer cells in tissue samples) vs. phosphocholine (Pchol, or PC) vs. choline (Chol). Cancerous and histo-benign tissue samples from 13 patients can be visually separated in observation plane. (**c**) The canonical (CANCOR) plot resulting from discriminant analysis of the three variables in Figure 9b. presents the maximum separation between the two groups**[5]**.

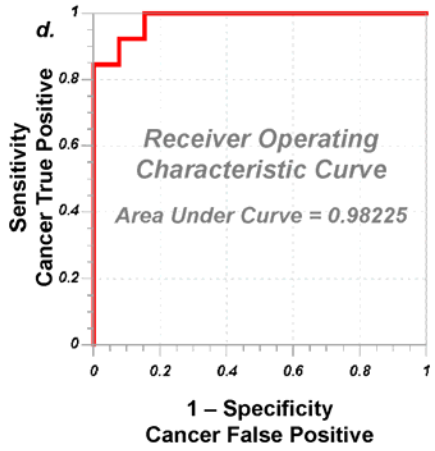

Figure 9. (**d**) The resulting receiver operating characteristic (ROC) curves indicates the accuracy of using the three variables in Figure 9b. to positively identify cancer samples**[5]**.

Feasibility Tests on Studies of Prostate Biopsy Samples.

In principle, HRMAS and quantitative pathology studies of prostate biopsy samples bears no difference from analyses of small surgical samples. However, due to the delicate geometrical shape of the prostate biopsy cores, additional care needs to be exercised during the procedures of tissue transfer. We tested the entire procedure by acquiring three cores from two freshly removed prostatectomy specimens. Examples are illustrated in **Figure 10**, clearly demonstrating our technological feasibility and capability to conduct the tasks proposed in our aim.

Figure 10. (A) "Bench-top biopsy" removed a tissue core from a prostate after prostatectomy. (B) The Bx core was transferred into a 4mm HRMAS rotor. (C) Spectra with 600 and 700 Hz spinning were recorded; the tissue core was (D) wished out from the rotor after HRMAS analyses and (E) fixed in formalin; (F) an H&E image of the Bx core, with a scale bar denoted 2mm.

In preparation for the proposed ex vivo biopsies from prostatectomy specimens, we have tested the entire procedure on surgical samples. **Figure 11** demonstrates an example of such investigations. In this evaluation, sextant biopsies were taken from the inked prostate at the locations marked by pins. The sites A and B (circled) in the middle of the prostate presented spectra that are clearly different as can be seen for the region including creating, cholines and inositols. The quantitative pathology results indicated that the major difference was the presence of 4% (by volume) cancer cells in sample from site B, while the amounts of epithelia and stromas between these two analyzed samples were comparable. This example again revealed the capability of the spectral data in detecting malignant components when present.

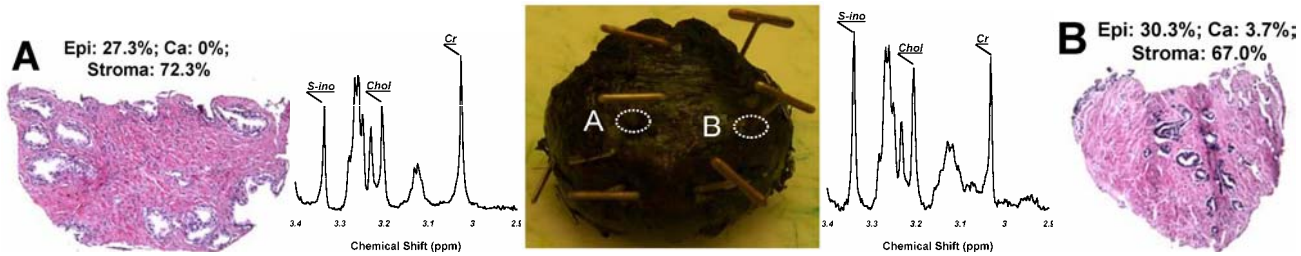

Figure 11. An example of a test of ex vivo biopsies on a prostatectomy specimen. Spectral differences observed with samples collected from the middle of the prostatectomy ex vivo biopsies (A and B) can be associated with the presence of cancer cells at B site.

Metabolic Profiles Are More Sensitive Than Histopathology [5]

We examined correlations between PCs and pathological tumor stage [AJCC/TNM staging system (6^{th} ed.)]. We observed the following with statistical significance for all the samples included (n=199): PC2 can differentiate T2c cancer (prostate-confined; both lobes) from T3 (invading extraprostatic tissue) and T2ab (prostate-confined; one lobe). PC5 (reflects changes in lactate, choline, inositol, lipids, etc.) can differentiate T2ab cancer from T2c and T3 (**Figures 12a** and **b**). Since PC2 was observed to correlate with vol% of epithelium (Table 1), we verified that observed differentiation among tumor stages was independent of epithelial content (e.g. T2ab: 21.88±2.59%; T2c: 20.21±1.91%). Upon analysis of histo-benign samples (n=179) similar differentiations persisted for both PCs (**Figures 12c** and **d**). Furthermore, when the same PCs were applied to histo-benign samples of GS 6 and 7 (n=162), both PCs distinguished the least aggressive tumors (i.e. GS 6 and T2ab tumors) from those in more aggressive groups (GS 6 T2c, GS 6 T3, and GS 7 tumors) (**Figures 12e** and **f**). For the last group, the ROC curve analysis of PC5 indicated that the overall accuracy (area under the curve, AUC) for identifying (GS6, T2ab) tumors (n=42) from (GS6, T2c), (GS6, T3) and (GS7) tumors (n=120) was 65.4%. By further restricting the ROC analysis to include only samples from patients of PSA levels ≤10.0 ng/ml (n=95), the AUC level increased to 71.5% (**Figure 13**). These AUC levels were very close to current literature values (62.7-73.8%) in predictions of patient pathological stages with Gleason scores at biopsy based on large patient populations (from 114 to 1283). The observation of PC2 positive correlation with benign epithelia, and at the same time its apparent differentiation power among tumor stages,are not in conflict, if we view the pathology invention of tumor stage as a means of indicating the degree of malignancy rather than merely the size of tumors, as in T2a, T2b, and T2c, which were the parameters the current pathology can measure. If a higher PC2 value can be more broadly viewed as less

malignant, in addition to more benign epithelia, then the higher PC2 values for T2ab than T2c should not cause too much surprise, while T3 stages designate different pathological considerations that may not be numerically compared with T2c's.

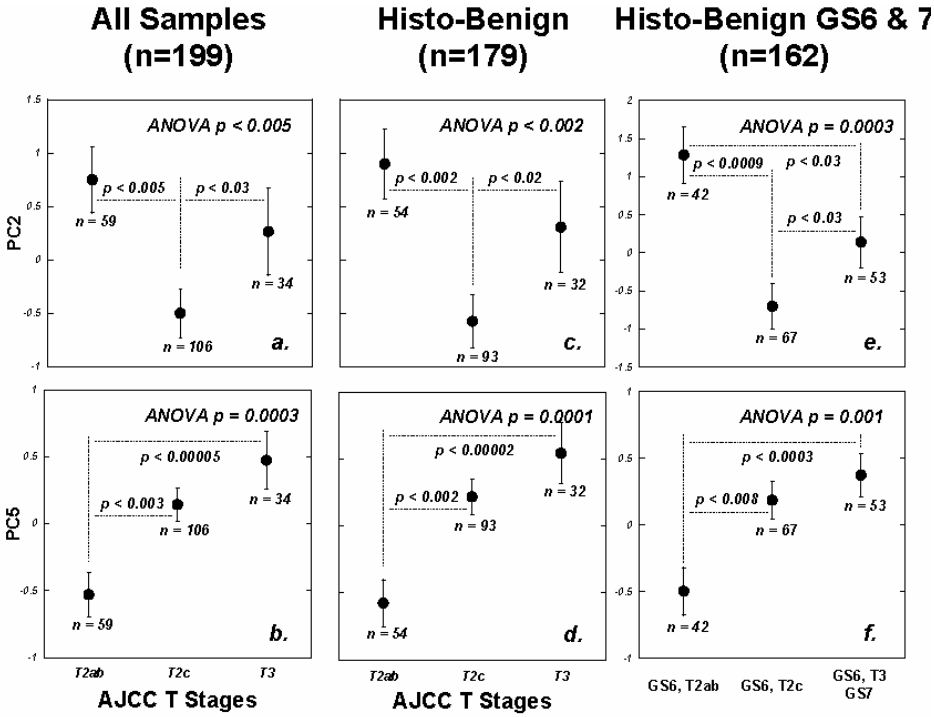

Figure 12. Principal Component 2 (PC2) and Principal Component 5 (PC5) as predictors of tumor stage: (**a**.) PC2 can differentiate T2c stage tumors from T2ab and T3 tumors as defined by AJCC/TNM staging system (6th ed.) with all samples analyzed; while (**b**.) PC5 can differentiate T2ab from T2c and T3 stages. Similar capabilities exist with histo-benign samples (**c**, **d**), and with histo-benign GS 6 and 7 samples (**e, f**). In the latter, PC2 and PC5 can differentiate among three tumor groups: 1) GS 6, T2ab, 2) GS 6, T2c, and 3) GS 6, T3 plus GS 7 tumors.

It is of note that, in contrast to published works relying on observation and evaluation of cancer cells in specimens, our results are based on chemical analyses of histo-benign tissues from PCa patients, which may resemble cases of false-negative biopsies.

In addition to the pathological stages, we noticed that, although not yet incorporated in AJCC/TMN staging, tumor perineural invasion (TPNI) indicates prostate tumor aggressiveness. Unfortunately, tumor heterogeneity may prevent visualization of invasion in biopsy samples. Our evaluation yielded a statistically significant correlation between PC14 levels and TPNI status for all samples (n=199) (**Figure 14a**), the 179 histo-benign samples (**Figure 14b**), and more interestingly, the 42 histo-benign samples from GS 6/T2ab tumors (**Figure 14c).** This last observation, combined with results shown in Figures 12e and f, may have great clinical significance in identifying and managing less aggressive GS 6 tumors. Similar to the above discussion regarding PC2, here we wish to point out that the negative correlation of PC14 with the amounts of cancer cells, or higher malignancy, agrees with the fact that the clinically worse group with "+" TPNI has lower PC14 values.

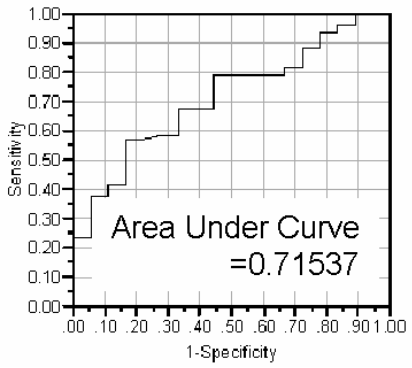

Figure 13. An ROC curve identifying (GS6, T2ab) tumors for PSA ≤10.0 ng/ml patients.

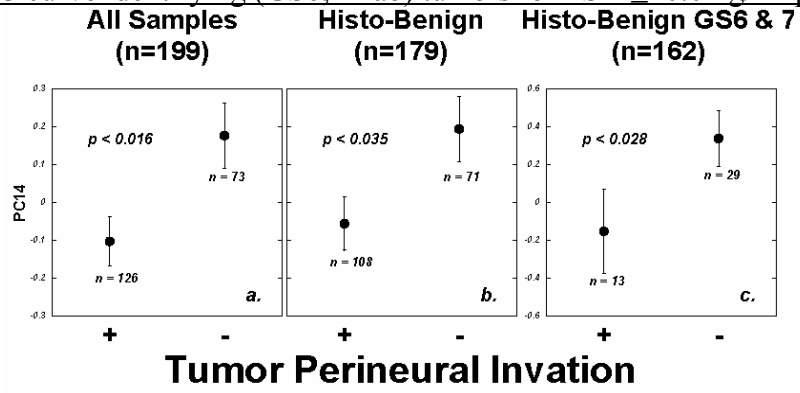

Figure 14. Principal Component 14 (PC14) as a predictor for TPNI. PC14, linearly correlated with volume % of cancer cells in tissue samples, can predict TPNI status with statistical significance particularly among GS 6 and T2ab samples (c).

Metabolomic Imaging in Human Prostate Cancer Detection

This is a new research direction that we developed based on the above presented human prostate cancer metabolomic studies funded by this award. Metabolomics evaluates physiological or pathological conditions by profiling an entire, measurable metabolome, rather than by focussing upon individual metabolites or isolated metabolic pathways. Metabolomic imaging uses abstract values of condition-specific biomolecular profiles to map anatomic structures and reveal the potential involvement of defined medical conditions for examined anatomy. Here, we introduce the use of metabolomic imaging for the examination of human prostatectomy specimens. The distribution of human prostate cancer (multi-focal and heterogeneous) prevents its reliable detection by current *in vivo* radiological techniques. Even gross pathology of removed prostates does not identify locations of the malignancy. Our results with metabolomic imaging in examinations of human prostatectomy specimens suggest an important clinical potential for this abstract imaging paradigm. Further, this paradigm may readily be extended beyond metabolomics to include other measurable, molecular parameters.

In the era of personalized medicine, there is a recognized need to establish and utilize novel biomedical parameters for the management of such controversial diseases as human prostate cancer. The controversies presently surrounding this malignancy occur at many levels, chief among them the following two concerns. First, the implementation of serum prostate specific antigen (PSA) testing has shifted diagnosis towards earlier disease stages. However, retrospective studies have shown that some human prostate tumors may grow at such slow rates, confined within the prostate, that they never become clinically significant during a given patient's lifetime. While statistical data clearly indicate that many in the PSA testing population are likely to have the more indolent tumors, current diagnostic modalities cannot distinguish these lesions from fast-growing, lethal ones. Second, since serum PSA values are known to be prostate specific, but not cancer specific, i.e. other

prostate conditions can also elevate serum PSA readings, thus a PSA elevation does not warrant a prostate removal. Furthermore, due to cancer heterogeneity, the positive rate for each biopsy core of a cancer patient is currently estimated to be around 10% of the PSA testing population. These and other concerns underscore the inability of current radiological techniques to visualize tumor lesions. The concerns may diminish if new radiological paradigms permit observation and evaluation of suspicious, potential lesions that can aid in directing biopsy prior to prostatectomy.

Recent developments of genomics and proteomics in medical investigations have fostered a philosophical acceptance of the clinical values of results from non-hypothesis-driven research. For instance, in the global evaluation of genomic results presented as the now familiar cluster diagrams, the limitation of current genetics with respect to the exact functions of each measured gene has been acknowledged. However, current gaps in our knowledge do not eclipse the implication of genomic profiles for indicating physiological and pathological conditions, perhaps even clinical outcomes of patients. This philosophical shift, which emphasizes the global evaluation of entire measured molecular parameters, can be applied to the analysis of disease-related metabolite changes in the form of metabolomics.

In **Figure 15**, we represent our prostate cancer metabolomic findings in terms of the relative metabolite intensities directly applicable to the present study, rather than the concentrations previously reported in **Figures 8** and **9**. **Figure 15** makes evident the advantage of a metabolomic profile represented by Canonical Score 1 (**Figure 15a**) over a single metabolite, phosphocholine (PChol) alone (**Figure 15b**), for differentiating cancer from histologically benign samples within the group. The overall accuracy, presented by Area Under Curve (AUC) in the Receiver Operating Characteristic (ROC) curve, increases from 80% (PChol alone) to 92% (Metabolomic profiles). Canonical score 1 as a specifically defined metabolomic profile was calculated by using the intensity of PChol, principal components (PCs) 6 and 11; both PCs were found to correlate linearly with the volume percentage of cancer glands in the samples: $p<0.017$, and 0.007, respectively. In **Figure 15a**, we also presented the median (M, filled Purple circle) and standard deviation (SD, Purple bars), as determined from all samples.

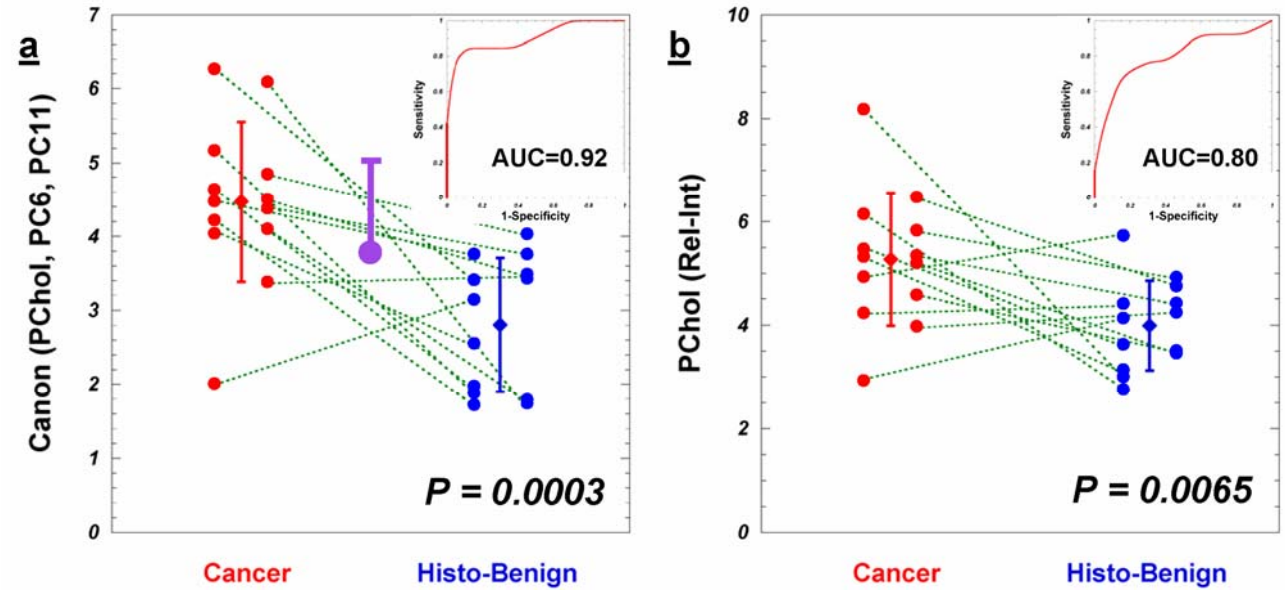

Figure 15. **Metabolomic profiles are more sensitive than individual metabolites in differentiating cancer (Red) from histological benign (Blue).** Proton MRS obtained from 13 pairs

of cancer and histo-benign prostate intact tissue samples obtained from 13 patients, originally reported in Ref [**[5]**] in terms of metabolite concentrations, are re-analyzed according to the relative metabolite intensity (individual resonance peaks normalized by the entire metabolite spectral region). (**a**). Metabolomic profile – Canonical Score 1 – is produced by PChol, and principal components 6 and 11. Both PC6 and PC11 are found to linearly correlate with the amount of cancer glands in the analyzed samples. (**b**). PChol represents the most sensitive individual metabolite in differentiating the two groups. Comparing **b** with **a**, the improved differentiating sensitivity in **a** is evident as being presented by the increase AUC in the inserted ROC curves. The median and the standard deviation of profile values calculated from all samples are indicated in **a** by Purple filled circle and bars, respectively.

We tested the concept of MRS-based metabolomic imaging with five human prostates, removed by prostatectomy surgeries from patients with biopsy-proven cancer in the prostate. Fresh specimens of the entire prostate were transferred on ice into a human 7-tesla MR scanner. A single loop surface coil was placed in the middle and around the prostate, though which localized MRS studies were acquired for three coronal prostate planes (the center-plane, approximately at the coil level, and two side-planes, each 6 mm above and below the center-plane). Each plane, of a thickness of 3 mm, consisted of 16x16 voxels (3x3x3 mm^3), as shown in **Figure 16a**. In this figure, data from voxels within the white border are included in the initial processing to visualize each spectrum.

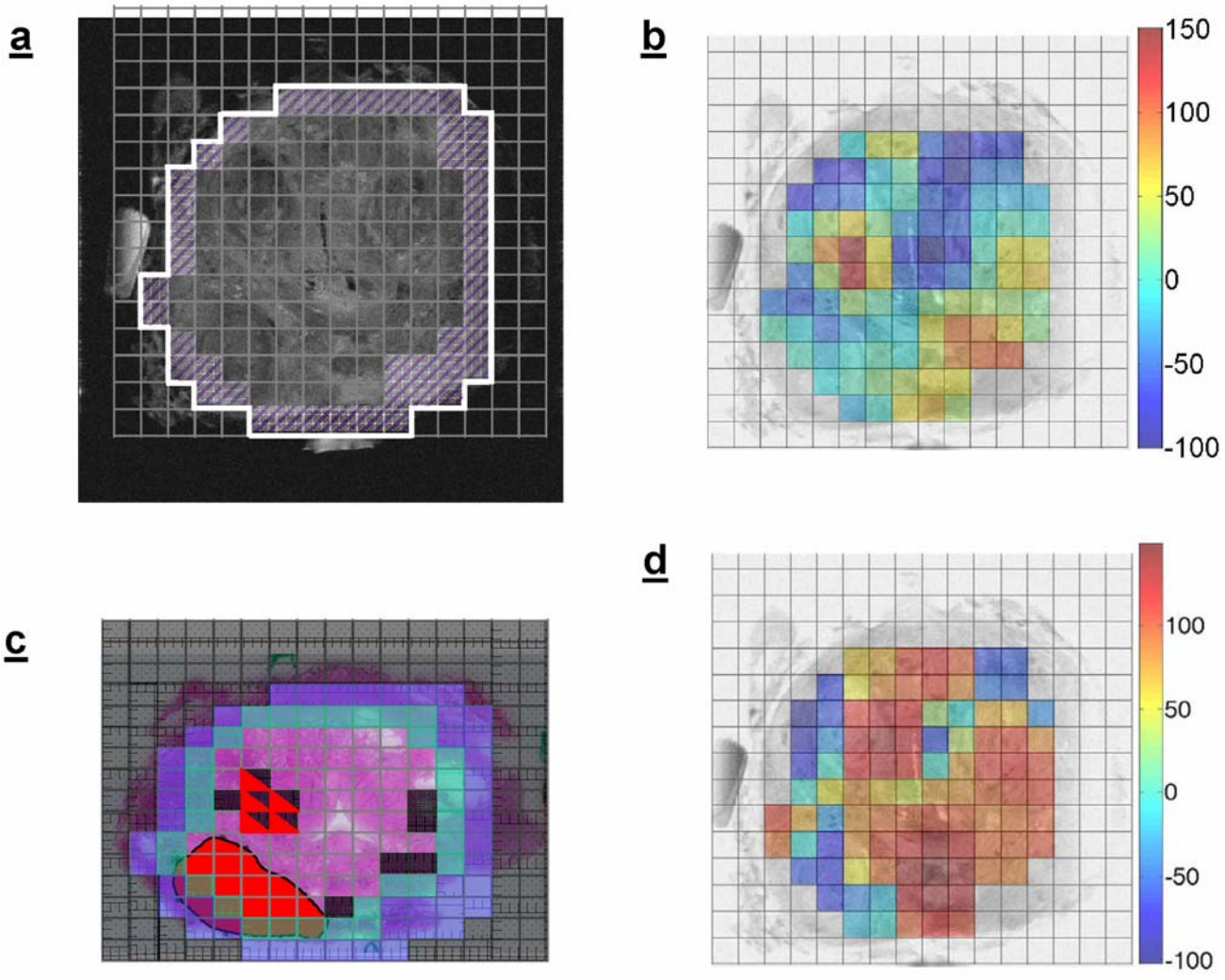

Figure 16. Metabolomic imaging of cancer from excised human prostate. (**a**). MRI of the prostate (orientation) cross-section overlaid with a grid indicating the locations of 16x16 voxels for which localized MRS was acquired for each voxel. The White border delineates the outline of the prostate cross-section. Data within the border were processed to produce a spectrum for each voxel. Due to the magnetic susceptibility interference, shaded voxels (tissue-air interface) of featureless spectra were eliminated from further analysis. (**b**). The values of the metabolomic profile were calculated by using parameters generated by Figure 1a for all voxels inward from the rim, and mapped onto the MR image. (**c**). Metabolomic profiles are plotted onto the whole-mounted prostate histology image of the approximately the same prostate cross-section level as in **a** with histology identified cancer region circled in Red. The voxels having profile values higher than median plus one time of standard deviation are labeled in Black. Black-Red Triangle forms a region of malignant suspicion that contain voxels that are at least one voxel layer inward from the rim (voxels in Green), in order to reduce out-of-voxel and susceptibility affects caused by voxels labeled in Purple (same as those shaded in **a**). The reasons and confounding factors that may cause the deviation of profile identified region from cancer histology region are discussed in the text. (**d**). A CC/C map is presented for comparison with **b**, see text for details.

To avoid any unknown, potential interference with the clinical pathology examination following MRS measurements, we did not immerse the prostates in magnetic-susceptibility compensated fluid while measuring them. Also, owing to susceptibility effects at the tissue-air interface, spectra in the shaded voxels in the **Figure 16a** were too featureless to be included for further analysis. The decision to eliminate these voxels from further analysis was made before the pathology results from the prostates were known.

Spectra from the remaining voxels were subjected to metabolite intensity analysis, from which prostate cancer metabolomic profiles were calculated. No metabolomic profile that had been constructed directly with data from the same experimental conditions as the current localized multi-voxel MRS was available for this exploratory study. Thus, as the first level of approximation, we borrowed prostate cancer metabolomic profiles (Canonical Score 1 in **Figure 15a**), determined from intact tissue MRS obtained at a higher field strength (14T) with higher spectral resolution achieved by sample magic angle spinning. The calculated profile value for each voxel was weighted by the values of its surrounding voxels and the results mapped onto the MR image, as shown in **Figure 16b**. As in **Figure 15a**, the more positive the profile value (in color Red), the higher we deemed the potential for a positive prostate cancer result.

In the current two-dimensional study, spectra in the center-plane were the data of choice and used when possible. This was due to their unique location, which was positioned close to the MR coil level. Measurements of spectra for side-planes were planed to increase detection of cancerous lesions in the studied planes, whether or not they were contained in the center-plane (information which could not have been known at the time of MRS measurement, prior to histology). Findings at whole-mounted histopathology evaluation of multiple levels of the five prostates revealed that the center-planes of two prostates contained no cancerous lesions. For these two prostates, both side-planes, on opposite sides of the center-plane, were included in the data analysis in order to reduce artifacts or bias that might be caused by the distance of a side-plane from the coil level. Thus, with five prostates, seven 16x16 voxel planes were analyzed. **Figure 16c** shows histopathology results for the same prostate level examined by MRS in **Figure 16a**. In **Figure 16c**, the histologically identified cancer lesion in the left-lower corner is marked in red; the shaded areas in **Figure 16a** are shown in Purple. Metabolite intensities from center voxels, bordered by and including the voxel

rims (in Green), were used to calculate the value of the prostate metabolomic profile for each voxel shown in **Figure 16b**.

Figure 15a shows the relationship between the median (M), standard deviation (SD) and differentiations of cancer from histologically benign samples. This median is more heavily weighted towards cancer (with equal numbers of cancer and histologically benign samples) than that in **Figure 16c**, where the cancer voxels are much fewer than those of histologically benign.

By calculating the value of median plus one standard deviation (M+SD) as a preliminary threshold, we identified those voxels (marked in Black in **Figure 16c**) which possessed values higher than M+SD. To reduce the effect of out-of-voxel contributions from boundary voxels (in purple) affected by magnetic susceptibility, we excluded the rim voxels (in green) from the M+SD calculation. To further eliminate possible interference slipping through the rim voxels, only those voxels which had values higher than (M+SD) and were also located at least one voxel layer inside of the rim (in green) were considered to be of independent value for further analysis (labeled in red-black triangles in **Figure 16c**). However, when voxels with values greater than M+SD were all located in the layer immediately inside the rim, this layer was excluded, and M and SD values were recalculated for the remaining voxels.

Figure 16d showed the resulting map generated by using a metabolite formula, CC/C: the ratio of spectral regions choline-to-creatine over citrate, proposed for in vivo prostate cancer detection with MRS imaging (MRSI) (compare with **Figure 16b**). We also analyzed the CC/C maps in the same manner as the metabolomic profile presented below; however, none of the CC/C results from these cases reached any statistical significance and so will not be further discussed.

On the seven planes analyzed for the five prostates, we identified seven tumor regions on five planes. For each tumor region, we measured its two-dimensional size, in mm^2, from the histological image, and estimated the partial size of those regions that extended inward beyond the rim voxels (Green, in **Figure 16c**).

From the metabolomic profile analysis conducted on the seven planes, and without knowing any histological conclusions, we identified 11 profile-elevated regions consisting of more than two consecutive voxels, each having a profile value greater than M+SD determined from the corresponding plane. Based on the level of elevation for each involved voxel and the number of connected voxels, we defined a Malignancy Index as the product of the sum of the profile values of the connected voxels that are all greater than M+SD, and the voxel size in mm^2. This Index can be viewed as a value that scales the absolute elevation of the metabolomic profile and may be used to compare different planes from different cases. We measured the distances from the centers of these profile-elevated regions to the centers of their potential corresponding tumor lesions on the same plane. We also calculated the shortest distances between the edges of these regions and lesions. These distances, together with the Malignancy Index are listed in the Table2.

Case number	Histo V(mm^2)	Histo/ MRS	Lesion number	Lesion Size(mm^2)	Lesion Inside(mm^2)	M+SD	Malignancy Index	Distance (center, mm)	Distance (close-edge, mm)
1a	6.8	75.6	1	101.4	27.2	36.5	852.7	7.4	0
						50.8			
						38.1			
			2	27.0	0	34.9	237.3	7.9	4.5
1b	7.3	81.1	--	--	--	54.5	1761.5	--	--
						61.2			
						47.1			
						78.5			
			--	--	--	38.0	519.0	--	--
						33.1			
2a	6.3	70.0	1	56.7	22.1	63.5	2125.6	8.6	1.3
						70.8			
						53.4			
						75.3			
						74.4			
2b	7.4	82.2	--	--	--	40.2	499.5	--	--
						27.3			
3	6.4	71.1	1	31.8	1.2	71.1	794.2	10.7	8.5
						53.0			
			2	12.8	9.6	--	0	--	--
4	6.2	68.9	1	98.6	52.7	64.9	2840.84	9.0	1.1
						144.6			
						129.7			
						54.1			
						64.9			
5	5.4	60.0	1	2.0	0	14.7	195.5	16.5	10.5
						21.5			
						23.6	597.2	18.5	11.5
						14.7			
						30.4			
						22.5			
						19.4			

Table 2. Metabolomic and histology measurements.

Figure 17 summarizes selected correlations of statistical significance concluded from data in Table 2. Due to the above mentioned intrinsic magnetic susceptibility interference that affect the reliability of data close to the rim of the analyzed prostate planes and a number of other confounding factors such as magnetic field inhomogeneity and specimen shrinkage during histology process (an average reduction of 27.3±7.7% was recorded in this study), the locations of metabolomic profile-elevated regions of cancer suspicion are not expected to coincide exactly with the malignant regions presented on the histological images. The potential corresponding relationship between the two regions may be evaluated and validated by the measured distances both between the centers and shortest edges of the two regions. Evaluation of these distance revealed that the larger the tumor sizes, the shorter the measured distances, with the examples of shortest edge distances shown in **Figure 17a**. **Figure 17b** presents a similar linear relationship between the shortest edge distances and the partial lesion sizes inside the rim. However, in addition to the seemingly linear correlation, data in this figure may also be viewed as two distinctive groups: those where no lesion extended into the rim and those with reasonable sizes of partial lesions inside the rim. For the former group, the shortest distance ranged between 4 to 12 mm, which challenges the validity of these regions to be considered as true malignancy representation, while for the latter group, the distances reduced to less than 2 mm and reconfirmed their potential links to the presence of malignancy.

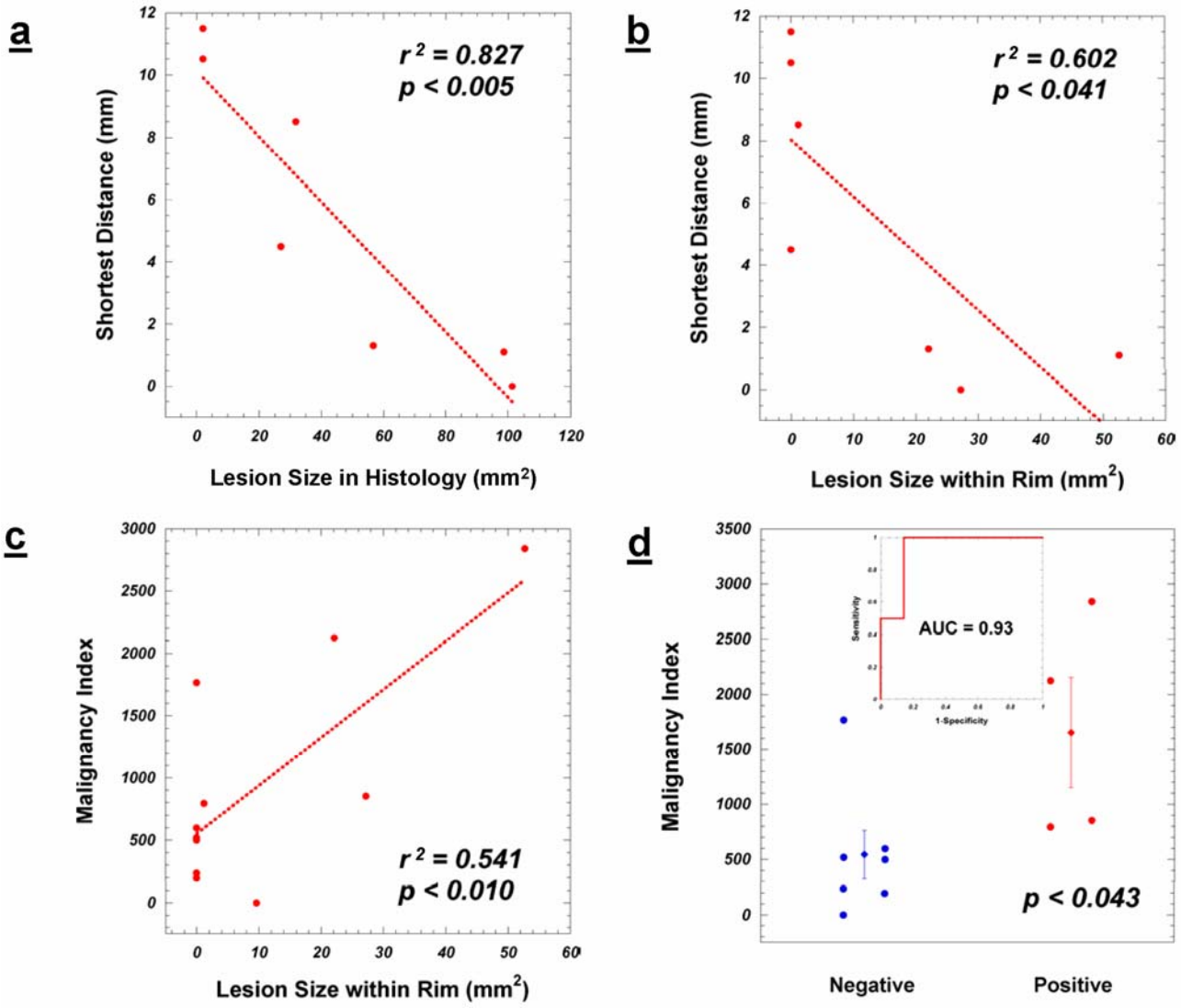

Figure 17. **Correlations of metabolomic profiles with histology**. (**a**). The shortest distances between the edges of metabolomic profile identified suspicious regions and histologically defined cancer regions on the same plane linearly correlated with the sizes of cancer measured on the examined plane, which indicates the validity of considering these profile-elevated regions to be linked with the concerned cancer regions. (**b**). The indication can be further evaluated by considering the relationship between these shortest distances and the partial cancer sizes that are located inside the rim, see text for discussion. (**c**). A linear relationship between Malignancy Index and the partial cancer sizes suggests the index can indicate the existence of malignancy. (d). This indication is further investigated as a threshold for cancer detection. See text for details.

The current study was inspired by the potential utility of metabolomic imaging in disease diagnosis, particularly in the detection of human prostate cancer for which no existing radiological protocol can effectively direct biopsy to sites that are likely cancer positive. Although the above analyses of the sizes of metabolomic regions and shortest edge distances may indicate the overall area of biopsy interest, in clinical reality it may be necessary to further evaluated and separate these metabolomic profile-elevated regions into different categories according to their malignant potentials for within any measured plane, disregarding the presence and absence of malignancy, some voxel regions will possess profile values of great then its own M+SD. Thus, in **Figure 17c**, the utility of Malignancy Index for such a differentiation is introduced. Furthermore, as a conclusion of data presentation,

with **Figure 17d** we can conservatively estimate that by using Malignancy Index defined from metabolomic profile, cancer lesions with extensions into the rim and with an overall size of more than twice of the MRS voxel sizes (18 mm^2), can be detected (within the area defined by the metabolomic profile-elevated region plus a perimeter of less than 2.7±1.9 mm) with an overall accuracy of 93%.

As an exploratory study of the concept of metabolomic imaging with removed human prostates, our evaluation is limited by a large number of confounding factors. In addition to the already discussed factors (such as the magnetic susceptibility, field inhomogeneity, specimen shrinkages during histology, the utilization of metabolomic profiles established under different experimental conditions, etc), other issues including the affects of tumor grades, pathology stages, patient medical histories, etc. were beyond the level that our current metabolomic knowledge on human prostate cancer to comfortably address. However, some of these recognized confounding issues may only be addressed by the future in vivo implementation of the tested concept. For instance, the magnetic susceptibility complication caused by tissue-air interface may be much less of a concern with in vivo MRS measurement and thus the MR spectra from the edge voxels of the prostate may also be usable for the complete inspection of the entire prostate rather than to be eliminated as seen above.

The concept of metabolomic imaging has evolved MRS and MRSI from an imaging of a defined metabolite, metabolite regions, or ratios of metabolites, into a mapping of an abstract value defined for a particular medical condition. Because of this transformation into the abstract, the concept of metabolomic imaging presented here and its potential clinical usage is not limited to the MRS measurable metabolites. This imaging paradigm may be applied to any, or any group or groups of, biomedical and/or molecular parameters so long as these parameters can be measured in vivo from known anatomic locations in clinic, in either two-dimensional or three-dimensional spaces, and the formula(s) to construct them into an abstract profile specific to the concerned medical condition is established.

KEY RESEARCH ACCOMPLISHMENTS:

-- Publication of the first population study of prostate cancer metabolite profiles in Cancer Research (April 15, 2005).

-- Identification of the linear relationship between ODC gene expression levels in benign prostate epithelia and prostate cancer growth rates.

-- Verification of the feasibility in conducting HRMAS spectroscopy and histpathology studies on human thin core biopsies.

-- Continuations in sample collections, spectroscopy and quantitative pathology analyses.

-- Development of novel metabolomic imaging paradigm.

REPORTABLE OUTCOME:

Publications:

In the past three years, in direct relation to the proposed project, we have published nine articles and three book chapters:

1. Taylor JL, Wu CL, Cory D, Gonzalez RG, Bielecki A, Cheng LL. High-resolution magic angle spinning proton NMR analysis of human prostate tissue with slow spinning rates. *Magn Reson Med* 2003;**50**:627-632.
2. Wu CL, Taylor JL, He WL, Zepeda AG, Halpern EF, Bielecki A, Gonzalez RG, Cheng LL. Proton high resolution magic angle spinning nmr analysis of fresh and previously frozen tissue of human prostate. *Magn Reson Med* 2003;**50**:1307-1311.
3. Burns MA, He W, Wu CL, Cheng LL. Quantitative pathology in tissue MR spectroscopy based human prostate metabolomics. *Technol Cancer Res Treat* 2004;**3**: 591-598.
4. Burns MA, Taylor JL, Wu CL, Zepeda AG, Bielecki A, Cory D, Cheng LL. Reduction of spinning sidebands in proton NMR of human prostate tissue with slow high resolution magic angle spinning. *Magn Reson Med* 2005; **54:**34-42.
5. Cheng LL, Burns MA, Taylor JL, He WL, Halpern EF, McDougal WS, Wu, CL. Metabolic characterization of human prostate cancer with tissue magnetic resonance spectroscopy. *Cancer Res.* 2005; **65**:3030-3034.
6. Loening NM, Chamberlin AM, Zepeda AG, Gonzales RG, Cheng LL. Quantification of phosphocholine and glycerophosphocholine with ^{31}P edited ^{1}H NMR spectroscopy. *NMR Biomed*. 2005; **18**:413-420.
7. Lentz MR, Taylor JL, Feldman DA, Cheng LL. Current clinical applications of *in vivo* magnetic resonance spectroscopy and spectroscopic imaging. *Curr Med Imag Rev*. 2005;**1**:271-302.
8. Cheng LL, Burns MA, Lean CL. High resolution magic angle spinning (HRMAS) proton MRS of surgical specimens. In: C Mountford & U Himmelreich (eds) "Medical Uses", (vol II), Modern Magnetic Resonance, G Webb (ed), Springer, London, 2006.
9. Cheng LL, Pohl U. The role of NMR-based metabolomics in cancer. In Handbook of Metabonomics and Metabolomics, Lindon JC, Nicholson J, Holmes E (eds), Elsevier, Amsterdam, 2007.
10. Jordan K, He W, Halpern E, Wu C, Cheng L. Evaluation of tissue metabolites with high resolution magic angle spinning MR spectroscopy human prostate samples after three-year storage at -80C. *Biomarker Insights* 2007;**2**:147-154.
11. Jordan KW, Cheng LL. NMR-based metabolomics approach to target biomarkers for human prostate cancer. *Expert Rev Prot* 2007, In press.
12. Jordan KW, Cheng LL. Metabolic characterization of prostate cancer: magnetic resonance spectroscopy. In: Cancer Imaging (vol II), MA Hayat (ed), Elsevier, In press.

In addition, our work from or partially from this award has been accepted for presentations:

13. Jordan KW, Cheng LL. Evaluation of Human Prostate Tissue Metabolites with High Resolution Magic Angle Spinning MR Spectrscopy After Three-Year Storage at -80C. Presentation at the 14th Annual Meeting of ISMRM, 2006.
14. Cortez-Retamozo VF, Jordan KW, He WL, Wu CL, Cheng LL. Evaluating human prostate cancer growth with ornithine decarboxilase. The 97th AACR Annual Meeting, Washington DC, 2006.
15. Jordan KW, Ratai E, Sheng J, Jenkins BG, Dai G, Ying LL, Wu CL, Cheng LL. Metabolomic Imaging. Presentation at the 15th Annual Meeting of ISMRM, 2007.

Furthermore, two patents have been applied:

16. Cheng LL, Pohl U, Wu CL. Method for the diagnosis and prognosis of cancer. PCT/US2006/41655.
17. Cheng LL, Wu CL, Jenkins BG, Dai G, Halpern EF. System, method and software arrangement for analyzing and correlating molecular profiles associated with anatomical structures. PCT/US2006/013517.

Invited Lectures:

18. Departmental Seminar
    "In the Beginning … - NMR on Cancer"
    Department of Biophysics and Physicology
    Boston University School of Medicine
    Boston, Massachusetts
    2005
19. The 5th Bi-Annual 2005 Minnesota Workshop on High Field MR Imaging and Spectroscopy and MR Imaging of Brain Function
    Department of Radiology
    University of Minnesota
    Minneapolis, Minnesota.
    October 14-16, 2005
20. "Metabolomic Profiling of Human Cancer with ex vivo Tissue MR Spectroscopy"
    Frontiers of Metabolomics for Cancer Research
    National Cancer Institute
    National Institute of Health
    Rockville, Maryland
    October 24-25, 2005
21. Departmental Seminar
    "Metabolomic of Prostate Cancer"
    Department of Urology
    Boston University School of medicine
    2006
22. Departmental Seminar
    "Magnetic Resonance on Cancer Metabolomics"
    Department of Biomedical Engineering
    Case Western Reserve University
    2006
23. Invited Lecture, The 2006 International Workshop on
    Functional Lung Imaging at Penn
    "Tissue and Serum Metabolomic Profiles of Lung Cancer"
    University of Pennsylvania
    2006
24. Invited Lecture, The First International Workshop on Hyperpolarized Carbon-13 and its Application in Metabolic Imaging
    "Metabolomic Imaging in Disease Diagnosis"
    University of Pennsylvania

2006

NIH R01 Grant Award:

25. NCI/NIH R01CA115746 (Cheng)
Characterizing Prostate Cancer by ex vivo MRS Signatures
2006-2011

CONCLUSION:

In the past three years of the award, in accordance with our proposed research pans, we have achieved overall successes. These achievements have been summarized in the "Reportable Outcomes". More importantly, based on the data gathered here, we have invented the concept of metabolomic imaging, which in addition to generating more NIH supports for our future research, will greatly impact the field of diagnostic radiology.

REFERENCES:

1. Jordan K, He W, Halpern E, Wu C, Cheng L. Evaluation of tissue metabolites with high resolution magic angle spinning MR spectroscopy human prostate samples after three-year storage at -80C. Biomarker Insights 2007;2:147-154.
2. Loening NM, Chamberlin AM, Zepeda AG, Gonzalez RG, Cheng LL. Quantification of phosphocholine and glycerophosphocholine with 31P edited 1H NMR Spectroscopy. NMR Biomed 2005:In press.
3. Burns MA, Taylor JL, Wu CL, Zepeda AG, Bielecki A, Cory DG, Cheng LL. Reduction of Spinning Sidebands in Proton NMR of Human Prostate Tissue With Slow High-Resolution Magic Angle Spinning. Magnetic Resonance in Medicine 2005;53:In Press.
4. Cheng LL, Burns MA, Taylor JL, He W, Halpern EF, McDougal WS, Wu CL. Metabolic characterization of human prostate cancer with tissue magnetic resonance spectroscopy. Cancer Res 2005;65(8):3030-3034.
5. Cortez-Retamozo V, Jordan K, He W, Wu C, Cheng L. the 97th AACR Annual Meeting. 2006; Washington, DC.
6. Taylor JL, Wu CL, Cory D, Gonzalez RG, Bielecki A, Cheng LL. High-resolution magic angle spinning proton NMR analysis of human prostate tissue with slow spinning rates. Magn Reson Med 2003;50(3):627-632.
7. Wu CL, Taylor JL, He W, Zepeda AG, Halpern EF, Bielecki A, Gonzalez RG, Cheng LL. Proton High Resolution Magic Angle Spinning NMR Analysis of Fresh and Previously Frozen Tissue of Human Prostate. Magn Reson Med 2003;50:1307-1311.
8. Burns MA, He W, Wu CL, Cheng LL. Quantitative pathology in tissue MR spectroscopy based human prostate metabolomics. Technol Cancer Res Treat 2004;3(6):591-598.

APPENDICES:

1. Taylor JL, Wu CL, Cory D, Gonzalez RG, Bielecki A, Cheng LL. High-resolution magic angle spinning proton NMR analysis of human prostate tissue with slow spinning rates. *Magn Reson Med* 2003;**50**:627-632.
2. Wu CL, Taylor JL, He WL, Zepeda AG, Halpern EF, Bielecki A, Gonzalez RG, Cheng LL. Proton high resolution magic angle spinning nmr analysis of fresh and previously frozen tissue of human prostate. *Magn Reson Med* 2003;**50**:1307-1311.
3. Burns MA, He W, Wu CL, Cheng LL. Quantitative pathology in tissue MR spectroscopy based human prostate metabolomics. *Technol Cancer Res Treat* 2004;**3**: 591-598.
4. Burns MA, Taylor JL, Wu CL, Zepeda AG, Bielecki A, Cory D, Cheng LL. Reduction of spinning sidebands in proton NMR of human prostate tissue with slow high resolution magic angle spinning. *Magn Reson Med* 2005; **54:**34-42.
5. Cheng LL, Burns MA, Taylor JL, He WL, Halpern EF, McDougal WS, Wu, CL. Metabolic characterization of human prostate cancer with tissue magnetic resonance spectroscopy. *Cancer Res.* 2005; **65**:3030-3034.
6. Loening NM, Chamberlin AM, Zepeda AG, Gonzales RG, Cheng LL. Quantification of phosphocholine and glycerophosphocholine with ^{31}P edited ^{1}H NMR spectroscopy. *NMR Biomed*. 2005; **18**:413-420.
7. Lentz MR, Taylor JL, Feldman DA, Cheng LL. Current clinical applications of *in vivo* magnetic resonance spectroscopy and spectroscopic imaging. *Curr Med Imag Rev*. 2005;**1**:271-302.
8. Cheng LL, Burns MA, Lean CL. High resolution magic angle spinning (HRMAS) proton MRS of surgical specimens. In: C Mountford & U Himmelreich (eds) "Medical Uses", (vol II), Modern Magnetic Resonance, G Webb (ed), Springer, London, 2006.
9. Cheng LL, Pohl U. The role of NMR-based metabolomics in cancer. In Handbook of Metabonomics and Metabolomics, Lindon JC, Nicholson J, Holmes E (eds), Elsevier, Amsterdam, 2007.
10. Jordan K, He W, Halpern E, Wu C, Cheng L. Evaluation of tissue metabolites with high resolution magic angle spinning MR spectroscopy human prostate samples after three-year storage at -80C. *Biomarker Insights* 2007;**2**:147-154.
11. Jordan KW, Cheng LL. NMR-based metabolomics approach to target biomarkers for human prostate cancer. *Expert Rev Prot* 2007, In press.
12. Jordan KW, Cheng LL. Metabolic characterization of prostate cancer: magnetic resonance spectroscopy. In: Cancer Imaging (vol II), MA Hayat (ed), Elsevier, In press.
13. Cheng LL, Pohl U, Wu CL. Method for the diagnosis and prognosis of cancer. PCT/US2006/41655.

Magnetic Resonance in Medicine 50:627–632 (2003)

High-Resolution Magic Angle Spinning Proton NMR Analysis of Human Prostate Tissue With Slow Spinning Rates

Jennifer L. Taylor,[1] Chin-Lee Wu,[1] David Cory,[2] R. Gilberto Gonzalez,[3] Anthony Bielecki,[4] and Leo L. Cheng[1,3*]

The development of high-resolution magic angle spinning (HR-MAS) NMR spectroscopy for intact tissue analysis and the correlations between the measured tissue metabolites and disease pathologies have inspired investigations of slow-spinning methodologies to maximize the protection of tissue pathology structures from HR-MAS centrifuging damage. Spinning sidebands produced by slow-rate spinning must be suppressed to prevent their complicating the spectral region of metabolites. Twenty-two human prostatectomy samples were analyzed on a 14.1T spectrometer, with HR-MAS spinning rates of 600 Hz, 700 Hz, and 3.0 kHz, a repetition time of 5 sec, and employing various rotor-synchronized suppression methods, including DANTE, WATERGATE, TOSS, and PASS pulse sequences. Among them, DANTE, as the simplest scheme, has shown the most potential in suppression of tissue water signals and spinning sidebands, as well as in quantifying metabolic concentrations. Magn Reson Med 50: 627–632, 2003. © 2003 Wiley-Liss, Inc.

Key words: HR-MAS; proton MRS; human prostate; slow spinning

The use of ex vivo high-resolution magic angle spinning (HR-MAS) in proton NMR studies of intact tissue results in highly resolved spectra comparable to those observed with solutions of tissue chemical extractions (1–8). However, unlike destructive chemical extractions, the HR-MAS method largely preserves histopathological structures intact, granting the opportunity for samples to be histopathologically examined after NMR measurement, which is extremely important, particularly for studies of human neoplastic diseases because of the well-known heterogeneous characteristics within individual tumors.

The HR-MAS method achieves high spectral resolution from biological tissues by eliminating spectral broadening largely caused by magnetic susceptibility. In the frequency domain of an NMR spectrum, spinning splits the broad resonance into a center peak at the isotropic resonance frequency and a number of spinning sidebands (SSBs) separated by the spinning rate. If the spinning frequency is greater than the frequency region of cellular metabolites, the SSB will be pushed outside of the region of interest, so that the region consists of only individual isotropic resonance peaks. In studies of biological cells and/or tissues, water, arising from either the media or the tissue itself, is the most intense resonance and the component contributing to the largest observed SSB. To eliminate the complication of water SSB on spectra of cellular metabolites, spinning rates that are equal to or above 5 ppm (3.0 kHz at 14.1T) have commonly been employed.

It has also been noted experimentally that spectral broadening primarily induced by bulk magnetic susceptibility can be substantially reduced with a sample-spinning rate of a few hundred Hz. In other words, if the complex issue of water SSB could be resolved, HR-MAS proton NMR spectra for most intact tissue could be measured at a spinning rate at least an order of magnitude lower than is commonly used. A reduction in sample spinning rates by 5–10-fold represents a 25–100-fold decrease in spinning-induced centrifugal stress. Since centrifugal stress may damage the organizational structure of connective tissue, although perhaps not disrupt cells, reducing spinning centrifugal stress can better preserve tissue pathological structures, which will translate into a more accurate evaluation of their pathologies (9).

We studied slow HR-MAS with various SSB suppression methodologies on human prostate tissues. We evaluated and compared rotor-synchronized DANTE (delays alternating with nutations for tailored excitation) (10,11), rotor-synchronized WATERGATE (water suppression by gradient-tailored excitation) (12), 1D-TOSS (total sideband suppression) (13), and 2D-PASS (phase-adjusted spinning sidebands) (14) sequences with presaturation for water suppression. Among these techniques, we found the rotor-synchronized DANTE sequence to be the most robust technique in terms of the reproducibility of SSB suppression and simplicity in concept and execution. Results of DANTE measurements at spinning rates of 600 and 700 Hz are reported here.

MATERIALS AND METHODS

Tissue Protocol

Samples from 22 prostatectomy cases were used in the study. Among them, for the first 13 cases two samples from each case were analyzed separately at low speeds (600, then 700 Hz) or at high speed (3.0 kHz), and the histopathological integrity of each sample was compared with the integrity observed from the adjacent tissue that was not subjected to spinning. For the remaining nine

[1]Department of Pathology, Massachusetts General Hospital, Harvard Medical School, Boston, Massachusetts.

[2]Department of Nuclear Engineering, Massachusetts Institute of Technology, Cambridge, Massachusetts.

[3]Department of Radiology, Massachusetts General Hospital, Harvard Medical School, Boston, Massachusetts.

[4]Francis Bitter Magnet Laboratory, Massachusetts Institute of Technology, Cambridge, Massachusetts.

Grant sponsor: PHS/NIH; Grant numbers: CA77727; CA80901; RR00995.

*Correspondence to: Leo L. Cheng, Pathology Research, CNY-7, 149 13th Street, Charlestown, MA 02129. E-mail: cheng@nmr.mgh.harvard.edu.

Received 28 October 2002; revised 2 May 2003; accepted 2 May 2003.

DOI 10.1002/mrm.10562

Published online in Wiley InterScience (www.interscience.wiley.com).

cases, one sample from each case was measured both at low (600, then 700 Hz) and then at high (3.0 kHz) spinning rates in order to evaluate the observed metabolite intensities from the same tissue under different rates of spinning.

HR-MAS Proton NMR

The NMR experiments were carried out on a Bruker (Billerica, MA) AVANCE spectrometer operating at 600 MHz (14.1T). A 4 mm zirconia rotor was used with Kel-F plastic inserts which created a spherical sample space of ~10 μl located at the center of the detection coil. A small (~10^{-1} mg) silicone rubber sample was permanently affixed inside one of the Kel-F spacers, positioned within the detection coil but not in contact with the sample, to function as an external standard for both frequency reference (0.06 ppm from TMS) and quantification. Tissue samples, ~8–10 mg, were used directly from freezers without further preparation. Sample packing was performed on a metal surface covered with gauze and resting on dry ice. Approximately 1.0 μl of D_2O was added into the rotor for ^2H field locking. Within less than 3 min after the completion of tissue packing, the rotor containing the tissue sample and D_2O was introduced into the probe precooled to 3°C. After waiting an additional ~3 min for temperature equilibration, the NMR spectra were measured. All NMR measurements were carried out at 3°C for better tissue preservation. At this temperature, spectral line-width of tissue water and the D_2O lock solvent indicated that the sample was not in a frozen state. While the freezing point of D_2O is nominally 3.8°C, its freezing point is evidently depressed by dispersal in tissue fluids. The rotor-spinning rate was regulated by a MAS controller (Bruker), and verified by measurements of inter-SSB distances from spectra with an accuracy of ±1.0 Hz. Each spectrum was acquired with 32 transients and a repetition time of 5 sec.

The DANTE pulse sequence achieves resonance selectivity based on the timing of RF pulses. We used rotor-synchronized DANTE, i.e., the interpulse spacings were set equal to the rotor cycle time. This has the effect of suppressing signal components spaced at intervals of the rotor frequency and centered on the spectrometer frequency. In our experiments, we set the spectrometer frequency on the water resonance. The water peak and all of its SSBs are therefore suppressed, but so, too, are any other resonances that occur close to those frequencies. A rotor-synchronized CPMG filter (10 ms) was included in the pulse sequence after the execution of the DANTE pulses to reduce broad resonances associated with probe background, rotor, and/or macromolecules. One thousand DANTE pulses of 1.5 μs (8.4° flip angle) were used. Figure 1 shows the diagram of the pulse sequence, including both CPMG and DANTE components.

Spectroscopic data were processed by using the Nuts software (Acorn NMR, Livermore, CA) according to the following procedures. All free induction decays were subjected to 1 Hz apodization before Fourier transformation, baseline correction, and phase adjustment. Resonance intensities reported here represent integrals of curve-fittings with Lorentzian-Gaussian line-shapes.

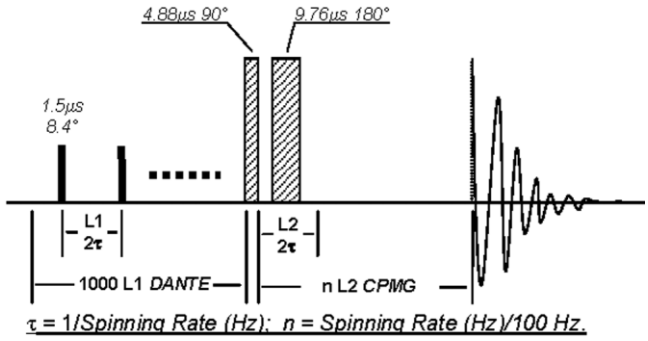

FIG. 1. A diagram of the rotor-synchronized CPMG-DANTE pulse sequence used in the study.

Histopathology

In this study, evaluation of tissue histopathology was focused on the comparison of varying HR-MAS-induced spinning centrifugal stresses on the resulting histopathology integrity. To achieve this aim with the first 13 cases, as previously described, both high rate and low rate HR-MAS experiments were conducted on separate but adjacent tissue samples. Specifically, specimens of ~30 mg from each case were cut with a surgical blade into three approximately equal portions. While one sample was used directly for histopathology evaluation, the other two were used to measure HR-MAS spectra at different spinning rates at 3°C. One sample was spun at 600 Hz for about 45 min, then at 700 Hz for about 15 min, while the other was spun at 3.0 kHz for 1 hr. These two spun samples, as well as the nonspinning sample, were processed according to routine histopathological procedures, cut into 7-μm sections on a cryotome, and stained with hematoxylin and eosin. A set of three individual cuts spaced 100 μm apart was obtained from each sample. These three sets of histopathological images from each case were compared by the pathologist in a random order to determine the effect of HR-MAS rates on the pathology structures. The pathologist was blinded from the history of samples and asked simply to identify the worst tissue quality among the three sets for each case in terms of tissue histopathological integrity by visual examination.

RESULTS

Spinning Effects on Tissue Histopathological Appearance

Figure 2 shows an example of the effects of HR-MAS stress on tissue morphology. All three images were obtained with the same clinical case, from adjacent tissue, and under the same magnification. Figure 2a shows a histopathological image of human prostate tissue that was obtained directly from frozen sample without being subjected to a spinning test. The image shows normal glandular structures with well-defined epithelial cells. Figure 2b shows the adjacent tissue of the same specimen after an HR-MAS experiment of slow spinning rates (600, 700 Hz). The image exhibits morphological structures similar to that of the original sample (Fig. 2a). Figure 2c shows another adjacent sample of the same specimen after its HR-MAS analysis at a higher spinning frequency of 3.0 kHz.

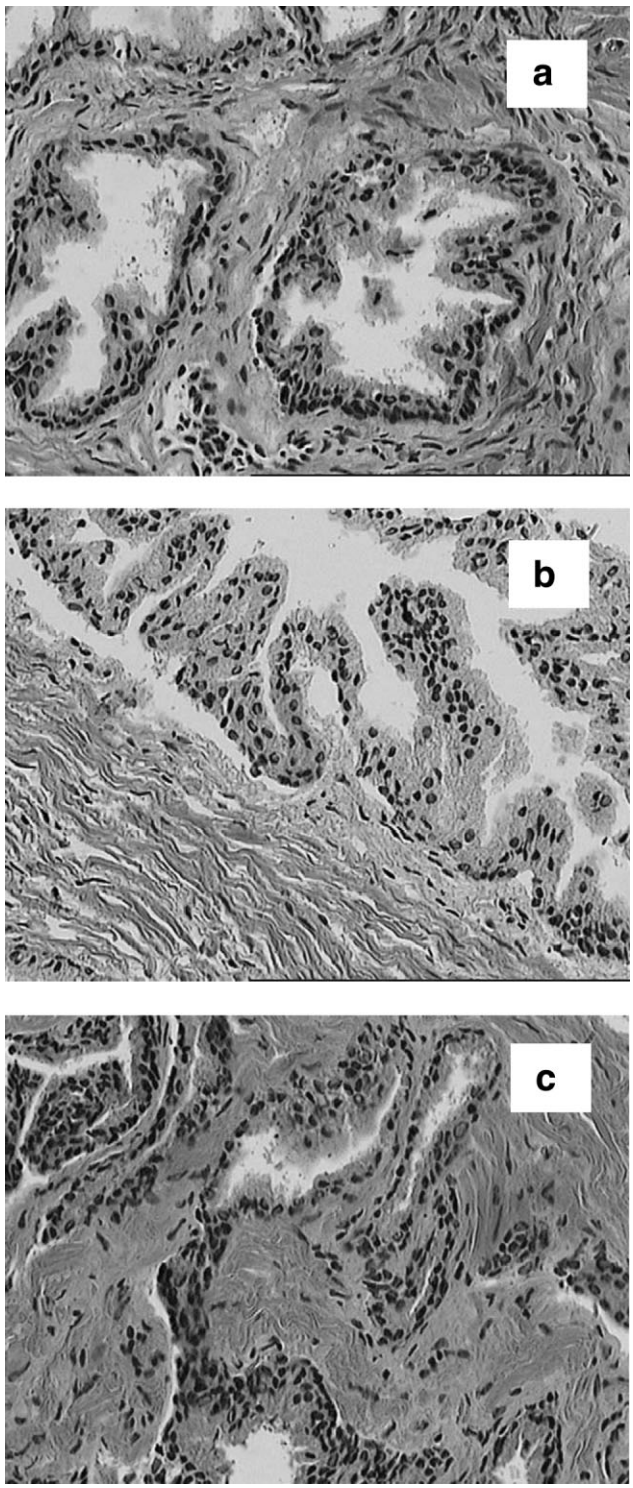

FIG. 2. The effects of HR-MAS stress on tissue morphology. **a:** A human prostate tissue sample taken directly from a tissue bank without HR-MAS testing. The tissue showed highly organized ductal cellular structures with well-defined epithelial layers. **b:** Another sample from the same patient but after an HR-MAS experiment, which involved spinning at 600 Hz for 45 min and then 700 Hz for 15 min. The tissue still exhibits a normal ductal structure that cannot be differentiated from the original sample (**a**). **c:** A sample, again from the same clinical case, after MAS analysis at higher spinning frequency, 3.0 kHz, for 1 hr. The tissue ductal structures are visibly distorted compared with the natural specimens. (Images presented at the same magnification.)

The distortion of ductal epithelial structures is visible when compared with ducts in Fig. 2a,b. Similar spinning effects on prostate tissue and the compromised histopathological integrity with 3.0 kHz spinning frequency were observed consistently with all 13 cases. Specifically, the pathologist always identified the tissue set after 3.0 kHz spinning to be the worst in pathological integrity for all cases. However, it should also be pointed out that such a compromise in histopathological structures did not hinder the pathologist's ability to differentiate, for instance, cancer from normal cells at cellular levels. Only the macrostructures, such as estimation of the amount of normal epithelial ducts, are affected by the fast spinning.

DANTE Spectra

At slow spinning rates, such as 600 Hz, HR-MAS single-pulse proton spectra of tissues are dominated by a large water peak and its SSB, typically with large amplitudes over a range of several ppm, as shown in Fig. 3a. The water centerband can be suppressed reasonably well with presaturation (with 5-sec CW during recycle delay time and a power level of 60 dB reduction from that of excitation pulses). Presaturation also reduces the SSB intensities, but these reductions were not sufficient to create clean spectra for metabolite quantification (see Fig. 3b). With DANTE pulses, as shown in Fig. 4a,b, although residual water SSB are still observable, they are reasonably small compared with those shown in Fig. 3. In either the 600 or 700 Hz spectrum, DANTE suppression leaves invalid regions that cannot be used for metabolite measurement. These two spin rates were selected to meet the following criteria: 1) the difference between the spin rates (100 Hz) is much greater than the water and metabolite linewidths ($<$10 Hz), and also greater than the width of the spectral regions attenuated by the DANTE pulse sequence (42 Hz); 2) arbitrary multiples of the two spin rates approach no closer than the difference between spin rates, except at their least

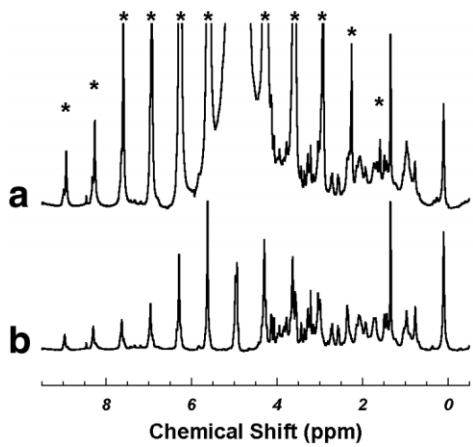

FIG. 3. **a:** An HR-MAS single-pulse proton spectrum of prostate tissue dominated by a large water peak and its SSB at 600 Hz. **b:** Suppression of water centerband with presaturation. Presaturation also reduces the SSB intensities, but these reductions were not sufficient to create clean spectra for metabolite quantification. Asterisk denotes spinning sidebands in this figure and in those that follow.

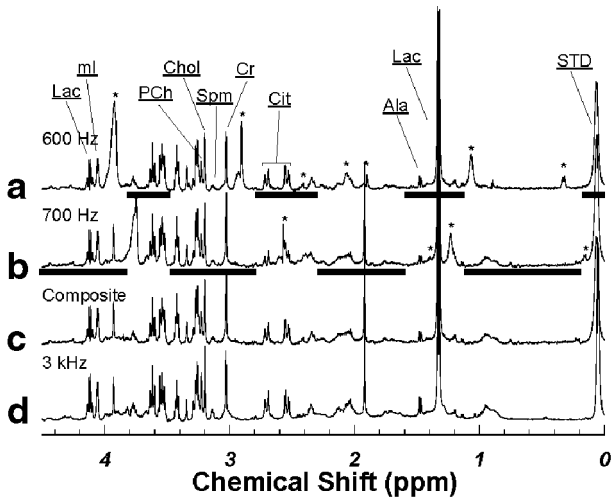

FIG. 4. Human prostate rotor-synchronized DANTE spectra at spinning rates of (**a**) 600 Hz, and (**b**) 700 Hz. **c:** A spectrum composed from (**a**) and (**b**) to be visually compared with (**d**) a spectrum obtained at spinning rate of 3.0 kHz. Abbreviations: Lac, lactate; ml, myo-inositol; PCh, phosphorylcholine; Chol, choline; Spm, spermine; Cr, creatine; Cit, citrate; Ala, alanine; STD, rubber standard. Spectral regions of **a** and **b** used to generate **c** are labeled with horizontal bars beneath them. The following symbols are used to denote SSB: "*," tissue water; "+," STD; and "#," Lac at 1.33 ppm.

common multiple; 3) the least common multiple of the two spin rates (4.2 kHz, or 7 ppm) is greater than the width of the region of water and metabolite peaks (3.0 kHz, or 5 ppm); and 4) the two spinning rates are close enough that the intensities of a particular tissue metabolite measured from both spectra are identical. These criteria ensure that every point in the region-of-interest will be free of water SSB and DANTE holes in at least one of the two spectra. Thus, the two spectra together may be used to estimate intensities for each metabolite peak, except for a small region near the water centerband. However, this issue of the distortion of spectral regions near the water centerband is common with any scheme of water suppression.

Figure 4c shows a composite spectrum, which was assembled simply by cutting and pasting valid regions of the 600 and 700 Hz HR-MAS spectra. These valid regions were free of SSB from tissue water and the external standard, as indicated by the horizontal bars under Fig. 4a,b, respectively. Figure 4c shows a close similarity to the 3.0 kHz spectrum, shown in Fig. 4d. Here we wish to point out that, in our experience studying human prostate samples, we have not seen severe spectral complication due to SSB from metabolites (except lactate at 1.33 ppm; cf. Fig. 4a,b). This phenomenon further proves that the primary effect of HR-MAS in biological tissue analysis is to average magnetic susceptibility of mobile cellular metabolites, rather than to overcome solid effects of metabolite molecules as in the case of solid-state NMR. However, should visible SSBs from metabolites present, the currently identified spectral regions under the tested spinning rates may still contain metabolite SSB. Nevertheless, we consider that Fig. 4c serves only as a visual illustration of a complete, sideband-free spectrum. A quantitative evaluation of a particular metabolite can be carried out directly from at least one of the two original spectra at a 600 or 700 Hz spinning rate, where SSBs do not overlap with the resonance of interest. Therefore, although the cutting and pasting process plays a helpful role for visualization of the results, it is not a necessary or a recommended method for the quantification of tissue metabolites. It should always be possible, by selecting a certain spinning rate, to quantify a defined metabolic marker (or markers) with a single DANTE-CPMG spectrum.

Metabolite Intensities

The accuracy of cellular metabolite intensities measured at slow HR-MAS rates can be evaluated by comparing them with those measured at "traditional" or high HR-MAS spinning rates. Figure 5 plots the sum of metabolite intensities identified in Fig. 4 as a function of sample weights, measured at slow spinning rates (600, 700 Hz), as well as 3.0 kHz, under otherwise identical experimental conditions (DANTE presaturation time and T_2 filter time). Only samples with weight <11 mg are included in the figure because the sample space created by the spherical inserts is $\sim$10 μl. For samples with weights much more than 10 mg, we observed that some of the tissue and/or fluids were squeezed out of the space into the well of the sealing screw in the upper insert. Figure 5 shows that the linear relationship under slow spinning condition passes much closer to the origin. Therefore, the correlation between sample weights and the total resonance intensity is better preserved under slow spinning conditions.

We next compared the intensities of individual metabolite resonances measured at slow spinning rates (600, 700 Hz) with those at 3.0 kHz for the same tissue samples from nine clinical cases. Linear regression results (slow rates: vertical, vs. 3.0 kHz rate: horizontal) of the comparisons for selected metabolite intensities normalized by the intensities of the external rubber standard (STD) measured at 600 Hz and 3.0 kHz are listed in Table 1. By adjusting

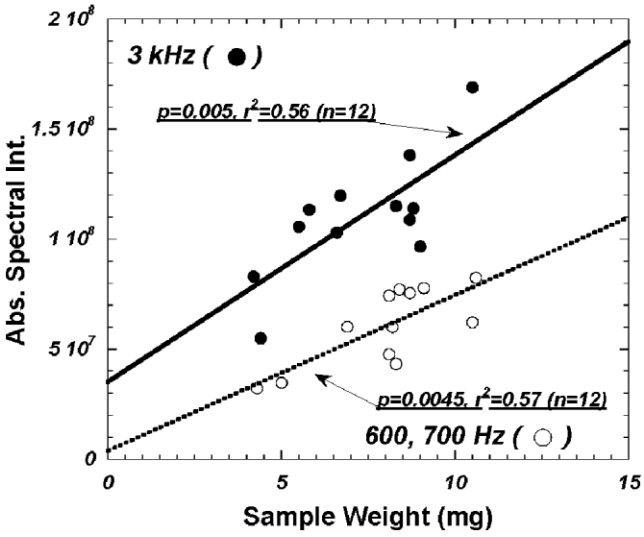

FIG. 5. Results of the total spectral intensities (i.e., the sum of metabolites labeled in Fig. 4) as a function of sample weights, measured at spinning rates of 600, 700 Hz, and 3.0 kHz.

Table 1
Comparison of Linear Regressions (Slow Rates: Vertical, vs. 3.0 kHz Rate: Horizontal) for Selected Metabolites Normalized by the Intensities of the External Rubber Standard (STD)

Met. reson. (ppm)	*P* value	R^2	Slope[a] Mean	Slope SE	Intercept Mean	Intercept SE
Lac (4.10–4.14)	0.0013	0.97	1.27	0.25	−0.11	0.07
mI (4.06)	0.0002	0.88	**1.00**[b]	**0.14**	**0.00**	**0.02**
Pch (3.22)	0.0025	0.75	**1.24**	**0.27**	**−0.02**	**0.03**
Chol (3.20)	<0.0001	0.95	1.20	0.11	−0.05	0.03
Spm (3.10–3.14)	0.0055	0.69	0.48	0.12	**0.01**	**0.01**
Cr (3.03)	0.055	0.43	0.65	0.28	**0.04**	**0.04**
Cit (2.52–2.71)	<0.0001	0.86	0.67	0.09	0.06	0.03
Acet (1.92)	<0.0001	0.97	0.65	0.04	0.06	0.03
Ala (1.47–1.49)	0.0002	0.87	**0.95**	**0.14**	−0.02	0.01
Lac (1.32–1.34)	0.0004	0.86	0.77	0.12	**−0.05**	**0.15**

[a]Statistically significant linear correlations with slopes close to 1 are observed with some metabolites, while slopes deviating from unity are observed with the others, for which the 3.0 kHz spinning rate produces slightly higher intensities.
[b]Boldface data in the table indicate either slopes are statistically indifferent (considering the range of mean based on ±SE) from 1, or the intercepts are indifferent from 0.

the gain of the spectrometer receiver, the absolute STD intensities at both spinning rates are approximately the same ($2.6 \pm 0.3 \times 10^7$ for 600 Hz, and $2.8 \pm 0.4 \times 10^7$ for 3.0 kHz). Statistically significant linear correlations with slopes close to 1.0 are observed with some metabolites, while slopes deviating from unity are observed with the others in which 3.0 kHz spinning rate produces slightly higher intensities. Histopathological analysis on these nine samples indicated a similarity in their pathological compositions ($14.0 \pm 5.1\%$ epithelium and $86.0 \pm 5.1\%$ stroma).

DISCUSSION AND CONCLUSIONS

There are several possible mechanisms by which HR-MAS may alter tissue morphologies. However, regardless of the mechanisms involved with a particular type of biological tissue, or in an individual sample, the faster the spinning rate, the larger the effect on the destruction of tissue morphology. Drastic morphological changes can also affect tissue MR-related physical parameters, such as T_1, T_2, and diffusion coefficients, etc., that in turn will require different instrumental parameters, or will affect signal intensities. Therefore, a reduction in HR-MAS rate can potentially result in better preservation of both tissue morphological structures and MR parameters. Although the DANTE experiment can be measured at any slow rate of spinning, the reduction of HR-MAS rate is limited by the linewidth of tissue static spectra, i.e., the spinning rates in Hz needs to be higher (larger) than the static resonance linewidth in order for the principle of HR-MAS to be effective. On the other hand, as in vivo methods continue to improve, it will become increasingly necessary to correlate ex vivo results with in vivo observations. It follows logically that: the slower the spinning rate of the ex vivo tests, the higher the accuracy for the in vivo comparison.

In general, there can be quantitation errors at low spinning rates, due to either slow molecular tumbling, diffusion in inhomogeneous fields, or residual (incompletely averaged) dipolar couplings and/or chemical shift anisotropy. Slow tumbling and residual couplings are more likely to be problematic for large molecules like lipids, while diffusion is more significant for small molecules.

Our results in Fig. 5 indicate that spinning either fast or slow gives spectral intensities that are proportional (within the data scatter) to sample mass, and therefore quantitation should be possible under either spinning condition. The data obtained with faster spinning generally has higher intensity. This is expected, since faster HR-MAS rotation tends to reduce the effects of field inhomogeneities and dipolar couplings further, leading to the increase of the observed metabolic intensities.

Similar differences in individual metabolites measured at different HR-MAS rates and normalized by the STD intensity measured at the same spinning rate can be seen in Table 1. Since the absolute signal intensity of the rubber standard measured at 3.0 kHz is three times higher (3.06 ± 0.23) than its value obtained at 600 Hz under the same receiver gain, slopes smaller than 1.0 indicate that the metabolite intensities of these metabolites increased more than three times when the spinning rate increased from 600 Hz to 3.0 kHz. The observed differences in metabolite slopes should reflect the intrinsic differences in the physical state among these metabolites.

In conclusion, our results indicate that the rotor-synchronized DANTE sequence appears to be a useful method for generating HR-MAS spectra of human tissue with the simplicity and reproducibility valuable for disease diagnosis in a clinical setting.

ACKNOWLEDGMENTS

The authors thank Dr. Eva Ratai for careful reading of the manuscript.

REFERENCES

1. Sitter B, Sonnewald U, Spraul M, Fjosne HE, Gribbestad IS. High-resolution magic angle spinning MRS of breast cancer tissue. NMR Biomed 2002;15:327–337.
2. Waters NJ, Holmes E, Waterfield CJ, Farrant RD, Nicholson JK. NMR and pattern recognition studies on liver extracts and intact livers from rats treated with alpha-naphthylisothiocyanate. Biochem Pharmacol 2002;64:67–77.

3. Tzika AA, Cheng, LL, Goumnerova L, Madsen JR, Zurakowski D, Astrakas LG, Zarifi MK, Scott RM, Anthony DC, Gonzalez RG, Black PM. Biochemical characterization of pediatric brain tumors by using in vivo and ex vivo magnetic resonance spectroscopy. J Neurosurg 2002;96: 1023–1031.
4. Morvan D, Demidem A, Papon J, De Latour M, Madelmont JC. Melanoma tumors acquire a new phospholipid metabolism phenotype under cystemustine as revealed by high-resolution magic angle spinning proton nuclear magnetic resonance spectroscopy of intact tumor samples. Cancer Res 2002;62:1890–1897.
5. Chen JH, Enloe BM, Fletcher CD, Cory DG, Singer S. Biochemical analysis using high-resolution magic angle spinning NMR spectroscopy distinguishes lipoma-like well-differentiated liposarcoma from normal fat. J Am Chem Soc 2001;123:9200–9201.
6. Griffin JL, Williams HJ, Sang E, Nicholson JK. Abnormal lipid profile of dystrophic cardiac tissue as demonstrated by one- and two-dimensional magic-angle spinning (1)H NMR spectroscopy. Magn Reson Med 2001;46:249–255.
7. Schiller J, Naji L, Huster D, Kaufmann J, Arnold K. 1H and 13C HR-MAS NMR investigations on native and enzymatically digested bovine nasal cartilage. Magma 2001;13:19–27.
8. Barton SJ, Howe FA, Tomlins AM, Cudlip SA, Nicholson JK, Bell BA, Griffiths JR. Comparison of in vivo 1H MRS of human brain tumours with 1H HR-MAS spectroscopy of intact biopsy samples in vitro. Magma 1999;8:121–128.
9. Wind RA, Hu JZ, Rommereim DN. High-resolution (1)H NMR spectroscopy in organs and tissues using slow magic angle spinning. Magn Reson Med 2001;46:213–218.
10. Bodenhausen G, Freeman R, Morris GA. A simple pulse sequence for selective excitation in Fourier transform NMR. J Magn Reson 1976;23: 171–175.
11. Morris GA, Freeman R. Selective excitation in Fourier transform nuclear magnetic resonance. J Magn Reson 1978;29:433–462.
12. Piotto M, Saudek V, Sklenar V. Gradient-tailored excitation for single-quantum NMR spectroscopy of aqueous solutions. J Biomol NMR 1992; 2:661–665.
13. Dixon WT. Spinning-sideband-free and spinning-sideband-only NMR spectra in spinning sample. J Chem Phys 1982;77:1800–1809.
14. Antzutkin ON, Shekar SC, Levitt MH. Two-dimensional sideband separation in magic-angle-spinning NMR. J Magn Reson 1995;115A: 7–19.

Magnetic Resonance in Medicine 50:1307–1311 (2003)

Proton High-Resolution Magic Angle Spinning NMR Analysis of Fresh and Previously Frozen Tissue of Human Prostate

Chin-Lee Wu,[1] Jennifer L. Taylor,[1] Wenlei He,[1] Andrea G. Zepeda,[1] Elkan F. Halpern,[2] Anthony Bielecki,[3] R. Gilberto Gonzalez,[2] and Leo L. Cheng[1,2*]

The previously observed improvement in spectral resolution of tissue proton NMR with high-resolution magic angle spinning (HRMAS) was speculated to be due largely to freeze-thawing artifacts resulting from tissue storage. In this study, 12 human prostate samples were analyzed on a 14.1T spectrometer at 3°C, with HRMAS rates of 600 and 700 Hz. These samples were measured fresh and after they were frozen for 12–16 hr prior to thawing. The spectral linewidths measured from fresh and previously frozen samples were identical for all metabolites except citrate and acetate. The metabolite intensities of fresh and freeze-thawed samples depend on the quantification procedures used; however, in this experiment the differences of means were <30%. As expected, it was found that tissue storage impacts tissue quality for pathological analysis, and HRMAS conditions alone are not sufficiently destructive to impair pathological evaluation. Furthermore, although storage conditions affect absolute metabolite concentrations in NMR analysis, relative metabolite concentrations are less affected. Magn Reson Med 50:1307–1311, 2003. © 2003 Wiley-Liss, Inc.

Key words: HRMAS; proton NMR; human prostate; tissue freezing; intact tissue

Shortly after high-resolution magic angle spinning (HRMAS) was introduced for intact-tissue, ex vivo, proton NMR for biomedical research, investigators examining rodent renal cortex tissue cautioned that the improvement in spectral resolution obtained with HRMAS might be a result of artifacts due to freeze-thawing processes in tissue storage (1). They reported that a large number of cellular metabolites were only visible or had drastically increased intensities (as much as 300%) after freeze-thawing (1). Although the authors of that study did not question the contribution of HRMAS in achieving a high spectral resolution that had not been observed previously with intact tissue (regardless of the type and/or storage process used) prior to the development of HRMAS, they did bring up an issue of great clinical relevance. The authors warned that if HRMAS were to be used in clinical evaluations, any possible perturbing effect resulting from sample storage (particularly the freeze-thawing process commonly used in the research phase of preclinical studies) should be carefully evaluated. Since the publication of that initial study, a number of researchers have expressed similar concerns and have attempted to address this issue (2–4).

The physics supporting this speculation are well understood. If the freeze-thawing process alters the physical state of tissue cellular metabolites, their NMR parameters might change, and therefore their spectral profiles might be different. It is important to evaluate such potential artifacts in order to establish disease-based tissue cellular metabolite databases for future clinical use. To confirm and measure these artifacts (if they exist), and demonstrate the harmlessness of the tissue-freezing process on measurable NMR cellular metabolites, careful measurements may need to be conducted individually for each tissue type of interest.

Our interest in the study of human prostate cancer prompted us to design this study to evaluate possible freeze-thawing effects on NMR measurements of human prostate tissue.

METHODS

Tissue Protocol

For the current study, NMR analysis of human prostate surgical specimens was approved by the Institutional Review Board of the Massachusetts General Hospital. Twelve human prostate specimens were collected in the operating room during five prostatectomies, representing different prostate zones (central, transitional, and peripheral). Each specimen (~50 mg) was divided into four pieces of approximately equal size. Sample 1 was directly fixed in 10% buffered formalin for histopathology; sample 2 was snap-frozen and stored at −80°C for spectroscopy analysis the next day; and samples 3 and 4 were kept in closed vials, placed on ice, and measured by HRMAS proton NMR within 2 hr after tissue resection. After NMR analysis, sample 3 was fixed in formalin; sample 4 was frozen at −80°C for 12–16 hr, and was spectroscopically reevaluated the next day. Whenever possible, sample 4 was directly frozen in the HRMAS rotor to avoid sample loss during the unpacking and repacking processes. Upon completion of HRMAS NMR analyses for samples 2 and 4 on the second day, they were also formalin-fixed for histopathology. According to this design, samples 2 and 3 represent frozen and fresh tissue, respectively, and in sample 4 the freeze-thawing effects were evaluated in the same sample. Lastly, sample 1 mimicked a routine clinical pathology procedure, and was used as a reference for evaluating tissue

[1]Department of Pathology, Massachusetts General Hospital, Harvard Medical School, Boston, Massachusetts.

[2]Department of Radiology, Massachusetts General Hospital, Harvard Medical School, Boston, Massachusetts.

[3]Francis Bitter Magnet Laboratory, Massachusetts Institute of Technology, Cambridge, Massachusetts.

Grant sponsor: PHS/NIH; Grant numbers: CA77727; CA80901; RR00995.

Chin-Lee Wu and Jennifer L. Taylor contributed equally to this work.

*Correspondence to: Leo L. Cheng, Pathology Research, CNY-7, 149 13th St., Charlestown, MA 02129. E-mail: cheng@nmr.mgh.harvard.edu

Received 20 March 2003; revised 31 July 2003; accepted 7 August 2003.

DOI 10.1002/mrm.10645

Published online in Wiley InterScience (www.interscience.wiley.com).

histopathological conditions influenced by freeze-thawing and spinning processes.

HRMAS Proton NMR

The NMR experiments were carried out on a Bruker (Billerica, MA) AVANCE spectrometer operating at 600 MHz (14.1T). A 4-mm zirconia rotor was used with Kel-F plastic inserts, which created a spherical sample space of ~10 μl located at the center of the detection coil. A small (~0.1 mg) silicone rubber sample was permanently fixed inside one of the Kel-F spacers, positioned within the detection coil but not in contact with the sample, to function as an external standard for both frequency reference (0.06 ppm from TMS) and quantification. Approximately 1.0 μl of D_2O was added into the rotor with the tissue sample for ^2H field locking. Within 3 min after tissue packing, the rotor containing the tissue sample and D_2O was introduced into the probe, precooled to 3°C, and spectroscopically measured. All NMR measurements were carried out at 3°C to ensure better tissue preservation. The rotor spinning rate was regulated by a MAS controller (Bruker) and verified by measuring inter-SSB distances from the spectra, with an accuracy of ±1.0 Hz. A TR of 5 s, and 32 transients were used to acquire each spectrum.

Spectra were collected with spinning rates of 600 and 700 Hz, and with or without a rotor synchronized DANTE sequence of 1000 DANTE pulses of 1.5 μs (8.4° flip angle) (5). A rotor-synchronized CPMG filter (10 ms) was included in the pulse sequence after the execution of the DANTE frequency-selective pulses to reduce broad resonances associated with probe background, rotor, and/or macromolecules. Spectra measured at 600 Hz spinning without DANTE were used to quantify the total NMR signal intensity, including tissue water, its sidebands, and all of the metabolites [M_0].

The spectroscopic data were processed with Nuts software (Acorn NMR Inc., Livermore, CA) according to the following procedure: All free induction decays (FIDs) were subjected to 1 Hz apodization before Fourier transformation, baseline correction, and phase adjustment. The resonance intensities reported here represent integrals of curve-fittings with Lorentzian-Gaussian lineshapes. Resonance intensities, which depended on the particular spectral regions, were analyzed from one of the two spectra where there was no effect of water spinning sidebands (SSBs) and DANTE suppression, as previously described (5). About 50 of the most intensive resonance peaks in the spectral region between 0.5–4.5 ppm were thus quantified. The sum of these resonances was used to estimate the total metabolite intensity [M_{met}]. The absolute concentration for metabolite a, [M_a], was estimated according to the metabolite intensity measured in DANTE spectra [$M_{a\mathrm{DANTE}}$], the total NMR signal intensity [M_0] from the single pulse measurement, and the intensities of rubber standard measured under both conditions, [STD_0] and [$\mathrm{STD}_{\mathrm{DANTE}}$], respectively, by using: $[M_a] = ([M_{a\mathrm{DANTE}}]/[\mathrm{STD}_{\mathrm{DANTE}}])*([\mathrm{STD}_0]/[M_0])$. The relative metabolite intensity [M_{a_rel}] was calculated by: $[M_{a\_\mathrm{rel}}] = [M_{a\mathrm{DANTE}}]/[M_{\mathrm{met}}]$.

Histopathology

In this study we focused on the effects of the tissue freeze-thawing process and HRMAS on the quality of histopathological images. Fixed tissue samples were cut into 7-μm sections and stained with hematoxylin and eosin. A set of three individual cuts, 100 μm apart, was obtained from each sample. Histopathological images of four sample sets from each specimen were compared by a genitourinary pathologist in random order and blinded fashion to determine the quality of the images on a scale of 1 to 5, with 5 being the best. The pathologist graded the histological quality by examining nuclear and cytologic features. Scale 5 is equivalent to the quality of routine, fresh clinical pathology samples that are fixed in formalin. Scale 3 is equivalent to the quality of a routine frozen-section slide of snap-frozen tissue. Scale 4 indicates a quality between scales 3 and 5. Scale 2 represents quality that is inferior to scale 3 but is sufficient for recognizing cell types and architecture. Scale 1 indicates histology that is insufficient for cell and tissue recognition.

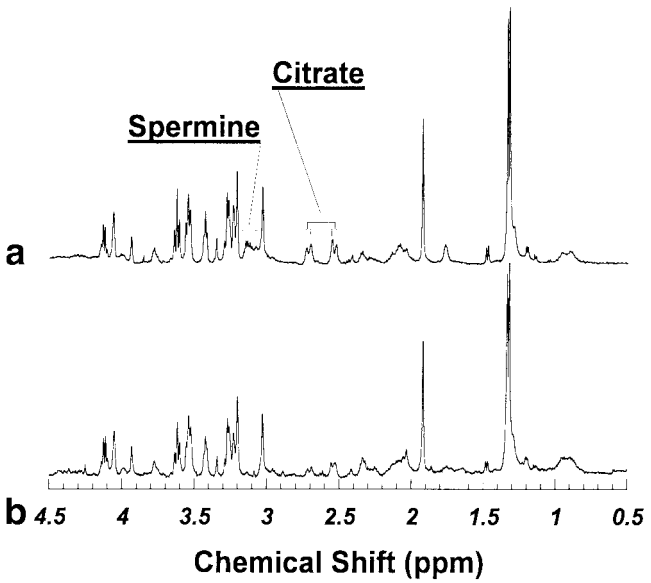

FIG. 1. Human prostate tissue HRMAS proton spectra measured (**a**) fresh, and (**b**) thawed after being frozen overnight. Both spectra are from the same sample.

RESULTS

Figure 1 shows the composite spectra (5) generated from DANTE spectra obtained with HRMAS rates of 600 and 700 Hz for one tissue sample (sample 4) that was both fresh and freeze-thawed, as described previously. Figure 1a displays the composite spectrum of fresh tissue, and Fig. 1b shows the same tissue thawed after being frozen overnight. The resolution values of the spectra are similar; however, close evaluation reveals that there may be some reduction in resonance intensity for certain metabolites (such as spermine and citrate) and the broad peak at 1.68–1.78 ppm after the freeze-thaw process. In addition, there appear to be alterations in the resonance profiles at the spectral region of 2.01–2.37 ppm as a result of the freeze-thaw process.

We compared the spectral resolution in terms of changes in linewidths for different metabolites before and after the

Table 1
Linear Correlations Between Absolute Metabolite Concentrations Measured Before and After Sample Freeze (N = 12)

Metabolite Resonance (ppm)	P value[a]	R^2	Slope[b]		Intercept[b]	
			Mean	SE	Mean	SE
Lac(4.10–4.14)	0.0045	0.57	**1.10**	**0.30**	**−0.96**	**4.12**
mI(4.06)	0.024	0.41	0.58	0.22	6.21	2.72
3.60–3.63[c]	0.0008	0.69	0.69	0.14	5.45	3.59
3.34	0.0075	0.57	0.74	0.22	1.67	1.65
3.26–3.27	0.016	0.49	0.55	0.19	**0.14**	**2.88**
Pch(3.22)	0.0019	0.68	**0.81**	**0.19**	**2.49**	**2.78**
Chol(3.20)	0.10	0.24	0.41	0.23	11.6	4.40
Spm(3.05–3.14)	<0.0001	0.86	0.55	0.07	**−1.07**	**4.64**
Cr(3.03)	0.0021	0.63	0.59	0.14	4.17	2.17
Cit(2.52–2.71)	<0.0001	0.86	0.67	0.09	**1.47**	**3.03**
2.31–2.37	0.037	0.40	**0.85**	**0.35**	**3.41**	**3.55**
2.01–2.14	0.0075	0.57	0.74	0.22	9.21	9.17
Acet(1.92)	<0.0001	0.97	**0.98**	**0.05**	**−0.28**	**0.65**
1.68–1.78	0.0001	0.82	0.57	0.09	2.34	2.47
Ala(1.47–1.49)	0.0004	0.73	**0.85**	**0.16**	**1.13**	**1.22**
Lac(1.32–1.34)	0.0004	0.73	**1.04**	**0.20**	**−3.74**	**16.67**
1.19–1.20	0.0003	0.75	**1.03**	**0.19**	**−0.17**	**0.59**
1.04–1.05	<0.0001	0.90	0.82	0.09	**0.23**	**0.28**
Lipid(0.90)	0.0022	0.63	1.38	0.34	**−2.63**	**5.00**

[a]Linear analyses conducted by plotting intensity after freezing (vertical) against that of fresh (horizontal), a slope of <1.0 indicated a reduction in intensity after sample freeze.
[b]Bold faced data in the table indicate either slopes are statistically indifferent (considering the range of Mean based on ± SE) from 1, or the intercepts are indifferent from 0.
[c]Resonance peaks not yet positively identified with metabolites.

freeze-thawing process. We found that except for two metabolites—citrate (19% reduction in linewidth after freeze-thawing, N = 92, one-way ANOVA, $P < 0.04$) and acetate (36% reduction, N = 32, one-way ANOVA, $P < 0.05$)—there was no indication that freeze-thawing improved spectral resolution, i.e., there was no statistically significant line-narrowing effect associated with tissue freezing (as determined by ANOVA) that would support the concerns raised by previous studies (1).

The changes observed in metabolite intensities in the same tissue samples before and after freezing (sample 4 type) are summarized in Tables 1 and 2. Table 1 shows the results of linear regression analyses on the estimated absolute metabolite concentrations (6). These linear analyses were conducted by plotting intensity after freezing (vertical) against that of fresh (horizontal). Therefore, a slope of <1.0 indicates a reduction in intensity after the sample was frozen. The boldface data in the table indicate slopes that are not statistically different (considering the range of mean based on ±SE) from one, or intercepts that are not different from zero. The data in the table appear to indicate that freezing resulted in reductions (20–45%) in absolute metabolite concentrations [M_a] for more than half of the analyzed metabolites, while only one resonance peak (lipid at 0.9 ppm) showed a slight increase in concentration (with a slope of 1.38 ± 0.34). Similar (but slightly better) correlation results obtained from analyses of the relative metabolite intensities [M_{a_rel}] before and after the freeze-thawing process were observed, as shown in Table 2.

The current histopathological evaluations of tissues (fresh from surgery, and analyzed by HRMAS NMR without freezing and after freeze-thaw treatment) were aimed at identifying the effects of these processes on histopathological integrity, as illustrated by an image-quality index on a scale of 1 to 5. The results indicate that fresh tissues that were spun at 600 Hz (<25 min) and then at 700 Hz (<5 min) produced high-quality images that were indistinguishable from those of the original tissue (indices: 4.75 ± 0.16 vs. 4.58 ± 0.19) (Fig. 2). However, freezing the tissue compromises the quality of the resulting images (3.75 ± 0.26), which agrees with the accepted wisdom in clinical pathology.

DISCUSSION AND CONCLUSIONS

Sample-freezing processes can potentially alter the physical state of tissue cellular metabolites, as well as the environment of tissue water. For instance, the freezing process may interrupt the linkages of metabolites and water with cell membranes and/or macromolecules, such as proteins. A change in the physical state of a metabolite and/or tissue water viscosity may lead to a change in NMR-related physical parameters, such as relaxation times and diffusion coefficients. Ultimately, the observed spectral profiles may be different. Therefore, the freeze-thawing effects previously observed in the rodent renal cortex were neither a surprise nor an issue unique to HRMAS NMR analysis (1). This may indicate that such effects, if they exist, may not be observable at low spectral resolution with conventional NMR without the assistance of HRMAS.

An evaluation of possible freeze-thawing effects on intact-tissue HRMAS spectra may include the following two aspects: spectral resolution and resonance intensities. Our results from human prostate tissue (see Fig. 1) suggest that for most analyzed metabolites there are no obvious in-

Table 2
Linear Correlations Between Relative Metabolite Intensities Measured Before and After Sample Freeze (N = 12)

Metabolite Resonance (ppm)	P value[a]	R^2	Slope[b]		Intercept[b]	
			Mean	SE	Mean	SE
Lac(4.10–4.14)	0.0041	0.62	0.76	0.20	1.55	0.89
mI(4.06)	0.0003	0.75	1.28	0.23	**−0.16**	**0.94**
3.60–3.63[c]	0.0047	0.57	0.76	0.21	2.09	1.70
3.34	0.0046	0.61	**0.88**	**0.24**	**0.45**	**0.57**
3.26–3.27	0.028	0.40	0.60	0.23	1.82	0.92
Pch(3.22)	0.0008	0.73	**0.84**	**0.17**	**0.98**	**0.78**
Chol(3.20)	0.0020	0.63	**0.87**	**0.21**	1.97	1.38
Spm(3.05–3.14)	<0.0001	0.89	0.70	0.08	**−0.15**	**1.13**
Cr(3.03)	<0.0001	0.80	0.86	0.13	0.67	0.57
Cit(2.52–2.71)	0.0002	0.76	**0.88**	**0.16**	**−0.12**	**1.31**
2.31–2.37	0.078	0.31	**0.83**	**0.42**	1.72	1.45
2.01–2.14	0.0002	0.80	1.30	0.21	**−2.22**	**2.89**
Acet(1.92)	<0.0001	0.95	1.31	0.10	**−0.28**	**0.32**
1.68–1.78	0.0029	0.64	0.57	0.14	1.41	0.82
Ala(1.47–1.49)	0.0004	0.74	0.81	0.15	0.58	0.35
Lac(1.32–1.34)	0.0023	0.62	**0.80**	**0.20**	6.56	5.46
1.19–1.20	0.0009	0.69	**0.93**	**0.20**	**0.07**	**0.24**
1.04–1.05	0.0002	0.77	0.72	0.13	0.14	0.12
Lipid(0.90)	0.0008	0.69	1.30	0.27	**−0.33**	**1.55**

[a]Linear analyses conducted by plotting intensity after freezing (vertical) against that of fresh (horizontal), a slope of <1.0 indicated a reduction in intensity after sample freeze.
[b]Bold faced data in the table indicate either slopes are statistically indifferent (considering the range of Mean based on ± SE) from 1, or the intercepts are indifferent from 0.
[c]Resonance peaks not yet positively identified with metabolites.

creases in spectral resolution associated with tissue freezing, i.e. the resonance linewidths for these metabolites do not become narrower after the tissue is freeze-thawed compared to those measured in fresh tissue. However, such reductions were indeed observed with citrate and acetate, which indicates that these metabolites may have increased mobility after the freeze-thawing process. This observation is very important because citrate is a well-recognized prostate metabolite marker (7–11). Further studies of citrate (for example, including measurements of associated relaxation times) are warranted. If this finding is confirmed, it may increase our understanding of citrate, and its function and associations within prostate cells (12,13).

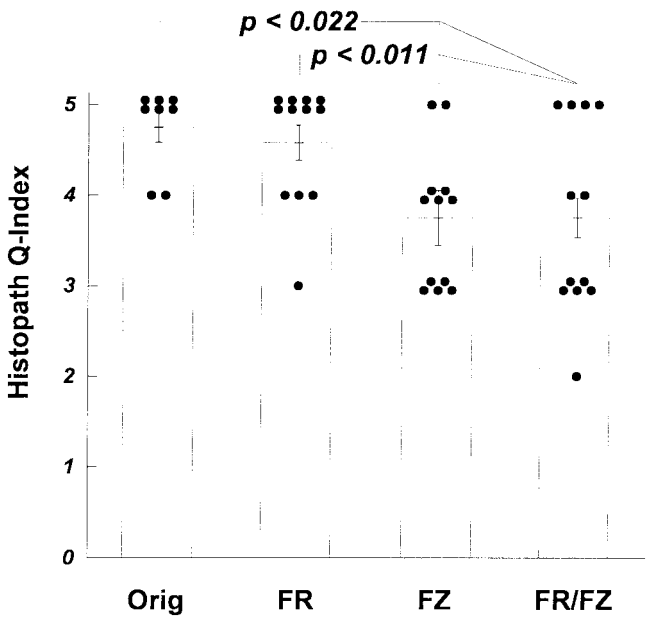

FIG. 2. Histopathological evaluations of tissues fresh from surgery (Orig) and analyzed by HRMAS NMR without freezing (FR) and after freeze-thaw treatment (FZ + FR/FZ). The histopathological images were graded on a scale of 1 to 5, with 5 indicating best quality.

The calculation of resonance intensity is a more complicated process than the measurement of resonance linewidth. We explored two different types of calculations: absolute concentration and relative intensity. Clearly, the calculation of the absolute metabolite concentration depends on the assumption of an important factor that is believed to be "absolute," measurable, and constant. Normally, the sample weight is used as such a factor. For this study, we considered using sample weight; however, in our particular situation, measurements of sample weight were found to be less practical because of the small size of the tested tissue (~10 mg) and the associated measurement error. It was not difficult to estimate the measurement error in the sample weight, since the sample was packed into the sample rotor, which weighed about 10^3 times more than the sample. In addition, we could not let tissue samples be exposed to air for an extended amount of time (minutes) for multiple measurements because that would certainly have resulted in a loss of tissue water. We therefore chose to use the total spectral intensity, including water and its SSB [M_0] measured at 600 Hz spinning rate, and without the DANTE pulse sequence, to calculate the metabolite concentrations (Table 1).

The measurements of slopes and intercepts presented in Table 1 indicate that the degradation of tissue caused by the freeze-thaw process may modify the environment of

metabolites to various degrees, and cause the NMR parameters associated with these metabolites to change. However, the data in this table suggest that there is a general reduction for almost all of the analyzed metabolites after tissue freeze-thawing, with the mean for the mean values of the slopes being 0.79 ± 0.05. These calculated values may be skewed because of the change in the water environment of the tissue, i.e., the [M_0] values were increased, perhaps due to the reduction of water viscosity after freeze-thawing. This speculation was supported to a certain degree by our data regarding the relative metabolite intensity [M_{a_rel}] in Table 2, where [M_0] values were not entered into the calculations. The slopes in Table 2 are closer to 1.0 than those in Table 1. In fact, the mean for the mean values of the slopes is now 0.89 ± 0.05. Overall, the results presented in both tables indicate that even if there were metabolite changes associated the freeze-thaw process, these changes (increase or decrease) were <50% of the values measured with fresh tissues for all of the analyzed metabolites. Although these changes may present a significant issue for researchers seeking absolute metabolic quantifications, they are certainly much smaller than the worrisome reported increases of as much as 300% (1).

Finally, our histopathology data indicate that there is a measurable difference between fresh and freeze-thawed prostate tissue in terms of the quality of the histopathological images. These data confirm our previous observation that mechanical spinning of human prostate tissue in a 4-mm rotor at a rate of ≤700 Hz for ~30 min does not produce tissue damage that compromises the integrity of the tissue histopathology (5).

In conclusion, we have shown that the freeze-thaw process in tissue does not appear to change the overall spectral resolutions measured by resonance linewidths. However, there were a few exceptions (such as citrate and acetate), which warrant further investigation. We have also shown that while there are differences in metabolite intensities between fresh and freeze-thawed samples, these differences are more pronounced with absolute concentrations than with relative intensities. The possible freeze-thawing effect on the measured concentration of an individual metabolite of clinical interest should be evaluated and accounted for in practice to further the utility of ex vivo HRMAS in clinical applications.

ACKNOWLEDGMENT

The authors thank Dr. Eva Ratai for her careful reading of the manuscript.

REFERENCES

1. Middleton DA, Bradley DP, Connor SC, Mullins PG, Reid DG. The effect of sample freezing on proton magic-angle spinning NMR spectra of biological tissue. Magn Reson Med 1998;40:166–169.
2. Garrod S, Humpfer E, Spraul M, Connor SC, Polley S, Connelly J, Lindon JC, Nicholson JK, Holmes E. High-resolution magic angle spinning 1H NMR spectroscopic studies on intact rat renal cortex and medulla. Magn Reson Med 1999;41:1108–1118.
3. Waters NJ, Garrod S, Farrant RD, Haselden JN, Connor SC, Connelly J, Lindon JC, Holmes E, Nicholson JK. High-resolution magic angle spinning (1)H NMR spectroscopy of intact liver and kidney: optimization of sample preparation procedures and biochemical stability of tissue during spectral acquisition. Anal Biochem 2000;282:16–23.
4. Sitter B, Sonnewald U, Spraul M, Fjosne HE, Gribbestad IS. High-resolution magic angle spinning MRS of breast cancer tissue. NMR Biomed 2002;15:327–337.
5. Taylor JL, Bielecki A, Wu CL, Gonzalez RG, Cheng LL. Ex vivo HRMAS MRS analysis of intact tissue at slow sample spinning rates. In: Proceedings of the 10th Annual Meeting of ISMRM, Honolulu, 2002. p 135.
6. Cheng LL, Ma MJ, Becerra L, Ptak T, Tracey I, Lackner A, Gonzalez RG. Quantitative neuropathology by high resolution magic angle spinning proton magnetic resonance spectroscopy. Proc Natl Acad Sci USA 1997;94:6408–6413.
7. Lynch MJ, Nicholson JK. Proton MRS of human prostatic fluid: correlations between citrate, spermine, and myo-inositol levels and changes with disease. Prostate 1997;30:248–255.
8. Zaider M, Zelefsky MJ, Lee EK, Zakian KL, Amols HI, Dyke J, Cohen G, Hu Y, Endi AK, Chui C, Koutcher JA. Treatment planning for prostate implants using magnetic-resonance spectroscopy imaging. Int J Radiat Oncol Biol Phys 2000;47:1085–1096.
9. Mueller-Lisse UG, Vigneron DB, Hricak H, Swanson MG, Carroll PR, Bessette A, Scheidler J, Srivastava A, Males RG, Cha I, Kurhanewicz J. Localized prostate cancer: effect of hormone deprivation therapy measured by using combined three-dimensional 1H MR spectroscopy and MR imaging: clinicopathologic case-controlled study. Radiology 2001; 221:380–390.
10. Swanson MG, Vigneron DB, Tran TK, Sailasuta N, Hurd RE, Kurhanewicz J. Single-voxel oversampled j-resolved spectroscopy of in vivo human prostate tissue. Magn Reson Med 2001;45:973–980.
11. Kurhanewicz J, Swanson MG, Nelson SJ, Vigneron DB. Combined magnetic resonance imaging and spectroscopic imaging approach to molecular imaging of prostate cancer. J Magn Reson Imaging 2002;16: 451–463.
12. Costello LC, Franklin RB. Testosterone and prolactin regulation of metabolic genes and citrate metabolism of prostate epithelial cells. Horm Metab Res 2002;34:417–424.
13. Costello LC, Franklin RB, Narayan P. Citrate in the diagnosis of prostate cancer. Prostate 1999;38:237–245.

Technology in Cancer Research & Treatment
ISSN 1533-0346
Volume 3, Number 6, December (2004)

Quantitative Pathology in Tissue MR Spectroscopy Based Human Prostate Metabolomics§

www.tcrt.com

Melissa A. Burns, B.A.[1]
Wenlei He, M.D., Ph.D.[1,2]
Chin-Lee Wu, M.D., Ph.D.[1,2]
Leo L. Cheng, Ph.D.[1,3,*]

Departments of:
[1]Pathology
[2]Urology
[3]Radiology
Massachusetts General Hospital
Harvard Medical School
Pathology Research
CNY-7, 149, 13th Street
Charlestown, MA 02129 USA

At present, the clinical utility of metabolomic profiles of human prostate tissue relies on the establishment of correlations between metabolite data and clinical measurements, particularly pathological findings. Because metabolomics is a quantitative study, its clinical value can be rigorously investigated by determining its association with other quantitative measures. The human visual assessment of prostate tissue, however, introduces both inter- and intra-observer biases that may limit the reliability of its quantitations, and therefore, the strength of its correlations with metabolomic profiles. The aim of this study was to develop a simple, feasible protocol for the computer-aided image analysis (CAIA) of prostate pathology slides in order to achieve quantitative pathology from tissue samples, following metabolomic measurement with high-resolution magic angle spinning (HRMAS) magnetic resonance spectroscopy (MRS). Thirty-eight samples from 29 prostatectomy cases were studied with HRMAS MRS. After spectroscopy analysis, samples were serial-sectioned, stained and visually assessed by pathologists. Cross-sections from these samples were then measured with the CAIA protocol. Results showed a two-fold difference between human visual assessments of the area percentages of tissue pathologies and CAIA area percentages obtained for the same features. Linear correlations were found between both metabolites indicative of normal epithelium and those indicative of prostate cancer, and the CAIA quantitative results. CAIA based quantitative pathology is more reliable than human visual assessment in establishing correlations useful for disease diagnosis between prostate pathology and metabolite concentrations.

Key words: Image analysis, Pathology, Human prostate, Computer-Aided, Magnetic resonance, Metabolomics.

Introduction

The emergence of the fields of human genomics, proteomics and metabolomics has aided the discovery of potential molecular markers for disease, thus defining the diagnostics and prognostics of the current era of molecular pathology.

Genomic advancements, such as the identification of gene mutations, contribute to the understanding of genetic markers of disease and disease risks. However,

* Corresponding Author:
L. L. Cheng, Ph.D.
Email: cheng@nmr.mgh.harvard.edu

Abbreviations: MRS, Magnetic resonance spectroscopy; CAIA, Computer-aided image analysis; HRMAS, High-resolution magic angle spinning; PSA, Prostate-specific antigen; PCa, Prostate cancer; GU, Genitourinary; IRB, Institutional Review Board; STD, External standard; ROI, Regions of interest; H&E, Hematoxylin and eosin; Cit, Citrate; Cho, Choline; PCh, Phospocholine.

§We wish to dedicate this work to the memory of Mr. Randall K. "Randy" Burns, the beloved father of M. A. Burns, who died of prostate cancer on February 21, 2004, at age 57.

such knowledge may not reflect the present clinical status and the biochemical activity of disease, or the potential capacity of this activity to forecast patient prognosis and disease progression, particularly in oncogenesis (1, 2).

Proteomics, however, has produced molecular biological knowledge that may be more relevant to the cancer clinic. Currently, tests which detect and quantify a single protein, such as prostate-specific antigen (PSA) present in blood, have been used in prostate cancer (PCa) screening. However, these screening tests are known to be of low specificity, though this may be improved by combining them with other evaluations such as biopsy (3-7) in order to reduce the incidence of false-positives generated by the presence of benign conditions (8, 9). Furthermore, even with the aid of biopsy, current molecular screenings used in the PCa clinic are unable to determine virulent from indolent cancers, which may result in the over-treatment (*i.e.*, interventions for tumors that would otherwise go unnoticed in a patient's lifetime) of as many as 30% of PCa cases (10, 11).

Metabolomics, in studying the complement of all measurable metabolites, seeks to define the levels, activities, interactions, and regulation of all metabolites in a biological system, and to investigate any changes in these quantities or activities in response to internal and external stimuli, such as disease processes. Metabolomic changes can be considered the ultimate response, a kind of molecular phenotype, of biological systems to both genetic and environmental stimuli. As such, it is expected that metabolomic changes most often occur before the manifestation of any morphological changes. Thus, metabolomic evaluation can be extremely useful, especially in the diagnosis and prognosis of human malignancies, where prognostic factors may be more strongly determined by the patient, the treatment, and the environment than by the tumor itself (12). At present, metabolomic technologies are represented almost entirely by magnetic resonance spectroscopy (MRS) and, to some extent by mass spectrometry. MRS is an objective technique, able to detect and quantify biochemical species, thereby capable of generating metabolomic profiles of normal tissue and of disease (13). High-resolution magic angle spinning (HRMAS) proton MRS for intact tissue analysis generates tissue spectra well enough resolved to allow the identification and quantification of individual metabolites from unaltered human specimens, while preserving tissue pathological structure, so that MRS results can be correlated directly with subsequent histopathological measurements.

Metabolomic studies have made evident the difference in emphasis between the pathological evaluations in the current era of molecular pathology, and those of the morphological pathology of the past century. The traditional morphology-based pathology, reporting mostly the presence or absence of certain pathological features, has been the gold standard in the diagnosis of human malignancies. However, its analysis is limiting to the interpretation of results measured in the fields of "-omics," because parameters measured by proteomics and metabolomics are continuous, proportional to the mass of the analyzed sample, and in flux throughout the development and progression of disease. Therefore, the quantitative evaluation of pathological features is particularly appropriate to the study of tissue metabolomics, and is required in order to maximize the utility of spectroscopic results.

Computer-aided image analysis (CAIA) has been recognized in the era of molecular pathology as a useful tool for providing objective and quantitative data. While most studies employing CAIA have focused on its ability to detect subtle changes in cell nuclear morphology that may not be visible to the human eye, CAIA is able also to identify and quantify cellular components, with objectivity and virtual independence from inter- and intra-observer variabilities.

In this study, we tested a CAIA protocol developed for differentiating and quantifying cellular components (normal glands, stroma, and cancer glands) of H/E stained prostate tissue sections. We examined correlations of the quantitative results obtained using the CAIA protocol, with those obtained by the visual assessments of experienced GU pathologists. More importantly, we demonstrated that the results of CAIA pathology correlated more strongly than the pathologists' visual quantifications with tissue metabolic intensities, measured with HRMAS proton MRS from the same specimens. Therefore, the development and implementation of CAIA procedures for quantitative pathology may be critical to the further realization of tissue metabolomic's potential for understanding and diagnosing disease.

Materials and Methods

Tissue Protocol

MRS analysis and histopathological evaluation of human prostate samples were approved by the Institutional Review Board (IRB) at the Massachusetts General Hospital.

Tissue samples (n=38 from 29 prostatectomy cases) were snap frozen in liquid nitrogen and stored at -80 °C until spectroscopic analysis. Following spectroscopic analysis, tissue samples were fixed in 10% formalin, embedded in paraffin, cut into 5-micron sections at either 100 (20/38 samples), or 200 (18/38 samples) micron intervals, and stained with hematoxylin and eosin (H&E). The percentages of areas (area%) representing normal epithelial glands (including lumen), stroma, and cancer glands (including lumen) in each cross-section were estimated independently to the nearest 5% by two GU pathologists, who had neither

prior knowledge of the spectroscopic results nor the other pathologist's reading. The independent readings were then averaged to obtain an area% for each cross-section.

CAIA was then applied to the tissue cross-sections. Of the 38 tissue samples selected for CAIA tests, the 15 cancer-negative samples were selected randomly from more than 200 measured samples, while the 23 cancer-positive samples represent all cancer-positive samples observed before the manuscript was prepared. All samples had undergone the same spectroscopy and histopathology procedures before they were used to test CAIA. Prostate cancer cases were selected for CAIA after cancer was diagnosed by the participating pathologists; however, CAIA results were generated independently from the quantitative measurements given by the pathologists.

High Resolution Magic Angle Spinning (HRMAS) Proton MRS

The MRS experiments were carried out on a Bruker (Bruker BioSpin Corp., Billerica, MA) AVANCE spectrometer operating at 600 MHz (14.1T). The sample was placed in a 4 mm zirconia rotor with Kel-F plastic inserts which created a spherical sample space of ~10 µl located at the center of the detection coil. A small (~0.1 mg) silicone rubber sample was permanently fixed inside one of the Kel-F spacers, positioned within the detection coil but not in contact with the sample, to function as an external standard (STD) for both frequency reference (0.06 ppm from TMS) and quantification. Prostate tissue samples (8-10 mg) were used directly from freezers without further preparation. Approximately 1.0 µl of D_2O was added to each sample for ^2H field locking. The sample was introduced into the probe pre-cooled to 3 °C for HRMAS MRS measurements at that temperature. The rotor spinning rate accuracy (±1.0 Hz) was controlled with an MAS controller and verified with the positions of spinning sidebands in the spectra.

Spectra were acquired with the spectrometer frequency set exactly on the water resonance. Of the 15 cancer-negative samples reported for correlations between CAIA and human visual assessment, 12 were measured under the same spectroscopic conditions with a spinning rate of 3kHz, and thus were selected for the analysis of correlations between quantitative pathology and tissue metabolite concentrations. Similarly, 19 of the 23 cancer-positive samples, reported for correlations between CAIA and human visual assessment, were analyzed using a rotor-synchronized Carr-Purcell-Meibom-Gill sequence with a total of 20ms delay after the 90° excitation pulse, and with a spinning rate of 700Hz. These 19 spectra also were selected for tissue metabolic concentration analysis. Each spectrum was acquired with 32 transients and a repetition time of 5s.

Spectroscopic data were processed using the Nuts software (Acorn NMR Inc., Livermore, CA) according to the following procedures. All free induction decays were subjected to 0.5 Hz apodization before Fourier transformation, baseline correction, and phase adjustment. Resonance intensities reported here represent integrals of curve-fittings with Lorentzian-Gaussian line-shapes normalized by the STD intensity measured for each sample. All intensities reported here in the context of quantification were area intensities obtained from curve fitting. Tissue cellular metabolite concentrations were calculated based on the intensity ratios of metabolites over the intensity of the H_2O peak at ~5.0ppm.

Computer Aided Image Analysis

Quantitative pathological analysis was applied using an Olympus BX41 Microscope Imaging System (Olympus American, Inc., Melville, NY) in conjunction with image analyzer MicroSuite™ (Soft Imaging System Corp., Lakewood, CO). Digital photographs were taken of each cross-section at 10× magnification. It was necessary to take multiple photographs in order to capture the entire cross-section. The multiple image alignment feature, available in MicroSuite™, confirmed that the entire cross-section had been captured without overlapping regions.

For each image of normal prostate tissue, regions of interest (ROI) were selected and initial color thresholds set for the differential detection of stroma, glandular epithelium, and glandular lumen. Using these color thresholds, the classification type "3Phases" was created. In addition, the "define measurement, detection, and classification settings" were specified as follows: minimum pixel size: 100 pixels, border particles: truncated, search area: ROI, pixel connectivity includes "diagonals [8]," Criterion set at "Phases," classification set at "3Phases," filled style, and ID particle > 100 pixels. Each image underwent the above "3Phases" detection protocol with RGB/HSI filters and ROI were adjusted in each case for optimal detection. Using the "Measure Area/Perimeter" tool, the total area of the image was calculated. All data generated from images within an individual cross-section were summed to generate the total area, and the area and area% stroma, glandular epithelium, and glandular lumen of each cross-section. Similarly, all data from individual cross-sections within a sample were summed, thus establishing a total representative volume, and the volume and volume percentage (vol%) of each individual component.

For cancerous tissues (determined by human visual assessment) a distinct classification system was created. ROI were selected within a cancerous tissue cross-section that, in general, were representative of expected prostate cancer tissue characteristics. Initial color thresholds were set using these ROI to detect both cancerous cells and their respective lumenal area, creating the classification type "cancer glands." All "define measurement, detection, and classification settings"

were the same as for normal tissues except classification type was set at "cancer glands," and minimum pixel size and ID particle size > were set at 50 pixels in order to accommodate small cancerous foci. As with the normal tissue, when the "cancer glands" classification protocol was applied to an image, ROI were manually selected, and RGB/HSI filters were adjusted for optimal detection of cancerous glands. Data from individual images within a cross-section and separately, data from individual cross-sections within a sample, were summed in order to calculate the area and area%, and volume and volume%, respectively, of cancer cells and lumen.

Due to the lengthy procedure for analyzing images of cancerous, H&E-stained samples, not all cross-sections of a case were measured individually; instead images from each sample were selected on the basis of the area% cancer determined by the pathologists, such that a new cross-section was selected for analysis for every difference greater than 10%. In general, two to three cross-sections were selected from each sample consisting of between six and thirteen cross-sections. The volume% of cancer cells and lumen for the sections that were not measured with CAIA were estimated based on results of adjacent and quantified sections.

Results

Determining Optimal Frequency of Pathology Serial-sectioning Using CAIA

Figure 1, an example of "3Phases" CAIA, and "cancer glands," shows the results of the CAIA classification scheme applied to a cross-section of human prostate tissue containing both normal and cancerous glands. Particularly, stroma, normal glandular epithelium (red), and normal glandular lumen (yellow) were identified using "3Phases" classification protocol, as seen in (b). Image (c) shows an image of a tissue section that underwent "cancer glands" classification, with cancer cells and lumen labeled in blue and light blue, respectively.

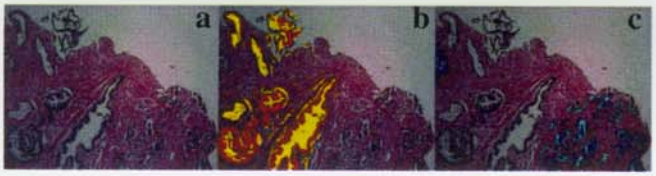

Figure 1: A digital photograph of the upper right quadrant of a cross section of prostate tissue with both cancerous and normal glands was taken using an Olympus BX41 Microscope Imaging System (Olympus American, Inc., Melville, NY) with 10× magnification (**a**). Using image analyzer MicroSuite™ (Soft Imaging System Corp., Lakewood, CO) "3Phases" classification analysis was performed on the image, resulting in the labeling of all normal glands (**b**) and stroma (not labeled in the image). In addition, the "cancer glands" classification scheme was also applied; image (**c**). For clarification regarding "3Phases" and "cancer glands" classification analyses, refer to ***Materials and Methods*** section of text.

To determine the effect of reducing the frequency of pathology serial sectioning on the reconstructions of volume percentages of tissue features, all slides from the 15 cancer-negative human prostate tissue samples were analyzed using the "3Phases" classification scheme. Ten samples were cut at intervals of 200 µm, while the remaining five were cut at 100 µm intervals. In Figure 2, vol% of epithelium (from CAIA) with and without lumen of every sample were plotted (on the horizontal axis) against vol% epithelium with and without lumen, calculated using only odd-numbered sections (on the vertical axis) for both 100 µm (a, b) and 200 µm (c, d) interval sections. The linearity of all four plots indicates that sections cut at 100 µm intervals were not remarkably different from those cut at 200 µm intervals, and similarly, vol% components from those cut at 200 µm intervals varied little when examined at 400 µm intervals. Hence, Figure 2 illustrates that CAIA may be used to estimate the optimal frequency of serial sectioning for the quantification of tissue pathologies. In this case, the results showed that for analyzing normal tissues using CAIA, a frequency of 400 µm would be sufficient for the calculation of the vol% of cellular components. It is possible that cancerous glands may be smaller and shallower than normal glands. However, visual assessment of adjacent pathology images suggests that similar area% were

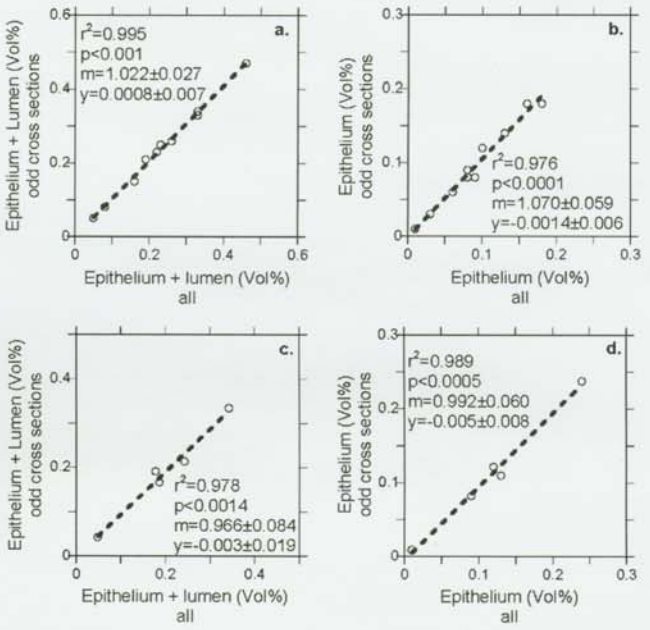

Figure 2: Highly significant direct correlations were observed between both total vol% of normal epithelium and lumen and vol% of normal epithelium and lumen, calculated using only odd cross-sections at intervals of both 200 microns and 400 microns, (**a**) and (**c**) respectively. Similarly, (**b**) and (**d**) show that slopes of virtually m=1 were also observed between total vol% and odd cross-section vol% of normal epithelium only cut at intervals of 200 and 400 microns, respectively. Essentially, this suggests that sectioning need only occur at 400 micron intervals, as there exist no appreciable differences in percent composition at 100, 200, or 400 micron intervals.

seen at sequential intervals both for cross-sections cut every 100 μm and those cut every 200μm.

CAIA Determinations of the Percentages of Areas/Volumes of Prostate Tissue Features are Strongly Correlated with the Determinations of Human Visual Assessment

Despite the linear correlations between results of CAIA and human estimations, it was found that there were significant differences between human pathological assessment of the area% of pathological features of interest and CAIA quantification of the same feature areas. This is shown in Figures 3 and 4, where the area% (i.e. cross-sections) and vol% (i.e. samples) of normal epithelium + lumen and cancer cells + lumen are presented, respectively.

Figures 3(a) and (b) show statistically significant linear relationships of the area% (a), R^2=0.67 p<0.0001, and vol% (b), R^2=0.67 p<0.0002, of normal glands (epithelium and lumen) as measured by CAIA, with the average of the pathologists' estimates of these values. When comparing CAIA (y-axis) with the pathologists' estimates (x-axis), both area% and vol% of normal glands indicated similarly sloping linear relationships, 0.46±0.03 and 0.49±0.10; that is, values from the human estimates amounted to about twice those determined by CAIA.

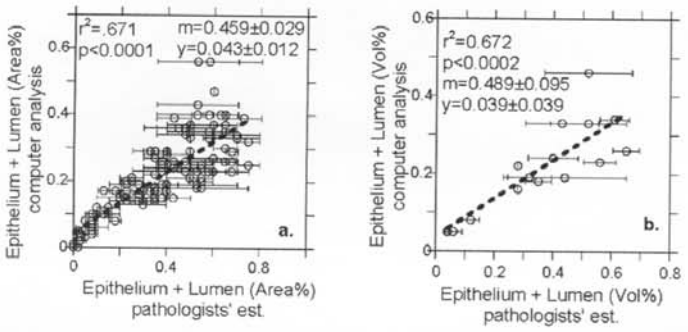

Figure 3: The observed linear correlations between both area% and vol% of normal glands from pathologists' estimations and area% and vol% of normal glands from "3Phases" computer analysis, (**a**) and (**b**) respectively. Similar slopes from (**a**), 0.459±0.029, and (**b**), 0.489±0.095, suggest that there tends to be approximately a two-fold difference of the percentages of normal epithelium and lumen between human pathological assessments and CAIA results.

Similarly, Figure 4 shows linear relationships between the averages of the pathologists' estimates of both area% and also vol% cancer glands (cells and lumen), and the results generated by CAIA, R^2=0.59 p<0.0001 and R^2=0.93 p<0.0001, respectively. The slopes for area% and vol% of cancer glands were 0.48±0.06 and 0.44±0.03, respectively. Again, these statistically significant slope values suggest that there is a two-fold difference between visual assessment and computer quantification.

Correlation of Metabolite Intensities to Prostate Pathology

Since HRMAS proton MRS does not alter prostate tissue intactness and pathological architectures, subsequent pathological assessment can be performed on the same samples to evaluate the critical correlations between metabolite concentration and vol% of cellular pathologies. The spectrum in Figure 5 is an example of the metabolic region of interest (4.8 ppm to -0.2 ppm) with a number of tissue cellular metabolites labeled: citrate (Cit), polyamines including spermine, choline (Cho) and phospocholine (PCh). These metabolites were chosen because they have been shown to be associated with prostate cancer growth (14-18). The metabolic intensities for those four metabolites were normalized by the intensity of the water peak at ~5.0 ppm (from a fully-relaxed spectrum, not shown) in order to derive the absolute metabolic concentration. In Figure 6, metabolic concentrations for Cit and polyamines were plotted against

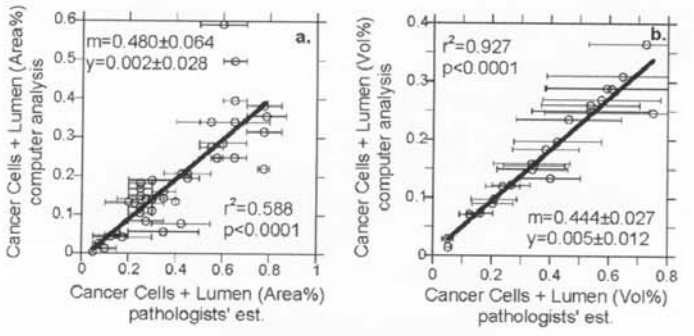

Figure 4: Statistically significant linear correlations observed between area% and vol% of cancer glands (cancer cells + lumen) as estimated by human pathological assessment and area% and vol% of cancer glands as detected using "cancer glands" classification scheme, (**a**) and (**b**) respectively. Slopes of 0.480±0.064 (**a**) and 0.444±0.027 (**b**) show two-fold difference between human assessments and CAIA results also exists for estimating the percentage of cancerous glands in human prostate tissue.

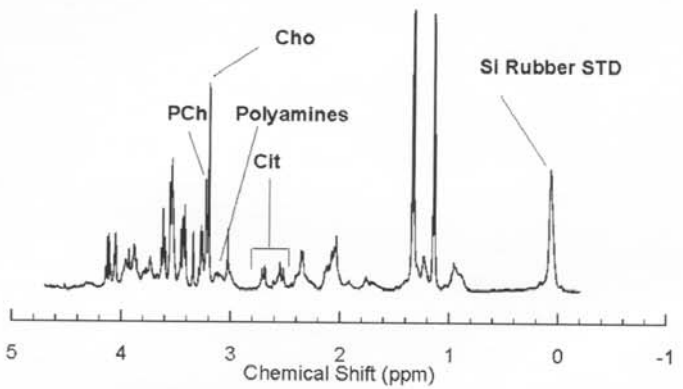

Figure 5: Proton HRMAS spectrum of a sample of cancerous human prostate tissue with metabolites of interest, as well as the SI Rubber STD, labeled. The spectrum was measured using a rotor-synchronized CPMG sequence with a total of 20ms delay after the 90° excitation pulse and with a spinning rate of 700Hz.

the vol% of epithelium with lumen (Fig. 6a), and without lumen (Fig. 6b) calculated by CAIA. Linear correlations were observed between concentrations of both Cit and polyamines and the vol% of epithelium with and without lumen. However there were no linear correlations observed between metabolic concentration and vol% lumen, which may suggest that both Cit and the polyamines, thought to be secreted metabolites, are secreted as a function of the amount of normal epithelia present in the tissue (19, 20).

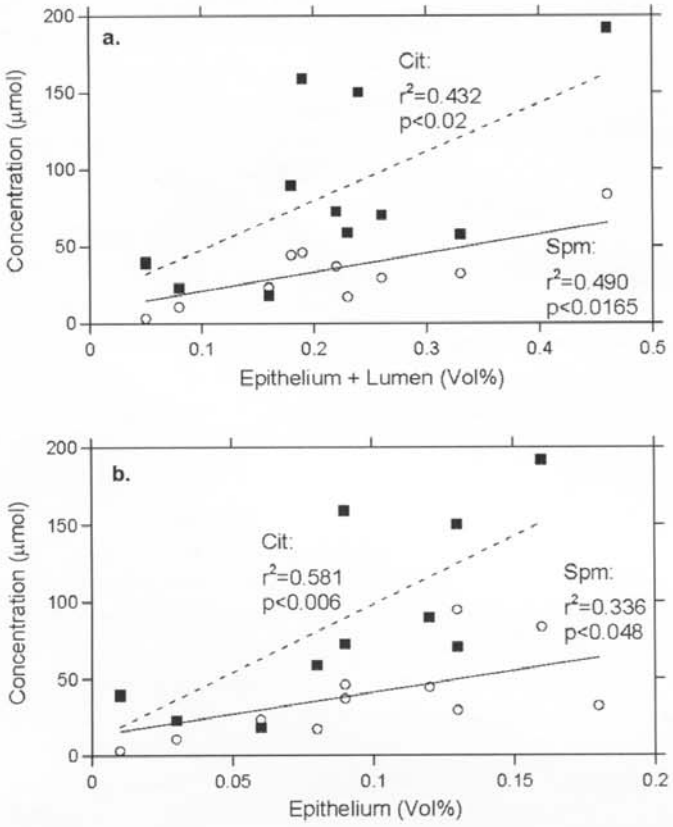

Figure 6: Linear correlations between concentration (µmol) of polyamines (Spm, ?) and citrate (Cit, ?) and vol% of normal glands (**a**) and of normal tissue epithelium only (**b**), measured from the same tissue sample after NMR measurement using "3Phases" computer analysis.

Figure 7 shows linear correlations observed between the vol% cancer (with and without lumen) calculated from CAIA, and Cho and PCh + Cho, respectively. Of importance, when the metabolic concentrations were plotted against the vol% cancer determined by human visual assessment, no correlations existed. Additionally, there was no correlation observed between vol% lumen and metabolic concentrations when vol% was determined by human estimation. Again, these observations suggest both that CAIA may be more sensitive than human visual quantification of pathological features and that the levels of Cho and PCh present in a tissue sample are intrinsically related and proportional to the amount of cancerous cells in that sample. This is consistent with the known fact that malignant transformation is connected to substantial geometric remodeling of the pore, or lumenal space (21).

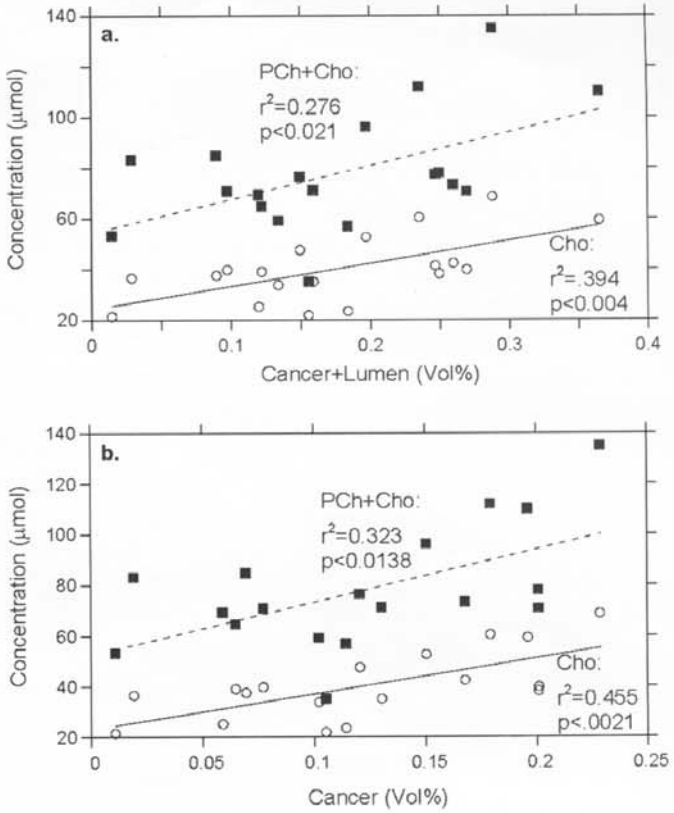

Figure 7: Linear correlations between the concentrations (µmol) of choline (Cho, ?) and the sum of phosphocholine plus choline (PCh + Cho, ?) and the vol% of cancer glands (**a**) and of cancer cells only (**b**) measured from the same tissue sample after NMR measurement using image analyzer MicroSuite™ and the "cancer glands" classification scheme. No correlation was identified when human pathologists' estimations were used in place of the computer-aided quantitative pathology measurements.

Discussions

The method presented, CAIA for quantitative pathology, has the ability to provide a powerful adjunct tool for metabolomic research using HRMAS proton MRS. Although this study was developed due to the necessity of performing tissue pathological quantification after HRMAS MRS measurements in order to identify potential biomolecular markers for disease diagnosis, its conclusions are generally applicable to other molecular pathology studies where both the presence and quantity of certain pathological features are of interest. Currently, human visual assessment of prostate pathology is used for comparison with metabolite concentration. However, human visual assessment introduces both inter- and intra- observer biases that may inhibit the determination of statistically significant correlations. The CAIA method described here provides a simple, reproducible, and reliable method of pathological assessment that is free of both inter- and intra-observer biases.

Validity and Current Limitations of Computer-aided Quantitative Pathology using MicroSuite™

Currently, limitations in the software available for CAIA necessitate a reliance on human visual assessment to distinguish normal from cancerous glands in clinic. This distinction is based on tissue architecture and cellular characteristics, and cannot be made simply based on the color of the H&E staining and the lumenal areas, as in CAIA. Therefore, it is essential that tissue undergoing CAIA be classified as cancer-negative or cancer-positive before CAIA, and that glands of images coded using "cancer glands" classification schemes be assessed after CAIA for the detection of any false positives, as was done in this study by the participating pathologists.

This limitation may be alleviated when other cancer cell specific immuno-stainings are incorporated. However, even at present, while the aid of expert pathologists is still necessary for the determination of normal versus cancerous glands, the computer classification protocols "3Phases" and "cancer glands" have shown the ability to produce objective results free of inter-observer bias. Since the computer classification schemes have fixed parameters that are used for every image, are the same for every tissue being studied, and are independent of the person performing the CAIA, inter-, as well as intra-, observer biases are not of concern. For instance, to determine whether CAIA is more consistent than human visual assessment, one sample of normal human prostate tissue containing 13 cross-sections was reanalyzed using the "3Phases" classification protocol. In addition, these cross-sections were also reread at a later date by one of the pathologists who initially read this sample. From the given results, the reproducibility of the CAIA is markedly better than inter-observer bias (m=0.91±0.08, y-intercept=0.04±0.03 versus m=0.62±0.06, y-intercept=0.15±0.04 for CAIA and visual, respectively), and slightly better than intra-observer bias for which both measurements approach unity and the origin, but for which $r^2_{\text{computer analysis}}$ is slightly more significant than $r^2_{\text{intraobserver bias}}$ (r^2=0.92 and r^2=0.90, respectively).

Potentially, technical advances in image analysis software will allow the fully automated detection of cellular components, including the detection of cancerous cells and/or glands with specific immunochemical stainings. However, with the minimal costs of H&E staining, the method used in this study, selecting for CAIA the cross-sections that represent large differences in area% of cellular components within a sample, is reliable based upon the correlations observed between vol% cancer and the metabolites Cho and PCh + Cho.

Correlations Between Tissue Pathology and Metabolite Concentrations

Using human visual assessment to estimate the vol% of tissue components for a sample, such as a prostate biopsy core, may be unreliable. Although calculating vol% is possible with the aid of a simple computer analysis to map the area of each tissue section within a sample, additional errors are introduced, making this method less reliable than the CAIA method presented in this report. Additionally, accurate determination of area% of epithelium or cancer without lumen is very difficult with human visual assessment due to the generally ring-like structures of the glandular epithelium and cancer cells. However, using the classification schemes presented in this report, determining the area% of such cellular components is facile. The ease and accuracy with which this determination is made allowed for the novel determination that the lumenal areas, both normal and cancerous, do not contribute to the correlations observed between metabolic concentrations and prostate pathologies. Such observations fuel metabolomics, which is concerned with metabolite levels that are continuously changing and evolving as a disease develops and progresses.

Pathologists do not often consider the area and volume percentages of each pathological structure as components of the whole tissue section or biopsy core, respectively. Rather, they rely on qualitative descriptions rather than quantitative data when making a diagnosis. Although quantitation is not of the interest of the traditional anatomic pathology, it has gained attention in the era of molecular pathology, in which both genomic expressions and proteomic profiles are presented quantitatively. Here we suggest that by comparing quantitative pathological data with metabolomic profiles, new diagnostic criteria may be established. However, as a preliminary evaluation, only the simple, linear regression method is used to demonstrate this principle. Such a simplified treatment of the complexity of cellular metabolism inevitably injects errors in the results, which likely explain the observed R^2 values presented in Figures 6 and 7 for metabolite correlations. Nevertheless, with the establishment of the principle and the implementation of sophisticated paradigms for tissue metabolite analyses, in the near future, metabolic criteria may be used in prostate biopsy to provide a more definitive diagnosis and allow for closer monitoring of suspicious foci than is currently possible.

Conclusions

The reported results indicate that CAIA for use in quantitative pathology may provide more reliable results than human visual assessment, and may allow for the observation of stronger correlations between prostate pathologies and metabolite concentrations measured with HRMAS proton NMR spectroscopy. In addition, this method is useful in the determination of certain technical aspects, such as the optimal frequency of pathology sections, and the determination of which specific components, for example epithelium or

lumen, correlate with the measured metabolite intensities. Furthermore, the ease and efficiency with which different classification schemes can be created allow for future extension to other cancers, diseases, and types of tissue.

Acknowledgements

We wish to thank Ms. D. Ashley Feldman for editorial assistance. This work is supported in part by PHS/NIH grants CA095624 and EB002026; and in part by a DOD grant W81XWH-04-1-0190.

References

1. Dove, A. Proteomics: Translating Genomics into Products? *Nat. Biotechnol. 17*, 233-236 (1999).
2. Binz, P. A., Muller, M., Walther, D., Bienvenut, W. V., Gras, R., Hoogland, C., Bouchet, G., Gasteiger, E., Fabbretti, R., Gay, S., Palagi, P., Wilkins, M. R., Rouge, V., Tonella, L., Paesano, S., Rossellat, G., Karmime, A., Bairoch, A., Sanchez, J. C., Appel, R. D., and Hochstrasser, D. F. A Molecular Scanner to Automate Proteomic Research and to Display Proteome Images. *Anal. Chem. 71*, 4981-4988 (1999).
3. Steinert, R., von Hoegen, P., Fels, L. M., Gunther, K., Lippert, H., and Reymond, M. A. Proteomic Prediction of Disease Outcome in Cancer: Clinical Framework and Current Status. *Am J Pharmacogenomics 3*, 107-115 (2003).
4. Stenman, U. H., Leinonen, J., Alfthan, H., Rannikko, S., Tuhkanen, K., and Alfthan, O. A Complex Between Prostate-specific Antigen and Alpha 1-antichymotrypsin is the Major Form of Prostate-specific Antigen in Serum of Patients with Prostatic Cancer: Assay of the Complex Improves Clinical Sensitivity for Cancer. *Cancer Res. 51*, 222-226 (1991).
5. Catalona, W. J., Partin, A. W., Slawin, K. M., Brawer, M. K., Flanigan, R. C., Patel, A., Richie, J. P., deKernion, J. B., Walsh, P. C., Scardino, P. T., Lange, P. H., Subong, E. N., Parson, R. E., Gasior, G. H., Loveland, K. G., and Southwick, P. C. Use of the Percentage of Free Prostate-specific Antigen to Enhance Differentiation of Prostate Cancer from Benign Prostatic Disease: A Prospective Multicenter Clinical Trial. *Jama 279*, 1542-1547 (1998).
6. Israeli, R. S., Powell, C. T., Corr, J. G., Fair, W. R., Heston, W. D. Expression of the Prostate-specific Membrane Antigen. *Cancer Res. 54*, 1807-1811 (1994).
7. Ito, K., Yamamoto, T., Ohi, M., Takechi, H., Kurokawa, K., Suzuki, K., and Yamanaka, H. Natural History of PSA Increase With and Without Prostate Cancer. *Urology 62*, 64-69 (2003).
8. Carter, H. B. and Isaacs, W. B. Improved Biomarkers for Prostate Cancer: A Definite Need. *J. Natl. Cancer Inst. 96*, 813-815 (2004).
9. Zackrisson, B., Aus, G., Lilja, H., Lodding, P., Pihl, C. G., and Hugosson, J. Follow-up of Men with Elevated Prostate-specific Antigen and One Set of Benign Biopsies at Prostate Cancer Screening. *Eur. Urol. 43*, 327-332 (2003).
10. Draisma, G., Boer, R., Otto, S. J., van der Cruijsen, I. W., Damhuis, R. A., Schroder, F. H., and de Koning, H. J. Lead Times and Overdetection Due to Prostate-specific Antigen Screening: Estimates from the European Randomized Study of Screening for Prostate Cancer. *J. Natl. Cancer Inst. 95*, 868-878 (2003).
11. Etzioni, R., Penson, D. F., Legler, J. M., di Tommaso, D., Boer, R., Gann, P. H., and Feuer, E. J. Overdiagnosis Due to Prostate-specific Antigen Screening: Lessons from U.S. Prostate Cancer Incidence Trends. *J. Natl. Cancer Inst. 94*, 981-990 (2002).
12. Fiehn, O. Metabolomics – The Link Between Genotypes and Phenotypes. *Plant Mol. Biol. 48*, 155-171 (2002).
13. Defernez, M. and Colquhoun, I. J. Factors Affecting the Robustness of Metabolite Fingerprinting Using 1H NMR Spectra. *Phytochemistry 62*, 1009-1017 (2003).
14. van der Graaf, M., van den Boogert, H. J., Jager, G. J., Barentsz, J. O., and Heerschap, A. Human Prostate: Multisection Proton MR Spectroscopic Imaging with a Single Spin-echo Sequence – Preliminary Experience. *Radiology 213*, 919-925 (1999).
15. Males, R. G., Vigneron, D. B., Star-Lack, J., Falbo, S. C., Nelson, S. J., Hricak, H., and Kurhanewicz, J. Clinical Application of BASING and Spectral/Spatial Water and Lipid Suppression Pulses for Prostate Cancer Staging and Localization by *In Vivo* 3D 1H Magnetic Resonance Spectroscopic Imaging. *Magn. Reson. Med. 43*, 17-22 (2000).
16. Hahn, P., Smith, I. C., Leboldus, L., Littman, C., Somorjai, R. L., and Bezabeh, T. The Classification of Benign and Malignant Human Prostate Tissue by Multivariate Analysis of 1H Magnetic Resonance Spectra. *Cancer Res. 57*, 3398-3401 (1997).
17. Cheng, L. L., Wu, C., Smith, M. R., and Gonzalez, R. G. Nondestructive Quantitation of Spermine in Human Prostate Tissue Samples Using HRMAS 1H NMR Spectroscopy at 9.4 T. *FEBS Lett. 494*, 112-116 (2001).
18. Swanson, M. G., Vigneron, D. B., Tabatabai, Z. L., Males, R. G., Schmitt, L., Carroll, P. R., James, J. K., Hurd, R. E., and Kurhanewicz, J. Proton HR-MAS Spectroscopy and Quantitative Pathologic Analysis of MRI/3D-MRSI-targeted Postsurgical Prostate Tissues. *Magn. Reson. Med. 50*, 944-954 (2003).
19. Lao, L., Franklin, R. B., and Costello, L. C. High-affinity L-aspartate Transporter in Prostate Epithelial Cells that is Regulated by Testosterone. *Prostate 22*, 53-63 (1993).
20. Cohen, R. J., Fujiwara, K., Holland, J. W., and McNeal, J. E. Polyamines in Prostatic Epithelial Cells and Adenocarcinoma: The Effects of Androgen Blockade. *Prostate 49*, 278-284 (2001).
21. Mattfeldt, T., Schmidt, V., Reepschlager, D., Rose, C., and Frey, H. Centred Contact Density Functions for the Statistical Analysis of Random Sets. A Stereological Study on Benign and Malignant Glandular Tissue Using Image Analysis. *J. Microsc. 183*, 158-169 (1996).

Date Received: August 23, 2004

Magnetic Resonance in Medicine 54:34–42 (2005)

Reduction of Spinning Sidebands in Proton NMR of Human Prostate Tissue With Slow High-Resolution Magic Angle Spinning

Melissa A. Burns,[1] Jennifer L. Taylor,[1] Chin-Lee Wu,[1] Andrea G. Zepeda,[1] Anthony Bielecki,[3] David Cory,[4] and Leo L. Cheng[1,2*]

High-resolution magic angle spinning (HRMAS) NMR spectroscopy has proven useful for analyzing intact tissue and permitting correlations to be made between tissue metabolites and disease pathologies. Extending these studies to slow-spinning methodologies helps protect tissue pathological structures from HRMAS centrifuging damage and may permit the study of larger objects. Spinning sidebands (SSBs), which are produced by slow spinning, must be suppressed to prevent the complication of metabolic spectral regions. In this study human prostate tissues, as well as gel samples of a metabolite mixture solution, were measured with continuous-wave (CW) water presaturation on a 14.1T spectrometer, with HRMAS spinning rates of 250, 300, 350, 600, and 700 Hz, and 3.0 kHz. Editing the spectra by means of a simple minimum function (Min(A, B, . . ., N) for N spectra acquired at different but close spinning rates) produced SSB-free spectra. Statistically significant linear correlations were observed for metabolite concentrations quantified from the Min(A, B, . . ., N)-edited spectra generated at low spinning rates, with concentrations measured from the 3 kHz spectra, and also with quantitative pathology. These results indicate the empirical utility of this scheme for analyzing intact tissue, which also may be used as an adjunct tool in pathology for diagnosing disease. Magn Reson Med 54:34–42, 2005.

Key words: HRMAS; proton MRS; human prostate; slow spinning; pathology

The utility of high-resolution magic angle spinning (HRMAS) proton NMR spectroscopy for the analyzing intact biological tissues is being demonstrated increasingly by spectroscopic laboratories in the field of medical MR (1–11). Correlations between tissue metabolites measured with this spectroscopic method and tissue pathologies have been identified, demonstrating the potential of this method for supplementing histopathological evaluations. The most significant asset of this method is that it does not jeopardize the structural integrity of the tissue, and therefore makes it possible to evaluate tissue samples histopathologically after they have been studied spectroscopically (12). Therefore, the use of slow-spinning measurements for optimally protecting histopathological tissue structures from possible damage resulting from high-rate spinning has become the subject of research. Studies in this area have also evaluated the possibility of conducting HRMAS measurements on objects larger than surgical specimens (13–15).

MAS, a line-narrowing technique, has the potential to reduce line-broadenings due to both homogeneous and inhomogeneous interactions. Homogeneous line-broadenings, which result from fast spin diffusions (e.g., dipolar couplings) and exchanges, generate the final isotropic lineshape, and obscure the identification of contributions from individual spins. In theory, inhomogeneous line-broadenings can be traced to individual spins that are either oriented differently to the magnetic field (e.g., chemical shift anisotropy), or are experiencing a different field strength (e.g., magnetic susceptibility). With MAS on protons, homogeneous line-broadenings (particularly from dipolar interactions at natural abundance) are too large in scale to be narrowed with the currently achievable spinning rates. As a result, the proton signals from proteins and cell membranes cannot be detected with an HRMAS measurement—even, for instance, at spinning rates of >5 kHz. The enhancement in tissue measurements observed with HRMAS at a spinning rate of a few hundred Hertz is the result of the averaging of inhomogeneous interactions (mostly magnetic susceptibility effects) in cytoplasm and biological fluids. Experimental results have shown that a reduction in spinning rates with HRMAS does not interfere with the ability of HRMAS to reduce spectral line-broadenings due to inhomogeneous interactions (13–16). Furthermore, such reductions in the effects of these inhomogeneous interactions do not happen at a specific, determined spinning rate, but rather occur gradually with the increase of the spinning rate, and are maximized when all of the interactions are experimentally accounted for.

Basic physics suggests that the probability that structural damage will result from the centrifugal stress of spinning greatly decreases as the spinning rate is lowered. Therefore, there seems to be an optimal spinning rate below the maximum rate required for the complete reduc-

[1]Department of Pathology, Massachusetts General Hospital, Harvard Medical School, Boston, Massachusetts, USA.

[2]Department of Radiology, Massachusetts General Hospital, Harvard Medical School, Boston, Massachusetts, USA.

[3]Francis Bitter Magnet Laboratory, Massachusetts Institute of Technology, Cambridge, Massachusetts, USA.

[4]Department of Nuclear Engineering, Massachusetts Institute of Technology, Cambridge, Massachusetts, USA.

Grant sponsor: PHS/NIH; Grant numbers: CA77727; CA80901; CA095624; EB002026; Grant sponsor: DOD; Grant number: W81XWH-04-1-0190.

*Correspondence to: Leo L. Cheng, Pathology Research, CNY-7, 149 13th Street, Charlestown, MA 02129. E-mail: cheng@nmr.mgh.harvard.edu.

Received 15 March 2004; revised 25 January 2005; accepted 27 January 2005.

DOI 10.1002/mrm.20523
Published online in Wiley InterScience (www.interscience.wiley.com).

tion of inhomogeneous interactions. At this optimal point, the spinning rate is fast enough to produce a tissue spectral resolution that is adequate for identifying metabolites for pathology, and slow enough to preserve tissue pathology structures. However, to study biological tissues at spinning rates <1 kHz, effective suppression of spinning sidebands (SSBs), particularly those from water signals, is essential in order to eliminate interference with metabolite peaks of interest.

Recently the results of an HRMAS proton NMR study of human prostate tissues obtained under spinning rates of 600 and 700 Hz, with the assistance of a rotor-synchronized delays alternating with nutation for tailored excitation (DANTE) sequence, were reported (16). A robust performance by the technique in terms of the reproducibility of SSB suppression and the simplicity of its concept and execution was observed. With this approach, spectral regions that were free of water SSBs were selected alternately between the 600- and 700-Hz generated spectra. The effectiveness of this approach for biological systems in which SSBs of metabolites other than water are negligible was demonstrated. However, it was acknowledged that the effectiveness of the approach will diminish for systems in which SSBs from tissue metabolites or surgical alcohol contamination are present. In addition, although the empirical selection of spectral regions is effective, it has elicited concerns regarding the objectivity of the procedure.

In the 1980s, S. Patt (personal communication) suggested that SSBs in solid-state NMR could be removed with a novel mathematical scheme by editing two spectra (A, B), obtained at different spinning rates, with the formula: $(A + B - |A - B|)/2$. However, the suggestion received little attention. Upon reviewing this mathematical scheme, it became apparent to us that the proposed formula is equal to the function of Min(A, B), the point-by-point minimum of spectra A and B. This recognition also led to a simple and critical extension of the scheme to Min(A, B,. . ., N). The results obtained from Min(A, B) and/or Min(A, B,. . ., N) on gel samples of a metabolite mixture solution, as well as from human prostate samples, are presented in this report.

MATERIALS AND METHODS

Tissue Protocol

The NMR analysis of human prostate surgical specimens was approved by the Institutional Review Board (IRB) of Massachusetts General Hospital. Tissue samples were snap-frozen in liquid nitrogen and stored at −80°C. Thirty-one prostate samples were used in the study. At the completion of the spectroscopic analysis, tissue samples were fixed in 10% formalin, embedded in paraffin, cut into 5-μm-thick sections at 100-μm intervals, and stained with hematoxylin and eosin. Cross sections of each sample were quantified from pathology slides using an Olympus BX41 Microscope Imaging System (Olympus American, Inc., Melville, NY, USA) equipped with the image analyzer MicroSuite™ (Soft Imaging System Corp., Lakewood, CO, USA). The percentage of the area representing cancer cells, normal epithelial cells, and stroma in each cross section was estimated visually to the nearest 5% by a pathologist who had no knowledge of the spectroscopic results. The reported vol% of each pathological presentation was calculated based on the size of the cross section and the corresponding area percentage of each pathological feature.

Preparation of a Standard Gel Mixture Solution of Common Metabolites

A gel mixture solution of 10 commonly observed cellular metabolites was prepared to test the quantitative capability of HRMAS proton NMRS and, in particular, the examined spectral editing scheme. The following compounds (approximately 1 mM each) were dissolved in 100 ml distilled water: phosphocreatine, L-glutamic acid, sodium citrate, L-glutamine, taurine, myo-Inositol, N-acetylaspartate, phosphorylcholine, glycerophosphorylcholine, and lactic acid. About 1.5 g of agarose was added to the mixture. The pH of the mixture solution was adjusted to ~7.0. The mixture was heated until the agarose dissolved, and then was cooled to form a gel solution. The gel of the mixture solution was kept at 4°C. The measured concentrations determined from the spectroscopy data were between 6.7 and 26.2 mM based on the tested range of spinning rates.

HRMAS Proton NMR

The NMR experiments were carried out on a Bruker (Bruker BioSpin Corp., Billerica, MA, USA) AVANCE spectrometer operating at 600 MHz (14.1T). The HRMAS probe had three frequency channels: ^{1}H, ^{13}C (not used in these experiments), and ^{2}H. The samples were placed into a 4-mm zirconia rotor with Kel-F plastic inserts, which created a spherical sample space of ~10 μl located at the center of the detection coil. A small (~0.1 mg) silicone rubber sample was permanently fixed inside one of the Kel-F spacers, positioned within the detection coil but not in contact with the sample, to function as an external standard (STD) for both frequency (0.06 ppm from TMS) and quantification. Different amounts of the gel-solution sample (6–10 mg) were measured. Prostate tissue samples (8–10 mg) were obtained directly from the freezers without further preparation. The weights of the tissue samples were estimated based on the weight of the empty rotor and the weights of the rotor with the samples, before and after the HRMAS measurements. Because of the weight difference between the rotor and the tissue samples (about 1000 times), and the apparent loss of sample weight after the HRMAS measurements (likely due to water condensation on the outside wall of the rotor, which contained frozen tissue when it was weighed before the HRMAS analysis), the error in weight is generously estimated as 0.5 mg. Approximately 1.0 μl of D_2O was added to each sample for ^{2}H field locking. The sample was introduced into the probe, which was precooled to 3°C for NMR measurements at that temperature. The rotor spinning rate accuracy (±1.0 Hz) was controlled with a MAS controller and was verified with the positions of the SSBs in the spectra.

Spectra were acquired with the spectrometer frequency set exactly on the water resonance. Two types of spectra were acquired: 1) CW water presaturation, followed by a

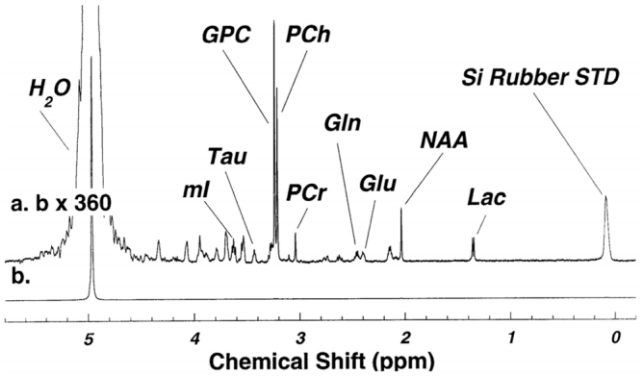

FIG. 1. Proton HRMAS spectrum of the prepared standard gel solution of commonly observed tissue cellular metabolites (as labeled) at 3.0 kHz. The spectrum was measured with a rotor-synchronized CPMG sequence with a total delay time of 20 ms. Spectrum **a** represents a 360-fold vertical expansion of the fully relaxed spectrum (**b**).

single 90° excitation pulse (used for both tissue and gel-solution samples), and 2) rotor-synchronized Carr-Purcell-Meiboom-Gill sequence (CPMG), with a 20-ms delay after the 90° excitation pulse (used only with the gel-solution samples). The CPMG sequence with a very short delay is used to reduce broad resonances caused by the probe background. Metabolite concentrations may be estimated from such a CPMG spectrum by reference to the intensity of water signals, while estimations from water presaturated spectra rely on the simultaneous measurement of the external standard.

Ten gel-solution samples of different weights were measured at spinning rates of 600 and 700 Hz, and 3.0 kHz with both CW water presaturation and rotor-synchronized CPMG pulse sequences. Of these, three were measured at the following additional spinning rates, with only the rotor-synchronized CPMG pulse sequence: 250, 300, 350, 800, and 900 Hz, and 1.0, 1.2, 1.4, 1.6, 1.8, 2.0, 2.4, 2.8, and 3.2 kHz. Of note, when total spectral absolute intensities of different spinning rates were compared, a decreasing trend was observed after 2.4 kHz. This reduction was likely the result of the sample leakage from the center of the rotor to the ends due to the spinning rate increase. Hence, data from 2.8 and 3.2 kHz spectra were not included in further calculations. The CW water presaturation sequence was used to analyze the human prostate tissue samples. Of the reported 31 human prostate samples, two samples were measured at spinning rates of 250, 300, 350, 600, and 700 Hz, and 3.0 kHz. Fourteen samples were measured at spinning rates of 600 and 700 Hz, and 3.0 kHz, and 15 samples were measured at spinning rates of 250, 300, and 350 Hz. Of note, the reported 17 samples measured at 250–350 Hz were the only samples analyzed thus far at those spinning rates, while the 16 samples evaluated at 600 and 700 Hz, and 3.0 kHz were the first samples from a series of studies involving 298 tissue specimens to date measured according to the Min(A, B) scheme. Each spectrum was acquired with 32 transients and a repetition time (TR) of 5 s.

The spectroscopic data were processed using the Nuts software (Acorn NMR Inc., Livermore, CA, USA) according to the following procedures: All free induction decays (FIDs) were subjected to 0.5–1 Hz apodization before Fourier transformation, baseline correction, and phase adjustment were performed. Min(A, B, . . ., N) was applied to the data in the frequency domain using Nuts software after all individual spectra had been processed. The resonance intensities reported here represent integrals of curve-fittings with Lorentzian-Gaussian line-shapes, normalized by the STD intensity measured for each sample. All intensities reported here in the context of quantification refer to area integrated intensities. Tissue metabolite concentrations were calculated based on the integrated intensity ratios of metabolites over the STD, as explained in detail in the following section.

RESULTS

Evaluation of the Standard Gel Solution, and Calibration of the Silicone Rubber STD in the Sample Rotor

Figure 1 shows a spectrum of the prepared metabolite gel solution measured at a spinning rate of 3.0 kHz with the CPMG sequence without water presaturation. The spectrum in Fig. 1a, which is a vertical expansion of the entire spectrum (b), clearly shows the resonances of all of the prepared metabolites, although the integrated intensity of citrate appears to be less than its expected concentration. In addition, a prominent $-CH_3$ resonance peak from a piece of silicone rubber STD (~0.1 mg) that was permanently fixed inside the sample rotor was observed. Since the physical nature of the STD is that of a solid, its inte-

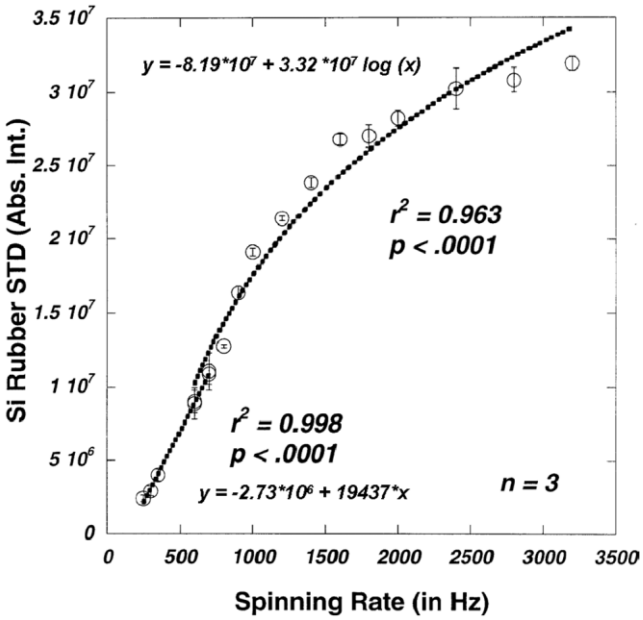

FIG. 2. The center band peak area integrated intensity of a silicon rubber standard (STD) as a function of the rotor spinning rate. The STD (~0.1 mg) was permanently fixed inside one of the Kel-F spacers to function as an external standard for both frequency and metabolite quantification. It appears that the spinning rate and the STD integrated intensity follow a linear relationship in the spinning rate region of 250–700 Hz, and then becomes logarithmic for spinning rates above 700 Hz.

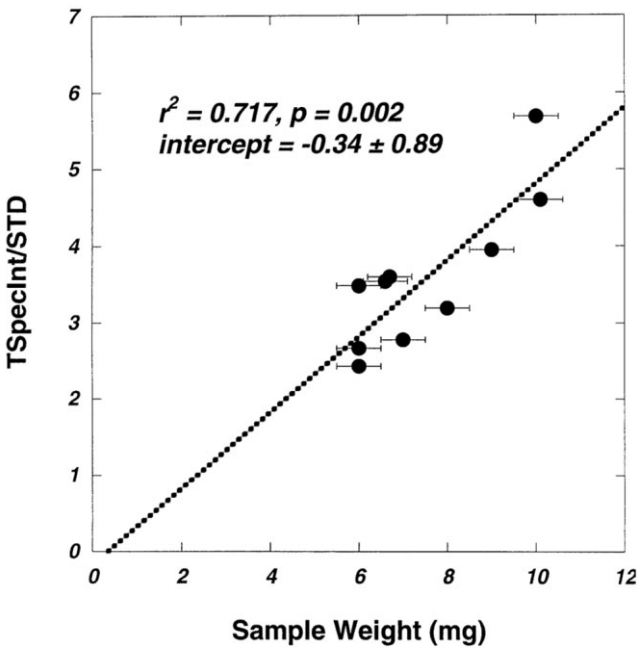

FIG. 3. The observed linear correlation between the sample weight (the mathematical average before and after spinning) and the total proton spectral integrated intensity measured at −0.2 to 4.8 ppm (excluding water signals) under the HRMAS spinning rate of 3.0 kHz from the prepared standard gel solution of metabolites measured with water presaturation.

grated intensity (at ~0 ppm) is heavily dependent on the spinning rate, as shown in Fig. 2. The relationship between the spinning rate and the STD absolute spectral integrated intensity has both linear (for the spinning rate region of 250–700 Hz) and logarithmic (for spinning rates above 700 Hz) components. Of particular interest in the present work, it was found that the STD's integrated intensity at 3.0 kHz was (3.06 ± 0.23) times higher than that measured at 600 Hz (16).

The overall quantitativeness of the HRMAS measurements was tested by varying the sample weights of the metabolite gel solution. A linear relationship was observed between the sample weight and the ratio between the summed spectral integrated intensities of all metabolite peaks and those of the STD measured at 3.0 kHz with the water presaturation sequence, as shown in Fig. 3.

The relationship between the sample spinning rate and the measured metabolite integrated intensities in the gel samples, as represented by both the concentrations (calculated according to the integrated intensity of the water resonance measured from the CPMG sequence) and the relative integrated intensities (Rel. Int., obtained as a ratio over the STD integrated intensity measured with the water presaturation sequence at 600 Hz), was examined. An example of this analysis applied to the lactate data ($N = 3$) is shown in Fig. 4. Both plots in the figure show a very similar logarithmic relationship of statistical significance between the increased spinning rate and the evaluated integrated intensities. The apparent integrated intensities (in both concentration and Rel. Int.) at different spinning rates (e.g., 600 Hz and 3.0 kHz) can be estimated for different metabolites according to these logarithmic curves. The linear relationship between the metabolic Rel. Int. and the metabolic concentration obtained from five measured metabolites at 600 Hz and 3.0 kHz is shown in Fig. 5. This linear relationship is critical for using the STD to estimate metabolite concentrations in intact tissue from spectra for which water presaturation is applied to improve the detectability of endogenous metabolites.

Measurement of Prostate Tissue at Low Spinning Rates

By varying the sample weight and spinning rate, and performing a spectroscopic analysis of the standard gels, we

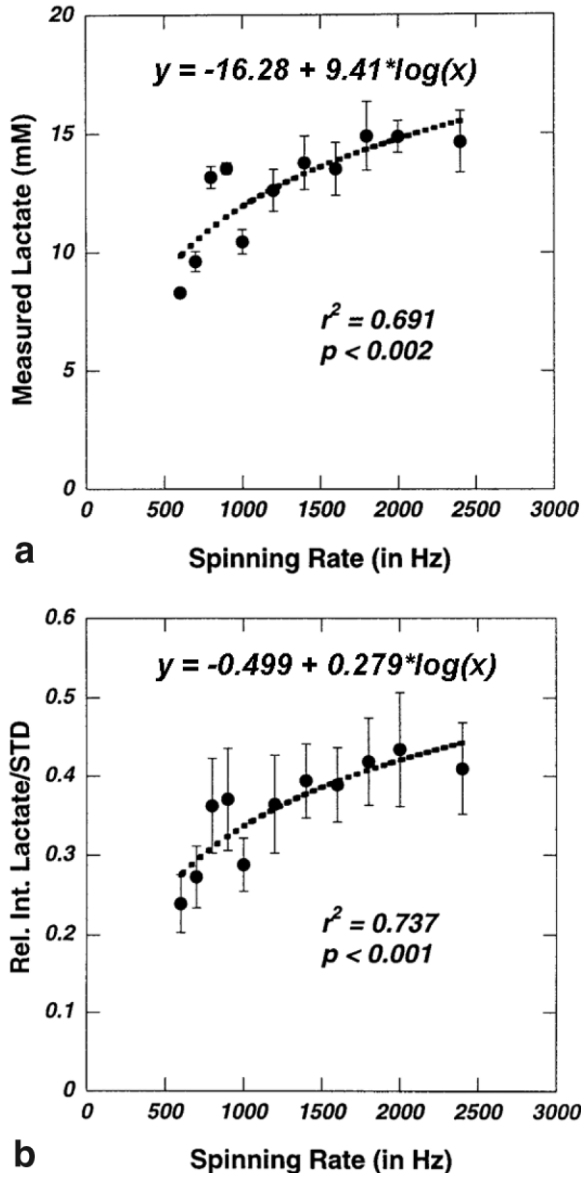

FIG. 4. Comparisons between the measured metabolite (lactate, $N = 3$) integrated intensities in absolute concentrations and relative intensities. (**a**) Absolute concentrations measured from the CPMG sequence and according to the water resonance intensity, and (**b**) relative intensity measured from the water presaturation sequence and according to STD integrated intensity measured at 600 Hz from the standard gel solution as functions of the HRMAS spinning rate.

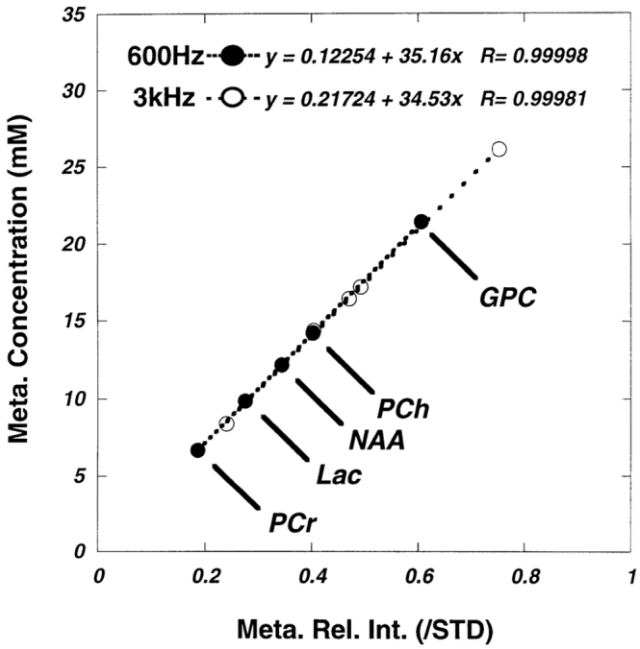

FIG. 5. Linear correlations observed between the relative metabolic integrated intensities as ratios over STD and the metabolite concentration estimated from the observed integrated intensities of water signals. These linear correlations were calculated based on the statistically significant curve-fitting results from the five measured metabolites as exemplified in Fig. 4 for lactate.

were able to identify the relationships necessary to quantify individual metabolites from human prostate tissue spectra edited with the Min(A, B,. . ., N) mathematical scheme. Figure 6 presents the results from the human prostate tissue sample that had the largest residual water SSBs after presaturation. Spectra A (Fig. 6a) and B (Fig. 6b) were measured at spinning rates of 600 and 700 Hz, respectively, where SSBs from water and the external standard were clearly observed. Figure 6d shows a spectrum of the same sample measured at the 3.0 kHz spinning rate, where all of the SSBs were pushed outside the region of interest (ROI; 4.8 ppm – (–)0.2 ppm). However, Fig. 6d was plotted with a different vertical scale to enable a comparison of the overall metabolite profiles with Fig. 6c. A visual inspection reveals no difference between Fig. 6d and c, where c represents the resulting spectrum after Min(A, B) editing. Additionally, Fig. 6e represents the digital inspection of these spectra (c and d). Although the differences between the two spectra are observable, they are minimal and can be neglected without compromising any resulting data. This Min(A, B) editing approach was further applied to three spectra (A, B, and C) (Fig. 7) generated at spinning rates of 250 Hz, 300 Hz, and 350 Hz, respectively. All three spectra showed visible SSBs. However, after the Min(A, B, C) editing scheme was applied to the three spectra, all SSBs were eliminated, as shown in Fig. 7d.

Tissue metabolite concentrations were estimated based on their ratio integrated intensities over the STD, measured both at low spinning rates (600 and 700 Hz) according to Min(A, B), and at 3.0 kHz. The comparison of metabolite concentrations measured with Min(A, B) to those obtained at 3 kHz is shown for the examples of polyamines and citrate in Fig. 8. Comparisons for other metabolites are presented in Table 1. The results in the table are represented by linear regression analyses performed between the two sets of data collected from the 16 samples. These linear regressions were constructed with the 3.0 kHz data on the horizontal, and the Min(A, B) results on the vertical. Hence, if the Min(A, B) value of a particular metabolite is identical to that measured at 3.0 kHz, the slope of the linear regression will be one and the intercept will be zero. On the other hand, a slope of <1 indicates that the integrated intensity of the metabolite measured at 3 kHz has a higher value than that determined with Min(A, B) at 600–700 Hz. For almost all of the evaluated metabolites, higher apparent concentrations were observed under the 3.0 kHz measurement conditions. This was not surprising because it is widely acknowledged that an increase in spinning rate can potentially increase the observable amount of a metabolite, which is affected by the greater minimization of bulk magnetic susceptibility effects and other physical, environmental effects, such as viscosity.

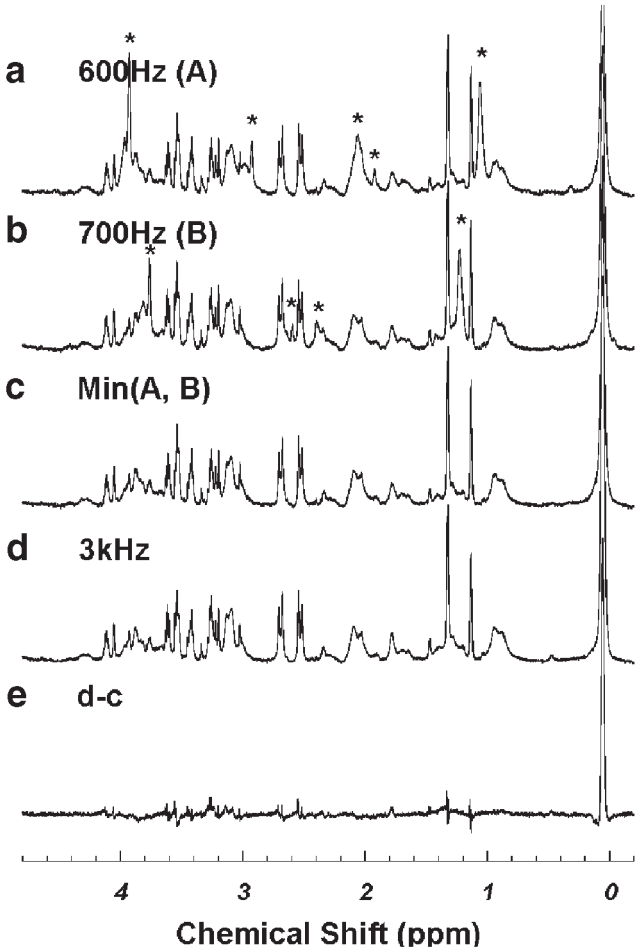

FIG. 6. Human prostate CW water presaturated spectra at spinning rates of (**a**) 600 Hz (A), and (**b**) 700 Hz (B). **c:** A spectrum that was edited, using A and B, with Min(A, B) to be visually compared with **d**, a spectrum obtained at a spinning rate of 3.0 kHz, plotted with a different vertical scale in order to produce **e**, a digital analysis presents the differences between spectra d and c. * SSBs from tissue water and rubber standard signals.

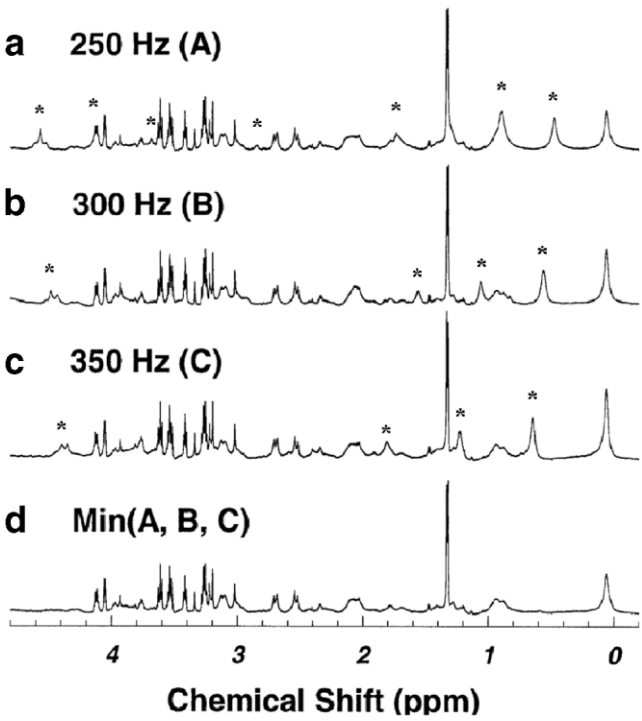

FIG. 7. Human prostate CW water presaturated spectra at spinning rates of (**a**) 250 Hz (A), (**b**) 300 Hz (B), and (**c**) 350 Hz (C). **d:** The resulting spectrum after the Min(A, B, C) editing scheme was applied to A–C. * SSBs from tissue water and rubber standard signals.

The two samples measured at 250, 300, 350, 600, and 700 Hz, and 3.0 kHz demonstrated linear relationships between the metabolic Rel. Int. at 600–700 Hz and 3 kHz, and also between the metabolic Rel. Int. at 250–350 Hz and at 3 kHz obtained with 16 quantified metabolite resonances (32 data points) from the Min(A, B, . . .,N)-edited spectra. Interestingly, while the Rel. Int. at 600–700Hz in Fig. 9 show a overall slope value (0.58) that is similar to those seen in Table 1 (average = 0.79) for concentrations, the Rel. Int. at 250–350 Hz indicates a slope of 0.31, suggesting that the apparent metabolic Rel. Int. measured at 250–350 Hz was much smaller than that measured at 3.0 kHz. Of note, the STD integrated intensities used in the figure were calibrated according to the STD-spinning rate relation curve presented in Fig. 2.

Correlation of Prostate Metabolite Integrated Intensities Measured at Low Spinning Rates With Prostate Pathology

We evaluated the utility of prostate metabolite data obtained with the Min(A, B, C) editing scheme at spinning rates of 250, 300, and 350 Hz by testing the data's correlation with the volume percent of tissue pathological structures. Statistically significant linear correlations between normal epithelium (vol%) and polyamines and citrate are shown in Fig. 10. These are in close agreement with previously reported results obtained at 9.4T (400 MHz) field strength, under a spinning rate of 2.5 kHz (12).

DISCUSSION

The goal of this work was to establish a simple, reproducible, and empirical spectroscopic scheme that can effectively evaluate intact tissue metabolite concentrations measured at slow spinning, which is desirable for protecting tissue pathological structures from the damages of fast mechanical spinning, and for applying spinning to larger objects. This study was conceived because of the need to evaluate pathological tissue after HRMAS analysis to gauge the potential of the metabolite measurements for aiding disease diagnosis. As an empirical approach, the mathematic validity of the scheme from the precise concepts of NMR physics is beyond the scope of the current report.

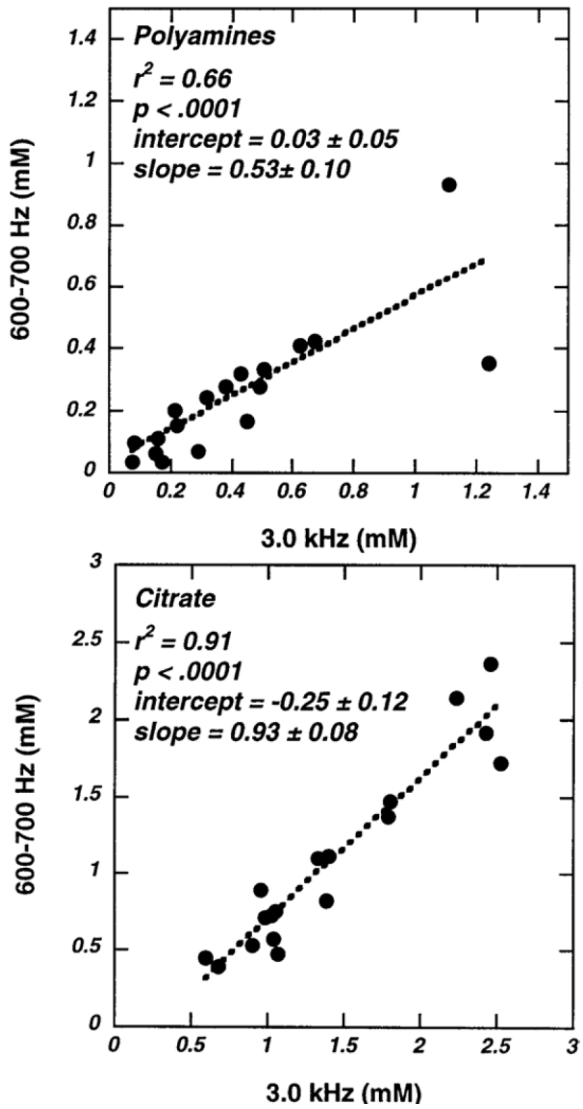

FIG. 8. Comparisons between concentrations of prostate metabolites, polyamines, and citrate measured with sample spinning at 3.0 kHz and those measured at 600 and 700 Hz and determined by Min(A, B) editing. If the Min(A, B) value of a particular metabolite is identical to that measured at 3.0 kHz, the slope of the linear regression would be one and the intercept would be zero. A slope of <1.0 indicates that the measured spectral integrated intensity at a higher (3.0 kHz) spinning rate is greater than that obtained at slower (600–700 Hz) spinning rates. It may be true that the more the slope falls below a value of 1.0, the more "solid-like" is the physical state of the metabolite.

Table 1
Comparison of Linear Regressions (Slow Rates–Vertical, vs. 3.0 kHz Rate–Horizontal) for Selected Metabolites*

Met. reson. (ppm)	*P* value	R^2	Slope[a]		Intercept[b]	
			Mean	SE	Mean	SE
Lac (4.10–4.14)	<0.0001	0.89	0.91	0.08	−0.24	0.17
ml (4.06)	<0.0001	0.77	1.00	0.14	**−0.18**	**0.18**
3.60–3.63	<0.0001	0.70	0.79	0.13	**−0.07**	**0.34**
3.52–3.54	<0.0001	0.84	0.87	0.10	**−0.09**	**0.32**
Tau (3.41–3.43)	<0.0001	0.80	0.87	0.11	**−0.08**	**0.11**
sl (3.34)	<0.0001	0.84	0.73	0.08	**0.00**	**0.01**
Pch (3.22)	0.0002	0.59	0.83	0.18	**−0.03**	**0.04**
Chol (3.20)	<0.0001	0.81	0.65	0.08	**0.01**	**0.02**
PM (3.09–3.14)	<0.0001	0.66	0.53	0.10	**0.03**	**0.05**
Cr (3.03)	<0.0001	0.87	0.76	0.08	**0.02**	**0.03**
Cit (2.52–2.71)	<0.0001	0.91	0.93	0.08	−0.25	0.12
Glu (2.33–2.36)	<0.0001	0.80	0.86	0.11	**−0.02**	**0.04**
Ala (1.47–1.49)	<0.0001	0.77	0.44	0.06	0.04	0.02
Lac (1.32–1.34)	<0.0001	0.76	0.91	0.13	−0.47	0.32

*The comparisons were made based on the estimated metabolite concentrations.
[a]Statistically significant linear correlations with slopes deviating from unity are observed indicating that the 3.0 kHz spinning rate produces higher metabolite integrated intensities.
[b]Bold faced data in the table indicate the intercepts are indifferent from 0.

Restrictions on Min (A, B,. . ., N)

The principle of Min(A, B,. . ., N) will work only if the following experimental conditions are met: 1) The spectra (A, B,. . .,N) are obtained from the same sample under the same experimental conditions, other than spinning rate. 2) The line-width for an individual resonance is the same (within measurement error) in all spectra, i.e., there is no additional visible narrowing of either homogeneous or inhomogeneous broadenings at higher spinning rates. For instance, in this study the line width at half maximum (LWHM) for creatine at 3.03 ppm in intact tissue was measured to be 3.73 ± 0.98 Hz at 600 Hz spinning, and 3.83 ± 0.95 Hz at 700 Hz spinning. 3) The spinning rates are decided such that there is no SSB overlap point present in the ROIs in all N spectra. 4) There are no negative resonances in the spectra. Therefore, the spectra should be identical when measured within a reasonable range of spinning rates (e.g., 600 and 700 Hz) if the integrated intensities of SSBs from metabolites can be neglected when compared with the isotropic resonance integrated intensity. The contributions of SSBs from any source (i.e., water, external standard, any metabolites, or even contamination) will result in the increase of local spectral integrated intensity.

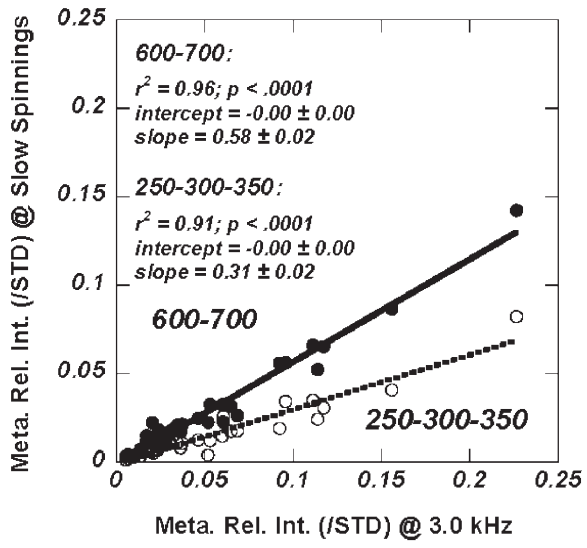

FIG. 9. Linear correlations between relative metabolic integrated intensities determined at an HRMAS spinning rate of 3.0 kHz and those measured at slower spinning rates (as ratios over the STD calibrated according to Fig. 2), i.e., Min(A, B) measured at 600 and 700 Hz, and Min(A, B, C) measured at 250, 300 and 350 Hz, for 16 metabolites from two cases.

Min(A, B,. . ., N) vs. DANTE

In comparison with the previously reported DANTE method, which was optimized mainly for the elimination of SSBs from water and the external standard (STD), the Min(A, B,. . ., N) editing procedure can produce more accurate results for cases in which not only SSBs of water and/or STD, but also SSBs of tissue metabolites or other contaminants are of concern (16). However, the DANTE approach still may prove to be a method of choice for future applications of HRMAS spectroscopy in the clinical setting, where a defined metabolic marker(s) can be quantified with the measurement of one spectrum of an appropriately selected spinning rate. The advantages of the two-spectra Min(A, B) method are apparent, particularly during the research phases of surveying and discovering the marker(s). In addition, the Min(A, B) method can easily be extended to a general scheme of Min(A, B,. . ., N), as was demonstrated in this study using spinning rates of 250, 300, and 350 Hz. Future studies using this method may provide evidence for optimal spinning rates, such that tissue degradation is minimized and metabolic integrated intensity is maximized.

Quantitative evaluations of the relative metabolite integrated intensities (i.e., [metabolite]/[STD]) in the current

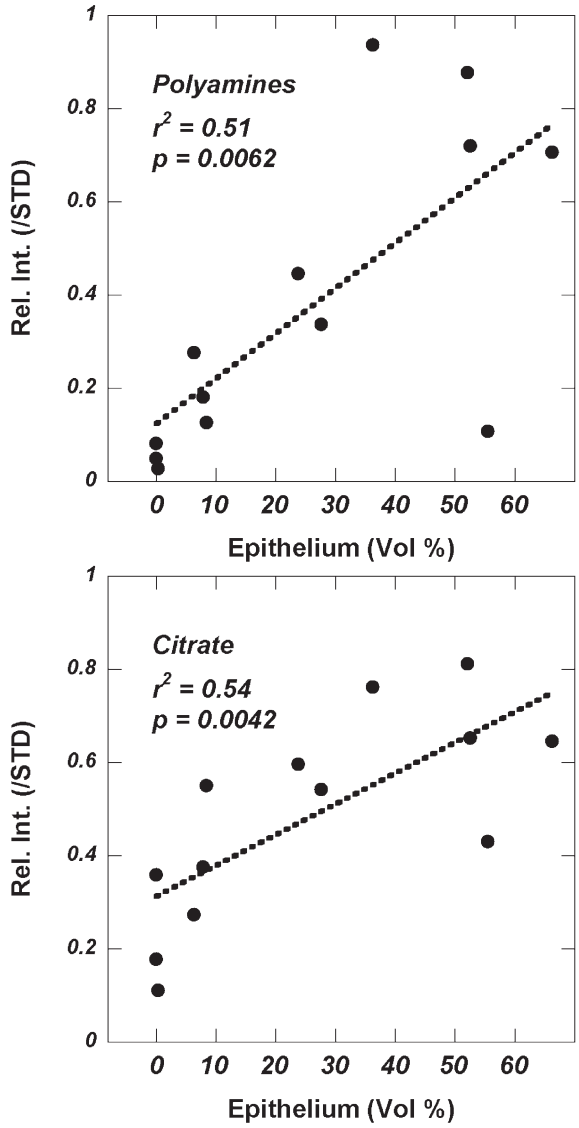

FIG. 10. Linear correlations between relative metabolic integrated intensities of polyamines and citrate with the volume percentage of tissue epithelium measured from the same tissue samples after NMR measurements.

analyses and those presented in the previous report of DANTE-CPMG measurements (16) revealed that the previous method could result in a reduction of metabolite integrated intensities by approximately 43% compared to the current Min(A, B) measurements of a single excitation pulse without CPMG. The reductions were likely the result of T_2 losses due to the rotor-synchronized CPMG of 10 ms.

Metabolite Integrated Intensities

The data presented in Table 1 were collected from the linear regression analysis of metabolite integrated intensities measured at spinning rates of 600–700 Hz with Min(A, B) vs. those obtained at the 3.0 kHz spinning rate. Since the metabolite integrated intensities of both the high and low spinning rates were normalized by the STD integrated intensity from direct measurement or projection, respectively, these integrated intensities represented the concentrations of the measured metabolites. Hence, a slope of <1.0 indicates that the measured spectral integrated intensity at the higher (3.0 kHz) spinning rate was greater than that obtained at the lower (600–700 Hz) spinning rates. In general, it may be expected that the further the slope shrinks from 1.0, the more inhomogeneous the interactions experienced by the metabolite will be (e.g., as in a viscosity-related limitation on molecular mobility). For instance, a recent study of the human prostate indicated that polyamines are secreted in prostatic secretory granules of approximately 1 μm, a degree of spatial constriction that would result in the minimization of metabolite movements (17). If this is true, we may expect that the values of metabolic slopes will vary with different tissue types. Studies in this direction may have the potential to increase our understanding of the physical nature of these endogenous cellular metabolites; however, this is beyond the scope of the current evaluation. Nevertheless, this difference in the measured metabolite integrated intensities at different spinning rates is expected, and should not affect the accuracy of the HRMAS method for diagnosing disease as long as the metabolite data are acquired at the same spinning rate.

Correlation of Metabolite Integrated Intensity to Tissue Pathologies

Since the Min(A, B, . . ., N) editing approach minimizes tissue degradation caused by high spinning rates, the same tissue samples can undergo pathological assessment, thus allowing for the study of any correlations between individual metabolite Rel. Int. and vol% of a specific tissue component, such as glandular epithelium or cancer cells. Expanding on this concept, the use of more detailed pathological assessments than the vol% of a tissue component (such as immunohistochemical stainings) for comparison with metabolite integrated intensities may aid in disease diagnosis and patient prognosis.

Nonlinearity of Min(A, B,. . ., N) and Fitting of Min(A, B,. . ., N) Spectra With Lorentzian-Gaussian Functions

Careful consideration must be given to the nonlinear nature of the minimum function, Min(A, B,. . ., N), as it relates to measurement accuracy and statistical treatment of metabolite concentration. The validity of the Min(A, B,. . ., N) function relies heavily on the assumption that the component spectra differ only in the SSB frequencies. It is easy to conceptualize that various instrument errors (e.g., baseline or phasing errors) and spectroscopic effects (e.g., changes in peak amplitude or line-width associated with MAS rate changes) may, after processing with Min(A, B,. . ., N), introduce errors in spectral integrated intensities, leading to errors in metabolite concentration estimates. Furthermore, the Min(A, B,. . ., N) function is not appropriate for processing spectra with negative peaks unless additional nonlinear treatment (e.g., taking absolute value spectra) is executed.

The effects of the nonlinearity of Min(A, B,. . ., N) on spectral noise deserve special attention. In the presence of noise, spectra that are run at different spinning rates but

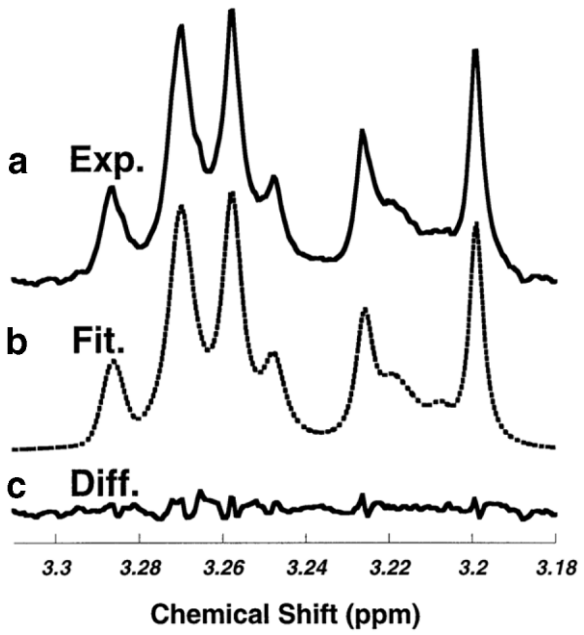

FIG. 11. Example of Lorentzian-Gaussian curve-fitting results for a Min(A, B,. . ., N)-edited spectrum. **a:** The 3.31–3.18 ppm spectral region from Fig. 7d. **b:** The Lorentzian-Gaussian curve-fitting results of a. **c:** Spectrum representing the difference between a and b. These differences are minimal and are typically observed with any curve-fitting process.

are otherwise identical will differ on a point-by-point basis. As Min(A, B,. . ., N) selects the lowest point, it introduces a negative bias that is uniform across the spectrum. If uncorrected, this will result in a negative bias in the metabolite measurement, with a magnitude that depends on the width and shape of the metabolite peak. The nonlinearity of the minimum function changes the noise statistics as well. A spectrum with normal (Gaussian) background noise, processed with Min(A, B,. . ., N), yields a spectrum with a non-Gaussian noise distribution, making statistical analysis more difficult but not impossible (given certain treatments of numerical methods). However, these theoretical concerns may not impair the empirical utility of the scheme in biological tissue analysis. Figure 11 illustrates that while there is some difference between the resulting Min(A, B,. . ., N) spectra (a region of Fig. 7d) obtained from a sample (Fig. 11a), and that obtained through curve-fitting (Fig. 11b) of the spectra, it is minimal and typical of any curve-fitting process (Fig. 11c). Thus, the production of spectra with non-Gaussian noise distribution resulting from the application of Min(A, B,. . ., N) should not remarkably affect metabolite integrated intensities. Therefore, since the interests and the purpose of this report are focused on the application of this empirical spectroscopic method in medical pathology, any further discussion of the nonlinearity of Min(A, B,. . ., N) and its correction may exceed the intended scope of this study.

CONCLUSIONS

The reported results indicate that by editing two or three slow-spinning tissue HRMAS spectra with a simple mathematical function Min(A, B, . . ., N), the SSBs can be eliminated to produce an SSB-free tissue NMR spectrum that may be sensitive enough for the purpose of disease diagnosis. Tests of the proposed scheme on both a standard gel solution of commonly observed tissue metabolites and intact human prostate tissue samples revealed the empirical usefulness of the scheme. The results further suggest that the metabolite integrated intensities thus observed can be correlated with quantitative histopathological data obtained from the same tissue after NMR measurement.

REFERENCES

1. Coen M, Lenz EM, Nicholson JK, Wilson ID, Pognan F, Lindon JC. An integrated metabonomic investigation of acetaminophen toxicity in the mouse using NMR spectroscopy. Chem Res Toxicol 2003;16:295–303.
2. Huster D, Schiller J, Arnold K. Comparison of collagen dynamics in articular cartilage and isolated fibrils by solid-state NMR spectroscopy. Magn Reson Med 2002;48:624–632.
3. Kurhanewicz J, Swanson MG, Nelson SJ, Vigneron DB. Combined magnetic resonance imaging and spectroscopic imaging approach to molecular imaging of prostate cancer. J Magn Reson Imaging 2002;16:451–463.
4. Sitter B, Sonnewald U, Spraul M, Fjosne HE, Gribbestad IS. High-resolution magic angle spinning MRS of breast cancer tissue. NMR Biomed 2002;15:327–337.
5. Waters NJ, Holmes E, Waterfield CJ, Farrant RD, Nicholson JK. NMR and pattern recognition studies on liver extracts and intact livers from rats treated with alpha-naphthylisothiocyanate. Biochem Pharmacol 2002;64:67–77.
6. Tzika AA, Cheng LL, Goumnerova L, Madsen JR, Zurakowski D, Astrakas LG, Zarifi MK, Scott RM, Anthony DC, Gonzalez RG, Black PM. Biochemical characterization of pediatric brain tumors by using in vivo and ex vivo magnetic resonance spectroscopy. J Neurosurg 2002;96:1023–1031.
7. Morvan D, Demidem A, Papon J, De Latour M, Madelmont JC. Melanoma tumors acquire a new phospholipid metabolism phenotype under cystemustine as revealed by high-resolution magic angle spinning proton nuclear magnetic resonance spectroscopy of intact tumor samples. Cancer Res 2002;62:1890–1897.
8. Chen JH, Enloe BM, Fletcher CD, Cory DG, Singer S. Biochemical analysis using high-resolution magic angle spinning NMR spectroscopy distinguishes lipoma-like well-differentiated liposarcoma from normal fat. J Am Chem Soc 2001;123:9200–9201.
9. Griffin JL, Walker L, Shore RF, Nicholson JK. High-resolution magic angle spinning 1H-NMR spectroscopy studies on the renal biochemistry in the bank vole (*Clethrionomys glareolus*) and the effects of arsenic (As3+) toxicity. Xenobiotica 2001;31:377–385.
10. Schiller J, Naji L, Huster D, Kaufmann J, Arnold K. 1H and 13C HR-MAS NMR investigations on native and enzymatically digested bovine nasal cartilage. MAGMA 2001;13:19–27.
11. Barton SJ, Howe FA, Tomlins AM, Cudlip SA, Nicholson JK, Bell BA, Griffiths JR. Comparison of in vivo 1H MRS of human brain tumours with 1H HR-MAS spectroscopy of intact biopsy samples in vitro. MAGMA 1999;8:121–128.
12. Cheng LL, Wu C, Smith MR, Gonzalez RG. Non-destructive quantitation of spermine in human prostate tissue samples using HRMAS 1H NMR spectroscopy at 9.4 T. FEBS Lett 2001;494:112–116.
13. Wind RA, Hu JZ, Rommereim DN. High-resolution (^{1})H NMR spectroscopy in organs and tissues using slow magic angle spinning. Magn Reson Med 2001;46:213–218.
14. Hu JZ, Rommereim DN, Wind RA. High-resolution 1H NMR spectroscopy in rat liver using magic angle turning at a 1 Hz spinning rate. Magn Reson Med 2002;47:829–836.
15. Hu JZ, Wind RA. Sensitivity-enhanced phase-corrected ultra-slow magic angle turning using multiple-echo data acquisition. J Magn Reson 2003;163:149–162.
16. Taylor JL, Wu CL, Cory D, Gonzalez RG, Bielecki A, Cheng LL. High-resolution magic angle spinning proton NMR analysis of human prostate tissue with slow spinning rates. Magn Reson Med 2003;50:627–632.
17. Cohen RJ, Fujiwara K, Holland JW, McNeal JE. Polyamines in prostatic epithelial cells and adenocarcinoma; the effects of androgen blockade. Prostate 2001;49:278–284.

Metabolic Characterization of Human Prostate Cancer with Tissue Magnetic Resonance Spectroscopy

Leo L. Cheng,[1,2] Melissa A. Burns,[1] Jennifer L. Taylor,[1] Wenlei He,[1,3] Elkan F. Halpern,[2] W. Scott McDougal,[3] and Chin-Lee Wu[1,3]

Departments of [1]Pathology, [2]Radiology, and [3]Urology, Massachusetts General Hospital, Harvard Medical School, Boston, Massachusetts

Abstract

Diagnostic advancements for prostate cancer have so greatly increased early detections that hope abounds for improved patient outcomes. However, histopathology, which guides treatment, often subcategorizes aggressiveness insufficiently among moderately differentiated Gleason score (6 and 7) tumors (>70% of new cases). Here, we test the diagnostic capability of prostate metabolite profiles measured with intact tissue magnetic resonance spectroscopy and the sensitivity of local prostate metabolites in predicting prostate cancer status. Prostate tissue samples (n = 199) obtained from 82 prostate cancer patients after prostatectomy were analyzed with high-resolution magic angle spinning proton magnetic resonance spectroscopy, and afterwards with quantitative pathology. Metabolite profiles obtained from principal component analysis of magnetic resonance spectroscopy were correlated with pathologic quantitative findings by using linear regression analysis and evaluated against patient pathologic statuses by using ANOVA. Paired t tests show that tissue metabolite profiles can differentiate malignant from benign samples obtained from the same patient (P < 0.005) and correlate with patient serum prostate-specific antigen levels (P < 0.006). Furthermore, metabolite profiles obtained from histologically benign tissue samples of Gleason score 6 and 7 prostates can delineate a subset of less aggressive tumors (P < 0.008) and predict tumor perineural invasion within the subset (P < 0.03). These results indicate that magnetic resonance spectroscopy metabolite profiles of biopsy tissues may help direct treatment plans by assessing prostate cancer pathologic stage and aggressiveness, which at present can be histopathologically determined only after prostatectomy. (Cancer Res 2005; 65(8): 3030-4)

Introduction

Prostate-specific antigen screening has effectively increased detection of prostate cancer at early stages. However, histopathology cannot reliably direct treatment in the prostate-specific antigen testing era: more than 70% of the newly diagnosed tumors receive a Gleason score (GS) of 6 or 7, yet clinical outcomes for these patients differ markedly (1). The limited prognostic insight of such clinical measures as prostate-specific antigen, Gleason score, and digital rectal exams often occasions either unnecessarily aggressive or dangerously conservative interventions (2–7). Prostate tumor heterogeneity further compromises histopathology in comprehensive evaluations as prostate cancer cells often elude biopsy, producing false negatives (8–10). More reliable and informative prognostic tools are needed. Changes in tumor metabolism, downstream from genomic and proteomic transformations, are thought to reflect disease-related biochemical reactivity, to precede histologically observable changes in cell morphology, and thus to offer an early means for predicting tumor behaviors (11).

Recently, high-resolution magic angle spinning proton magnetic resonance spectroscopy was developed for intact tissue analysis (12, 13). Magic angle spinning, originally used to reduce resonance line width in solid-state nuclear magnetic resonance, subjects samples to mechanical rotations (approximately in kilohertz) at the magic angle (54 degrees 44 minutes) away from the direction of the static magnetic field of the spectrometer while spectroscopy is recorded. Applied to intact tissues, high-resolution magic angle spinning can produce highly resolved spectra, allowing identification of individual metabolites while preserving tissue pathologic morphology.

We evaluated the diagnostic utility of prostate tissue metabolite profiles measured with high-field (14.1 T), high-resolution magic angle spinning proton magnetic resonance spectroscopy. Unaltered prostatectomy samples were analyzed spectroscopically, then histopathologically. Prostate metabolite profiles obtained from principal component analysis of tissue spectra were correlated with pathology quantities and with patient serum prostate-specific antigen levels. Finally, the diagnostic potentials of tissue metabolite profiles in predicting pathologic stage and tumor perineural invasion were investigated.

Materials and Methods

Sample collection. This study of human prostate tissue with magnetic resonance spectroscopy was reviewed and approved by the Institutional Review Board at Massachusetts General Hospital. Samples (n = 199, from 82 cancer prostatectomies) were collected from different prostate zones of the following patient population: (A) Gleason score: 5 [2 cases, 5 samples]; 6 [51, 126]; 7 [21, 53]; 8 [4, 9]; and 9 [4, 6]; and (B) American Joint Committee on Cancer/Tumor-Node-Metastasis (AJCC/TNM) stages (6th ed.): T_{2ab} [24 cases, 59 samples], T_{2c} [44, 112], T_{3a} [10, 17], T_{3b} [3, 5], and T_{3ab} [1, 6]. The few T_{3a}, T_{3b}, and T_{3ab} cases identified were combined and regarded in the study as T_3. Surgical tissue samples were snap frozen in liquid nitrogen and stored at −80°C until magnetic resonance spectroscopy. Patient clinical statuses were obtained from pathology reports.

High-resolution magic angle spinning proton magnetic resonance spectroscopy. A Bruker (Billerica, MA) AVANCE spectrometer operating at 600 MHz (14.1 T) was used for all magnetic resonance experiments. Tissue samples were placed into a 4-mm rotor with 10-μL plastic inserts. One-microliter D_2O was added for field locking. Spectra were recorded at 3°C with the spectrometer frequency set on the water resonance and a rotor-synchronized DANTE experimental protocol was applied with spinning at 600 and 700 Hz (±1.0 Hz; ref. 14). Thirty-two transients were averaged at a repetition time of 5 seconds.

Spectra were processed with AcornNMR-Nuts (Livermore, CA) according to the following procedures: 0.5-Hz apodization before Fourier

Requests for reprints: Leo L. Cheng, Pathology Research CNY-7, 149 13th Street, Charlestown, MA 02129. Phone: 617-724-6593; Fax: 617-726-5684; E-mail: cheng@nmr.mgh.harvard.edu.

transformation, baseline correction, and phase adjustment. Resonance intensities used in the study were integrals of curve fittings with Lorentzian-Gaussian line shapes measured from either 600- or 700-Hz high-resolution magic angle spinning spectrum (14).

Quantitative histopathology. Following spectroscopy, samples were fixed in 10% formalin, embedded in paraffin, cut into 5-μm sections at 100-μm intervals throughout the entire sample, and stained with H&E.

An Olympus BX41 Microscope Imaging System (Melville, NY), in conjunction with the image analyzer SoftImaging-MicroSuite (Lakewood, CO), was used to quantify sample cross sections. A pathologist with no knowledge of the spectroscopic results visually estimated to the nearest 5% the percent area representing cancer cells, normal epithelial cells, and stroma in each cross section. The percent volume of these features was calculated from the sizes of the cross sections and the corresponding percent area of each pathologic feature.

Statistical analysis. The aim of the present work was to correlate spectral metabolite profiles with tissue pathologies and patient clinical statuses. Prior to investigating such correlations, the metabolite matrix was subjected to statistical data treatment—principal component analysis—to reduce the complexity of spectral data.

Because certain pathologic processes can manifest simultaneous changes in multiple measurable metabolites, a change in a single metabolite may not represent the underlying process. Principal component analysis attempts to identify combinations (principal components) of the measured concentrations that may reflect distinct pathologic processes if they exist in the set of the samples. A positive contribution of a certain metabolite indicates the elevation of the metabolite within the component (process), and a negative contribution suggests suppression.

The components are ordered by the extent to which they are associated with variability in the observed cases. The more metabolites affected by a process (the more associated with a principal component), the greater the association. The stronger the change in the metabolites caused by a process, the greater the association. Additionally, the incidence of the process is a factor in the associated variability: extremely rare and extremely common processes cause little variability whereas processes that are seen in 50% of the cases have the greatest associated variability.

Principal components may differ from the actual underlying processes in one important respect. Principal components are required to be independent. Actual processes may affect some metabolites in common. For instance, one process might elevate metabolites A, B, C, and D, while suppressing E and F. A second process might elevate A and B, while suppressing C, D, E, and F. As both affect A, B, E and F in the same way, it is likely that the principal component analysis results identify a strong component, expressing an elevation of A and B with the simultaneous suppression of E and F. Another, possibly weaker, component might express metabolites C and D and would distinguish the first process from the second.

The hypothesis that different prostate pathologic features (percent volume epithelia, cancer cells, stroma) possess different metabolite profiles can thus be tested by using linear regression analysis against these principal components. Paired Student's t tests were used to evaluate the ability of cancer-related principal component 13 and its major contributing metabolites (phosphocholine and choline) to differentiate cancerous from histologically benign samples obtained from the same patient, whereas discriminant analyses were used to generate a canonical plot to achieve the maximum separation between the two groups, with accuracy being analyzed by receiver operating characteristic curves (15). Student's t tests were used

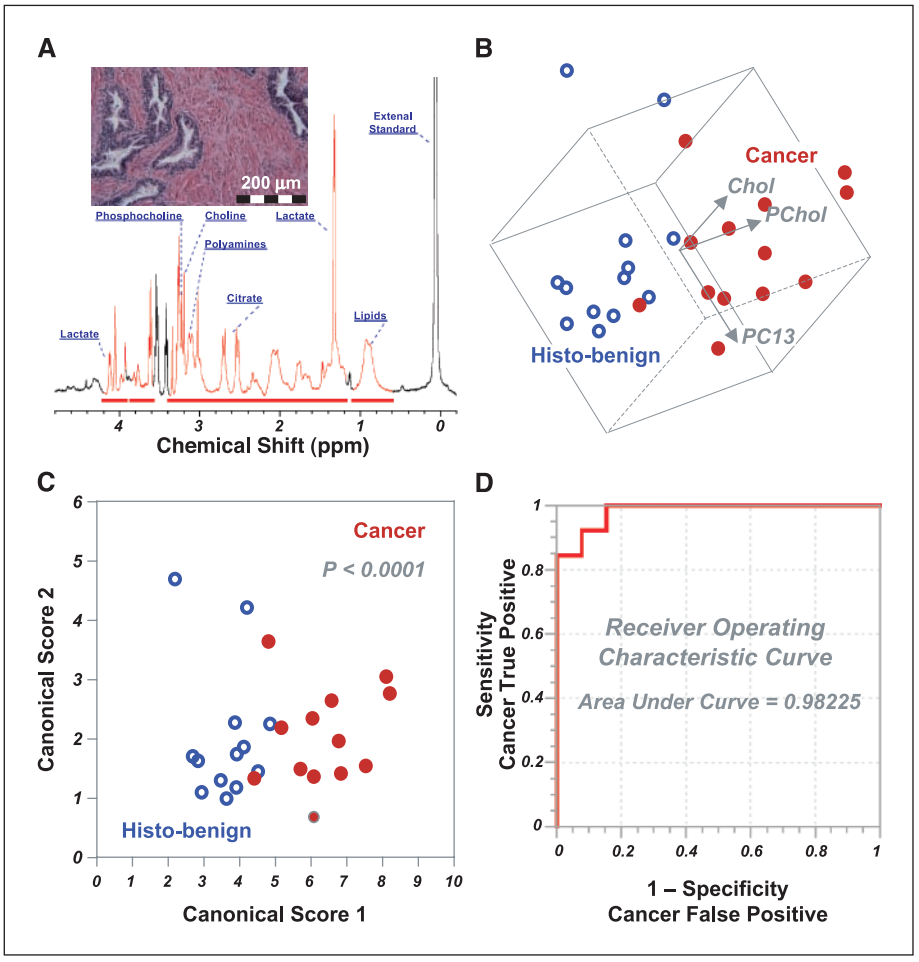

Figure 1. *A*, high-resolution magic angle spinning ^{1}H MR spectrum of intact tissue obtained from the removed prostate of a 61-year-old patient with GS 6 T_{2b} tumors. Histopathology analysis of the tissue sample (*insert*) after its spectroscopy measurement revealed that the sample contained 40% histopathologically defined benign epithelium and 60% stromal structures, with no identifiable cancerous glands. Cellular metabolites mentioned in the text are labeled on the spectrum. The 36 most intense resonance peaks or metabolite groups above the horizontal bars were selected for analyses, whereas the other regions were excluded from calculation, partly due to surgery-related alcohol contamination. *B*, three-dimensional plot of principal component 13 (PC13 correlates linearly with percent volume of cancer cells in tissue samples) versus phosphocholine versus choline. Cancerous and histologically benign (histo-benign) tissue samples from 13 patients can be visually separated in observation plane. The paired Student's t test results (cancer versus histo-benign from the same patients) for principal component 13, phosphocholine, and choline are 0.012, 0.004, and 0.001. Only results from these 13 patients could be evaluated with paired tests for other cancer positive samples were collected from patients from whom no histo-benign samples were analyzed. *C*, the canonical plot resulting from discriminant analysis of the three variables in *B* presents the maximum separation between the two groups. *D*, the resulting receiver operating characteristic curves indicates the accuracy of using the three variables in *B* to positively identify cancer samples.

to investigate the relationship between cancer-related principal component 14 and tumor perineural invasion. The abilities of principal components 2 and 5 to differentiate between pathologic stages were tested using ANOVA. Statistical analyses were carried out using SAS-JMP (Cary, NC).

Results and Discussion

High-resolution tissue proton magnetic resonance spectroscopy and principal component analysis. High-resolution magic angle spinning magnetic resonance spectroscopy permits the acquisition of high-resolution proton spectra from intact tissue, while preserving tissue architectures for subsequent histopathologic analysis (Fig. 1*A*). To achieve high resolution before high-resolution magic angle spinning, tissue metabolites were analyzed in solutions of chemical extraction so that results depended on the applied procedures and their completeness. Furthermore, tumor heterogeneity limits the usefulness of extraction approaches.

Histomorphologic evaluations proved critical for the correct interpretation of spectroscopic data obtained from the same samples. In this study, 20 of 199 analyzed samples from prostate cancer patients contained cancerous glands, whereas the rest (n = 179) represented histologically benign tissue obtained from cancerous prostates. This frequency reflects the infiltrative, heterogeneous nature of prostate cancer; producing no visible mass, its architecture precludes cancer-selective tissue removal and thus accounts for the clinical complexity of prostate biopsy (8–10).

Principal component analysis was carried out on the concentrations of the 36 most intense resonance peaks or groups assigned to specific metabolites to generate principal components representing different variations of tissue metabolite profiles. Because of the existence of pathologic variations among the samples, certain principal components may capture these variations. For instance, principal component 2, reflecting changes in polyamines, citrate, etc., was found to differentiate epithelia from stroma with statistical significance (16.5% of variance; epithelia: r = 0.381, P < 0.0001; stroma: r = −0.303, P < 0.0001), in agreement with previous observation (16). Moreover, both principal component 13 and principal component 14 differentiate cancer from stroma (cf. principal component 14 represents 1.54% of variance; cancer: r = −0.160, P = 0.0243; stroma: r = 0.217, P = 0.0021). The difference of variance representation (16.5% versus 1.54% of the total variability of the standardized 36 metabolites for principal components 2 and 14, respectively) agrees with the fact that only 10% of the samples were identified as cancer positive, whereas >90% of them were designated epithelium positive. Of note, not all principal components are related with the evaluated pathologies. Many of them may indicate intrinsic differences that are not evaluated or variables, such as spectrometer instabilities, that are not the subjects of interest.

Differentiating cancer from histologically benign samples. By using histologically defined noncancer (histo-benign) samples from 13 of 20 patients from whom histologically cancer-positive samples were also analyzed, we observed a separation between the cancerous and histo-benign groups on a plane of a three-dimensional plot (Fig. 1*B*) of principal component 13 versus phosphocholine and choline. Both metabolites were found to be the major contributors to principal components 13 and 14, in agreement with descriptions by the current *in vivo* and *ex vivo* magnetic resonance spectroscopy literature of their relationship with malignancy (18). Further, both principal components were linearly correlated (P: 0.04, 0.02) with percent volume of cancer cells. Application of discriminant analysis to the three variables indicated a classification accuracy of 92.3% (Fig. 1*C*). An overall accuracy of 98.2% for the identification of cancer samples was obtained from a receiver operating characteristic curve generated from the three variables (Fig. 1*D*).

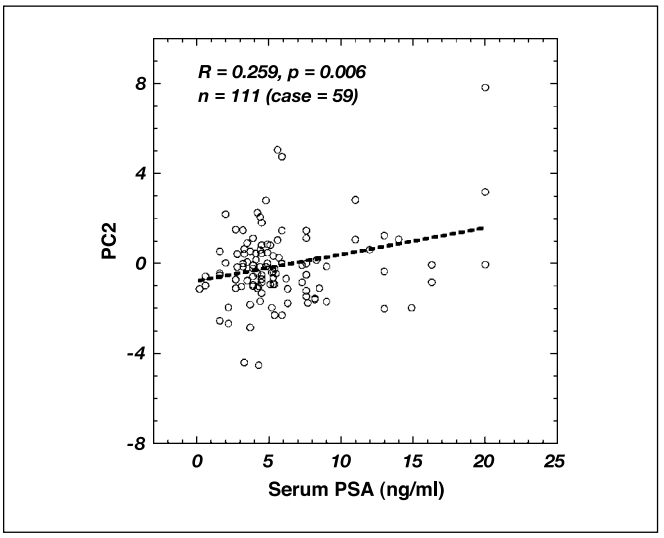

Figure 2. Statistically significant correlation between the patient serum prostate-specific antigen levels before prostatectomy and the metabolite profiles represented by principal component 2 (*PC2*), as measured from 111 histo-benign prostate tissue samples obtained from 59 prostatectomy cases for prostate cancer. Plotted principal component 2 values represent the linear combinations of metabolite concentrations according to the principal component 2 formula obtained from principal component analysis.

Correlating with patient serum prostate-specific antigen levels. From the 82 prostatectomy cases studied, we identified 59 cases for which the serum prostate-specific antigen levels of patients before surgery were available. Among these, 111 histo-benign tissue samples from different prostate zones (central, transitional, and peripheral) were identified. We evaluated the relationship between prostate-specific antigen levels and tissue metabolite profiles, and found that principal component 2 was linearly correlated, with statistical significance, to prostate-specific antigen results (Fig. 2). Because principal component 2 is linearly correlated with the percent volume of histo-benign epithelial cells, as previously presented, we verified that no coincidental correlation occurred between prostate-specific antigen levels and epithelial percent volume among these measured samples.

Identifying tumor pathologic stages and predicting tumor perineural invasion. We examined the correlation between principal components and tumor pathologic stage (AJCC/TNM staging system). With all 199 samples, we observed that principal component 2 differentiated T_{2c} cancer (prostate-confined; both lobes) from T_3 (invading extraprostatic tissue, P < 0.03) and T_{2ab} cancer (prostate confined; one lobe, P < 0.005). Principal component 5 also differentiated T_{2ab} cancer from T_{2c} (P < 0.003) and T_3 cancer (P < 0.00005). Again, we verified that the observed principal component 2 differentiation among tumor stages was independent of epithelial content (e.g., T_{2ab}, 21.88 ± 2.59%; T_{2c}, 20.21 ± 1.91%).

More interestingly, on analysis of the histo-benign samples (n = 179), similar differentiations persisted for both principal

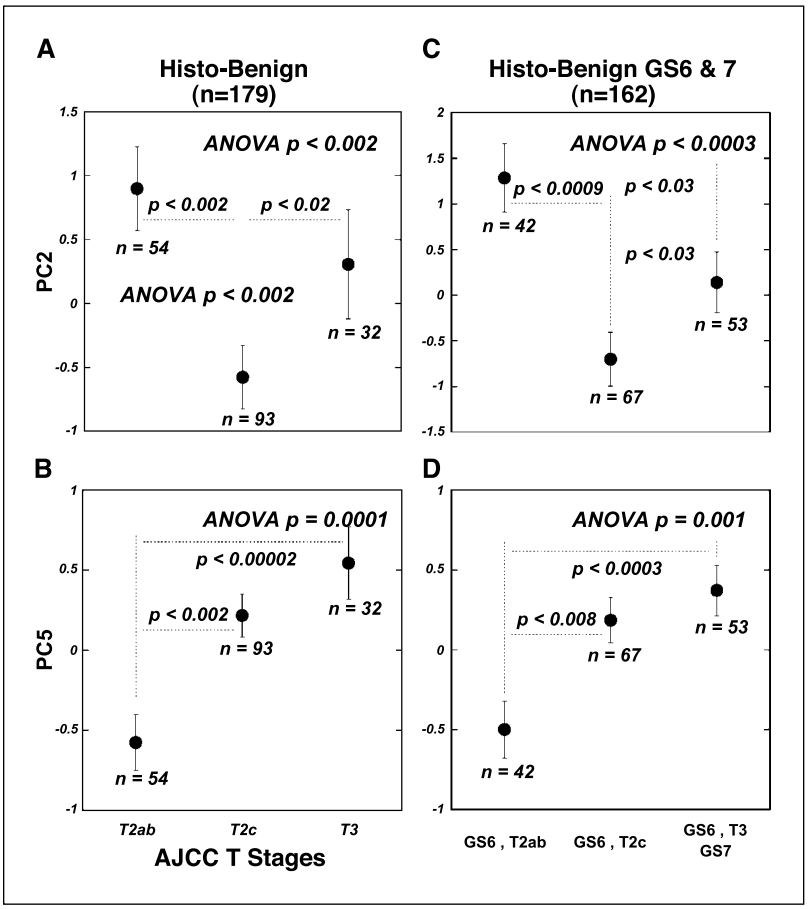

Figure 3. Principal components 2 and 5 as predictors of tumor stage. Principal component 2 (*A*) can differentiate T_{2c} stage tumors from T_{2ab} and T_3 tumors, whereas principal component 5 (*B*) can differentiate T_{2ab} from T_{2c} and T_3 stages, as defined by AJCC/TNM staging system with histo-benign samples, and with histo-benign GS 6 and 7 samples (*C* and *D*). In the latter, principal components 2 and 5 can differentiate among three tumor groups: GS 6 T_{2ab}, GS 6 T_{2c}, and GS 6 T_3 plus GS 7 tumors.

components (Fig. 3*A* and *B*). Furthermore, when the same principal components were applied to histo-benign samples of GS 6 and 7 tumors (n = 162), both principal components identified the least aggressive tumor (i.e., GS 6 T_{2ab} tumors, n = 42) from those of the more aggressive groups (GS 6 T_{2c}, GS 6 T_3, and GS 7 tumors; Fig. 3*C* and *D*).

Tumor perineural invasion status, although not yet incorporated in AJCC/TMN staging, indicates prostate tumor aggressiveness and aids treatment planning (17). Unfortunately, tumor heterogeneity prevents the visualization of invasion in biopsy samples. Our evaluation yielded a statistically significant correlation between principal component 14 levels and invasion status for all 199 samples (126 "+" and 73 "−"; $P < 0.01$), for 179 histo-benign samples (103 "+" and 71 "−"; $P < 0.035$), and more interestingly, for 42 histo-benign samples from GS 6 T_{2ab} tumors (13 "+" and 29 "−"; $P < 0.028$). This last observation, combined with results shown in Fig. 3*E* and *F*, may have great clinical significance in identifying and managing the less aggressive tumor group within the >70% newly diagnosed moderately differentiated tumors.

Our findings, with respect to tumor pathologic stages and perineural invasion, present an important indication of the technique's potential to improve current pathology in prostate cancer diagnosis. Despite its significance in treatment planning, tumor pathologic stage can now only be assessed from resected prostate. Our observations indicate that metabolite profiles may provide a "second opinion" for prostate biopsy evaluation. They further suggest that an additional biopsy core, obtained to generate metabolite profiles, could help predict tumor stage for cancer-positive patients, even if the core itself is histo-benign.

In this report, we emphasize the phrase "histo-benign" to introduce the fact that the noncancer status of these tissue samples was based on histologic examination. We also emphasize that currently our metabolite results are analyzed according to histopathology, which remains the "gold standard" for cancer diagnosis and treatment planning. However, evaluation of the metabolite paradigm presented, and its usefulness in the oncology clinic, may require reconsideration of the boundaries of histopathology and metabolites. Current wisdom concerning the development and progression of malignancy, such as the widely proposed stroma effects, may assist this transformation (19, 20).

Our data leave unanswered questions. First, we cannot be certain from where, in proximity to cancer glands, our histo-benign samples were obtained. Therefore, we cannot predict whether observed metabolite alterations are global or focal. Additionally, comparisons between cancer-positive and histo-benign samples rely entirely on tissue from prostate cancer patients due to the lack of normal controls and the disqualifying metabolic degradation of tissue upon death. Our limited number of cancer-positive samples has also prevented determination of prostate pathologic stage based exclusively on cancer-positive samples.

We have nevertheless shown that metabolites measured with tissue magnetic resonance spectroscopy correlate with histopathology findings and that metabolite profiles reveal overall tumor clinicopathologic status and aggressiveness before either is

visible to histopathology. We believe the data presented here show the diagnostic and prognostic potential of the metabolite protocol. However, its clinical utility can be assessed only through longitudinal patient follow-up. Only correlations between tumor metabolites and patient outcome will allow us to establish the sensitivity and specificity of diagnostic and prognostic values for tumor metabolites, independent of current pathology.

Acknowledgments

Received 11/16/2004; revised 2/4/2005; accepted 2/16/2005.

Grant support: Public Health Service/NIH grants CA80901, CA095624, and EB002026, and DOD grant W81XWH-04-1-0190.

The costs of publication of this article were defrayed in part by the payment of page charges. This article must therefore be hereby marked *advertisement* in accordance with 18 U.S.C. Section 1734 solely to indicate this fact.

We thank Dr. Kurt J. Isselbacher for encouragement, guidance, and support.

References

1. Pound CR, Partin AW, Eisenberger MA, Chan DW, Pearson JD, Walsh PC. Natural history of progression after PSA elevation following radical prostatectomy. Jama 1999;281:1591–7.

2. Carter HB, Isaacs WB. Improved biomarkers for prostate cancer: a definite need. J Natl Cancer Inst 2004;96:813–5.

3. Incrocci L, Slob AK. Incidence, etiology, and therapy for erectile dysfunction after external beam radiotherapy for prostate cancer. Urology 2002;60:1–7.

4. Eton DT, Lepore SJ. Prostate cancer and health-related quality of life: a review of the literature. Psychooncology 2002;11:307–26.

5. Ko YJ, Bubley GJ. Prostate cancer in the older man. Oncology (Huntingt) 2001;15:1113–9, 23–4; discussion 24–6, 31.

6. Ransohoff DF, McNaughton Collins M, Fowler FJ. Why is prostate cancer screening so common when the evidence is so uncertain? A system without negative feedback. Am J Med 2002;113:663–7.

7. Smith RA, Cokkinides V, Eyre HJ. American Cancer Society guidelines for the early detection of cancer, 2003. CA Cancer J Clin 2003;53:27–43.

8. Zackrisson B, Aus G, Lilja H, Lodding P, Pihl CG, Hugosson J. Follow-up of men with elevated prostate-specific antigen and one set of benign biopsies at prostate cancer screening. Eur Urol 2003;43:327–32.

9. Mazal PR, Haitel A, Windischberger C, et al. Spatial distribution of prostate cancers undetected on initial needle biopsies. Eur Urol 2001;39:662–8.

10. Steiner H, Moser P, Hager M, et al. Clinical and pathologic features of prostate cancer detected after repeat false-negative biopsy in a screening population. Prostate 2004;58:277–82.

11. Mountford C, Doran S, Lean C, Russell P. Cancer pathology in the year 2000. Biophys Chem 1997;68:127–35.

12. Cheng LL, Lean CL, Bogdanova A, et al. Enhanced resolution of proton NMR spectra of malignant lymph nodes using magic-angle spinning. Magn Reson Med 1996;36:653–8.

13. Cheng LL, Ma MJ, Becerra L, et al. Quantitative neuropathology by high resolution magic angle spinning proton magnetic resonance spectroscopy. Proc Natl Acad Sci U S A 1997;94:6408–13.

14. Taylor JL, Wu CL, Cory D, Gonzalez RG, Bielecki A, Cheng LL. High-resolution magic angle spinning proton NMR analysis of human prostate tissue with slow spinning rates. Magn Reson Med 2003;50:627–32.

15. McNeil BJ, Keller E, Adelstein SJ. Primer on certain elements of medical decision making. N Engl J Med 1975;293:211–5.

16. Cheng LL, Wu C, Smith MR, Gonzalez RG. Non-destructive quantitation of spermine in human prostate tissue samples using HRMAS ^{1}H NMR spectroscopy at 9.4 T. FEBS Lett 2001;494:112–6.

17. Beard CJ, Chen MH, Cote K, et al. Perineural invasion is associated with increased relapse after external beam radiotherapy for men with low-risk prostate cancer and may be a marker for occult, high-grade cancer. Int J Radiat Oncol Biol Phys 2004;58:19–24.

18. Podo F. Tumour phospholipid metabolism. NMR Biomed 1999;12:413–39.

19. Wong YC, Wang XH, Ling MT. Prostate development and carcinogenesis. Int Rev Cytol 2003;227:65–130.

20. Cooper CR, Chay CH, Gendernalik JD, et al. Stromal factors involved in prostate carcinoma metastasis to bone. Cancer 2003;97:739–47.

NMR IN BIOMEDICINE
NMR Biomed. 2005;**18**:413–420
Published online 1 August 2005 in Wiley InterScience (www.interscience.wiley.com). DOI:10.1002/nbm.973

Quantification of phosphocholine and glycerophosphocholine with ^{31}P edited ^{1}H NMR spectroscopy

Nikolaus M. Loening,[1]* Anne M. Chamberlin,[1] Andrea G. Zepeda,[2] R. Gilberto Gonzalez[3], and Leo L. Cheng[2,3]

[1]Department of Chemistry, Lewis & Clark College, 0615 SW Palatine Hill Road, Portland, OR 97219, USA
[2]Department of Pathology, Massachusetts General Hospital, Harvard Medical School, Boston, MA 02129, USA
[3]Department of Radiology, Massachusetts General Hospital, Harvard Medical School, Boston, MA 02129, USA

Received 8 December 2003; Revised 15 March 2004, 9 July 2004, 5 April 2005; Accepted 26 May 2005

ABSTRACT: Choline and the related compounds phosphocholine (PC) and glycerophosphocholine (GPC) are considered to be important metabolites in oncology. Past studies have demonstrated correlations linking the relative ratios and concentrations of these metabolites with the development and progression of cancer. Currently, *in vivo* and tissue *ex vivo* magnetic resonance spectroscopy methods have mostly centered on measuring the total concentration of these metabolites and have difficulty in differentiating between them. Here, a new scheme that uses ^{31}P edited ^{1}H spectroscopy to quantify the concentrations of choline, PC and GPC in biological samples is reported and its applicability is demonstrated using samples of human brain tumor extracts. This method is particularly well-suited for analytical situations where the PC and GPC resonances are not sufficiently resolved and/or are obscured by other metabolites. Consequently, this scheme has the potential to be used for the analysis of choline compounds in *ex vivo* tissue samples. Copyright © 2005 John Wiley & Sons, Ltd.

KEYWORDS: ^{31}P edited ^{1}H NMR; INEPT; choline compounds; human brain tumor extracts

INTRODUCTION

Choline and the related compounds phosphocholine (PC) and glycerophosphocholine (GPC) are essential nutrients that function as substrates in many major bio-metabolic pathways. These choline-compounds participate in a number of biological processes ranging from the normal development of the brain and liver in infants[1] to various pathological conditions such as the progression of neoplasm.[2] Although the biochemical functions of these compounds have been studied for decades, their unique importance has only come to light over the past 20 years with the application of NMR spectroscopy to medical science.

The relationship between the concentrations of choline-compounds and pathology has been measured and documented for many medical conditions, such as HIV infections,[3] traumatic brain injuries,[4] schizophrenia,[5] neuro-degenerative[6] and neuro-genetic[7] disorders, chronic fatigue[8] and multiple sclerosis,[9] as well as for the processes of normal development[10] and aging.[11] However, one of the most studied connections has been with cancer.[12–18] In general, the concentrations of choline-compounds are elevated in cancer and, more importantly, *ex vivo* studies of tissue extract samples suggest that the ratio of the phosphoryl derivatives indicates the status of the disease.[19–21] The signals of the methyl [$-N(CH_3)_3$] protons has been used to differentiate choline (3.185 ppm) from PC (3.208 ppm) and GPC (3.212 ppm) in *ex vivo* analyses.[22] Unfortunately, present NMR-based *in vivo* techniques cannot differentiate the methyl protons of choline from those of PC and GPC as their signals are separated by less than 0.03 ppm. For *ex vivo* samples of intact tissue the methyl protons of choline can be differentiated from those of the other choline compounds using high-resolution magic angle spinning proton NMR spectroscopy. Differentiating between the methyl protons of PC and GPC is a great challenge because of their very small chemical shift separation (0.007 ppm, see Results section).[23,24] Therefore, even at moderate field strengths (e.g. 300 MHz), the resonances are difficult to resolve. This means that it is currently almost impossible to quantify these metabolites simultaneously *in vivo*. Although *ex vivo* quantification of all three compounds

**Correspondence to:* N. M. Loening, Department of Chemistry, Lewis & Clark College, 0615 SW Palatine Hill Road, Portland, OR 97219, USA.
E-mail: loening@lclark.edu
Contract/grant sponsor: NIH; *contract/grant number:* F32 NS42425-01.
Contract/grant sponsors: Camille and Henry Dreyfus Foundation; NIH NIBIB; *contract/grant number:* EB002026.
Contract/grant sponsor: NIH NCI; *contract/grant numbers:* CA77727, CA095624, CA83159.

Abbreviations used: GPC, glycerophosphocholine; INEPT, insensitive nuclei enhanced by polarization transfer; PC, phosphocholine.

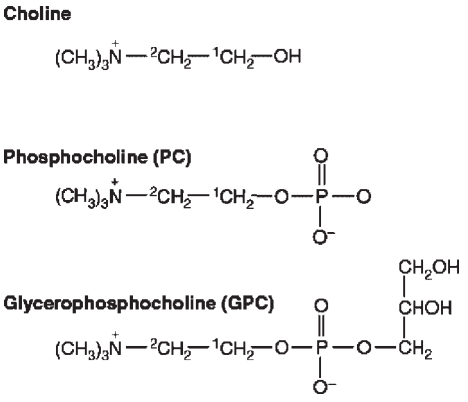

Figure 1. Molecular structures of choline, PC, and GPC. The ^{31}P edited ^{1}H experiment discussed in the text uses INEPT steps to transfer magnetization from the $^{1}CH_2$ protons to the phosphorous nuclei and back, and selectively refocuses the scalar couplings between the $^{1}CH_2$ and $^{2}CH_2$ protons during the transfers

is possible using the methyl proton signals, it is difficult and requires techniques such as post-processing peak deconvolution or two-dimensional spectroscopy.[25–28]

Here, we introduce a scheme that can efficiently differentiate and quantify PC and GPC, and we demonstrate its applicability to both model compounds and extracts of human brain tissue. The crux of this method is the use of phosphorous (^{31}P) edited proton (^{1}H) NMR spectroscopy to measure signals from the $^{1}CH_2$ protons (see Fig. 1) of PC and GPC. These protons have a spectral separation that is about 20 times greater than that between the methyl protons (0.13 vs 0.007 ppm). The ^{31}P editing is accomplished using the scalar couplings between the ^{31}P nucleus and the $^{1}CH_2$ protons in PC and GPC. Although the sensitivity of this technique suffers compared with the direct analysis of the methyl protons, the better resolution of the $^{1}CH_2$ protons allows for analysis in situations where the individual methyl proton resonances from the three choline compounds are not sufficiently resolved. Consequently, we believe this approach may be helpful in the future for *ex vivo* analyses of intact tissue samples and, if sensitivity issues can be resolved, has the potential to be incorporated into *in vivo* examinations.

EXPERIMENTAL

The experiments were carried out using vertical standard-bore Bruker Avance NMR spectrometers. The standard samples were studied using a 300 MHz (7.05 T) system equipped with a Bruker broadband inverse-geometry *z*-axis gradient probe. The brain tissue extract samples were studied using a 600 MHz (14.1 T) system equipped with a Bruker ^{31}P/^{13}C/^{15}N–^{1}H inverse-geometry *z*-axis gradient probe. The pulse sequence developed for the experiment is shown in Fig. 2. It consists of two INEPT steps[29] that transfer the initial ^{1}H magnetization to ^{31}P and then back to ^{1}H. Inserted into these INEPT steps are selective 180° pulses that only affect the $^{2}CH_2$ protons and, consequently, refocus the homonuclear scalar couplings between the $^{1}CH_2$ and $^{2}CH_2$ protons. These selective pulses are essential because the ^{1}H–^{1}H couplings are similar in size to the ^{31}P–^{1}H couplings. Without the selective pulses the effect of the ^{1}H–^{1}H couplings during the INEPT delays would be to transform the single quantum coherences arising from the $^{1}CH_2$ protons into multiple quantum coherences. Pulsed field gradients are used in conjunction with phase cycling to eliminate unwanted signals in the ^{31}P edited ^{1}H spectra. The gradients G_1 and G_2 impart a phase label to the ^{31}P magnetization that is later refocused after the magnetization has been transferred to ^{1}H by the final coherence selection gradient, G_3. Finally, a zero-quantum filter is included at the end of the sequence to further attenuate contributions from undesired coherence transfer pathways.[30]

A recycle time of 10 s was used for both the regular and ^{31}P edited experiments to ensure that the sample magnetization was at equilibrium before every scan. During the

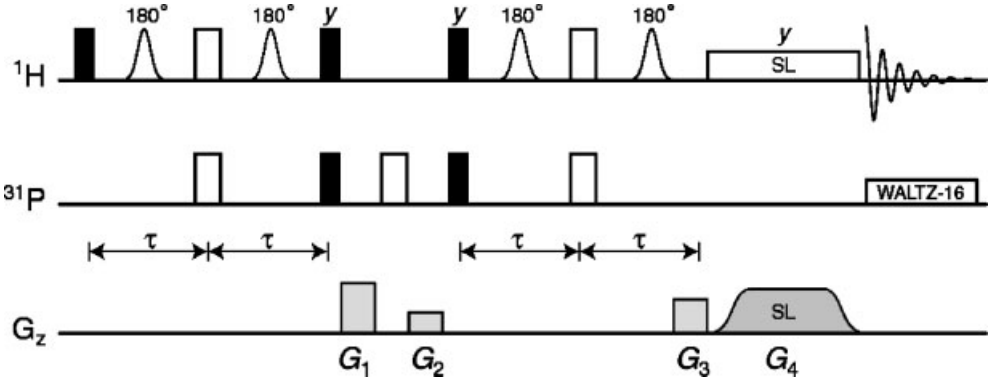

Figure 2. The pulse sequence used to acquire the ^{31}P edited ^{1}H spectra. For the ^{1}H and ^{31}P channels, solid rectangles correspond to 90° radiofrequency pulses, open rectangles correspond to 180° pulses, and Gaussian shapes represent selective 180° pulses. The spin-lock pulse is denoted by 'SL'. The phase of all pulses is *x* unless indicated otherwise

recycle delay, the water resonance was saturated with a weak radio frequency field ($\gamma B_1/2\pi = 50$ Hz). Low power Waltz-16 decoupling[31] ($\gamma B_1/2\pi = 625$ Hz) was used on the ^{31}P channel during ^{1}H acquisition to narrow the lines of the PC and GPC $^{1}CH_2$ resonances; this resulted in an increase (20%) in the sensitivity of the experiment. For the high-power pulses, the radiofrequency field strength ($\gamma B_1/2\pi$) was 40 kHz for ^{1}H and 10 kHz for ^{31}P on the 14 T instrument, and 35 kHz for ^{1}H and 20 kHz for ^{31}P on the 7 T instrument. For the ^{31}P experiments, Waltz-16 decoupling ($\gamma B_1/2\pi = 2500$ Hz) was used on the ^{1}H channel.

In the ^{31}P edited ^{1}H experiment, Gaussian 180° pulses were used to selectively decouple the ^{1}H homonuclear scalar couplings during the INEPT steps. The selective pulses were 5 ms on the 14 T system and 10 ms on the 7 T system; for both systems the pulses were applied at 3.3 ppm. Consequently, these pulses refocused the $^{2}CH_2$ protons of choline, PC, and GPC, but left the $^{1}CH_2$ protons of these molecules unperturbed. The gradients G_1, G_2, G_3 and G_4 were set to 35, 15, 20, and 1 G cm^{-1} and were 2.47, 2.47, 1, and 10 ms in length, respectively. The first three gradients were shaped to a half-sine bell; the shape of the fourth gradient was constant over the central 80% of the pulse and was smoothly ramped on and off at the ends of the pulse.

The sample temperature was maintained at 10 °C with a cooling gas flow rate of 535 l h^{-1} for the experiments at 14 T to minimize any potential problems owing to sample degradation. The experiments at 7 T were performed at 25 °C. The temperature was controlled to better than ± 0.2 °C during the experiments; temperature stability is important for quantitation as the efficiency of the heteronuclear transfer steps varies with temperature.

Standards

The standard samples consisted of between 0 and 5 mM PC, between 0 and 5 mM GPC, and 3.1 mM choline in 10% D_2O–90% H_2O. D_2O was included in the sample for the purpose of locking the magnet field. All spectra for the standards were acquired with 16 scans (each spectrum required just under 3 min to complete). The pH of each sample was adjusted to be in the range 6–7.5 by the addition of small amounts of HCl or NaOH.

Solutions of human brain tumor metabolites

Eleven samples of human glioma (malignant brain tumor) extracts were prepared using the FastPrep™ and Speed Vac® systems (Thermo Savant, Holbrook, NY, USA) according to the following procedure. Between 100 and 200 mg of frozen tissue samples from surgeries or autopsies were transferred into Lysing Matrix D tubes (Qbiogene, Carlsbad, CA, USA) along with 1.2 ml methanol. The sample tubes were then placed in the FastPrep™ system and processed for 35 s on speed dial 4.0. This was repeated at least three times until no visible tissue pieces remained. Next, a modified methanol–chloroform extraction was carried out.[32] The resulting aqueous layer of brain metabolites was dried with the Speed Vac® system and redissolved in D_2O. The pH of these samples was adjusted to be in the range 7–8. Since this preparation method is not a calibrated protocol for metabolite quantification, we observed a decrease in the absolute metabolite concentrations. For instance, the mean concentration for total choline was determined to be 0.31 ± 0.07 mM, which is only 25% of the literature values (1.24 ± 0.10 mM) for extracts of tumor tissues of similar type.[33–35] Although this reduction in concentration resulted in much longer experiment times, it did not interfere with the aim of this work, which was to test the capability of the ^{31}P edited ^{1}H spectral protocol to quantify PC and GPC concentrations of tissue extract samples. ^{1}H spectra for the brain extracts were acquired using 1024 scans, resulting in an experiment time of 3.2 h. ^{31}P edited ^{1}H spectra were acquired using between 3096 and 5192 scans, resulting in experiment times ranging from 9.8 to 16.3 h.

RESULTS

^{31}P edited spectra of the standards

The method described in this report concentrates on the measurement of signals from the $^{1}CH_2$ protons instead of the more intense signals that arise from the methyl protons. Focusing on the $^{1}CH_2$ protons has two main advantages. First, as seen in the regular ^{1}H spectrum shown in Fig. 3(a), the signals from the $^{1}CH_2$ protons are dispersed over a range of 0.13 ppm instead of the 0.007 ppm range of the methyl protons. This suggests that the measurement of the $^{1}CH_2$ protons is better suited for situations, such as *ex vivo* tissue analyses, where the spectral resolution is limited to the point that the individual methyl resonances cannot be resolved. The second advantage is that the $^{1}CH_2$ protons for PC and GPC have observable ($\sim$6.1 and 6.3 Hz, respectively [22]) couplings to the ^{31}P nucleus, which allows for the use of ^{31}P editing. This fact is important as, without ^{31}P editing, the ^{1}H signals of the choline-compounds (especially those from the $^{1}CH_2$ resonances but also the methyl resonances) are mingled with signals from other metabolites, making quantification more difficult and less reliable.

The main disadvantage of our method is that the integral of the $^{1}CH_2$ protons is 4.5 times smaller than the integral of the methyl protons [note the separate intensity scale used for the methyl region in Fig. 3(a)]. Nevertheless, the quality of the ^{31}P editing allows the relatively weak $^{1}CH_2$ peaks to be easily resolved and measured in a ^{31}P edited ^{1}H spectrum. With ^{31}P editing,

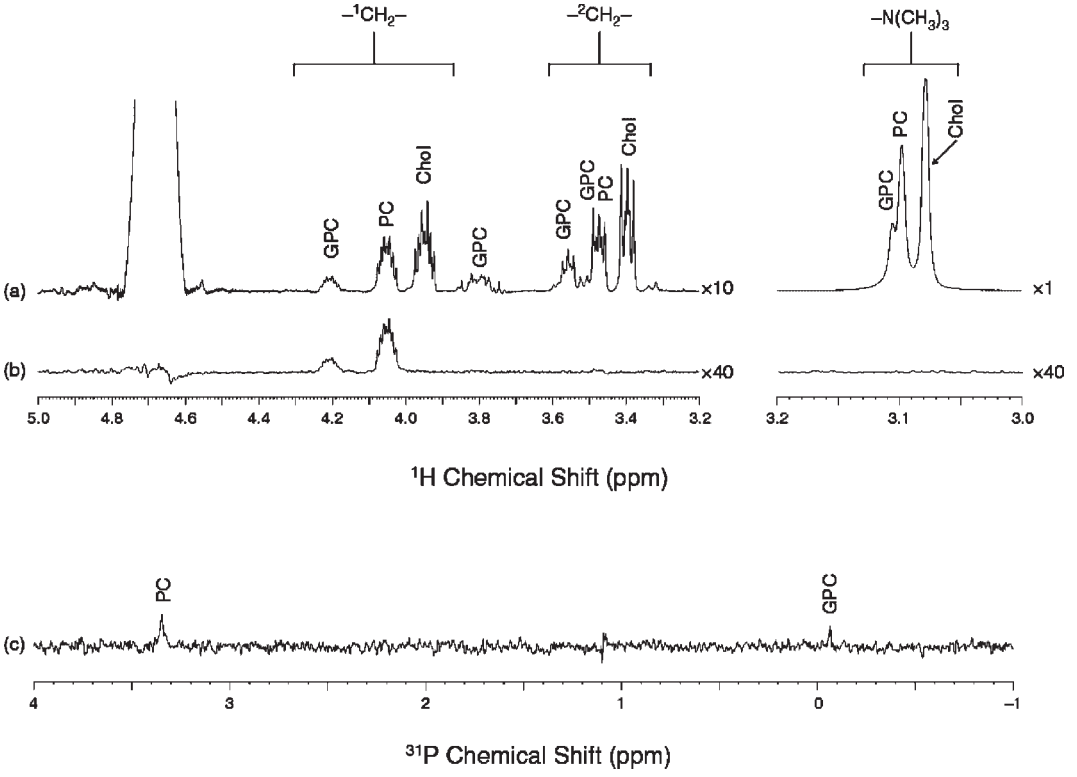

Figure 3. (a) ^{1}H, (b) ^{31}P filtered ^{1}H, and (c) ^{31}P spectra for a standard sample of 3.1 mM choline, 2.0 mM PC, and 1.0 mM GPC in 10% D_2O–90% H_2O. Each spectrum was acquired in 16 scans and with heteronuclear decoupling at 300 MHz for ^{1}H. The lack of resolution in the methyl region (3.12–3.06 ppm) is what makes it hard to use the methyl peaks to quantify the concentrations of choline, PC, and GPC in tissue samples. In spectrum (a), the additional GPC peaks at 3.78 ppm and overlapping the $^2CH_2$ resonances at 3.5 ppm arise from the glycerol moiety. The relative scales for spectra (a) and (b) are indicated at the right of each part. All spectra were processed with 0.5 Hz of line broadening; baseline correction was used for spectrum (a) to compensate for the intense water signal at 4.7 ppm

the only peaks that remain in the ^{1}H spectrum are those from the $^1CH_2$ protons of PC and GPC. The signal from the $^1CH_2$ protons of choline, which would have appeared at 3.95 ppm, is completely removed, as are the intense methyl signals at ~3.1 ppm from all three choline compounds. The small artifact at 4.7 ppm in the ^{31}P edited ^{1}H spectrum is all that remains of the water signal after suppression by presaturation and coherence transfer pathway selection. This artifact has an integral close to zero and is 0.5 ppm downfield from the signals of interest, so it does not affect the integration of the GPC and PC signals.

Signals from choline are removed in the ^{31}P editing step, so it is not possible to determine its concentration directly from the ^{31}P edited ^{1}H spectrum. However, the quantitative relationship between the ^{31}P edited and the regular ^{1}H spectra can be exploited to determine the choline concentration. This can be accomplished by determining the PC and GPC concentrations from the edited spectrum, and then using this information to subtract their contributions from the total integrated intensity of the methyl protons in the regular ^{1}H spectrum. The remaining intensity corresponds to the concentration of choline. As a result, it is possible to determine the relative concentrations of all three species in cases where the individual methyl signals are not resolved.

Quantification of the amount of choline, PC, and GPC in a sample using ^{31}P edited ^{1}H spectra depends on the transfer efficiency of the INEPT steps. This transfer efficiency, in turn, depends on the ^{31}P–^{1}H coupling constants, pulse imperfections, and the transverse and longitudinal relaxation rates. The coupling constants are largely insensitive to sample conditions and the INEPT steps are reasonably tolerant of variations in pulse calibration, so the main difficulty with establishing the transfer efficiency stems from variations in the relaxation rates. For the range of concentrations used in our samples we found that the transfer efficiencies were independent of the relative concentrations of choline, PC, and GPC. However, relaxation rates (and therefore the transfer efficiency) depend on temperature so it is important to establish the transfer efficiency for whatever temperature is used for the experiment. For our experiments with brain tissue samples, which were kept at 10 °C, we observed signal intensities in the ^{31}P edited spectra that were 13.4 and 18.5% of the unedited signal intensities for

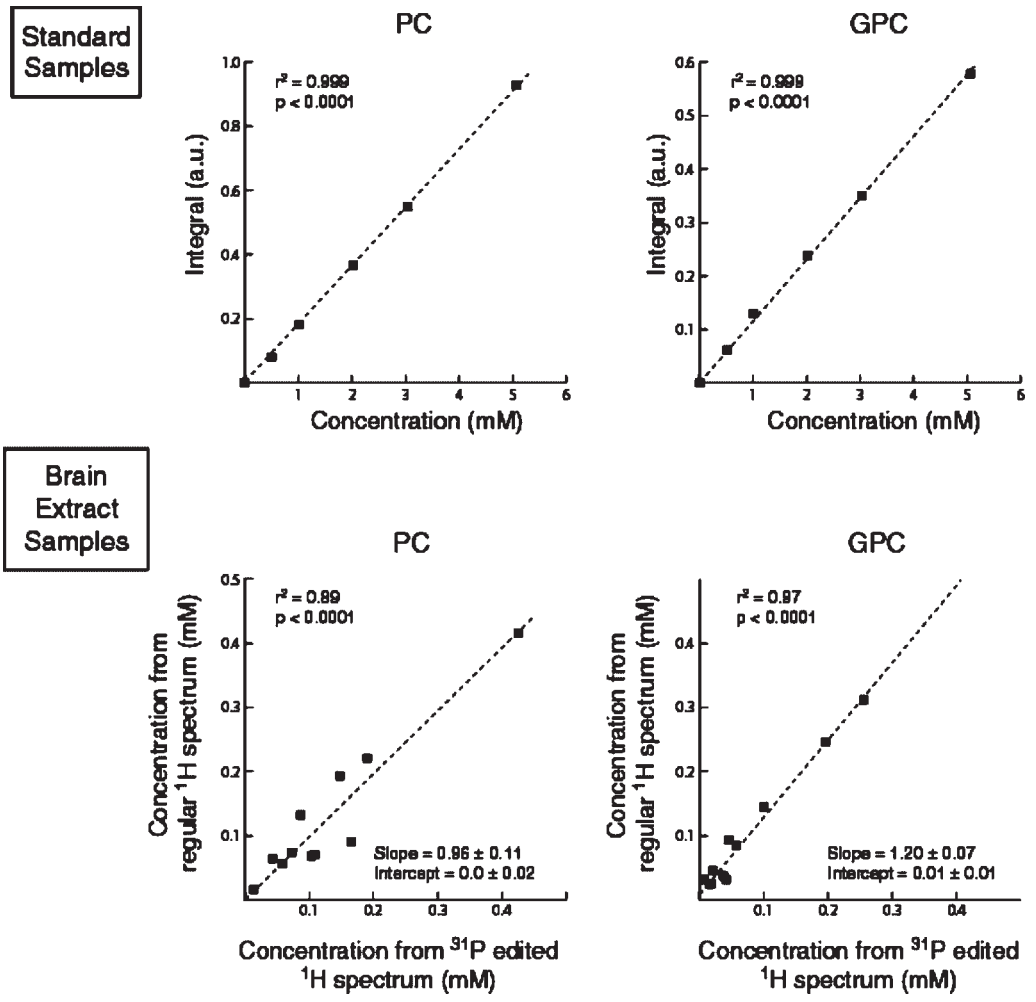

Figure 4. At the top are graphs demonstrating the linear response of the integrals from $^{1}CH_2$ peaks in the ^{31}P edited H spectra for the standard samples (0–5 mM PC, 0–5 mM GPC and 3.1 mM choline in 10% D_2O–90% H_2O) at 300 MHz. At the bottom are graphs showing how the concentrations of PC and GPC, determined by fitting the methyl peaks in regular ^{1}H spectra, compare with the concentrations determined using the integrals of the $^{1}CH_2$ peaks in the ^{31}P edited ^{1}H spectra. These results were determined from spectra acquired at 600 MHz for ^{1}H for the brain extract samples described in the text. The dotted lines indicate the results from linear regression analyses of the data; the result of each analysis is shown with the relevant graph

PC and GPC, respectively. These results are 54 and 74% of the theoretical maximum transfer efficiency of 25% (see Discussion section). At 25 °C, the transfer efficiencies (PC = 24.1% and GPC = 20.1%) were much closer to the theoretical value, as would be expected based on the connection between temperature and relaxation rates for small molecules in solution.

The top half of Fig. 4 demonstrates the linear relationship between the PC and GPC peak integrals in the ^{31}P edited ^{1}H spectra and the PC and GPC concentrations for a series of standard samples.

Analyses of human brain extracts

We tested the applicability of ^{31}P editing for the quantification of PC and GPC in biological systems using a series of 11 human glioma extract samples. Representative 600 MHz ^{1}H spectra for one of these samples are shown in Fig. 5. From the subspectrum shown in Fig. 5(b), it is clear that the $^{1}CH_2$ resonances are overlapped by peaks from other metabolites in the regular ^{1}H spectrum; this problem also affects the methyl resonances, although to a smaller extent. The complexity of the spectrum makes it difficult to quantify the relative amounts of the choline compounds using just the regular ^{1}H spectrum.

In the ^{31}P edited ^{1}H spectrum [Fig. 5(c)], the $^{1}CH_2$ resonances are clearly resolved and the relative amounts of PC and GPC can be easily quantified. The additional peaks at 4.095 and 3.96 ppm arise from other phosphorous containing brain metabolites such as, possibly, phosphoethanolamine (PE) and glycerophosphoethanolamine (GPE). [22] If these additional peaks prove to be due to PE and GPE, then the use of ^{31}P editing for quantification is even better justified. This is because the methyl signals of

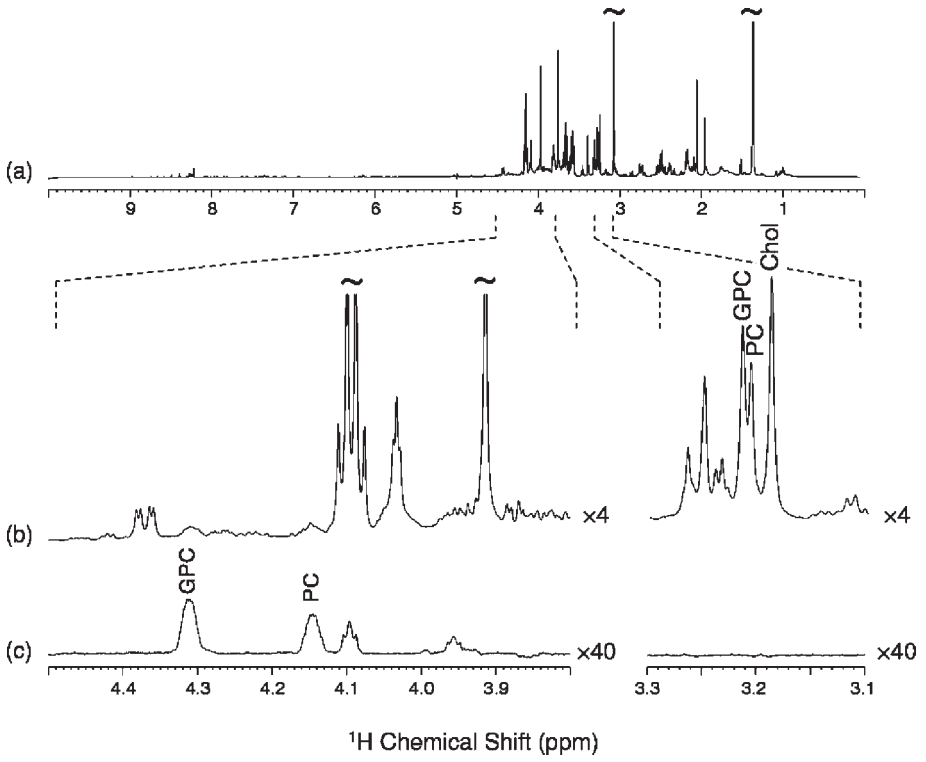

Figure 5. The 600 MHz regular (a) and ^{31}P edited ^{1}H (c) spectra obtained for a human glioma extract sample. Spectrum (b) highlights two regions of the regular spectrum with the scale increased by a factor of 4. The scale of the ^{31}P edited ^{1}H spectrum shown as spectrum (c) is increased by a factor of 40 relative to spectrum (a). Peaks other than those from PC and GPC in the ^{31}P edited ^{1}H spectrum arise from other phosphorous-containing brain metabolites in the sample

PE and GPE interfere with the quantification of the PC, GPC, and choline methyl peaks in regular ^{1}H spectra.[22] In contrast, the PE and GPE peaks that appear in the ^{31}P edited ^{1}H spectrum are well-resolved and, consequently, do not affect the quantification of the $^{1}CH_2$ resonances from PC and GPC.

The graphs shown in the bottom half of Fig. 4 demonstrate the correlation between the results of fitting the methyl peaks in the regular ^{1}H spectra (as has been done in the past) vs the results from the ^{31}P edited ^{1}H experiment. The variation seen in these graphs is not surprising owing to difficulties in quantifying the methyl peaks in the regular ^{1}H spectra. These difficulties are due to: (1) the lack of baseline resolution between the methyl peaks, and (2) the presence of other components that overlap the methyl peaks. These difficulties can be expected to be greatly exacerbated when using an instrument at lower field or in the analysis of *ex vivo* tissue samples.

DISCUSSION

^{31}P spectroscopy vs ^{31}P edited ^{1}H spectroscopy

As the ^{31}P resonances of PC and GPC differ from one another by $\sim$3.5 ppm, it could be argued that a better approach for the quantification of PC and GPC would be to directly observe the ^{31}P signal.[2,36–39] In fact, with the development and availability of high field MR imagers, it has been demonstrated recently that PC and GPC can be observed in *in vivo* ^{31}P spectroscopy at 7 T from a voxel size of 27 ml.[40] However, it may be better to utilize the improved sensitivity of ^{1}H nuclei for detection due to the higher magnetogyric ratio of ^{1}H, especially if an inverse geometry probehead is in use (as is often the case for *ex vivo* studies). This is clearly demonstrated in Fig. 3. The signal-to-noise ratio for the peaks in the ^{31}P edited ^{1}H spectrum [Fig. 3(b)] is roughly 10 times greater than the signal-to-noise ratio of the resonances in the ^{31}P spectrum [Fig. 3(c)] when the line broadening is optimized. The signal-to-noise ratio was calculated as the ratio of the PC or GPC peak intensity to the root-mean-square noise of a signal-less spectral region. As quantitative work usually makes use of integrals instead of intensities, the comparison of these techniques based on their signal-to-noise ratios underestimates the advantages of the ^{31}P-filtered ^{1}H experiment because the peaks in the ^{31}P spectrum are approximately 10 times narrower than the $^{1}CH_2$ peaks in the ^{31}P filtered ^{1}H spectrum. In addition, ^{31}P nuclei typically relax more slowly than ^{1}H nuclei, so ^{31}P edited ^{1}H spectra will have a further signal-to-noise advantage compared with ^{31}P spectra when comparing data acquired with the same amount of experiment time instead of the same number of scans.

Signal intensities in ^{31}P edited ^{1}H spectra

The use of a ^{31}P filter for editing in these experiments reduces the signal intensity due to the added restrictions to the coherence transfer pathway. In theory, the edited spectrum should have 50% of the intensity of the unedited spectrum if only phase cycling is used for selecting the coherence transfer pathway. However, we found that it was useful to supplement the phase cycling with pulsed field gradients to further attenuate artifacts in the spectrum. However, this comes at the price of an additional two-fold reduction in signal intensity, resulting in a total theoretical transfer efficiency of 25%.

INEPT transfer vs Hartman–Hahn mixing

We note that we also attempted to use heteronuclear Hartman–Hahn mixing[41] for the heteronuclear transfer steps. However, the measured transfer efficiency was around 3%, much lower than the efficiency of INEPT transfers. The inefficiency of heteronuclear Hartman–Hahn mixing compared with INEPT is attributable to the longer periods required to complete the heteronuclear magnetization transfer as well as to interference from homonuclear Hartman–Hahn mixing.

Realistic experiment times

The use of a non-quantitative extraction procedure for the preparation of the human glioma samples used in this study led to relatively low metabolite concentrations. Consequently, the ^{1}H spectra for the brain extracts were acquired using 1024 scans, resulting in an experiment time of 3.2 h, and the ^{31}P edited ^{1}H spectra were acquired using between 3096 and 5192 scans, resulting in quite lengthy experiment times of between 9.8 and 16.3 h. Owing to the low metabolite concentrations, as well as other factors, the measurement times used for these experiments are much longer than what will typically be needed. If samples were used with metabolite concentrations similar to those reported in the literature (which are about four times higher than the concentrations of the brain extract samples used for this study), then a spectrum equivalent to the results shown in Fig. 5 could be achieved while reducing the experiment time by a factor of 16. In addition, the signal-to-noise ratio (SNR) shown in Fig. 5 is greater than what is actually needed for quantification. If half the SNR were deemed acceptable for quantification, than the experiment time could be reduced by a factor of 4. Combined, these two changes would reduce the experiment time by a factor of 64, shortening a 9.8 h experiment to a much more reasonable 9.5 min experiment. In addition, experiment times can be further reduced by using shorter recycle delays as long as all samples are analyzed using the same conditions.

CONCLUSION

We have demonstrated a scheme that uses ^{31}P edited ^{1}H NMR spectroscopy to quantify the concentrations of phosphocholine and glycerophosphocholine in biological samples. In addition, the concentration of choline can be indirectly determined using this method. This method is particularly well-suited for analytical situations in which the $^{1}CH_2$ resonances are obscured by other metabolites and/or the methyl resonances are not sufficiently resolved. We believe this method will be applicable for the analysis of choline compounds in *ex vivo* tissue samples. In addition, if problems of sensitivity are resolved, this method may have potential for the *in vivo* non-destructive quantification of choline, PC and GPC.

Acknowledgements

The authors thank Prof*s*. Robert G. Griffin and Franca Podo for useful discussion and Dr. Anthony Bielecki for assistance. N.M.L. thanks the National Institutes of Health for support via a National Research Service Award post-doctoral fellowship (F32 NS42425-01) and the Camille and Henry Dreyfus Foundation for support through a Faculty Start-Up Award. This work is supported in part by NIH NCI grants CA77727, CA095624, CA83159, and by NIH NIBIB grant EB002026.

REFERENCES

1. Holmes HC, Snodgrass GJ, Iles RA. Changes in the choline content of human breast milk in the first 3 weeks after birth. *Eur. J. Pediatr.* 2000; **159**(3): 198–204.
2. Podo F. Tumour phospholipid metabolism. *NMR Biomed.* 1999; **12**(7): 413–439.
3. Chang L, Ernst T, Witt MD, Ames N, Walot I, Jovicich J, DeSilva M, Trivedi N, Speck O, Miller EN. Persistent brain abnormalities in antiretroviral-naive HIV patients 3 months after HAART. *Antivir. Ther.* 2003; **8**(1): 17–26.
4. Brenner T, Freier MC, Holshouser BA, Burley T, Ashwal S. Predicting neuropsychologic outcome after traumatic brain injury in children. *Pediatr. Neurol.* 2003; **28**(2): 104–114.
5. Delamillieure P, Constans JM, Fernandez J, Brazo P, Benali K, Courtheoux P, Thibaut F, Petit M, Dollfus S. Proton magnetic resonance spectroscopy (^{1}H MRS) in schizophrenia: investigation of the right and left hippocampus, thalamus, and prefrontal cortex. *Schizophr. Bull.* 2002; **28**(2): 329–339.
6. Firbank MJ, Harrison RM, O'Brien JT. A comprehensive review of proton magnetic resonance spectroscopy studies in dementia and Parkinson's disease. *Dement. Geriatr. Cogn. Disord.* 2002; **14**(2): 64–76.
7. Brockmann K, Dechent P, Meins M, Haupt M, Sperner J, Stephani U, Frahm J, Hanefeld F. Cerebral proton magnetic resonance spectroscopy in infantile Alexander disease. *J. Neurol.* 2003; **250**(3): 300–306.
8. Chaudhuri A, Condon BR, Gow JW, Brennan D, Hadley DM. Proton magnetic resonance spectroscopy of basal ganglia in chronic fatigue syndrome. *Neuroreport* 2003; **14**(2): 225–228.
9. Arnold DL, De Stefano N, Narayanan S, Matthews PM. Proton MR spectroscopy in multiple sclerosis. *Neuroimag. Clin. N. Am.* 2000; **10**(4): 789–798, ix–x.

10. Filippi CG, Ulug AM, Deck MD, Zimmerman RD, Heier LA. Developmental delay in children: assessment with proton MR spectroscopy. *AJNR Am. J. Neuroradiol.* 2002; **23**(5): 882–888.
11. Sijens PE, den Heijer T, Origgi D, Vermeer SE, Breteler MM, Hofman A, Oudkerk M. Brain changes with aging: MR spectroscopy at supraventricular plane shows differences between women and men. *Radiology* 2003; **226**(3): 889–896.
12. Galanaud D, Chinot O, Nicoli F, Confort-Gouny S, Le Fur Y, Barrie-Attarian M, Ranjeva JP, Fuentes S, Viout P, Figarella-Branger D, Cozzone PJ. Use of proton magnetic resonance spectroscopy of the brain to differentiate gliomatosis cerebri from low-grade glioma. *J. Neurosurg.* 2003; **98**(2): 269–276.
13. Rijpkema M, Schuuring J, Van Der Meulen Y, Van Der Graaf M, Bernsen H, Boerman R, Van Der Kogel A, Heerschap A. Characterization of oligodendrogliomas using short echo time ^{1}H MR spectroscopic imaging. *NMR Biomed.* 2003; **16**(1): 12–18.
14. Lindskog M, Kogner P, Ponthan F, Schweinhardt P, Sandstedt B, Heiden T, Helms G, Spenger C. Noninvasive estimation of tumour viability in a xenograft model of human neuroblastoma with proton magnetic resonance spectroscopy (^{1}H MRS). *Br. J. Cancer* 2003; **88**(3): 478–485.
15. Howe FA, Barton SJ, Cudlip SA, Stubbs M, Saunders DE, Murphy M, Wilkins P, Opstad KS, Doyle VL, McLean MA, Bell BA, Griffiths JR. Metabolic profiles of human brain tumors using quantitative *in vivo* ^{1}H magnetic resonance spectroscopy. *Magn. Reson. Med.* 2003; **49**(2): 223–232.
16. El-Sayed S, Bezabeh T, Odlum O, Patel R, Ahing S, MacDonald K, Somorjai RL, Smith IC. An *ex vivo* study exploring the diagnostic potential of ^{1}H magnetic resonance spectroscopy in squamous cell carcinoma of the head and neck region. *Head Neck* 2002; **24**(8): 766–772.
17. Katz-Brull R, Lavin PT, Lenkinski RE. Clinical utility of proton magnetic resonance spectroscopy in characterizing breast lesions. *J. Natl. Cancer Inst.* 2002; **94**(16): 1197–1203.
18. Nakagami K, Uchida T, Ohwada S, Koibuchi Y, Suda Y, Sekine T, Morishita Y. Increased choline kinase activity and elevated phosphocholine levels in human colon cancer. *Jpn. J. Cancer Res.* 1999; **90**(4): 419–424.
19. Sabatier J, Gilard V, Malet-Martino M, Ranjeva JP, Terral C, Breil S, Delisle MB, Manelfe C, Tremoulet M, Berry I. Characterization of choline compounds with *in vitro* ^{1}H magnetic resonance spectroscopy for the discrimination of primary brain tumors. *Invest. Radiol.* 1999; **34**(3): 230–235.
20. Morvan D, Demidem A, Papon J, De Latour M, Madelmont JC. Melanoma tumors acquire a new phospholipid metabolism phenotype under cystemustine as revealed by high-resolution magic angle spinning proton nuclear magnetic resonance spectroscopy of intact tumor samples. *Cancer Res.* 2002; **62**(6): 1890–1897.
21. Katz-Brull R, Margalit R, Degani H. Differential routing of choline in implanted breast cancer and normal organs. *Magn. Reson. Med.* 2001; **46**(1): 31–38.
22. Govindaraju V, Young K, Maudsley AA. Proton NMR chemical shifts and coupling constants for brain metabolites. *NMR Biomed.* 2000; **13**(3): 129–153.
23. Cheng LL, Ma MJ, Becerra L, Ptak T, Tracey I, Lackner A, Gonzalez RG. Quantitative neuropathology by high resolution magic angle spinning proton magnetic resonance spectroscopy. *Proc. Natl. Acad. Sci. USA* 1997; **94**(12): 6408–6413.
24. Sitter B, Sonnewald U, Spraul M, Fjosne HE, Gribbestad IS. High-resolution magic angle spinning MRS of breast cancer tissue. *NMR Biomed.* 2002; **15**(5): 327–337.
25. Ala-Korpela M, Posio P, Mattila S, Korhonen A, Williams SR. Absolute quantification of phospholipid metabolites in brain-tissue extracts by ^{1}H NMR spectroscopy. *J. Magn. Reson. B* 1996; **113**(2): 184–189.
26. Moreno A, Lopez LA, Fabra A, Arus C. ^{1}H MRS markers of tumour growth in intrasplenic tumours and liver metastasis induced by injection of HT-29 cells in nude mice spleen. *NMR Biomed.* 1998; **11**(3): 93–106.
27. Morvan D, Demidem A, Papon J, De Latour M, Madelmont JC. Melanoma tumors acquire a new phospholipid metabolism phenotype under cystemustine as revealed by high-resolution magic angle spinning proton nuclear magnetic resonance spectroscopy of intact tumor samples. *Cancer Res.* 2002; **62**(6): 1890–1897.
28. Morvan D, Demidem A, Papon J, Madelmont JC. Quantitative HRMAS proton total correlation spectroscopy applied to cultured melanoma cells treated by chloroethyl nitrosourea: demonstration of phospholipid metabolism alterations. *Magn. Reson. Med.* 2003; **49**(2): 241–248.
29. Morris GA, Freeman R. Enhancement of nuclear magnetic-resonance signals by polarization transfer. *J. Am. Chem. Soc.* 1979; **101**: 760–762.
30. Davis AL, Estcourt G, Keeler J, Laue ED, Titman JJ. Improvement of z filters and purging pulses by the use of zero-quantum dephasing in inhomogenous B_1 and B_0 fields. *J. Magn. Reson.* 1993; **A105**: 167–183.
31. Shaka AJ, Keeler J, Freeman R. Evaluation of a new broad-band decoupling sequence—Waltz-16. *J. Magn. Reson.* 1983; **53**: 313–340.
32. Le Belle JE, Harris NG, Williams SR, Bhakoo KK. A comparison of cell and tissue extraction techniques using high-resolution ^{1}H-NMR spectroscopy. *NMR Biomed.* 2002; **15**(1): 37–44.
33. Peeling J, Sutherland G. High-resolution ^{1}H NMR spectroscopy studies of extracts of human cerebral neoplasms. *Magn. Reson. Med.* 1992; **24**(1): 123–136.
34. Sutton L, Wehrli S, Gennarelli L, Wang Z, Zimmerman R, Bonner K, Rorke L. High-resolution ^{1}H-magnetic resonance spectroscopy of pediatric posterior fossa tumors *in vitro*. *J. Neurosurg.* 1994; **81**(3): 443–448.
35. Kinoshita Y, Yokota A. Absolute concentrations of metabolites in human brain tumors using *in vitro* proton magnetic resonance spectroscopy. *NMR Biomed.* 1997; **10**(1): 2–12.
36. Ronen SM, Leach MO. Imaging biochemistry: applications to breast cancer. *Breast. Cancer Res.* 2001; **3**(1): 36–40.
37. Leach MO, Verrill M, Glaholm J, Smith TA, Collins DJ, Payne GS, Sharp JC, Ronen SM, McCready VR, Powles TJ, Smith IE. Measurements of human breast cancer using magnetic resonance spectroscopy: a review of clinical measurements and a report of localized ^{31}P measurements of response to treatment. *NMR Biomed.* 1998; **11**(7): 314–340.
38. Bhujwalla ZM, Aboagye EO, Gillies RJ, Chacko VP, Mendola CE, Backer JM. Nm23-transfected MDA-MB-435 human breast carcinoma cells form tumors with altered phospholipid metabolism and pH: a ^{31}P nuclear magnetic resonance study *in vivo* and *in vitro*. *Magn. Reson. Med.* 1999; **41**(5): 897–903.
39. Lehtimaki KK, Valonen PK, Griffin JL, Vaisanen TH, Grohn OH, Kettunen MI, Vepsalainen J, Yla-Herttuala S, Nicholson J, Kauppinen RA. Metabolite changes in BT4C rat gliomas undergoing ganciclovir-thymidine kinase gene therapy-induced programmed cell death as studied by ^{1}H NMR spectroscopy *in vivo*, *ex vivo*, and *in vitro*. *J. Biol. Chem.* 2003; **278**(46): 45915–45923.
40. Lei H, Zhu XH, Zhang XL, Ugurbil K, Chen W. *In vivo* ^{31}P magnetic resonance spectroscopy of human brain at 7 T: an initial experience. *Magn. Reson. Med.* 2003; **49**(2): 199–205.
41. Ernst M, Griesinger C, Ernst RR. Optimized heteronuclear cross polarization in liquid. *Mol. Phys.* 1991; **74**: 219–252.

Current Clinical Applications of *In Vivo* Magnetic Resonance Spectroscopy and Spectroscopic Imaging

Margaret R. Lentz[1], Jennifer L. Taylor[2], D. Ashley Feldman[3] and Leo L. Cheng[1, 3, *]

Departments of [1]Radiology, [3]Pathology, Massachusetts General Hospital, Harvard University, Boston, Massachusetts, [2]Department of Cancer Biology and Pritzker School of Medicine, The University of Chicago, Chicago, Illinois

Abstract: Magnetic resonance imaging (MRI) infused Radiology with rejuvenating vigor in the 1980s, owing credit to a couple of magnetic resonance spectroscopy (MRS) experiments performed in 1973. MRI has since been embraced by the radiology and medical communities. If the goal of MRS is to measure many chemicals in a homogeneous magnetic field, then the function of MRI is, in general, to measure one chemical – water – in an artificially created inhomogeneous field.

Combining spectroscopy principles with technologies developed over the past two decades for MRI presented the philosophical appeal of non-invasively measuring metabolic molecules in living tissue, and led to the explosive developments in the last decade of *in vivo* MRS, and more recently MRSI, in the settings of diagnostic radiology.

This review is intended to discuss the basic technologies of the current trends in the field of *in vivo* MRS and MRSI, especially the inherent predilections of individual techniques to the study of certain disease states. Following a historical introduction, individual techniques and their clinical applications, found in publications between January 2000 and October 2004, are reviewed in connection with related *ex vivo* results, after which the practical aspects of *in vivo* MRS and MRSI in clinical settings are discussed.

Keywords: Magnetic resonance spectroscopy, magnetic resonance spectroscopic imaging, brain, cancer, clinical applications, *in vivo*.

1. INTRODUCTION

1.1. Time Before Magnetic Resonance

If we adopt arbitrarily that human civilization has a 5, 000-year history, then consider the recent and rapid progress of medicine in reference even to our own lifetimes, we are left straining to imagine what medical feats were performed before the birth of a "little" trick now known as radiology. The Renaissance curiosity of human anatomy and desire to depict it accurately was historically unique, and many believe that the scientific, and therefore modern notion of medicine was born with Leonardo Da Vinci's anatomical maps. However, if for medicine, to penetrate the skin was to see, then for 400 years after Da Vinci's suggestive drawings, the scalpel remained medicine's only way to see.

Light streamed in at the dawn of the 20th century first with Roentgen's breakthrough mass-density (absorption) based X-ray[1], and subsequently with the Becquerel[2] and Curies[3]' discovery of radioactivity. X-ray dominated medical diagnostics for the first eight decades of the 20th century. Particularly, the invention of computers in the 1970s led to the development of the x-ray based computed tomography (CT)[4], which emerged as a powerful tool, bringing a third dimension to the classical two-dimensional x-ray films.

Radiology, from the 2nd half of the 20th century, has become a substitute word for non-invasive diagnosis. Although excessive exposure to x-rays causes irreversible damage to living organisms, the benefits of examining, without surgery, the internal structure of the body outweigh the risks. This newly broad definition of radiology exceeded the parameters of its simple and direct reference of association to radioactivity. In fact, every technology developed to render "non-invasive" diagnoses has been embraced by radiology and enlisted into its service. These umbrella-crowders include ultrasound, positron emission tomography (PET), and most notably, MRI. Of these new technologies, MRI is regarded as the most versatile, sharing not only the historical idealism of non-invasive diagnosis, but also having in common with x-ray the electromagnetic spectrum. However, in opposition to x-ray, MRI resides at the low energy end of the spectrum, in the range of the radio

*Address correspondence to this author at the Pathology Research CNY-7, 149 13th Street, Charlestown, MA 02129, USA; Tel: 617-724-6593; Fax: 617-726-5684; E-mail: cheng@nmr.mgh.harvard.edu

[1] **Wilhelm Conrad Röntgen** (1845-1923), The Nobel Prize in Physics 1901 "in recognition of the extraordinary services he has rendered by the discovery of the remarkable rays subsequently named after him."(http://nobelprize.org/physics/laureates/1901/index.html)

[2] **Antoine Henri Becquerel** (1852-1908), The Nobel Prize in Physics 1903 "in recognition of the extraordinary services he has rendered by his discovery of spontaneous radioactivity." (http://nobelprize.org/physics/laureates/1903/index.html)

[3] **Pierre Curie** (1859-1906), **Marie Curie** (1867-1934), The Nobel Prize in Physics 1903 "in recognition of the extraordinary services they have rendered by their joint researches on the radiation phenomena discovered by Professor Henri Becquerel."(http://nobelprize.org/physics/laureates/1903/index.html)

[4] **Allan M. Cormack** (1924-1998), **Godfrey N. Hounsfield** (1919-2004), The Nobel Prize in Physiology or Medicine 1979 "for the development of computer assisted tomography." (http://nobelprize.org/medicine/laureates/1979/index.html)

1573-4056/05 $50.00+.00

frequency. Accordingly, one might claim that it was MRI which assisted radiology in becoming truly non-invasive.

The underlying technology of MRI is fundamentally different from that of x-ray. Since x-ray is mass-density based, when the mass within a particular region of an object is more dense, less ray penetrates this region, resulting in its appearing light in the eventual image. MRI is based on the quantum mechanic properties of the nucleus, which govern its behavior (orientation profile) when it is placed in an externally applied magnetic field. Acquisition of an image using MRI is not as straightforward as it is for x-ray. To understand MRI, particularly the topics of this review, MRS and MRSI, it is necessary to discuss very briefly the related physical principles. Expert readers may wish to proceed directly to the second section: The Current Clinical Usage of MRS and MRSI, while more determined learners may wish to read dedicated monographs on the principles of MRS.

1.2. A Few Principles of Magnetic Resonance

To physicists and chemists, MRS has been known as nuclear magnetic resonance (NMR) since its development in the 1940s. It is based on the quantum mechanic properties of nuclei, first predicted by theory and later observed experimentally in 1946 with technologies developed during World War II[5]. As NMR became clinically relevant, the word "nuclear" was abandoned to prevent misguided apprehensions arising from the common association, after WWII, of "nuclear" with nuclear fission. Thus, NMR became MRS both in the public arena and in certain scientific circles. MRI, discovered in the early 1970s[6], is an extension of NMR and is now commonly used for clinical diagnosis.

For a nucleus that possesses angular momentum (a.k.a. spin), quantum mechanics predicts that the energy levels of this nucleus will degenerate in a magnetic field. The splitting of these energy levels depends on the strength of the applied magnetic field (B_o), as well as the intrinsic properties of the nucleus, such as the gyromagnetic ratio. If a nucleus is unperturbed in the field, it will tend to stay at the lowest energy level, which is said to be in alignment with the field. Fortunately for biological investigations, most biologically relevant elements have isotopes (such as ^{1}H, ^{13}C, ^{31}P, ^{17}O, and ^{15}N) that possess this property (spin). To accomplish a transition between the degenerate energy levels, energy, in the range of radiofrequencies (rf), needs to be supplied.

The introduction of Fourier Transform (FT) to spectral acquisition has proved critical to the fundamental developments of modern MRS and MRI[7]. With FT, energy (in the form of the so-called "rf pulses") of different levels is supplied simultaneously and perpendicular to B_o, to the object of interest. The nucleus will resonate when the energy of this pulse equals the energy difference between these levels. The applied rf pulse, which is composed of a broad range of frequencies, will cause all nuclei of interest (e.g. ^{1}H) to resonate simultaneously. When the rf pulse is turned off, the spins of the resonating nuclei immediately begin to realign with B_o, and dephase due to field inhomogeneities. The rate at which the spins realign with B_o is termed T1 relaxation, or the longitudinal relaxation rate. The dephasing process that these spins undergo is termed T2 relaxation or transverse relaxation. The relaxation rates for a given nucleus depend on the surrounding physical and chemical environments.

The paramount importance of relaxation in terms of MR imaging was the discovery that relaxation rates vary with tissue type and disease [1]. Of particular interest for clinical evaluation was the observed increase in relaxation rates in the malignant cells. A large amount of work has been devoted to developing rf pulse sequences for MRS and MRI, based on the exploitation of these relaxation rates. The decay of the object or region's net magnetization due to these relaxation effects is called the free induction decay (FID), which is obtained in the time domain. Using FT techniques, the FID is converted into the frequency domain, generating the peaks which one sees in an MR spectrum. The effective magnetic field strength experienced by a particular nucleus is the sum of B_o and the induced fields resulting from the motions of electrons surrounding the nucleus. Therefore, the chemical environment has a perceptible influence on the field experienced by a particular nucleus and hence, the same nucleus may experience slightly different fields in different chemical environments. The end result is a slight difference in the energy level splitting. This phenomenon is known as chemical shift. Chemical shifts are very useful in MRS because they allow for the identification of different nuclei and functional groups within a molecule. With *in vivo* MRS, several molecules or metabolites are measured, many of which have overlapping resonances. A typical ^{1}H MRS measured at 1.5T with a clinical scanner is shown in (Fig. **1**).

In order to obtain a narrow linewidth in a MR spectrum, the object of interest must experience a homogeneous magnetic field. The extent to which the applied magnetic field is inhomogeneous will be reflected in the degree of broadening of the linewidth of each peak in the spectrum. To obtain the most homogeneous field in the volume of interest (VOI), a technique called shimming is used in both MRS and MRI, which uses many channels of electrical currents to generate induced fields in different directions in order to compensate for the inhomogeneities of B_o.

MR images are generated by applying a linearly varying magnetic field, known as a gradient, to the uniform field, B_o. Nuclei are localized by spatial encoding of the frequency of nucleus rotation in the FID signal. To obtain an axial MR image, one gradient in the z-direction is used for slice selection, while a gradient in the x-direction is used for frequency encoding, and a gradient in the y-direction is used for phase encoding. The phase encoding gradient is applied for a short period of time, and is turned off prior to data acquisition. This allows spatial localization of the nuclei, and thus, following a two-dimensional FT, an image of the object is digitally generated. A more detailed description of MRI

[5] Felix Bloch (1905-1983), Edward Mills Purcell (1912-1997), The Nobel Prize in Physics 1952 "for their development of new methods for nuclear magnetic precision measurements and discoveries in connection therewith. " (http://nobelprize.org/physics/laureates/1952/index.html)

[6] Paul C. Lauterbur (1929-), Sir Peter Mansfield (1933-), The Nobel Prize in Physiology or Medicine 2003 "for their discoveries concerning magnetic resonance imaging." (http://nobelprize.org/medicine/laureates/2003/index.html)

[7] Richard R. Ernst (1933-), The Nobel Prize in Chemistry 1991 "for his contributions to the development of the methodology of high resolution nuclear magnetic resonance (NMR) spectroscopy." (http://nobelprize.org/chemistry/laureates/1991/index.html)

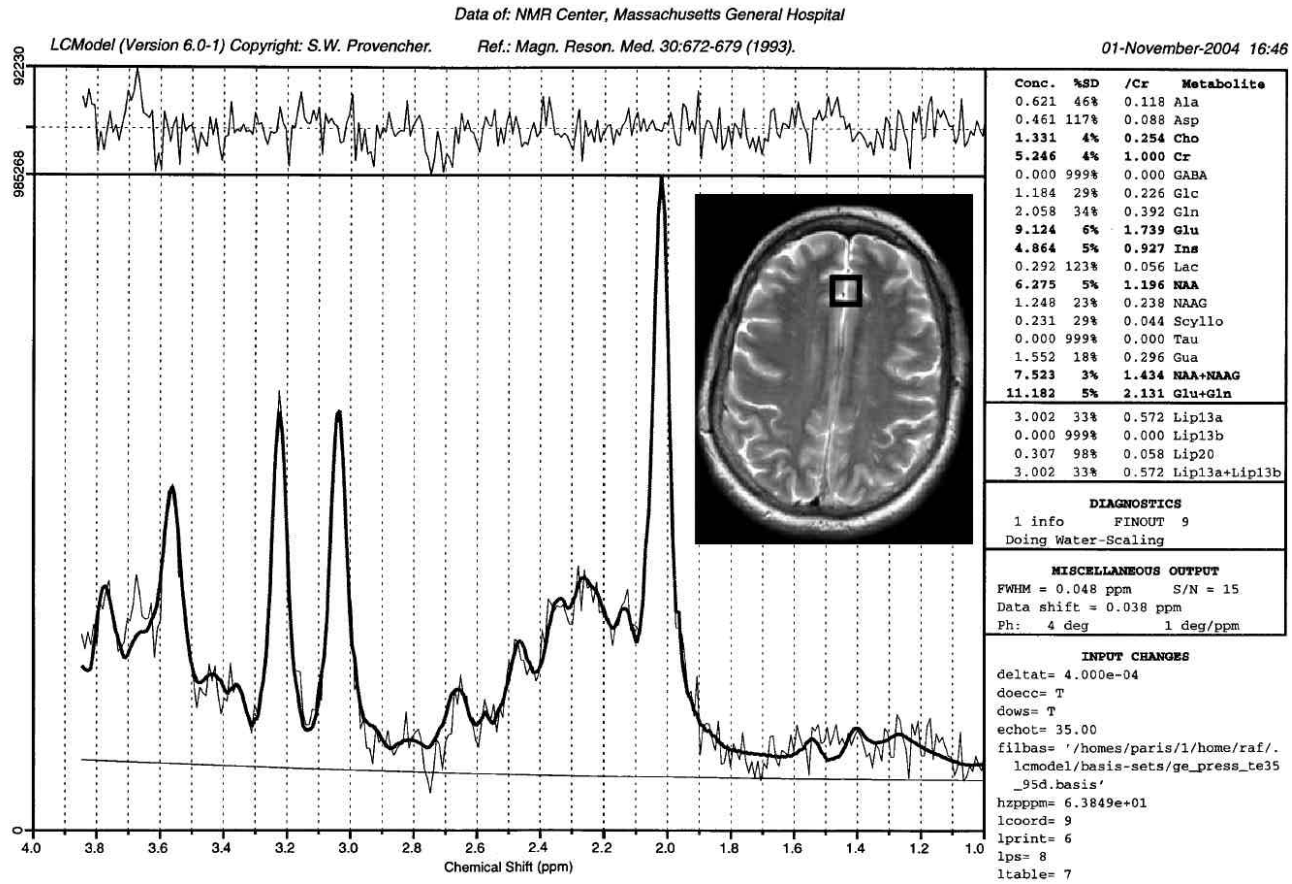

Fig. (1). A typical single-voxel ^{1}H MR spectrum measured from the frontal cortex of a healthy volunteer in a clinical GE 1.5T scanner. The brain region from where the spectrum was acquired is labeled with a square voxel, along with the caluclated metabolite concentrations from curve fittings using computer software LCModel [89, 90].

can be found in a variety of MR textbooks [2-4]. Readers with interest in the quantum mechanic principles of MR theory can find discussions in classical MR monographs [5, 6].

MRS has opened many frontiers in chemical investigation, while, ironically, the tremendous success of MRI in medicine reduced such investigations to a single chemical: water. In any biological object, such as a human body, there are many other interesting and potentially important chemicals than water. Therefore, built on the successes of MRI, progress in the past decade has brought *in vivo* MRS and spectroscopic imaging (MRSI) onto the radiology stage.

In radiology, MRS is employed to study cellular chemistry. MRS may be able to supply a chemical fingerprint of the biochemical state of the sample studied. The implications for the understanding of cellular metabolism and physiology are staggering. MRS has the potential to help define mechanistic details of disease progression and function as a non-invasive means of monitoring the effectiveness of treatments and therapies. What better non-invasive means exist to help unite the study of anatomic structure with function than the use of *in vivo* MRS and MR imaging?

1.3. Towards a Working Knowledge of MRS/MRSI

Reviewing the literature of MRS can be confusing even to readers familiar with it, particularly because of the non-standardized terminology used by researchers to describe experiments during the rapid development of the field. For a clinician interested in translating results “from bench to bedside”, the task of understanding the utility of MR technologies from a literature search can be daunting. In this review, we intend to demystify the acronyms of these techniques, and focus on areas where current research is being translated to clinical practice.

Most magnets currently used for clinical MRI are also equipped with the hardware and software necessary for acquiring MRS, as would be performed on a vertical magnet spectrometer found in the basement of a chemistry department at any university.

The majority of MRSI currently performed is the so-called metabolic imaging. Several variations of this technique exist, and some confusion is present in the terminology. However, the general approach is to use a multi-voxel spectroscopy sequence in which the VOI is localized from the MR images and selective saturation bands are used for outer voxel suppression. Other than additional

complexity due to its multi-voxel nature, MRSI is not fundamentally different from single-voxel MRS. MRSI is often referred to in the literature as chemical shift imaging (CSI), or occasionally as *in vivo* MRS, making it easily mistaken for single-voxel MRS experiments. MRSI has found its most important clinical applications in neurological and oncological evaluations, because of its ability to distinguish between normal and abnormal metabolic profiles at high spectral resolutions. In this review, we will use MRSI to refer only to multi-voxel techniques, and "*in vivo* MRS" or simply "MRS" to refer to single-voxel evaluations if the latter is clearly distinushable from *ex vivo* MRS beased on the context.

In addition to MRSI, there have been developments in other types of metabolic imaging that are gaining popularity, among them, the most noteable echo planar spectroscopic imaging (EPSI). EPSI is based on Mansfield's technique which allows the simultaneous and rapid acquisition of spatial and spectral data. Furthermore, availability of high field strengths and an interest in measuring low gyromagnetic nuclei of biological importance, such as ^{31}P and ^{13}C, have also shown promise for advancing the clinical utility of *in vivo* MRS and spectroscopic imaging.

While the focus of this review is ^{1}H on *in vivo* MRS and MRSI, it is important to note that MRS experiments have been carried out both on solutions of purified chemical extracts from excised tissue samples, and on intact tissue specimens for more than 20 years, yielding a wealth of results. These experiments are typically described as "*ex vivo* MRS" or "MRS on extracted metabolites". Interested readers are encouraged to examine the many excellent reviews of these topics. Because of the limited scope of this review, we do not intend to cover these results, except for those observed with intact tissue specimens that may have direct benefits for the discussion of *in vivo* observations.

The following sections will outline details of *in vivo* MRS and MRSI techniques, their clinical utility, and our comments regarding clinical applications of these techniques. Because of the enormous volume of published clinical results and because of our limits, we will focus in this review on clinical concerns and the applications of *in vivo* MRS and MRSI, with particular consideration to many of the results published between January 2000 and October 2004. Reviews of clinical work prior to 2000 can be found in a large number of excellent, already published reviews.

2. THE CURRENT CLINICAL USAGE OF MRS AND MRSI

Experimentation with *in vivo* proton (^{1}H) MRS was initiated after the development of ^{1}H MRI, roughly 20 to 30 years ago. It is difficult to determine specifically when and by whom the first, single-voxel *in vivo* (human) MRS was observed. However, it most certainly predated the observations of MRSI in the early 1980s both on ^{1}H and ^{31}P [7, 8]. Many reasons can be cited for presence of ^{31}P in the sequence of developments of MRS, including the importance of phosphorus in biological processes, and limits of several techniques essential for ^{1}H measurements, such as water suppression, automated shim routines and development of localization methods in the early age of surface coil techniques [9-11]. The massive physiological concentration of hydrogen within living organisms, and the large natural abundance of its MR active isotope, ^{1}H, with its high gyromagnetic ratio makes it remarkably suitable for MRS studies. In the mid 1980's, many of the techniques essential for proton measurements were developed, making the clinical use of ^{1}H MRS and MRSI a testable concept [12-14]. By 1983, the first *in vivo* ^{1}H MRSI was reported on a human forearm [7]. This technique was based on a simple modification of the three-dimensional fourier zeugmatography method outlined in 1979 [15, 16], and latter described in a theoretical paper in 1982 [17].

The reports discussed in this review, if not otherwise specified, were measured at the magnetic field strength of 1.5T (T – Tesla, the unit for magnetic field strength, named after Nikola Tesla 1856-1943). To give context to this magnitude, the average Earth field strength is on the order of 0.00005T. For readers who still remember the details of their experience with NMR in organic chemistry lab, 1.5T is equivant to 64 MHz, for it is the resonance frequency of ^{1}H at this field strength.

2.1. Proton Single Voxel Spectroscopy – *In Vivo* MRS

Diseases that cause a functional disturbance at the cellular level are potential systems for *in vivo* MRS evaluations. The need for non-invasive diagnostic tools is the driving force for much of *in vivo* MRS investigation. Currently, the widest clinical application of MRS is to the study of neurological conditions ranging from stroke, ischemic brain injury, HIV and infectious diseases, Central nervous system (CNS) degenerative brain diseases, and peripheral nervous system diseases like multiple sclerosis. Another area to which MRS is already widely applied is human oncological evaluations, for instance, of brain tumors and prostate cancer for which treatment options are limited and non-invasive diagnostic methods are greatly appreciated. Recently, MRS reports have been seen in studies of human breast and cervical cancers.

2.1.1 Techniques

In vivo MRS is performed using clinical imaging systems, or scanners, and more often than not results are combined with imaging studies. The major, and perhaps only difference between *in vivo* MRS of a human and MRS measurements in a chemistry department with a sample tube is the necessity to localize a VOI within the body for *in vivo* MRS. In contrast, MRS of a chemical is performed on the entire volume of the sample. The same whole-sample approach is also practiced occasionally in biomedicine when a global value is desired, for instance in measuring and monitoring the total brain n-acetyl aspartate (NAA) level in volunteers [18], and in multiple sclerosispatients [19]. However, generally, *in vivo* MRS obtains a FID of a single-voxel VOI that is defined by the user from a previously acquired scout image, using one of two localization pulse sequences: point-resolved spectroscopy (PRESS), or stimulated echo acquisition mode (STEAM). These pulse sequences were developed in the 1980s for the purpose of exciting nuclei only in the assigned VOI [20, 21]. When reviewing reports of measurements with these methods, readers inevitably will encounter the abbreviations TR, TE

and sometimes TM, which mean recycle time, echo time, and mixing time, respectively. These terms refer to the delays in the pulse sequences used to record the localized FIDs. There is another localization approach, (ISIS for image selective *in vivo* spectroscopy) which excites an entire region, and subsequently subtracts signals originating from beyond the VOI, but this approach has been applied less frequently in recent years.

After the identification of the VOI, and before the acquisition of the FID, the user needs to perform magnet shimming, most likely, in a modern imager, by invoking the automatic shimming procedure to ensure that the applied field in the VOI is maximally homogenous. Another technical point that merits emphasis is that since MRS is not a technique of high signal-to-noise ratios (SNR), most often, signal averaging is necessary, which understandably requires the VOI, in other words the subject, to be motionless during the period of data acquisition.

As previously indicated, where *ex vivo* data is available, we will review clinical results of *in vivo* MRS (as well as of MRSI in Section 2.2) for a particular disease in the context of its *ex vivo* measurements. However, we will restrict our discussions to intact tissue studies either with conventional MRS or with the recently developed high resolution magic angle spinning (HRMAS) MRS approach, and exclude measurements on tissue chemical extracts. Solutions of tissue extracts can produce high-resolution spectra, allowing for the identification of individual metabolites which is unachievable from the broad-line spectra of conventional MRS. However, the extraction process is destructive and has been found to alter the spectroscopic results to an unknown degree [22], depending on the procedure used and the thoroughness of extraction. The tested benefit of the HRMAS MRS approach is that it allows for the identification of individual metabolites from intact tissue studies, as with extract solutions, while also preserving the tissue structure, making possible subsequent pathological studies of the same tissue.

2.1.2. Clinical Applications

Because the ability to detect a chemical depends directly on its abundance in a sample, single-voxel techniques, which acquire data from a relatively large area, are ideally suited for examining less prevalent metabolites, and for detecting other non-proton nuclei of low natural abundance. The primary function of *in vivo* MRS has been to identify metabolic markers of diseases, and to distinguish pathological from normal tissue. Because of the complex pathophysiology of human disease, it is not surprising that the search has met with only limited success.

With the amount of information that can be obtained using *in vivo* MRS, it may be difficult for a person interested in a particular disease to know where to begin an MRS experiment. In the next several sections we will look at the most relevant ways MRS contributes to the clinical setting, and discuss the particular metabolites that are most interesting to study in some of the systems in which MRS is most commonly used. Here, we wish to emphasize that in most cases or in general, there is not a single metabolite whose presence or absence alone directly corresponds to the presence or absence of a particular disease condition. However, there seem to be exceptions.

2.1.2.1. Neurological Disorders

In the brain, for example, the amino acid NAA is interpreted as a marker of neuronal cell health, and its changes have been recorded in both neuronal injury and death. Although tissue contains many cell types, the finding that NAA in the adult brain is detectable only in neurons and not in glial cells, the two major components of brain tissue, provided excellent support for the use of NAA to study pathologies targeting neurons [23, 24]. Other metabolites of importance in brain MRS include myo-inositol (MI, a sugar present only in glia), choline-compounds (Cho), and creatine (Cr) as well as lactate (Lac), which although are not specific to neural cells, are often elevated in the pathological processes of inflammation and necrosis, respectively [25].

The substantial clinical contribution of ^{1}H MRS of the brain is due in part to the difficulty of obtaining brain biopsy specimens, which has driven researchers to find a means to investigate neurological disorders non-invasively. Other reasons explaining the large number of neurological studies using MRS are the brain's homogeneous nature (relative to other organs) and its lack of major physiological motions. Having these requirements and advantages, brain studies provided the impetus for technological improvements and innovations in many areas of MRS including developments of pulse sequences, outer volume suppression methods for better suppression of lipids from nearby tissue, functional imaging, and the use of high field magnets (e.g. 3T or higher). In general, high field experiments improve not only image quality by increasing SNR, but also spectral quality by resolving spectral components that normally overlap at 1.5T.

In vivo MRS studies of brain have penetrated almost every subject of neurology and neuropathology. *In vivo* MRS may be particularly well suited for studies of neurological conditions that affect a large volume of tissue somewhat uniformly. However, even our limited survey of this body of work has presented us with a rich coverage of MRS clinical investigations of various neurological diseases. The topics include neuro-anatomy, vascular, infectious, demyelination, degenerative diseases, metabolic disorders, trauma, epilepsy, psychiatry, and the impact on the brain of non-neurological diseases such as pulmonary, liver, and cardiac conditions.

Neuro-Anatomy Studies

The rationale of employing the single-voxel procedure is very well illustrated by a number of neuro-anatomy studies, including those which have measured metabolite levels of human fetal brains at 30 to 40+ weeks gestational age [26-29], of healthy elderly subjects in two VOIs [30], and of the cervical spinal cord [31].

The single-voxel approach is best suited for investigations in which either a large sample size is preferred for achieving an optimal SNR, as in fetal brain studies, or the structure of the experimental object is irregular and small in certain dimensions, exemplified by the spinal cord. It was found that with the cervical spinal cord, because of the susceptibility effects of the surrounding tissue, the optimal result could be obtained with the elongated voxel (9x7x35

mm^3) placed at the inferior end of vertebral C2. The study used PRESS and demonstrated that the concentration of NAA in the cord is lower than that in the brainstem, but higher than that in the cortex and cerebellum. Cr in the cord was lower than in the cerebellum, but no statistical differences were observed with cortex and brainstem [31].

In fetuses, the underdeveloped brains are known to be have a high concentration of water, and measurable metabolite concentrations are expected to be lower than in adult brains, hence the largest possible voxel sizes are desirable. Larger voxel size would also translate into high SNR and would require less measurement time. Shorter measuring time was also critical in reducing the effects of motion by the fetus. A number of commonly observed brain metabolites, including MI, Cho, Cr, and NAA, were quantified and expressed as functions of fetal gestational age for 35 normally developing fetuses, with VOI between 15 and 40cc, which to some degree reflected the growth of the brain during the third trimester. The most interesting result was that among these quantified metabolites, only the increase with age of neuron-specific NAA was determined statistically significant. In this study, both STEAM (TR/TE/TM: 2500/20/30ms) and PRESS (TR/TE: 2500/15ms) were used. No observable difference between the two methods was noticed [28].

Vascular Disease

Single-voxel MRS can be used to detect sensitively the Lac signal to observe the recovery of brain tissue following a stroke from the acute stage through the subacute and chronic stages of neuronal recovery [32]. MRS has also been used, with a double-blind, placebo-controlled study, to assess the effect of a sodium dichloroacetate infusion on the Lac level of the lesion. Reductions were seen with high doses, and with patients treated within the first two days following infarction [33]. However, MRS results so far have shown that with ischemic stroke, the level of Lac never returns to normal. Here, the advantage of employing single-voxel measurements is evident because the interest is localized on the lesion and the study's question is focused on the measurement and interpretation of the temporal changes. To improve the sensitivity of MRS evaluation of stroke, diffusion weighted imaging (DWI) has been introduced to identify regions of ischemia for the placement of MRS VOI. DWI is the most sensitive test for detecting the occurrence of an ischemic stroke within a few hours of a cerebrovascular event. The sensitivity of DWI to stroke can be utilized in the selection of VOI for metabolic MRS studies, in order that they may find more sensitive predictors of neurological deficits resulting from stroke injury [34].

MRS can be used also to probe the pathogenesis of stroke [35]. Like NAA to neurons, MI is proposed to be a metabolite specific to the glial cells. However, declaring MI a marker of cell density can be problematic. Glial cells increase the production of MI in response to osmolarity changes, which often accompany brain injury. In addition, glial cells proliferate in response to neuron damage in a process known as reactive gliosis. In many studies, the proposed role of the metabolite measured in MRS is an indicator of pathology, but when the metabolite's synthesis is altered or degraded in response to cellular injury, as may be the case in stroke, the relationship of the metabolite to the pathogenic process is obscured. Understanding the physiology of the pathogenic process aids in the interpretation of metabolite ratios, or "markers", in terms of their relationship to the disease. The role of a measured metabolite is not only to be an empirical statistic associated with the disease, but also to provide possible directions toward therapy design and patient follow-up.

Trauma

While Lac can be used as a marker for brain recovery from stroke, it also appears to have predictive value in determining the outcome of patients who have suffered from perinatal asphyxia and pediatric closed head injury [36-40]. However, this predictive power was found lacking in cases of adult traumatic brain injury. While some reports indicate changes in Lac in this group, others reported conflicting observations [41-45].

Infectious Disease

The most publicized infectious disease MRS has been utilized to understand is HIV infection and the dementia it causes (NeuroAIDS) [46-48]. The selection of the single-voxel MRS approach in these studies was motivated by the aim of measuring possible correlations between cerebral metabolites in well hypothesized brain regions (frontal lobe and basal ganglia) with cognitive function and clinical variables, such as CD4 counts, plasma and CSF viral loads [46, 47].

In a correlation study, 45 antiretroviral-naïve HIV patients were recruited. The study was designed to test, and later confirmed the hypothesis that MI and Cho, suspected glial markers, should be elevated due to glial proliferation caused by virus infection. Measuring patients before antiretroviral treatments avoided possibly confounding factors introduced by treatment agents. The authors warned that future MRS studies of HIV patients should consider using metabolite concentrations rather than the ratios over Cr, since Cr may also change during the course of the disease [46].

A MRS study involving a consortium of eight medical centers throughout the U.S has been reported. It was designed to evaluate the effect of an AIDS Clinical Trials Group (ACTG) phase II trial of memantine, a N-methyl D-aspartate (NMDA) receptor antagonist, as treatment of neuroAIDS. The first consortium's report on 58 patients indicated that neuroAIDS might correlate with significantly elevated Cho/Cr and MI/Cr levels in the basal ganglia, and NAA/Cr reduction and MI/Cr elevation in the frontal white matter. Although these results of the study were useful confirmations of the predictions based on previous measurements, the valuable contribution of this multi-center report reached beyond its tabularized results, presenting a quality control paradigm that may be adopted by future multi-center MRS studies or clinical trials of other diseases [47].

Brain abscesses, another form of infectious disease, have also been evaluated by MRS. With brain abscesses, the benefit of a single-voxel is evident by the presence of lesions, easily identifiable by imaging [49, 50]. Unlike

HIV/AIDS studies, abscess studies often have the opportunity to obtain pus samples for *ex vivo* analyses. *Ex vivo* analysis of these pus samples using high field MRS methods (for instance at 4.7T) can produce high resolution spectra, from which metabolites can be identified, even verified with two-dimensional correlation spectroscopy. In combining the applications of *in vivo* and *ex vivo* MRS, it was possible to differentiate anaerobic and aerobic sterile brain abscesses based on their metabolite patterns [50].

Demyelinating Disease

Multiple sclerosis (MS) is perhaps the best-known demyelination disease. Since MS is a global white matter disease, it is best suited for multi-voxel analysis, as will be discussed in the later sections. Nevertheless, single-voxel approaches have been employed to study identifiable lesions caused by the disease. It has been shown with measurements of NAA, Cho and Cr in the parieto-occipital region, that NAA/Cr, Cho/Cr, and NAA can differentiate primary from secondary progressive lesions, and NAA/Cr as well as the absolute concentration of NAA can differentiate normal-appearing white matter (NAWM) from both primary and secondary progressive lesions [51]. Another interesting study reported the relationship between NAA levels and the major CNS myelin protein, proteolipid protein (PLP1), and concluded that axonal degeneration might occur due to the lack of PLP1. By using an animal model of PLP1 deficiency, they concluded that the degeneration process is length-dependent, but not associated with significant demyelination [52]. However, a reported measurement of the whole-brain NAA level did not find correlation with MS clinical status scale scores for 49 relapsing-remitting MS patients [19].

Neuro-degenerative Disease

The class of diseases described as neuro-degenerative presents a number of familiar names, Alzheimer [53-58], Parkinson [59, 60], ALS [61-66], etc., all of which have been actively pursued by single-voxel MRS.

Among the Alzheimer (AD) reports, we noticed a longitudinal (a one-year gap between studies of the same subject) quantitative study of hippocampus of nine probable AD patients with 14 age-matched control subjects. Lower hippocampal NAA levels for the cognitively impaired patients were observed relative to controls, however the changes within the one-year period were not significant [56]. An interesting report of 18 AD patients and 12 healthy controls dealt with glutamate and glutamine measurements at 0.5T [53]. Glutamate is an energy metabolite and the most abundant neurotransmitter in the brain, while glutamine, a product of the glutamate cycle, is transferred from glial cells to neurons after exocytotic release of glutamate into the synaptic space. Both metabolites are critical for a number of neuronal functions, and are expected to play important roles in AD. In the report, the authors clearly demonstrated that while the sum of glutamate and glutamine (Glx) could be seen in the 0.5 T spectrum of cingulated cortex, and a significant reduction in Glx was found with AD patients. However, the same Glx signal was not observed with the same subjects in a 1.5 T spectrum. Including Glx, in addition to NAA and MI, for the metabolite diagnosis of AD resulted in an increase in sensitivity from 78% to 89%.

NAA is a proposed neuronal marker of injury, damage, and death, and nearly all MRS studies of AD seem to measure changes in NAA and discuss its changes. However, a study comparing elderly subjects with chronic hypertension, early AD and healthy controls (ten in each group) revealed significantly elevated MI/Cr ratios in both disease groups, but no differences in either NAA or Cho ratios between the three groups [55]. The lack of NAA reduction in early stages of AD may suggest that neuronal injury at the tested stage is not MRS apparent, or that neuronal death at the later AD stages is responsible for the commonly reported NAA decrease with AD. The latter conclusion is supported by autopsy studies of AD brain tissues. For instance, an *ex vivo* HRMAS study showed correlations between MRS data and stereological pathology for AD brains (n=7), and confirmed the proportionality of NAA concentration to neuronal density. This study also demonstrated the quantitative nature of the NAA and neuronal count relationship, as the linear correlation intercepted at zero (–0.29±1.15 _mol/g) [67].

It is not surprising to see NAA levels affected in Parkinson disease (PD), as it is also a neuro-degenerative disease. For example, a study comparing PD patients with (n=14) and without (n=12) dementia to healthy controls (n=13) suggested that NAA in the occipital region could identify PD patients with dementia, while no differences in MI levels were seen between the groups. The study suggested that by combining measurements of NAA with MI, PD might be differentiated from AD, where MI increases have been frequently observed [60]. The indicative value of NAA/Cho in the evaluation of PD after thalamotomy was reported in a study of 15 patients who underwent surgeries for control of Parkinsonian tremor, and the results were compared with 15 age-matched control subjects. It was indicated that patients who improved after stereotactic thalamotomy had significantly reduced post-surgical NAA/Cho values compared to levels measured prior to the procedure in both substantia nigra and thalamus, but not in putamen. However, the changes were not significant if evaluated by ratios of NAA/Cr and Cho/Cr [59]. Without the opportunity to evaluate brain tissues of PD patients (which is a general difficulty with studies of neurological disease), a recent report compared metabolite levels in cerebrospinal fluid (CSF) for PD patients and controls. However, this approach yielled no significant results [68].

Amyotrophic lateral sclerosis (ALS) is a neuro-degenerative disorder with unknown cause which has also been measured extensively by *in vivo* MRS [61-64, 66]. The hallmark of these studies is the observation of a decrease in NAA, or NAA/Cr, occasionally accompanied by observations of MI and Cho increases, particularly in motor cortices, and its correlations with clinically evaluated neurological functions [63, 64]. A recently reported longitudinal study evaluated the motor cortices of 70 ALS patients and 48 healthy controls [66]. These patients were divided according to the EL Escorial Criteria into subgroups of suspected, possible, probable, and definite ALS. The concentration results showed that both NAA and Cr were reduced in patients compared with controls, while no Cho differences were detected. When the results were arranged by metabolite ratios, they showed reductions of NAA/Cho

and NAA/Cr with all subgroups, while an increase in Cho/Cr was detected only with definite ALS patients. Sixteen of these patients were followed for an average of one year (12.1±8.7 months), and showed a further reduction in NAA/Cho of 9.1%. A 7.0% increase in Cho/Cr was found to correlate with disease progression [66]. The study indicated that *in vivo* MRS might eventually be used clinically as a means of non-invasively monitoring neuro-degeneration and the effects of therapy strategies, at least for ALS.

Metabolic Diseases

A number of *in vivo* MRS studies on metabolic diseases were found, including a study of adrenoleukodystrophy for the evaluation and prediction of patient outcomes with hematopoietic stem cell transplantation therapy [69], and the searches for the mechanism of cerebrotendinous xanthomatosis with NAA/Cr and Lac/Cr levels [70]. Studies were also seen in diabetes mellitus [71], and most interestingly, after the lengthy discussion of NAA, Cho, MI, and Cr, in phenylketonuria by measuring phenylalanine (Phe) signals resonating at the opposite spectral side of water signals from the other metabolites [72]. In this study, brain Phe levels presented as Phe/Cr ratios were measured from ten patients, four in earlier stages and six in later stages, each whose disease was detected and treated. The Phe/Cr ratios were correlated with clinical, biochemical, and MRI findings. The study showed that in both groups brain Phe/Cr levels correlated with plasma Phe concentrations, and with clinical phenotype for patients whose disease were detected in later stages.

Changes in brain metabolites due to non-neurological diseases have been investigated and measured extensively. These studies cover a wide spectrum of conditions represented by inflammatory diseases such as systemic lupus erythematosis with reduction in NAA and increases in MI and Cho [73, 74], chronic pain with reduction in NAA and glucose [75], chronic fatigue syndrome with increases in Cho/Cr [76], chronic obstructive pulmonary disease [77], liver cirrhosis with decreases in Cho and MI and increases in Glx [78-80], and dilated idiopathic cardiomyopathy with decreased Cr and lipid levels [81].

Psychiatry

The psychiatric topics addressed by *in vivo* MRS cover an array of conditions, although our inclusion of certain topics may be somewhat liberal, such as the observations in panic disorder of disorder-related reduction of γ-aminobutyric acid (GABA) in the occipital cortices for 14 patient-control pairs [82], and decreases of Cr in the right medial temporal lobe in patients (measured from 11 patient-control pairs) [83], or the evaluation of mood in terms of the Positive and Negative Affect Scale by the levels of Cho in the left frontal lobe [84], .

Studies of classical psychiatry also tested the utility and reproducibilty of MRS. NAA, Cho and Cr were evaluated in the left frontal white matter and caudate nucleus for schizophrenic patients, but no significant metabolite differences were observed between scans of a one-week gap for 12 patients. While NAA was found to have a small coefficient of variance in all brain regions examined, Cr and Cho measured in the left caudate nucleus were found to have larger variance (16-18%) [85]. Evaluations of NAA in the dorsolateral frontal lobe for children with attention-deficit/hyperactivity disorder (ADHD) have also been reported. 23 patients and 24 controls were enrolled in the study, but no significant difference between them was recorded [86].

As a prominent category of neurological disorders, epilepsies present a clinical phenotype that may be caused by a variety of neurological conditions. This presents epilepsy as a fundamentally global disease of the CNS, which is therefore best suited for MRSI examinations, rather than a local disorder of certain brain structures for which the single-voxel approach would have many advantages. We noticed that most often epilepsy is reported in the temporal lobe (TLE), according to clinical observations, and there have been single-voxel studies of TLE reported, for instance the study of the complementary roles of MRS and diffusion-weighted MRI [87], and the comparison between MRS and PET [88]. However, a large volume of epilepsy studies have utilized the MRSI approach, and we will defer our detailed epilepsy discussion to the later MRSI section.

In conclusion, in single-voxel MRS applications to neurological conditions, other than for a few specific diseases, the majority of measurements are centered on the analyses of NAA, Cho, Cr, and MI, which most of time are the only resolved signals in an *in vivo* brain spectrum. Nevertheless, efforts have been employed to identify other brain metabolites, for instance, those in brain tumors, using automated spectral analysis programs based on model compound measurements. One of the most popular and commonly used spectral analysis programs for MRS is the linear combination (LC)Model [89, 90]. To conduct an analysis of this type, a basis-set specific to each scanner should be constructed using *in vivo* phantom measurements on the scanner for every expected metabolites. The knowledge of the chemical shift values for these model compounds is necessary, and interested readers are encouraged to start the pursuit from reviewing the existing data reported for *in vitro* measurements of brain metabolites [91].

With the status of current MRS techniques, it is impossible to definitively diagnose a neurological disease based purely on the changes observed in a limited number of metabolites. However, as discussed, the reported changes in different brain regions even for a single metabolite may be meaningfully indicative of the underlying disease. Therefore, to achieve disease diagnosis, or to test the ability of MRS in disease detection, the simultaneous mapping of different metabolites in different brain regions may be necessary, which is the strength of MRSI.

2.1.2.2. Oncological Diseases

The brain has more restricted physiological motion, and a more homogeneous structure compared to other organs, which is why it has been the subject of a large number of MRS studies. This fact, combined with the ability to visualize easily a lesion on the brain and to prescribe a VOI through MR images, encouraged the extensive pursuits of MRS studies of brain tumors. If the heterogeneity within a single tumor is the focus of the examination, MRSI tends to

be the more desirable evaluation method. The main advantage of single-voxel measurement in tumors is that it leads to a spectrum with a higher SNR than that usually achievable with MRSI.

Single-voxel MRS is not a screening tool. Mostly, it is used to further investigate suspicious lesions identified in brain images. Therefore, the primary utility of MRS is to differentiate a tumor lesion from other brain mass presented in an image. There are two other main functions of MRS: to achieve non-invasive diagnosis of the tumor, and to monitor both the response of the tumor and other changes in the brain resulting from therapy. It warrants emphasis that until now all studies had either the nature of feasibility evaluations, or the status of clinical trials. To the best of our knowledge, there exists no clinically approved MRS protocol in oncological clinics. Therefore, in most of the reported studies, the accuracy of MRS results was determined at final biopsy conclusion.

Brain Tumors

MRS covers the entire spectrum of functions that a radiology tool is expected to contribute to the oncological clinic. These functions include: detection of neoplasm, characterization of tumors, and monitoring the effectiveness of therapy. Since the most commonly encountered brain tumors are gliomas, the majority of MRS studies on brain tumors are centered on this type of tumors, although we noticed that the approach developed for them has been applied to the evaluations of non-malignant brain lesions, such as neurofibromatoses [92] and epileptogenic hypothalamic hamartomas [93].

The detection of tumors from metabolite measurements has been reported in the context of differentiating lesions of tumors from those of other origins, such as large inflammatory lesions [94] and inflammatory demyelinating disease [95] that mimic tumors in both CT and MR images. It has been reported that in order to differentiate cerebral ischemia lesions from tumors, the apparent diffusion coefficients (ADC) of NAA and Cr must be taken into consideration [96]. The technique of measuring brain metabolites with single-voxel MRS has also been applied to the detection and identification of pediatric brain tumors. However, because of the developing status of brain metabolism in children, a study of this nature must include age-matched control subjects [97].

Many recent reports on the diagnosis or characterization of brain tumors by their types and grades have included large patient numbers, on the order of more than 100 [98-100]. The different types of tumors studied were astrocytomas (WHO II), anaplastic astrocytomas (WHO III), glioblastomas (GBM, WHO IV), medulloblastomas, meningiomas (MNG), and metastases (MET). The evaluated brain metabolites included Cho, Cr, NAA, Lac, lipids, and in some studies alanine and Glx. When metabolite results were included in the diagnostic parameters obtained from MRI, it was reported that the number of correct diagnoses increased (15.4%), while the number of incorrect and equivocal diagnoses decreased (6.2% and 16%, respectively), from diagnoses using MRI parameters alone [100].

An elaborate algorithm for discrimination of the most common brain tumors has been proposed based on the measured values of metabolites [99]. Another study, although with a smaller number of patients (n=42), also reached a diagnostic scheme by involving a 2D plot of (alanine+lactate+lipids) vs. MI/Cho. The resulting 2D field was divided into four areas: WHO II, III, MNG, and a mixture of GBM and MET, where GBM and MET were the worst possible conditions [101]. Furthermore, the specific ability of MRS to identify lipid signals for both the diagnosis of GBM and the possible transformation of low-grade tumors to GBM, was reported [102].

These *in vivo* observations were in close agreement with *ex vivo* MRS analyses of human brain tissue performed in the past ten years. For instance, examination of brain tumor tissues by MR spectrometers similar to those used for chemical analyses, suggested the diagnostic importance of lipid metabolites. Correlations between the MR lipid signal intensities and the amount of necrosis in astrocytomas were reported in 42 cases, where the intensity of the mobile fatty acyl –(CH=CH)– resonance differentiated with statistical significance three tumor groups with varying amounts (0%, 1-5% and 10-40%) of necrosis [103].

Recently, with the development of HRMAS, ^{1}H MRS for intact tissue analysis[8], high resolution brain tumor spectra can be measured, for the first time, with detailed profiles of both water-soluble metabolites, as can be obtained from extract solutions, and lipids. A study of 19 brain tumors, including astrocytomas, GBM, MNG, schwannomas, and normal brain, reported that metabolite concentrations both in absolute units and relative ratios normalized to the Cr (3.03 ppm). Metabolite concentrations from intact tissues, and from tissue extracts of the same tumors were compared to each other and to the literature values. While the concentrations of some metabolites measured by HRMAS MRS were similar to those measured from extracts, concentrations of others were much higher in tissue than they were in extracts. However, it should be noticed that the capability for metabolite concentrations to differentiate tumor types was reported based on clinical data, rather than on detailed histopathology of the tissue samples examined by *ex vivo* MRS [104]. Because of tumor histopathological heterogeneities, the reported correlations might be considered only as a proof of concept, in light of a later report which analyzed quantitative histopathological data obtained from the same brain tumor specimen after the *ex vivo* MRS study. Quantitative histopathological evaluation accounted for the observed spectral differences measured between different regions of a single tumor as consequences of extensive tumor microheterogeity. Particularly, correlations were observed between the amount of tumor necrosis and the concentrations of mobile lipids (R^2=0.961, $p<0.020$) and Lac (R^2=0.939, $p<0.032$), and between the numbers of glioma cells and the ratio of the phosphocholine to choline resonances (R^2=0.936, $p<0.033$) [105]. The strong

[8] Magic-angle spinning, originally used to reduce resonance line-width in solid-state NMR, subjects samples to fast mechanical rotations (~kHz) at the magic-angle, (54°44') away from the direction of the spectrometer's static magnetic field while spectroscopy is recorded. When applied to intact tissues, HRMAS can produce high spectral resolution metabolite spectra that allow identification of individual metabolites, while leaving tissue pathological structures intact.

linear correlation between tissue necrosis (%area) and lipids (mM) indicates that the amount of tissue necrosis can be estimated using the measured concentration of lipids from MRS, which agrees well with *in vivo* results.

The diagnostic value of automated pattern recognition analysis of brain tumor single-voxel MRS has been tested and reported by a study involving three clinical centers [106]. This study included 144 patients of four different tumor types: WHO II, GBM, MNG, and MET, and reported an accuracy of over 92.3% in characterizing individual cases according to the automated pattern recognition.

Of special interest in tumor detection and diagnosis is the elevation of Cho observed *in vivo*. These compounds are associated with cellular proliferations, although the exact biochemical events underlying these experimental observations are still unknown. However, with brain tumor studies, the correlation between Cho and cellular proliferation seems strong as a number of studies have shown the linkage between elevated Cho levels and proliferative activity, measured by the immunohistochemical marker Ki-67 (MIB-1) [107, 108]. However, one must exhibit caution in examining reported results of this nature because of the heterogeneity of the disease, and the lager (>1000) differences in scale between the measured volumes of MRS (>1 cm^3) and immunohistochemistry (~1 mm^2).

The elevation of a unique metabolite, glutathione, observed in *in vivo* MRS, has been associated with the diagnosis of meningiomas, a finding reported by a study of a small number of cases (n=6). Although the presence of the compound was not obvious upon visual evaluation, it was revealed and quantified by curve fits of the LCModel. The MRS results on glutathione were shown to be in agreement with the published data obtained with other chemical methods [109].

In addition to using sophisticated spectral analysis software, such as the LCModel, to achieve diagnostic conclusions, investigators may need to consider the experimental conditions upon which the spectral data are obtained. These considerations have a fundamental importance to any conclusions that one may hope to reach. Since almost all *in vivo* MRS are measured with a certain echo time, the relaxations that occur during those echoes reduce the measured concentrations from their intrinsic levels. Hence, corrections may be necessary. However, since such corrections can only be achieved with time-consuming calibrations, they are not feasible to conduct experimentally for each individual case. Instead, corrections according to tissue types may be measured and used [110] to validate the diagnostic values of tissue metabolite levels for certain diseases. These tissue-type specfic correlations permit the comparison of results, where the values are recorded under the same experimental conditions with the same amounts of relaxation time.

Another commonly encountered possible experimental artifact relates to the measurement sequence of MR examinations. As previously discussed, the advantage of MRS is to further investigate the chemical composition of a lesion identified by MRI. Nowadays, most MRIs are measured with the assistance of agents that enhance the contrast of the diseased lesion for interpretation of disease anatomy. The possible influence of these administered contrast agents to the resulting spectral data needs to be carefully evaluated before the data is employed for the dissemination of information about the disease. In reference to the commonly used Gd-DTPA agent, it was found that although it broadened the linewidth of Cho in gliomas, the changes in the peak areas of Cho were not significant [111]. Similar evaluation needs to be undertaken for other agents before there is any attempt to correlate MRS chemical data with diseases.

In vivo MRS measurable brain tumor metabolic profiles have been tested as a non-invasive means, both for children and adults, of monitoring tumors and their responses to therapies, including radiation effects [112-114], and chemotherapy differences [115, 116]. The potential contribution of MRS non-invasive monitoring towards the design of brain tumor treatments is apparent in its alleviation of the requirement of invasive biopsies. However, compared with diagnostic studies, these reports of monitoring trials included relatively small patient numbers. Hence, the potential influence of MRS in the brain tumor clinic still needs to be evaluated with large patient populations.

Breast Cancer

Breast cancer is another oncological area in which MRS reports on primary lesions and lymph nodes have been frequently published [117-119]. However, MRS technologies for breast examinations are not as mature as those utilized in brain studies because of the challenge introduced by the abundance of mobile lipids found in the breast. A new spectral strategy has been proposed to reduce the confounding effects of lipids to other metabolites in breast lesion MRS [120].

Fortunately, or perhaps unfortunately from the MR technique point of view, the *in vivo* MR spectrum of breast cancer is often very simple consisting only of lipids and Cho, and therefore although data evaluations present a somewhat simple task, the options to correlate these evaluations with clinical data are limited. A study of 38 patients showed that by using the elevated Cho levels, the sensitivity and specificity in differentiating breast malignancy from benign lesions were 83 and 87%, respectively [118]. Another study of 105 subjects, examined at a field strength of 4T (a higher field strength can produce better resolved MRS for better observation of different resonance peaks), confirmed these observations. It showed that Cho levels were significantly more elevated in the malignant breast lesions than in the benign abnormalities and normal breast tissues [117]. Elevated Cho levels were also reported with lymph nodes in the evaluations performed in breast cancer patients. Combining *in vivo* Cho data with the fine-needle aspiration biopsy (FNAB) results, the report concluded that the overall accuracy of *in vivo* MRS detection of malignancy was 90% [119].

The diagnostic function of Cho measured from *in vivo* MRS of breast cancer has been corroborated by *ex vivo* studies. Since the high lipid content of human breast tissue also complicates *ex vivo* analysis, FNAB needed to be obtained in order to acquire a breast tissue spectrum that was

diagnostically meaningful [121]. In a study of 218 FNAB samples from 191 patients with benign lesions, ductal carcinoma in situ (DCIS), and invasive carcinoma found that the resonance peak height ratio threshold of 1.7 (3.25 ppm vs. 3.05 ppm; or Cho vs. Cr), could be used to differentiate benign lesions from carcinoma with 95% sensitivity and 96% specificity. However, this single ratio identifier only worked if the SNR, particularly for Cho peaks at 3.25 ppm, was above 10. To extend the MRS differentiation capability below this limit, and more importantly, to search for a more robust diagnostic protocol for computer spectrum analysis, a more elaborated three-stage statistical classification strategy (SCS) that utilizes the entire MR spectrum rather than just two peaks is necessary. The advantages of SCS for relating broad line ^{1}H FNAB MR spectra to breast cancer diagnosis and possibly prognosis are discussed [121]. However, the more advanced the SCS is, the less evident were the direct connections with individual metabolites.

Similar conclusions of the role of Cho on breast cancer may be more clearly presented with HRMAS MRS studies. Even with lipid-rich tissue, HRMAS MRS has successfully produced high-resolution ^{1}H spectra. Results from a study at 9.4T of 19 cases of ductal carcinomas showed that both the high fat contents and the individual cellular metabolites could be measured from the same spectrum. In particular, phosphocholine could be quantified separately from choline; the ratio between phosphocholine and choline was found to correlate with tumor grades [122].

A more recent detailed HRMAS MRS study at 14.1T of 10 ductal carcinomas compared HRMAS MR spectra with those obtained using conventional MRS of perchloric acid tissue extracts. The study concluded that for breast tissue, HRMAS MRS was able to achieve spectral resolutions approaching those obtained using conventional MRS of extracts. 2D J-resolved and correlation (COSY) MRS were used to accurately assign metabolites [123].

Other Solid Tumors

In addition to brain tumors and breast cancer, single-voxel MRS studies of many other solid tumors have been reported over the past years, including cervical cancers [124-126], bone and soft tissue tumors [127], lymphomas [128], head and neck lymph node metastases [129], female intrapelvic tumors [130], and rectal adenocarcinomas [131]. Generally, these studies are more challenging than brain tumor MRS, because the regions of interest are located physically near the centers of physiological motions, and the SNR limitations of MRS require more signal averaging. To address complicationsarising from these motions, a breathhold (20 seconds) MRS scheme was proposed for 3T investigations, and was tested on patients with abdominal and thoracic metastatic lesions due to renal cell carcinomas [132].

Human cervical cancer specimens have been analyzed with *ex vivo* MRS since 1990 [133]. Broad-line resonances corresponding to lipid contribution at 0.9 ppm (-CH_3), 1.3 ppm (-CH_2-), and 3.8-4.2 ppm (CH) were found to distinguish invasive from preinvasive epithelial malignancy [134].

An interesting recent study combined both *in vivo* MRS and *ex vivo* HRMAS MRS analyses of human invasive and preinvasive cervical cancer of 51 subjects (nine normal controls, 10 preinvasive, and 32 invasive) (Fig. **2**). The study reported that by measuring triglyceride-CH_2 (1.3 ppm) *in vivo* with endovaginal coils, the presence of cancer could be predicted with sensitivity and specificity of 77.4 and 93.8%, respectively. *Ex vivo* measurements of the same resonance from biopsy samples presented 100% sensitivity, while the specificity of this marker was only 69% [125].

In addition to the discussed *ex vivo* MRS studies of cervical biopsies examined with the HRMAS technique, there are a number of recent *ex vivo*reports on HRMAS studies with statistically significant results [135, 136]. Of particular interest is a study that advanced from evaluations of a single (or a small number of) metabolite(s), to the use of principal component analysis (PCA) to analyze the entire spectrum. The loading profile of the principal component (PC) that can differentiate cancer from non-cancer samples is comprised primarily of Lac, the methyl and methylene groups of lipids, and, to a lesser extent, the choline-containing compounds, representing 63% of the variations in the spectra. In cervical cancer cases, this PC evaluation had higher scores, implying that the diagnostic compounds are present in elevated levels in the cancerous samples.

2.1.2.3. Other Clinical Conditions

In addition to its neurological and oncological applications, single-voxel MRS has been used for other medical evaluations, including the measuring of total body fat and muscle contents [137-141], and the composition of gallbladder bile [142, 143]. As a non-invasive procedure, MRS provided a platform with which Cho and lipids in bile were quantified.

2.1.3. Comments on Advantages and Limitations

Not surprisingly, some of the first 1H MRS experiments were tested on the brain, and the brain continues to be a good system for study with single-voxel MRS, despite the popularity of multivoxel methods. Because of the importance of the potential ability to perform "virtual", non-invasive biopsies, high resolution single-voxel methods will continue to be appropriate in brain.

It should be cautioned that relying on MRS alone for the oncological evaluation of malignancies other than brain tumors may not be necessary, since biopsy or surgical samples are relatively easy to access, and pathology studies can be done for evaluation. Hence, *in vivo* MRS criteria can be evaluated and verified with *ex vivo* analyses. But, with neurological conditions, even brain tumors, tissue sampling for *ex vivo* analyses is often not an option; hence, the ensuthssism towards the metabolic characterization of brain disease with *in vivo* MRS techniques is rational.

2.2. Proton Multi-Voxel Metabolite Imaging – MRSI

Although single-voxel MRS yields relatively high resolution spectra with clearly resolved metabolite peaks, multivoxel approaches have gained popularity due to their surveying ability. Currently multivoxel approaches represent the most common application of MR spectroscopy to the evaluation of clinical disease.

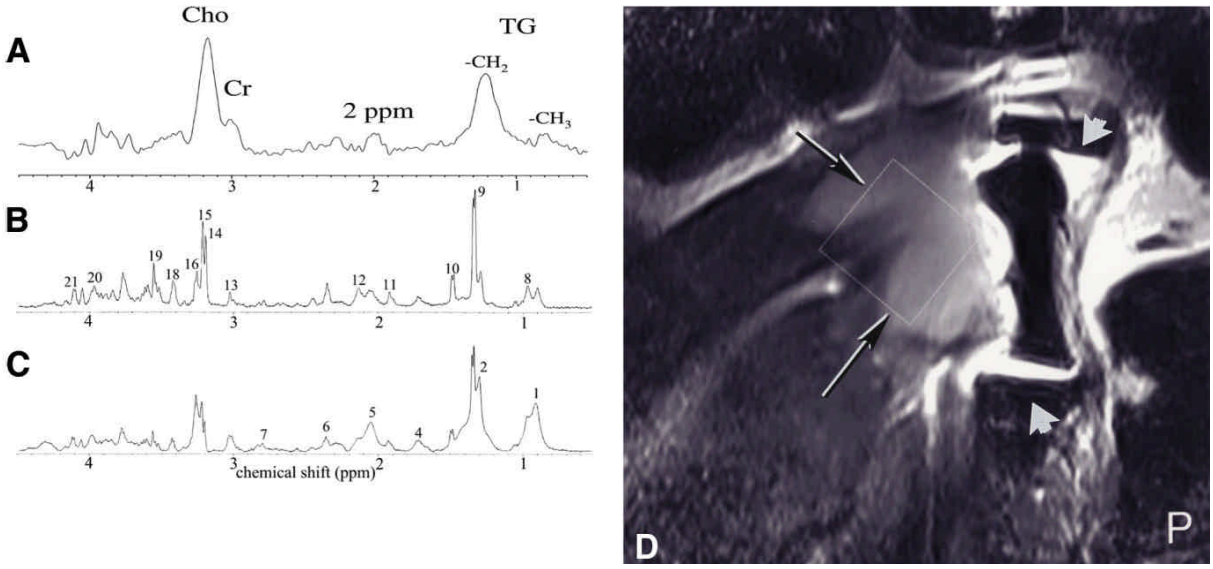

Fig. (2). ^{1}H MR spectra of cervical cancer. A). *in vivo* PRESS (TR=1600ms, TE=135ms); B) *ex vivo* CPMG at TE=135ms; C). *ex vivo* single pulse; D). A T2-weighted fast spin echo image (TR=4000ms, effective TE=88ms) used a 37mm diameter endovaginal coil (arrowheads) showed an irregular mass of tumor centrally within the cervix (arrors) filling 70% of the *in vivo* MRS VOI (marked square). (From Figure 3 in Mahon MM *et al*. [125]).

Despite the ability to correlate high resolution *in vivo* MRS acquired from large voxels with *ex vivo* tissue MRS metabolite profiles and with pathological evaluations, researchers recognized limitations of these methods for many pathologies in which there was heterogeneity of the lesion contained in the single large voxel. In brain, for instance, inflammation and edema often complicate stroke. Inflammatory cells, as well as normal tissue still present in the ischemic area contaminate the spectra from stroke voxels. Metabolite concentrations obtained from these spectra could be difficult to interpret because the individual contributions of normal and ischemic neural tissue, as well as inflammatory infiltrate, are impossible to deduce without histopathological investigation. In addition to problems of metabolite concentration, metabolite location is also problematic in studies using large voxels; that is, when one detects the presence of a particular metabolite, one cannot determine with any certainty from which cells, or even from which part of the voxel, the particular signal arises.

In addition to its surveying character, multivoxel studies can also take into account lesion heterogeneity by obtaining spectra from many relatively smaller voxels, often arranged in a two-dimensional grid. This technique, known as metabolic imaging or chemical shift imaging has the added advantage of being able to generate maps of metabolites of interest by specialized processing methods. The intensities of metabolite peaks in each spectrum can be mapped onto an image of the sampled region, similar to the activation maps familiar from the now-popular functional (f)MRI. For instance, one can acquire a 4x4 grid of 16 spectra, with a spatial resolution on the order of a cubic centimeter, approximately an order of magnitude lower than that attained with single-voxel techniques. By observing the change in metabolite peaks across the entire VOI, one can begin to correlate more clearly lesion pathogenesis with spectral findings. Since the SNRs of MRS spectra are directly related to the amount of the analyzed sample, by sacrificing in SNR with measurements of smaller volumes, one can approach the tangible goal of performing "virtual biopsy" of multiple regions with metabolic imaging, or MRSI. However, readers should be aware that this improved spatial resolution is at the expense of spectral resolution of the spectrum of each voxel.

2.2.1. Techniques

The general technique of MRSI is similar to the single-voxel MRS applications. A VOI is localized using either PRESS or STEAM sequences, modified to obtain spectra from the multiple small voxels of the matrix placed onto the VOI. As in single-voxel MRS, outer volume suppression techniques can be applied to avoid partial volume artifacts from the region outside the defined VOI. Upon detection of a VOL from a scout MRI, the user can visualize and place a grid onto the VOI. Some specialized techniques allow shaping of the region (to circles or free-form areas, rather than rectangular regions) or tilting of the grid over the VOI. The pulse sequence typically consists of 8-10 phase-encoding steps that generate an 8x8 to 10x10 array of rectangular voxels positioned over the defined VOI. One spectrum will be obtained from each voxel to achieve a spatial resolution on the order of a cubic centimeter, or smaller. The arrangement of the voxels in a grid-pattern has led to the term 2D-MRSI to distinguish single-voxel *in vivo* MRS from multi-voxel MRSI. Three-dimensional (3D) MRSI methods are also possible on some research scanner systems at this moment. In this review, we will consider both 2D and 3D phase-encoding techniques together.

With a single pulse sequence, multiple spectra are acquired simultaneously from the VOI indicated by the grid. Improvements in methods have allowed increasingly shorter acquisition times, enabling higher spectral resolution from

the ability to average over a larger number of acquisitions in a clinically tolerable time window. Ideally, combined MRI and MRSI evaluations can be conducted in less than one hour to minimize patient discomfort during data acquisition.

2.2.2. Clinical Applications

The same theme present in the use of single-voxel methods applies to multivoxel MRSI applications as well, in that MRSI studies are predominantely applied to investigations of brain pathology and solid cancers. This technique has particular relevance in cancers where single-voxel studies are clearly insufficient to address lesion heterogeneity and to survey the surroundings of solid tumors. Because of its sensitivity and higher spatial-spectral resolution, the technique has shown promise in aiding diagnosis, staging and even grading of malignant disease, as well as treatment planning, MR guided biopsy, and the monitoring of treatment response.

We will continue our clinical review on the path laid out in the presentation of single-voxel applications, beginning with neurological disorders, then proceeding to oncological diseases and finally, other clinical conditions. However, though we will attempt to categorize studies according to disease type, our review efforts will focus on the new insights of biomedical processes and new knowledge about diseases revealed by MRSI, which were not available with single-voxel MRS. When reviewing MRSI reports, the most important concept of which readers may wish to constantly remind themselves is that MRSI is a "mapping" approach targeted at evaluations of global changes of multiple regions, which should be familiar to radiologists who are used to image examinations.

2.2.2.1 Neurological Disorders

Neuro-Anatomy Studies

Before we discuss evaluations of various disorders, we wish to mention that we noticed a large number of neuro-anatomy studies that used MRSI to measure metabolite concentrations [144, 145] or ratios [146] in different brain regions simultaneously. Metabolite differences for NAA, Cho, Cr, Glx and MI were observed in these studies with healthy subjects. Documenting these regional differences is very important since these normal levels and their variations are the basis upon which detection and determination of abnormalities may be possible. A further level of complication is the changes of brain neurochemistry with age. This simple concept is readily acceptable to anyone, however documentation of these changes demands great efforts. Again, as a mapping task, many MRSI reports have been devoted to the topic, with subjects ranging from premature neonates (30-34 weeks of postconceptional age) to senior citizens of 89 y.o. [147-151]. In these studies, NAA, Cho, Cr, and occasionally MI are measured and their changes, correlated with age. However, from the existing data, even though some of these studies by the standard of a single project are extensive, for instance, with inclusion of 68 subjects covering three adult age groups [150], or 90 subjects of ages 4 to 88 years [148], we are compelled to comment that more studies may be needed to generate complete human brain metabolic maps for different age groups. The existing data is composed of measurements from different brain regions, and was analyzed and reported non-uniformly, with either metabolite ratios or concentrations.

Vascular Diseases and Traumas

Studies of vascular diseases and traumas have been reported. All of these studies shared the common theme of evaluation of the overall brain response to these conditions and attacks, rather than only a focus on lesions or the affected regions. For instance, in a study of nine patients with intracerebral hemorrhages, MRSI in combination with diffusion-weighted MRI revealed that the secondary neuronal injury after the onset may not follow the proposed mechanism of ischemia, for instead of observing the expected reduction in ADCs and the presence of Lac, as demonstrated with only one patient (Fig. **3**), the measurements of the areas surrounding the hemorrhages in eight others revealed the opposite [152]. A Lac increase was observed in 11 patients suffering from chronic cerebral infarction, and was found in correlation with the decrease of vascular reactivity quantified by PET [153]. A stroke MRSI study assisted by regional cerebral blood flow (rCBF) measured with SPECT (single-proton emission computer tomography) showed that a perfusion defect in the region of cortical diaschisis correlates with the NAA/Cr decrease in the white matter in the region [154]. Trauma effects on brain metabolites were surveyed for as many as 25 brain regions with MRSI after mild closed head injuries [155]. With Lac/NAA mappings before and after surgery, it was concluded that the often observed neurodevelopmental impairment following surgical repair of congenital heart disease might be attributable to conditions preexistent to the heart surgeries [156].

Demyelinating Disease

As we previously explained, since multiple sclerosis (MS) could be a global demyelination disorder, MRSI should be more suitable than single-voxel evaluations in assessing the brains of patients with this disease. MRSI has been tested in almost every aspect of the MS clinic, including: 1). investigations of MS metabolite patterns for diagnosis of primary progressive (PPMS), relapsing-remitting (RRMS), and secondary progressive (SPMS); 2). analyses of patients at early stages; 3). predictions of disease progression; and 4). evaluations of therapy efficacy. In all these studies, since MS is a white matter disorder, most often the measurements were centered on the so call "normal-appearing white matter (NAWM), " as defined from MR images.

Primary progressive disease is characterized by a gradual progression of the disease from its onset with no superimposed relapse and remission. A 3D MRSI study of 34 PPMS patients and ten controls of the central brain region (a total VOI 160 cc) at the middle of the corpus callosum presented a statistically significant 12% NAA/Cr decrease in the examined area of patients compared with controls. This total VOI in patients consists mostly of NAWM, gray matter (GM) and CSF, with less than 2% T2 MRI identified lesions [157]. Of note, this study measured patients both with 3D MRSI and 3D EPSI, which will be discussed latter, however there was no difference in the calculated NAA/Cr results

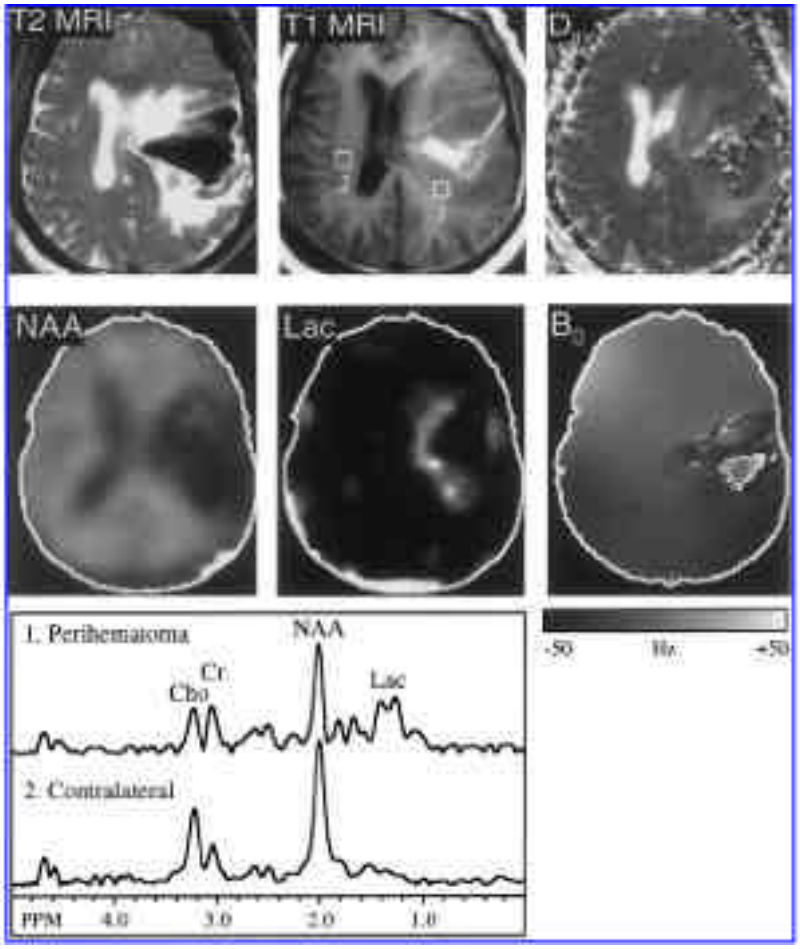

Fig. (3). T2-, T1-weighted, Dav (a.k.a. ADC) images; proton MRSI (NAA, lactate); B_0 field map; and selected proton spectra from perihematoma and contralateral VOI in a patient four days after symptom onset. Hematoma is dark on T 2-weighted images and shows a large local disturbance of field homogeneity (presumably due to the presence of paramagnetic deoxyhemoglobin). Dav or proton spectra could not be evaluated in the hematoma because of focal-field inhomogeneity. However, perihematoma regions show increased signal on T 2-weighted images, increased Dav, and increased lactate. Lactate is definitively assigned on the basis of a chemical shift of 1.33 ppm and 7-Hz J coupling. (From Figure 2 in Carhuapoma JR *et al*. [152]).

between the two approaches. When NAA and Cr were analyzed separately, the observed increase in NAWM Cr with PPMS patients (n=15) when compared with RRMS patients (n=13) and 20 control subjects supported the hypothesis that gliosis increases during this phase of the disease, whereas reduction in NAA in the lesions of both patient groups reflects the axonal loss that results in progressive disability [158].

Representing a more easily identifiable patient group, RRMS patients are the focus of many studies, either alone [159-163] or in comparisons with secondary progressive SPMS subjects [164-168]. RRMS is different from SPMS by its characteristic of relapse with appearance of new symptoms or worsening of preexisting ones, followed by periods of remission during which time the person fully or partially recovers from the deficits acquired during the relapse. However, SPMS is characterized by a steady progression of clinical neurological damage with most of these patients having previously experienced RRMS for a number of years.

Using 3D MRSI measurements of a total of 480cc, the overall reduction of NAA was 9%, with increases in Cr (22%) and Cho (32%), when NAWM from 11 RRMS patients were compared with measurements from nine control subjects. Observations of the study suggested that changes of Cho in NAWM preceded those of NAA and atrophy, and that Cho was the only metabolite among the three analyzed to have the power to differentiate RRMS from controls (100% specificity and 90% sensitivity) [160]. Another 2D MRSI analysis of voxels immediately superior to the roof of the lateral ventricles, confirmed the reduction of NAA in NAWM, while reporting that no statistical significances in Cr and Cho were observed. On the other hand, an increase of MI in NAWM was reported, as were reductions of Cho, NAA, and Glx in the cortical GM. In addition, Cr and Glx in GM, and MI in NAWM were found to significantly correlate with functional composite scores [161].

3D MRSI was attempted to evaluate lesions of RRMS patients during high-dose methylprednisolone therapy. With

MS, methylprednisolone is used because of its capacity to close the damaged blood-brain barrier and reduce inflammation. In this study of 14 RRMS patients, 29 contrast-enhancing and 24 non-enhancing lesions were analyzed along with NAWM. The study measured NAA, Cho, Cr, and Lac. Although, NAA/Cr did display lower values in both types of lesions than NAWM, and Cho/Cr had higher values in the enhanced lesions than in both the non-enhanced ones and NAWM, no treatment related metabolite change was recorded [163]. The differences between RRMS and SPMS were reported in the study of normal-appearing corpus callosum (NACC), and NAWM outside of the corpus callosum for 12 RRMS and 12 SPMS patients, and 15 healthy controls. For SPMS patients, NAA/Cr levels were lower in both measured regions compared with the controls, however the same reduction was only detected in NACC for the RRMS patients ($p<0.001$) along with decreased levels of Cho/Cr ($p=0.003$) [168].

In a study with a larger population of patients (88 RRMS and SPMS), reductions in NAA/Cr were detected before patients experienced significant disabilities, and in particular, the ratio was found to be linearly correlated with mild disabilities, represented by values of below 5 in the Expanded Disability Status Scale (EDSS) [165]. The predictive value of MRSI for the population of RRMS and SPMS was demonstrated by a study of the corpus callosum and the adjacent periventricular NAWM of 12 patients. It showed that NAWM voxels with significant higher Cho/Cr values presented MRI visible lesions in the following scans after six months than the unchanged voxels ($p<0.001$), and higher Cho/Cr values in voxels with lesions also resulted in lesion volume increases after 6 months ($p<0.009$) [167]. These results indicate the better sensitivity of MRSI than conventional MRI towards pathological changes in tissue, and were in agreement with the knowledge of the focal pre-lesion myelin membrane pathology.

A MRSI and fMRI study of nine RRMS and SPMS patients without impaired hand functions reported an interesting observation [166]. It was found that fMRI activation of the ipsilateral sensorimotor cortex with simple hand movements of patients was increased fivefold from controls (20.0 ± 24.3 vs. 3.8 ± 4.2), and was negatively correlated with the decreases in NAA ($p=0.0001$). This observation suggest the existence of a compensatory cortical adaptive response, and the authors further hypothesized that such responses may explain the discrepancy between the observation of MRI lesions and the clinical measures of disability.

Neuro-Degenerative Diseases

Applications of MRSI evaluations in neuro-degenerative disorders have been seen in AD [169-172] and ALS patients [65, 173-175]. When comparing large numbers of AD patients ($n=56$) and controls ($n=54$), it was apparent that NAA reductions in AD were region selective and concentrated in the medial temporal lobes and GM in the parietal lobes with no effect to WM and no changes in the frontal lobes. It was reported that by inclusion of NAA reduction to the volume measurements of the hippocampus, the accuracy of the classification of AD patients from controls improved from 89% to 95% [169]. When MRSI measurements were combined with FDG (18F-2-fluoro-2-deoxy-D-glucose) PET analysis, significant correlations between metabolite ratios (Cho/Cr and NAA/Cho) and regional cerebral glucose metabolism quantified from PET were observed [172].

The advantage of global evaluation with MRSI was also demonstrated in ALS studies. For instance, NAA/(Cho+Cr) ratios were found to be significantly reduced in the motor cortex of ALS patients when compared with those in controls [173, 174], and furthermore, with longitudinal evaluations, decreases in all three metabolites were detected in motor cortex, but not in the non-motor regions [174].

Of particular interest, a study compared results obtained with single-voxel to those obtained with MRSI for 12 patients and ten controls. The single-voxels were placed bilaterally in the precentral gyrus, from which NAA/Cho, NAA/Cr, and Cr/Cho were determined. While no statistically significant differences were observed with these ratios between the ALS patients and the controls, MRSI measurements found that patients with clinically pronounced upper motoneuron signs had significantly lower ($P = 0.037$) NAA/Cr ratios in the more affected hemisphere [65].

MRSI has also been used in the evaluation of a proposed ALS therapy [176]. The therapy study was designed based on the hypothesis that ALS might be the result of excessive glutamate-mediated excitotoxicity. Gabapentin (GBP), a structural analog of the neurotransmitter GABA, was shown to modulate the GABA and glutamate neurotransmitter systems by reducing the synthesis of glutamate and hastening its degradation, thereby reducing fasciculation and muscular cramps for ALS patients. However, MRSI analysis of eight patients placed on this drug and 14 controls concluded that the difference in NAA/Cr between patients and controls observed before and after treatment did not change. It also noted that no improvement in patient clinical condition was seen [176].

Metabolic Diseases

An interesting MRSI study of metabolic disorder was reported on the evaluations of 76 women heterozygous for x-linked adrenoleukodystrophy (X-ALD). Although in general, x-linked disorders transmitted by female carriers affect only males, the study showed the reduction of NAA levels in the corticospinal projection fibers of these subjects who had normal MRI examinations [177]. In addition, the utility of MRSI in the evaluation of X-ALD patients (mostly men) has been tested [178, 179], and it was found that NAA/Cr can be used to measure disease progression [178].

A report of MRSI study on phenylketonuria concluded that in order to detect phenylalanine, the sum of all 256 MRSI voxels was necessary to achieve a sufficient SNR [180]. This presented the best illustration of the limitation of MRSI, when low metabolic concentrations in each voxel prevent the production of a visible MRSI map.

Psychiatry

Metabolite variations in schizophrenic patients have been probed with MRSI. In adults, NAA reductions were seen in hippocampus and thalamus, and in the latter, Cho was also reduced [181]. In children, however, the most prominent

changes were increases in Cr and Cho. It was measured that Cr increased 14.3% in superior anterior cingulated and Cho increased 30.3% in superior anterior cingulated, 13.3% in frontal cortex, and 13.5% in caudate head[182]. The increase in Cr was explained by the abnormal local cellular energy demands, while Cho results were in agreement with the hypothesis that children with early schizophrenia experience phospholipid membrane disturbances. MRSI has been used to evaluate brain responses to psychiatric treatments for schizophrenia patients [183, 184]. Higher NAA levels in dorsolateral prefrontal cortex were measured when patients were on antipsychotic treatments for more than four weeks [183]. This observation supports the belief that reduction in NAA may represent not only neuronal damage and death, but neuronal injuries that could be reversed with treatment.

Studies of other psychiatric conditions have also been reported, including the evaluation of a panic treatment [185], the measurement of Cr in autism where it was observed to be higher (21.1%) in the head of the right caudate nucleus and lower in the body of the left caudate nucleus (17.9%) and right occipital cortex (16.6%) [186], the increased Cho in medial thalamus with child obsessive-compulsive disorders [187], and investigations of unipolar and bipolar disorders [188-191]. With bipolar disorders, it was shown that Cho/Cr levels measured in the left cingulated cortex correlated with depression ratings, and the levels on Cho/Cr in the right cingulated cortex were higher in patients not on medication than in those on medications. Both patient cohorts had higher Cho/Cr levels than controls [190].

Although this psychiatry section may not be entirely appropriate to contain the following result, we cannot find a better-suited part of the review in which to discuss it. A hippocampus study of five ecstasy users showed that there was no measurable brain metabolic change with the users when compared with controls [192]. Perhaps, neuronal damage had not yet caught up with these particular subjects, at least in the tested brain region.

Epilepsy

Epilepsy presented as a neurological condition can be the result of many different neurological diseases. The survey of brain metabolite alterations for epilepsy patients may be the first step in understanding the causes of the condition, which may lead to the design of treatment plans. Hence, it is not surprising to see that a large number of MRSI studies have been devoted to the mapping of different types of epilepsies [193-200], to the investigation of metabolite correlations with brain neuro-electrical currents measured by EEG [201, 202], and to the development of metabolite prediction markers for surgical planning [203-207].

MRSI metabolite patterns were observed with epilepsy patients that verified clinical observations and confirmed hypothesis. Idiopathic generalized epilepsy (IGE) is considered to be related to the thalamo-cortical circuitry. A MRSI study of 20 IGE patients revealed the reduction of NAA/Cr in thalamus compared with controls, while no significant NAA/Cr difference was found with other examined brain regions [194]. Temporal lobe epilepsy (TLE) is the most frequent cause of focal and refractory seizures. The pathology of TLE frequently finds mesial temporal sclerosis in temporal lobectomy specimens. Mesial temporal sclerosis displays neuronal loss in the hippocampal formation. A study of 15 patients with mesial temporal lobe epilepsy (mTLE) found that in the ipsilateral hippocampus, NAA concentration was 27.3% lower in patients compared with its concentration in controls ($P < 0.001$), and 18.5% lower compared with that in the contralateral side ($P < 0.01$). Using only hippocampal data, 60% of the cases of mTLE were correctly lateralized. Lateralization, determined using whole temporal lobe data, had 87% sensitivity and 92% specificity. Of note, in addition to hippocampus, NAA was bilaterally reduced in the frontal, parietal, and occipital lobes of patients with mTLE compared with that in controls ($P < 0.01$) [198]. The importance of lateralization in epilepsy evaluation has encouraged investigations in accurate analysis of MRSI data. A study of 9 patients and an equal number of controls compared visual inspections by three radiologists with computer quantification of NAA/(Cho+Cr) ratios for each voxel. The result showed that visual inspection correlated with the measured ratios, and thus concluded that while visual inspection can be preformed routinely by experienced radiologists with high accuracy, metabolite ratios from MRSI may provide more quantifiable assessments of the spatial distribution of the disease [200].

Another study intended to investigate the cause of TLE either as the result of an early injury or due to ongoing neuronal damage from seizures. With 82 consecutive patients of medically intractable, non-foreign-tissue TLE, the study was able to conclude that ipsilateral and contralateral NAA/Cr was negatively correlated with duration of epilepsy. Furthermore, it was found that patients with frequent seizures presented lower NAA/Cr than patients with no or rare seizures. The results suggest that although an early injury may cause asymmetric temporal lobe damage that is present at the onset of epilepsy, generalized seizures may induce additional neuronal damage, marking progression over the course of the disease [193].

Since EEG is used clinically to provide measures of epilepsy, the relationship between clinical EEG results and MRSI evaluation of brain areas is of great interest. A study of temporal and frontocentroparietal regions for 51 patients of TLE, extra-TLE and multilobar epilepsy reported that 38% of TLE and 50% of extra-TLE presented low NAA/Cr areas outside of the EEG defined disease areas [201]. However, the clinical implication of this observed discrepancy for treatment planning still needs more detailed investigation.

A number of reports have suggested the value of MRSI measured metabolites in predicting patient surgical outcomes. A comparative study of 32 patients undergoing epilepsy surgeries divided these patients in two groups: seizure-free or not seizure-free, with 16 patients in each group. The results showed that after surgeries, NAA/Cr in temporal lobe is significantly higher with the seizure-free group than with the non-seizure-free group, and in the seizure-free group the post-surgical NAA/Cr levels were higher than their pre-surgical values [205]. Patients (n=6) who underwent Gamma Knife radiosurgery on amygdale and hippocampus for mTLE were followed by MRSI for three years. The most significant spectroscopic changes were

reported to be in the first year after the irradiation, with the formation of edema and strong lipid signals in the spectra. Then, the subsequent changes presented were decreases in NAA, Cr, and Cho in the ipsilateral region of the brain to the irradiation. However, the most unexpected observation was the increases of NAA in the contralateral side after irradiation. The author explained this phenomenon as possible evidence that chronic seizure might cause secondary contralateral dysfunction. Irradiation eliminated seizures and allowed contralateral neurons to return to normal functioning [207]. Once again, a relationship between NAA and neuronal injury/recovery was proposed.

2.2.2.2. Oncological Diseases

Brain Tunors

MRSI has been extensively applied in human brain tumor studies. Our inexhaustive literature search produced more than three dozen reports since January, 2000. This clearly indicates the very large research efforts in the area, considering brain tumors represent only less than 1.4% of malignancy and less than 2.3% malignancy related deaths, for instance in the US [208]. But, as previously explained, brain, and particularly brain tumor, provided us with an almost ideal living phantom that allows the MRSI technique to be tested, developed and implemented.

Brain tumor MRSI studies have covered many clinical aspects. However, analyses of tumor metabolites still have fundamental importance in characterization of the diseases. For example, pediatric pilomyxiod astrocytomas were found to have less Cho, NAA, and Cr than pilocytic astrocytomas [209]. In addition to the expected NAA reduction and Cho increase in oligodendrogliomas, these tumors were found with increased Glx. The levels of Glx in the low grade oligodendrogliomas were higher than those in the low grade astrocytomas [210]. Gliomatosis cerebri were found to be differentiable from low grade gliomas [211]. However, evaluated from the current reports, it is apparent that the investigations of brain tumor MRSI have turned more directly towards clinical applicationss in the last couple of years.

The concept of trading single-voxel spectral resolution for MRSI spatial resolution was appreciated in brain tumor evaluations with detailed correlations of tumor metabolites with histopathological examinations of tissue samples obtained from MRSI voxels. For better correlations, MRSI compatible stereotactic biopsy approaches have been developed and applied [212, 213]. Furthermore, to account for tumor heterogeneity (may be determined macro-heterogeneity according to the histopathology scale), three dimensional MRSI techniques have been tested with voxel sizes between 0.2-1.0 cc [147, 214-216]. In order to achieve diagnosis or to be able to label different voxels for different pathological conditions, such as tumor, normal brain, or necrosis, MRSI data need to be processed with accuracy and reproducibility, from which numerical threshold values for tumor detection can be empirically determined [217], such as the Cho/NAA Index (CNI) proposed to identify tumor voxels. It was reported that by using the CNI threshold value, 2.5, on 68 newly diagnosed tumors, MRSI had 90% sensitivity and 86% specificity [216]. Another study of 18 glioma patients showed correlations between an increase in Cho, and the increased expression of proliferative index MIB-1 [218].

Applications of knowledge acquired through tumor metabolite pattern analyses, and from observed correlations with tumor pathology extended logically into evaluations of their capacity to predict patient outcomes and to monitor therapy response. However, before treatment planning, accurate assessment of tumor size and its extensions into the surrounding tissue is necessary. There are studies that have directly utilized the advantage of high spatial resolution, the distinguishing feature of MRSI. These studies aimed to improve tumor volume assessments based on MRSI quantified metabolite abnormalities, either for the planning of primary tumor treatments [219-222] or for the detection of residual disease after surgery [223].

While most of these works measured MRSI against conventional MRI, an interesting study compared MRSI with MEG (magnetoencephalography, measuring brain activities in terms of slow, fast waves and spike) for measurements of astrocytomas and meningiomas. It showed that brain pathological activities observed in MEG were localized in surrounding regions of the bulk of tumors, where mild reduction of NAA and slight accumulation of Lac were measured. The study suggested these areas might be considered as border zones between normal tissue and tumor tissues [220].

It was demonstrated with evaluations of pathologies of 247 tissue samples from 31 glioma patients, that with voxel sizes of 0.8 cc, MRSI data can better identify tumor boundaries than results from conventional MRI alone, and Cho signals can be used to detect the presence of tumor infiltrations into the surrounding tissues [219]. Another study of glioma patients (n=34, 22 WHO III and 12 GBM) concluded that although T2-weighted MRI presented tumor risk regions more than 50% larger than those proposed by MRSI, in 88% patients MRSI regions extended outside of the T2 regions by as much as 28 mm [221]. Similarly, discrepancies between MRI and MRSI were reported for the identification of residual tumors after surgeries [223]. Therefore, these two methodologies clearly report different cellular populations. However, pathological evaluations to determine which assessment is more meaningful and important to patient survival can be difficult to conduct even with primary tumor cases in which imaging results are known prior to surgery. This is due to special surgical procedures involving brain tumors. Except for the removal of the not so frequently observed solid lesions, the most useful tool to a neurosurgeon is not a scalpel, but rather a suction tip. Furthermore, the critical and mystical importance of the brain does not always allow us to plan surgeries according to the combined maximal area. Nevertheless, with low grade gliomas, the MRSI-defined, metabolically (e.g. high CNI) active tumors were restricted mainly to the T2 enhanced lesions with less then 2 cm extensions to the outside. This led the proposal to construct a clinical target volume by including both areas of T2 enhancing and metabolically active extensions. It was rationalized that this proposed volume would result in a reduction in the size and a change in the shape of the currently used standard clinical

target volumes, generated by adding uniform margins of 2-3 cm to the T2 lesions [224].

The proposed CNI measured before and after surgery has been tested for its value in predicting survival for glioma patients. The CNI maps generated for patients undergoing either regular or gamma knife surgeries, and in some studies combining with ADC and rCBV measurements, were evaluated against patient survival data [225-227]. In addition to Cho, the resonance peak representing the combination of Lac and lipid has also shown sensitivity in prognostics of glioma patients [226, 228].

More often than not, even for operable gliomas, patients are treated with radiation therapy after surgery because of the understandable neurooncological conflict between the concept of "clean margins" emphasized with other oncological surgeries, and the preservation of brain functions. However, radiation therapy delivers the same fatal effects to both cancer cells and normal tissues. Therefore, a major task in the neurooncological clinic is to differentiate recurrent tumors from lesions caused by radiation. Unfortunately, conventional imaging methods such as CT, MRI, PET, etc. cannot distinguish between the two types of lesions. This is a very active area for MRSI to contribute in clinical decision making. Both resonance peaks of Cho and Lac-lipids have shown ability to differentiate between the two types, with a Cho increase indicating tumor, and a Lac-lipid increase suggesting necrosis, in the latter cases there most likely to be radiation necroses [229-232]. In addition to evaluating radiation therapy effects on glioma patients, MRSI was also tested for monitoring chemotherapy of high grade gliomas with high-dose orally administered tamoxifen. Clinically, it was observed that there were no differences between responders and nonresponders in terms of age, sex, tumor type, mean tumor volume, mean Karnofsky scale score, mean number of weeks postradiotherapy, or mean amount of prior radiation exposure. However, metabolites measured with MRSI differed significantly between the two groups before and during treatment. Furthermore, the study indicated that linear discriminant analyses, based on patients' MRSI results, could accurately predict individual response to tamoxifen both before treatment, and at very early treatment stages (2 and 4 weeks) [233].

Pediatric brain tumors as a distinct group have also been investigated by MRSI studies. These studies included measurements of their metabolite patterns [234, 235], analyses of tumor progression [236], evaluations of therapies [237], and prediction of survival [238].

Prostate Cancer

Another major focus of MRSI in clinical oncology has been in the area of prostate cancer. Since prostate cancer presents the major male malignancy in many areas of the world, extensive MRS studies, both *in vivo* and *ex vivo*, have been reported.

Ex vivo studies are aimed at establishing metabolite markers of prostate cancer. An interesting study of intact prostate tissue, combining conventional MRS and high-pressure liquid chromatography (HPLC) analysis, aimed to measure the relationship between polyamines (PA) and prostate cancer [239]. Although PA were observed in the *ex vivo* MRS and measured to have statistically significant drops in cancer samples with HPLC. However, no correlation between PA levels measured by MRS and those determined by HPLC was presented for the same cases due to the limited number of samples analyzed. Nevertheless, the study suggested the existence of a potential prostate biomarker, as well as a direction for future studies.

A recent conventional MRS study measured 71 prostate samples from 41 patients who underwent both cancer and non-cancer prostate surgeries [240]. Using peak ratios Cho/Cr and lipid/lysine, they were able to differentiate malignant from benign tissues with 97% sensitivity and 88% specificity.

Experiments of HRMAS *ex vivo* MRS analysis on human prostate tissues were reported in a qualitative study that also measured two dimensional correlation spectroscopy [241]. Another HRMAS MRS study of human prostate tissues from 16 patients was the first to perform quantitative pathology on the MRS specimens and to include multiple subjects [242]. The results of the study proved the validity of HRMAS MRS for the accurate determination of tissue histopathology. Both citrate (Cit) and PA were quantified from the tissue HRMAS MR spectra and were shown to be linearly correlated with the amounts of prostate normal epithelium. Recently, an interesting study of HRMAS MRS of tissues from 26 patients was published. In this study, prostate tissues were harvested post surgically under the guidance of 3D-MRSI from lesions that had been analyzed using *in vivo* MRS prior to prostatectomy. By combining the MRS results with quantitative pathology of the same tissue after spectroscopy, metabolite discriminators (i.e. ratios of Cit, PA, and Cho to Cr) were found to differentiate normal prostate epithelial tissue from cancer and stromal tissue. Furthermore, a correlation between the intensity of MIB-1 immunohistochemical staining and the ratio of Cho/Cr resonances was reported, supporting their findings *in vivo*. These conclusions were dependent on the assumption that the Cr concentration did not change during the disease process, which awaits verification [243].

With knowledge of prostate metabolites, obtained from *ex vivo* analyses and the identification of *in vivo* visible prostate metabolites: Cho, Cr, Cit and PA, in the past years the MRSI efforts have been seen in the further development of technology for more accurate tumor detection; in the attempt to establish a consultation role in patient treatment planning; and in tests of efficacy for the monitoring of treatments.

Technology developments cover a wide array of topics, including data acquisition methods, such as water and fat suppression and localizations [244, 245], MRSI reader accuracy [246], and tests of surface pelvic phase array vs. endorectal signal receiving coils [247]. Of particular interest, the coil test study showed that at 1.5T with measurements of 35 prostate cancer patients and five controls, there was no measurable difference between the two types of coils in terms of detection accuracy. A study testing dynamic contrast-enhanced (DCE) MRI and 2D MRSI was performed on 23 cancer patients, with cancer regions histopathologically quantified by whole-mount sections after radical prostatectomy. It concluded that by combining high-

resolution spatio-vascular information from DCE MRI, with a (Cho+Cr)/Cit threshold of 0.68, an indicator of tumor presence, cancer voxels could be reliably located and characterized [248].

Detection of prostate cancer from biopsy with patients considered to be at risk who have elevated PSA levels is challenging due to the extremely heterogeneous characteristics of the disease. Such tissue heterogeneity results in both high rates of false negative biopsies and for many patients, repeated biopsies. MRSI's non-invasive "biopsy" ability was tested with 24 consecutive patients who had at least one prior negative prostate biopsy, and presented with PSA levels between 4 and 40 ng/ml. Based on the MRSI finding, 10-core biopsies were carried out. By combining MRSI and MRI, the final analysis showed 100% sensitivity, 70.6% specificity, 58.3% positive and 100% negative predictive values, and the accuracy was determined to be 79.2% [249].

The utilization of prostate MRSI in patient treatment planning has been seen in the contribution of prostate metabolite information to the placement of radiation seeds in brachytherapy. Optimization procedures were developed that incorporated MRSI with ultrasound or CT images by coregistrations [250-252]. Furthermore, MRSI results have impacted brachytherapy directly by defining areas in the cancerous prostate in which boost doses should be introduced [253].

Patients undergoing a variety of prostate cancer treatments have been monitored by MRSI evaluations. A very recent study of 21 patients treated with an external radiation beam concluded that, in one hemiprostate, three or more voxels (size: 0.32 cc/ea) suspicious of containing cancer has 89% sensitivity and 82% specificity for the diagnosis of local tumor recurrence [254]. Another recent report presented the conclusion that MRSI examinations might provide an earlier indication of tumor response to brachytherapy than PSA response (28.9 months vs. 42.5 months) [255]. With hormone-deprivation therapy, comparisons between 65 treated, and 30 untreated patients showed that treatments resulted in time-dependent metabolite loss of all *in vivo* visible metabolites. While healthy and malignant tissues showed different time courses in the losses, Cit displayed more rapid reduction than the rates for Cho and Cr because of the known hormonal effects on Cit production, and the loss of its secluded prostate glandular ducts due to therapy [256].

Breast Cancer

The feasibility of MRSI has been tested in the diagnoses of other malignancies. A recent report on breast cancer showed that Cho was significantly more elevated in the malignant tissue than in benign tissue with measurements of 15 patients. However, the challenges for MRSI utilization in breast cancer were clearly illustrated by the study, with three out of 18 examined patients (~16.6%) not able to produce sufficient MRSI data, and with reporting Cho in terms of SNR, rather than in concentrations [257].

2.2.2.3. Other Clinical Conditions

Besides the above reviewed MRSI applications in the clinic, we also notice its attempts in the evaluation of many other anatomic structures and conditions, such as knee joints for suspected internal derangement measured on an open magnet of 0.35T [258], bone marrow [259], spinal vertebra [260], muscles [261-264], and intramyocellular lipid levels [265]. However, other than the knee joint report, all the other reports dealt with the development and implementation of various MRSI methodologies, and were too early for actual clinical measurements for disease detection and diagnosis.

2.2.3. Echo Planer Spectroscopic Imaging – EPSI

The ability to localize metabolite concentrations to small voxels in an image represents a great technological advantage in the ability to generate maps of metabolite concentrations in the VOI. Spatial resolution of spectra (or spatial-spectral resolution) becomes a limiting factor in the ability to specifically localize a metabolite within a voxel. To address this limitation of MRSI, other forms of metabolite imaging have been developed and attempted to be employed in the clinic.

The most promising, recently developed metabolite imaging method is EPSI. EPSI, based on Mansfield's technique [266], is able to simultaneously and rapidly acquire spatial and spectral data at high resolutions, because all phase-encoding information is obtained in a single excitation. Because EPSI generates a frequency spectrum at each pixel in an image, with resulting voxel sizes on the order of 1 mm^3, maps of spectral components are created with extremely high spatial resolution to aid in the evaluation of metabolite changes.

Traditional MRSI relies on conventional MR imaging to locate a VOI for spectroscopic investigation, and to handle the post-spectral acquisition alignment of spectra with the original image to represent data and generate metabolite maps. EPSI however has the advantage of simultaneously acquiring spatial and spectral data from a single excitation. Following excitation, a readout gradient is applied in one spatial direction, and a series of phase encoding steps generates a train of spin echo images. By sampling along the echo images, a change of the signal over time is generated. Thus, following three dimensional FT, a frequency spectrum is generated at every pixel in an image with resulting voxel sizes on the order of 1 mm^3 depending on the field of view.

Recently, technical developments of EPSI have been witnessed in a number of research groups [267-270], with preliminary applications in brain imaging [271, 272] and in breast cancer detection [273-275]. Particularly, in the breast cancer study, eight patients having suspicious lesions were compared with six healthy female volunteers. The result showed that with high spatial-spectral resolutions achievable with EPSI, observation of tumor anatomic details was greatly improved [273]. An example of an infiltrating ductal carcinoma is shown in (Fig. **4**). In the figure, EPSI is compared with T1-weighted fat saturated MRI, illustrating the superior ability of EPSI to present clearly the cancer lesion. It is apparent that with the inclusion of spectral information that eliminates the chemical shift effect, which causes blurring at the fat-water interfaces, the resulting resolution and anatomical detail are better displayed in EPSI. Another reason for the observation of high-resolution EPSI is that the magnetic susceptibility gradients minimized for

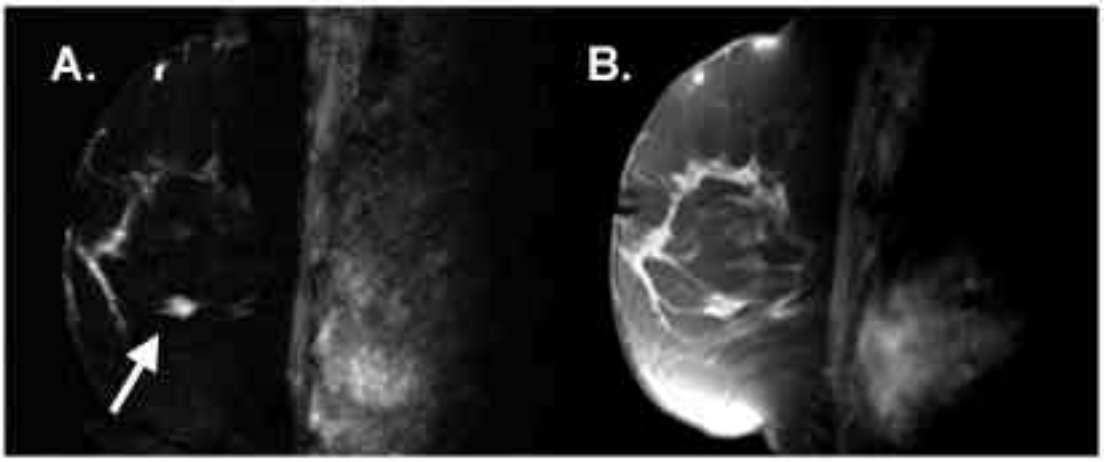

Fig. (4). A comparison between A). EPSI, and B). the standard clinical post-contrast, T1-weighted fat saturated images obtained from an infiltrating ductal carcinoma (arrow) (The images were kindly provided by Drs. Milica Medved and Gregory S. Karczmar at The University of Chicago).

EPSI images are synthesized from only one frequency component, rather than from the whole water resonance, which may be significantly broadened. With the demonstrated EPSI advantage, researchers at the University of Chicago, have begun integrating EPSI into clinical evaluations of patients with suspicious breast lesions identified with mammography.

EPSI has its own set of unique challenges and limitations. The bandwidth of the spectral acquisitions is sufficiently wide, for example, to separate the ^{1}H containing components of water and fat. The sensitivity, however, is low as for any other kind of metabolite imaging because of the low abundance of other materials. The gain in high spatial resolution still results in the sacrifice of spectral SNR and sensitivity. However EPSI shows great promise in its ability to clearly resolve anatomical structures from variations in water and fat chemical shift, and intensity across an image. Additionally, images generated from EPSI acquisitions do not require contrast agent injection or fat suppression. Images of water peak height or integrals can be made equal in spatial resolution to the T1-weighted image obtained from the first echo method, with fat and other metabolites now removed. This is especially useful as a conventional imaging technique, eliminating the need for tedious and frustratingly inconsistent fat saturation methods.

3. ISSUES REGARDING CLINICAL MRSI USE

3.1 A Few Practical Guidelines

MRS Training and Education

The development of MRS as a clinical diagnostic tool for radiology is currently in its infancy, despite its continuing success in researche. Spectroscopists, clinicians and scientists who have dedicated much effort to learning these techniques can easily perform an *in vivo* MRS/MRSI experiment. However, implementation of MRS on a broad clinical scale, or in multi-center studies is often far more challenging. There are many factors that should be considered before a spectrum of reasonable quality can be observed. Particularly, the one issue that is most often missed by reviewers is the need for training and education of the novice MRS users. Facilities, such as Massachusetts General Hospital's (MGH) Neuroradiology department, have started to employ dedicated clinical spectroscopists, on duty to maintain the MRS systems for all clinical scanners, monitor spectral analysis and quality, develop and implement new MRS protocols, and train neuroradiology residents, fellows, and all MR technicians in the acquisition of accurate and reliable MR spectra. The majority of technicians and clinicians are unfamiliar with MR spectra, and require education to differentiate a spectrum containing quality data from one of mostly noise. Training topics should include the effects of poor voxel placement, sources of artifacts such as motion and susceptibility [276, 277], lipid inclusion, and the status of magnet shimming. Post-processing of spectra, with consideration of phasing and scaling, should also be addressed in training. The establishment of websites at MGH for MR technicians with "quick reference" guides to voxel placement has also helped to improve the quality of ^{1}H MRS/MRSI.

Little guidance currently exists in the clinician's education that promotes a physician in determining when an MRS examination should be prescribed, and how should the result of the study be interpreted and incorporated in clinical decision making [278]. If MRS is to become a widely used clinical tool, further training and education may be necessary for clinicians to understand applications and limitations of MRS in following the progression or treatment of various diseases. Another issue that clinicians must be aware of is the complexity involved in translating MRS research results to patients cares [278]. Direct translation of statistically significant MRS research results typically found in large cohorts to an individual patient can often be difficult due to the inherent biologic variability among patients.

Localization

Many techniques have been developed for the purpose of localization in both single-voxel MRS and multivoxel MRSI. Early localization techniques revolved around the use of surface coils and ^{31}P MRS, but the most utilized techniques

today in single-voxel ^{1}H spectroscopy are PRESS and STEAM techniques. Both techniques excite only the VOI with frequency selective rf pulses. The flip angles, sequence timing and placement of gradient pulses are different for each technique. The nature of the echo signal is the major difference between the two techniques. Refocusing the complete net echo signal forms the echo in PRESS. STEAM, on the other hand only preserves part of the magnetization to produce the stimulated echo. This causes the SNR of PRESS to be greater than that for STEAM (theoretically by a factor of 2). Advantages and disadvantages for the use of each technique can be found in many publications [279-284]. MRSI uses either of these techniques, but is modified to obtain spectra from multiple smaller voxels placed within the VOI.

Water Suppression

The large concentration of water compared to the miniscule amount of metabolites that exists in tissues present a great challenge to performing ^{1}H MRS/MRSI. In clinical ^{1}H MRS, measurement sequences must include ways to suppress the predominant water signal. Water suppression does not have to be complete, and a method that allows for 50-100-fold reduction in the water peaks amplitude may be sufficient. A small water peak can be used for frequency and phase corrections before being subtracted from the MR signal. This technique reduces baseline distortions that can resulted from water suppression. The most commonly used water suppression method is achieved by eliminating the water signal prior to exciting and observing the FID. This is achieved through the use of a chemical shift selective saturation (CHESS) pulse, which is followed by a dephasing gradient pulse [12]. Effective water suppression can also be achieved with other techniques such as water suppression enhanced through T1 effects (WET) [285], and with the use of multiple repetitions of selective pulse and dephasing gradient. Drastic reduction of water signal in spectroscopy with the stimulated echo acquisition mode, or DRYSTEAM, uses this multiple pulse technique [286].

Multi-center Studies

The translation of meaningful research observations into clinically applicable examinations for any disease or condition need verification both with sufficient numbers of subjects and from different clinical centers. When considering the application of MRS/MRSI on a multi-center scale, the chances for errors increase exponentially. Multiple cites, having people with various levels of training, who have varying ideas of what parameters ensure a high quality spectrum, each with different hardware specifications (coils, magnets, etc.), all increase the chance of injecting serious error into the results. An effective means of avoiding error is declaring one site the principal site, which will design the necessary protocol and disseminate it to the other sites. Metabolite phantoms, all created from the same solution at the same time, should be shipped to all centers, and routine spectroscopy quality control analyses should be performed on the phantom in order to assess inter-site reliability and instrument stability of each site at all time. The data from both the phantom and the enrolled patients should be analyzed by a designated site for spectral quantification to ensure that the same fitting parameters are used in analyzing the data [47].

3.2. Challenges to MRS and MRSI as Clinical Evaluation Tools

Narrow Chemical Shift Imaging Range

Most metabolites of interest found in a ^{1}H MRS spectrum occur in a small chemical shift range of 10-15 ppm. Quantification of ^{1}H spectra obtained using a high field instrument is easier than *in vivo* due to the increased resolution in the spectrum. However, most clinical MRS occurs on magnets with lower field strengths (1.5 T or less), which results in a spectrum with overlapping peaks for metabolites, thereby causing quantification difficulties. The impact of this issue may be reduced by different approaches. The selective editing or suppression of specific resonances can allow for easier and more accurate assessment of metabolites. Spectral editing can be achieved by designing pulse sequences which exploit T1 and T2 relaxation differences of metabolites, spin coupling, quantum coherence [287, 288], and resonance frequencies [289]. For instance, these techniques allow drug-induced variations in GABA to be monitored and detected in the human brain, giving insights into the effects of therapy on patients with epilepsy [290]. *In vivo* ^{1}H 2D MR correlation spectroscopy was found to facilitate separation of metabolite and macromolecule peaks overlapping with GABA and creatine in the 1D spectrum [291, 292]. This technique was successfully used to follow epilepsy patients treated with a ketogenic diet [291].

As MR technology and application in radiology departments progress, the use of higher field magnets (3.0 T and above) will become more prevalent. For instance, the use of a 4 T scanner has made it is possible to improve Cho quantification in breast cancer [117]. However, with higher fields, the use of higher order shims must be considered to achieve increased spectral, spatial and temporal resolution [293, 294]. Transitions to higher field will also benefit MRS studies involving nuclei with low gyromagnetic ratios such as ^{13}C and ^{31}P [295-297]. Although difficulties arise with the use of high field magnets, several studies have demonstrated that these limitations can be overcome with time and effort [294, 298].

Methods for Archiving Data

Picture archiving and communication system (PACS) is crucial for the daily clinical image operations of a clinical radiologist. While radiologists have used this method for years as a practical way to work in different physical locations at once, the archiving of spectroscopic data, especially the large volumes of MRSI data, has been difficult and is usually a problem left to each site. It is often achieved by having the MR technicians post-process the data, and through the use of software to generate images of the spectrum, they can be posted on the web and viewed from other sites. Working towards this goal, a web archival and interface system was created and implemented in the Department of Radiology at University of California, Los Angeles [299] that allowed for retrieval of MRSI data by radiologists via any PC from internet. This system allows the users to specify the voxel location that they wish to observe, to view both the spectra and all corresponding images, and to

provide integral and ratio data of the metabolites measured from spectra. It permits MRSI data to be viewed world wide, but requires security measures to ensure patient confidentiality. However, this system does not allow a user to reprocess the raw data, since what the user actually views are pictures of the processed raw data. This technique obviously has many limitations and a better solution is necessary for clinicians to be able to post-process the data themselves after they have been trained to perform the task.

Quality Assurance of Spectral Data

Little has been published on the issues of quality assurance or even to define the spectral quality that must be obtained to ensure accurate results [300-303]. It is admittedly true that when experts in the field of MRS are asked to define the qualities which make up a "good" spectrum, the reply is that it depends on a multitude of factors such as use of short or long echo time (TE), use of *in vivo* MRS or MRSI, and even which organs/tissue types are being examined. An excellent review was recently published with the hope of beginning a much needed dialogue between these experts to form a general consensus of parameters and quality factors needed for clinical MRS use [276]. This review not only discusses causes of artifacts and problems in automated fitting models, but also delineates criteria for quality assurance and rejection of data.

Diagnosis using Automated Pattern Recognition Techniques

Radiologists quite often rely on visual examination to interpret a spectrum, which is a biased approach that lacks quantification and is based solely on the training of the individual. Automated pattern recognition techniques for diseases, such as brain tumor classification, have been proposed [304], but have relied on manual prepossessing of the phasing or measuring peak areas [305]. Reports exist for the INTERPRET project, which has developed a system for the classification of brain tumors based on comparing an unknown spectrum of a tumor to a database of tumor spectra each with a known pathology classification [106, 306]. In one report, brain tumors were classified as either meningioma, or astrocytomas, based on the automated pattern recognition. The system relied on the use of a training data set that consisted of 94 spectra gathered from 3 different sites. When 50 other cases were used to test the recognition system, linear discriminate analysis successfully classified 48/50 in the test set, as proven by histopathology, and the remaining two were considered to be atypical cases. Testing spectra obtained from multiple sites indicated that the differences in spectral patterns are greater between tumor types than for acquisition parameters [106].

Quantification and Interpretation of Spectra

Clinicians and scientists who have a more intimate understanding of MRS utilize many methods for quantification of *in vivo* MR spectra [117, 307-314]. A relative calculation can be performed in which metabolite peaks of interest are integrated and are normalized to a metabolite that is assumed to be unchanged by the disease. Cr is typically the metabolite of choice for normalization because it is believed that its concentration does not vary with age. The results of a recent 3D ^{1}H MRS study, however, indicate that Cr may not be a reliable denominator because its concentration varies among normal volunteers [315].

Another means of spectral quantification is the use of absolute units. An example of this is to express the metabolite contents as a percentage based on the area of the unsuppressed water signal, without further corrections or conversions. Many prefer absolute concentration measurements instead, but this approach also has complications due to overlapping resonances found within spectra, inherit propogation of errors due to correction factors used, and unpredictable forms of both line shape and baseline.

Several fitting routines have been developed such as linear combination LCModel [89, 90] and the PROBE package from GE [316]. Before spectral fitting occurs, it is imperative to pay attention to the quality of spectra, or else the likelihood of inaccurate results within a study increases. Spectral features that may influence accurate fitting include distortions due to motion [277, 317, 318], artifacts [276], poor signal to noise ratio, broad peak linewidths, and lipid contamination from the scalp. The macromolecule signal contribution in a spectrum should also be considered when quantifying and interpreting a spectrum [319, 320], as it has been found to change with certain diseases.

An alternative means of quantifying metabolites and statistically significant finding differences between optimally obtained spectra is to perform principal component analysis. Some groups have begun using this method [321, 322]. The primary benefit is that it introduces the least amount of error in the interpretation of the spectra because it relies on all the data set, not just individual, user-selected metabolites to account for the amount of variation among the peaks in a set of spectra. While this still does not overcome the problem of improperly obtaining and processing spectra, it does address the issue of quantification. Full disclosure of processing parameters, in addition to acquisition parameters is also vital.

Patient Issues

Even with all the scientific and technological difficulties solved, there is still an issue of primary importance for the patient, which must be resolved before MRS can be used routinely in clinic, at least in the United States. The principal difficulty is due to the lack of reimbursement by many insurance policies for MRS studies, which ultimately places the financial burden on the patient [278]. This issue, although will determine the ultimate success of MRS and MRSI in medical practices, is indeed beyond our expertise.

ACKNOWLEDGMENTS

We wish to express our thanks to Drs. Bruce Rosen, Lawrence Wald, Bruce Jenkins, Andrew Maudsley, Milica Medved and Gregory Karczmar for valuable discussions, to Drs. Gilberto Gonzalez, Eva Ratai, Sarah Pilkenton and Julian He for careful reading and commenting on portions the manuscript. We gratefully acknowledge and appreciate the editing assistance from Mr. Erhan Ermis. This work was supported in part by PHS/NIH grants CA095624 and in part by a DOD grant W81XWH-04-1-0190.

ABBREVIATIONS

AD = Alzheimer disease

ADC	=	Apparent diffusion coefficient
ALS	=	Amyotrophic lateral sclerosis
B_o	=	Externally applied magnetic field
Cho	=	Choline (*in vivo* including phosphocholine and glycerophosphocholine)
Cit	=	Citrate
CNI	=	Choline-to-NAA index
CNS	=	Central nervous system
Cr	=	Creatine (*in vivo* including phosphocreatine)
CSI	=	Chemical shift imaging
DCE	=	Dynamic contrast-enhanced
DWI	=	Diffusion-weighted imaging
EDSS	=	The expanded disability status scale
EPSI	=	Echo planar spectroscopic imaging
FID	=	Free induction decay
FNAB	=	Fine-needle aspiration biopsy
FT	=	Fourier transform
GABA	=	γ-aminobutyric acid
GBM	=	Glioblastoma multiforme (WHO IV)
Glx	=	Glutamate and/or glutamine (*in vivo*)
GM	=	Gray matter
HPLC	=	High-pressure liquid chromatography
HRMAS	=	High resolution magic angle spinning
IGE	=	Idiopathic generalized epilepsy
Lac	=	Lactate
LCModel	=	Linear combination model
MET	=	Metastasis
MGH	=	Massachusetts general hospital
MI	=	Myo-inositol
MNG	=	Meningioma
MRS	=	Magnetic resonance spectroscopy
MRSI	=	Magnetic resonance spectroscopic imaging
MS	=	Multiple sclerosis
mTLE	=	Mesial temporal lobe epilepsy
NAA	=	N-acetyl aspartate
NAWM	=	Normal appearing white matter
NMR	=	Nuclear magnetic resonance
PA	=	Polyamines
PC	=	Principal component
PCA	=	Principal component analysis
PD	=	Parkinson disease
Phe	=	Phenylalanine
PPMS	=	Primary progressive multiple sclerosis
PRESS	=	Point-resolved spectroscopy
PSA	=	Prostate specific antigen
rCBF	=	Regional cerebral blood flow
rf	=	Radiofrequency
RRMS	=	Relapsing-remitting multiple sclerosis
SNR	=	Signal to noise ratio
SPMS	=	Secondary progressive multiple sclerosis
STEAM	=	Stimulated echo ecquisition eode
T1	=	Longitudinal relaxation time
T2	=	Transverse relaxation time
T	=	Tesla, the unit for magnetic field strength
TE	=	Echo time
TLE	=	Temporal lobe epilepsy
TM	=	Mixing time
TR	=	Recycle time
VOI	=	Volume of interest
WHO	=	World health organization
WM	=	White matter

REFERENCES

[1] Damadian R. Tumor detection by nuclear magnetic resonance. Science 1971; 171(976): 1151-1153.

[2] Callaghan PT. Principles of Nuclear Magnetic Resonance Microscopy. New York: Oxford University Press Inc.; 2003. 1-492 p.

[3] Haacke EM, Brown RW, Thompson MR, Venkatesan R. Magnetic Resonance Imaging: Physical Principles and Sequence Design. New York, NY: John Wiley & Sons, Inc.; 1999. 1-914 p.

[4] Salibi N, Brown MA. Clinical MR Spectroscopy: First Principles. New York: John Wiley & Sons, Inc.; 1998. 1-220 p.

[5] Ernst RR, Bodenhausen G, Wokaun A. Principles of Nuclear Magnetic Resonance in One and Two Dimension. New York: Clarendon Press; 1988. 1-610 p.

[6] Slichter CP. Principles of Magnetic Resonance. Cardona M, Fulde P, von Klitzing K, Queisser HJ, editors. New York: Springer-Verlag New York Berlin Heidelberg; 1990. 1-655 p.

[7] Pykett IL, Rosen BR. Nuclear magnetic resonance: *in vivo* proton chemical shift imaging. Work in progress. Radiology 1983; 149(1): 197-201.

[8] Maudsley AA, Hilal SK, Simon HE, Wittekoek S. *In vivo* MR spectroscopic imaging with P-31. Work in progress. Radiology 1984; 153(3): 745-750.

[9] Gordon RE. Topical magnetic resonance. Biosci Rep 1982; 2(9): 701-706.

[10] Gordon RE, Hanley PE, Shaw D, Gadian DG, Radda GK, Styles P, Bore PJ, Chan L. Localization of metabolites in animals using 31P topical magnetic resonance. Nature 1980; 287(5784): 736-738.

[11] Cox SJ, Styles P. Toward biochemical imaging. J Magn Reson 1980; 40: 209-212.

[12] Haase A, Frahm J, Hanicke W, Matthaei D. 1H NMR chemical shift selective (CHESS) imaging. Phys Med Biol 1985; 30(4): 341-344.

[13] Bottomley PA; General Electric Company, assignee. Selective volume method for performing localized NMR spectroscopy. United States patent 4480228. 1984 October 30, 1984.

[14] Frahm J, Merboldt KD, Hanicke W, al. e. Stimulated echo imaging. J Magn Reson 1985; 64: 81-95.

[15] Maudsley AA, Oppelt A, Ganssen A. Rapid measurement of magnetic field distribtions using nuclear magnetic resonance. Forsch u Entwickl - Ber Bd 1979; 8(6): 326-331.

[16] Maudsley AA, Hilal SK, Simon HE; Philips Medical Systems, Inc., assignee. NMR Imaging Methods. United States patent 4585992. 1986 April 29, 1986.

[17] Brown TR, Kincaid BM, Ugurbil K. NMR chemical shift imaging in three dimensions. Proc Natl Acad Sci U S A 1982; 79(11): 3523-3526.

[18] Gonen O, Viswanathan AK, Catalaa I, Babb J, Udupa J, Grossman RI. Total brain N-acetylaspartate concentration in normal, age-grouped females: quantitation with non-echo proton NMR spectroscopy. Magn Reson Med 1998; 40(5): 684-689.

[19] Bonneville F, Moriarty DM, Li BS, Babb JS, Grossman RI, Gonen O. Whole-brain N-acetylaspartate concentration: correlation with T2-weighted lesion volume and expanded disability status scale score in cases of relapsing-remitting multiple sclerosis. AJNR Am J Neuroradiol 2002; 23(3): 371-375.

[20] Bottomley PA. Spatial localization in NMR spectroscopy *in vivo*. Ann N Y Acad Sci 1987; 508: 333-348.

[21] Matthaei D, Frahm J, Haase A, Merboldt KD, Hanicke W. Multipurpose NMR imaging using stimulated echoes. Magn Reson Med 1986; 3(4): 554-561.

[22] Cheng LL, Ma MJ, Becerra L, Ptak T, Tracey I, Lackner A, Gonzalez RG. Quantitative neuropathology by high resolution magic angle spinning proton magnetic resonance spectroscopy. Proc Natl Acad Sci U S A 1997; 94(12): 6408-6413.

[23] Urenjak J, Williams SR, Gadian DG, Noble M. Specific expression of N-acetylaspartate in neurons, oligodendrocyte-type-2 astrocyte progenitors, and immature oligodendrocytes *in vitro*. J Neurochem 1992; 59(1): 55-61.

[24] Urenjak J, Williams SR, Gadian DG, Noble M. Proton nuclear magnetic resonance spectroscopy unambiguously identifies different neural cell types. J Neurosci 1993; 13(3): 981-989.

[25] Galanaud D, Nicoli F, Le Fur Y, Guye M, Ranjeva JP, Confort-Gouny S, Viout P, Soulier E, Cozzone PJ. Multimodal magnetic resonance imaging of the central nervous system. Biochimie 2003; 85(9): 905-914.

[26] Heerschap A, Kok RD, van den Berg PP. Antenatal proton MR spectroscopy of the human brain *in vivo*. Childs Nerv Syst 2003; 19(7-8): 418-421.

[27] Kok RD, van den Bergh AJ, Heerschap A, Nijland R, van den Berg PP. Metabolic information from the human fetal brain obtained with proton magnetic resonance spectroscopy. Am J Obstet Gynecol 2001; 185(5): 1011-1015.

[28] Kok RD, van den Berg PP, van den Bergh AJ, Nijland R, Heerschap A. Maturation of the human fetal brain as observed by 1H MR spectroscopy. Magn Reson Med 2002; 48(4): 611-616.

[29] Kreis R, Hofmann L, Kuhlmann B, Boesch C, Bossi E, Huppi PS. Brain metabolite composition during early human brain development as measured by quantitative *in vivo* 1H magnetic resonance spectroscopy. Magn Reson Med 2002; 48(6): 949-958.

[30] Valenzuela MJ, Sachdev PS, Wen W, Shnier R, Brodaty H, Gillies D. Dual voxel proton magnetic resonance spectroscopy in the healthy elderly: subcortical-frontal axonal N-acetylaspartate levels are correlated with fluid cognitive abilities independent of structural brain changes. Neuroimage 2000; 12(6): 747-756.

[31] Cooke FJ, Blamire AM, Manners DN, Styles P, Rajagopalan B. Quantitative proton magnetic resonance spectroscopy of the cervical spinal cord. Magn Reson Med 2004; 51(6): 1122-1128.

[32] Graham GD, Hwang JH, Rothman DL, Prichard JW. Spectroscopic assessment of alterations in macromolecule and small-molecule metabolites in human brain after stroke. Stroke 2001; 32(12): 2797-2802.

[33] Graham GD, Barker PB, Brooks WM, Morris DC, Ahmed W, Bryniarski E, Hearshen DO, Sanders JA, Holshouser BA, Turkel CC. MR spectroscopy study of dichloroacetate treatment after ischemic stroke. Neurology 2000; 55(9): 1376-1378.

[34] Parsons MW, Li T, Barber PA, Yang Q, Darby DG, Desmond PM, Gerraty RP, Tress BM, Davis SM. Combined (1)H MR spectroscopy and diffusion-weighted MRI improves the prediction of stroke outcome. Neurology 2000; 55(4): 498-505.

[35] Rumpel H, Lim WE, Chang HM, Chan LL, Ho GL, Wong MC, Tan KP. Is myo-inositol a measure of glial swelling after stroke? A magnetic resonance study. J Magn Reson Imaging 2003; 17(1): 11-19.

[36] Ashwal S, Holshouser BA, Shu SK, Simmons PL, Perkin RM, Tomasi LG, Knierim DS, Sheridan C, Craig K, Andrews GH, Hinshaw DB. Predictive value of proton magnetic resonance spectroscopy in pediatric closed head injury. Pediatr Neurol 2000; 23(2): 114-125.

[37] Barkovich AJ, Westmark KD, Bedi HS, Partridge JC, Ferriero DM, Vigneron DB. Proton spectroscopy and diffusion imaging on the first day of life after perinatal asphyxia: preliminary report. AJNR Am J Neuroradiol 2001; 22(9): 1786-1794.

[38] Kadri M, Shu S, Holshouser B, Deming D, Hopper A, Peverini R, Ashwal S. Proton magnetic resonance spectroscopy improves outcome prediction in perinatal CNS insults. J Perinatol 2003; 23(3): 181-185.

[39] Malik GK, Pandey M, Kumar R, Chawla S, Rathi B, Gupta RK. MR imaging and *in vivo* proton spectroscopy of the brain in neonates with hypoxic ischemic encephalopathy. Eur J Radiol 2002; 43(1): 6-13.

[40] Maneru C, Junque C, Bargallo N, Olondo M, Botet F, Tallada M, Guardia J, Mercader JM. (1)H-MR spectroscopy is sensitive to subtle effects of perinatal asphyxia. Neurology 2001; 57(6): 1115-1118.

[41] Brooks WM, Stidley CA, Petropoulos H, Jung RE, Weers DC, Friedman SD, Barlow MA, Sibbitt WL, Jr., Yeo RA. Metabolic and cognitive response to human traumatic brain injury: a quantitative proton magnetic resonance study. J Neurotrauma 2000; 17(8): 629-640.

[42] Garnett MR, Blamire AM, Corkill RG, Cadoux-Hudson TA, Rajagopalan B, Styles P. Early proton magnetic resonance spectroscopy in normal-appearing brain correlates with outcome in patients following traumatic brain injury. Brain 2000; 123 (Pt 10): 2046-2054.

[43] Garnett MR, Blamire AM, Rajagopalan B, Styles P, Cadoux-Hudson TA. Evidence for cellular damage in normal-appearing white matter correlates with injury severity in patients following traumatic brain injury: A magnetic resonance spectroscopy study. Brain 2000; 123 (Pt 7): 1403-1409.

[44] Garnett MR, Corkill RG, Blamire AM, Rajagopalan B, Manners DN, Young JD, Styles P, Cadoux-Hudson TA. Altered cellular metabolism following traumatic brain injury: a magnetic resonance spectroscopy study. J Neurotrauma 2001; 18(3): 231-240.

[45] Son BC, Park CK, Choi BG, Kim EN, Choe BY, Lee KS, Kim MC, Kang JK. Metabolic changes in pericontusional oedematous areas in mild head injury evaluated by 1H MRS. Acta Neurochir Suppl 2000; 76: 13-16.

[46] Chang L, Ernst T, Witt MD, Ames N, Gaiefsky M, Miller E. Relationships among brain metabolites, cognitive function, and viral loads in antiretroviral-naive HIV patients. Neuroimage 2002; 17(3): 1638-1648.

[47] Lee PL, Yiannoutsos CT, Ernst T, Chang L, Marra CM, Jarvik JG, Richards TL, Kwok EW, Kolson DL, Simpson D, Tang CY, Schifitto G, Ketonen LM, Meyerhoff DJ, Lenkinski RE, Gonzalez RG, Navia BA. A multi-center 1H MRS study of the AIDS dementia complex: validation and preliminary analysis. J Magn Reson Imaging 2003; 17(6): 625-633.

[48] Samann PG, Schlegel J, Muller G, Prantl F, Emminger C, Auer DP. Serial proton MR spectroscopy and diffusion imaging findings in HIV-related herpes simplex encephalitis. AJNR Am J Neuroradiol 2003; 24(10): 2015-2019.

[49] Gupta RK, Vatsal DK, Husain N, Chawla S, Prasad KN, Roy R, Kumar R, Jha D, Husain M. Differentiation of tuberculous from pyogenic brain abscesses with *in vivo* proton MR spectroscopy and magnetization transfer MR imaging. AJNR Am J Neuroradiol 2001; 22(8): 1503-1509.

[50] Garg M, Gupta RK, Husain M, Chawla S, Chawla J, Kumar R, Rao SB, Misra MK, Prasad KN. Brain abscesses: etiologic categorization with *in vivo* proton MR spectroscopy. Radiology 2004; 230(2): 519-527.

[51] Cucurella MG, Rovira A, Rio J, Pedraza S, Tintore MM, Montalban X, Alonso J. Proton magnetic resonance spectroscopy in primary and secondary progressive multiple sclerosis. NMR Biomed 2000; 13(2): 57-63.

[52] Garbern JY, Yool DA, Moore GJ, Wilds IB, Faulk MW, Klugmann M, Nave KA, Sistermans EA, van der Knaap MS, Bird TD, Shy ME, Kamholz JA, Griffiths IR. Patients lacking the major CNS myelin protein, proteolipid protein 1, develop length-dependent axonal degeneration in the absence of demyelination and inflammation. Brain 2002; 125(Pt 3): 551-561.

[53] Antuono PG, Jones JL, Wang Y, Li SJ. Decreased glutamate + glutamine in Alzheimer's disease detected *in vivo* with (1)H-MRS at 0.5 T. Neurology 2001; 56(6): 737-742.

[54] Block W, Traber F, Flacke S, Jessen F, Pohl C, Schild H. In-vivo proton MR-spectroscopy of the human brain: assessment of N-acetylaspartate (NAA) reduction as a marker for neurodegeneration. Amino Acids 2002; 23(1-3): 317-323.

[55] Catani M, Mecocci P, Tarducci R, Howard R, Pelliccioli GP, Mariani E, Metastasio A, Benedetti C, Senin U, Cherubini A. Proton magnetic resonance spectroscopy reveals similar white matter biochemical changes in patients with chronic hypertension and early Alzheimer's disease. J Am Geriatr Soc 2002; 50(10): 1707-1710.

[56] Dixon RM, Bradley KM, Budge MM, Styles P, Smith AD. Longitudinal quantitative proton magnetic resonance spectroscopy of the hippocampus in Alzheimer's disease. Brain 2002; 125(Pt 10): 2332-2341.

[57] Kantarci K, Jack CR, Jr., Xu YC, Campeau NG, O'Brien PC, Smith GE, Ivnik RJ, Boeve BF, Kokmen E, Tangalos EG, Petersen RC. Regional metabolic patterns in mild cognitive impairment and Alzheimer's disease: A 1H MRS study. Neurology 2000; 55(2): 210-217.

[58] Waldman AD, Rai GS. The relationship between cognitive impairment and *in vivo* metabolite ratios in patients with clinical Alzheimer's disease and vascular dementia: a proton magnetic resonance spectroscopy study. Neuroradiology 2003; 45(8): 507-512.

[59] Baik HM, Choe BY, Son BC, Jeun SS, Kim MC, Lee KS, Kim BS, Lee JM, Lee HK, Suh TS. Proton MR spectroscopic changes in Parkinson's diseases after thalamotomy. Eur J Radiol 2003; 47(3): 179-187.

[60] Summerfield C, Gomez-Anson B, Tolosa E, Mercader JM, Marti MJ, Pastor P, Junque C. Dementia in Parkinson disease: a proton magnetic resonance spectroscopy study. Arch Neurol 2002; 59(9): 1415-1420.

[61] Bowen BC, Pattany PM, Bradley WG, Murdoch JB, Rotta F, Younis AA, Duncan RC, Quencer RM. MR imaging and localized proton spectroscopy of the precentral gyrus in amyotrophic lateral sclerosis. AJNR Am J Neuroradiol 2000; 21(4): 647-658.

[62] Ellis CM, Simmons A, Glover A, Dawson JM, Williams SC, Leigh PN. Quantitative proton magnetic resonance spectroscopy of the subcortical white matter in motor neuron disease. Amyotroph Lateral Scler Other Motor Neuron Disord 2000; 1(2): 123-129.

[63] Abe K, Takanashi M, Watanabe Y, Tanaka H, Fujita N, Hirabuki N, Yanagihara T. Decrease in N-acetylaspartate/creatine ratio in the motor area and the frontal lobe in amyotrophic lateral sclerosis. Neuroradiology 2001; 43(7): 537-541.

[64] Sarchielli P, Pelliccioli GP, Tarducci R, Chiarini P, Presciutti O, Gobbi G, Gallai V. Magnetic resonance imaging and 1H-magnetic resonance spectroscopy in amyotrophic lateral sclerosis. Neuroradiology 2001; 43(3): 189-197.

[65] Kenn W, Ochs G, Pabst TA, Hahn D. 1H spectroscopy in patients with amyotrophic lateral sclerosis. J Neuroimaging 2001; 11(3): 293-297.

[66] Pohl C, Block W, Karitzky J, Traber F, Schmidt S, Grothe C, Lamerichs R, Schild H, Klockgether T. Proton magnetic resonance spectroscopy of the motor cortex in 70 patients with amyotrophic lateral sclerosis. Arch Neurol 2001; 58(5): 729-735.

[67] Cheng LL, Newell K, Mallory AE, Hyman BT, Gonzalez RG. Quantification of neurons in Alzheimer and control brains with ex vivo high resolution magic angle spinning proton magnetic resonance spectroscopy and stereology. Magn Reson Imaging 2002; 20(7): 527-533.

[68] Garseth M, Sonnewald U, White LR, Rod M, Zwart JA, Nygaard O, Aasly J. Proton magnetic resonance spectroscopy of cerebrospinal fluid in neurodegenerative disease: indication of glial energy impairment in Huntington chorea, but not Parkinson disease. J Neurosci Res 2000; 60(6): 779-782.

[69] Wilken B, Dechent P, Brockmann K, Finsterbusch J, Baumann M, Ebell W, Korenke GC, Pouwels PJ, Hanefeld FA, Frahm J. Quantitative proton magnetic resonance spectroscopy of children with adrenoleukodystrophy before and after hematopoietic stem cell transplantation. Neuropediatrics 2003; 34(5): 237-246.

[70] De Stefano N, Dotti MT, Mortilla M, Federico A. Magnetic resonance imaging and spectroscopic changes in brains of patients with cerebrotendinous xanthomatosis. Brain 2001; 124(Pt 1): 121-131.

[71] Geissler A, Frund R, Scholmerich J, Feuerbach S, Zietz B. Alterations of cerebral metabolism in patients with diabetes mellitus studied by proton magnetic resonance spectroscopy. Exp Clin Endocrinol Diabetes 2003; 111(7): 421-427.

[72] Leuzzi V, Bianchi MC, Tosetti M, Carducci CL, Carducci CA, Antonozzi I. Clinical significance of brain phenylalanine concentration assessed by *in vivo* proton magnetic resonance spectroscopy in phenylketonuria. J Inherit Metab Dis 2000; 23(6): 563-570.

[73] Mortilla M, Ermini M, Nistri M, Dal Pozzo G, Falcini F. Brain study using magnetic resonance imaging and proton MR spectroscopy in pediatric onset systemic lupus erythematosus. Clin Exp Rheumatol 2003; 21(1): 129-135.

[74] Axford JS, Howe FA, Heron C, Griffiths JR. Sensitivity of quantitative (1)H magnetic resonance spectroscopy of the brain in detecting early neuronal damage in systemic lupus erythematosus. Ann Rheum Dis 2001; 60(2): 106-111.

[75] Grachev ID, Fredrickson BE, Apkarian AV. Abnormal brain chemistry in chronic back pain: an *in vivo* proton magnetic resonance spectroscopy study. Pain 2000; 89(1): 7-18.

[76] Puri BK, Counsell SJ, Zaman R, Main J, Collins AG, Hajnal JV, Davey NJ. Relative increase in choline in the occipital cortex in chronic fatigue syndrome. Acta Psychiatr Scand 2002; 106(3): 224-226.

[77] Shim TS, Lee JH, Kim SY, Lim TH, Kim SJ, Kim DS, Kim WD. Cerebral metabolic abnormalities in COPD patients detected by localized proton magnetic resonance spectroscopy. Chest 2001; 120(5): 1506-1513.

[78] Tarasow E, Panasiuk A, Siergiejczyk L, Orzechowska-Bobkiewicz A, Lewszuk A, Walecki J, Prokopowicz D. MR and 1H MR spectroscopy of the brain in patients with liver cirrhosis and early stages of hepatic encephalopathy. Hepatogastroenterology 2003; 50(54): 2149-2153.

[79] Rovira A, Grive E, Pedraza S, Alonso J. Magnetization transfer ratio values and proton MR spectroscopy of normal-appearing cerebral white matter in patients with liver cirrhosis. AJNR Am J Neuroradiol 2001; 22(6): 1137-1142.

[80] Spahr L, Vingerhoets F, Lazeyras F, Delavelle J, DuPasquier R, Giostra E, Mentha G, Terrier F, Hadengue A. Magnetic resonance imaging and proton spectroscopic alterations correlate with parkinsonian signs in patients with cirrhosis. Gastroenterology 2000; 119(3): 774-781.

[81] Walecki J, Michalak MJ, Michalak E, Bilinska ZT, Ruzyllo W. Usefulness of 1H MR spectroscopy in the evaluation of myocardial metabolism in patients with dilated idiopathic cardiomyopathy: pilot study. Acad Radiol 2003; 10(10): 1187-1192.

[82] Goddard AW, Mason GF, Almai A, Rothman DL, Behar KL, Petroff OA, Charney DS, Krystal JH. Reductions in occipital cortex GABA levels in panic disorder detected with 1h-magnetic resonance spectroscopy. Arch Gen Psychiatry 2001; 58(6): 556-561.

[83] Massana G, Gasto C, Junque C, Mercader JM, Gomez B, Massana J, Torres X, Salamero M. Reduced levels of creatine in the right medial temporal lobe region of panic disorder patients detected with (1)H magnetic resonance spectroscopy. Neuroimage 2002; 16(3 Pt 1): 836-842.

[84] Jung RE, Yeo RA, Love TM, Petropoulos H, Sibbitt WL, Jr., Brooks WM. Biochemical markers of mood: a proton magnetic resonance spectroscopy study of normal human brain. Biol Psychiatry 2002; 51(3): 224-229.

[85] Mullins PG, Rowland L, Bustillo J, Bedrick EJ, Lauriello J, Brooks WM. Reproducibility of 1H-MRS measurements in schizophrenic patients. Magn Reson Med 2003; 50(4): 704-707.

[86] Yeo RA, Hill DE, Campbell RA, Vigil J, Petropoulos H, Hart B, Zamora L, Brooks WM. Proton magnetic resonance spectroscopy investigation of the right frontal lobe in children with attention-deficit/hyperactivity disorder. J Am Acad Child Adolesc Psychiatry 2003; 42(3): 303-310.

[87] Kantarci K, Shin C, Britton JW, So EL, Cascino GD, Jack CR, Jr. Comparative diagnostic utility of 1H MRS and DWI in evaluation of temporal lobe epilepsy. Neurology 2002; 58(12): 1745-1753.

[88] Park SW, Chang KH, Kim HD, Song IC, Lee DS, Lee SK, Chung CK, Yu IK, Han MH, Park YH. Lateralizing ability of single-voxel proton mr spectroscopy in hippocampal sclerosis: comparison with

mr imaging and positron emission tomography. AJNR Am J Neuroradiol 2001; 22(4): 625-631.

[89] Provencher SW. Estimation of metabolite concentrations from localized *in vivo* proton NMR spectra. Magn Reson Med 1993; 30(6): 672-679.

[90] Provencher SW. Automatic quantitation of localized *in vivo* 1H spectra with LCModel. NMR Biomed 2001; 14(4): 260-264.

[91] Govindaraju V, Young K, Maudsley AA. Proton NMR chemical shifts and coupling constants for brain metabolites. NMR Biomed 2000; 13(3): 129-153.

[92] Alkan A, Sarac K, Kutlu R, Yakinci C, Sigirci A, Aslan M, Ozcan H, Yologlu S. Proton MR spectroscopy features of normal appearing white matter in neurofibromatosis type 1. Magn Reson Imaging 2003; 21(9): 1049-1053.

[93] Freeman JL, Coleman LT, Wellard RM, Kean MJ, Rosenfeld JV, Jackson GD, Berkovic SF, Harvey AS. MR imaging and spectroscopic study of epileptogenic hypothalamic hamartomas: analysis of 72 cases. AJNR Am J Neuroradiol 2004; 25(3): 450-462.

[94] Gajewicz W, Papierz W, Szymczak W, Goraj B. The use of proton MRS in the differential diagnosis of brain tumors and tumor-like processes. Med Sci Monit 2003; 9(9): MT97-105.

[95] Hayashi T, Kumabe T, Jokura H, Fujihara K, Shiga Y, Watanabe M, Higano S, Shirane R. Inflammatory demyelinating disease mimicking malignant glioma. J Nucl Med 2003; 44(4): 565-569.

[96] Harada M, Uno M, Hong F, Hisaoka S, Nishitani H, Matsuda T. Diffusion-weighted *in vivo* localized proton MR spectroscopy of human cerebral ischemia and tumor. NMR Biomed 2002; 15(1): 69-74.

[97] Wilken B, Dechent P, Herms J, Maxton C, Markakis E, Hanefeld F, Frahm J. Quantitative proton magnetic resonance spectroscopy of focal brain lesions. Pediatr Neurol 2000; 23(1): 22-31.

[98] Murphy M, Loosemore A, Clifton AG, Howe FA, Tate AR, Cudlip SA, Wilkins PR, Griffiths JR, Bell BA. The contribution of proton magnetic resonance spectroscopy (1HMRS) to clinical brain tumour diagnosis. Br J Neurosurg 2002; 16(4): 329-334.

[99] Majos C, Alonso J, Aguilera C, Serrallonga M, Perez-Martin J, Acebes JJ, Arus C, Gili J. Proton magnetic resonance spectroscopy ((1)H MRS) of human brain tumours: assessment of differences between tumour types and its applicability in brain tumour categorization. Eur Radiol 2003; 13(3): 582-591.

[100] Moller-Hartmann W, Herminghaus S, Krings T, Marquardt G, Lanfermann H, Pilatus U, Zanella FE. Clinical application of proton magnetic resonance spectroscopy in the diagnosis of intracranial mass lesions. Neuroradiology 2002; 44(5): 371-381.

[101] Howe FA, Barton SJ, Cudlip SA, Stubbs M, Saunders DE, Murphy M, Wilkins P, Opstad KS, Doyle VL, McLean MA, Bell BA, Griffiths JR. Metabolic profiles of human brain tumors using quantitative *in vivo* 1H magnetic resonance spectroscopy. Magn Reson Med 2003; 49(2): 223-232.

[102] Murphy PS, Rowland IJ, Viviers L, Brada M, Leach MO, Dzik-Jurasz AS. Could assessment of glioma methylene lipid resonance by *in vivo* (1)H-MRS be of clinical value? Br J Radiol 2003; 76(907): 459-463.

[103] Kuesel AC, Briere KM, Halliday WC, Sutherland GR, Donnelly SM, Smith ICP. Mobile lipid accumulation in necrotic tissue of high grade astrocytomas. Anticancer Res 1996; 16: 1485-1490.

[104] Cheng LL, Chang IW, Louis DN, Gonzalez RG. Correlation of high-resolution magic angle spinning proton magnetic resonance spectroscopy with histopathology of intact human brain tumor specimens. Cancer Res 1998; 58(9): 1825-1832.

[105] Cheng LL, Anthony DC, Comite AR, Black PM, Tzika AA, Gonzalez RG. Quantification of microheterogeneity in glioblastoma multiforme with ex vivo high-resolution magic-angle spinning (HRMAS) proton magnetic resonance spectroscopy. Neuro-oncol 2000; 2(2): 87-95.

[106] Tate AR, Majos C, Moreno A, Howe FA, Griffiths JR, Arus C. Automated classification of short echo time in *in vivo* 1H brain tumor spectra: a multicenter study. Magn Reson Med 2003; 49(1): 29-36.

[107] Herminghaus S, Pilatus U, Moller-Hartmann W, Raab P, Lanfermann H, Schlote W, Zanella FE. Increased choline levels coincide with enhanced proliferative activity of human neuroepithelial brain tumors. NMR Biomed 2002; 15(6): 385-392.

[108] Shimizu H, Kumabe T, Shirane R, Yoshimoto T. Correlation between choline level measured by proton MR spectroscopy and Ki-67 labeling index in gliomas. AJNR Am J Neuroradiol 2000; 21(4): 659-665.

[109] Opstad KS, Provencher SW, Bell BA, Griffiths JR, Howe FA. Detection of elevated glutathione in meningiomas by quantitative *in vivo* 1H MRS. Magn Reson Med 2003; 49(4): 632-637.

[110] Isobe T, Matsumura A, Anno I, Yoshizawa T, Nagatomo Y, Itai Y, Nose T. Quantification of cerebral metabolites in glioma patients with proton MR spectroscopy using T2 relaxation time correction. Magn Reson Imaging 2002; 20(4): 343-349.

[111] Murphy PS, Dzik-Jurasz AS, Leach MO, Rowland IJ. The effect of Gd-DTPA on T(1)-weighted choline signal in human brain tumours. Magn Reson Imaging 2002; 20(1): 127-130.

[112] Davidson A, Payne G, Leach MO, McVicar D, Britton JM, Watson M, Tait DM. Proton magnetic resonance spectroscopy ((1)H-MRS) of the brain following high-dose methotrexate treatment for childhood cancer. Med Pediatr Oncol 2000; 35(1): 28-34.

[113] Rock JP, Scarpace L, Hearshen D, Gutierrez J, Fisher JL, Rosenblum M, Mikkelsen T. Associations among magnetic resonance spectroscopy, apparent diffusion coefficients, and image-guided histopathology with special attention to radiation necrosis. Neurosurgery 2004; 54(5): 1111-1117; discussion 1117-1119.

[114] Schlemmer HP, Bachert P, Herfarth KK, Zuna I, Debus J, van Kaick G. Proton MR spectroscopic evaluation of suspicious brain lesions after stereotactic radiotherapy. AJNR Am J Neuroradiol 2001; 22(7): 1316-1324.

[115] Kallen K, Burtscher IM, Holtas S, Ryding E, Rosen I. 201Thallium SPECT and 1H-MRS compared with MRI in chemotherapy monitoring of high-grade malignant astrocytomas. J Neurooncol 2000; 46(2): 173-185.

[116] Murphy PS, Viviers L, Abson C, Rowland IJ, Brada M, Leach MO, Dzik-Jurasz AS. Monitoring temozolomide treatment of low-grade glioma with proton magnetic resonance spectroscopy. Br J Cancer 2004; 90(4): 781-786.

[117] Bolan PJ, Meisamy S, Baker EH, Lin J, Emory T, Nelson M, Everson LI, Yee D, Garwood M. *In vivo* quantification of choline compounds in the breast with 1H MR spectroscopy. Magn Reson Med 2003; 50(6): 1134-1143.

[118] Cecil KM, Schnall MD, Siegelman ES, Lenkinski RE. The evaluation of human breast lesions with magnetic resonance imaging and proton magnetic resonance spectroscopy. Breast Cancer Res Treat 2001; 68(1): 45-54.

[119] Yeung DK, Yang WT, Tse GM. Breast cancer: *in vivo* proton MR spectroscopy in the characterization of histopathologic subtypes and preliminary observations in axillary node metastases. Radiology 2002; 225(1): 190-197.

[120] Bolan PJ, DelaBarre L, Baker EH, Merkle H, Everson LI, Yee D, Garwood M. Eliminating spurious lipid sidebands in 1H MRS of breast lesions. Magn Reson Med 2002; 48(2): 215-222.

[121] Mountford CE, Somorjai RL, Malycha P, Gluch L, Lean C, Russell P, Barraclough B, Gillett D, Himmelreich U, Dolenko B, Nikulin AE, Smith IC. Diagnosis and prognosis of breast cancer by magnetic resonance spectroscopy of fine-needle aspirates analysed using a statistical classification strategy. Br J Surg 2001; 88(9): 1234-1240.

[122] Cheng LL, Chang IW, Smith BL, Gonzalez RG. Evaluating human breast ductal carcinomas with high-resolution magic-angle spinning proton magnetic resonance spectroscopy. J Magn Reson 1998; 135(1): 194-202.

[123] Sitter B, Sonnewald U, Spraul M, Fjosne HE, Gribbestad IS. High-resolution magic angle spinning MRS of breast cancer tissue. NMR Biomed 2002; 15(5): 327-337.

[124] Allen JR, Prost RW, Griffith OW, Erickson SJ, Erickson BA. *In vivo* proton (H1) magnetic resonance spectroscopy for cervical carcinoma. Am J Clin Oncol 2001; 24(5): 522-529.

[125] Mahon MM, Cox IJ, Dina R, Soutter WP, McIndoe GA, Williams AD, deSouza NM. (1)H magnetic resonance spectroscopy of preinvasive and invasive cervical cancer: *in vivo*-ex vivo profiles and effect of tumor load. J Magn Reson Imaging 2004; 19(3): 356-364.

[126] Mahon MM, Williams AD, Soutter WP, Cox IJ, McIndoe GA, Coutts GA, Dina R, deSouza NM. 1H magnetic resonance spectroscopy of invasive cervical cancer: an *in vivo* study with ex vivo corroboration. NMR Biomed 2004; 17(1): 1-9.

[127] Oya N, Aoki J, Shinozaki T, Watanabe H, Takagishi K, Endo K. Preliminary study of proton magnetic resonance spectroscopy in bone and soft tissue tumors: an unassigned signal at 2.0-2.1 ppm

may be a possible indicator of malignant neuroectodermal tumor. Radiat Med 2000; 18(3): 193-198.

[128] Schwarz AJ, Maisey NR, Collins DJ, Cunningham D, Huddart R, Leach MO. Early *in vivo* detection of metabolic response: a pilot study of 1H MR spectroscopy in extracranial lymphoma and germ cell tumours. Br J Radiol 2002; 75(900): 959-966.

[129] Star-Lack JM, Adalsteinsson E, Adam MF, Terris DJ, Pinto HA, Brown JM, Spielman DM. *In vivo* 1H MR spectroscopy of human head and neck lymph node metastasis and comparison with oxygen tension measurements. AJNR Am J Neuroradiol 2000; 21(1): 183-193.

[130] Okada T, Harada M, Matsuzaki K, Nishitani H, Aono T. Evaluation of female intrapelvic tumors by clinical proton MR spectroscopy. J Magn Reson Imaging 2001; 13(6): 912-917.

[131] Dzik-Jurasz AS, Murphy PS, George M, Prock T, Collins DJ, Swift I, Leach MO, Rowland IJ. Human rectal adenocarcinoma: demonstration of 1H-MR spectra *in vivo* at 1.5 T. Magn Reson Med 2002; 47(4): 809-811.

[132] Katz-Brull R, Rofsky NM, Lenkinski RE. Breathhold abdominal and thoracic proton MR spectroscopy at 3T. Magn Reson Med 2003; 50(3): 461-467.

[133] Mountford CE, Delikatny EJ, Dyne M, Holmes KT, Mackinnon WB, Ford R, Hunter JC, Truskett ID, Russell P. Uterine cervical punch biopsy specimens can be analyzed by 1H MRS. Magn Reson Med 1990; 13(2): 324-331.

[134] Delikatny E, Russell P, Hunter J, Hancock R, Atkinson K, van Haaften-Day C, Mountford C. Proton MR and human cervical neoplasia. I. Ex vivo spectroscopy allows distinction of invasive carcinoma of the cervix from carcinoma in situ and other preinvasive lesions. Radiology 1993; 188: 791-796.

[135] Sitter B, Bathen T, Hagen B, Arentz C, Skjeldestad FE, Gribbestad IS. Cervical cancer tissue characterized by high-resolution magic angle spinning MR spectroscopy. MAGMA 2004; 16(4): 174-181.

[136] Mahon MM, deSouza NM, Dina R, Soutter WP, McIndoe GA, Williams AD, Cox IJ. Preinvasive and invasive cervical cancer: an ex vivo proton magic angle spinning magnetic resonance spectroscopy study. NMR Biomed 2004; 17(3): 144-153.

[137] Kamba M, Meshitsuka S, Iriguchi N, Koda M, Kimura K, Ogawa T. Measurement of relative fat content by proton magnetic resonance spectroscopy using a clinical imager. J Magn Reson Imaging 2000; 11(3): 330-335.

[138] Kamba M, Kimura K, Koda M, Ogawa T. Proton magnetic resonance spectroscopy for assessment of human body composition. Am J Clin Nutr 2001; 73(2): 172-176.

[139] Sinha R, Dufour S, Petersen KF, LeBon V, Enoksson S, Ma YZ, Savoye M, Rothman DL, Shulman GI, Caprio S. Assessment of skeletal muscle triglyceride content by (1)H nuclear magnetic resonance spectroscopy in lean and obese adolescents: relationships to insulin sensitivity, total body fat, and central adiposity. Diabetes 2002; 51(4): 1022-1027.

[140] Renema WK, Klomp DW, Philippens ME, van den Bergh AJ, Wieringa B, Heerschap A. Magnetization transfer effect on the creatine methyl resonance studied by CW off-resonance irradiation in human skeletal muscle on a clinical MR system. Magn Reson Med 2003; 50(3): 468-473.

[141] Rico-Sanz J, Moosavi M, Thomas EL, McCarthy J, Coutts GA, Saeed N, Bell JD. *In vivo* evaluation of the effects of continuous exercise on skeletal muscle triglycerides in trained humans. Lipids 2000; 35(12): 1313-1318.

[142] Prescot AP, Collins DJ, Leach MO, Dzik-Jurasz AS. Human gallbladder bile: noninvasive investigation *in vivo* with single-voxel 1H MR spectroscopy. Radiology 2003; 229(2): 587-592.

[143] Dzik-Jurasz AS, Prescot AP, Leach MO, Collins DJ. Non-invasive study of human gall bladder bile *in vivo* using (1)H-MR spectroscopy. Br J Radiol 2003; 76(907): 483-486.

[144] Jacobs MA, Horska A, van Zijl PC, Barker PB. Quantitative proton MR spectroscopic imaging of normal human cerebellum and brain stem. Magn Reson Med 2001; 46(4): 699-705.

[145] Wiedermann D, Schuff N, Matson GB, Soher BJ, Du AT, Maudsley AA, Weiner MW. Short echo time multislice proton magnetic resonance spectroscopic imaging in human brain: metabolite distributions and reliability. Magn Reson Imaging 2001; 19(8): 1073-1080.

[146] McLean MA, Woermann FG, Simister RJ, Barker GJ, Duncan JS. *In vivo* short echo time 1H-magnetic resonance spectroscopic imaging (MRSI) of the temporal lobes. Neuroimage 2001; 14(2): 501-509.

[147] Vigneron D, Bollen A, McDermott M, Wald L, Day M, Moyher-Noworolski S, Henry R, Chang S, Berger M, Dillon W, Nelson S. Three-dimensional magnetic resonance spectroscopic imaging of histologically confirmed brain tumors. Magn Reson Imaging 2001; 19(1): 89-101.

[148] Kadota T, Horinouchi T, Kuroda C. Development and aging of the cerebrum: assessment with proton MR spectroscopy. AJNR Am J Neuroradiol 2001; 22(1): 128-135.

[149] Horska A, Kaufmann WE, Brant LJ, Naidu S, Harris JC, Barker PB. *In vivo* quantitative proton MRSI study of brain development from childhood to adolescence. J Magn Reson Imaging 2002; 15(2): 137-143.

[150] Rotondo E, Bruschetta G, Sacca A, Bramanti P, Di Pasquale MR. Straightforward relative quantitation and age-related human standards of N-acetylaspartate at the centrum semiovale level by CSI (1)H-MRS. Magn Reson Imaging 2003; 21(9): 1055-1060.

[151] Schuff N, Ezekiel F, Gamst AC, Amend DL, Capizzano AA, Maudsley AA, Weiner MW. Region and tissue differences of metabolites in normally aged brain using multislice 1H magnetic resonance spectroscopic imaging. Magn Reson Med 2001; 45(5): 899-907.

[152] Carhuapoma JR, Wang PY, Beauchamp NJ, Keyl PM, Hanley DF, Barker PB. Diffusion-weighted MRI and proton MR spectroscopic imaging in the study of secondary neuronal injury after intracerebral hemorrhage. Stroke 2000; 31(3): 726-732.

[153] Mihara F, Kuwabara Y, Yoshida T, Yoshiura T, Sasaki M, Masuda K, Matsushima T, Fukui M. Correlation between proton magnetic resonance spectroscopic lactate measurements and vascular reactivity in chronic occlusive cerebrovascular disease: a comparison with positron emission tomography. Magn Reson Imaging 2000; 18(9): 1167-1174.

[154] Chu WJ, Mason GF, Pan JW, Hetherington HP, Liu HG, San Pedro EC, Mountz JM. Regional cerebral blood flow and magnetic resonance spectroscopic imaging findings in diaschisis from stroke. Stroke 2002; 33(5): 1243-1248.

[155] Govindaraju V, Gauger GE, Manley GT, Ebel A, Meeker M, Maudsley AA. Volumetric proton spectroscopic imaging of mild traumatic brain injury. AJNR Am J Neuroradiol 2004; 25(5): 730-737.

[156] Miller SP, McQuillen PS, Vigneron DB, Glidden DV, Barkovich AJ, Ferriero DM, Hamrick SE, Azakie A, Karl TR. Preoperative brain injury in newborns with transposition of the great arteries. Ann Thorac Surg 2004; 77(5): 1698-1706.

[157] Pelletier D, Nelson SJ, Oh J, Antel JP, Kita M, Zamvil SS, Goodkin DE. MRI lesion volume heterogeneity in primary progressive MS in relation with axonal damage and brain atrophy. J Neurol Neurosurg Psychiatry 2003; 74(7): 950-952.

[158] Suhy J, Rooney WD, Goodkin DE, Capizzano AA, Soher BJ, Maudsley AA, Waubant E, Andersson PB, Weiner MW. 1H MRSI comparison of white matter and lesions in primary progressive and relapsing-remitting MS. Mult Scler 2000; 6(3): 148-155.

[159] Kapeller P, McLean MA, Griffin CM, Chard D, Parker GJ, Barker GJ, Thompson AJ, Miller DH. Preliminary evidence for neuronal damage in cortical grey matter and normal appearing white matter in short duration relapsing-remitting multiple sclerosis: a quantitative MR spectroscopic imaging study. J Neurol 2001; 248(2): 131-138.

[160] Inglese M, Li BS, Rusinek H, Babb JS, Grossman RI, Gonen O. Diffusely elevated cerebral choline and creatine in relapsing-remitting multiple sclerosis. Magn Reson Med 2003; 50(1): 190-195.

[161] Chard DT, Griffin CM, McLean MA, Kapeller P, Kapoor R, Thompson AJ, Miller DH. Brain metabolite changes in cortical grey and normal-appearing white matter in clinically early relapsing-remitting multiple sclerosis. Brain 2002; 125(Pt 10): 2342-2352.

[162] Sharma R, Narayana PA, Wolinsky JS. Grey matter abnormalities in multiple sclerosis: proton magnetic resonance spectroscopic imaging. Mult Scler 2001; 7(4): 221-226.

[163] Schocke MF, Berger T, Felber SR, Wolf C, Deisenhammer F, Kremser C, Seppi K, Aichner FT. Serial contrast-enhanced magnetic resonance imaging and spectroscopic imaging of acute multiple sclerosis lesions under high-dose methylprednisolone therapy. Neuroimage 2003; 20(2): 1253-1263.

[164] Tedeschi G, Bonavita S, McFarland HF, Richert N, Duyn JH, Frank JA. Proton MR spectroscopic imaging in multiple sclerosis. Neuroradiology 2002; 44(1): 37-42.

[165] De Stefano N, Narayanan S, Francis GS, Arnaoutelis R, Tartaglia MC, Antel JP, Matthews PM, Arnold DL. Evidence of axonal damage in the early stages of multiple sclerosis and its relevance to disability. Arch Neurol 2001; 58(1): 65-70.

[166] Reddy H, Narayanan S, Arnoutelis R, Jenkinson M, Antel J, Matthews PM, Arnold DL. Evidence for adaptive functional changes in the cerebral cortex with axonal injury from multiple sclerosis. Brain 2000; 123 (Pt 11): 2314-2320.

[167] Tartaglia MC, Narayanan S, De Stefano N, Arnaoutelis R, Antel SB, Francis SJ, Santos AC, Lapierre Y, Arnold DL. Choline is increased in pre-lesional normal appearing white matter in multiple sclerosis. J Neurol 2002; 249(10): 1382-1390.

[168] Oh J, Pelletier D, Nelson SJ. Corpus callosum axonal injury in multiple sclerosis measured by proton magnetic resonance spectroscopic imaging. Arch Neurol 2004; 61(7): 1081-1086.

[169] Schuff N, Capizzano AA, Du AT, Amend DL, O'Neill J, Norman D, Kramer J, Jagust W, Miller B, Wolkowitz OM, Yaffe K, Weiner MW. Selective reduction of N-acetylaspartate in medial temporal and parietal lobes in AD. Neurology 2002; 58(6): 928-935.

[170] Colla M, Ende G, Bohrer M, Deuschle M, Kronenberg G, Henn F, Heuser I. MR spectroscopy in Alzheimer's disease: gender differences in probabilistic learning capacity. Neurobiol Aging 2003; 24(4): 545-552.

[171] Frederick B, Satlin A, Wald LL, Hennen J, Bodick N, Renshaw PF. Brain proton magnetic resonance spectroscopy in Alzheimer disease: changes after treatment with xanomeline. Am J Geriatr Psychiatry 2002; 10(1): 81-88.

[172] Mielke R, Schopphoff HH, Kugel H, Pietrzyk U, Heindel W, Kessler J, Heiss WD. Relation between 1H MR spectroscopic imaging and regional cerebral glucose metabolism in Alzheimer's disease. Int J Neurosci 2001; 107(3-4): 233-245.

[173] Schuff N, Rooney WD, Miller R, Gelinas DF, Amend DL, Maudsley AA, Weiner MW. Reanalysis of multislice (1)H MRSI in amyotrophic lateral sclerosis. Magn Reson Med 2001; 45(3): 513-516.

[174] Suhy J, Miller RG, Rule R, Schuff N, Licht J, Dronsky V, Gelinas D, Maudsley AA, Weiner MW. Early detection and longitudinal changes in amyotrophic lateral sclerosis by (1)H MRSI. Neurology 2002; 58(5): 773-779.

[175] Kalra S, Genge A, Arnold DL. A prospective, randomized, placebo-controlled evaluation of corticoneuronal response to intrathecal BDNF therapy in ALS using magnetic resonance spectroscopy: feasibility and results. Amyotroph Lateral Scler Other Motor Neuron Disord 2003; 4(1): 22-26.

[176] Kalra S, Cashman NR, Caramanos Z, Genge A, Arnold DL. Gabapentin therapy for amyotrophic lateral sclerosis: lack of improvement in neuronal integrity shown by MR spectroscopy. AJNR Am J Neuroradiol 2003; 24(3): 476-480.

[177] Fatemi A, Barker PB, Ulug AM, Nagae-Poetscher LM, Beauchamp NJ, Moser AB, Raymond GV, Moser HW, Naidu S. MRI and proton MRSI in women heterozygous for X-linked adrenoleukodystrophy. Neurology 2003; 60(8): 1301-1307.

[178] Eichler FS, Barker PB, Cox C, Edwin D, Ulug AM, Moser HW, Raymond GV. Proton MR spectroscopic imaging predicts lesion progression on MRI in X-linked adrenoleukodystrophy. Neurology 2002; 58(6): 901-907.

[179] Izquierdo M, Adamsbaum C, Benosman A, Aubourg P, Bittoun J. MR spectroscopic imaging of normal-appearing white matter in adrenoleukodystrophy. Pediatr Radiol 2000; 30(9): 621-629.

[180] Sijens PE, Oudkerk M, Reijngoud DJ, Leenders KL, De Valk HW, Van Spronsen FJ. 1H MR chemical shift imaging detection of phenylalanine in patients suffering from phenylketonuria (PKU). Eur Radiol 2004; 14(10): 1895-1900.

[181] Ende G, Braus DF, Walter S, Weber-Fahr W, Henn FA. Multiregional 1H-MRSI of the hippocampus, thalamus, and basal ganglia in schizophrenia. Eur Arch Psychiatry Clin Neurosci 2003; 253(1): 9-15.

[182] O'Neill J, Levitt J, Caplan R, Asarnow R, McCracken JT, Toga AW, Alger JR. 1H MRSI evidence of metabolic abnormalities in childhood-onset schizophrenia. Neuroimage 2004; 21(4): 1781-1789.

[183] Bertolino A, Callicott JH, Mattay VS, Weidenhammer KM, Rakow R, Egan MF, Weinberger DR. The effect of treatment with antipsychotic drugs on brain N-acetylaspartate measures in patients with schizophrenia. Biol Psychiatry 2001; 49(1): 39-46.

[184] Braus DF, Ende G, Weber-Fahr W, Demirakca T, Henn FA. Favorable effect on neuronal viability in the anterior cingulate gyrus due to long-term treatment with atypical antipsychotics: an MRSI study. Pharmacopsychiatry 2001; 34(6): 251-253.

[185] Layton ME, Friedman SD, Dager SR. Brain metabolic changes during lactate-induced panic: effects of gabapentin treatment. Depress Anxiety 2001; 14(4): 251-254.

[186] Levitt JG, O'Neill J, Blanton RE, Smalley S, Fadale D, McCracken JT, Guthrie D, Toga AW, Alger JR. Proton magnetic resonance spectroscopic imaging of the brain in childhood autism. Biol Psychiatry 2003; 54(12): 1355-1366.

[187] Smith EA, Russell A, Lorch E, Banerjee SP, Rose M, Ivey J, Bhandari R, Moore GJ, Rosenberg DR. Increased medial thalamic choline found in pediatric patients with obsessive-compulsive disorder versus major depression or healthy control subjects: a magnetic resonance spectroscopy study. Biol Psychiatry 2003; 54(12): 1399-1405.

[188] Vythilingam M, Charles HC, Tupler LA, Blitchington T, Kelly L, Krishnan KR. Focal and lateralized subcortical abnormalities in unipolar major depressive disorder: an automated multivoxel proton magnetic resonance spectroscopy study. Biol Psychiatry 2003; 54(7): 744-750.

[189] Bertolino A, Frye M, Callicott JH, Mattay VS, Rakow R, Shelton-Repella J, Post R, Weinberger DR. Neuronal pathology in the hippocampal area of patients with bipolar disorder: a study with proton magnetic resonance spectroscopic imaging. Biol Psychiatry 2003; 53(10): 906-913.

[190] Moore CM, Breeze JL, Gruber SA, Babb SM, Frederick BB, Villafuerte RA, Stoll AL, Hennen J, Yurgelun-Todd DA, Cohen BM, Renshaw PF. Choline, myo-inositol and mood in bipolar disorder: a proton magnetic resonance spectroscopic imaging study of the anterior cingulate cortex. Bipolar Disord 2000; 2(3 Pt 2): 207-216.

[191] Castillo M, Kwock L, Courvoisie H, Hooper SR. Proton MR spectroscopy in children with bipolar affective disorder: preliminary observations. AJNR Am J Neuroradiol 2000; 21(5): 832-838.

[192] Obergriesser T, Ende G, Braus DF, Henn FA. Hippocampal 1H-MRSI in ecstasy users. Eur Arch Psychiatry Clin Neurosci 2001; 251(3): 114-116.

[193] Bernasconi A, Tasch E, Cendes F, Li LM, Arnold DL. Proton magnetic resonance spectroscopic imaging suggests progressive neuronal damage in human temporal lobe epilepsy. Prog Brain Res 2002; 135: 297-304.

[194] Bernasconi A, Bernasconi N, Natsume J, Antel SB, Andermann F, Arnold DL. Magnetic resonance spectroscopy and imaging of the thalamus in idiopathic generalized epilepsy. Brain 2003; 126(Pt 11): 2447-2454.

[195] Li LM, Dubeau F, Andermann F, Arnold DL. Proton magnetic resonance spectroscopic imaging studies in patients with newly diagnosed partial epilepsy. Epilepsia 2000; 41(7): 825-831.

[196] Simister RJ, Woermann FG, McLean MA, Bartlett PA, Barker GJ, Duncan JS. A short-echo-time proton magnetic resonance spectroscopic imaging study of temporal lobe epilepsy. Epilepsia 2002; 43(9): 1021-1031.

[197] Woermann FG, McLean MA, Bartlett PA, Barker GJ, Duncan JS. Quantitative short echo time proton magnetic resonance spectroscopic imaging study of malformations of cortical development causing epilepsy. Brain 2001; 124(Pt 2): 427-436.

[198] Capizzano AA, Vermathen P, Laxer KD, Matson GB, Maudsley AA, Soher BJ, Schuff NW, Weiner MW. Multisection proton MR spectroscopy for mesial temporal lobe epilepsy. AJNR Am J Neuroradiol 2002; 23(8): 1359-1368.

[199] Pauli E, Eberhardt KW, Schafer I, Tomandl B, Huk WJ, Stefan H. Chemical shift imaging spectroscopy and memory function in temporal lobe epilepsy. Epilepsia 2000; 41(3): 282-289.

[200] Vikhoff-Baaz B, Malmgren K, Jonsson L, Starck G, Ljungberg M, Forssell-Aronsson E, Uvebrant P, Ekholm S. Lateralisation with magnetic resonance spectroscopic imaging in temporal lobe epilepsy: an evaluation of visual and region-of-interest analysis of metabolite concentration images. Neuroradiology 2001; 43(9): 721-727.

[201] Li LM, Cendes F, Andermann F, Dubeau F, Arnold DL. Spatial extent of neuronal metabolic dysfunction measured by proton MR

spectroscopic imaging in patients with localization-related epilepsy. Epilepsia 2000; 41(6): 666-674.

[202] Maton B, Gilliam F, Sawrie S, Faught E, Hugg J, Kuzniecky R. Correlation of scalp EEG and 1H-MRS metabolic abnormalities in temporal lobe epilepsy. Epilepsia 2001; 42(3): 417-422.

[203] Antel SB, Li LM, Cendes F, Collins DL, Kearney RE, Shinghal R, Arnold DL. Predicting surgical outcome in temporal lobe epilepsy patients using MRI and MRSI. Neurology 2002; 58(10): 1505-1512.

[204] Li LM, Cendes F, Antel SB, Andermann F, Serles W, Dubeau F, Olivier A, Arnold DL. Prognostic value of proton magnetic resonance spectroscopic imaging for surgical outcome in patients with intractable temporal lobe epilepsy and bilateral hippocampal atrophy. Ann Neurol 2000; 47(2): 195-200.

[205] Serles W, Li LM, Antel SB, Cendes F, Gotman J, Olivier A, Andermann F, Dubeau F, Arnold DL. Time course of postoperative recovery of N-acetyl-aspartate in temporal lobe epilepsy. Epilepsia 2001; 42(2): 190-197.

[206] Suhy J, Laxer KD, Capizzano AA, Vermathen P, Matson GB, Barbaro NM, Weiner MW. 1H MRSI predicts surgical outcome in MRI-negative temporal lobe epilepsy. Neurology 2002; 58(5): 821-823.

[207] Hajek M, Dezortova M, Liscak R, Vymazal J, Vladyka V. 1H MR spectroscopy of mesial temporal lobe epilepsies treated with Gamma knife. Eur Radiol 2003; 13(5): 994-1000.

[208] Jemal A, Tiwari RC, Murray T, Ghafoor A, Samuels A, Ward E, Feuer EJ, Thun MJ. Cancer statistics, 2004. CA Cancer J Clin 2004; 54(1): 8-29.

[209] Cirak B, Horska A, Barker PB, Burger PC, Carson BS, Avellino AM. Proton magnetic resonance spectroscopic imaging in pediatric pilomyxoid astrocytoma. Childs Nerv Syst 2004.

[210] Rijpkema M, Schuuring J, van der Meulen Y, van der Graaf M, Bernsen H, Boerman R, van der Kogel A, Heerschap A. Characterization of oligodendrogliomas using short echo time 1H MR spectroscopic imaging. NMR Biomed 2003; 16(1): 12-18.

[211] Galanaud D, Chinot O, Nicoli F, Confort-Gouny S, Le Fur Y, Barrie-Attarian M, Ranjeva JP, Fuentes S, Viout P, Figarella-Branger D, Cozzone PJ. Use of proton magnetic resonance spectroscopy of the brain to differentiate gliomatosis cerebri from low-grade glioma. J Neurosurg 2003; 98(2): 269-276.

[212] Son BC, Kim MC, Choi BG, Kim EN, Baik HM, Choe BY, Naruse S, Kang JK. Proton magnetic resonance chemical shift imaging (1H CSI)-directed stereotactic biopsy. Acta Neurochir (Wien) 2001; 143(1): 45-49; discussion 49-50.

[213] Burtscher IM, Skagerberg G, Geijer B, Englund E, Stahlberg F, Holtas S. Proton MR spectroscopy and preoperative diagnostic accuracy: an evaluation of intracranial mass lesions characterized by stereotactic biopsy findings. AJNR Am J Neuroradiol 2000; 21(1): 84-93.

[214] Dowling C, Bollen AW, Noworolski SM, McDermott MW, Barbaro NM, Day MR, Henry RG, Chang SM, Dillon WP, Nelson SJ, Vigneron DB. Preoperative proton MR spectroscopic imaging of brain tumors: correlation with histopathologic analysis of resection specimens. AJNR Am J Neuroradiol 2001; 22(4): 604-612.

[215] Li X, Lu Y, Pirzkall A, McKnight T, Nelson SJ. Analysis of the spatial characteristics of metabolic abnormalities in newly diagnosed glioma patients. J Magn Reson Imaging 2002; 16(3): 229-237.

[216] McKnight TR, von dem Bussche MH, Vigneron DB, Lu Y, Berger MS, McDermott MW, Dillon WP, Graves EE, Pirzkall A, Nelson SJ. Histopathological validation of a three-dimensional magnetic resonance spectroscopy index as a predictor of tumor presence. J Neurosurg 2002; 97(4): 794-802.

[217] McKnight TR, Noworolski SM, Vigneron DB, Nelson SJ. An automated technique for the quantitative assessment of 3D-MRSI data from patients with glioma. J Magn Reson Imaging 2001; 13(2): 167-177.

[218] Gupta RK, Cloughesy TF, Sinha U, Garakian J, Lazareff J, Rubino G, Rubino L, Becker DP, Vinters HV, Alger JR. Relationships between choline magnetic resonance spectroscopy, apparent diffusion coefficient and quantitative histopathology in human glioma. J Neurooncol 2000; 50(3): 215-226.

[219] Croteau D, Scarpace L, Hearshen D, Gutierrez J, Fisher JL, Rock JP, Mikkelsen T. Correlation between magnetic resonance spectroscopy imaging and image-guided biopsies: semiquantitative and qualitative histopathological analyses of patients with untreated glioma. Neurosurgery 2001; 49(4): 823-829.

[220] Kamada K, Moller M, Saguer M, Ganslandt O, Kaltenhauser M, Kober H, Vieth J. A combined study of tumor-related brain lesions using MEG and proton MR spectroscopic imaging. J Neurol Sci 2001; 186(1-2): 13-21.

[221] Pirzkall A, McKnight TR, Graves EE, Carol MP, Sneed PK, Wara WW, Nelson SJ, Verhey LJ, Larson DA. MR-spectroscopy guided target delineation for high-grade gliomas. Int J Radiat Oncol Biol Phys 2001; 50(4): 915-928.

[222] Law M, Yang S, Wang H, Babb JS, Johnson G, Cha S, Knopp EA, Zagzag D. Glioma grading: sensitivity, specificity, and predictive values of perfusion MR imaging and proton MR spectroscopic imaging compared with conventional MR imaging. AJNR Am J Neuroradiol 2003; 24(10): 1989-1998.

[223] Pirzkall A, Li X, Oh J, Chang S, Berger MS, Larson DA, Verhey LJ, Dillon WP, Nelson SJ. 3D MRSI for resected high-grade gliomas before RT: tumor extent according to metabolic activity in relation to MRI. Int J Radiat Oncol Biol Phys 2004; 59(1): 126-137.

[224] Pirzkall A, Nelson SJ, McKnight TR, Takahashi MM, Li X, Graves EE, Verhey LJ, Wara WW, Larson DA, Sneed PK. Metabolic imaging of low-grade gliomas with three-dimensional magnetic resonance spectroscopy. Int J Radiat Oncol Biol Phys 2002; 53(5): 1254-1264.

[225] Chan AA, Lau A, Pirzkall A, Chang SM, Verhey LJ, Larson D, McDermott MW, Dillon WP, Nelson SJ. Proton magnetic resonance spectroscopy imaging in the evaluation of patients undergoing gamma knife surgery for Grade IV glioma. J Neurosurg 2004; 101(3): 467-475.

[226] Li X, Jin H, Lu Y, Oh J, Chang S, Nelson SJ. Identification of MRI and 1H MRSI parameters that may predict survival for patients with malignant gliomas. NMR Biomed 2004; 17(1): 10-20.

[227] Oh J, Henry RG, Pirzkall A, Lu Y, Li X, Catalaa I, Chang S, Dillon WP, Nelson SJ. Survival analysis in patients with glioblastoma multiforme: predictive value of choline-to-N-acetylaspartate index, apparent diffusion coefficient, and relative cerebral blood volume. J Magn Reson Imaging 2004; 19(5): 546-554.

[228] Kuznetsov YE, Caramanos Z, Antel SB, Preul MC, Leblanc R, Villemure JG, Pokrupa R, Olivier A, Sadikot A, Arnold DL. Proton magnetic resonance spectroscopic imaging can predict length of survival in patients with supratentorial gliomas. Neurosurgery 2003; 53(3): 565-574; discussion 574-566.

[229] Lee MC, Pirzkall A, McKnight TR, Nelson SJ. 1H-MRSI of radiation effects in normal-appearing white matter: dose-dependence and impact on automated spectral classification. J Magn Reson Imaging 2004; 19(4): 379-388.

[230] Rock JP, Hearshen D, Scarpace L, Croteau D, Gutierrez J, Fisher JL, Rosenblum ML, Mikkelsen T. Correlations between magnetic resonance spectroscopy and image-guided histopathology, with special attention to radiation necrosis. Neurosurgery 2002; 51(4): 912-919; discussion 919-920.

[231] Virta A, Patronas N, Raman R, Dwyer A, Barnett A, Bonavita S, Tedeschi G, Lundbom N. Spectroscopic imaging of radiation-induced effects in the white matter of glioma patients. Magn Reson Imaging 2000; 18(7): 851-857.

[232] Weybright P, Maly P, Gomez-Hassan D, Blaesing C, Sundgren PC. MR spectroscopy in the evaluation of recurrent contrast-enhancing lesions in the posterior fossa after tumor treatment. Neuroradiology 2004; 46(7): 541-549.

[233] Preul MC, Caramanos Z, Villemure JG, Shenouda G, LeBlanc R, Langleben A, Arnold DL. Using proton magnetic resonance spectroscopic imaging to predict *in vivo* the response of recurrent malignant gliomas to tamoxifen chemotherapy. Neurosurgery 2000; 46(2): 306-318.

[234] Tzika AA, Zarifi MK, Goumnerova L, Astrakas LG, Zurakowski D, Young-Poussaint T, Anthony DC, Scott RM, Black PM. Neuroimaging in pediatric brain tumors: Gd-DTPA-enhanced, hemodynamic, and diffusion MR imaging compared with MR spectroscopic imaging. AJNR Am J Neuroradiol 2002; 23(2): 322-333.

[235] Tzika AA, Astrakas LG, Zarifi MK, Petridou N, Young-Poussaint T, Goumnerova L, Zurakowski D, Anthony DC, Black PM. Multiparametric MR assessment of pediatric brain tumors. Neuroradiology 2003; 45(1): 1-10.

[236] Tzika AA, Astrakas LG, Zarifi MK, Zurakowski D, Poussaint TY, Goumnerova L, Tarbell NJ, Black PM. Spectroscopic and perfusion

magnetic resonance imaging predictors of progression in pediatric brain tumors. Cancer 2004; 100(6): 1246-1256.

[237] Tzika AA, Zurakowski D, Poussaint TY, Goumnerova L, Astrakas LG, Barnes PD, Anthony DC, Billett AL, Tarbell NJ, Scott RM, Black PM. Proton magnetic spectroscopic imaging of the child's brain: the response of tumors to treatment. Neuroradiology 2001; 43(2): 169-177.

[238] Warren KE, Frank JA, Black JL, Hill RS, Duyn JH, Aikin AA, Lewis BK, Adamson PC, Balis FM. Proton magnetic resonance spectroscopic imaging in children with recurrent primary brain tumors. J Clin Oncol 2000; 18(5): 1020-1026.

[239] van der Graaf M, Schipper RG, Oosterhof GO, Schalken JA, Verhofstad AA, Heerschap A. Proton MR spectroscopy of prostatic tissue focused on the detection of spermine, a possible biomarker of malignant behavior in prostate cancer. Magma 2000; 10(3): 153-159.

[240] Swindle P, McCredie S, Russell P, Himmelreich U, Khadra M, Lean C, Mountford C. Pathologic characterization of human prostate tissue with proton MR spectroscopy. Radiology 2003; 228(1): 144-151.

[241] Tomlins A, Foxall P, Lindon J, Lynch M, Spraul M, Everett J, Nicholson J. High resolution magic angle spinning 1H nuclear magnetic resonance analysis of intact prostatic hyperplastic and tumor tissue. Analy Common 1998; 35: 113-115.

[242] Cheng LL, Wu C, Smith MR, Gonzalez RG. Non-destructive quantitation of spermine in human prostate tissue samples using HRMAS 1H NMR spectroscopy at 9.4 T. FEBS Lett 2001; 494(1-2): 112-116.

[243] Swanson MG, Vigneron DB, Tabatabai ZL, Males RG, Schmitt L, Carroll PR, James JK, Hurd RE, Kurhanewicz J. Proton HR-MAS spectroscopy and quantitative pathologic analysis of MRI/3D-MRSI-targeted postsurgical prostate tissues. Magn Reson Med 2003; 50(5): 944-954.

[244] Schricker AA, Pauly JM, Kurhanewicz J, Swanson MG, Vigneron DB. Dualband spectral-spatial RF pulses for prostate MR spectroscopic imaging. Magn Reson Med 2001; 46(6): 1079-1087.

[245] Males RG, Vigneron DB, Star-Lack J, Falbo SC, Nelson SJ, Hricak H, Kurhanewicz J. Clinical application of BASING and spectral/spatial water and lipid suppression pulses for prostate cancer staging and localization by *in vivo* 3D 1H magnetic resonance spectroscopic imaging. Magn Reson Med 2000; 43(1): 17-22.

[246] Dhingsa R, Qayyum A, Coakley FV, Lu Y, Jones KD, Swanson MG, Carroll PR, Hricak H, Kurhanewicz J. Prostate cancer localization with endorectal MR imaging and MR spectroscopic imaging: effect of clinical data on reader accuracy. Radiology 2004; 230(1): 215-220.

[247] Kaji Y, Wada A, Imaoka I, Matsuo M, Terachi T, Kobashi Y, Sugimura K, Fujii M, Maruyama K, Takizawa O. Proton two-dimensional chemical shift imaging for evaluation of prostate cancer: external surface coil vs. endorectal surface coil. J Magn Reson Imaging 2002; 16(6): 697-706.

[248] van Dorsten FA, van der Graaf M, Engelbrecht MR, van Leenders GJ, Verhofstad A, Rijpkema M, de la Rosette JJ, Barentsz JO, Heerschap A. Combined quantitative dynamic contrast-enhanced MR imaging and (1)H MR spectroscopic imaging of human prostate cancer. J Magn Reson Imaging 2004; 20(2): 279-287.

[249] Yuen JS, Thng CH, Tan PH, Khin LW, Phee SJ, Xiao D, Lau WK, Ng WS, Cheng CW. Endorectal magnetic resonance imaging and spectroscopy for the detection of tumor foci in men with prior negative transrectal ultrasound prostate biopsy. J Urol 2004; 171(4): 1482-1486.

[250] Zaider M, Zelefsky MJ, Lee EK, Zakian KL, Amols HI, Dyke J, Cohen G, Hu Y, Endi AK, Chui C, Koutcher JA. Treatment planning for prostate implants using magnetic-resonance spectroscopy imaging. Int J Radiat Oncol Biol Phys 2000; 47(4): 1085-1096.

[251] Mizowaki T, Cohen GN, Fung AY, Zaider M. Towards integrating functional imaging in the treatment of prostate cancer with radiation: the registration of the MR spectroscopy imaging to ultrasound/CT images and its implementation in treatment planning. Int J Radiat Oncol Biol Phys 2002; 54(5): 1558-1564.

[252] Zelefsky MJ, Cohen G, Zakian KL, Dyke J, Koutcher JA, Hricak H, Schwartz L, Zaider M. Intraoperative conformal optimization for transperineal prostate implantation using magnetic resonance spectroscopic imaging. Cancer J 2000; 6(4): 249-255.

[253] DiBiase SJ, Hosseinzadeh K, Gullapalli RP, Jacobs SC, Naslund MJ, Sklar GN, Alexander RB, Yu C. Magnetic resonance spectroscopic imaging-guided brachytherapy for localized prostate cancer. Int J Radiat Oncol Biol Phys 2002; 52(2): 429-438.

[254] Coakley FV, Teh HS, Qayyum A, Swanson MG, Lu Y, Iii MR, Pickett B, Shinohara K, Vigneron DB, Kurhanewicz J. Endorectal MR Imaging and MR Spectroscopic Imaging for Locally Recurrent Prostate Cancer after External Beam Radiation Therapy: Preliminary Experience. Radiology 2004.

[255] Pickett B, Ten Haken RK, Kurhanewicz J, Qayyum A, Shinohara K, Fein B, Roach M, 3rd. Time to metabolic atrophy after permanent prostate seed implantation based on magnetic resonance spectroscopic imaging. Int J Radiat Oncol Biol Phys 2004; 59(3): 665-673.

[256] Mueller-Lisse UG, Swanson MG, Vigneron DB, Hricak H, Bessette A, Males RG, Wood PJ, Noworolski S, Nelson SJ, Barken I, Carroll PR, Kurhanewicz J. Time-dependent effects of hormone-deprivation therapy on prostate metabolism as detected by combined magnetic resonance imaging and 3D magnetic resonance spectroscopic imaging. Magn Reson Med 2001; 46(1): 49-57.

[257] Jacobs MA, Barker PB, Bottomley PA, Bhujwalla Z, Bluemke DA. Proton magnetic resonance spectroscopic imaging of human breast cancer: a preliminary study. J Magn Reson Imaging 2004; 19(1): 68-75.

[258] Bredella MA, Losasso C, Moelleken SC, Huegli RW, Genant HK, Tirman PF. Three-point Dixon chemical-shift imaging for evaluating articular cartilage defects in the knee joint on a low-field-strength open magnet. AJR Am J Roentgenol 2001; 177(6): 1371-1375.

[259] Hilaire L, Wehrli FW, Song HK. High-speed spectroscopic imaging for cancellous bone marrow R(2)* mapping and lipid quantification. Magn Reson Imaging 2000; 18(7): 777-786.

[260] Lin CS, Fertikh D, Davis B, Lauerman WC, Henderson F, Schellinger D. 2D CSI proton MR spectroscopy of human spinal vertebra: feasibility studies. J Magn Reson Imaging 2000; 11(3): 287-293.

[261] Hu J, Xia Y, Shen Y, Li J, Zuo CS, Xuan Y, Jiang Q. Significant differences in proton trimethyl ammonium signals between human gastrocnemius and soleus muscle. J Magn Reson Imaging 2004; 19(5): 617-622.

[262] Vermathen P, Boesch C, Kreis R. Mapping fiber orientation in human muscle by proton MR spectroscopic imaging. Magn Reson Med 2003; 49(3): 424-432.

[263] Vermathen P, Kreis R, Boesch C. Distribution of intramyocellular lipids in human calf muscles as determined by MR spectroscopic imaging. Magn Reson Med 2004; 51(2): 253-262.

[264] Hu J, Jiang Q, Xia Y, Zuo C. High spatial resolution *in vivo* 2D (1)H magnetic resonance spectroscopic imaging of human muscles with a band-selective technique. Magn Reson Imaging 2001; 19(8): 1091-1096.

[265] Shen W, Mao X, Wang Z, Punyanitya M, Heymsfield SB, Shungu DC. Measurement of intramyocellular lipid levels with 2-D magnetic resonance spectroscopic imaging at 1.5 T. Acta Diabetol 2003; 40 Suppl 1: S51-54.

[266] Mansfield P. Spatial mapping of the chemical shift in NMR. J Phys D: Appl Phys 1983; 16: L235-L238.

[267] Du W, Du YP, Fan X, Zamora MA, Karczmar GS. Reduction of spectral ghost artifacts in high-resolution echo-planar spectroscopic imaging of water and fat resonances. Magn Reson Med 2003; 49(6): 1113-1120.

[268] Oshio K, Kyriakos W, Mulkern RV. Line scan echo planar spectroscopic imaging. Magn Reson Med 2000; 44(4): 521-524.

[269] Ebel A, Soher BJ, Maudsley AA. Assessment of 3D proton MR echo-planar spectroscopic imaging using automated spectral analysis. Magn Reson Med 2001; 46(6): 1072-1078.

[270] Ebel A, Maudsley AA. Improved spectral quality for 3D MR spectroscopic imaging using a high spatial resolution acquisition strategy. Magn Reson Imaging 2003; 21(2): 113-120.

[271] Ebel A, Maudsley AA. Comparison of methods for reduction of lipid contamination for *in vivo* proton MR spectroscopic imaging of the brain. Magn Reson Med 2001; 46(4): 706-712.

[272] Pelletier D, Nelson SJ, Grenier D, Lu Y, Genain C, Goodkin DE. 3-D echo planar (1)HMRS imaging in MS: metabolite comparison from supratentorial vs. central brain. Magn Reson Imaging 2002; 20(8): 599-606.

[273] Medved M, Du W, Zamora MA, Fan X, Olopade OI, MacEneaney PM, Newstead G, Karczmar GS. The effect of varying spectral resolution on the quality of high spectral and spatial resolution magnetic resonance images of the breast. J Magn Reson Imaging 2003; 18(4): 442-448.

[274] Du W, Du YP, Bick U, Fan X, MacEneaney PM, Zamora MA, Medved M, Karczmar GS. Breast MR imaging with high spectral and spatial resolutions: preliminary experience. Radiology 2002; 224(2): 577-585.

[275] Medved M, Newstead GM, Fan X, Du W, Du YP, MacEneaney PM, Culp RM, Kelcz F, Olopade OI, Zamora MA, Karczmar GS. Fourier components of inhomogeneously broadened water resonances in breast: a new source of MRI contrast. Magn Reson Med 2004; 52(1): 193-196.

[276] Kreis R. Issues of spectral quality in clinical 1H-magnetic resonance spectroscopy and a gallery of artifacts. NMR Biomed 2004; 17(6): 361-381.

[277] Doyle VL, Howet FA, Griffiths JR. The effect of respiratory motion on CSI localized MRS. Cooperative Group on MR Applications to Cancer. Phys Med Biol 2000; 45(8): 2093-2104.

[278] Alger JR. Regulatory, financial and ethical aspects of routine clinical magnetic resonance spectroscopy. NMR Biomed 2000; 13(5): III-V.

[279] Katz-Brull R, Lenkinski RE. Frame-by-frame PRESS 1H-MRS of the brain at 3 T: the effects of physiological motion. Magn Reson Med 2004; 51(1): 184-187.

[280] Longo R, Vidimari R. *In vivo* localized 1H NMR spectroscopy: an experimental characterization of the PRESS technique. Phys Med Biol 1994; 39(1): 207-215.

[281] Ernst T, Hennig J. Coupling effects in volume selective 1H spectroscopy of major brain metabolites. Magn Reson Med 1991; 21(1): 82-96.

[282] Moonen CT, von Kienlin M, van Zijl PC, Cohen J, Gillen J, Daly P, Wolf G. Comparison of single-shot localization methods (STEAM and PRESS) for *in vivo* proton NMR spectroscopy. NMR Biomed 1989; 2(5-6): 201-208.

[283] Yongbi NM, Payne GS, Collins DJ, Leach MO. Quantification of signal selection efficiency, extra volume suppression and contamination for ISIS, STEAM and PRESS localized 1H NMR spectroscopy using an EEC localization test object. Phys Med Biol 1995; 40(7): 1293-1303.

[284] Kwock L, Brown MA, Castillo M. Extraneous lipid contamination in single-volume proton MR spectroscopy: phantom and human studies. AJNR Am J Neuroradiol 1997; 18(7): 1349-1357.

[285] Ogg RJ, Kingsley PB, Taylor JS. WET, a T1- and B1-insensitive water-suppression method for *in vivo* localized 1H NMR spectroscopy. J Magn Reson B 1994; 104(1): 1-10.

[286] Moonen CTW, van Zijl PCM. Highly effective water suppression for *in vivo* proton NMR spectroscopy (DRYSTEAM). J Magn Reson 1990; 88: 28-41.

[287] Lei H, Peeling J. Off-resonance effects of the radiofrequency pulses used in spectral editing with double-quantum coherence transfer. J Magn Reson 2000; 144(1): 89-95.

[288] McLean MA, Busza AL, Wald LL, Simister RJ, Barker GJ, Williams SR. *In vivo* GABA+ measurement at 1.5T using a PRESS-localized double quantum filter. Magn Reson Med 2002; 48(2): 233-241.

[289] Sotak CH. Multiple quantum NMR spectroscopy methods for measuring the apparent self-diffusion coefficient of *in vivo* lactic acid. NMR Biomed 1991; 4(2): 70-72.

[290] Ranjeva JP, Confort-Gouny S, Le Fur Y, Cozzone PJ. Magnetic resonance spectroscopy of brain in epilepsy. Childs Nerv Syst 2000; 16(4): 235-241.

[291] Wang ZJ, Bergqvist C, Hunter JV, Jin D, Wang DJ, Wehrli S, Zimmerman RA. *In vivo* measurement of brain metabolites using two-dimensional double-quantum MR spectroscopy--exploration of GABA levels in a ketogenic diet. Magn Reson Med 2003; 49(4): 615-619.

[292] Hu J, Xu Y, Jiang Q, Sehgal V, Shen Y, Xuan Y, Xia Y. Spectral pattern of total creatine and trimethyl ammonium in multiple sclerosis. Magn Reson Imaging 2004; 22(3): 427-429.

[293] Marzola P, Osculati F, Sbarbati A. High field MRI in preclinical research. Eur J Radiol 2003; 48(2): 165-170.

[294] Di Costanzo A, Trojsi F, Tosetti M, Giannatempo GM, Nemore F, Piccirillo M, Bonavita S, Tedeschi G, Scarabino T. High-field proton MRS of human brain. Eur J Radiol 2003; 48(2): 146-153.

[295] Oz G, Henry PG, Seaquist ER, Gruetter R. Direct, noninvasive measurement of brain glycogen metabolism in humans. Neurochem Int 2003; 43(4-5): 323-329.

[296] Gruetter R, Seaquist ER, Kim S, Ugurbil K. Localized *in vivo* 13C-NMR of glutamate metabolism in the human brain: initial results at 4 tesla. Dev Neurosci 1998; 20(4-5): 380-388.

[297] Lei H, Zhu XH, Zhang XL, Ugurbil K, Chen W. *In vivo* 31P magnetic resonance spectroscopy of human brain at 7 T: an initial experience. Magn Reson Med 2003; 49(2): 199-205.

[298] Bartha R, Drost DJ, Menon RS, Williamson PC. Comparison of the quantification precision of human short echo time (1)H spectroscopy at 1.5 and 4.0 Tesla. Magn Reson Med 2000; 44(2): 185-192.

[299] Alger JR, Frew AJ, Cloughesy TF, Del Vecchio W, Villablanca JP, Curran JG. Novel methodology for the archiving and interactive reading of clinical magnetic resonance spectroscopic imaging. Magn Reson Med 2002; 48(3): 411-418.

[300] Podo F, Henriksen O, Bovee WM, Leach MO, Leibfritz D, de Certaines JD. Absolute metabolite quantification by *in vivo* NMR spectroscopy: I. Introduction, objectives and activities of a concerted action in biomedical research. Magn Reson Imaging 1998; 16(9): 1085-1092.

[301] Hajek M, Burian M, Dezortova M. Application of LCModel for quality control and quantitative *in vivo* 1H MR spectroscopy by short echo time STEAM sequence. Magma 2000; 10(1): 6-17.

[302] Griffiths JR, Tate AR, Howe FA, Stubbs M. Magnetic Resonance Spectroscopy of cancer-practicalities of multi-centre trials and early results in non-Hodgkin's lymphoma. Eur J Cancer 2002; 38(16): 2085-2093.

[303] de Certaines JD, Cathelineau G. Safety aspects and quality assessment in MRI and MRS: a challenge for health care systems in Europe. J Magn Reson Imaging 2001; 13(4): 632-638.

[304] Mader I, Roser W, Hagberg G, Schneider M, Sauter R, Seelig J, Radue EW, Steinbrich W. Proton chemical shift imaging, metabolic maps, and single voxel spectroscopy of glial brain tumors. Magma 1996; 4(2): 139-150.

[305] Preul MC, Caramanos Z, Collins DL, Villemure JG, Leblanc R, Olivier A, Pokrupa R, Arnold DL. Accurate, noninvasive diagnosis of human brain tumors by using proton magnetic resonance spectroscopy. Nat Med 1996; 2(3): 323-325.

[306] Devos A, Lukas L, Suykens JA, Vanhamme L, Tate AR, Howe FA, Majos C, Moreno-Torres A, van der Graaf M, Arus C, Van Huffel S. Classification of brain tumours using short echo time 1H MR spectra. J Magn Reson 2004; 170(1): 164-175.

[307] Tong Z, Yamaki T, Harada K, Houkin K. *In vivo* quantification of the metabolites in normal brain and brain tumors by proton MR spectroscopy using water as an internal standard. Magn Reson Imaging 2004; 22(7): 1017-1024.

[308] Beer M. Cardiac spectroscopy: techniques, indications and clinical results. Eur Radiol 2004; 14(6): 1034-1047.

[309] Kanowski M, Kaufmann J, Braun J, Bernarding J, Tempelmann C. Quantitation of simulated short echo time 1H human brain spectra by LCModel and AMARES. Magn Reson Med 2004; 51(5): 904-912.

[310] Geurts JJ, Barkhof F, Castelijns JA, Uitdehaag BM, Polman CH, Pouwels PJ. Quantitative 1H-MRS of healthy human cortex, hippocampus, and thalamus: metabolite concentrations, quantification precision, and reproducibility. J Magn Reson Imaging 2004; 20(3): 366-371.

[311] Schirmer T, Auer DP. On the reliability of quantitative clinical magnetic resonance spectroscopy of the human brain. NMR Biomed 2000; 13(1): 28-36.

[312] Duc CO, Trabesinger AH, Weber OM, Meier D, Walder M, Wieser HG, Boesiger P. Quantitative 1H MRS in the evaluation of mesial temporal lobe epilepsy *in vivo*. Magn Reson Imaging 1998; 16(8): 969-979.

[313] De Beer R, Barbiroli B, Gobbi G, Knijn A, Kugel H, Langenberger KW, Tkac I, Topp S. Absolute metabolite quantification by *in vivo* NMR spectroscopy: III. Multicentre 1H MRS of the human brain addressed by one and the same data-analysis protocol. Magn Reson Imaging 1998; 16(9): 1107-1111.

[314] Chard DT, McLean MA, Parker GJ, MacManus DG, Miller DH. Reproducibility of *in vivo* metabolite quantification with proton magnetic resonance spectroscopic imaging. J Magn Reson Imaging 2002; 15(2): 219-225.

[315] Li BS, Wang H, Gonen O. Metabolite ratios to assumed stable creatine level may confound the quantification of proton brain MR spectroscopy. Magn Reson Imaging 2003; 21(8): 923-928.

[316] Moats RA, Watson L, Shonk T, Tokuyama S, Braslau D, Eto R, Mandigo JC, Ross BD. Added value of automated clinical proton MR spectroscopy of the brain. J Comput Assist Tomogr 1995; 19(3): 480-491.

[317] Felblinger J, Kreis R, Boesch C. Effects of physiologic motion of the human brain upon quantitative 1H-MRS: analysis and correction by retro-gating. NMR Biomed 1998; 11(3): 107-114.

[318] Schwarz AJ, Leach MO. Implications of respiratory motion for the quantification of 2D MR spectroscopic imaging data in the abdomen. Phys Med Biol 2000; 45(8): 2105-2116.

[319] Hofmann L, Slotboom J, Boesch C, Kreis R. Characterization of the macromolecule baseline in localized (1)H-MR spectra of human brain. Magn Reson Med 2001; 46(5): 855-863.

[320] Hofmann L, Slotboom J, Jung B, Maloca P, Boesch C, Kreis R. Quantitative 1H-magnetic resonance spectroscopy of human brain: Influence of composition and parameterization of the basis set in linear combination model-fitting. Magn Reson Med 2002; 48(3): 440-453.

[321] Stoyanova R, Brown TR. NMR spectral quantitation by principal component analysis. III. A generalized procedure for determination of lineshape variations. J Magn Reson 2002; 154(2): 163-175.

[322] Griffin JL, Bollard M, Nicholson JK, Bhakoo K. Spectral profiles of cultured neuronal and glial cells derived from HRMAS (1)H NMR spectroscopy. NMR Biomed 2002; 15(6): 375-384.

Received: November 04, 2004 Accepted: February 14, 2004

Part II

High Resolution Magic Angle Spinning (HRMAS) Proton MRS of Surgical Specimens

Leo L. Cheng[1,2], Melissa A. Burns[1] and Cynthia L. Lean[3,4]
[1]*Departments of Pathology;*
[2]*Departments of Radiology Massachusetts General Hospital, Harvard Medical School Boston, Massachusetts 02114, USA;*
[3]*Institute for Magnetic Resonance Research, NSW 1590, Australia; and*
[4]*Department of Magnetic Resonance in Medicine, University of Sydney, NSW 2006, Australia*

List of Abbreviations

BPH	Benign prostatic hyperplasis
DCIS	Ductal carcinoma *in situ*
FNAB	Fine needle aspiration biopsy
GBM	Glioblastoma multiforme
HCA	Hierarchical cluster analysis
^{1}H MRS	Proton magnetic resonance spectroscopy
HPLC	High pressure liquid chromatography
(HR)MAS	(High resolution) Magic angle spinning
NAA	N-acetyl aspartate
PA	Polyamines
PC	Phosphocholine
PCA	Principal component analysis
PTC	Phosphatidylcholine
SCS	Statistical classification strategy
SSB	Spinning side bands

Introduction

Over the last two decades, a large body of *ex vivo* work and some *in vivo* work has demonstrated the utility of proton magnetic resonance spectroscopy (^{1}H MRS) in detecting and monitoring cellular chemical alterations associated with the development and progression of human malignant diseases [1–3]. Reports of conventional *ex vivo* ^{1}H MRS studies of human tissues, i.e. analysis of intact tissues with liquid-state MRS probes, have demonstrated that diagnosis, and for some organs, prognosis of malignant disease using metabolite ratios measured from spectra may reach 95% for both sensitivity and specificity. The accuracy can further be improved using an objective pattern recognition technique, statistical classification strategy (SCS) [2]. While tissue conventional MRS is fast and has shown the ability to diagnose accurately various human malignancies, it is limited by poor spectral resolution caused by the magnetic susceptibility effects of heterogeneous structures of the sample, and therefore detailed identification of individual metabolites is difficult. Metabolite profiling involving the measurement and quantification of tissue metabolites [4] is of increasing interest in the era of genomics and proteomics due to the direct involvement of tissue metabolites in tumor development and progression. High-resolution magic angle spinning (HRMAS) was developed to improve the spectral resolution of MR spectra of intact tissue by the reduction of susceptibility induced broadening such that individual metabolites may be identified and correlated with disease states.

Characterization of Human Malignancies

A malignant lesion exhibits unregulated growth characteristics both at primary and secondary (metastatic) sites. Initial attempts to characterize and understand tumor development and progression hinged therefore on lesion morphology and, as such, on histopathology using the light microscope, which has been the medical diagnostic "gold standard" for much of the 20th century. With the discovery of DNA and the advent of molecular genetics it became evident that tumor morphology represented only a single variable in the characterization of malignancies and could not report on risk factors or on the biological potential of a lesion. Predicting tumor behavior is essential for determining optimal disease management protocols and it is proteomics and spectroscopic metabolite profiling that have the potential to provide the information necessary for this endeavor. Metabolite profiling data, thus far, has been generated predominantly by studies involving MR spectroscopy and mass-spectrometry.

Specific Limitations of Histopathology

The principal limitation of histopathology is the restricted range of morphological changes that tissues can express. Pathologists attempt to extract a sophisticated pattern specific for an individual disease process from a continuum of morphological changes. These patterns overlap,

Graham A. Webb (ed.), Modern Magnetic Resonance, 1–14.

are susceptible to subjective assessment, and may be altered by sampling error. Patient assessment involves histological grading and clinicopathological staging. Tumor grading attempts to establish the aggressiveness of the tumor based on the degree of differentiation, or anaplasia, of tumor cells. However, such a distinction is subjective and often inconclusive. Staging of cancer determines the extent and spread of the disease, but it is unable to distinguish between recent but aggressive primary tumors and older but more slowly growing ones since clinical presentation of patients does not usually reveal how long a neoplasm has been present. Adequate staging of disease is often problematic. For instance, histopathological assessment of lymph nodes is subject to observer and sampling errors due to the large volumes of tissue to be assessed and the time and resource constraints that prevent thorough and complete examination. A retrospective study revealed that: "Serial sectioning of lymph nodes judged to be disease-free after routine examination revealed micrometastases in an additional 83 (9%) of 921 breast cancer subjects" [5].

Current histopathology has shown both conceptual and procedural inadequacies in providing optimal medical diagnosis. The development of new modalities capable of improving the accuracy of disease diagnosis is needed.

Cancer Pathology Determined by Conventional ^{1}H MRS

Conventional MRS measures cellular chemicals that are mobile on the MR time scale and their variations with changes in physiological or pathological function [6]. Although restricted by achievable spectral resolutions due to susceptibility induced broadening of resonances, many promising results have been obtained from conventional proton MRS studies of human malignant tissue and fine needle aspiration biopsies. The potential for diagnoses of malignant diseases in many organs has been demonstrated and more importantly, metabolic changes have been reported that were not morphologically manifested [7,8]. A study of aspiration biopsies from primary breast tumors not only determined diagnosis, but also reported on nodal involvement and tumor vascularization [9]. The sensitivity of MRS was demonstrated in a study using a rat model for lymph node metastasis where malignant cells in lymph nodes were detected with a greater sensitivity than histology. Micrometastases were detected that were not apparent even when the entire node was serially sectioned for examination by histology. The MR diagnoses were confirmed to be correct by xenografting nodal tissue into nude mice [10].

Historically, the limitation in spectral resolution of conventional proton MRS of tissue samples was realized as an obstacle to the identification of detailed cellular metabolism. A number of procedures, including sample packing and chemical extraction of tissue were investigated as ways to improve spectral resolution [11]. While solutions of tissue extracts did produce high-resolution spectra, the process was destructive and was found to alter the spectroscopic results to an unknown degree, depending on the procedure used and the thoroughness of extraction. Therefore, neither broad-line tissue analyses nor high-resolution measurements of extracts have been able to successfully evaluate malignant disease or exemplify the advantages of proton MRS in metabolite identification.

Methodology

Limited spectral resolution is a common problem in solid-state MRS for which many techniques have been proposed and tested. Among these magic angle spinning (MAS), a line-narrowing technique, was invented after the realization of the angle-dependent characteristics of the so-called "solid effects" that broaden the resonance lines [12,13]. These "effects" classically include dipolar coupling and chemical shift anisotropy, which always exist in solids. It was later shown that MAS could also reduce resonance line-broadenings caused by bulk magnetic susceptibility [14]. Specifically, in solids, spectral broadening due to these effects follows $(3\cos^2\theta - 1)$, where θ is the angle between the static magnetic field and the internuclear vector. Therefore, if a sample is spun mechanically at the "magic angle ($54^\circ 44'$, i.e. $3\cos^2(54^\circ 44') - 1 = 0$)," and at a rate faster than the broadening originating from these effects, the contribution of these effects to the spectral broadening can be reduced [15].

The HRMAS Method

The term HRMAS is currently used to refer to proton MRS of non-solution samples, such as biological tissues and cells, obtained with the application of MAS. It is important to note, however, that there are conceptual differences between classical MAS and tissue HRMAS used with proton spectroscopy [16]. The targets of MAS in classical proton solid-state studies are chemical shift anisotropies and dipolar couplings that are in ordinary solids >50 kHz. The application of MAS in solid-state studies has involved the use of high spinning rates and strong radio-frequency pulses in an attempt to decouple these homonuclear interactions. This is not the case, however, for the MAS study of cellular metabolites in biological tissues. Here, water-soluble molecules reside in the cytoplasm wherein their motion is restricted by magnetic susceptibilities caused by various interfaces with other cell structures and by inherent viscosity. Although classical "solid-effects" exist, for instance within cell membranes, they would

contribute only to an almost invisible spectral background that is too broad (~50 kHz) to be measurable in a typical HRMAS spectrum of metabolites (~5 kHz, or 10 ppm on a 500 MHz spectrometer). Overall, the magnitude of line-broadenings due to magnetic susceptibility is approximately 10^3 less than that caused by "solid-effects," and can be greatly reduced by MAS.

Experimental

Sample Preparation

Fresh and previously frozen samples may be measured directly with HRMAS MRS [17–21]. For the purpose of preserving the metabolite concentrations within tissues, samples should not be collected or stored in any liquid medium. In cases where the size of frozen tissue exceeds the sample size required for HRMAS MRS analysis, samples must be cut on a frozen surface to avoid multiple freezing and thawing. Such a surface can be made with a thin metal plate, covered with gauze and placed on top of dry ice.

Tissue samples may be washed briefly with D_2O prior to spectroscopy if they contain visible amounts of blood. However, exposure to D_2O should be brief to minimize the possible loss of cellular metabolites [22]. We have observed complete depletion of metabolites for human prostate samples (~10 mg blocks) submerged in ~2 ml D_2O for approximately 10 min.

As always, when working with human materials of potential biohazard, universal precautions need to be practiced at all times. In particular, tissue samples will undergo spinning and even at "slow spinning speeds" of less than 1 kHz, tissue fluid can leak from the rotor cap if the cap is not in tight-fit with the rotor (Figure 1). Thus the compatibility and seal between rotor and cap should be tested using a D_2O solution prior to tissue analysis. The test can be done by comparing the weights of the rotor with solution before and after HRMAS using the same experimental conditions (temperature and spinning speed) used for tissue analysis.

Fig. 1. Photograph of the rotor and a typical biopsy tissue sample that will be placed in the rotor using the tweezers for HRMAS MRS analysis.

To maximize spectral resolution, tissue samples should be limited to the physical boundaries of the receiving coils; for example by using Kel-F inserts to create a spherical sample when measuring samples on a Bruker spectrometer (Bruker BioSpin Corp., Billerica, MA). The use of a spherical sample is recommended for it minimizes shimming efforts as well as reduces the effect of the magnetic field inhomogeneity on the broadening of spectral lines.

Spectrometer Settings

Before tissue measurements, the HRMAS probe should be adjusted for its magic angle with potassium bromine (KBr) following the manufacturer's protocol for solid-state MRS. Ideally, measurements should be made at a low temperature (e.g. 4 °C) to reduce tissue degradation during acquisition.

The optimal spinning rate should be decided after consideration of several factors, including tissue type, metabolites of interest, and the plan for the tissue after HRMAS MRS analysis. Generally, the higher the spinning rate, up to 10 KHz as reported in the literature, the better the spectral resolution [23]. However, since high spinning rates can function as a centrifuge that can potentially disrupt tissue structures, if subsequent histopathological evaluation of the tissue is critical to the study, spinning rates must be reduced to limit any structural damage of the tissue that may interfere with histopathology. It is important to note that different tissue types endure different levels of stress. For instance, for the same spinning rate, skin tissue may be perfectly preserved in structure, while brain tissue can be completely destroyed. On the other hand, if less mobile metabolites such as lipids are the focus of HRMAS MRS evaluation, faster spinning rates may be necessary. The preservation of tissue architectures during HRMAS MRS is often critical and, as such, a number of studies have explored HRMAS MRS tissue analysis using moderate to slow spinning conditions [24–27]. These studies aimed to suppress spinning side bands (SSB) that overlapped with metabolite spectral regions of interest, using spinning rates that were not fast enough to "push" the 1st SSB beyond these regions. Interested readers should test these reported techniques for applicability to their specific tissue systems.

Optimal probe shimming is another critical factor that directly affects achievable spectral resolution. We have found that shimming on the lock or tissue water signal was not as sensitive as shimming on the splitting of the lactate doublet at 1.33 ppm, which fortunately presents in most excised biological tissues. However, in order to shim

interactively on the degree of splitting, it is necessary to work with the frequency domain. This should not present a challenge to most current spectrometers. Furthermore, it should be possible to establish autoshimming protocols based on this criterion.

It is now accepted that malignancy related cellular marker metabolites may not present simply as present or absent, but rather as continuous changes in intensity throughout disease development and progression. Quantification of these metabolites can be extremely important if they are to accurately diagnose and characterize stages of disease. Metabolite concentrations may be estimated from HRMAS MR spectra by using either the intensity of tissue water signals or an external standard (e.g. a small piece of silicone rubber) permanently attached to the inside of the rotor or attached to the rotor inserts. Such an external standard can be calibrated with known compounds of known concentrations. Interested readers can make such compounds by dissolving known amounts of relevant metabolites in agarose gel.

HRMAS MR spectra may be acquired with or without water suppression, depending on whether water intensities are required for the estimation of metabolite concentrations. A rotor-synchronized CPMG sequence may be applied to achieve a flat spectral baseline if there are undesired broad resonances from the probe background.

Histopathology

The clinical utility of high-resolution tissue metabolite profiles obtained with HRMAS MRS needs to be investigated and validated by means of accurate and detailed correlation with serial-section tissue pathologies. Such correlations are particularly important for studies of human malignancies due to the heterogeneity that may be inherent in the disease. Tissue pathology can vary greatly from region to region within a single tumor, and intertumor differences may be even more pronounced. An obvious advantage of HRMAS MRS is its preservation of tissue for subsequent histopathological analyses, allowing the establishment of correlations between metabolite profiles and quantitative pathologies [28–30].

Routine clinical histopathology data is most often inadequate. Routine histopathology, in particular 5 micron slices of the tissue biopsy, provides information about the presence or absence of certain features. These features may vary from slice to slice and therefore information from a small percentage of the tissue may not correlate with the spectral profile, which consists of the weighted sum of the profiles from all tissue slices or indeed the entire piece of tissue. Hence, for certain types of tissues, particularly neoplasm samples with known heterogeneities, histopathology needs to be evaluated quantitatively. This can be achieved laboriously by the histopathologist's examining serially sectioned tissue slices or possibly with the assistance of computer image analysis of these same sections. The sectioning frequency differs with tissue type and should be determined in consultation with the pathologist. For instance, the optimal sectioning frequency for human prostate was found to be between $200 \sim 400\ \mu m$.

Data Analysis

Histopathological analysis in cancer diagnosis relies on the observation of variations in colors and shapes using a light microscope. Importantly, to suspect disease the pathologist must observe widespread rather than isolated changes in color and/or shape, a process requiring keen pattern recognition. Similarly, pattern recognition methods are most often required to allow the diagnosis of malignancy from MRS tissue metabolite profiles. Development and progression of malignant disease involves the simultaneous evolution of many metabolic processes. Therefore, although some individual metabolites have been reported to correlate with disease types and stages [1,2] it is more likely that the overall metabolite profile rather than changes in single metabolites will be sensitive and specific for disease diagnosis [31,32]. Sophisticated statistical classification strategies (SCS) have been developed and applied to the analysis of conventional MRS of malignant tissues [33]. To date, however, principal component analysis (PCA) using readily available statistical programs has been sufficient for revealing accurate diagnostic information from HRMAS MRS data [34,35]. However, the application of SCS may further improve these accuracies.

HRMAS MRS of Human Surgical Specimens

Over recent years, HRMAS MRS has been applied biomedically to the analysis of human surgical samples, research animal tissues, and cultured cells. The scope of the methodology presented in this section will be limited to HRMAS MRS studies of human tissues and will be presented where possible in context with preceding studies of the same tissues using conventional MRS. Although presented in this context, comparison of the sensitivities and specificities obtained using conventional and HRMAS MRS are not at this stage warranted as unlike the mature discipline of conventional MRS, HRMAS MRS is still in its infancy and has reported only studies with restricted patient numbers. Although the capability of HRMAS has been clearly demonstrated in generating high-resolution spectra from which individual metabolites can be measured and such measurements were impossible with conventional methods, studies of large patient populations, as with conventional MRS studies, that allow evaluation of the sensitivity and specificity of the method have not

yet appeared in literature. Similarly, it is not as yet possible to provide the reader with one concise and optimal method for undertaking HRMAS MRS. Detailed methods are provided for each of the studies presented and these methods discussed in terms of the study aims. In an emerging discipline such as HRMAS MRS care must be taken to rigorously address methodological variables with respect to the type of tissue being analyzed and the specific information required. Increased spectral quality will most often be obtained with higher spinning speeds but this will be at the expense of tissue preservation allowing subsequent histopathological assessment of the tissue. Some tissues are less easily destroyed than others by high spinning speeds and thus preliminary experiments need to be undertaken to determine optimal parameters.

MRS analyses on tissue extracts have been studied for many years on many diseases, and have formed a large body of literature. Results from these studies are worthy of close examination and review but will not, however, be included in this review due to the following: the pathology of the tissue samples most often remains incomplete and/or the degree of extraction cannot be certain.

Brain

Human brain was the first study reported using proton HRMAS MRS to determine tissue pathology. Due to the relative motion stability and homogeneity compared to other organs, brain has dominated the development of *in vivo* MRS, and accordingly has inspired many *ex vivo* studies, primarily including neurodegenerative diseases and tumors, aimed at understanding metabolism and defining brain tissue chemistry.

The first HRMAS MRS human studies on brain tissues from autopsies described semi-quantitative evaluation of the pathology of a neurodegenerative disease, specifically Pick disease [36]. Through MRS measurements and traditional neurohistopathology, direct and semi-quantitative correlations were found to exist between the levels of N-acetyl aspartate (NAA) and the amount of surviving neurons in varying regions of examined brain as seen in Figure 2. The study also, for the first time, demonstrated that the spectral resolution of HRMAS proton MRS was comparable with that measurable with conventional proton MRS of tissue

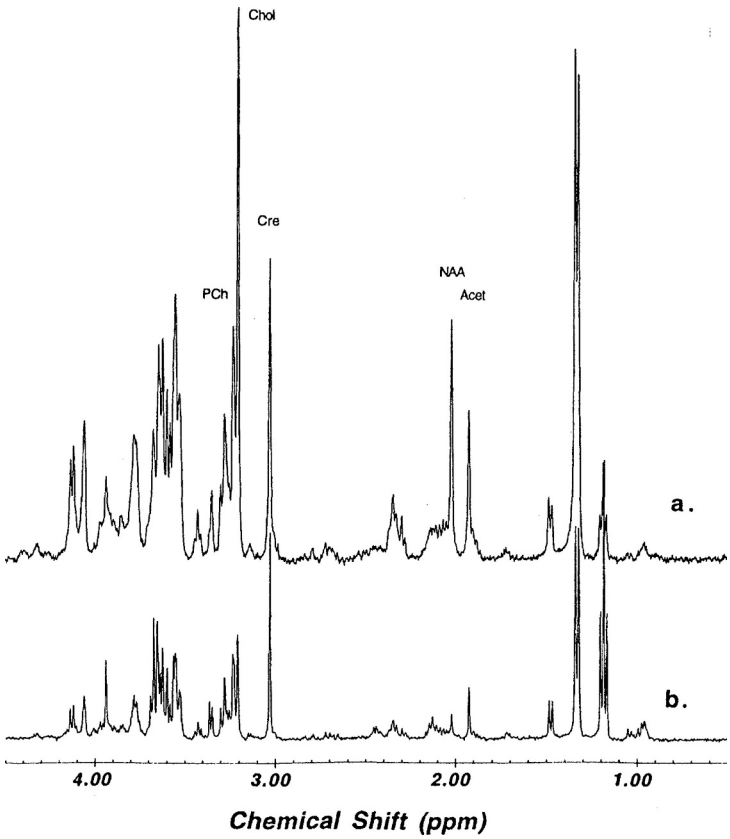

Fig. 2. Comparison of HRMAS MR spectra of brain tissue from the relatively unaffected primary visual cortex region (a) and the severely Pick disease affected rostral inferior temporal gyrus region (b), showing a marked decrease in NAA concentration, 8.48 μmol/g for spectrum a and 4.96 μmol/g for spectrum b. This decrease in NAA was found to correlate with an average neuronal count decrease of 33 neurons per 0.454 mm^2. The spectra were acquired at 2 °C, and were scaled according to concentration of creatine at 3.03 ppm for enhanced visualization. *Figure 4 from ref. [36]*

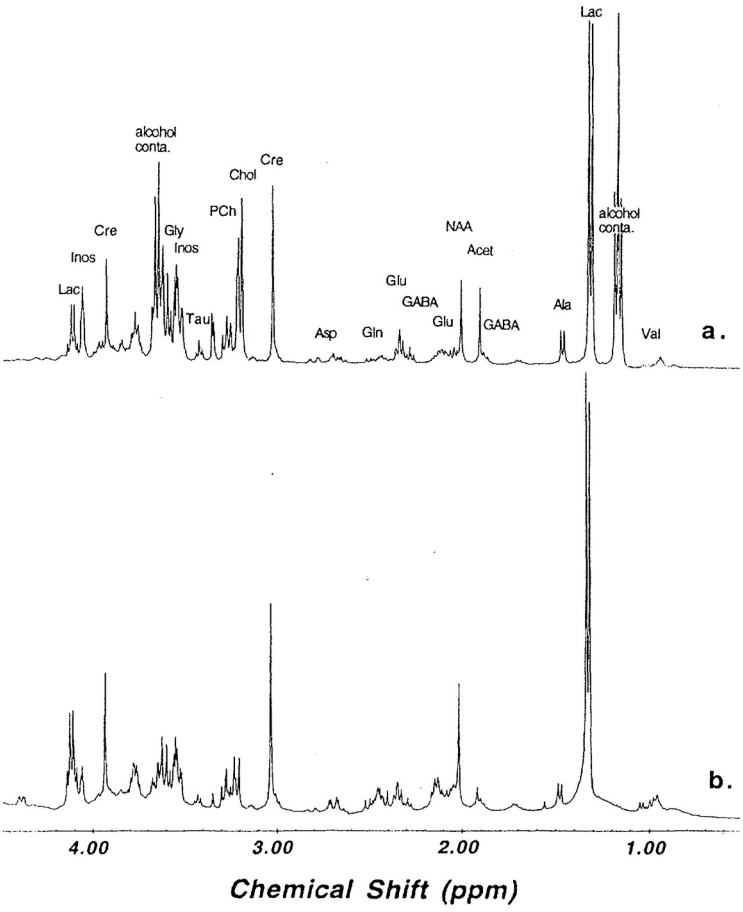

Fig. 3. Comparison of human brain proton MRS acquired with (a) HRMAS on intact tissue and (b) conventional method on extract solution. The spectral resolution was comparable while relative intensities for certain metabolites varied.

extracts (Figure 3), and superior to that obtained using conventional MRS of intact tissue (Figure 4). Another early study, also on autopsy brain tissues, correlated MRS data and stereological pathology for Alzheimer's disease and confirmed NAA concentration to be proportional to neuronal density (Figure 5). In this study, 7 human brains were examined, 3 of which were Alzheimer diseased and 4 which presented as normal human control brains. Figure 5 demonstrates the quantitative nature of the NAA and neuronal count relationship, as the correlation intercepted at zero (-0.29 ± 1.15 μmol/g) [37].

The MRS study of brain tumor intact tissues using conventional MRS suggested the diagnostic importance of lipid and lipid metabolites. Kuesel and colleagues reported correlations between MR lipid signal intensities and the amount of necrosis in astrocytomas [38]. With 42 cases, they showed that the intensity of the mobile fatty acyl –CH=CH- resonance at 5.3 ppm, differentiated 0, 1–5 and 10–40% of necrosis with statistical significance [39]. These results represented a great potential use for *ex vivo* MRS for astrocytoma diagnosis, in particular for differentiating Grade III and Grade IV tumors, which have radically different prognoses. The technique also ensured that necrotic foci often missed by clinical pathology were identified. Working with conventional MR spectra of brain tumor tissues, Rutter *et al.* attempted to categorize tumors according to 1D peak ratios (3.1–3.4 vs. 1.1–1.5 ppm), T_2 values of peaks at 1.3 ppm and cross-peaks on 2D COSY spectra (0.9 ppm with 1.35 ppm, representing methyl-methylene couplings; and 1.3 ppm with 2.05 ppm for couplings between methylene groups in fatty acids) [40]. With 38 samples studied from 33 subjects (including normal tissue, astrocytoma, GBM, meningiomas, and metastases), they were able to use peak ratios to

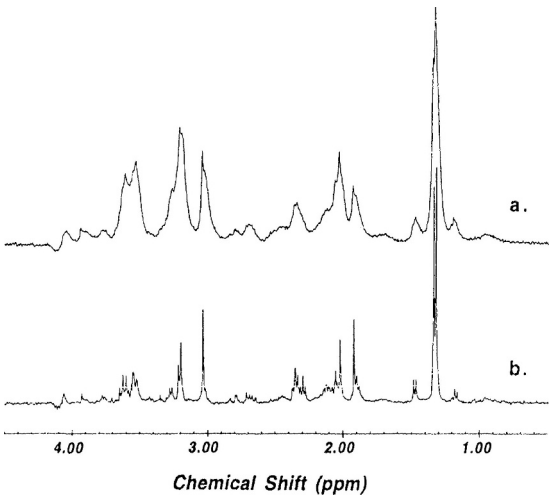

Fig. 4. Comparison of human brain proton MRS acquired with (a) conventional MRS and (b) HRMAS MRS. *Figure 2 from ref. [36].*

differentiate GBM from astrocytomas and normal tissues. They also found that the T_2 of the 1.3 ppm peak could be fitted by a double exponential function and that the long fraction of T_2 values could be used to group both GBM and metastasis from normal tissue. However, tissue spectra measured with conventional method of low resolution prevented these studies from observation of individual brain metabolites other than identification of broad lipid peaks.

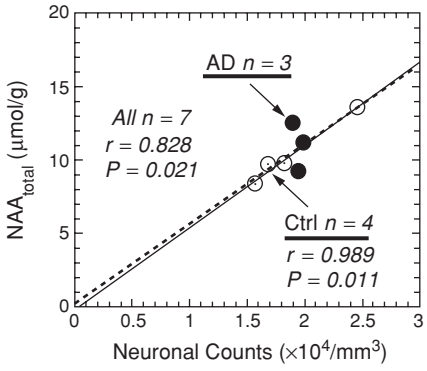

Fig. 5. A statistically significant linear correlation was found to exist between the number of neurons and the concentration of NAA_{total}, measured from 3 Alzheimer diseased and 4 normal control brains (the dotted line, $r = 0.828$, $P = 0.021$). The solid line represents the linear correlation obtained when only normal control brains were included ($r = 0.989$, $P = 0.011$). *Figure 3 from ref. [37].*

HRMAS MRS of brain tumors allowed for the first-time detailed profiles of water-soluble metabolites and lipids to be obtained from the same spectra [31]. In a study of 19 brain tumors, including astrocytomas, GBM, meningiomas, Schwannomas, and normal brain, metabolite concentrations both in absolute units and relative ratios normalized to the creatine resonance at 3.03 ppm were reported and T_2 values for these metabolites were measured *ex vivo* for the first time (Table 1). Metabolite concentrations from intact tissues and tissue extracts from the same tumors were compared to each other and to the literature values. While the concentrations for some metabolites, measured by HRMAS MRS, were similar to those in extracts, others showed much higher concentrations in tissue than in extracts. Metabolite concentrations and T_2 values accurately differentiated tumor types based on clinical data, but detailed histopathology of the tissue samples was not performed due to the false belief at the time that HRMAS MRS damaged tissue such that subsequent histopathological analysis was not possible.

The important fact that accurate histopathological evaluation of tissue samples after HRMAS MRS is possible and the necessity of performing quantitative pathology on the same tissues after MRS was reported by Dr. Anthony and colleagues [28]. Tissue pathologies from both HRMAS MRS analyzed tissue and adjacent tissue that had not undergone HRMAS MRS before histopathological evaluation were analyzed semi-quantitatively for each region of the brain tumor. The quantitative histopathological data obtained from the study showed that adjacent specimens from the same tumor region shared similar histopathological features. Although quantitative differences were noted, these differences were most likely due to extensive tumor microheterogeity and not the result of the HRMAS MRS procedure. Futhermore, correlations between the amount of tumor necrosis and the concentrations of mobile lipids ($R^2 = 0.961$, $p < 0.020$) and lactate ($R^2 = 0.939$, $p < 0.032$), as well as between the numbers of glioma cells and the ratio of phosphocholine (PC) to choline resonances ($R^2 = 0.936$, $p < 0.033$) were observed. The strong linear correlation between tissue necrosis (%area) and lipids (mM) indicated that the amount of tissue necrosis can be estimated using the measured concentration of lipids from HRMAS MRS, and that according to the long T_2s these lipids are relatively mobile consistent with them being products of cell membrane degradation. Additionally, the results of the correlation obtained between the number of glioma cells and the phospocholine to choline resonances suggested the importance of measuring and quantifying these two resonances separately, which is difficult with both *in vivo* and *ex vivo*

Table 1: Matrix of selected brain metabolite concentrations measured with HRMAS MRS for differentiation between different pathological specimens NAA, in the table, includes both measured resonances of NAA at 2.01ppm and acetate at 1.92 ppm (see text for details); Numbers in parentheses represent resonance chemical shift in ppm. The resonance at 3.93 is tentatively assigned to the Cr metabolite. As an example of the use of this matrix, the Chol resonance can be used to differentiate low-grade/anaplastic astrocytomas from GBMs with a significance of $p < 0.05$. Similarly, the glycine resonance (Gly) can be used to distinguish GBMs from Schwannomas with a $p < 0.005$

	Normal	LG and AA[a]	GBMs	Schwannomas	Meningiomas
Normal		NAA[b] Lac (1.33)[c]	Cr (?, 3.93)[c] Gly (3.55)[d] Chol (3.20)[b] Cr (3.03)[b] NAAf Lac (1.33)[b]	Chol (3.20)[b] NAA[b] Lac (1.33)[d]	Cr (?, 3.93)[b] Chol (3.20)[e] Glu (2.35)[d] Ala (1.48)[b]
LG&AA			Chol (3.20)[e]		Glu (2.35)[b]
GBMs				Gly (3.55)[d]	Gly (3.55)[b]
Schwannomas					
Meningiomas					

[a]LG and AA, low-grade/anaplastic astrocytomas
[b]$p < 0.05$, two-tailed student's t test.
[c]$p < 0.0005$, two-tailed student's t test.
[d]$p < 0.005$, two-tailed student's t test.
[e]$p < 0.05$, calculated according to one-tailed student's t test, based on the hypothesis that chol increases in tumors.
[f]$p < 0.00005$, two-tailed student's t test.

conventional MRS methods, but readily achievable with MAS.

It is expected that HRMAS MR spectra of tissue rather than MRS of tissue extracts will provide metabolite information more closely related to that in the *in vivo* brain. However, cautions should be exercised when comparing *in vivo* MRS and HRMAS MRS data, as *in vivo* MRS will always be broad-line in nature. Nevertheless, a number of studies, both in adult [41] and pediatric [42] brain tumors, have concluded that there is good agreement between *in vivo* and *ex vivo* tissue MR spectra with high-resolution *ex vivo* results providing both insight into which metabolites reside within the broad resonances observed *in vivo* and a link between *in vivo* MRS evaluations and neuropathologies.

Prostate

The search for marker metabolites of prostate cancer has been inspired by the current state of prostate cancer pathology, wherein more than 70% of newly diagnosed cases are categorized with similar Gleason scores (6 or 7), but for which individual patient outcomes within these tumors are drastically different and unpredictable.

Hahn and colleagues reported the first intact prostate tissue conventional MRS study of 66 benign prostatic hyperplasia (BPH) and 21 prostate cancer samples from 50 patients [43]. They divided the proton spectral region between 0.5 and 3.55 ppm into 50 equal subregions, and applied multivariate linear-discriminant analysis to the point-reduced spectra. The study found six spectral regions including those containing citrate, glutamate, and taurine to be sensitive in differentiating BPH from cancer with an overall accuracy of 96.6%. This algorithm was tested by the same research group on another group of 140 samples from 35 patients after radiotherapy to test for the sensitivity of spectroscopy analysis in differentiating cancer positive vs. cancer negative samples [44]. After eliminating 24 samples that did not have sufficient signal-to-noise ratios, they reported, with the remaining 116 spectra, the sensitivity and specificity of tissue spectra in identifying cancer samples to be 88.9 and 92%, respectively.

Van der Graaf and colleagues presented another interesting study of intact prostate tissue combining conventional MRS and high-pressure liquid chromatography (HPLC) analysis to measure the relationship between polyamines (PA) and prostate cancer [45]. Although they observed PA in the proton spectra and measured statistically significant drops of PA in cancer samples with HPLC, no correlation between PA levels measured by MRS and those determined by HPLC were presented for the same cases due to very limited number of samples analyzed. Nevertheless, the study suggested the existence

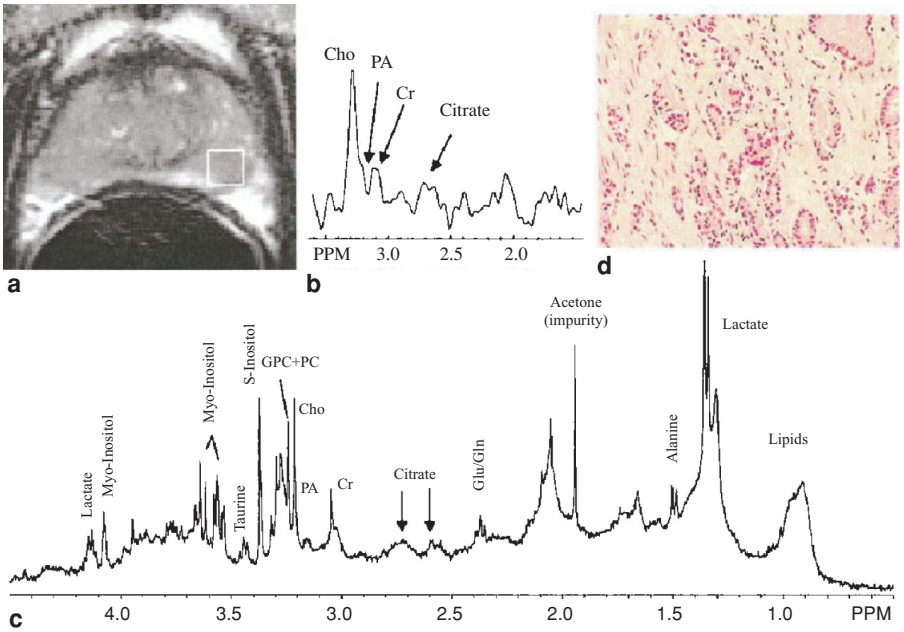

Fig. 6. Results from a presurgical 3D-MRSI of a 56-year-old prostate cancer patient were concordant with histopathologically classified malignancy of H and E stained tissue samples of excised tissue with Gleason 3 + 4 prostate cancer, **d**. Spectrum **b**, shows elevated levels of choline and low levels of citrate and polyamines relative to creatine in the 0.24 cm3 voxel of **a**. The postsurgical HRMAS MR spectrum (c) confirms the 3D-MRSI results with enhanced resolution that also identifies elevated levels of GPC + PC relative to choline. *Figure 2 from ref. [30].*

of a potential prostate biomarker that MRS may be able to quantify, as well as a direction for future studies. More recently, Mountford *et al.* reported a conventional MRS study of 71 prostate samples from 41 patients who underwent both cancer and non-cancer prostate surgeries [46]. By using peak ratios 3.2/3.0 ppm (choline-to-creatine) and 1.3/1.7 ppm (lipid-to-lysine), they were able to differentiate malignant from benign tissues with 97% sensitivity and 88% specificity.

Tomlins and colleagues experimented with proton HRMAS MRS analysis on human prostate tissues with both 1D and 2D MR spectroscopy. In their qualitative report, they confirmed the usefulness of HRMAS MRS in producing high-resolution spectra from intact human prostate tissues [47]. A second HRMAS MRS study of human prostate tissues from 16 patients was the first to include quantitative pathology on the MRS specimens and to include multiple subjects [29]. The results of the study proved the validity of HRMAS MRS for the accurate determination of tissue histopathology. Both citrate and spermine were quantified from the tissue HRMAS MR spectra and shown to be linearly correlated with the amounts of prostate normal epithelium. In 2003, Swanson and colleagues reported an interesting study of HRMAS MRS of tissues from 26 patients harvested post surgically under the guidance of 3D-MRSI from lesions that had been analyzed using *in vivo* MRS prior to prostatectomy. Figure 6 shows the resulting spectra from a 56-year-old prostate cancer patient [30]. By combining the MRS results with quantitative pathology of the same tissue after spectroscopy, metabolite discriminators (i.e. ratios of citrate, polyamine, and choline compounds to creatine) were found to differentiate normal prostate epithelial tissue from cancer and stromal tissue. Furthermore, a correlation between the intensity of MIB-1 immunohistochemical staining and the ratio of choline to creatine resonances was reported, supporting their findings *in vivo*. These results were dependent on the assumption that the creatine concentration did not alter during the disease process, which awaits verification.

Breast

Human breast tissue was difficult to analyze using conventional proton MRS due to high lipid content. As pioneers of this work, Mountford and colleagues noted that to acquire a spectrum that was diagnostically meaningful,

fine-needle aspiration biopsy (FNAB) instead of regular tissue samples had to be utilized [48]. In a study of 218 FNAB samples from 191 patients with benign lesions, ductal carcinoma *in situ* (DCIS), and invasive carcinoma, they found that by using the resonance peak height ratio threshold of 1.7 (3.25 vs. 3.05 ppm; or choline-compounds vs. creatine), benign lesions could be differentiated from carcinoma with 95% sensitivity and 96% specificity. However, this single ratio identifier only worked if the signal-to-noise ratio, particularly for choline peaks at 3.25 ppm, was above 10. To extend the MRS differentiation capability below this limit, and more importantly to search for a more robust diagnostic protocol of computerized spectral analysis, Mountford *et al.*, along with Smith *et al.* at the NRC, Canada, used a pattern recognition method, SCS, developed to utilize the entire MR spectrum instead of only the aforementioned two peaks for the purpose of analysis [9]. From measurements conducted on 140 samples, they reported an overall accuracy of 93% in distinguishing benign from malignant tumors using SCS. Furthermore, they reported that using SCS classifiers, lymph node involvement and tumor vascular invasion could be predicted with 95 and 94% overall accuracies, respectively. The advantage of SCS in relating proton FNAB spectra with breast cancer diagnosis and possibly prognosis is evident and its potential in clinical usage is apparent. However, the more advanced the SCS, the less evident were the direct connections with individual metabolites.

HRMAS MRS overcame many of the limitations of conventional MRS32. Even with such lipid-rich tissue, HRMAS MRS successfully produced high-resolution proton spectra. Results from a study at 400 MHz of 19 cases of ductal carcinomas showed that both the high fat contents and individual cellular metabolites could be measured from the same spectrum. Particularly, from these spectra, PC could be quantified separately from choline; and the ratio between PC and choline was found to correlate with tumor grades, as shown in Figure 7.

A more recent detailed HRMAS MRS study at 600 MHz of 10 ductal carcinomas by Sitter *et al.* compared HRMAS MR spectra with those obtained using conventional MRS of perchloric acid tissue extracts [20]. The study concluded that for breast tissue, HRMAS MRS was able to achieve spectral resolutions approaching those obtained using conventional MRS of extracts. 2D J-resolved and COSY MRS was used to accurately assign metabolites.

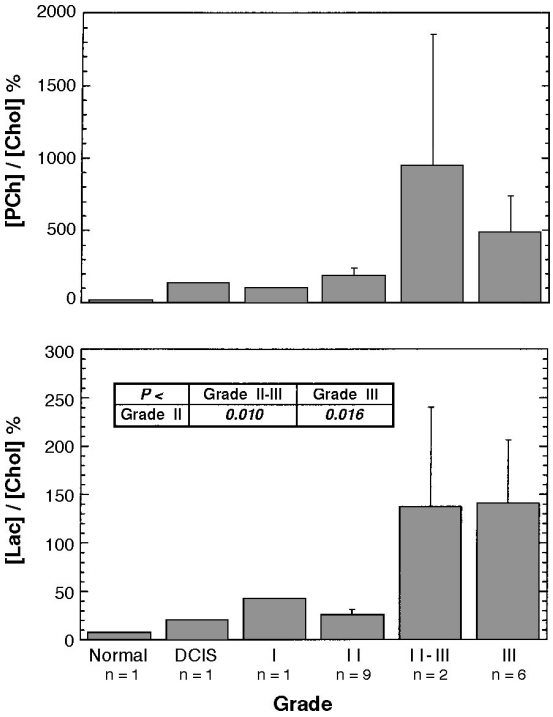

Fig. 7. Examples of observed correlations between histopathological grades of breast ductal carcinomas and the means for metabolic intensities, particularly PC over choline (A) and lactate over choline (B) measured with HRMAS MRS. Of note, the HRMAS method provided a means to differentiate PC from choline in the such a lipid-rich tissue. *Figure 4 from ref. [32].*

Cervix

Mountford and colleagues began analysis of human cervical biopsies with conventional proton MRS in the early 1990s [49]. Broad-line resonances at 0.9 ppm (CH3), 1.3 ppm (CH2), and 3.8–4.2 ppm (CH) were found to distinguish invasive from pre-invasive epithelial malignancy [50].

More recently, Sitter and colleagues reported the use of HRMAS MRS of cervical tissue from eight cancer and eight non-cancer patients [.35]. In addition to their presentation of detailed resonance assignments for cervical metabolites, they were able to use PCA to separate cancer from non-cancer samples with the first principal component (PC1). This principal component was comprised primarily of lactate, the methyl, and methylene groups of lipids, and, to a lesser extent, the choline-containing compounds. This component represented 63% of the variations in the spectra.

Kidney

HRMAS MRS analysis of kidney tissue has been shown to diagnose renal cell carcinoma based on an increased intensity of lipid resonances in malignant compared to

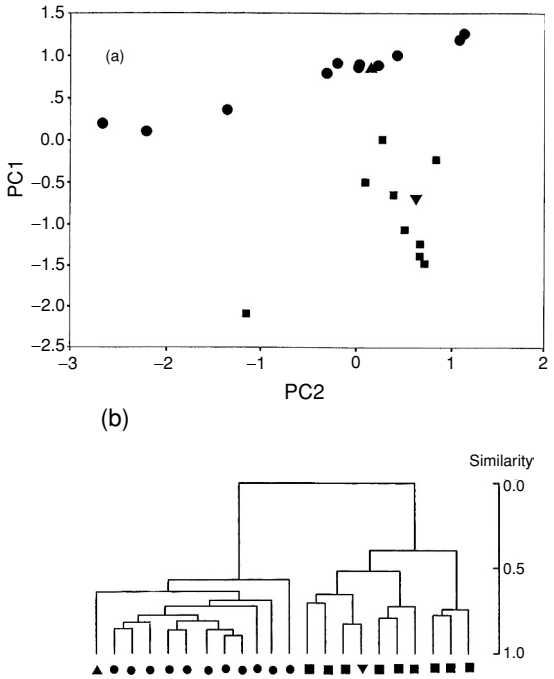

Fig. 8. Using PCA (a) and HCA (b), tumor samples can be differentiated from non-tumor samples. Key: (•) normal tissue; (■) renal cell carcinoma; (▲) sample from bladder metastasis in renal collecting duct; and (▼) lung metastasis in renal cortex. *Figure 3 from ref. [.35].*

control tissues [51,52]. These studies were not designed to test the utility of HRMAS MRS in the diagnosis of renal cell carcinoma, but rather to illustrate the feasibility of HRMAS MRS for assignment of resonances and identification of metabolites as well as to develop two-dimensional HRMAS MRS techniques for the assessment of intact tissues.

Later, a study of 22 paired control and tumor samples of human renal cortex used computer-based pattern recognition techniques to show that using PCA and hierarchical cluster analysis (HCA), tumor samples were differentiated from non-tumor samples, as shown in Figure 8 [34].

Sarcoma

HRMAS MRS has been shown to be a useful technique in the analysis of human sarcoma tissue. Singer and colleagues reported a comparison of 2D TOCSY spectra with and without HRMAS MRS, which demonstrated the superior resolution of the MAS technique by revealing less intense cross peaks that were not observed when the sample was not spun [53,54]. For this initial study, spectra of liposarcoma and lipoma were dominated by signals from lipids, interfering with the ability to observe resonances from other metabolites. More recently, Chen and colleagues have developed a double pulsed field gradient selective echo (DPFGSE) technique in combination with HRMAS MRS to selectively excite spectral regions that contain less abundant non-lipid metabolites [23]. With their new technique they were able to observe and quantify phosphatidylcholine (PTC), PC and choline, and found, using six paired samples from six patients, that the ratio of PTC/PC differentiated normal fat from lipoma-like well-differentiated liposarcoma with statistical significance ($p < 0.001$).

Lymph Nodes

Accurate detection of metastatic deposits in lymph nodes is often the most important predictor of cancer patient prognosis. Histopathology is subject to sampling and observer error and thus there is a real need for a new, rapid, and cost-effective method with high accuracy for this purpose.

An early study identifying malignant cells in lymph node tissue using 1D ^{1}H MRS was limited by high fat content of the tissue and the low spectral resolution obtained. Two-dimensional (2D) techniques successfully resolved resonances and allowed the complex spectra from lymph nodes to be assigned and correlated with detailed histopathology [10]. Choline and lactate were found to be key metabolites diagnostic of the presence of metastases in lymph nodes using the 2D method. However, these 2D MR experiments require long acquisition times (4–5 h) during which sample degradation may occur, potentially compromising the outcome of the measurement. In addition, conventional 1D and 2D techniques cannot address the problem of resonance broadening directly and thus useful diagnostic information may be missed.

Alternatively, MRS of FNAB of lymph node tissues has been used to diagnose the presence of metastases in lymph nodes from melanoma patients [55]. Spectra of node tissue containing metastatic melanoma were characterized by the presence of a distinct resonance from choline-containing metabolites at 3.2 ppm. The ratio of the integrals of resonances from lipid and metabolites (1.8–2.5 ppm region) and "choline" (3.1–3.3 ppm region) distinguished benign nodes (38.8 ± 34.3) from melanoma containing nodes (7.2 ± 6.8) with $p < 0.012$ (separate t-test) [55]. This method assumes the chemistry of the node detectable by MRS changes immediately upon the node being infiltrated by metastatic cells. This is supported by studies in a rat lymph node metastasis model where MRS detected the presence of malignant cells prior to clusters of metastatic cells being identified by histopathology.

Instead, single malignant cells were observed unclustered throughout the node, the presence of which was confirmed by growing these nodes in nude mice, which subsequently developed tumors. Datasets in the study of MRS on FNAB as a method of diagnosing lymph node metastases remain, however, small and until larger databases confirm these findings the possibility that the method introduces a sampling error cannot be excluded.

The application of HRMAS MRS to intact tissue analysis was in fact initiated from the proton MR detection of lymph node metastases in a rat model for breast cancer metastasis. Since then, HRMAS MRS has also been successfully applied to the proton MR analyses of human lymph nodes from breast cancer patients. Malignant nodes were distinguished from reactive nodes based on the peak height ratio of the smallest to largest peaks resolved in the 0.9 ppm resonance multiplied by the peak height ratio of the choline and creatine resonances at 3.2 and 3.0 ppm, respectively (Figure 9). Three of four axillary nodes from breast cancer patients that were clinically suspicious but diagnosed cancer free on routine histopathology had an HRMAS MRS ratio consistent with reactive nodes. The fourth node in this category was, by HRMAS MRS criteria, malignant. Review of the histology of these nodes using increased magnification and immunohistochemical staining identified malignancy in the fourth node missed during routine examination.

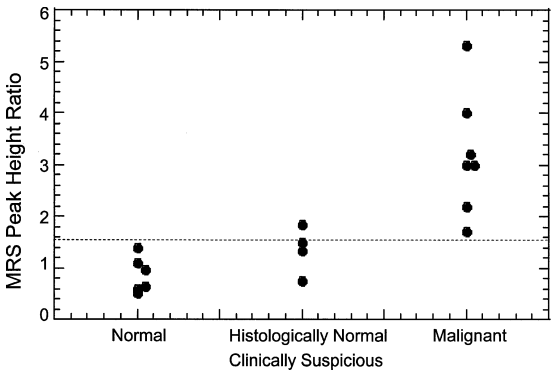

Fig. 9. HRMAS MRS of Human Lymph Nodes: Malignant nodes were distinguished from normal (reactive) nodes based on the MRS Peak Height Ratio (ratio of the smallest to largest peaks resolved in the 0.9 ppm resonance multiplied by the ratio of the choline and creatine resonances at 3.2 and 3.0 ppm). One of four axillary nodes that were clinically suspicious but cancer free on routine histopathology had an HRMAS MRS ratio consistent with malignancy. Review of the histology for all four nodes identified malignancy in this one node missed by routine histopathology.

Future Developments and Conclusions

The development of proton HRMAS MRS for tissue analysis has not only drastically simplified the procedure of obtaining high resolution cellular metabolite spectra directly from intact tissue, but more importantly allows quantitative pathology to be conducted on the same tissue after MRS measurements for correlation with individual metabolite concentrations or collective alterations in overall metabolite profiles. The high-resolution spectra generated by HRMAS MRS contain many more resonance peaks for analysis than conventional MRS. This greatly improves the likelihood that sophisticated data analysis methods can accurately distinguish between differing pathologies. However, the increased discriminatory power of the method relies on precise histopatholgical information about the tissue assessed by HRMAS MRS being available. This is only possible when detailed serial section histopathological methods are undertaken to substantially increase the precision of the information currently obtained from clinical pathology.

Glossary of Terms

Astrocytoma—The most common type of brain tumor in adults; astrocytomas, known for their marked potential for malignant progression and infiltrative nature, can be classified histopathologically into three grade of malignancy: WHO Grade II astrocytoma, WHO Grade III anaplastic astrocytoma, and WHO Grade IV GBM.

Benign Prostatic Hyperplasia—Enlargement of the prostate and more specifically, overgrowth of the epithelium and fibromuscular tissue of the transition zone and periurethral area.

Ductal Carcinoma *In Situ*—Noninfiltrative lesions composed of malignant epithelial cells that are confined to the mammary ducts and lobules.

Glioblastoma Multiforme—The most malignant grade of astrocytoma (WHO Grade IV), which has an overall survival time of less than 2 years for most patients. These tumors are histopathologically characterized according to their dense cellularity, high proliferative indices, endothelial proliferation, and most importantly the presence of focal tissue necrosis.

Lipoma—Commonly diagnosed benign tumors of adipose tissue that can develop anywhere in the body where fat is normally found.

Liposarcoma—A commonly diagnosed soft tissue sarcoma in adults which be found anywhere in the body and for which there exists several types with varying clinical outcomes.

Meningioma—Intracranial tumors that arise in the meninges and compress the underlying brain. In general, many of these tumors are benign, however, others are

malignant with the capability to metastasize, both locally and distally.

Metabolite Profiling—The study of small molecules, such as lipids, peptides, amino acids, and carbohydrates, which represent steady-state concentrations of intermediate products or end products of cellular processes and as a result can be thought of as the ultimate response to genetic and environmental stimuli.

Necrosis—Tissue and/or cell death.

Neoplasm—Literally meaning "new growth." An abnormal growth of tissue which may be benign or malignant.

Oncogenomics—The study of genes, gene sequences, and the underlying genetic alterations that appear to be involved in oncological pathways.

Reactive Nodes—Lymph nodes that have been immunologically challenged.

Schwannoma—Benign tumors that arise on peripheral nerves in general and on cranial nerves in particular, especially on the vestibular portion of the eighth cranial nerve.

Sensitivity—The term relating to the percentage of people with disease who test positive for the disease, i.e. the percentage of patients with cancer who have positive biopsy results.

Specificity—The term referring to the percentage of people without disease who test negative for the disease, i.e. patients without cancer with cancer negative biopsy results.

Acknowledgments

The authors thank their former and present staff, students, and collaborators involved in the research presented in this review whom have all worked diligently towards developing MRS and HRMAS MRS for determining tissue pathology. We also thank our colleagues and friends from around the world for allowing us to describe their work and for their many interesting discussions and contributions to this review. Particular thanks to Carolyn Mountford, Peter Russell, and Peter Malycha for their encouragement and support. We thank Sinead Doran and Deborah Edward for helping prepare the manuscript. LLC and MAB acknowledge grant supports from PHS/NIH CA095624 and from DOD W81XWH-04-1-0190.

References

1. Mountford C, Doran S, Lean C, Russell P. Chem. Rev. 2004;104:3677.
2. Lean C, Somorja R, Smith I, Russell P, Mountford C. In: AG Webb (Ed). Accurate Diagnosis and Prognosis of Human Cancers by Proton MRS and A Three Stage Classification Strategy, 2002.
3. Pomper MG. In VT DeVita Jr, S Hellman, SA Rosenberg (Ed). Functional and Metabolic Imaging. Philadelphia, 2001.
4. Nicholson JK, Lindon JC, Holmes E. Xenobiotica 1999;29: 1181.
5. Bettelheim R. Price K, Gelber R, Davis B, Castiglione M, Goldhirsch A, Neville A, Lancet 1990;335:1565.
6. Mountford C, Lean CL, Mackinnon W, Russell P. In G Webb (Ed). The Use of Proton MR in Cancer Pathology. London, 1993.
7. Russell P, Lean C, Delbridge L, May G, Dowd S, CE M. Am. J. Med. 1994;96:383.
8. Doran ST, Falk GL, Somorjai RL, Lean CL, Himmelreich U, Philips J, Russell P, Dolenko B, Nikulin AE, Mountford CE. Am. J. Surg. 2003;185:232.
9. Mountford CE, Somorjai RL, Malycha P, Gluch L, Lean C, Russell P, Barraclough B, Gillett D, Himmelreich U, Dolenko B, Nikulin AE, Smith IC. Br. J. Surg. 2001;88:1234.
10. Mountford C, Lean C, Hancock R, Dowd S, Mackinnon W, Tattersall M, Russell P. Invasion and Metastasis, 1993; 13:57.
11. Kuesel A, Kroft T, Saunders J, Prefontaine M, Mikhael N, Smith I. Magn. Reson. Med. 1992;27:340.
12. Andrew E, Bradbury A, Eades R. Nature 1958;182:1695.
13. Lowe I. Phy. Rev. Lett. 1959;2:285.
14. VanderHart D, Earl W, Garroway A. J. Magn. Reson. 1981;44:361.
15. Maricq M, Waugh J. J. Chem. Phys. 1979;70:3300.
16. Cheng LL, Lean CL, Bogdanova A, Wright SC Jr, Ackerman JL, Brady TJ, Garrido L. Magn Reson Med. 1996;36: 653.
17. Middleton DA, Bradley DP, Connor SC, Mullins PG, Reid DG, Magn. Reson. Med. 1998;40:166.
18. Garrod S, Humpfer E, Spraul M, Connor SC, Polley S, Connelly J, Lindon JC, Nicholson JK, Holmes E. Magn. Reson. Med. 1999;41:1108.
19. Waters NJ, Garrod S, Farrant RD, Haselden JN, Connor SC, Connelly J, Lindon JC, Holmes E, Nicholson JK. Anal. Biochem. 2000;282:16.
20. Sitter B, Sonnewald U, Spraul M, Fjosne HE, Gribbestad IS. NMR Biomed. 2002;15:327.
21. Wu CL, Taylor JL, He W, Zepeda AG, Halpern EF, Bielecki A, Gonzalez RG, Cheng LL. Magn. Reson. Med. In Press (2003)
22. Bourne R, Dzendrowskyj T, Mountford C. NMR Biomed. 2003;16:96.
23. Chen JH, Enloe BM, Fletcher CD, Cory DG, Singer S. J. Am. Chem. Soc. 2001;123:9200.
24. Wind RA, Hu JZ, Rommereim DN. Magn. Reson. Med. 2001;46:213.
25. Hu JZ, Rommereim DN, Wind RA. Magn. Reson. Med. 2002;47:829.
26. Hu JZ, Wind RA. J. Magn. Reson. 2003;163:149.
27. Taylor JL, Wu CL, Cory D, Gonzalez RG, Bielecki A, Cheng LL. Magn. Reson. Med. 2003;50:627.
28. Cheng LL, Anthony DC, Comite AR, Black PM, Tzika AA, Gonzalez RG, Neuro-oncol. 2000;2:87.
29. Cheng LL, Wu C, Smith MR, Gonzalez RG. FEBS Lett. 2001;494:112.
30. Swanson MG, Vigneron DB, Tabatabai ZL, Males RG, Schmitt L, Carroll PR, James JK, Hurd RE, Kurhanewicz J. Magn. Reson. Med. 2003;50:944.

Author: Please provide publisher place and location for ref. [2].

Author: Please provide publisher name for ref. [6].

Author: Please provide full name for "CE M." in ref. [7].

Author: Please update ref. [21].

31. Cheng LL, Chang IW, Louis DN, Gonzalez RG. Cancer Res. 1998;58:1825.
32. Cheng LL, Chang IW, Smith BL, Gonzalez RG. J. Magn. Reson. 1998;135:194.
33. Somorjai R, Dolenko B, Nikulin A, Pizzi N, Scarth G, Zhilkin P, Halliday W, Fewer D, Hill N, Ross I, West M, Smith I, Donnelly S, Kuesel A, Briere K. J. Magn. Reson. Imaging. 1996;6:437.
34. Tate AR, Foxall PJ, Holmes E, Moka D, Spraul M, Nicholson JK, Lindon JC. NMR Biomed. 2000;13:64.
35. Sitter B, Bathen T, Hagen B, Arentz C, Skjeldestad FE, Gribbestad IS. MAGMA. 2004;16:174.
36. Cheng LL, Ma MJ, Becerra L, Ptak T, Tracey I, Lackner A, Gonzalez RG. Proc. Natl. Acad. Sci. U.S.A. 1997;94:6408.
37. Cheng LL, Newell K, Mallory AE, Hyman BT, Gonzalez RG. Magn. Reson. Imag. 2002;20:527.
38. Kuesel A, Donnelly S, Halliday W, Sutherland G, Smith I. NMR Biomed. 1994;7:172.
39. Kuesel AC, Briere KM, Halliday WC, Sutherland GR, Donnelly SM, Smith ICP. Anticancer Res. 1996;16:1485.
40. Rutter A, Hugenholtz H, Saunders J, Smith I. J. Neurochem. 1995;64:1655.
41. Barton SJ, Howe FA, Tomlins AM, Cudlip SA, Nicholson JK, Bell BA, Griffiths JR. Magma 1999;8:121.
42. Tzika AA, Cheng LL, Goumnerova L, Madsen JR, Zurakowski D, Astrakas LG, Zarifi MK, Scott RM, Anthony DC, Gonzalez RG, Black PM. J. Neurosurg. 2002;96:1023.
43. Hahn P, Smith I, Leboldus L, Littman C, Somorjai R, Bezabeh T. Cancer Res. 1997;57:3398.
44. Menard C, Smith IC, Somorjai RL, Leboldus L, Patel R, Littman C, Robertson SJ, Bezabeh T. Int. J. Radia. Oncol. Biol. Phys. 2001;50:317.
45. van der Graaf M, Schipper RG, Oosterhof GO, Schalken JA, Verhofstad AA, Heerschap A. Magma 2000;10:153.
46. Swindle P, McCredie S, Russell P, Himmelreich U, Khadra M, Lean C, Mountford C. Radiology 2003;228:144.
47. Tomlins A, Foxall P, Lindon J, Lynch M, Spraul M, Everett J, Nicholson J. Analy. Common. 1998;35:113.
48. Mackinnon WB, Barry PA, Malycha PL, Gillett DJ, Russell P, Lean CL, Doran ST, Barraclough BH, Bilous M, Mountford CE. Radiology, 1997;204:661.
49. Mountford CE, Delikatny EJ, Dyne M, Holmes KT, Mackinnon WB, Ford R, Hunter JC, Truskett ID, Russell P. Magn. Reson. Med. 1990;13:324.
50. Delikatny E, Russell P, Hunter J, Hancock R, Atkinson K, van Haaften-Day C, Mountford C. Radiology, 1993;188:791.
51. Moka D, Vorreuther R, Schicha H, Spraul M, Humpfer E, Lipinski M, Foxall P, Nicholson J, Lindon J. Analy. Common. 1997;34:107.
52. Moka D, Vorreuther R, Schicha H, Spraul M, Humpfer E, Lipinski M, Foxall PJ, Nicholson JK, Lindon JC. J. Pharm. Biomed. Anal. 1998;17:125.
53. Millis KK, Maas WE, Cory DG, Singer S. Magn. Reson. Med. 1997;38:399.
54. Millis K, Weybright P, Campbell N, Fletcher JA, Fletcher CD, Cory DG, Singer S. Magn. Reson. Med. 1999;41:257.
55. Lean CL, Bourne R, Thompson JF, Scolyer RA, Stretch J, Li LX, Russell P, Mountford C. Melanoma Res. 2003;13:259.

Handbook of Metabonomics and Metabolomics
Chapter 13
The Role of NMR-based Metabolomics in Cancer

*L. L. Cheng**
Departments of Radiology and Pathology
Massachusetts General Hospital
Harvard Medical School
Boston, Massachusetts, U. S. A.

&

U. Pohl
Department of Histopathology
Addenbrooke's Hospital
Cambridge, U. K.

*** Dr. Cheng would like to acknowledge support from NIH grant CA211478 and DOD grant 212597, as well as the editorial assistance of Kate Jordan.**

Content:

In the era of "-omics"

Biological science in the 21st century has been marked by the amending of well-recognized scientific branches into newly created disciplines with the suffix of "-omics." As you may have already noticed, in less then half a decade such popularized disciplines as genomics and proteomics have been embraced by the scientific community, as well as the mass media, although the exact scopes and dimensions of these disciplines are still in the process of development. Not surprisingly, the topic of this book, metabolomics - a junior member of the "-omics" family- and the connection of metabolomics with the aspect of this chapter, human oncology, are even less concretely defined. To facilitate our discussions in this chapter we wish to define current cancer metabolomics as: a study of the global variations of metabolites, and a measurement of global profiles of metabolites from various known metabolic pathways under the influence of oncological developments and progressions. We wish to emphasize the keyword in this definition is "global", which is clearly different from other adjectives, such as "individual".

This seemingly simple definition may not be obvious when you try translating it into clinical research. In fact, if you proposed to search for cancer metabolite profiles before the turn of the 21st century you would probably be branded as conducting "fishing expeditions." Fortunately, the expedition phrase has gradually faded away from today's scientific colloquy and the disengagement between perceptions of common sense and the rules in scientific pursuits have been somewhat lessened in regard to metabolomics. As evidence, if you browse the website of the National Institute of Health (NIH) of the U.S.A., you will find the word "metabolomics" in the title of Requests for Applications (RFAs) published by the agency[1]; in addition, at the same time as this chapter is being prepared in October, 2005, a workshop titled "Frontiers in Metabolomics for Cancer Research" is being organized by the National Cancer Institute at NIH.

This change of heart regarding the "-omics" came as a direct result of the birth of genomics. The technological inventions, such as those accompanying the human genome project, have created this new scientific branch that captures the front pages of

[1] "Metabolomics Technology Development" http://grants.nih.gov/grants/guide/rfa-files/RFA-RM-04-002.html and "Genomic, Proteomic, and Metabolomic Fingerprints as Alcohol Biomarkers" http://grants.nih.gov/grants/guide/rfa-files/RFA-AA-06-001.html.

mass media news as well the covers of scientific journals. After the completion of the human genome project, the innovative use of the suffix "-omics" was created to reflect the processes of searching for correlations between the large arrays of genome data measured by these new technologies, with physiological and pathological conditions. Genomics, rather than genetics, has "granted licenses" to many pursuits of clinical importance that would otherwise be rejected by scientific communities because of their exploratory nature and the lack of hypotheses that could be clearly delineated. In other words, the introduction of these new "-omics" branches has ratified formerly inconceivable concepts, allowing scientists a greater breadth of exploration in areas into which they have only vague insight; these explorations do not come at the expense of good science, however, and the "-omics" studies still rely on sound data collection and valid, measurable parameters.

There are many genomics examples of gene expression studies for oncology that can be found in literatures in the past five years. For instance, in a seminal paper published in Nature in 2000, C. M. Perou et. al. reported results of DNA microarrays of 8,102 human genes analyzed using breast tissue samples from 42 individuals[1]. Among the measured genes they analyzed 1,753 (22% of 8,102) of them in an effort to establish "molecular portraits of human breast tumours," as shown in **Figure 1**. In this cluster analysis map each row represents a single gene, while each column came from a measured sample. Without getting into details it may be appreciated that, with the appearance of clustered red and green dots, the map seems to indicate the existence of certain patterns that are not completely random. In hindsight, considering research development experiences since the publication of the paper, one can ponder a number of issues regarding the published study that may have direct implications to the topic of this chapter. Firstly, considering biological variations among individuals, how representative the "portraits" could be if a number of tumors were only collected from a single case? Secondly, how valuable would the gene profiles be without knowing the pathological details from which the profiles were derived? These issues arises because of the existence of heterogeneity, a major characteristic of human malignancy, i.e. the pathological features and the amount of these features vary among different regions in the same tumor, especially since the study was conducted on homogenized tissue blocks[2]. Later studies have indicated that these problems could be resolved to satisfactory degrees. The first issue is administrative and somewhat easy to solve as long as multiple clinical cases are available to the study. To solve the second issue, a colleague of ours, D. C. Sgroi, has demonstrated the need for and the feasibility of sample preparation via a special protocol. With the assistance of laser capture microdissection techniques, Sgroi and his colleagues removed pathologically identified specific cell types from 36 breast cancer patients (**Figure 2**), and subjected these removed cells to 12,000-gene cDNA microarray analyses[3]. By analyzing the most varied 1,940 genes (16% of 12,000), they were able to propose genomic profiles for tumors of different grades, as shown in **Figure 3**. Although there are many other studies that may be discussed, these two reports contain some common features that may be appreciated for our subsequent discussion. First, more than 80% of measured parameters did not reach the final analyses, and second, at least, more than half of the genes that composed the final cluster maps were of unknown functions, according to the most conservative estimation.

This seemingly "new" concept for research designs (deviating from the dominated and accepted structure of hypothesis-driven research approaches) has in fact always been employed in medical science and medicinal practice during the progression of modern medicine. For instance, considering histopathology and patient prognostication, and even equipped with the most up-to-date knowledge of anatomic pathology, it is almost impossible for us to imagine how one would propose any intelligent hypothesis that could relate cellular morphological changes with disease processes at the dawn of the discovery of optical microscopes, or even today. Nevertheless, that did not prevent observation based anatomic pathology from becoming a discipline that dictates almost every aspect of oncological practice to this day (as will be discussed later in this chapter). Thus, we can appreciate the emphasis on the criteria of hypothesis-driven research as the philosophical practices accompanying the blooming of sciences in the 20th century. In addition we should also realize the vital value of scientific explorations and derivations from these observations both in the history and at present. And finally, as hypothesis driven research was a valuable tool of the past, so can we appreciate the transition in the 21st century to this new era of "-omics" and the immense scientific potential this era holds.

The current metabolomics

Examining the active field of current metabolomics from the same perspective that you may use to scrutinize the status of genomics, you may realize that the state of current metabolomic activities is fundamentally different from contemporary genomics or proteomics. To fully appreciate the status and utilize the capability of current metabolomics, we need to dwell a bit on the still young history of genomics.

The development of genomics relyed almost entirely on innovations in the technologies of molecular biology. One such innovation which is now widely used was the creation of gene microarrays, as exemplified in the previously discussed human breast cancer studies. The fundamental characteristic of these new array paradigms is their ability to measure a very large number of parameters at the same time. These parameters can either be the investigation of thousands of genes from one sample, or the simultaneous comparison of the expression of one gene for hundreds of tissue samples. These investigations produce massive amounts of data in a magnitude that was never before witnessed in the human pursuits of biological science. In the context of human pathology, this situation may resemble the overwhelming sensation that our predecessors might have experienced when optical microscopes were first introduced into gross anatomy. The rules of engagement were changed. Thus, the transition to morphological examination more than a century ago required digestion and evaluation efforts of many generations, in many decades, to present us with the current prominent status of anatomic pathology. While optical microscopes allowed pathological evaluations to intrude into smaller physical spaces, genomics expanded our ability to evaluate a vast amount of genetic parameters, for many of which our current genetic knowledge cannot provide insight. Hence, we may expect that the efforts of the coming generations may be necessary to fully comprehend the functional importance of these genes; although hopefully the ever-increasing pace of developments in science and technology may facilitate these digestion and evaluation efforts. For example, at the time this chapter is being prepared, we notice a current publication on *interactome* and *transcriptome* in Nature (11 August, 2005)[4]. In this work M. Vidal and colleagues expanded the previous

concept of interactome for studies of protein-protein interactions, a. k. a. *interactomics*, into evaluations of relationships of gene expression profiles, now known as *integrative interactomics,* to identify the functions of genes in *Caenorhabditis elegans*.

Fortunately, the current status of metabolomics is less complicated than the those of genomics and proteomics, which mostly present either dots of individual genes or proteins with *unknown* linkages among them, or genes/proteins with indiscernible functions that require interactomics to reveal them. As already stated in the beginning of this chapter, our interpretation of and emphasis for the current metabolomics is focused on evaluations of global variations and global profiles of metabolites from various *known* metabolic pathways in relationship with physiological and pathological processes. This "known" vs. "unknown" difference, in our opinion, is the unique characterization of metabolomics that philosophically differentiates it from the current concepts of genomics and proteomics.

This "known" status is due solely to the fact that, up till now, there have not been fundamental breakthroughs in the innovation of metabolite analysis. This situation is very unlike the fields of genomics and proteomics where breakthrough technical innovations have been witnessed in the past years. Methodologies used in current metabolite analyses were well-established in past decades. Because of this the metabolic knowledge currently studied by the methodologies of analytic chemistry are known, at least individually, for each metabolite based on characterization through many tests and proven metabolic pathways. These methodologies currently include nuclear magnetic spectroscopy (NMR), mass spectroscopy, and gas chromatography.

You may agree with the concept that the words "genomics" and "proteomics" first serve to capture the images of scientific frontiers whose constitutes and significance are still unclear. Second these terms emphasize the need to consider all the measurable parameters simultaneously. If you concur with these statements then from our above discussion you may realize that the same concept cannot be applied to the parallel expression – metabolomics – without alterations. At the present, conducted with the above-mentioned well-tested methodologies for metabolite analyses, the chance for the discovery of new metabolites in vast quantities as witnessed in the other "-omics" fields is relatively slim. However, this should not discourage the development of metabolomics from the philosophical aspect of the "-omics" concept on global interpretations of the organization of the current knowledge on the overall metabolite pathways. The task of primary importance in current metabolomics is to interpret the global metabolite alterations collectively in the context of their overall changes in relation to human physiological and pathological conditions. For the purpose of this chapter, it is to better understand the global inter-connectivity of metabolites from various known metabolic pathways during the development and progression of human malignancies. Such a concept reflects and agrees well with the somewhat ancient idea that the human body is a united organic entity within which all the biological processes are inter-connected and balanced to produce measurable metabolite profiles. It is this overall profile, likely not a single metabolite, that may alter cell chemistry and be informative as indicative of disease. We also wish to emphasize that our statement regarding the slim chance for discovering new metabolites with the current analytic methods merely reflects our assessment of the limitations of the existing analytic methodologies. It by no means indicates we should stop expanding our knowledge on human metabolism. On the

contrary, given the numbers of new genes and proteins being discovered, we believe the numbers of metabolites unknown to us may be too large to estimate.

A metabolite, according to Oxford English Dictionary, is "a substance that is a substrate or product of a metabolic reaction, or that is necessary to a metabolic reaction; *esp.* an intermediate or end product of a metabolic pathway (Draft Revision Dec. 2001)." The pictorial interpretations of this simple definition can be very complicated for many of us to grasp. Demonstrations of the current knowledge on human metabolism can be found in various maps and charts of metabolic pathways; charts such as the one comprehensively generated by Dr. Donald E. Nicholson of Leeds, England, in collaboration with the International Union of Biochemistry & Molecular Biology and with Sigma-Aldrich (**Figure 4**). Since any substance registered in such a chart, and possibly millions of the others that are still unknown to us, can potentially be the fair targets and subjects of metabolomics, the complex future of metabolomics seems impossible to comprehend at this moment. On the other hand, if we again consider that under normal conditions all of these pathways in a human body are initialized by dietary intakes, then such a puzzling chart may be simplified greatly to carbohydrates, lipids, proteins, amino acids, etc. Thus, it seems that any measurement of these substances, using any modality taught in college classes of analytical chemistry, can be potential subjects of and tools for metabolomics. In reality, we need to point out that, presently in 2005, the bulk of the so-called metabolomics data associated with human oncology is supplied by NMR analyses. We attribute this observation to the fact that there has been an established NMR community actively pursuing identification of cancer related metabolites far prior to the era of "-omics." We hope that by now you have noticed that whenever we mention metabolomics we define it as "the current metabolomics" or "metabolomics of today." This is due particularly to the above-mentioned fact of the prior existence of analytic technologies in metabolite chemistry. Many parts of our discussion should be viewed as applicable only to the present status of metabolomics. Although it is hard to predict the era to come, we are certain that technical developments will change the face as well as the contents of metabolomics in the near future. The situation of current and future metabolomics is concisely summarized by the previously mentioned NIH RFA: "Technologies currently in use for metabolomic analysis include NMR, chromatography and mass spectrometry, each of which has significant limitations in quantification, scope, and/or throughput. No one technology can effectively measure, identify and quantify, with sufficient sensitivity and precision, the diverse range of metabolites and their dynamic fluctuations in cells. An integrated set of technologies is needed to address the entire spectrum of challenges for metabolomics. Ideally, new technologies should yield quantitative, comprehensive data and be applicable to achieving anatomical resolution at the cellular and subcellular level"[2].

The current oncology

Any clinical procedure in modern medicine, including oncology, can be characterized into one of the following categories for disease management: screening,

[2] "Metabolomics Technology Development" http://grants.nih.gov/grants/guide/rfa-files/RFA-RM-04-002.html

diagnosis, or therapy. Developments in modern medicine, therefore, have been spinning around advancements in these areas. Surveying the current status of oncology, the impacts of new scientific knowledge and technology innovations are evident. Unfortunately the consequence of new knowledge and its impact on the life or the quality of life for patients may not always be as pleasant as expected. For instance, with the realization of the relationship between certain genetic mutations and breast cancer development, prophylactic mastectomy (preventive removal of breasts) has been offered to women who are considered to be at high risk. However, harboring certain genetic mutations does not mean that cancer is present, or will always occur. Hence, it may be argued that prophylactic mastectomy might not be necessary for all women in whom these mutations are detected. Therefore, it can be best argued that in such a case new and more accurate disease markers are urgently needed; specifically markers that are particularly sensitive in early detection of cancer and preferably pre-cancerous lesions. The pursuit of how best to incorporate scientific developments into oncological practices to serve patients and not merely to treat diseases presents not only as a medical or technological topic, but a medical philosophical and ethical issue as well.

Examining the effects of emerging disciplines on disease management, we find that histopathology (the current "gold standard" in cancer diagnosis) is no longer viewed as an optimal diagnostic tool. Histopathology provides accurate, literal pictures of the existing state of specimens under evaluation. However, its ability is limited when it comes to providing information that may delineate the preceding condition of the individual patient prior to the particular histopathological presentation or to suggesting the possible or probable disease course for an individual condition. Histopathology works statistically well in providing disease interpretations for a class of conditions or a group of patients. Particularly, the histopathological approach to cancer diagnosis has served oncology sufficiently in the past, when the oncological needs for decision-makings on therapies were a direct result of symptoms that had displayed clinical significance. However, these past successes have been challenged in the current era of cancer screening, when patient presentations are asymptomatic and the diseases are early enough to defy the statistical efficiency of the "snapshots." With the creation of new testing protocols there is now a societal demand for early diagnosis and individual disease management. For this reason, if you immerse yourself in oncological discussion in these days, often what you will hear is not how to treat this group of patients, but rather what is the best treatment plan for this *individual*. This situation can best be illustrated by some examples.

Prostate Cancer

When discussing the impact of the new screening era on oncology, no other type of cancer is more divisive than prostate cancer. The status of prostate cancer as a common, controversial malignancy has not changed since the second half of the 1980s when the blood test of prostate specific antigen (PSA) for cancer screening was introduced. In the United States alone in 2005, it is estimated that more than 635 men are diagnosed with the disease daily, and another 83 lose their lives to the disease[5]. Meanwhile, considerable concerns have been expressed regarding the adverse effects of surgical intervention for tumors that may never likely become life threatening, as the >150 radical prostatectomies performed each day in the U.S. result in impotence for >90 men, and/or incontinence of urine for >45 men.

Facing this complicated situation involving a common disease, instead of posting clinical questions that intrigue us, we encourage you to ponder simultaneously a number of factors related to prostate cancer: the increased incidence rate achieved with PSA screening led to the increase of "indolent" cancers in PSA screening populations; the seemingly steady death rate over the history (**Figure 5**); the adverse effects experienced by considerable numbers of patients as results of therapies; and the large body of autopsy evidence that shows about 20-30% of men before the PSA testing era harbored indolent prostate cancer in their gland. How should all these facts play into decision making in the prostate cancer clinic, both in terms of providing the most appropriate care for an individual patient and for the interests of healthcare costs of the society?

These issues were realized by the National Institute of Cancer (NCI) in the U.S. in the 1990s. At the request of the then NCI director, Dr. Richard Klausner, the NCI Prostate Cancer Progress Review Group (PRG) was formed in 1997 with more than twenty prominent scientists and patient advocates on prostate cancer. After more than one year of work, the PRG published a report titled, "Defeating Prostate Cancer: Crucial Directions for Research"[3]. In the PRG Report the panel notes that "[b]ased on autopsy studies it is estimated that as many as 1 in 4 men 30 years of age may harbor a small focus of PCa in their glands." Furthermore, "[t]he basic problem…is that while about 11 percent of all men will contract clinically significant PCa in their lifetime, only 3.6 percent will die of it. The challenge is to determine which of the 7 to 8 percent can safely go untreated." The Report cites "our inability to distinguish 'indolent' from 'aggressive' carcinomas," concluding that this can "lead to the adverse consequences of over-treatment" if "[the] tumor is one that will remain 'quiescent,' or clinically insignificant throughout [the patient's] natural life span."

The utility of PSA testing in detecting clinically significant prostate tumors has been clinically proven. However, in the PSA screening era, most newly diagnosed prostate cancer (more than 70% at conservative estimations) belong to a similar group according to Gleason histological grading, which current histopathology cannot further sub-categorize without additional surgical intervention. Furthermore, tumors of clinical significance may be neither lethal to their hosts, nor indicative for "definitive therapies" that may increase "morbidity, particularly incontinence and/or impotence," as being noted by the PRG report. In fact, the PGR report estimates that currently in the U.S. >30% of prostate cancer patients are over-treated. The urgent task set forth by the PRG report is to discover "new and better markers than PSA for the early diagnosis of patients who harbor fast-progressing and virulent forms of prostate cancer." These markers are expected to "refine" early detection with PSA testing by identifying cancers able to kill their hosts if left untreated, double-checking for overlooked virulent cancers, and in doing so furnishing "prognostic markers that can guide the therapy of patients in an individualized fashion". To realize this goal, the PRG advised the development and validation of molecular assays with the comments that "[e]valuation of limited disease in the prostate is prone to extensive sampling error caused by heterogeneity. The availability of micro-dissection techniques and/or aspiration biopsy, coupled with molecular analyses (i.e. PR-PCR) or array analysis), could provide new approaches to conventional tissue analysis." If these words from the 1990s are translated into today's

[3] http://prg.nci.nih.gov/pdfprgreports/1998prostate.pdf

vernacular, they likely indicate the future advances in prostate cancer clinic will be discovered through "-omics".

Breast Cancer

The numbers of NCI Progress Report Groups has grown to 12 that cover almost all types of human malignancies[4]. However, before the turn of the 21st century, there were only two issued in 1998. One of them was the previously discussed prostate cancer PRG, and the other, commissioned in the same period and published at the same time, was titled: "Charting the Course: Priorities for Breast Cancer Research"[5].

The status of breast cancer in women is very similar to that of prostate cancer in men. In the U.S., breast cancer has always been the most frequently diagnosed cancer in women, and was only reduced to the second leading cause of cancer death in 1980s after the increase of lung cancer incidence[6].

In this era of public awareness and improved screening technologies breast cancer, similar to prostate cancer, presents its own controversial issues. Controversies in the care of breast cancer patients can be visualized and understood, step-by-step, by following the practices in a comprehensive breast health clinic:

Very often one to several suspicious lesions are identified by self-examination, annual physical examination, and/or a mammography. Since no non-invasive diagnostic modality is now available, everyone agrees that a biopsy, whether a fine-needle aspiration (FNA) or more often a core needle biopsy (both possible in a doctors' office), is necessary.

Unfortunately, this may be the last universal agreement among caregivers, breast cancer patients, and their physicians regarding treatment options. Disagreements arise immediately at the interpretation of the observation of many FNA and core needle biopsy specimens. Discrepancies in these observations often result in open biopsies (operating room procedures) for these FNA and/or core needle inconclusive patients, who represent a very large population. Focused on the histopathology issues of breast cancer, the breast cancer PRG report recognized that light-microscope based diagnostic and prognostic "criteria are suboptimal," and recommended that "markers should be sought that will signal the presence and identity of specific types of lesions, indicate their prognosis if left untreated, and predict the likelihood that they will respond to particular types of therapy. Clinically useful markers will most likely be identified and characterized first in tissue samples obtained during biopsy or surgical procedures."

Another controversy in today's breast cancer clinic deals with the uncertainty of how to deal with the greatly increased number of ductal carcinoma in situ (DCIS) patients in the mammographic screening era. Twenty years ago DCIS represented only <1-5% of detected breast malignancies. The introduction and widespread availability of mammographic screening, which has greatly improved our ability to detect non-palpable and asymptomatic breast cancer, has increased the reported incidence of DCIS detection to >50% of all malignancies discovered by mammogram-directed biopsies. This increase has generated a spectrum of challenges to current surgical pathology, ranging from evaluation of breast biopsy specimens to direction of post-surgery therapy. For instance,

---

[4] http://planning.cancer.gov/disease/plans.shtml#prg.

[5] http://prg.nci.nih.gov/pdfprgreports/1998breastcancer.pdf

it is known that frozen section intra-operative evaluation, while generally reliable in diagnosing palpable breast masses, is of limited use in the diagnosis of non-palpable DCIS. The vast number of cases itself has also indicated that DCIS, rather than a simple breast cancer subtype, represents a collection of lesions with varied malignant potential and morphological heterogeneity. Thus, the interobserver reproducibility of histopathological diagnosis for DCIS is poor. Mastectomy is considered a curative treatment for DCIS, but its radical nature has recently been criticized as unnecessary overtreatment for many women with mammogram-detected, early stage DCIS. Ideally, all women diagnosed with non- or less aggressive DCIS could successfully be treated with breast-conserving treatment (BCT), but this course may not be successful for highly aggressive lesions. Commonly histopathology cannot classify variations in DCIS morphology, assess tumor aggressiveness, nor direct adjuvant systematic therapies (AST) for individual patients, particularly when the objectives for intervention emphasize consideration of a patient's comfort and quality of life. Regarding DCIS, the PRG summarized that "[t]hese women will have near normal survival but may experience short and long-term morbidity from treatment. DCIS is seriously understudied from a disease- and patient-focused outcomes perspective." The PGR further recommends research to integrate patient-focused data "with biological prognostic information to make the best treatment decisions" for these DCIS patients.

The increased number of tumors detected at early stages have also generated another controversy. Currently treatments for tumors at early stages (such as DCIS, and low grades) occupy an entirely different arena then they did two decades ago in the era predominated by total mastectomy. Breast-conserving treatment is considered to be a major aim of breast cancer treatment in the 21st century. The new BCT approach is clinically and scientifically sound, since it has been shown that patients with a grade I tumor have an 85% chance of surviving for 10 years after diagnosis; however, a grade III tumor reduces the chance of 10-year survival to 45%. An 85% likelihood for survival at 10 years following diagnosis can be considered a great achievement in our battle against breast cancer in light of cancer epidemiology. However, in reality clinicians and patients are more interested to know, not cancer statistics, but if THIS patient will survive for 10 years. Each patient represents 100% of her own statistics, and unfortunately, due to the extreme heterogeneity of the disease, the current pathology cannot differentiate the 85% survival from the 15% mortality group. Uncertainty as to the nature and aggressiveness of an individual woman's cancer, and the need to rely on historical statistical data, can result in undertreatment or overtreatment of the *individual* woman. For example, chemotherapy is routinely given to women with breast tumors over 1 cm and negative lymph nodes even though only 3-5% of those treated are expected to benefit. Conversely, chemotherapy is routinely withheld from women with tumors under 1 cm and negative lymph nodes, even though some will ultimately develop metastatic disease. New approaches to characterize tumors that better reflect their biological behavior are sorely needed. These needs were concisely summarized by the PRG as the opportunities in breast cancer research to: "Develop new methods to diagnose clinically significant breast disease and predict clinical outcome better than conventional histologic examination and the few available biomarker assays (e.g., SPF, ER, PgR, c-erbB-2) ;" and to discover "biomarkers that predict the clinical outcome of precancerous and

cancerous breast lesions if left untreated (i.e., prognostic factors) with a high degree of certainty."

This list of controversies related to the breast cancer clinic goes on, but we will stop after the next one concerning post-surgery adjuvant systemic therapy (AST). Current pathology, developed from observations over the last 100 years, has identified many prognostic factors for invasive breast cancer, such as tumor size, differentiation status, lymph node stage, vascular invasion, etc. However, these factors have proven to be too generalized in that they fail to consider the biochemical characteristic of an individual tumor. Since almost all the AST currently used in breast cancer clinic — chemo- and radiotherapy — are known to have association with morbidity, personalized therapeutic protocols based on tumor biomolecular signatures are clearly the hope of future breast cancer clinics, especially in the age of BCT. In addition, although there are a number of oncological drugs available, the current AST chemotherapies are still generally conducted on a trial-and-error basis for an individual patient. If one agent fails, valuable time in the window of treatment is lost. Clinicians thus face an urgent need to measure and understand the biological nature of a specific tumor in order to predict the potential efficacy of a particular agent for an individual patient. Again, the breast cancer PRG urges researchers to "learn more about the biology of breast cancer for the purpose of predicting clinical course and predicting response to therapy;**"** and to discover "biomarkers that predict the response of precancerous and cancerous breast lesions to specific types of therapy (i.e., predictive factors) with a high degree of certainty."

The arguments for and discussions of the need for new and better disease markers for every step of oncological clinics can be made for every type of cancer. Biomarkers that are urgently needed include those that are particularly sensitive in early detection of cancer and precancerous lesions, as well as biomarkers that may test the current oncological hypothesis that cancers may be controlled as chronic disorders, rather than being intervened as acute diseases.

From histological to molecular pathology

The discovery and invention of cancer screening protocols were the fruits of intensive cancer research efforts in the 1970s and 1980s that resulted in the advancements of knowledge in cancer biology and developments in biomedical technologies. The contributions of these screening practices in the identification of malignancies at their early stages, and in the improvement of disease control and patients' survival, were evident. For instance, at present, the percentage of women diagnosed with breast cancer is 1.5 times higher then it was 25 years ago, while the percentage of women who die of the disease has been reduced by about 15% from its value a quarter of a century ago. Similarly, as previously discussed, with the assistance of blood PSA tests, the detection of incidences of prostate cancer at relatively early stages has increased greatly. Thus, if we look narrowly at the ratio between the greatly increased incidences over the seemingly almost unaltered death numbers due to the disease it may be argued that the invention of PSA testing has guided many asymptomatic prostate cancer patients to seek early treatments, and the "cure rate" of the disease has improved. However, as already discussed, there are some troubling facts related to these early diagnoses that should lead us to pause and evaluate the current status of the clinic and the clinical impacts of early diagnoses. This data illustrates the fact that morphology-based histological pathology

served oncological practice sufficiently to the end of 1980s, or even the beginning of 1990s, prior to the establishment of the current concepts and practices of cancer screening. In those days, oncological clinics received patients either with palpable masses, or internal masses which had grown to become functionally destructive. In other words, before the start of the cancer-screening era, oncological clinics dealt with relatively later stage diseases. From these cases, pathological evidences and experiences were also accumulated from the corresponding stages of the diseases. Therefore, the criteria for cancer diagnoses that matured in those days is based heavily on later stage histological pathologies and needs to be up-dated to include new observations of vast amounts of tumors diagnosed at early stages.

Fortunately, crises and opportunities often come hand-in-hand. Developments in molecular biology, particularly in cancer biology, coincide with the progression of cancer screening evolution. These developments have greatly enlarged our breadth of knowledge, or, more conservatively, have begun to unveil mysteries surrounding the biological mechanism behind these morphological alterations. Applications for these developments in clinical practices have created new pathological branches that form current molecular pathology. A number of these new biological markers have been utilized in clinical evaluations. For instance, many common names, such as estrogen receptor (ER), P53, etc., have been integrated into comprehensive pathological evaluations for their empirical values in the patient prognostications of certain malignancies.

To systematically analyze the potential utility of cancer biological information bioinformatics obtained from genomics, proteomics, and/or metabolomics in assisting histopathology in oncological clinics, it may be helpful to analyze the relationship among these scientific branches. To begin these analyses, we need to assume that the metabolic activities in malignant cells are different from those in normal cells. We consider this hypothesis to be scientifically sound, reasonable and self-evident.

Based on this hypothesis, we wish to consider the sequence of events in cancer development and the roles metabolites play. Changes in metabolic profiles are the results of certain active metabolic pathways. For these pathways to be active, active enzymes are needed. To have enzyme activities, enzymes need to be synthesized. Furthermore, to synthesize enzyme proteins requires the existence of messenger RNAs (mRNAs), and forth the correct DNAs. On the other hand, with mutated DNA the required mRNA may not be available for the synthesis of the enzymatic proteins; thus as a result of the DNA mutation, certain metabolic pathways are blocked. We can only present this basic molecular biology concept as a chain of events, however, we wish to emphasize that by presenting in this way we do not suggest that there are measurable temporal sequences and delays in association with genes, proteins, and metabolites. Viewing the human body as a united entity, without the exact knowledge regarding the dynamic rates of these molecular (genomic, proteomic, and metabolomic) transformations, we can speculate that the entire process may occur simultaneously and be coupled with feed-back loops and parallel processes. This means that a logically clean chain of events is not always discernable; although we suspect that there must be a time window during which the presentation of malignancy transformations may be detectable by molecular biology means, while the revelation in cellular morphology is still uncertain. Thus, quantitative evaluations (proteomics, metabolomics) of the biological activities of an individual lesion

may provide more sensitive and predictive parameters that may be able to subcategorize histomorphology results.

From this above reasoning, we can likely conclude that in order to observe certain metabolic profiles during or after malignant transformations, their corresponding gene players need to be in the right time and place, i.e. these genomic factors may be the necessary condition for the formation of the related metabolomic results. Hence, the processes of malignancy formations and progressions will require every player involved in all these "-omics," and every interfering factor in the entire duration, to be in harmonic association. Factors from all these disciplines reflect the same biological process from different angles, and at different points in the malignancy formation. In the larger picture of genomics, proteomics, and metabolomics, genomics has a stronger predictive capability than proteomics or metabolomics, which are viewed more as studies of the *current state* of the malignancy (although this may change as our understanding of complex gene relationships develops). A complete assessment of the strengths and weaknesses of parameters measured from each discipline, and their correlations with histopathological observations and oncological realities, presents great potential for the improvement of cancer characterization to meet the needs of the current screening era.

Having discussed the general connections between all these disciplines and their relationship with human oncology, we would like to clearly state the importance of histopathology and its predominant role in the present practice of oncology. We are compelled to do so because one of us, as a clinical pathologist, reads pathology slides under microscopes everyday; more importantly we believe new disciplines should complement, not directly contradict, histopathology. Current histopathology, as previously explained, is the gold standard for the diagnosis of malignancy and the prognostication of a patient. The knowledge of this field is based on the collective and continuous contributions of human efforts over the past centuries. The very basic "do no harm" principle of modern medicine requires us to practice oncology exclusively based on the recommendations of histopathological conclusions until there is convincing clinical proof that other modalities can bring more benefit to the patients. Acknowledging that histopathology is a very subjective tool that leads to a lot of gray area, we conclude that histopathology is an excellent point from which to launch research in the areas of the "-omics" and, with time, new quantitative forms of measurements will be developed.

Chemical detection of cancer

To be trained as a board certified pathologist requires one's earnest efforts for more than a decade. However, after a few minutes with an effective pathologist anyone with genuine interest may be able to appreciate the unique cellular pattern presentation of cancer observable under a microscope. A nice depiction of the disease can be found on the cover of the first issue of Nature Review Cancer (**Figure 6**), where leg-like arrays of diseased cells spreading into the surrounding of the lesion pictorially exemplifies why "cancer" gets its name from the Greek word for "crab." Seeing cancer cells and the "crab" formation under a microscope irrefutably displays the presence of the condition. In contrast to visual presentations of the disease, the idea of diagnosis based on molecular biology or chemistry requires more imagination. Nevertheless, evidence of associations between the presence of certain proteins/metabolites and clinical conditions of cancers

has been broadly studied and reported. For instance, in 1993 C. E. Mountford and colleagues reported an interesting study involving magnetic resonance spectroscopy analysis of lymph node metastasis in a rat model. From their study they found the sensitivity of MRS in suggesting the existence of malignant cells in lymph nodes, what they termed "micrometastases," that were not apparent even when the entire node was serially sectioned and examined by histology. However, the MR conclusions were confirmed with the development of malignancy by xenografting nodal tissue into nude mice[7]. Studies such as this are extremely clinically relevant. In 1990, a retrospective study in Lancet revealed that: "Serial sectioning of lymph nodes judged to be disease-free after routine examination revealed micro-metastases in an additional 83 (9%) of 921 breast cancer subjects"[8].

The utility of biological markers in human cancer classification for the purpose of predicting patient outcomes have also been demonstrated in human clinical studies. An example of such evaluations in human brain tumors was published by one of us with D. N. Louis and colleagues in 2003. The study investigated the use of gene expression profiling of a 12,000 gene microarray in classifying a set of 50 high-grade gliomas (28 glioblastomas and 22 anaplastic oligodendrogliomas). By developing a prediction model, results of the study indicated that the inclusion of genomic profiles could produce brain tumor classification criteria that were more objective, explicit, and consistent with patient clinical outcomes than assessments made from standard pathology alone[9].

Chemical and molecular biological detections of cancer have also evolved in more clearly "seeing" tumours with the development of various molecular imaging methodologies, including infrared, mass spectroscopy, and magnetic resonance. The advantage of these imaging approaches is that they preserve the concept of recognizing the anatomic structures central to pathology evaluations by expanding the visible wavelength used in histopathology into the invisible domains of human vision. However, at present, there are still many limiting trade-off aspects regarding these attempts. Commonly, a better spatial resolution (or anatomic details) comes at the expense of a limited spectral resolution (differentiating different chemicals) for any imaging modality because of the intrinsic competition between signals and noises.

Applications for genomics and proteomics in human malignancy, as a rapidly emerging field, are beyond the scope of the current monograph on metabolomics. However, we wish to point out that the differences between proteomics and metabolomics, in our opinion, are not as fundamental as the differences between them and genomics. To simplify the difference between proteomics and metabolomics, if metabolomics concentrates on the understanding of molecules that are considered to be monomers (for instance, amino acids), then proteomics focuses on the research of some kind of polymers of these monomers (i.e. proteins). Therefore, any method developed in analytic chemistry, or found in an instrumental analysis textbook, can have its potential applications in both proteomics and metabolomics studies. However, there are exceptions.

One exception, a method that may only be used for metabolomics but not for proteomics analysese , happens to be the major topic that we will discuss in the rest of this chapter, i.e. cancer pathology measured with intact tissue high resolution magnetic resonance spectroscopy. In general, this approach is capable of analyzing cellular metabolites and tissue histopathology from the same sample. This methodology

eliminates the confounding factor of tumour heterogeneity by creating a correspondence between molecular profiles and histopathological patterns with separate samples from the same clinical case. We select this chemical methodology to illustrate applications for metabolomics on human cancer for several reasons. First, since it was proposed by one of us in mid 1990s, it has been rapidly utilized by many research laboratories around the world on a variety of human diseases including many types of malignancies. Second, we have not yet seen any other metabolic approach (mass spectroscopy, liquid chromatography, or infrared, etc) that can demonstrate the same degree of relevance to clinical oncology in terms of the potential to establish one-to-one correlations between metabolite profiles and tissue pathologies, since almost all of the other approaches require procedures of chemical extractions of tissue samples that have yet to be characterized by histopathology.

Magnetic resonance spectroscopy and cancer

Before we engage in the discussion of intact tissue high resolution magnetic resonance spectroscopy on identification and utilization of cancer metabolomics, we wish to overview briefly the field of magnetic resonance spectroscopy in cancer prior to the discovery of this methodology.

Magnetic resonance (MR) spectroscopy has also been known as NMR (nuclear magnetic resonance) to chemists and physicists decades before the medical use of magnetic resonance imaging (MRI). NMR signals are extremely sensitive to changes in chemical environments and have been widely applied in physical and chemical analyses before the invention of MRI. For the topic of this chapter we will confine ourselves to discussion of ex vivo tissue magnetic resonance spectroscopy and will not traverse the enormous field of medical imaginf.,. The ability of NMR to acquiring both metabolic and pathological parameters from the same sample gives NMR its potential to alter the principle of cancer diagnosis with metabolomics.

Prior to the "-omics" era magnetic resonance spectroscopy had shown the ability to quantify metabolites of different cell types and detect relatively small populations of abnormal cells. Diagnostic in vivo proton magnetic resonance spectroscopy studies of human malignancies have aimed at characterization of lesions and assessment of tumor grades and stages**.** However, these attempts have not yet the critical status where clinical decisions can be based solely on these measurements.

It has long been considered that fundamental in vivo improvements rely on the more accurate characterization and quantification of tumor metabolites measurable ex vivo at high magnetic field strength with high spectroscopic resolution. Ex vivo studies started more than two decades ago aimed to: correlate cancer pathologies with spectroscopically measurable metabolite alterations; elucidate the details of cancer metabolites so as to better to understand tumor biology; and improve designs of in vivo methodologies. The ex vivo studies conducted prior to the introduction of intact tissue high resolution magnetic resonance spectroscopy utilized the conventional NMR methodology designed to analyze aqueous homogeneous solutions. Unfortunately, such an approach rests on the false assumption that fundamental physical differences between aqueous solutions and non-liquid tissues are relatively insignificant. In reality, substantial differences exist between aqueous solutions and intact tissues. As an

unavoidable result, low spectral resolution data observed with non-liquid tissues preclude measurement of individual metabolites.

The invalidity of the above assumption (i.e. intact biological tissues and aqueous solutions may be treated similarly) did not go unrecognized before the discovery of intact tissue high resolution methodology. To overcome the issue of low resolution observed with intact tissue samples, and to achieve measurement of individual metabolites at high spectral resolution, tissue metabolites were analyzed in solutions of chemical extractions. Unfortunately there were other difficulties or uncertainties associated with extraction approaches. First, understandably, the measured spectral results depend on the applied extraction procedures and their completeness. Since the assurance of completeness may not be tested by any experimental design that involves the procedure itself, it may be accurate to state that extractions may alter measurable metabolites to an unknown degree. Second, and more importantly, as previously discussed, heterogeneity of human malignancies limits the usefulness of extraction approaches because the procedure prevents histopathological evaluation of the same specimen. Hence, even equipped with perfectly resolved spectra and precisely quantified metabolite concentrations, no one could rationalize the pathology compositions that generated this data. Regrettably, an extremely large body of extract studies on human malignancies, which could be misleading to various degrees, exists in the literature. In short, we will never know the exact pathological details corresponding with various chemical and biological profiles obtained for many types of human malignancies in hundreds, maybe thousands, of publications. Applications of conventional NMR on studies of animal models may not be assessed with equal alarm, as tumour heterogeneity often does not play a critical role in those models, sometimes referred to as "living Petri dishes."

Development of intact tissue MR spectroscopy

During his post-doctoral studies at the Massachusetts General Hospital and Harvard Medical School, one of us discovered that spectral resolution of proton (1H) NMR of intact tissue could be greatly enhanced by subjecting the unaltered intact tissue sample to a NMR technique known as magic angle spinning (MAS), which was previously developed for chemical studies of solids. This line-narrowing technique by mechanical sample rotation can generate spectral resolution sufficient for the identification and quantification of individual metabolites in *intact* biological tissue without needing to produce solutions of tissue extractions. This technique became known as high-resolution magic angle spinning (HRMAS). In a later study, with a critical observation made by D. C. Anthony, a neuropathologist and the then acting Chief of Pathology at Boston's Children Hospital, it was found that under a moderate rotation (for instance below 3 kHz for brain tumor tissues) tissue pathological structures did not undergo severe alterations. This meant routine histopathology could be conducted with samples after spectroscopy analyses. Only after this additional discovery was the HRMAS methodology established as a capable choice for recording sample metabolite concentrations and quantitative pathology from the same specimens in order to correlatespectroscopic data and quantitative pathology . This methodology has since been termed high resolution magic angle spinning proton magnetic resonance spectroscopy (a. k. a. HRMAS 1HMRS). For readers who wish to know more about the methodology, its physical description and experimental design, we suggest you consult

Chapter 4 in this monograph, titled "Analytical Methods – MAS NMR," by D. Cory and colleagues.

HRMAS 1HMR spectroscopy has multifold advantages. For instance, histopathology evaluations are the impressions of pattern recognitions by a trained observer, whereas spectroscopy examinations can express a medical condition by numerical values once the links are established. Therefore, a computer can readily assume further analyses of spectroscopy results, while computerization of histopathological evaluations, is still difficult for us to envision. Furthermore, the above-mentioned numerical nature of spectroscopic evaluation of tissue status may be more objective and repeatable than the "artistic" nature of histopathological evaluations. Even more importantly, HRMAS 1HMRS will likely constitute parameters for patient prognostication that will be complimentary to or more sensitive/accurate than those in current clinical practice. Furthermore.

It also needs to be realized that, although drastic improvements in tissue metabolic analyses have been fostered by the introduction of this method, the discussed tissue magnetic resonance spectroscopy is not the "silver bullet" that can solve all the remaining issues with cancer diagnosis. There are still many intrinsic limitations associated with intact tissue spectroscopy analyses. For example, utilizing this analytic approach alone will not solve the widely recognized "sampling error" problem associated with histopathology, i.e. histopathology results can only be as good as a measure of features that present themselves on the evaluated tissue slides. Due to the heterogeneous nature of human malignancies, false negative conclusions may be reached if the sampled tissue specimens contain no cancer cells, particularly during biopsies. This clinical issue clearly cannot be overcome by utilizing a different analytic protocol. In fact, we suspect that similarly as histopathology, any molecular pathology evaluation will also encounter sampling errors of its own kind. Similarly, as we previously reported that different regions possess different metabolite profiles that correlate with differences in tissue pathologies observed in a case of human brain tumor, we suspect that heterogeneities in genomic and proteomic profiles may also exist, hence susceptible to sampling errors. Interesting questions to consider are how much overlap exists among these heterogeneities, which one is less heterogeneous throughout the lesion, and which one may have the largest field effect that extending the malignant information beyond the perimeters of the optical or human vision visible lesions.

From tissue MR spectra to cancer metabolomics

The status of cancer metabolite studies can best be presented by reviewing current publications of research using intact tissue MR spectroscopy. First of all, these studies have covered many types of human cancers including: brain, prostate, cervix, breast, kidney, and sarcomas. Next, we notice the gradual shift in the nature of studies away from "proof-of-concept" examinations, with small numbers of subjects, toward evaluations of clinical populations with cases number ranging from 50+. We also observe a gradual change in the overall perception of the MR spectroscopy methodology. MR spectroscopy is now being recognized for its unique advantage in establishing correlations between cellular metabolites and tissue pathologies measured from the same sample. Finally, a trend in the research design of extreme metabolomics importance is also emerging: the traditional NMR approach of attempting to relate changes in single

metabolites with the disease conditions has been substituted by the concept of analyzing the *global* metabolite profiles and seeking to reveal the changes in these *overall* profiles that are associated with the physiological and pathological conditions of interest. It is precisely this last trend, which agrees with our definition of metabolomics, that has convinced us metabolomics has reached the status where it can claim membership in the "-omics" family. These methodological evolutions in the studies of human malignancies illustrate the maturation process through which a technical discovery may ultimately deliver important health advances.

There is a two-fold motivation for investigations of NMR-visible metabolites in biological tissues. The original inspiration responded to the conviction that these metabolites might be of pathological importance and useful to improving the accuracy of disease diagnoses. Research endeavors towards this direction started in the late 1970s and early 1980s. Subsequently, in the 1990s, rapid technical innovations in MR imaging motivated researchers to try and understand the spectroscopic features observed in the newly developed localized in vivo MR spectroscopy, and attempt to design new in vivo strategies for spectroscopy measurement of targeted specific metabolites. Both motivating factors consider human malignant conditions the most suitable systems to test hypotheses and develop techniques because samples from the identifiable lesions associated with the diseases can be either removed for ex vivo analysis or localized from MR images for in vivo evaluations. Furthermore, imaging visible sites of lesions also allows the identification and selection of "normals," or disease-free sites from the same subject, such as the contralateral site in the cases of brain tumors, to be used as paired controls to reveal disease related metabolite alterations. For these reasons, and also due to the relative cardiac/respiratory motion stability and tissue homogeneity of the brain compared to other organs, human brains and brain tumors have been the main spectroscopy research targets (although brain tumors represent only about 1% of all malignancies).

Since studies of the brain have dominated the development of in vivo MRS both in concept and technology, it was logical that a number of initial intact tissue HRMAS MR spectroscopy studies of human oncology were devoted to analyses of human brain tumors. Another advantage of studies with brain tissue is the lack of adipose tissue, which can mask spectral regions of interest in tissue such as breast tissue, which makes measurement of cellular metabolites less challenging. Therefore, without extensive masking of cellular metabolite signals by the presence of fatty acid peaks, the net effect of signal peak narrowing produced by the application of the HRMAS technique was evident and easy to visualize, which contributed to the general acceptance of the approach as a valid innovation for analyses of intact human pathological tissues (**Figure 7**). Later, with the acceptance of the concept, it was proven that using HRMAS even in breast tissues the peak widths from fat signals could be reduced to result in spectral windows where metabolite signals were visible.

The benefit and rational of studying brain tumors encountered one critical logistic issue that was somewhat unique to this particular malignancy: tissue availability. Unlike treatment of any other malignant conditions, neurosurgeons, or more precisely patients, cannot afford to remove additional brain tissue just to create a clean margin. Hence, instead of using scalpels, the surgeons often resort to the assistance of suction tips to remove minimal but absolutely necessary amounts of cancerous tissue. Hence, excess

tumor material after pathological diagnosis is often very limited and not readily available for research. This perhaps also explains our observation of literature on HRMAS tissue spectroscopy studies of human brain tumors. Most studies evaluate different aspects of the feasibility of methodology with small patient numbers (e.g. for each type and grade), such as the validity of measuring spectral and pathological data from the same specimens and the correlations between in vivo and ex vivo spectroscopic observations. We have not yet seen a report of an ex vivo tissue study with significantly large patient numbers that can address the issue of biological variations. This situation also reflects the fact that brain tumors are not a common cancer compared with other malignancies, hence the overall patient population is much lower than in other common diseases, such breast and prostate cancers. Technical developments and feasibility studies addressing issues encountered during studies of a particular malignancy have also been seen in reports on other more common types of cancers, for instance, the effects of tissue degradation on the measured cellular metabolite profiles, and the developments of slow rate HRMAS methodology during human prostate cancer studies.

The effect and function of HRMAS can be visualized as "squeezing" a broad resonance peak into a center band surrounded by a number of side bands distanced by the sample rotation rate, as illustrated in **Figure 8**. These side bands can severely hinder the interpretation of observations if they fall into regions where metabolite signals of interest reside. Therefore, in common practice, sample rotation rates are chosen such that they are fast enough to "push" the first pair of side bands at each side of the center band outside the spectral regions of interest, which means the utilization of rotation rates between 3~5 kHz. At these rotation rates pathological identification of cancer cells is possible, but some tissue types display evidence of the centrifugal stress experienced by tissues. For instance, in prostate tissue the glandular structures, particularly the glandular spaces, were significantly altered. These pathological structures are extremely important for the establishment of correlations with tissue metabolic profiles. Therefore, maximal preservation and accurate histopathological quantification is required. To do this, following the basic principles of physics, one needs to consider reducing the structural damage from the centrifugal stress of sample rotation by using reduced rotation rates. Without involving too much detail on the physics of HRMAS, experimental results have shown that for many types of human tissue a reduction in rotation rates to less than 1 kHz does not decrease the ability of HRMAS to produce spectra of narrow peaks, while the details of tissue pathological structures are largely preserved. Several studies on the development of slow HRMAS methodologies have been reported, and these methodologies have been utilized in evaluations of large patient populations. It should be realized that results of these technical developments and feasibility evaluations are likely to be tissue type specific, hence the applicability to different types of tissue samples needs to be tested individually. For example, results published by one of us on techniques of slow HRMAS developed for human prostate cancer analyses also worked well with brain tissues for both tissue types are characterized by lack of adipose components[10, 11]. The proposed scheme is rendered ineffective, however, with the reported slow rotation rates, on samples rich in adipose tissue, such as those of breast or skin. On the other hand, samples of this nature may be more durable to mechanical stresses, hence their pathological structures are less vulnerable to higher rates of HRMAS sample rotation.

The above discussion directly addresses an important issue related to evaluation of tissue metabolite profiles and pathological quantities from the same sample. We have rationalized the tremendous significance of such a sequential analytic protocol in the evaluations of human cancers due to the heterogeneous characteristics of malignant diseases. While we have emphasized the capability of the HRMAS NMR approach in addressing this fundamental need, we are also aware that among the several dozens of research articles of HRMAS NMR on human cancers, only a handful of them were conducted according to this protocol. The rest of them followed the "classical" approach where results of metabolites and pathologies are obtained from adjacent samples, as in studies involving tissue chemical extractions. Although our previous arguments still hold true, many reports show correlations between the measured tissue metabolite concentrations and patient cancer status so clearly and convincingly we would be hard pressed to discount them. To reconcile the seeming conflict between the concept and reality one must consider, these observations might suggest a "field effect", i.e. the malignancy related tissue metabolite profiles, or cancer metabolomics, are delocalized from cancer cells and extend to their surrounding histopathologically benign tissues. Although the suggestion of the existence of "field effects" in cancer metabolomics can only be considered a hypothesis, it is certainly not a foreign concept, particularly regarding the widely accepted and studied cancer-stroma effects in today's molecular oncology.

An additional troubling issue in current literature is a derivation from our "global" concept of metabolomics. In many studies a number of individual metabolites were measured in an attempt to associate them with the malignant condition. Although these studies may not represent the perfect approach for metabolomics, they contain valid observations. These results likely reflect the fact that many metabolites previously linked to malignancy could indeed be the major contributors to the characteristic metabolite profiles of a particular condition. This is verified by the following example, which we hope illustrates our suggested approach for studies of human cancer metabolomics:

Recently, one of us published a report on the study of human prostate cancer with intact tissue HRMAS NMR spectroscopy[12]. In short, this study included 199 prostate tissue samples obtained from 82 prostate cancer patients after prostatectomy. The study was conducted by first analyzing samples with HRMAS NMR spectroscopy, and then with quantitative pathology. Metabolite concentrations were calculated from the spectroscopy data and their profiles were generated by statistics with principle component analysis (PCA). Quantitative pathological evaluations of these tissue samples indicated that 20 samples of the total 199 samples from prostate cancer patients contained cancerous glands, while the rest (n=179) represented histologically benign tissue obtained from cancerous prostates. This was not surprising as it agrees with the frequency seen in biopsy in prostate cancer clinic and reflects the infiltrative, heterogeneous nature of prostate cancer. Following spectroscopy and pathology analyses, tissue metabolite profiles were correlated with quantitative pathology findings using linear regression analysis, and evaluated against patient pathological statuses by using analysis of variance (ANOVA). Paired-t-tests were then used to show the ability of tissue metabolite profiles to differentiate malignant from benign samples obtained from the same patient (**Figure 9**), and correlated with patient serum PSA levels. Finally, metabolite profiles obtained

from histologically benign tissue samples were used to delineate a subset of less aggressive tumors and predict tumor perineural invasion within the subset.

Reflecting on the discussions in this section, we wish to emphasize a number of points within this example that directly address our concept of cancer metabolomics.

Firstly, it is feasible and clinically important to conduct intact tissue studies of a large patient population, from which results results may be revealed that potentially revolutionize oncological treatment.

Second, histomorphological evaluations are critical for the correct interpretation of spectroscopic data obtained from the same samples and to define cancer metabolomic profiles.

Third, correct data statistical analysis is crucial to generate tissue metabolomic profiles. There are many bio-statistical approaches that one can use to achieve this purpose, in the example, principle component analysis (PCA) was used. The selection of PCA for the analyses of spectroscopy data in the example was based on the aim of the work: to correlate spectral metabolite profiles with tissue pathologies and patient clinical statuses. Based on our definition of cancer metabolomics, malignant pathological processes manifest simultaneous changes in multiple measurable metabolites, and a change in a single metabolite may not represent the underlying process. To test this hypothesis, PCA attempts to identify combinations (principal components or PCs) of the measured concentrations that may reflect distinct pathological processes if they exist in the set of the samples. Positive contributions of certain metabolites indicate the elevations of these metabolites within the component (process), and negative contributions suggest suppressions. For instance, the study has shown that the cancer-related principle components 13 and 14 both had metabolites phosphocholine (PChol) and choline (Chol) as their major positive contributors in agreement with current in vivo and ex vivo MRS literature's descriptions of the relationship of these metabolites with malignancy.

Finally, the reported capability of certain metabolite profiles (represented as principle components) to differentiate various pathological tumor stages seems to support the hypothesis of the existence of "field effects". However, the scale and the extent of these effects are still largely undefined.

Future directions and implications

In summary, we organized this chapter in light of the potential metabolomics applications to malignancy diagnosis with tissue samples. We consider intact tissue HRMAS NMR is still the best, and the only known, method that can provide both metabolite and pathology data from the same samples. Because our aims are orientated around this specific aspect of extreme oncological importance, we did not include discussions on chemical measurements of body fluids or other liquid samples, and their potential usages in clinic.

Within this specific scope, with the apparently sufficient developments of the spectroscopy methodology, the emphasis of cancer metabolomics in the near future will be focused on answering four key issues:

In connection with evaluations of current histopathology and within the parameters thus defined, the first task of cancer metabolomics is to test the sensitivities of metabolite profiles in subcategorizing tumor conditions for patients in the same

histopathological groups. Secondly, research in this field will attempt to identify metabolomic profiles reflecting the status of tumor biology that can be used to indicate the tumor's sensitivity to a particular treatment protocol. The third task will likely concentrate on the identification of metabolomic profiles that may be more sensitive than histopathology evaluations in indicating pre-cancerous conditions. Finally, we envision that in order to gain more comprehensive understanding on cancer biology in terms of disease mechanisms and treatment strategies, increasing research efforts will focus on aspects that connect metabolomics with genomics and proteomics, particularly in clinical and pre-clinical areas where the concepts of non-invasive diagnoses of human malignancies with molecular imaging have been forcefully pursued. With the future of metabolomics now at hand it is reasonable to assume that metabonomics will have major contributions to the history of medical science.

References

1. Perou CM, Sorlie T, Eisen MB, van de Rijn M, Jeffrey SS, Rees CA, Pollack JR, Ross DT, Johnsen H, Akslen LA, Fluge O, Pergamenschikov A, Williams C, Zhu SX, Lonning PE, Borresen-Dale AL, Brown PO,Botstein D. Molecular portraits of human breast tumours. Nature 2000;406(6797):747-752.
2. Perou CM, Jeffrey SS, van de Rijn M, Rees CA, Eisen MB, Ross DT, Pergamenschikov A, Williams CF, Zhu SX, Lee JC, Lashkari D, Shalon D, Brown PO,Botstein D. Distinctive gene expression patterns in human mammary epithelial cells and breast cancers. Proc Natl Acad Sci U S A 1999;96(16):9212-9217.
3. Ma XJ, Salunga R, Tuggle JT, Gaudet J, Enright E, McQuary P, Payette T, Pistone M, Stecker K, Zhang BM, Zhou YX, Varnholt H, Smith B, Gadd M, Chatfield E, Kessler J, Baer TM, Erlander MG,Sgroi DC. Gene expression profiles of human breast cancer progression. Proc Natl Acad Sci U S A 2003;100(10):5974-5979.
4. Gunsalus KC, Ge H, Schetter AJ, Goldberg DS, Han JD, Hao T, Berriz GF, Bertin N, Huang J, Chuang LS, Li N, Mani R, Hyman AA, Sonnichsen B, Echeverri CJ, Roth FP, Vidal M,Piano F. Predictive models of molecular machines involved in Caenorhabditis elegans early embryogenesis. Nature 2005;436(7052):861-865.
5. Jemal A, Tiwari RC, Murray T, Ghafoor A, Samuels A, Ward E, Feuer EJ,Thun MJ. Cancer statistics, 2004. CA Cancer J Clin 2004;54(1):8-29.
6. Jemal A, Murray T, Ward E, Samuels A, Tiwari RC, Ghafoor A, Feuer EJ,Thun MJ. Cancer statistics, 2005. CA Cancer J Clin 2005;55(1):10-30.
7. Mountford C, Lean C, Hancock R, Dowd S, Mackinnon W, Tattersall M,Russell P. Magnetic resonance spectroscopy detects cancer in draining lymph nodes. Invasion & Metastasis 1993;13:57-71.
8. Bettelheim R, Price K, Gelber R, Davis B, Castiglione M, Goldhirsch A,Neville A. the International (Ludwig) Breast Cancer Study Group, Prognostic importance of occult axillary lymph node micrometastases from breast cancer. Lancet 1990;335:1565-1568.
9. Nutt CL, Mani DR, Betensky RA, Tamayo P, Cairncross JG, Ladd C, Pohl U, Hartmann C, McLaughlin ME, Batchelor TT, Black PM, von Deimling A,

Pomeroy SL, Golub TR, Louis DN. Gene expression-based classification of malignant gliomas correlates better with survival than histological classification. Cancer Res 2003;63(7):1602-1607.
10. Taylor JL, Wu CL, Cory D, Gonzalez RG, Bielecki A,Cheng LL. High-resolution magic angle spinning proton NMR analysis of human prostate tissue with slow spinning rates. Magn Reson Med 2003;50(3):627-632.
11. Burns MA, Taylor JL, Wu CL, Zepeda AG, Bielecki A, Cory DG,Cheng LL. Reduction of Spinning Sidebands in Proton NMR of Human Prostate Tissue With Slow High-Resolution Magic Angle Spinning. Magnetic Resonance in Medicine 2005;53:In Press.
12. Cheng LL, Burns MA, Taylor JL, He W, Halpern EF, McDougal WS,Wu CL. Metabolic characterization of human prostate cancer with tissue magnetic resonance spectroscopy. Cancer Res 2005;65(8):3030-3034.
13. Cheng LL, Ma MJ, Becerra L, Ptak T, Tracey I, Lackner A,Gonzalez RG. Quantitative neuropathology by high resolution magic angle spinning proton magnetic resonance spectroscopy. Proc Natl Acad Sci U S A 1997;94(12):6408-6413.
14. Zheng L. Solid state NMR studies of proton diffusion [PhD]. Waltham: Brandeis University; 1993.

Figure Legends

Figure 1. The 1,753-gene cluster diagram revealing gene expression in 84 experimental samples of breast cancer reported by C. M. Perou et.al. Each row represents a single gene, and each column an experimental sample. The colored bars on the right identified the gene clusters corresponding to (from the top): endothelial, stromal/fibroblast, basal epithelial, B-cells, adipose-enriched/normal breast, macrophage, T-cells, and luminal epithelial cells (From Figure 1b)[1].

Figure 2. Laser capture microdissection identified normal breast epithelium (white arrows) and abnormal epithelium (black arrows) from ADH, DCIS, and IDC from a single breast specimen. Images of precapture (lane a), postcapture (lane b), and the captured epithelial compartments (lane c) are shown (From Figure 1)[3].

Figure 3. Two-dimensional clustering of 61 samples and the top 200 genes correlating with tumor grade (From Figure 3)[3].

Figure 4. A metabolic pathway chart produced by Dr. Donald E. Nicholson of Leeds, England, in collaboration with the International Union of Biochemistry & Molecular Biology and with Sigma-Aldrich.

Figure 5. Statistical data on human prostate cancer in the U. S. (Based on the data kindly provided by A. Jemal, also see[6]).

Figure 6. The cover of the first issue of Nature Review Cancer (October 2001).

Figure 7. A comparison of brain tissue MR spectra obtained with a sample a) static; and b) with 2.5 kHz rotation at the magic angle (54º44' away from the direction of the magnet field.) (From Figure 1)[13].

Figure 8. An illustration of the effects of magic angle spinning on the appearance of spectral patterns measured with crystalline powder samples of barium chlorate monohydrate at room temperature with sample spinning rate from 0 to 10 kHz (From Figure 2-5)[14].

Figure 9. (**a.**) High-Resolution Magic Angle Spinning (HRMAS) 1H MR spectrum of intact tissue obtained from the removed prostate of a 61 y.o. patient with Gleason score 6, T2b tumors. Histopathology analysis of the tissue sample (insert) after its spectroscopy measurement revealed that the sample contained 40% histopathologically defined benign epithelium and 60% stromal structures, with no identifiable cancerous glands. Cellular metabolites mentioned in the text are labeled on the spectrum. The 36 most intense resonance peaks or metabolite groups above the horizontal bars were selected for analyses, while the other regions were excluded from calculation, partly due to surgery-related alcohol contamination. (**b**) 3D plot of Principal Component 13 (PC13 correlates linearly with vol% of cancer cells in tissue samples) vs. phosphocholine (Pchol) vs. choline (Chol). Cancerous and histologically benign (histo-benign) tissue samples from 13 patients can be visually separated in observation plane. The paired Student's t-test (cancer vs. histo-benign from the same patients) results for PC13, PChol and Chol are: 0.012, 0.004, and 0.001. Only results from these 13 patients could be evaluated with paired tests, for other cancer positive samples were collected from patients with whom no histo-benign samples were analyzed. (**c**) The canonical plot resulting from discriminant analysis of the three variables in Fig. 1b. presents the maximum separation between the two groups. (**d**) The resulting receiver operating characteristic (ROC) curves indicates the accuracy of

using the three variables in Fig. 1b. to positively identify cancer samples (From Figure 1)[12].

Figure 1.

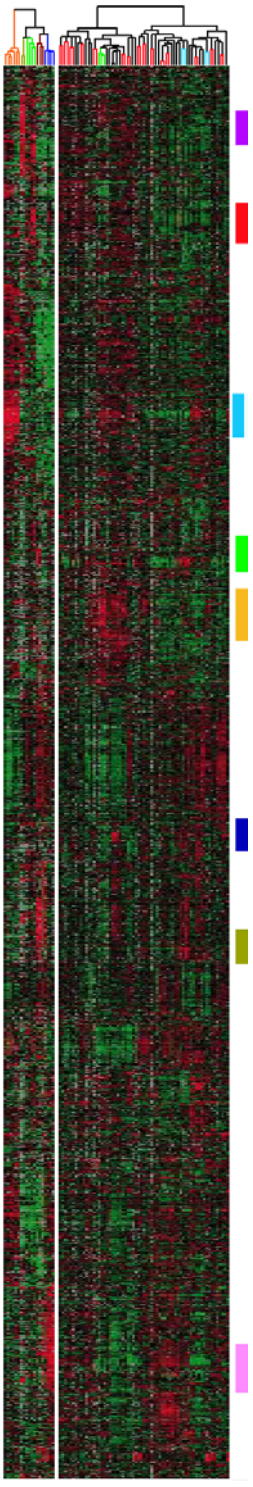

Figure 2.

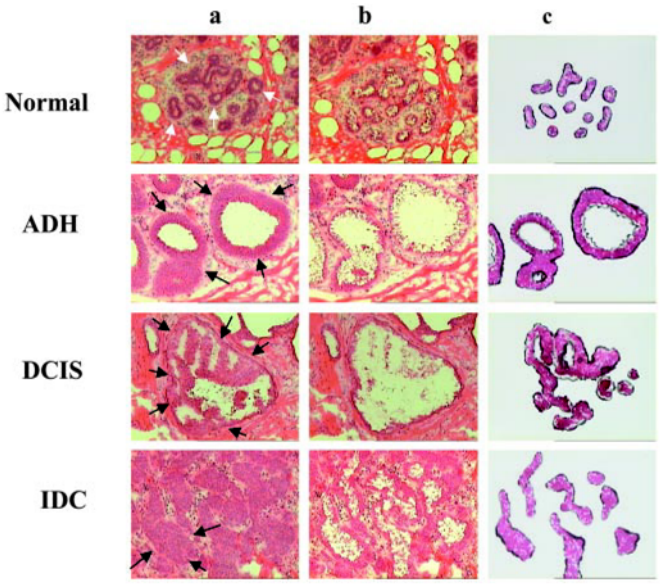

Figure 3.

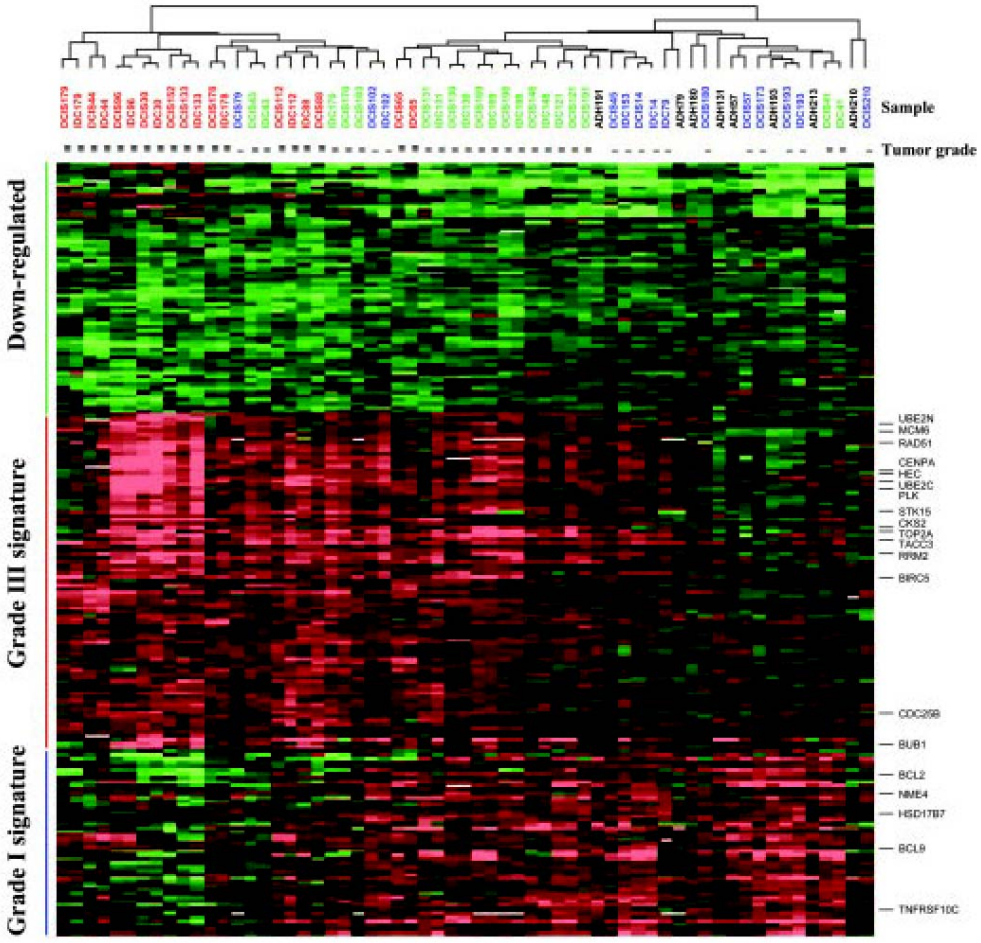
Sample
Tumor grade
Down-regulated
Grade III signature
Grade I signature
UBE2N
MCM6
RAD51
CENPA
HEC
UBE2C
PLK
STK15
CK82
TOP2A
TACC3
RRM2
BIRC5
CDC20
BUB1
BCL2
NME4
HSD17B7
BCL9
TNFRSF10C

Figure 4.

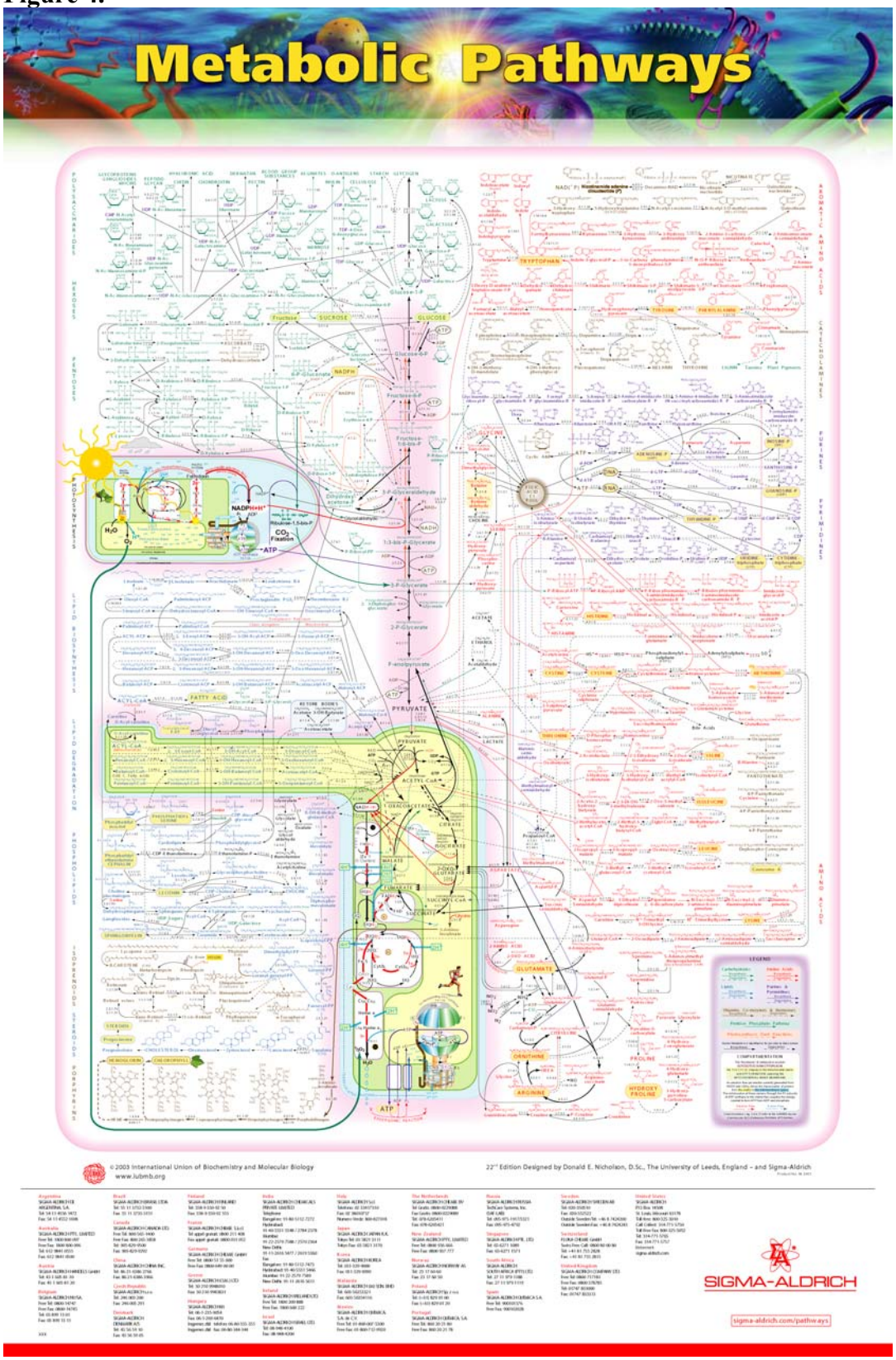

Figure 5.

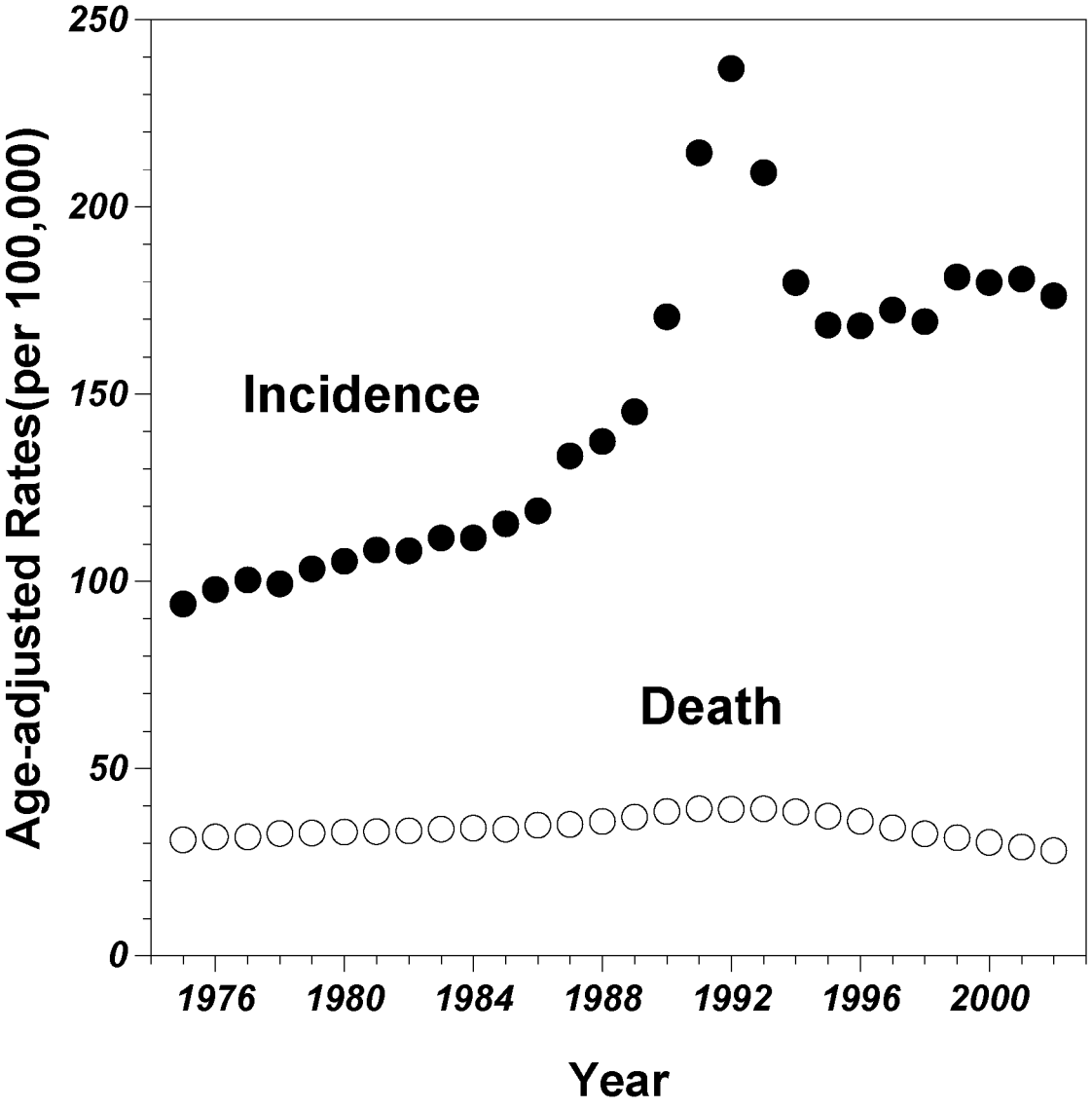
250
200
150
100
50
0
Age-adjusted Rates(per 100,000)
Incidence
Death
1976
1980
1984
1988
1992
1996
2000
Year

Figure 6.

Figure 7.

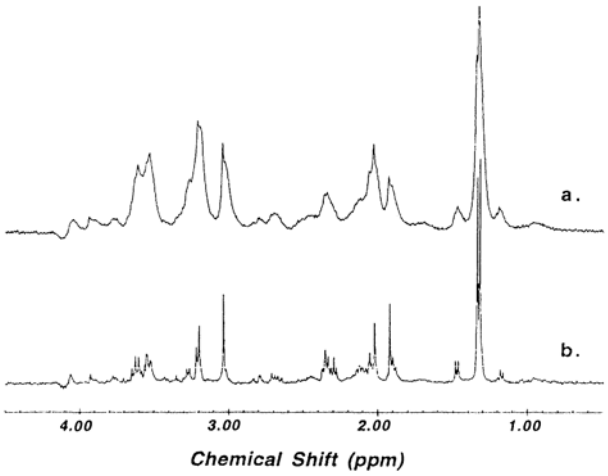

Figure 8.

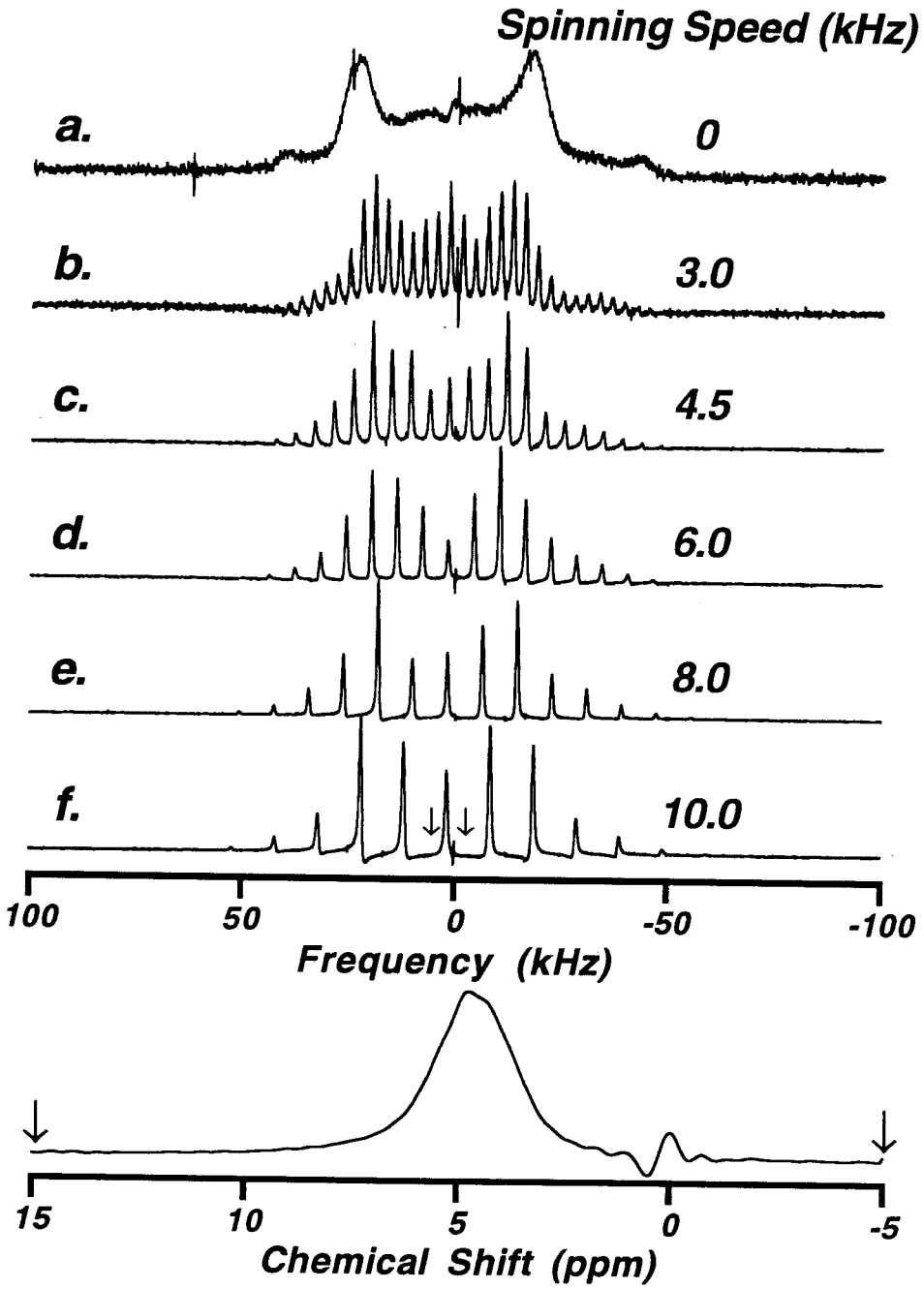
Spinning Speed (kHz)
a.
0
b.
3.0
c.
4.5
d.
6.0
e.
8.0
f.
10.0
100
50
0
-50
-100
Frequency (kHz)
15
10
5
0
-5
Chemical Shift (ppm)

Figure 9.

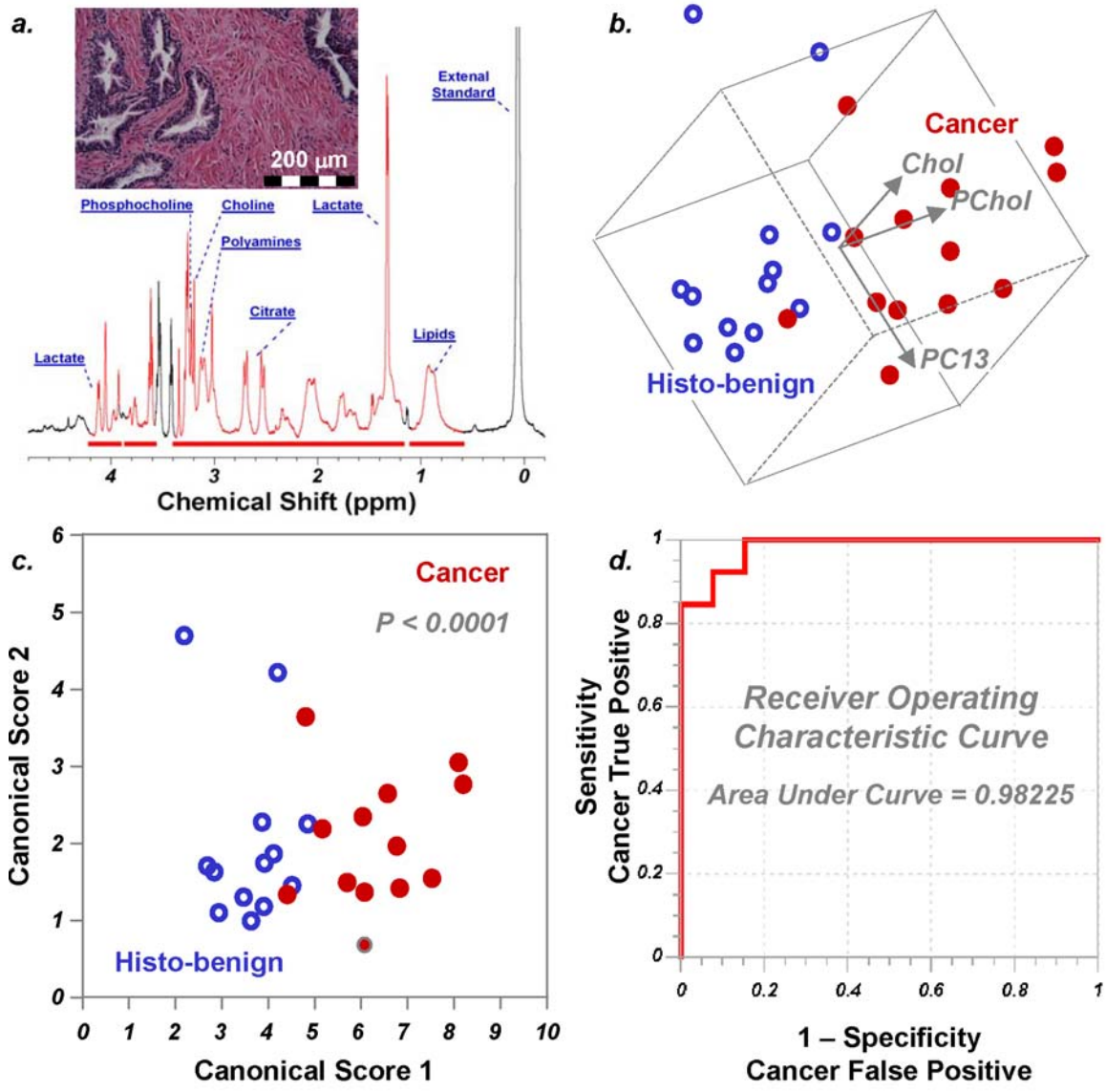
a.
200 µm
Extenal Standard
Phosphocholine
Choline
Lactate
Polyamines
Citrate
Lipids
Lactate
Chemical Shift (ppm)
b.
Cancer
Chol
PChol
PC13
Histo-benign
c.
Cancer
P < 0.0001
Histo-benign
Canonical Score 2
Canonical Score 1
d.
Receiver Operating Characteristic Curve
Area Under Curve = 0.98225
Sensitivity
Cancer True Positive
1 – Specificity
Cancer False Positive

Evaluation of Tissue Metabolites with High Resolution Magic Angle Spinning MR Spectroscopy Human Prostate Samples After Three-Year Storage at –80 ºC

Kate W. Jordan[1], Wenlei He[1], Elkan F. Halpern[2], Chin-Lee Wu[1] and Leo L. Cheng[1,2,]

Departments of [1]Pathology and [2]Radiology Massachusetts General Hospital, Harvard Medical School Boston, Massachusetts.

Abstract: Accurate interpretation and correlation of tissue spectroscopy with pathological conditions requires disease-specific tissue metabolite databases; however, specimens for research are often kept in frozen storage for various lengths of time. Whether such frozen storage results in alterations to the measured metabolites is a critical but largely unknown issue. In this study, human prostate tissues from specimens that had been stored at –80 ºC for 32 months were analyzed with high resolution magic angle spinning (HRMAS) magnetic resonance (MR) spectroscopy, and compared with the initial measurements of the adjacent specimens from the same cases when snap frozen in the operation room and kept frozen for less than 24 hours. Results of the current study indicate that that the storage-induced metabolite alterations are below the limits that tissue MR spectroscopy can discriminate. Furthermore, quantitative pathology evaluations suggest the observed alterations in metabolite profiles measured from the adjacent specimens of the same prostates may be accounted for by tissue pathological heterogeneities and are not a result of storage conditions. Hence, these results indicate that long-term frozen storage of prostate specimens can be quantitatively analyzed by HRMAS MR spectroscopy without concerns regarding significant metabolic degradation or alteration.

Abbreviations: HRMAS: (high resolution magic angle spinning); MR: (magnetic resonance); CPMG: (Carr-Purcell-Meiboom-Gill).

Keywords: High resolution magic angle spinning, magnetic resonance spectroscopy, human prostate, metabolites, tissue frozen storage.

Introduction

Since the introduction of the high resolution magic angle spinning (HRMAS) methodology to investigate biological tissue samples (Cheng et al. 1996), a concern frequently posed has been the possible effects of sample storage duration on the measured metabolite concentrations. This concern is scientifically logical and clinically relevant because of the increasing tests and evaluations of the HRMAS spectroscopy methodology for its biomedical utilities and the observed correlations between the measured tissue metabolite changes and their underlying pathological alterations.

A large body of research has suggested the potential utility of using tissue metabolic profiles thus defined to indicate and predict the existence of certain pathological conditions (Swanson et al. 2003; Sitter et al. 2004; Tugnoli et al. 2004; Cheng et al. 2005; Duarte et al. 2005; Keshari et al. 2005; Tugnoli et al. 2005; Sitter et al. 2006). Therefore, the promising and practical utilities of this methodology in disease diagnosis, patient prognostication, and therapy monitoring have been progressively recognized.

We realize that as interest in disease-related HRMAS MR spectroscopy grows the HRMAS methodology is often being tested at a research stage. As such, more often then not, human specimens of interest from surgeries and/or biopsies, or even from autopsies, are used. However, most of these specimen cannot be analyzed immediately without frozen storage durations due to various technical, administrative, or logistical reasons. Very often research projects, particularly retrospective studies, also use frozen human samples, such as those collected by various tumor banks, stored in either liquid nitrogen (–196 ºC) or –80 ºC freezers for months or even years. At present there are no data to either support or contradict the rationale for using these samples, as the existence or non-existence of frozen storage induced metabolic alternations is largely unknown.

Correspondence: Leo L. Cheng, Pathology Research, CNY-7, 149 13th Street, Charlestown, MA 02129. Tel: 617-724-6593; Fax: 617-726-5684; Email: cheng@nmr.mgh.harvard.edu

Here, we report a study that we designed to measure prostate tissue metabolite profile for samples kept at –80 ºC during a storage period of three years. In this study, we used a set of well-characterized human prostate tissue specimens from prostatectomies of cancer patients. In 2002, in order to evaluate tissue freeze-thawing processes via the measured metabolite concentrations, we collected and analyzed 12 fresh human prostate specimens from five patients and reported those results in an article in 2003 (Wu et al. 2003). After that study, the extra specimens were in frozen storage at –80 ºC from 2002 to 2005.

Experimental

Tissue protocol

MR spectroscopic analyses of surgical specimens from human prostates were approved by the Institutional Review Board (IRB) at Massachusetts General Hospital. Twelve human prostate specimens were collected in 2002 in the operating room from different prostatic zones (central, transitional and peripheral) of five prostatectomy cases. Among these 12 specimens, 11 specimens left remaining tissue samples after the 2002 study (Wu et al. 2003). These samples have been stored at –80 ºC from July 2002 to March 2005. For the current study, a total of 15 samples cut from these 11 specimens were analyzed with spectroscopy (duplicates were measures from four samples with extra material).

HRMAS proton NMR

The spectroscopic experimental protocol is exactly the same as used in the 2002 study. Briefly, MR experiments were carried out on a Bruker (Billerica, MA) AVANCE spectrometer operating at 600 MHz (14.1T). A 4 mm zirconia rotor was used with Kel-F plastic inserts which created a spherical sample space of ~10 μl located at the center of the detection coil. A small (~0.1 mg) silicone rubber sample was permanently fixed inside one of the Kel-F spacers, positioned within the detection coil but not in contact with the sample, which functioned as an external standard for both frequency reference (0.06 ppm from TMS) and concentration quantification. Approximately 1.0 μl of D_2O was added into the rotor with the tissue sample for ^2H field locking. All spectroscopy measurements were carried out at 3 ºC for better tissue preservation. The rotor-spinning rate was regulated by a MAS controller (Bruker), and verified by the measurement of inter-SSB distances from spectra, with an accuracy of ±1.0 Hz. A repetition time of five seconds and 32 transients were used to acquire each spectrum.

Spectra were collected with spinning rates of 600 and 700 Hz, with or without a rotor synchronized DANTE sequence (1000 DANTE pulses of 1.5 μs, 8.4º flip angle) (Taylor et al. 2003). A rotor-synchronized CPMG filter (10 ms) was included in the pulse sequence after the execution of the DANTE frequency-selective pulses to reduce broad resonances associated with probe background, rotor, and/or macromolecules. Spectra measured at 600 Hz spinning without DANTE were used to quantify the total metabolite signal intensity including tissue water, its sidebands, and all the metabolites.

Spectroscopic data were processed with Nuts software (Acorn NMR Inc. Livermore, CA) according to the following procedures. All free induction decays were subjected to 1Hz apodization before Fourier transformation, baseline correction, and phase adjustments of both zero and first order. Resonance intensities reported here represent integrals of curve-fittings with Lorentzian-Gaussian line-shapes. All spectra were processed manually and objectively, as in the 2002 study, without knowledge of tissue pathological information. As previously reported, resonance intensities, depending on the particular spectral regions, were analyzed from one of the two spectra where there was no effect of water spinning sidebands (SSB) and DANTE suppression (Taylor et al. 2003). The absolute concentration for a metabolite was estimated according to the metabolite intensity measured in DANTE spectra, the total MR spectral signal intensity from the single pulse measurement, and the intensities of the rubber standard measured under both conditions, according to the formula below:

$$[M] = \left[(\boldsymbol{I}_M / n) / \boldsymbol{I}_{STD} \right]_{\mathrm{w/o\ H_2O}} \left[\boldsymbol{I}_{STD} / \boldsymbol{I}_{H_2O/2} \right]_{H_2O} {}^{*}55.56 \times 10^3 \ (\mu\mathrm{mol/g})$$

where $\mathbf{I}_M$ represents measured intensities for metabolites, $\mathbf{I}_{STD}$ is the measured intensity of the external rubber reference, n is the number of protons giving rise to the resonance, $\boldsymbol{I}_{H_2O/2}$ is the intensity of water, and 55.56×10^3 (μmol/g) is the concentration of water.

Histopathology

After spectroscopy analyses all 15 samples were fixed in formalin for histopathology evaluations. Fixed tissue samples were embedded in paraffin, cut into 5 μm sections, and stained with Hematoxylin and Eosin. Sets of serial-sections cut 100 μm apart were obtained from each sample. Volume percentages of histological features were quantified from these histopathological images (Burns et al. 2004).

Results and Discussions

Figure 1 compares two proton HRMAS spectra acquired from the adjacent specimens of the same prostate after tissue samples were frozen at –80 ºC either for less than 24 hours in July 2002 (Fig. 1b, same as presented in Figure 1b in the previous report (Wu et al. 2003)), and for more than 32 months until March 2005 (Fig. 1a). The tissue metabolite profiles in these spectra showed little difference, suggesting that discriminating the possible metabolite degradations over a tissue –80 ºC storage period up to 32 months may be below the capability of current analyses. However, identical prostate metabolite profiles obtained 32 months apart from adjacent samples of the same prostate were not observed with every pair tested.

To investigate the discrepancy, as the HRMAS methodology allows post-acquisition histopathological evaluations, we performed quantitative pathology evaluations on the measured samples. Histopathological examinations of serial

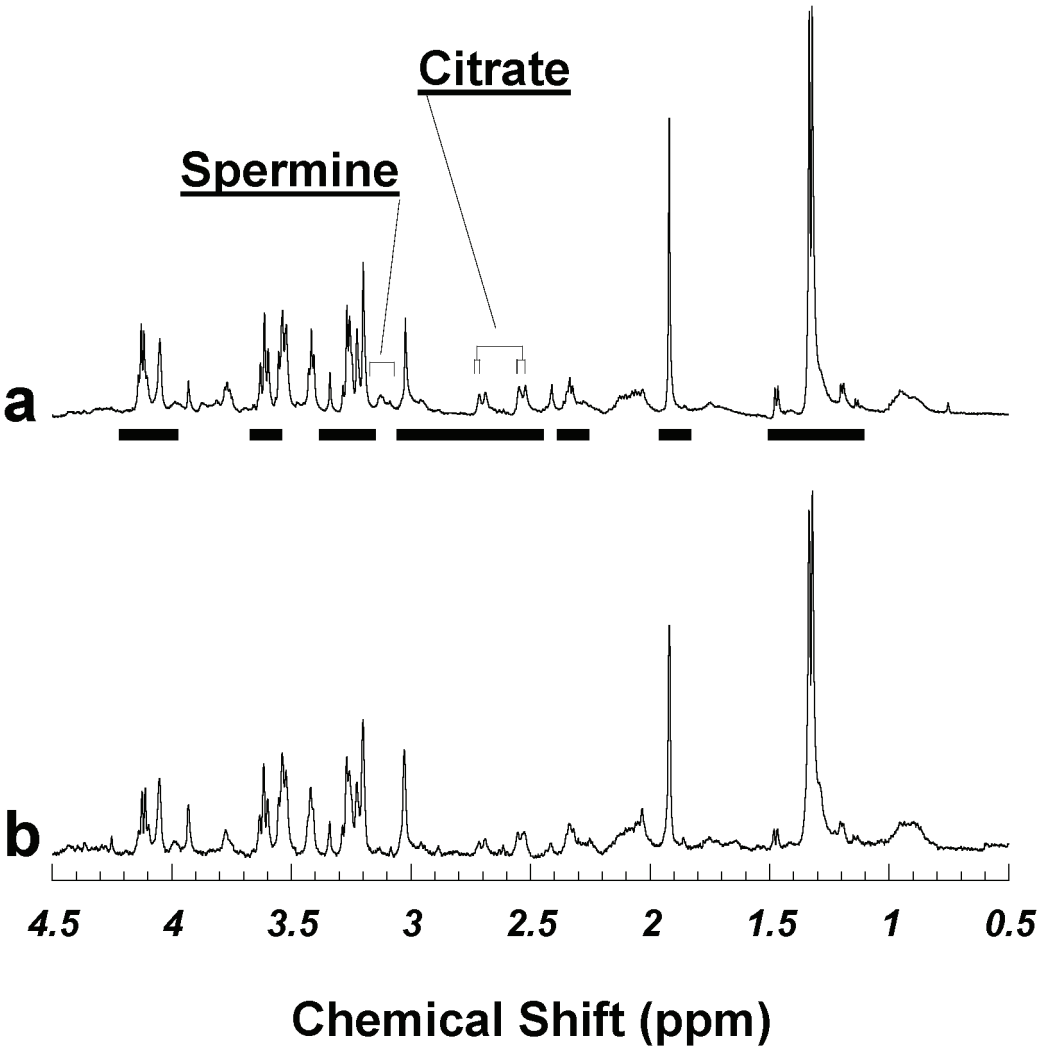

Figure 1. Visually undifferentiated human prostate tissue HRMAS proton spectra from two cuts of the same surgical specimen of a cancerous prostate measured (a) in 2005 after being stored at –80 ºC for 32 months, and (b) in 2002 when the sample was thawed after being frozen overnight. Quantitative pathology detected no histopathologically identifiable cancerous glands in either sample; other than stromal cells, the majority of prostate pathology in both samples was histopathologically benign epithelia, which comprised 46.1 and 33.8%, for (a) and (b), respectively. Figure 1 (b) was adopted from Figure 1 (b) of Ref. (Wu et al. 2003). Metabolite intensities analyzed in the current study are labeled with horizontal bars under spectrum 1a.

sections produced from these tissue samples after their spectroscopy analyses indicated that among all the tested samples there were no cancerous glands present. This was not surprising given the heterogeneous nature of the prostate and the fact that only 10% of research samples were found to have histologically positive cancer glands (Cheng et al. 2005). Hence, the major quantifiable histopathological differences among the current research samples were the variations in the volume percentage ratios between histopathologically benign prostate epithelial glands and stromal cells (Table 1). Quantitative histopathology results showed that the amounts of benign epithelia were (a) 46.09 and (b) 33.75% (vol) in Figure 1 for the two samples measured for in 2005 and 2002, and the relative percentage difference was about 15% (= (46.09 – 33.75)/(46.09 + 33.75)), as shown in Table 1. This table reflected heterogeneity in pathological compositions between adjacent tissues of the same prostate for the 15 pairs of samples reported. In this table we summarize all 15 tested samples and their counter measurements evaluated in 2002, together with the calculated pathological absolute differences represented by benign epithelial percentages (Diff. Epith. %), and the relative differences in terms of the absolute differences normalized by the sum of the values of the both years.

Based on observations obtained with sample pairs represented by Figure 1, we hypothesize that spectroscopic differences observed between samples measured in 2002 and 2005 were predominately caused by variations in pathological composition. We tested this hypothesis in Table 2, which compares the evaluated paired t-tests results of the 13 most intense resonance peaks measured from the HRMAS spectra for all 15 sample pairs with seven pairs with relative percentage differences of histological features less than 20%. If a statistically significant difference for a particular metabolite existed between the two tested groups, i.e. groups measured in 2002 *vs*. those in 2005, a paired t-test can be used to detect this existence. However, if the resulting p-value is greater than 0.05 (after a Bonferroni correction for multiple comparisons), it would indicate that either there is no statistically significant difference between the two groups of interest, or the test does not have enough statistical power to reveal the difference. In Table 2, some metabolites, such as creatine (Cr, 3.03 ppm) and citrate (Cit, 2.70 – 2.73 ppm), displayed seemingly significant differences (even after Bonferroni corrections) between the two groups when considering all 15 sample pairs. These significances do not persist when more restrictive controls on the allowable variations in pathological compositions are applied by including only sample pairs of the relative pathological differences <20%.

Considering the subgroup of seven tissue sample pairs with less than 20% relative pathological variations within each pair, Figure 2 plots the relationship of relative metabolite intensities (resonance peaks normalized by the total spectral inten-

Table 1. Quantitative pathology results of prostate sample pairs measured in 2002 and 2005. No histopahtologically identifiable cancer glands were detected in these samples, and the major pathological components were histologically benign epithelia and stroma. The quantitative results are presented as the percentage of benign epithelia as Epith. 2002 (% Vol) and Epith. 2005 (%Vol), respectively. Diff. Epith. %: the absolute values of the epithelial difference between each sample pair. The relative difference is presented as the ratio of the absolute difference over the sum of epithelial percentages for each pair; (a) two values indicate specimens were analyzed twice in 2005; (b) Bold identifies samples with values <20% of relative epithelial differences.

Specimen No.	Epith. 2002 (% Vol)	Epith. 2005 (% Vol)	Diff. Epith. %	|Epith. 2002 – Epith. 2005| (Epith. 2002 + Epith. 2005)%
1	4.01	46.98, 11.69[a]	42.97, 7.68	84.27, 48.92
2	3.49	32.60, 23.28	29.11, 19.79	80.66, 73.93
3	3.84	14.88	11.04	58.97
4	26.64	24.61	2.03	3.96[b]
5	38.31	40.00	1.69	2.16
6	0.00	16.11, 4.74	16.11, 4.74	100.00, 100.00
7	27.76	33.12	5.36	8.80
8	23.67	18.89, 18.30	4.78, 5.37	11.23, 12.79
9	8.69	8.49	0.20	1.164
10	33.75	46.09	12.34	15.46
11	10.00	41.19	31.19	60.93

Table 2. The p-values of paired t-tests for the 13 most intense resonance peaks measured from the HRMAS spectra. Based on the principle of Bonferroni correction to account for the possible existence of type I error, a p-value of <0.0038 represents statistical significance.

	AllSamples (n = 15)	**|Epith. 2002 – Epith. 2005| (Epith. 2002 + Epith. 2005) <20% (n = 7)**
Lac(4.10–4.14)	0.0092	0.1661
MI(4.05)	0.5567	0.3429
3.29	0.0234	0.0690
3.27	0.8176	0.2990
3.25–3.26	0.1066	0.6920
Pch(3.22)	0.2646	0.8499
Chol(3.20)	0.0560	0.2975
Spm(3.05–3.14)	0.2023	0.1431
Cr(3.03)	0.0027	0.0120
Cit(2.70–2.73)	0.0042	0.0734
Acet(1.92)	0.0724	0.2857
Ala(1.47–1.49)	0.6829	0.5520
Lac(1.32–1.34)	0.3878	0.8709
Mean	0.2451	0.3580
Standard Dev	0.2807	0.2936

sity excluding tissue water signals) measured from 2002 spectra against those obtained in 2005. The statistically significant linear relationship between the two data sets, with slope equal to unity and intercept close to 0, indicates the absence of tissue metabolite changes after frozen storage of 32 months.

Following the analytic procedures used for the 2002 report (Wu et al. 2003), in Table 3, we further examined concentrations of 21 prostate metabolites summarized in the 2002 report for seven sample pairs of relative differences of pathological volume percentages less than 20% within each pair (in Table 1). Metabolite concentrations obtained in 2002 are compared with those measured in 2005, together with their respective p values of paired t-tests included. Also included in this table are the power calculations to determine the levels of Type II errors, if any, for each measured metabolite. Specifically, based on the standard deviations measured with the seven-pairs of samples, using two-sided evaluation of a 5% significant level, and at an 80% power level, the minimal detectable differences in metabolite concentrations for each metabolites are presented in the table as the percentage of the 2002 values. For instance, the detectable difference 38.9% in the first row of the table for lactate indicates that based on the current study we can conclude there is no lactate change measured in 2005 that is greater than 38.9% of its value in 2002, i.e. either less than 7.86 mM or greater than 17.88 mM. Similarly, for phosphocholine (Pch, 3.22 ppm), we can conclude that there are no changes that are greater than 95.1% of its 2002 value; and for choline (3.20 ppm), no changes detected that are larger than 67.1%. Of a particular interest, we can confidently conclude that with alanine our data indicate that no changes measured in 2005 are greater that 75.7% of the 2002 values. This is very important evidence supporting our hypothesis that no MR spectroscopy visible tissue degradation occurs during long term storage; as with our tissue MR spectroscopy experience, alanine and other free amino acids are the first metabolites that present due to the break down of proteins, as shown in Figure 3. Comparing spectra in Figure 3, particularly in the boxed-in region, with the corresponding regions in spectra in Figure 1, it is not difficult to recognize the metabolite changes resulting from tissue degradations at 4 ºC after 12 hours under the 3.6 kHz HRMAS experimental condition.

There are a number of related issues that are worthy of discussion. First, examination of Table 1 reveals that although our data analysis made the best effort to reduce the influence of pathological heterogeneity by grouping the seven sample pairs having relative differences <20%, this difference still varied from 2.16% to 15.46%. More importantly, the absolute epithelial volume

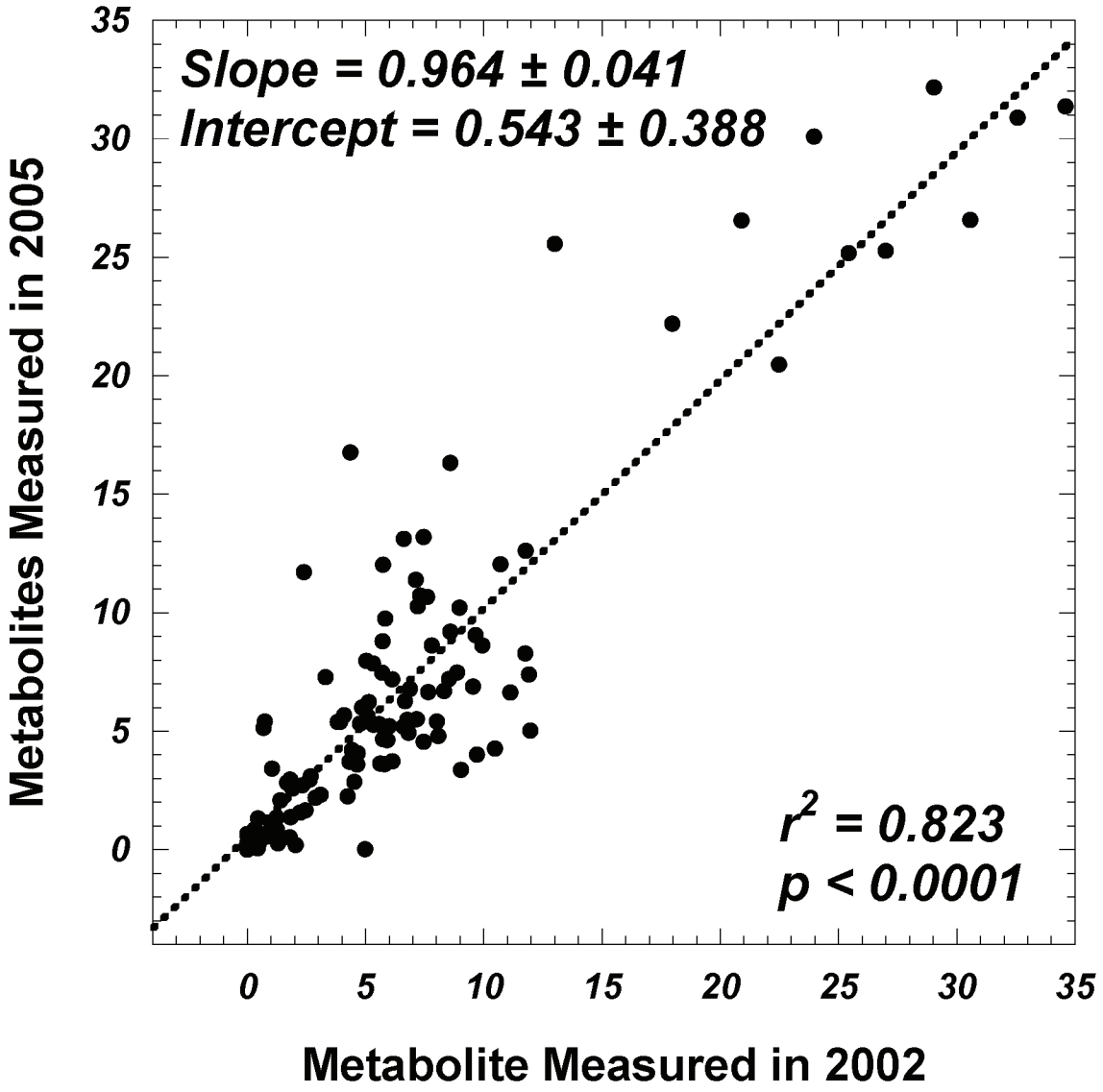

Figure 2. A linear correlation between metabolite intensities (normalized by total spectral intensity excluding tissue water signals) measured in 2002 with those measured in 2005 for seven pairs of tissue samples; within each pair the changes in volume percentages of histological features are <20%.

percentage in the analyzed samples varied from 8.49% to 46.09%. This difference undoubtedly contributed to the increase in the calculated standard deviations, which in turn affect the estimations of the minimal detectable limits. However, these confounding factors of bio-diversity and tissue heterogeneity are intrinsically associated with clinical studies and cannot be extricated, although special considerations may be applied to reduce the effects. Secondly, instead of investing in rigorous efforts to reduce the confounding factors in order to measure the true values of storage related tissue metabolite differences, if in existence, one may wish to consider there are acceptable levels of uncertainty, as long as they does not interfere with the clinical significance of the resulted metabolite profiles (Cheng et al. 2005).

Combining data in Table 3, which sets the boundary for the possible existence of type II errors associated with each analyzed metabolite, with Figure 2 that indicates the overall preservation of tissue metabolites during storage, we can conclude that there seem to be no HRMAS-quantifiable statistically significant prostate metabolite differences that can be contributed to sample storage at –80 ºC for 32 months. We have also noted that some standard deviations in Table 3

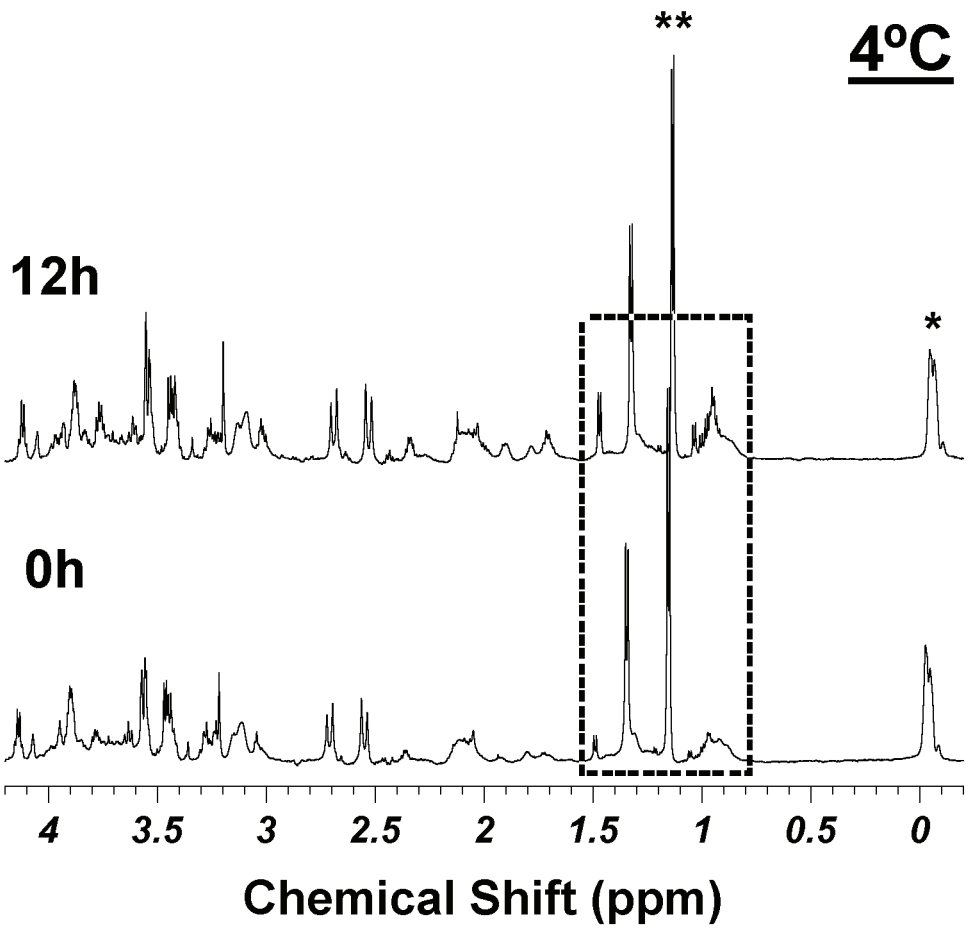

Figure 3. Intact prostate tissue HRMAS spectra measured at 4°C at 0 and 12 hours. *denotes an external rubber standard; **indicates alcohol contaminations. Comparison between these two spectra reveals metabolite products due to tissue degradations. Readers are instructed to pay special attention to the boxed-in spectral regions, where the increased intensities of free amino acids such as alanine (1.48 ppm), valine (0.96 ppm) etc. are clearly visible in the 12 h spectrum.

are greater than the mean; this is due to the small sample number (n = 7) and the skewed concentration distributions that deviated away from a normal bell curve distribution.

However, we wish to emphasize that the above conclusion regarding a lack of significant measurable metabolite changes over long term frozen storage can only be utilized within the current experimental conditions. For instance, since the tested prostate specimens contained no histologically visible cancer glands, theoretically, we cannot simply extend the experimental observations directly to cancer cells. However, based on observations here reported, we may suggest that quantification of prostate pathologies may be more critical for the correct interpretation of tissue spectroscopy results than any possible storage effects. Furthermore, although the concept that storage of tissue samples at –80 ºC halts the processes of metabolite pathways may be applicable to other types of tissues, the universal applicability is not self-evident and cannot be directly extended from the current results measured on prostate tissues. Separate studies on the types of tissues of interest are necessary to verify the concept.

Conclusion

Analyzing and comparing human prostate tissue spectra from specimens that have been stored at –80 ºC for 32 months after their initial spectroscopy measurements when snap frozen for less than 24 hours has led us to conclude that the possible frozen storage induced metabolite alterations are as minimal as tissue MR spectroscopy can distinguish. Such alterations, even if in existence, are much less critical to the interpretation of tissue HRMAS spectroscopy for pathological purposes than the influence of innate pathological heterogeneities.

Table 3. The concentrations of 21 prostate metabolites for seven sample pairs with relative differences of epithelial volume percentages less than 20% within each pair. Metabolite concentrations (means and standard deviations) obtained in 2002 are compared with those measured in 2005 together with their respective p-values (without Bonferroni corrections) of paired t-tests. Also included in this table are the power calculations to determine the levels of Type II errors for each measured metabolite. These calculations are based on the standard deviations measured with the seven-pairs of samples, using two-sided evaluation of a 5% significant level, and at an 80% power level to determine the minimal detectable differences in metabolite concentrations for each metabolites and presented in the table as the percentage of the 2002 values. These 21 metabolites included all the reported metabolites in Ref. (Wu et al. 2003).

	2005		2002		Paired	Detectable
	Mean	SD	Mean	SD	t-Test	Diff (%)
Lac(4.10–4.14)[a]	14.29	3.98	12.87	6.68	0.38	38.9
MI(4.05)	10.30	2.77	12.57	5.39	0.31	54.4
3.60–3.63[b]	16.98	6.78	20.17	13.57	0.56	78.8
3.34	5.18	2.08	5.49	1.95	0.82	61.9
3.29	1.11	0.63	2.53	2.13	0.13	108
3.27	8.79	2.38	11.17	5.60	0.30	62.8
3.25–3.26	12.22	3.32	13.95	5.85	0.26	33.8
Pch(3.22)	1.05	0.28	1.44	1.05	0.38	95.1
Chol(3.20)	1.53	0.22	1.70	0.91	0.64	67.1
Spm(3.05–3.14)	1.75	2.69	2.21	1.72	0.52	103
Cr(3.03)	2.66	0.92	5.19	3.69	0.08	76.3
Cit(2.70–2.73)	4.87	1.86	3.44	1.66	0.19	94.4
2.31–2.37	5.60	2.13	10.17	3.32	0.06	48.1
2.01–2.14	29.67	14.92	42.51	6.99	0.13	47.3
Acet(1.92)	1.36	3.02	1.19	2.54	0.44	58.8
1.68–1.78	10.89	7.11	10.98	7.34	0.98	124
Ala(1.47–1.49)	1.00	0.42	1.52	1.13	0.18	75.7
Lac(1.32–1.34)	17.45	4.18	20.53	9.80	0.37	51.6
1.19–1.20	2.70	2.30	2.13	2.67	0.35	91.1
1.04–1.05	0.51	0.32	1.59	2.21	0.25	183
Lipid(0.90)[c]	22.87	5.11	14.65	6.55	0.03	84.6

Acknowledgement

This work was supported by PHS/NIH grants: CA095624 and EB002026; a DOD grant W81XWH-04-1-0190, and the MGH A.A. Martinos Center for Biomedical Imaging.

References

Burns, M.A., He, W., Wu, C.L. et al. 2004. Quantitative pathology in tissue MR spectroscopy based human prostate metabolomics. *Technol. Cancer Res. Treat.*, 3:591–8.

Cheng, L.L., Anthony, D.C., Comite, A.R. et al. 2000. Quantification of microheterogeneity in glioblastoma multiforme with ex vivo high-resolution magic-angle spinning (HRMAS) proton magnetic resonance spectroscopy. *Neuro-oncol.*, 2:87–95.

Cheng, L.L., Burns, M.A., Taylor, J.L. et al. 2005. Metabolic characterization of human prostate cancer with tissue magnetic resonance spectroscopy. *Cancer Res.*, 65:3030–4.

Cheng, L.L., Lean, C.L., Bogdanova, A. et al. 1996. Enhanced resolution of proton NMR spectra of malignant lymph nodes using magic-angle spinning. *Magn. Reson. Med.*, 36:653–8.

Duarte, I.F., Stanley, E.G., Holmes, E. et al. 2005. Metabolic assessment of human liver transplants from biopsy samples at the donor and recipient stages using high-resolution magic angle spinning 1H NMR spectroscopy. *Anal. Chem.*, 77:5570–8.

Keshari, K.R., Zektzer, A.S., Swanson, M.G. et al. 2005. Characterization of intervertebral disc degeneration by high-resolution magic angle spinning (HR-MAS) spectroscopy. *Magn. Reson. Med.*, 53:519–27.

Sitter, B., Bathen, T., Hagen, B. et al. 2004. Cervical cancer tissue characterized by high-resolution magic angle spinning MR spectroscopy. *MAGMA*, 16:174–81.

Sitter, B., Lundgren, S., Bathen, T.F. et al. 2006. Comparison of HR MAS MR spectroscopic profiles of breast cancer tissue with clinical parameters. *NMR Biomed.*, 19:30–40.

Swanson, M.G., Vigneron, D.B., Tabatabai, Z.L. et al. 2003. Proton HR-MAS spectroscopy and quantitative pathologic analysis of MRI/3D-MRSI-targeted postsurgical prostate tissues. *Magn. Reson. Med.*, 50:944–54.

Taylor, J.L., Wu, C.L., Cory, D. et al. 2003. High-resolution magic angle spinning proton NMR analysis of human prostate tissue with slow spinning rates. *Magn. Reson. Med.*, 50:627–32.

Tugnoli, V., Mucci, A., Schenetti, L. et al. 2004. Molecular characterization of human gastric mucosa by HR-MAS magnetic resonance spectroscopy. *Int. J. Mol. Med.*, 14:1065–71.

Tugnoli, V., Schenetti, L., Mucci, A. et al. 2005. A comparison between in vivo and ex vivo HR-MAS 1H MR spectra of a pediatric posterior fossa lesion. *Int. J. Mol. Med.*, 16:301–7.

Wu, C.L., Taylor, J.L., He, W. et al. 2003. Proton High Resolution Magic Angle Spinning NMR Analysis of Fresh and Previously Frozen Tissue of Human Prostate. *Magn. Reson. Med.*, 50:1307–1311.

NMR-based metabolomics approach to target biomarkers for human prostate cancer

K.W. Jordan and L.L. Cheng

Key Words:

- Metabolomics
- Metabolites
- Nuclear Magnetic Resonance (NMR)
- Magnetic Resonance Spectroscopy (MRS)
- Magnetic Resonance Spectroscopic Imaging (MRSI)
- Prostate Cancer (PCa)

In the era of genomics and proteomics, metabolomics offers a unique way to probe the underlying biochemistry of malignant transformations. In the context of oncological-metabolomics, the study of the global variation of metabolites involved in the development and progression of cancers, few existing techniques offer as much potential to discover biomarkers as nuclear magnetic resonance (NMR or MR) techniques. The most fundamental MR methodologies with regard to human prostate cancer (PCa) are magnetic resonance spectroscopy (MRS) and magnetic resonance spectroscopic imaging (MRSI). Recent *in vivo* explorations have examined crucial metabolites that may indicate cancerous lesions and have the potential to direct treatment; while *ex vivo* studies of prostatic fluids and tissues have defined novel diagnostic parameters and indicated MR methodologies will be paramount in future PCa management.

Prostate cancer is the most common cancer among men in America. An estimated 218,000 cases of PCa will be diagnosed in 2007; during that same year over 27,000 men will die from the disease[1]. The lifetime risk of developing PCa is 20% in the US, and the US National Institutes of Health (NIH) and Department of Defense spend almost $500 million on research into the malignancy every year[2,3] . Despite these facts and figures, the mortality rate of patients afflicted with cancer has remained stagnant for nearly 30 years, illustrated by Figure 1[4]. The development of the prostate specific antigen (PSA) test was a remarkable achievement, the main consequence of which was an increase in the early diagnosis of prostate cancers. However, clinicians continue to lack a method to non-invasively determine the biological status of cancer and the extent to which it is present in the prostate. In addition, tumor markers are needed to accurately differentiate the aggressive tumors, which require immediate action, from those that can be managed with watchful waiting without the potential to reach clinical significance during the patient's life time. The National Cancer Institute's Prostate Cancer Progress Review Group (PRG) has outlined "crucial directions for research," including discovering markers to identify assertive tumors, improving prognostic markers to guide individual therapy, and improving diagnostic modalities to ensure no prostate cancers are missed[5]. Various techniques are currently being explored for their ability to meet the needs defined by the PRG, among them NMR-based approaches are unique and promising.

METABOLOMICS FOR PROSTATE CANCER

History of Metabolomics

Metabolomics, a science that utilizes fundamental analytical techniques to probe the chemical fingerprint of a sample, has developed in the remarkable era of genomics and proteomics[6]. Steve Oliver, of Manchester University, defined the term "metabolomics" as

the study of "the complete set of metabolites/low-molecular weight intermediates, which are context dependent, varying according to the physiological, developmental or pathological state of the cell, tissue, organ or organism"[7]. Metabolomics is a method used to probe the underlying biochemistry of processes taking place on the cellular level. Similar to genomics and proteomics, which are broad based analyses of the genome and proteome, metabolomics is an examination of the entire measurable metabolome: it is the comprehensive profiling of the various interconnected pathways comprising metabolism. Due to its nature the metabolome is dynamic and changes can be induced by innate factors or the environment. The term metabolite applies to the molecules that are products, reactants, intermediates or waste in metabolism. A primary metabolite is one involved in normal homeostatic mechanisms including development and reproduction (e.g.: hormones); while secondary metabolites usually perform ecological functions (e.g.: antibiotics).

Metabonomics is a term often used synonymously with metabolomics, a term coined by Lindon, Nicholson, and colleagues; however the science of metabonomics differs from metabolomics in that metabolomics profiles the metabolites present at the moment of analysis, while metabonomics quantifies the history of time-dependent changes taking place in a cell due to various endogenous and exogenous factors[8]. For the purposes of this manuscript the term metabolomics will be used, even in the context of discussing time-specific changes to the metabolome.

Ignoring feedback loops and parallel processes, we can generally consider metabolites are downstream products of genomic and proteomic changes, they are in fact products of the execution of various signals a cell is receiving. Each cellular process has a metabolic signature associated with it, and an analysis of the concentrations of metabolites present can be used to create a metabolic profile, which can then be used as a biomarker for that process. Metabolites, therefore, are the signatures of a cell at the moment of analysis. To literally illustrate the dynamics of metabolites, Figure 2 shows one component of a biochemical pathways chart for choline (a metabolite commonly studied in NMR due to its established link to cancerous developments[9,10]) and several of its derivatives. Charts illustrating the metabolic pathways of the known metabolome demonstrate the current knowledge on human metabolism that has been investigated thus far. Metabolic pathway charts, such as this one, exemplify how individual metabolites relate to one another and overall cellular metabolism. While genomic and proteomic explorations continually yield newly discovered genes and proteins, the majority of the metabolites comprising the possible human metabolome have been examined for decades and can now be related to specific homeostatic and disease mechanisms using metabolomic technologies.

As a modern science, metabolomics developed after the advent of the genomics era, following the completion of the human genome project. The theoretical basis for correlating metabolites to cellular developments is more historic, however. In 1949 Linus Pauling attributed a molecular mechanism to the causal agent of sickle cell anemia and subsequently determined that a chromatographic (metabolic) profile of bodily fluid could predict or even diagnose a disease[11]. Later Pauling and his colleague, A. Robinson, published the first study analyzing metabolites in bodily fluid in 1971, and later conducted nineteen published investigations into the role of metabolites in disease and physiology[12]. In 1985, R.F. Derr generated the metabolic control theory currently viewed as fundamental to the development of metabolomics[13]. Additionally, at the time of this article's publication, the techniques used to explore the metabolome (mass spectrometry, NMR, etc.) have existed for over half a century[14,15]. Metabolomics may be considered a "new" science due to both the technical advances in the field of NMR in recent years, and -perhaps more poignantly- the shifting focus to increasingly microscopic explorations of disease.

From genes to proteins to metabolites, so the scientific interest shifts from genomics to proteomics to metabolomics. An indication of such is the significant research support metabolomics currently receives: in 2005 the NIH designated its first $70 million to advance metabolomic technologies[16]. The results of ongoing interest in metabolomics is evident in both the contemporary publication record and the impressive completion, in January 2007, of the Human Metabolome Database, a project spearheaded by the Wishart group that provides a comprehensive record of the 2180 endogenous human metabolites[17](available www.hmdb.ca).

Metabolomic Methodologies

While this article focuses on the role of nuclear magnetic resonance techniques and their applications to prostate metabolomics, other metabolomic methodologies exist. In contrast to other means by which the metabolome can be analyzed, NMR has two exceedingly significant advantages. The first benefit of using NMR is the ability to rapidly identify and quantify the majority of metabolites present in the samples studied. The spectrum produced during an NMR experiment represents all the metabolites above the detection limit. Within the spectrum the metabolites have established chemical shifts, such that the location of the metabolite within the spectrum is a characteristic of that metabolite, as is the structure of the Fourier transformed signal (for example lactate resonances in a 1HNMR spectrum are found as a doublet at ~1.31 ppm and a quartet at ~4.09 ppm) (site Metabolite Shift Paper). Regardless of the specific application of NMR (*in vivo*, *ex vivo*, cell lines, tissues, etc.) the signals from metabolites are conservative, there is no variation in the response of a specific metabolite other than the area under the peak, which is indicative of the concentration of the metabolite present in the sample.

The second fundamental advantage of using NMR is the minimal sample preparation required. Nuclear magnetic resonance can be performed on unaltered specimens, which allows for future use of the same sample (for example an intact tissue sample studied can be subjected to pathological analysis because the tissue architecture has not been disturbed),

Contrasting with the above benefits of NMR are the characteristics of mass spectrometry (MS), which is the principle alternative to NMR for metabolomic studies. Mass spectrometry involves the conversion of molecules into ions and the measurement of the mass-to-charge ratio of the ion in order to determine the physical composition of a sample[14]. Mass spectrometry has several forms including gas chromatography MS (GC-MS), liquid chromatography MS (LC-MS), high performance LC-MS (HPLC-MS), ultra high performance MS (UPLC-MS), ion mobility MS (IMS), tandem MS, and direct infusion MS (DIMS), among others[18]. All forms of MS provide a sensitive means by which to measure metabolites, sometimes with lower detection limits than those that can be used in NMR[8]. However, the chief deficits of MS are the necessity (with most forms of MS) for a separation phase and the lack of uniform-detection[8]. Mass spectrometry analyses require extensive sample preparation and, therefore, alteration. The differing properties of the metabolites within the sample alter the response of the metabolites to their ionization. Hence mass spectrometry is a useful tool for providing rapid metabolic structural information (including empirical formula), but is less useful for providing a full metabolic profile of a sample[18]. Metabolomic studies using MS are much less prolific than those using NMR[19,20].

Metabolomic Statistical Tools

Metabolomic techniques generate vast amounts of information to which rigorous statistical methods must be applied to establish meaningful correlations between metabolites

and pathological conditions. It is unlikely that metabolomic biomarkers will consist of an individual metabolite, instead a metabolic profile can serve as a biomarker, requiring multivariate methods of analysis. Two groups of methods are 'supervised' versus 'unsupervised;' unsupervised methods establish if any intrinsic clustering of the data is relevant to the study, while supervised methods calibrate a model based on the metabolic data and known clinical outcomes in order to establish separation between groups[8,18].

The goal of many metabolomic studies is to generate either a disease marker or a prognostication factor using unsupervised methods. In order to do this the data must be put into a manageable cohort. A popular data-reduction technique is Principle Component Analysis (PCA), which constructs independent principle components (PC) where each PC expresses variance within the data set. Each point of data (it can be a spectrum, or a single metabolite, or a group of metabolites, etc.) is factored into the PC by a loading value, which itself demonstrates the variance of the data point. A point that associates strongly with a PC will make a larger contribution to the PC. A positive loading factor means the data point is enhanced in the PC, while a negative value indicates suppression. For example, a PCA of a group of metabolites will generate PCs, which can be correlated with specific pathologies. If a PC is correlated with cancer, for example, the metabolites that have highly positive values are strong contributors to the malignant cancer profile; conversely those with negative values are metabolites decreased in the malignant condition. The correlation between PCs and the conditions of interest is established using linear regression analysis, and a paired student's *t* test can evaluate the significance of the ability of PCs to differentiate conditions from one another (e.g. cancer from normal). Maximum separation within a group is determined by discriminant analysis and a receiver operating characteristic curve (ROC) determines the accuracy via a graphical display of sensitivity versus 1-specificity [21]. An example of the results of this type of analysis can be found in Figure 3.

Algorithms including partial least squared (PLS) and SIMCA are useful supervised statistical methods where several groups are generated. First a training set establishes models of the metabolic association with a condition and groups samples accordingly. Next each group established by the training set is validated and fine-tuned. Finally the test set is subjected to fitting to assess the accuracy of the models. SIMCA creates multivariate boundaries within the training set which are later validated; while PLS operates on the basis of relating dependent versus independent variables[8]. Other types of less popular algorithms are artificial neural networks (ANN), rule induction-based algorithms, and evolutionary computation[18].

Metabolic Changes in Prostate Cancer

The prostate is an exocrine gland of the male reproductive system responsible for secreting prostatic fluid into male ejaculate. Prostatic fluid comprises 25-30% of human seminal fluid and is important for stabilizing DNA-containing chromatin of sperm cells, coagulating the semen to keep it in the vaginal canal, and assisting the formation of disulphide cross-links in sperm fusion[22]. Anatomically the prostate is divided into three zones by the pattern of smooth muscle fiber extension into the gland: the peripheral zone comprises the majority of the gland, the central zone surrounds the ejaculatory duct, and the transitional zone surrounds the urethra. More than 75% of prostate cancers are adenocarcinomas originating from the secretory epithelium of the peripheral zone; 15% are derived from the transitional zone; and very few originate from central zone tissue[23].

Before the introduction of the metabolomics concept. the role of several metabolites in malignant transformation had been characterized, although the metabolic pathways in prostate cancer are not as well developed as those in other malignancies[24]. In the healthy

prostate there are high levels of citrate as a result of zinc inhibition preventing the oxidation of citrate in the Kreb's cycle. Citrate and zinc are found in high concentrations in healthy prostatic tissue and fluid (citrate concentration in normal prostatic tissue is 8,000 to 15,000 nmol/g, versus 150 to 450 nmol/g in other soft tissues of the body)[25]. The change from citric-production to citric-oxidation is the most consistent modification in malignant prostate tissue, with PCa tissue usually containing 1,000 to 2,000 nmol/g[25]. High levels of zinc in prostate cells lines have shown the potential to inhibit malignant development[26,27]. Furthermore, the alternation to a citric-oxidizing state is associated with increased oxygen expenditure which may increase the prostate tumor angiogenesis[25].

Elevated choline is another metabolic marker of prostate cancer. Choline, phsophocholine and glycerophosphocholine are associated with alterations in cell membrane synthesis accompanying cancerous developments[9,10]. Creatine, polyamines (spermine, spermidine, and putrescine), taurine and myo-inositol have also been examined for their role in prostate cancer development;differentiation of benign and malignant tissues can be based on the polyamines as they are elevated in benign conditions and reduced in PCa[28,29]. Polyamines are the metabolites that play an important part in forming the disulphide links in sperm fusion and adhesion proteins[22].

Characterizing the metabolic activities of prostate cancers has been tested using one or two metabolites (such as *in vivo* studies) and the entire measurable metabolic profile, metabolomics, (such as published *ex vivo* analyses). Regardless of the number of metabolites studied, metabolic analysis with MR techniques yields a powerful tool that may have the potential to ease the often complex management of prostate cancers.

Prostate Cancer Status and Features

Prostate cancer is an extremely heterogeneous, often multi-focal, disease. Current screening tests, such as serum prostate specific antigen (PSA) testing and digital rectal exams (DRE) are marred by a lack of specificity. PSA is *prostate* specific but is not *cancer* specific. Benign conditions such as benign prostate hyperplasia (BPH) and prostatitus can elevate PSA levels. Abnormal findings from PSA and DRE often lead to unnecessarily intervention as only 25-50% of men with abnormal DRE are proven to have cancer[30]. Benign conditions associated with normal aging are a predominant barrier to successful diagnosis of PCa. Benign prostate hyperplasia occurs in the epithelial and mesencymal areas of the organ and has no etiological connection to cancer[31]. Symptoms of benign conditions are often coincidental with symptoms of PCa including enlarged prostate, frequent urination, and elevated PSA levels.

Modern diagnosis of prostate cancer is based on the gold-standard pathological examination of core biopsies. However, such a task is complicated by the limitations of histopathology: sampling errors result in false-negatives, and staging accuracy and biopsy sensitivity is determined by tumor-volume[32]. Clinical identification of PCa based on transrectal ultrasound (TRUS)-guided biopsy has a high sampling error and false-negative rate. Initial TRUS-guided biopsies detect PCa in only 22-34% of patients whose cancers are later confirmed by additional clinical measures[33-35]. It is not uncommon for patients to have up to four biopsies before their cancer is discovered, at which point they have lost critical treatment time.

Furthermore, once prostate cancer is diagnosed the issue of treatment garners more debate. PSA screening has lead to an increase in early disease diagnosis, but has not yielded an improvement in mortality rates[36]. A likely cause of this dissociation is an inability to distinguish the more aggressive from more indolent cancers. Seventy percent (70%) of PCa's determined by Gleason score are described as moderately differentiated[37]. The clinical

outcomes among patients with this type of cancer run the gamut; some patients will have no symptoms from the disease throughout their life, while for others the disease is fatal. The Gleason score system grades cancers according to their architectural features on a 1 to 5 scale; a score of 1 indicates a well-differentiated area, while a 5 signifies an almost complete loss of glandular structure. The Gleason score is determined by grading the primary and secondary growth patterns then summing the grades; the Gleason score system is widely debated and highly variable because a Gleason score is based only on predominant features and would not account for a higher grade growth pattern if it were present only in small foci[38,39]. Several nomograms are currently being analyzed to determine if combining information from various prognostic factors can gauge the outcome of various treatments; however no published nomograms have been successful at differentiating survivability among prostate cancers[40-42].

It is most likely that the majority of patients would benefit from treatment, but what type? Watchful waiting, radiation therapy (EBRT, IMRT, brachytherapy), or prostatectomy? It is estimated 30% of PCa patients are over-treated[43]; as a result of prostatectomy 90 men each day in the US will experience impotence and 45 will become incontinent[44]. These are alarming statistics for patients and clinicians, especially in light of a 2004 study that established men would prefer decreased lifetime with potency to increased lifetimes with impotency[45].

A thin needle biopsy may indicate the presence of cancer, but does little to indicate the extent of the disease within the gland. At the time of diagnosis the cancer may be present in a single foci, throughout the prostate or spreading beyond the gland. An obvious, and effective, measure of PCa aggressiveness is its scope within and beyond the diseased organ[46]. While not a biomarker in the strictest sense, a measure of cancer aggressiveness is exceedingly important for individualized PCa treatment planning. Treatment of PCa with surgical prostatectomy is undertaken as long as the patient has no detectable extracapsular invasion of the cancer. For instance, patients whose disease extends only minimally beyond the gland have a high cure rate with surgery[47,48]. Patients whose cancer spreads significantly into tissues surrounding the prostate have a high recurrence rate after surgery and may opt treatments other than surgery. Malignant invasion into the seminal vesicles is an extremely important prognostic factor as vesicular invasion corresponds with distant metastasis and development of local recurrence.

A "good" marker for prostate cancer could, therefore, either be a diagnostic marker, one that indicates tumor virulence, or one that helps direct treatment. Tissue metabolomics analyzed with MR techniques may offer a means by which to search for such a biomarker(s).

NUCLEAR MAGNETIC RESONANCE APPROACHES

Theory of Nuclear Magnetic Resonance

The terms nuclear magnetic resonance or magnetic resonance imply a number of techniques used by several scientific communities, among them MRI, MRS and MRSI, all of which can be performed *in vivo* or *ex vivo*. In general, magnetic resonance describes the reaction of nuclei when they are placed in an external magnetic field, then perturbed by a second oscillating field.

At rest, nuclei have both magnetic and angular moment. The angular momentum is generated by the electrons as they move around the nucleus. The nuclear magnetic moment is generated by all of the protons and neutrons in the nucleus. When a sample is placed in an external magnetic field (B_0) the angular momentum aligns with the B_0 field and the nuclear momentum splits into degenerated states. The splitting results in an energy differential

between these two states equivalent to a radiofrequency (RF). If energy of that RF is applied as a B_1 field to the sample, the nuclei can absorb the energy and transition between the states. When the nuclei are absorbing RF energy they are said to be "on resonance" and their absorption-emission behaviors may be recorded to present a “spectrum”. The MR spectrum of a sample result when the precise radiofrequencies of energy corresponding to transitions between respective energy states for all nuclei in the sample is applied.

Most clinical applications of MR involve the pulse, Fourier transform (FT) technique. Pulse NMR records all the nuclei of interest simultaneously, versus the original MR form called continuous-wave, which excited each frequency individually. In pulse MR the B_1 field is introduced by applying a sinusoidal RF current, through a coil, much greater than that used on continuous wave (CW) MR. The frequency of the RF pulse excites the nuclei to be on resonance in the excited state. When the pulse is turned off the nuclei attempt to return to their ground state and require a set length of time for the nuclei to relax back to equilibrium (Figure 4a). During this time, the nuclei emit energy signals that can be registered in the time domain as a signal/time plot known as the free induction decay (FID). After the FID is induced and recorded it is translated into a frequency-dependent pattern (a spectrum) using the Fourier transformation (Figure 4b).

The nuclear decay to the ground state can be viewed as taking place on both the z direction (i.e. the direction of the external magnetic field) and on a plane (x-y) perpendicular to the field direction. The FID generated during nuclear relaxation processes can provide such useful information as chemical shifts, conformational changes in macromolecules, bond distances, spin-spin couplings (e.g. the interaction of two hydrogen nuclei on the same molecule splitting the spectral lines), molecular diffusion, and molecular correlation times. Most often the three types of relaxation time discussed in regard to MRS are: T_1, T_2, and T_2*.

T_1 is the first order relaxation, commonly referred to as spin-lattice relaxation time; it is the time required for the nuclei to return to equilibrium by exchanging energy with their surroundings. The lattice is a general term for the nucleus’ surroundings, which can absorb energy given off by the nuclei, this includes other nuclei (but only those tumbling at a rate equal to one or two times the Larmor frequency).

T_2 occurs via relaxation between nuclei which are tumbling at much slower rates than Larmor frequency. As nuclei relax they do not remain in phase with one another, as each experience a slightly different local magnetic field and precesses at its own specific frequency.

T_2* is the relaxation time that acknowledges both the T_2 and the fact that a magnetic field can never, in reality, be perfectly homogenous, therefore, nuclei in different physical locations of the field experience differing net magnetism, thus, have different resonance frequencies. At the moment of the initial RF pulse all nuclei are rotated a certain degree from the z direction, as they rotate (or more precisely precess) they become dephased in the x-y plane; Fig 2 pictorially represents the fan-like array of de-phased spins. Within the sample the nuclei that precess at the same speed, which have the same Larmor frequency and experience the same magnetization, are called spin isochromats. When discussing dephasing and the relaxation back to 0 in the x-y plane it is these isochromats to which we are specifically referring.

Magnetic Resonance Spectroscopy

Magnetic resonance spectroscopy provides extensive chemical information about the sample studied as it reveals information about the concentrations of all metabolites in the sample. Proton (1H), ^{31}Phosphorus and ^{13}Carbon (13C) are the most common nuclei studied using MRS. Figure 3a shows an example of a spectra produced by a type of *ex vivo* MRS

(high resolution magic angle spinning or HRMAS) ideal for studying intact biological tissues; the resonance peaks of several metabolites are labeled. Water is suppressed in a proton spectrum because it exists in such a high concentration that the water peak, to the point of their being impossible to differentiate, dwarfs metabolites.

The benefit of vast information provided by MRS is coupled with several deficits. Data analysis for MRS is more time consuming. Analyzing metabolites visually can easily identify which are increased or decreased compared to the baseline, but quantification or semi-quantification is necessary to accurately identify the metabolome of the sample.

Magnetic Resonance Imaging

Magnetic resonance imaging is a not a metabolomic technique in that it provides an illustration of areas inside the body by exciting the nuclei in water, and water is not a metabolite. Magnetic resonance imaging is, however, a nuclear magnetic resonance approach that is used as an alternative or in conjunction with metabolomic approaches and will, therefore, be discussed briefly in this article.

The density of water in different anatomic structures having different physical properties may appear bright or dark, depending on the type of RF pulses applied. The contrast creates an image that in turn aids in analyzing the health of the imaged structures. The information provided by MRI is not, however, considered as biochemically in-depth as a complete metabolic analysis achieved with MRS, or partially with MRSI. Magnetic resonance images contrast surrounding images with one another, but the biochemical information that reveals the activity of the cell in that area cannot be recorded with routine MRI.

Magnetic Resonance Spectroscopic Imaging

Magnetic resonance spectroscopic imaging in some ways combines both imaging and spectroscopy. MRSI provides limited spectroscopic data (usually one to three metabolites) that is overlaid onto the anatomical image provided by MRI. A region of interest is broken into small areas, voxels, and spectroscopy is taken within each voxel to reveal concentrations of some metabolites. For prostate MRSI spectroscopy is most often taken at differing angles to provide a three-dimensional grid of the entire gland. The deficit of MRSI is the complicated interpretation of the data. Heterogeneous organs, such as the prostate, can contain multiple tissue types within the same voxel, each influencing the metabolic concentrations of the one to three metabolites measured. An example of prostate MRSI is found in Figure 5. Magnetic resonance spectroscopic imagining, due to the limited number of metabolites currently examined *in vivo*, may not always be considered a true metabolomics technique. However, increasing the number of metabolites examined *in vivo* such that a larger portion of the metabolome is probed could yield a future where MRSI provides as in-depth analysis of the biochemistry of the organ or tissue examined.

BIOMARKERS DEFINED IN VIVO

MRI of the Prostate

Currently most prostate MRIs are conducted at the field strength of 1.5 T, using a phase arrayed pelvic coil in combination with the endorectal coil. Imaging of the prostate focuses on the peripheral zone, though recent studies have shown tumors in the transistional zone can also be found with MRI especially if a contrast agent is used[49]. For the purposes of

discussion below, however, all references to MRI of the prostate conventionally refer to the peripheral zone. T2 weighted imaging (T2W) may distinguish normal from cancerous prostatic tissue. In the prostate normal tissue is bright, versus the dark images that result from the tumor[50]. The decrease in image brightness corresponds to the increasing density of water in diseased areas. However, other, non-malignant, conditions can affect the interpretation of T2W images. Furthermore, though the zonal anatomy is captured with accuracy, studies have shown that even among tumors greater than 0.5 cm^3, only 70% can be diagnosed based entirely on imaging[51]. Rather than as an alternative to biopsy, current prostate MRI could serve to increase the accuracy of histopathology by targeting a specific area for biopsy, thereby reducing sample errors[52].

The Role of Magnetic Resonance Spectroscopic Imaging

During an MR examination chemical (metabolic) data in addition to the imaging can be measured to maximize the information provided by the exam. While imaging is based entirely on the behaviors of water, metabolites of high concentrations can be evaluated using either MRSI or MRS to explore the biochemical behaviors of the tissues. Magnetic resonance spectroscopic imaging is the most commonly coupled spectroscopic technique accompanying MRI *in vivo*.

The three metabolites most commonly visualized in MRSI of the prostate are citrate, choline and creatine. In order to detect their resonances the metabolites must be present in concentrations of 1 mM or greater and water must be suppressed (the usual concentration of water in the body is 10^5 times the concentration of the metabolites of interest). In prostate spectroscopy, citrate levels are usually decreased in malignant conditions and choline is increased. At common clinical field strengths, and with variations in the quality of the spectroscopy, many resonances overlap in regions of interest. Ratios of metabolites are often examined in lieu of individual metabolite concentrations due to the difficulty of absolute quantitation and the trends in certain metabolites under malignant developments. The ratio of the choline-creatine region to citrate ([Cho + Cr]/Cit) is the most commonly used spectral analysis clinically and has been shown to correlate with Gleason score. Voxels are classified as normal, suspicious for cancer, very suspicious for cancer, or non-diagnostic[53]. The threshold for delineating a voxel as suspicious for cancer is a (Cho + Cit)/Cre ratio 2 standard deviations (SD) above the average ratio for normal tissue; a ratio of 3 SD above normal is considered very suspicious for cancer[54]. Voxels are non-diagnostic if no metabolite signals register of the signal-to-noise ratio exceeds 5. Figure 5 shows the MRSI voxel overlay on anatomical images; the spectra of healthy tissue and malignant tissue are juxtaposed.

The value of MRSI lies in the supplement it provides to MRI: incorporating MRSI into an MRI exam has reportedly shown to significantly increase the number of cancers identified, and help provide information predictive of Gleason score prior to a biopsy being obtained[55]. Magnetic resonance imaging and spectroscopic imaging are both enhanced by their combination. Magnetic resonance imagine alone has a sensitivity around 75% and a specificity around 60%; MRSI has a higher specificity (75%), but a lower sensitivity (63%)[55]. Combined the MRI/MRSI modality reached a reported specificity of 91% and sensitivity of 95%[55].

A notable example where MRSI is superior when it is autonomous from MRI is in the diagnosis of PCa recurrence following radiation therapy. Local recurrence following radiation therapy is difficult to find via biopsy due to sampling error and an uncertain timeline for tumor recurrence[56]; imaging modalities are defunct due to a reduction in imaging signal intensity in atrophied glands and fibrosis, the normal side effects of radiation therapy[57]. MR spectroscopic examination allow the quantification of the key diagnostic

metabolites (choline, creatine and citrate) even after the prostatic duress inflicted by radiation treatments. This novel application of MRSI is applicable in a small percentage of patients, only 17% of newly diagnosed patients choose beam therapy and 50% of those patients will have PSA relapse within five years[58]. Additionally, diagnosis could be aided here by MRS, which would yield information on additional PCa markers such as the polyamines.

Magnetic Resonance Spectroscopy *in vivo* (single voxel)

A full spectroscopic examination of all the metabolites found *in vivo* can also be performed, but data analysis and interpretation are more challenging. For the detection of PCa, single voxel *in vivo* MRS has a reported sensitivity, specificity, and accuracy up to 89%, 77%, and 83%, respectively[59]; however, this study used a late-stage patient cohort and it should be emphasized that specificity and sensitivity for early stage cancers would most likely be lower than the values reported. As the ability to gather data on the entire metabolome *in vivo* is increased the value of MRS will be greatly enhanced. Magnetic resonance spectroscopy may, in the future, be used to identify markers that can be searched for using MRI/MRSI. With technological advances in field strength and resolution, increasing numbers of metabolites defined as potential cancer markers by MRS (such as the polyamines) could be searched for using MRI/MRSI.

BIOMARKERS DEFINED EX VIVO

Fluid-Based Studies

Human seminal fluid, because of its high concentration of prostatic fluid, is an appropriate avenue to search for PCa markers. The first studies linking metabolites found in seminal fluid to prostate tumorogenesis were undertaken prior to 1930[60]. Proton MRS has furthered the possible explorations of metabolites contained in prostatic fluids, and has yielded exciting results[28,60,61]. MRS is used because of its dynamic nature: the complex nature of a biofluid can be dissected analytically to reveal the underlying molecular processes. Samples of prostatic fluid can be obtained using prostate massage, or via conventional ejaculation, without significant alternation to metabolite concentrations[22]. For the purposes of analyzing prostatic changes, prostatic fluid is more ideal than seminal fluid as seminal fluid contains contributions from other organs (bulborethral glands, testes and seminal vesicles).

Several metabolites that have been defined as cancer-markers in tissues have preliminarily been found to have potential as cancer-markers in prostatic fluid. Most notably the citrate and spermine levels in prostatic fluid are significantly correlated with a patient's PCa status. Citrate concentrations in seminal fluid have been found to differentiate between PCa patients, healthy controls, and men with BPH[60]. Even more impressively, studies have suggested that the citrate concentration in whole, unaltered seminal fluid outperforms prostate specific antigen as a PCa marker[61].

The advantages of searching seminal fluid for PCa markers are obvious: seminal fluid samples can be obtained non-invasively compared to biopsy. Furthermore, MRS has no inter-observer reproducibility issues. The potential to use citrate concentration in seminal fluid as a screening tool may be novel and effective, which raises question as to why it has not been executed. The seeming cause is the level of personal comfort breached by using this particular biofluid. It is extremely plausible that the volunteering of ones seminal fluid could be viewed as crossing the boundary of a patient's personal space. More conclusive evidence

especially that which determines a threshold value of citrate level indicating disease, needs to be collected. Given the promising outcome of studies of individual metabolites in prostatic/seminal fluid, the predictive value of a complete metabolomic profiling study of prostatic fluid could be immense.

Tissue-Based Studies

The physical state of tissue must be considered for successful applications of NMR on excised tissues. Classical NMR developed for analysis of aqueous solutions, where molecules can tumble freely and are liberated from intermolecular interactions. Solids often undergo anisotropic affects whereby nuclei from the same functional group in different surroundings within the compound experiencing different effects of the magnetic field. Line broadening results in spectra undergoing anisotropic affects, often to the point that metabolites overlap and become indistinguishable. Though not characterized as a solid, biological tissues are subject to anisotropic afects to various degrees. One way to overcome this is to make an aqueous extract from the tissue, whereby cells are lysed and their metabolites are dissolved in solution. Unfortunately this precludes pathological observation of the tissue following spectroscopic analysis. Microscopic examination are extremely important in order to account for the heterogeneity presented in a tissue; otherwise, the metabolites analyzed might be erroneously associated with malignancy when, in fact, the sample might have been entirely benign, and vice versa.

Anisotropic, or context-dependent, affects can be epitomized by dipolar interactions. It was discovered that dipolar interactions, and in fact all of the anisatropic effects in solids resulting in spectral line broadening, can be overcome by mechanically rotating, or spinning, the sample 54.7° away from the applied magnetic field[62]. Thus 54.7° is known as the "magic angle". The increased resolution with spinning allows for the quantificiation of many metabolites that are otherwise impossible to differentiate in a broad line spectrum. The adoption of the technique for the study of unaltered biological tissues was developed in the late 1990s and is termed high resolution magic angle spinning proton magnetic resonance spectroscopy (HRMAS 1HMRS)[63,64]. Spinning rates in HRMAS 1HMRS are chosen such that they do not damage tissue architecture, leaving samples in a condition that allows them to be analyzed pathologically to overcome heterogeneity issues previously discussed[28,65]. The methodology is widely used to probe various cancers, including those of the prostate.

For example, a reported study used HRMAS 1HMRS to define PCa markers in combination with a number of other MR technologies. Tissues were targeted for excision using MRI and MRSI, and HRMAS 1HMRS was applied to the tissues *ex vivo* to analyze the predictive capacity of HRMAS 1HMRS. Malignant tissue could be significantly distinguished from normal using HRMAS 1HMRS on the basis of higher levels of citrate and the polyamines in normal gland, and increased choline compounds (choline, GPC, and phosphocholine) in cancer, if the sample had more than 20% cancer by volume pathologically[66]. Several metabolites, such as the polyamines, not quantifiable *in vivo* were also reported, and the ability to analyze a wider array of metabolites could lead to the elucidation of the underlying biology of prostate tumorogensis, and the improvement of *in vivo* MRS/MRSI. The ability for MRI/MRSI to target normal and cancerous tissues were 90% and 71% accurate, respectively, thus *ex vivo* spectroscopy acted as an adjuvant to MRI/MRSI.

Recently the capacity of HRMAS 1HMRS based prostate metabolomics presented by principle components of the tissue spectral profile in predicting disease status has been demonstrated. It was found that by analyzing the compilation of all metabolites found in the sample, metabolic profiles can differentiate malignant from benign samples, correlate with

patient PSA level, differentiate between indolent and aggressive tumors, and predict tumor perinural invasion[21]. The ability to predict perinerual invasion is important for classification, though not incorporated in traditional staging, because it indicates tumor aggressiveness and alters treatment planning. The impressive aptitudes of HRMAS 1HMRS indicate it would be beneficial as a second opinion to biopsy histology, one which could successfully subcategorize otherwise indistinguishable tumors from one another. In the case of HRMAS 1HMRS the entire measurable metabolome comprises the cancer marker. This is similar to the familiar "heat maps" generated by genomic analyses. The various processes taking place all manifest in metabolic changes which may be less meaningful if they are analyzed individually. Single metabolites, while powerful tools, lack the precision of metabolic profiles. Figure 3 displays the spectra, histopathology, and statistical data from 13 patients whose cancer was analyzed using metabolic profiles generated by principle component analysis of HRMAS 1HMRS data.

Drug Targets

Ex vivo MRS can be used to monitor the effects of PCa treatments, and to elucidate the mechanism of action and target for drugs with known potency. In many cases drugs that differ only slightly from one another may have drastically different cellular effects; the metabolites produced by each treatment can indicate the cellular developments the drug induces, thereby differentiating drugs from one another and indicating them for use among different populations of PCa patients.

Differentiating agents are a useful example of the power of MRS as a tool to target PCa markers which are, in turn, targeted for therapy. Differentiating agents promote cell differentiation and apoptosis, often through methods that are poorly understood even at the stage of clinical trials. Phenylacetate (PA) and phenylbutrate (PB) are two aromatic acids that act as differentiation inducers of prostate cancer cells. Behaviors of each compound have been determined by treating PCa cells *ex vivo* and monitoring the effects with 1H and 31P diffusion-weighted MRS. MRS analysis revealed significant metabolic changes in the signals from lactate, mobile lipids and neutral amino acids, fatty acids, total choline, and glycerophosphorylcholine (GPC)[67]. The results were compared to electron and light microscopy to associate metabolic changes with morphological variations. Further analysis of the spectroscopy and microscopy data indicate that PB treatment causes an arrest in the G1 phase of the cell cycle leading to induction of apoptosis[67]. PA treatment, on the other hand, lead to an accumulation of G2/M cells and did not induce apoptosis[67]. Thus, the two differentiating agents, while structurally similar, affect different stages of the cell cycle. Of key importance here is the fact that MRS is able to monitor metabolic changes and analyze toxicological effects of potential chemotherapeutic agents.

Hormone refractory cancer is a subclass of PCa with a poor prognosis, and drugs to treat this specific form of malignancy are being developed. MRS has been used as a non-invasive monitor of drug efficacy to discriminate if genetic prodrug activation therapy (GPAT) could be used to treat hormone refractory prostate cancer[68]. Disease management with GPAT has demonstrated tumor-specific immune response, and works by inserting 'suicide' genes (usually the herpes simplex virus thymadine kinase enzyme/ ganciclovir prodrug system) into tumor cells. Cells treated with GPAT die during the cell cycle, while also initiating an immune response important for the 'bystander effect' and, potentially, distant metastasis. However, clinical trails of the early 2000s produced limited clinical response, and MRS was proposed as a means to monitor the system and address efficacy issues. In this specific case monitoring was done with MRS *in vivo* in animals from two mouse models. Significant changes were observed in tumor ATP/Pi and phosphomonester

(PME)/phosphate ratios. Tumors of treated animals displayed an increase in the ATP/Pi, while the PME/phosphate ratio decreased; contrarily, tumors of the control animals had a decrease in the ATP/Pi ratio and no change over time of the PME/phosphate ratio[68]. Changes to the PME/phosphate ratio are often associated with an increased response to PCa treatment and this, combined with other data, indicates GPAT induces metabolic effects similar to those produced with other chemotherapies.

Monitoring drug treatment can be accomplished using MRS *in vivo* or *ex vivo*, with cell lines, animal models, or even during clinical trials. If undertaken *in vivo* MRSI could prove a useful adjunct to conventional MRS for the purpose of examining a drugs toxicological effects. An issue unique to prostate cancer is the lack of interest in developing new chemotherapeutic approaches to PCa. As prostatectomy is the most common treatment, patients can be understandably unwilling to opt for a drug regime if their entire tumor can be removed, especially as the side effects to chemotherapy can be as harrowing as those produced by prostatectomy. If drugs can be validated before clinical implementation with means such as MRS, to the point that they are as successful as prostatectomy, then there could be a shift in the treatment paradigm.

EXPERT OPINION

Redefining PCa management in light of NMR discoveries is a logical step in the advancement of the prostate cancer clinic. Metabolic processes taking place that have yet to manifest in pathological changes to tissues yield important information about the biochemistry of a disease. Through individual analysis by NMR techniques it is possible to generate a metabolomic profile of a patient's cancer that takes into account far more information than provided by histopathology of a biopsy. In the era of personalized medicine it is crucial to direct patients to the most appropriate therapy for their lifestyle and cancer type. Gleason score may not be a good predictor of a patient's prognosis, but metabolic changes, viewed globally in terms of metabolomics, seen with MRI, MRSI, or MRS may provide the differentiation ability currently lacking in clinical PCa management. Incorporation of these techniques can be seen as costly, but no more so than the potentially unnecessary surgeries and biopsies taking place everyday and the money spent on treatments whose outcome could have been predicted.

FIVE-YEAR VIEW

Ex vivo metabolomic biomarkers will continue to be discovered, which can then be searched for *in vivo* by combining MRI/MRSI to the diagnosis, staging, and treatment planning for individual patients. The value of this approach will continue to be demonstrated until it is finally viewed as an acceptable expense for all patients with increased PSA level. New prostate cancer screening tools will be developed on the basis of NMR metabolomics, most likely those biomarkers that can be found in prostatic fluids or perhaps even blood. As technology advances in the coming decades, the ability to probe deeper into the metabolome *in vivo* will result in metabolic profiles that characterize a patient’s cancer, in the same way that genetic testing will soon allow a person to access information specific to their genome.

KEY ISSUES

- Current paradigms for prostate cancer (PCa) diagnosis and treatment planning are insufficient and may lead to patient over treatment and a lack of personalized cancer management.
- Metabolomic techniques are a way to probe the underlying biochemistry of tumors to offer a complete, individualized analysis of a patient's cancer.
- Metabolomic techniques can use multivariate statistical analysis to generate metabolic profiles of homeostatic and diseased states.
- Magnetic resonance spectroscopy (MRS) *ex vivo* can be used to identify prostate metabolomic biomarkers for screening tools, to direct drug treatment planning, and to refine *in vivo* techniques.
- Magnetic resonance imaging (MRI) in conjunction with magnetic resonance spectroscopic imaging (MRSI), based on prostate metabolomics, may direct biopsies and stage cancer prior to histopathological identification of PCa.

REFERENCES

Papers of interest have been highlighted as:

* of interest

** of considerable interest

1. *Cancer Facts & Figure 2007* American Cancer Society, Atlanta, GA, (2007).
2. *Federal Research Funding* National Prostate Cancer Coalition, Washington, DC, (2007).
3. Jemal A, Tiwari R, Murrary T, Ghafoor A, Samuels A, Ward E *et al.* Cancer Statistics, 2004. *CA Cancer Journal for Clinicians* 54, 8-29 (2004).
4. Jemal A. (personal communication with L. Cheng) (2005).
5. Report of the Prostate Cancer Progress Review Group. Defeating Prostate Cancer: Crucial Directions for Research.National Cancer Institute.August 1998
6. Raamsdonk LM, Teusink B, Broadhurst D, Zhang N, Hayes A, Walsh MC *et al.* A functional genomics strategy that uses metabolome data to reveal the phenotype of silent mutations. *Nat Biotechnol* 19, 45-50 (2001).
7. Oliver S. Functional Genomics: all the king's horses and all the king's men can put Humpty together again. *Mol Cell* 12, 1343-4 (2003).
8. Lindon JC, Holmes E, Bollard ME, Stanley EG, Nicholson JK. Metabonomics technologies and their applications in physiological monitoring, drug safety assessment and disease diagnosis. *Biomarkers* 9, 1-31 (2004).

** Current methodologies, statistics, and applications of metabonomics.

9. Glunde K, Jacobs MA, Bhujwalla ZM. Choline metabolism in cancer: implications for diagnosis and therapy. *Expert Rev Mol Diagn* 6, 821-9 (2006).
10. Glunde K, Serkova NJ. Therapeutic targets and biomarkers identified in cancer choline phospholipid metabolism. *Pharmacogenomics* 7, 1109-23 (2006).
11. Pauling L, Itano HA, et al. Sickle cell anemia a molecular disease. *Science* 110, 543-8 (1949).
12. Pauling L, Robinson A, Teranishi R, Cary P. Quantitative analysis of urine vapor and breath by gas-liquid partition chromatography. *Proc Natl Acad Sci* 68, 2374-2376 (1971).

13. Durr R. Modern metabolic conrol-theory. 1. Fundamental theorems. *Biochemical Archives* 1, 239-247 (1985).
14. de Hoffman E, Stroobant V. *Mass Spectrometry: Principles and Applications* John Wiley and Sons, (2001).
15. Farrar T. *Introduction to Pulse NMR Spectroscopy* The Farragut Press, Madison, WI, (1997).

** Thorough introduction to the theory and practice of magnetic resonance techniques.

16. Daviss B. Growing pains for metabolomics. *Scientist* 19, 25-28 (2005).
17. Wishart DS, Tzur D, Knox C, Eisner R, Guo AC, Young N *et al.* HMDB: the Human Metabolome Database. *Nucleic Acids Res* 35, D521-6 (2007).
18. Hollywood K, Brison DR, Goodacre R. Metabolomics: current technologies and future trends. *Proteomics* 6, 4716-23 (2006).
19. Fiehn O. Metabolomics--the link between genotypes and phenotypes. *Plant Mol Biol* 48, 155-71 (2002).
20. Plumb R, Granger J, Stumpf C, Wilson ID, Evans JA, Lenz EM. Metabonomic analysis of mouse urine by liquid-chromatography-time of flight mass spectrometry (LC-TOFMS): detection of strain, diurnal and gender differences. *Analyst* 128, 819-23 (2003).
21. Cheng LL, Burns MA, Taylor JL, He W, Halpern EF, McDougal WS *et al.* Metabolic characterization of human prostate cancer with tissue magnetic resonance spectroscopy. *Cancer Res* 65, 3030-4 (2005).

** Prominent *ex vivo* study indicating the high potential for metabolomics based biomarker discoveries.

22. Lynch MJ, Nicholson JK. Proton MRS of human prostatic fluid: correlations between citrate, spermine, and myo-inositol levels and changes with disease. *Prostate* 30, 248-55 (1997).
23. Carroll P, Lee K, Fuks Z, Kantoff P. Cancer of the Prostate In *Cancer: Principle and Practice of Oncology.* DeVita V, Hellman S, Rosenberg Seds (ed). Lippincott Williams & Wilkins, Philadelphia, 2001).
24. Dang CV, Semenza GL. Oncogenic alterations of metabolism. *Trends Biochem Sci* 24, 68-72 (1999).
25. Costello LC, Franklin RB. The intermediary metabolism of the prostate: a key to understanding the pathogenesis and progression of prostate malignancy. *Oncology* 59, 269-82 (2000).
26. Costello LC, Liu Y, Zou J, Franklin RB. Evidence for a zinc uptake transporter in human prostate cancer cells which is regulated by prolactin and testosterone. *J Biol Chem* 274, 17499-504 (1999).
27. Ishii K, Usui S, Sugimura Y, Yoshida S, Hioki T, Tatematsu M *et al.* Aminopeptidase N regulated by zinc in human prostate participates in tumor cell invasion. *Int J Cancer* 92, 49-54 (2001).
28. Cheng LL, Wu C, Smith MR, Gonzalez RG. Non-destructive quantitation of spermine in human prostate tissue samples using HRMAS 1H NMR spectroscopy at 9.4 T. *FEBS Lett* 494, 112-6 (2001).
29. Swanson MG, Zektzer AS, Tabatabai ZL, Simko J, Jarso S, Keshari KR *et al.* Quantitative analysis of prostate metabolites using 1H HR-MAS spectroscopy. *Magn Reson Med* 55, 1257-64 (2006).
30. DeVita VT, Hellman S, Rosenberg SA. *Cancer Principles & Practice of Oncology* Lippincott, Williams & Wilkins, Philadelphia, (2005).
31. Tumors of the Prostate. In *WHO Classification of Tumors.* Eble N, Suater G, Epstein Jeds (ed). IARC Press, Lyon, 159 (2004).

32. Steiner H, Moser P, Hager M, Berger AP, Klocker H, Spranger R *et al.* Clinical and pathologic features of prostate cancer detected after repeat false-negative biopsy in a screening population. *Prostate* 58, 277-82 (2004).
33. Djavan B, Ravery V, Zlotta A, Dobronski P, Dobrovits M, Fakhari M *et al.* Prospective evaluation of prostate cancer detected on biopsies 1, 2, 3 and 4: when should we stop? *J Urol* 166, 1679-83 (2001).
34. Keetch DW, Catalona WJ, Smith DS. Serial prostatic biopsies in men with persistently elevated serum prostate specific antigen values. *J Urol* 151, 1571-4 (1994).
35. Roehl KA, Antenor JA, Catalona WJ. Serial biopsy results in prostate cancer screening study. *J Urol* 167, 2435-9 (2002).
36. Shibata A, Ma J, Whittemore AS. Prostate cancer incidence and mortality in the United States and the United Kingdom. *J Natl Cancer Inst* 90, 1230-1 (1998).
37. Pound CR, Partin AW, Eisenberger MA, Chan DW, Pearson JD, Walsh PC. Natural history of progression after PSA elevation following radical prostatectomy. *Jama* 281, 1591-7 (1999).
38. Gleason DF. Classification of prostatic carcinomas. *Cancer Chemother Rep* 50, 125-8 (1966).
39. Gleason DF, Mellinger GT. Prediction of prognosis for prostatic adenocarcinoma by combined histological grading and clinical staging. *J Urol* 111, 58-64 (1974).
40. Kattan MW, Eastham JA, Stapleton AM, Wheeler TM, Scardino PT. A preoperative nomogram for disease recurrence following radical prostatectomy for prostate cancer. *J Natl Cancer Inst* 90, 766-71 (1998).
41. Kattan MW, Potters L, Blasko JC, Beyer DC, Fearn P, Cavanagh W *et al.* Pretreatment nomogram for predicting freedom from recurrence after permanent prostate brachytherapy in prostate cancer. *Urology* 58, 393-9 (2001).
42. Kattan MW, Zelefsky MJ, Kupelian PA, Scardino PT, Fuks Z, Leibel SA. Pretreatment nomogram for predicting the outcome of three-dimensional conformal radiotherapy in prostate cancer. *J Clin Oncol* 18, 3352-9 (2000).
43. Carter HB, Walsh PC, Landis P, Epstein JI. Expectant management of nonpalpable prostate cancer with curative intent: preliminary results. *J Urol* 167, 1231-4 (2002).
44. Ransohoff DF, McNaughton Collins M, Fowler FJ. Why is prostate cancer screening so common when the evidence is so uncertain? A system without negative feedback. *Am J Med* 113, 663-7 (2002).

* An intriguing examination of the decisions that are made by PCa patients and clinicians regarding PCa diagnosis and treatment.

45. Sculpher M, Bryan S, Fry P, de Winter P, Payne H, Emberton M. Patients' preferences for the management of non-metastatic prostate cancer: discrete choice experiment. *Bmj* 328, 382 (2004).
46. Scher HI, Heller G. Clinical states in prostate cancer: toward a dynamic model of disease progression. *Urology* 55, 323-7 (2000).
47. Blute ML, Bergstralh EJ, Iocca A, Scherer B, Zincke H. Use of Gleason score, prostate specific antigen, seminal vesicle and margin status to predict biochemical failure after radical prostatectomy. *J Urol* 165, 119-25 (2001).
48. Han M, Partin AW, Zahurak M, Piantadosi S, Epstein JI, Walsh PC. Biochemical (prostate specific antigen) recurrence probability following radical prostatectomy for clinically localized prostate cancer. *J Urol* 169, 517-23 (2003).
49. Akin O, Sala E, Moskowitz CS, Kuroiwa K, Ishill NM, Pucar D *et al.* Transition zone prostate cancers: features, detection, localization, and staging at endorectal MR imaging. *Radiology* 239, 784-92 (2006).

50. Katz S, Rosen M. MR imaging and MR spectroscopy in prostate cancer management. *Radiol Clin North Am* 44, 723-34, viii (2006).
** Comprehensive examination of the current role of various MR techniques in PCa management.
51. Coakley FV, Kurhanewicz J, Lu Y, Jones KD, Swanson MG, Chang SD *et al.* Prostate cancer tumor volume: measurement with endorectal MR and MR spectroscopic imaging. *Radiology* 223, 91-7 (2002).
52. Akin O, Hricak H. Imaging of prostate cancer. *Radiol Clin North Am* 45, 207-22 (2007).
53. Kurhanewicz J, Vigneron DB, Hricak H, Narayan P, Carroll P, Nelson SJ. Three-dimensional H-1 MR spectroscopic imaging of the in situ human prostate with high (0.24-0.7-cm3) spatial resolution. *Radiology* 198, 795-805 (1996).
54. Males RG, Vigneron DB, Star-Lack J, Falbo SC, Nelson SJ, Hricak H *et al.* Clinical application of BASING and spectral/spatial water and lipid suppression pulses for prostate cancer staging and localization by in vivo 3D 1H magnetic resonance spectroscopic imaging. *Magn Reson Med* 43, 17-22 (2000).
55. Scheidler J, Hricak H, Vigneron DB, Yu KK, Sokolov DL, Huang LR *et al.* Prostate cancer: localization with three-dimensional proton MR spectroscopic imaging--clinicopathologic study. *Radiology* 213, 473-80 (1999).
56. Catton C, Milosevic M, Warde P, Bayley A, Crook J, Bristow R *et al.* Recurrent prostate cancer following external beam radiotherapy: follow-up strategies and management. *Urol Clin North Am* 30, 751-63 (2003).
57. Pucar D, Shukla-Dave A, Hricak H, Moskowitz CS, Kuroiwa K, Olgac S *et al.* Prostate cancer: correlation of MR imaging and MR spectroscopy with pathologic findings after radiation therapy-initial experience. *Radiology* 236, 545-53 (2005).
58. Coakley FV, Teh HS, Qayyum A, Swanson MG, Lu Y, Roach M, 3rd *et al.* Endorectal MR imaging and MR spectroscopic imaging for locally recurrent prostate cancer after external beam radiation therapy: preliminary experience. *Radiology* 233, 441-8 (2004).
59. Squillaci E, Manenti G, Mancino S, Carlani M, Di Roma M, Colangelo V *et al.* MR spectroscopy of prostate cancer. Initial clinical experience. *J Exp Clin Cancer Res* 24, 523-30 (2005).
60. Averna TA, Kline EE, Smith AY, Sillerud LO. A decrease in 1H nuclear magnetic resonance spectroscopically determined citrate in human seminal fluid accompanies the development of prostate adenocarcinoma. *J Urol* 173, 433-8 (2005).
61. Kline EE, Treat EG, Averna TA, Davis MS, Smith AY, Sillerud LO. Citrate concentrations in human seminal fluid and expressed prostatic fluid determined via 1H nuclear magnetic resonance spectroscopy outperform prostate specific antigen in prostate cancer detection. *J Urol* 176, 2274-9 (2006).
** A paramount paper illustrating the potential for fluid based studies to lead to future screening tools that may out perform PSA testing.
62. Andrew E, Bradbury A, Eades R. Removal of dipolar broadening of nuclear mangetic resonance spectra of solids by specimen rotation. *Nature* 183, 1802-1803 (1959).
63. Cheng LL, Lean CL, Bogdanova A, Wright SC, Jr., Ackerman JL, Brady TJ *et al.* Enhanced resolution of proton NMR spectra of malignant lymph nodes using magic-angle spinning. *Magn Reson Med* 36, 653-8 (1996).
64. Cheng LL, Ma MJ, Becerra L, Ptak T, Tracey I, Lackner A *et al.* Quantitative neuropathology by high resolution magic angle spinning proton magnetic resonance spectroscopy. *Proc Natl Acad Sci U S A* 94, 6408-13 (1997).

65. Cheng LL, Anthony DC, Comite AR, Black PM, Tzika AA, Gonzalez RG. Quantification of microheterogeneity in glioblastoma multiforme with ex vivo high-resolution magic-angle spinning (HRMAS) proton magnetic resonance spectroscopy. *Neuro-oncol* 2, 87-95 (2000).
66. Swanson MG, Vigneron DB, Tabatabai ZL, Males RG, Schmitt L, Carroll PR *et al.* Proton HR-MAS spectroscopy and quantitative pathologic analysis of MRI/3D-MRSI-targeted postsurgical prostate tissues. *Magn Reson Med* 50, 944-54 (2003).
67. Milkevitch M, Shim H, Pilatus U, Pickup S, Wehrle JP, Samid D *et al.* Increases in NMR-visible lipid and glycerophosphocholine during phenylbutyrate-induced apoptosis in human prostate cancer cells. *Biochim Biophys Acta* 1734, 1-12 (2005).
68. Eaton JD, Perry MJ, Todryk SM, Mazucco RA, Kirby RS, Griffiths JR *et al.* Genetic prodrug activation therapy (GPAT) in two rat prostate models generates an immune bystander effect and can be monitored by magnetic resonance techniques. *Gene Ther* 8, 557-67 (2001).
101. *Cancer Facts & Figure 2007.* American Cancer Society, Atlanta, GA, 2007. Available at: http://www.cancer.org/downloads/STT/CAFF2007PWSecured.pdf
102. *Federal Research Funding.* National Prostate Cancer Coalition, Washington, DC, 2007. Available at: www.fightprostatecancer.org
103. *Biochemical Pathways- Metabolic Pathways* (ExPASy and Roche Applied Science). Available at: http://www.expasy.ch/cgi-bin/show_thumbnails.pl
104. Nicholson D. *Metabolic Pathways Chart.* International Union of Biochemistry & Molecular Biology and Sigma-Aldrich, 2004. Available at: http://www.sigmaaldrich.com/img/assets/4202/MetabolicPathways_6_17_04_.pdf

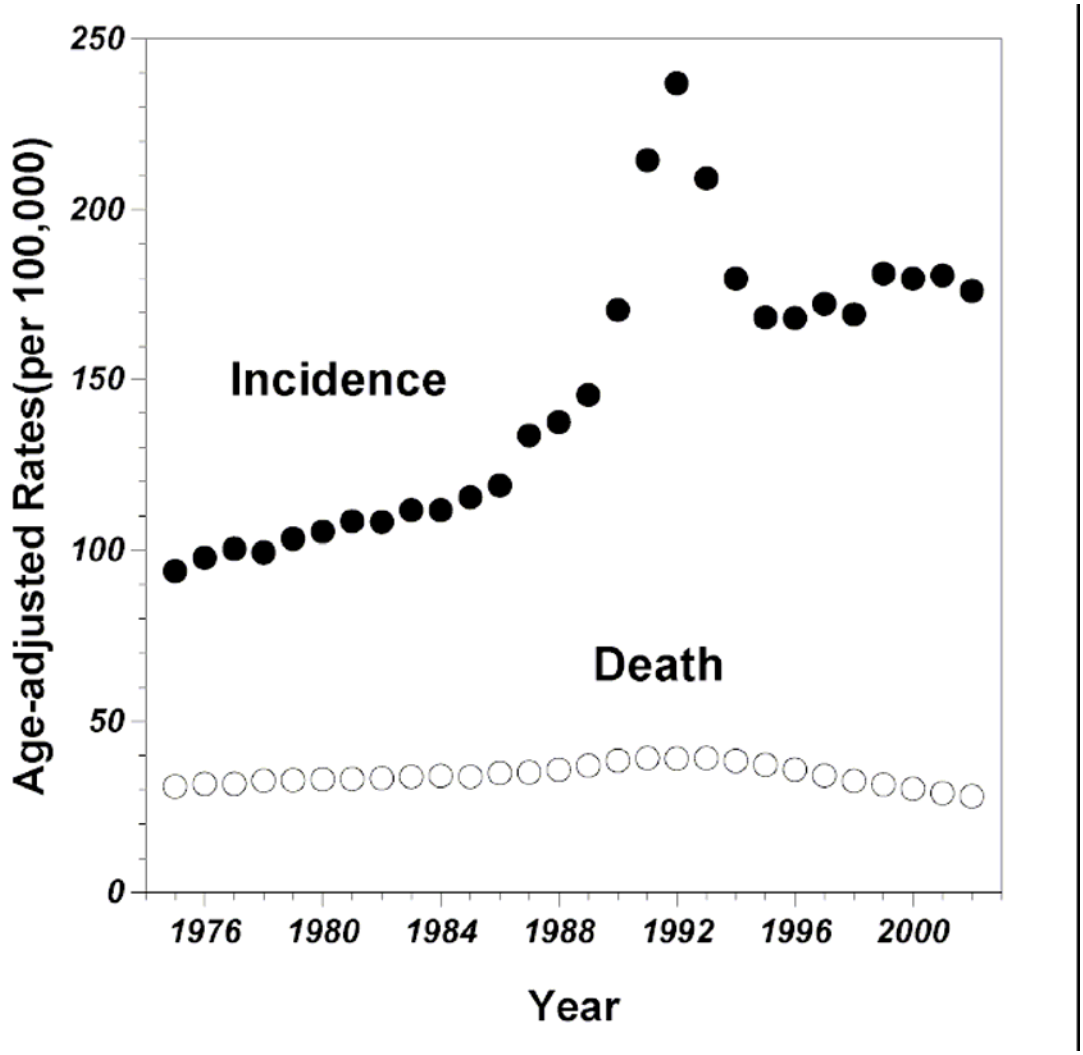

Figure 1: Human prostate cancer incidence and death rates from 1975 to 2002, showing an increase in incidence over the years (presumably due to increased early diagnosis) but a steady rate of mortality. Produced with permission from A. Jemal, also see [3-4].

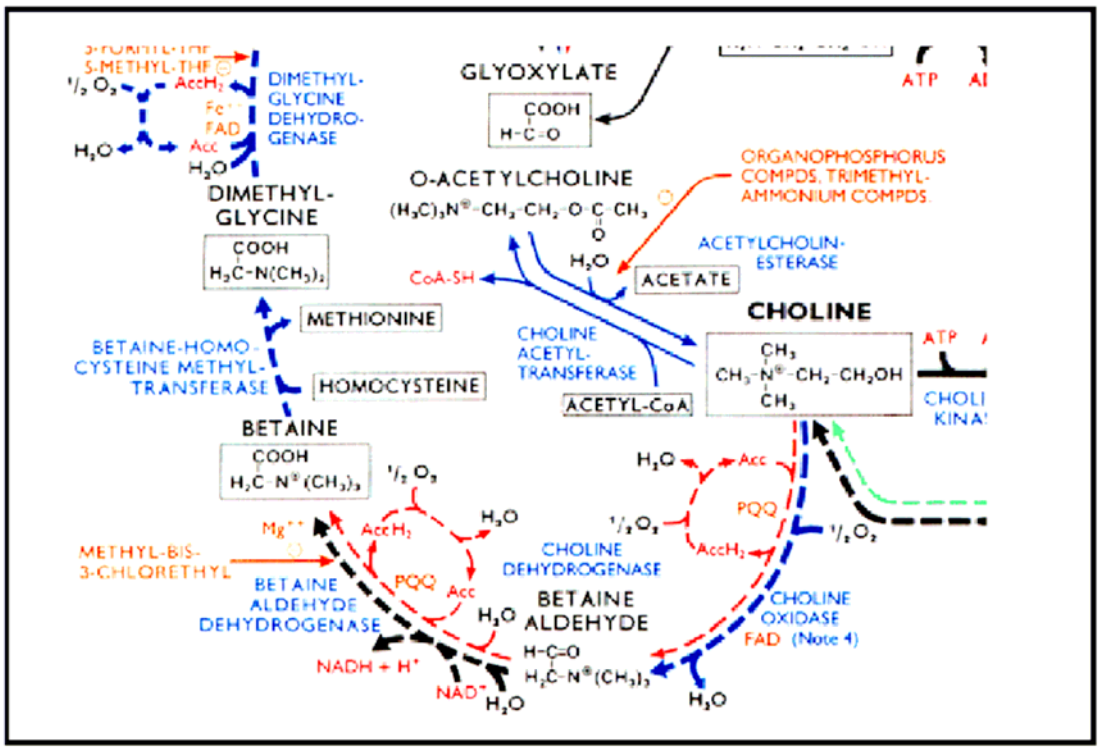

Figure 2: Biochemical pathways chart for choline and several of its derivatives, produced by and reprinted with permission from Roche. Pathway charts of metabolism are available from Roche and Sigma at [103-104] respectively.

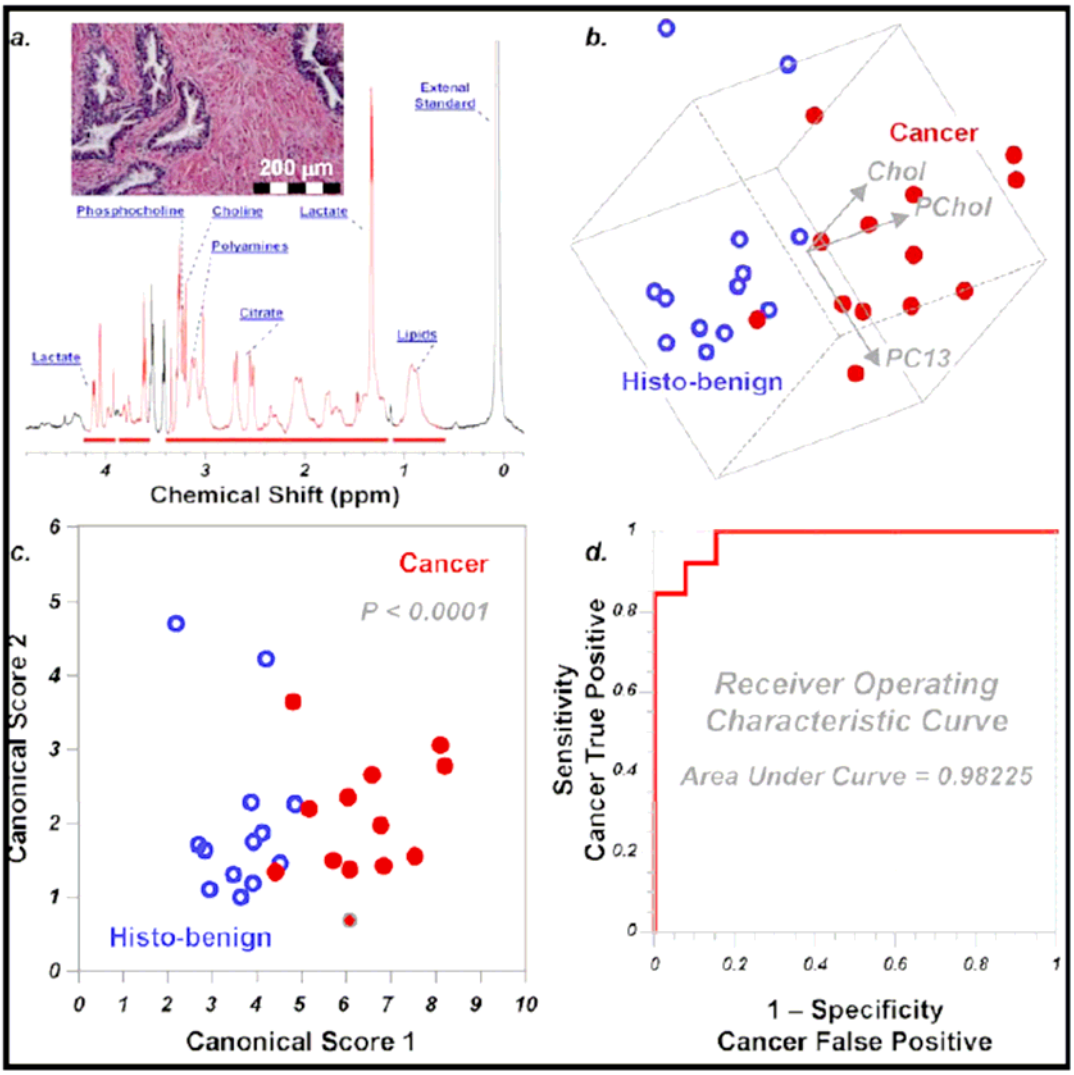

Figure 3: Results from HRMAS 1HMRS experiments; a) spectra observed and histopathology of tissue obtained from 61-year-old patient with Gleason score 6 PCa, b) 3D plot of principle component 13, which correlated linearly with vol% cancer, vs. phosphocholine (Pchol) vs. choline (Chol) for 13 tissue samples, c) canonical plot from discrimination analysis of the three variables in Fig 4b presents maximum separation between groups, and d) resulting receiver operating characteristic (ROC) curves indicating the accuracy of using the three variables in 4b to positively identify cancer samples. Also see [21].

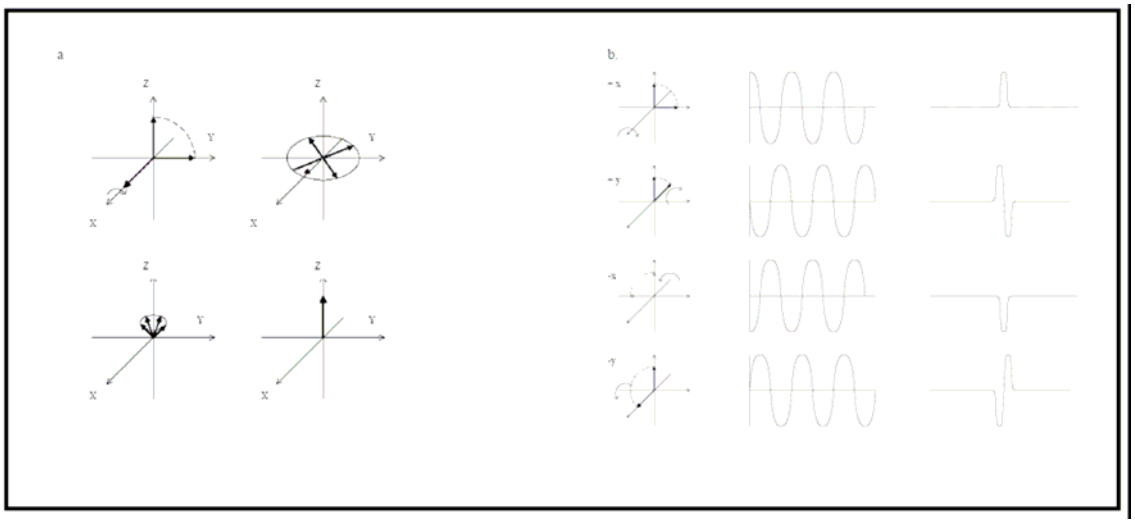

Figure 4: a) A 90° RF pulse applied to nuclei in a magnetic field result in the spins dephasing from one another, precessing and finally return to equilibrium; b) the behavior of spins in the rotating frame, the FID signal generated, and the spectral signal after Fourier transformation for nuclei in the x and y axis (+x, +y, -x, and –y). Adapted from [15].

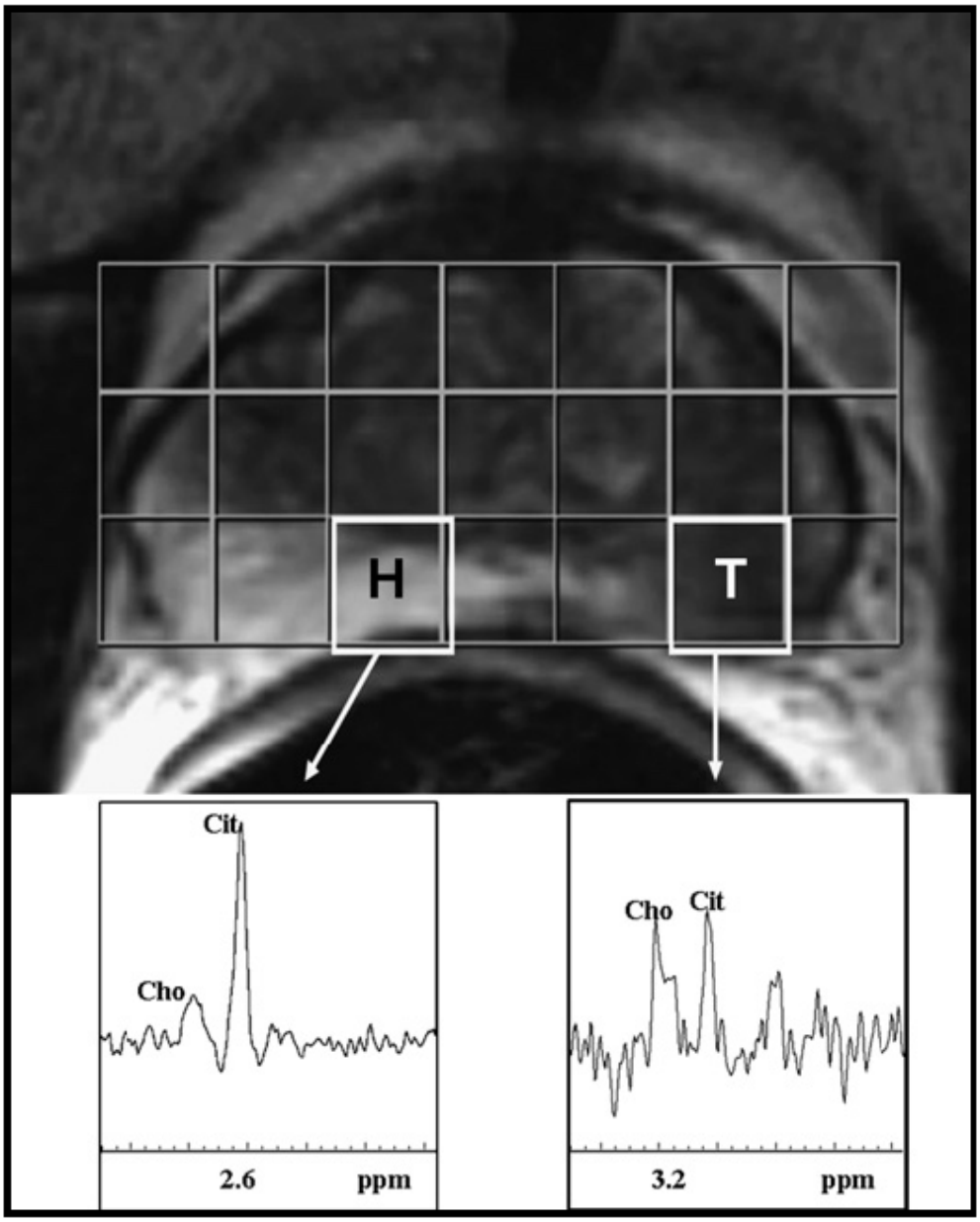

Figure 5: MRSI of Gleason score 9 prostate cancer in a 59-year-old male: H) spectra of healthy tissue of the right peripheral zone, and T) reduced citrate and increased choline in tumor tissue of the left peripheral zone. Reprinted from [52] with permission from Elsevier.

Cancer Imaging Vol. 2
Metabolic Characterization of Prostate Cancer: Magnetic Resonance Spectroscopy
K.W. Jordan & L.L. Cheng

I. INTRODUCTION

1.1 From Metabolites to Metabolomics

To evaluate prospectively the clinical utility of magnetic resonance spectroscopy one must first understand the rationale for how metabolomics in the era of genomics and proteomics offer a potentially powerful tool for disease evaluation. Simplifying the complex networks of biological metabolisms that control and regulate a human life by ignoring feedback loops and parallel processes, we can generally consider metabolites (such as those found in one's bodily fluids or tissues) are downstream products of genomic and proteomic changes. However, compared with genes and proteins, the advantage of metabolites is that they are, in many ways, the stepping-stones of cellular pathways through which the current, existing molecular processes can be probed. We define current oncological-metabolomics as the study of the global variations of metabolites, and a measurement of global profiles of metabolites from various metabolic pathways under the influence of oncological developments and progressions. The intrinsic interconnectivity of the entire metabolism, both physiological and pathological, of a human body under the influence of oncological processes is reflected in the emphasized word "global" in the above definition. Metabolomics is a science that evolved from studies of individual metabolites and their specific relationship with physiology and pathology into a discipline that now surveys the entire measurable metabolite profile for correlations with biomedicine.

1.2 Metabolomics for Prostate Cancer

The majority of prostate cancers (PCs), > 70%, are adenocarcinomas originating from the secretory epithelium of the peripheral zone; 15% arise from the transitional zone; and very few cancers derive from central zone tissue (Carroll et al., 2001). Despite this seemingly straight-forward analysis of the prostate, in clinical reality the disease is very heterogenous. Prostate cancer is a pathologically multifocal disease that can be found throughout the gland. The innate heterogeneity of prostate cancer complicates disease diagnosis. While 1 in 4 men may harbor PC in their gland, only 3.6% of those diagnosed will die of the disease and an estimated 30% of PC patients are over-treated (Carter et al., 2002). Regrettably there are currently no clinical paradigms to assess the virulent from indolent cancers. Each day > 150 radical prostatectomies are performed in the U.S. resulting in impotence and/or incontinence of urine for more than 95 and 45 men, respectively (Ransohoff et al., 2002).

Understandably, these are alarming statistics for both patients and clinicians. The NCI's Prostate Cancer Progress Review Group (PRG) (1998) has, therefore, outlined "crucial directions for research" which include: discovering new markers to differentiate less harmful from aggressive tumors, improving prognostic markers to better guide individual therapy, and improving diagnosis to ensure destructive PC's are not missed. Of all the various avenues that could be pursued, metabolomics offer a unique, sensitive, and specific solution to the issues raised by the PRG. In this chapter we show that metabolomics can be evaluated with magnetic resonance spectroscopy (MRS) which has demonstrated its potential to refine the PC clinic and may offer new paradigms with which diagnosis and management of the disease may be advanced to a new, high level.

1.3 Malignant Changes in Prostate Metabolism

Magnetic resonance spectroscopy, also known as nuclear magnetic resonance (NMR), was discovered independently by Felix Bloch and Edward Mills Purcell in 1945 (Sohlman, 2003). Following the development of NMR, German and English researchers in the 1970s found that small changes in cellular pathways could lead to large changes in metabolic concentrations (Daviss, 2005). This crucial discovery became the foundation of metabolomics as it describes the ability of metabolites to signify otherwise undetectable biological changes in cellular processes.

A number of specific metabolites have particularly significant importance in studying the prostate. Historically, citrate and choline have the most well-categorized biochemical role in prostate malignant transformation. In the epithelial cells of a healthy prostate there is a high cellular accumulation of zinc (Franklin et al., 2005). High levels of zinc inhibit oxidation of citrate in the Krebs cycle, leading to high levels of citrate, which is secreted into prostatic fluid. The metabolic transformation from citric-production to citric-oxidization is the most consistent modification from normal to malignant prostate tissue. Elevated levels of choline are associated with changes in cell membrane synthesis accompanying cancerous development (Podo, 1999). In addition to citrate and choline, other common metabolites that have been evaluated as diagnostic markers for prostate cancer include creatine, the choline-containing compounds phosphochline and glycerophosphocholine, spermine, spermadine, taurine, and myo-inositol. Integrating the polyamines allows the differentiation of cancer from healthy or benign prostatic hyperplasia tissue, as the polyamine levels are elevated in benign conditions but are reduced in malignant situations (Cheng et al., 2001). Polyamines stabilize membranes of both cells and organelles, and assist the formation of disulfide crosslinks (such as those important to sperm fusion and adhesion proteins). Significant data from cell-extract studies have shown that the alterations in prostate cellular metabolism that accompany malignant changes are in fact cancer specific, and are not due to changes in cellular volume or doubling time (Ackerstaff et al., 2001).

When investigating metabolic alterations in relation with physiological and pathological conditions, the predecessors to current PC spectroscopy often focused on individual metabolites, usually choline, creatine, and citrate. As spectroscopy developed, analysis of concentrations of individual metabolites gave way to examining ratios of metabolites to one another. Current *in vivo* spectroscopy continues to use the ratios of choline, citrate, and creatine to one another as their litmus test. Probing the concentrations of other metabolites, such as the polyamines, in *in vivo* spectroscopy is not easy due to the fact that at 1.5T (T, Tesla, is the unit of magnetic field strength) the polyamine resonances overlap with the peaks for choline and creatine.

Ex vivo spectroscopy of biological samples, utilizing the advantages of high field strength and better achievable field homogeneity, can reveal dozens of cellular metabolites that are not distinguishable *in vivo*. *Ex vivo* studies can be performed either on intact tissue samples or on solutions of tissue extracts. These solutions or intact tissues if analyzed effectively with appropriate methodologies, are likely to produce spectra with >100 resonance peaks. The collections of these peaks, reflecting the MRS visible cellular metabolomics of the analyzed samples from an individual, vary according to individual biological diversity, disease status, and pathological conditions. Thus, instead of considering each individual metabolite independently, one needs to collectively and simultaneously evaluate them as an entire group. Fortunately, there do exist statistical models and methods that can readily be used for this type of data mining and analysis (e.g., principal component analysis).

II. MAGNETIC RESONANCE SPECTROSCOPY

2.1 Magnetic Resonance Spectroscopy

Innate nuclear momentum is known to have different states that become degenerated, for instance, into □ and □ states for protons, when the nucleus is placed in an external magnetic field (B_0). This splitting of momentum states results in an energy differential in which more atoms exist in the lower energy state (populations are now given by Boltzmann's law, $N^-/N^+ = e^{-E/kT}$, T: absolute temperature). The effective field at the nucleus is in reality not the full strength of the applied field due to electron circulation; the net magnetic field is referred to as *B*. The electron density at each nucleus varies, an effect referred to as chemical shift. In a given magnetic field, B_0, the energy needed to transfer between □ and □ states is proportional not to B_0, but to the field strength *B*.

Magnetic resonance occurs between the states when a second magnetic field, B_1, is applied through a coil at a radio frequency (RF) that matches the required energy to transition between the α and β states:

$$\Delta E = h\,\nu,$$

where *h* is Planck constant, and ν is the resonance frequency that can be written as:

$$\nu = \gamma B / 2\pi.$$

In this formula, γ is the gyromagnetic ratio that relates directly to the type of the examined nucleus. The equation $\nu = \gamma B / 2\pi$ is known as the Larmor equation; which is fundamental to MR spectroscopy, where chemical environments affect *B* through chemical shift □, and hence alter the Larmor frequency, ν.

The samples studied by MRS are not homogenous; the MR spectra are produced by the nuclei, for instance protons, with different Larmor frequencies in a given molecule or a mixture of different molecules. Each nucleus in a different chemical environment will have a unique Larmor frequency, in an applied B_0 field, and resonate when the applied B_1 energy matches that frequency. A nucleus is said to be "on resonance" when it is absorbing RF energy. Magnetic resonance uses the response of the magnetic moment of a nucleus when placed in a static external magnetic field and perturbed by a second oscillating field. Because the level of the response of a particular nucleus depends on its type as well as the chemical environment in which it resides, and by measuring a range or a spectrum of the responding levels for a given sample, the identification of the contained chemical components can be determined.

2.2 Pulse and Fourier Transform Magnetic Resonance Spectroscopy

Magnetic resonance spectroscopy was initially practiced using the continuous-wave (CW) technique, meaning either: a) the magnetic field was constant and the oscillating wave was swept to detect on resonance molecules; or, more commonly, b) the oscillating field was fixed at a certain frequency and the magnetic field was swept. In CW MRS each Larmor frequency of interest must be probed individually. The CW modality lost favor to pulse MRS by the 1970s. Pulse MRS, as indicated by its title, instead of swiping through magnetic fields, pulses the applied RF B_1 field through the sample with a short square pulse that, according to the mathematics of Fourier transform, contains all the frequencies of interest. Therefore, all the Larmor frequencies can be excited simultaneously and nuclear behavior can be recorded after the RF B_1 field is turned off.

The advantages of Pulse MRS over CW MRS are evident. The most obvious improvement being an increase in the S/N, resulting in the capability to do more measurements

per unit of time. The signal is the measurable output of the nuclei, while noise is the appearance of outside interference on the spectra. Signal-to-noise ratio (S/N) increases with the number of scans performed, proportional to $\sqrt{N}$. Pulse MRS allows one to take more scans in a dramatically reduced time period compared to CW MRS (seconds vs. minutes or longer); thus, pulse MRS provides a remarkably impressive S/N benefit. Besides this advantage, the most important contribution of pulse MRS is its ability to manipulate nuclei of interest and force them to yield the desired chemical information, which we will discuss later.

In pulse MRS the B_1 field is introduced by applying a sinusoidal RF current much greater than that used in CW MRS. The frequency of the RF pulse excites the nuclei to be on resonance for a time, *t,* which rotates the net magnetization of the nuclei $\gamma B_1 t$. For example, a pulse that can rotate the nuclei 90° is called a 90° (or $\pi/2$) pulse. Doubling the time the RF is applied will result in doubling the degree to which the nuclei are rotated (e.g., a π pulse turns the nuclei 180°). When the pulse is turned off the nuclei attempt to return to their ground state and require a set length of time for the nuclei to relax back to equilibrium (**Figure 1**). During this time, the nuclei emit energy signals that can be registered in the time domain as a signal/time plot known as the free induction decay (FID). The FID measured from a sample is the algebraic sum of all the decaying waves for the measured nuclei. After the FID is induced and recorded it is translated into a frequency-dependent pattern (a spectrum) using the Fourier transformation (**Figure 2**). Fourier transformation is a very powerful tool because it allows us to relate the frequency and time domains to extract meaningful spectra, and also because it integrates the complex amalgam of sinusoidal patterns produced by each individual molecule as their nuclei decay to produce the spectra.

The nuclear decay to the ground state takes place in two arenas, the z direction (i.e., the direction of the external magnetic field) and a plane (x-y) perpendicular to the field direction. The relaxation times of the nuclei with regard to the z-direction and the x-y plane can provide such useful information as chemical shifts, conformational changes in macromolecules, bond distances, spin-spin couplings (the interaction of two hydrogen nuclei on the same molecule splitting the spectral lines), molecular diffusion, and molecular correlation times. Most often the three types of relaxation time discussed in regard to MRS are: T_1, T_2, and T_2*.

T_1 is the first order relaxation, commonly referred to as spin-lattice relaxation time; it is the time required for the nuclei to return to equilibrium by exchanging energy with their surroundings. The lattice is a general term for the nucleus' surroundings, which can absorb energy given off by the nuclei. In addition to nuclear effects of magnetization, MRS must also acknowledge innate thermodynamic processes taking place. T_1 time is the relaxation order that reestablishes thermal equilibrium. After T_1 time the magnetization has been reestablished in the z direction and thermo-equilibrium is restored; however, since the signals can only be detected in the x-y plane, one can use a second pulse to rotate the already recovered nuclear magnetizations away from the z direction after a certain recovery time. Variations in the length of this recovering time allow one to measure the T_1 value.

T_2 takes into account nuclei relaxing back to equilibrium not with their external environment but instead with each other, among the like nuclei. As nuclei relax they do not remain in phase with one another, as each experience a slightly different local magnetic field and rotates at its own Laramour frequency. T_2 is always less than or equal to T_1.

T_2* is the relaxation time that acknowledges both the natural line width (T_2) and the fact that a magnetic field can never, in reality, be perfectly homogenous. Therefore, nuclei in different parts of the field experience differing net magnetism, thus, have different resonances.

At the moment of the initial RF pulse all nuclei are rotated a certain degree from the z direction, as they rotate (or more precisely precess) they become dephased in the x-y plane; Fig 2 pictorially represents the fan-like array of dephased nuclei. As previously described this means certain nuclei will, in essence, precess more quickly than others (the portions of the sample experiencing the greatest net magnetization precess most rapidly). Within the sample the nuclei that precess at the same speed, which have the same Larmor frequency and experience the same magnetization, are called spin isochromats. When discussing dephasing and the relaxation back to 0 in the x-y plane it is these isochromats to which we are specifically referring.

Increasing field homogeneity will bring T_2* closer to T_2. However, the mechanical and technical aspects of increasing field homogeneity have a limit. Therefore, spin-echo techniques are used to diminish the effects of field inhomogeneity. Spin echo techniques involve multiple pulses that reverse the order of the spin isochromats. This is accomplished in the following way: first, the sample is pulsed to a certain extent (usually 90°) after which the spin isochromats dephase. After a certain time, *t*, during which the spin isochromats become out of phase with each other, but *before* they have a chance to internally dephase, there is a second, 180° pulse applied along the x' direction in the x'-y' plane (x' being the plane in the rotating frame of the coil and sample, versus the x plane of the static magnet). The net magnetization in the z' direction is inverted and has no effect on the experiment, while the order of the spin isochromats is now reversed so that the fastest isochromats are behind the slowest. The benefit of this rearrangement is that the faster spin isochromats catch up with the slower ones and result a refocused magnetization along the y' direction at time 2*t*. The representation of the spin echo is an inverted FID. Several pulse techniques have been created to generate what is known as an echo train.

An echo train consists of the FIDs produced by a pulse sequence rephrasing the isochromats at multiples of time, *t*. The maximal echo amplitude in the spin echo should decay at a time constant that is consistent with T_2. The Carr-Purcell echo train combines 180° pulses with 180° phase shifts (e.g., echo one +x, echo two –x) and diminishes any pulse errors resulting from field inhomogeneity or pulse length discrepancies; alternatively phase shifting all echo pulses so they are 90° with respect to the initial pulse simplifies the process (e.g., all echoes are in the direction of the initial FID), this is known as the very common Meiboom-Gill modification of the Carr-Purcell sequence (CPMG).

A further importance of pulse MRS is the ability to decrease the time requisite for accumulating FIDs. In order for an FID to be complete, enough time must lapse between pulses for the magnetization to accrue along the z direction. This is not as large a problem in liquids as it is in solids because in liquids T_1 is closer to T_2*. To overcome the FID time requirement in samples such as non-liquid biological samples, one must force the system to return to thermal equilibrium faster then is natural. Driven equilibrium Fourier transform (DEFT) involves the initiation of a pulse echo sequence, and at the peak of a spin echo a 90° pulse rotates the nuclei back to the z direction, preparing the sample to start the process of gather FID again.

2.3 Magnetic Resonance Spectroscopy of Non-aqueous Solutions and Solids

In the above discussion, we categorically considered that identical molecules, or nuclei in the same chemical functional group of molecules, are physically the same, i.e., they are identical and have exactly the same Larmor frequency. In reality the closest system that may mimic such an ideal condition is an aqueous solution, where molecules of interest are all surrounded by solvent molecules and are a distance away from each other. Thus, by the additional assistance of

molecular tumbling, these molecules, and hence their nuclei of the same functional group, may be considered identical. In a non-ideal case there exist differences in the chemical shift factor □ for these nuclei. This is known as an anisotropic effect, and it results in nuclei of the same type resonating at a range of Larmor frequencies. This fact is reflected in an MR spectrum, where the resonance peak corresponding to these nuclei is broadened, as a spectrum is in fact a pictorial presentation of population distributions. This phenomenon is seen everywhere from classical solids, to biological samples of non-aqueous solution, to *in vivo* MRS of any physiological structures and organs.

Considerations of MRS for non-aqueous solution can be applied to the study of any biological tissues. For this reason, historically it has been common for researchers to investigate solutions of tissue extracts instead of dealing with biological tissues, which are of a semi-solid nature. However, while individual metabolites can be quantified within the extract solution using this method, the metabolites are altered to an unknown (unquantifiable) degree when going through the extraction processes. Furthermore, extraction methods destroy tissue pathological structures and preclude histopathological evaluation of the analyzed samples, preventing a correlation between the spectra and the pathology that produced it. This issue might not present a problem if tumors consisted of pathologically homogenous structures. Unfortunately, when dealing with human malignancies, tissue heterogeneity must be assumed and accounted for when analyzing MR spectra. While hundreds, if not thousands, of past publications were based on extraction MRS, the ability to compare biological and metabolic process with their underlying pathology (which may be considered essential) has been forever lost.

2.4 Magnetic Resonance Spectroscopy with Magic Angle Spinning

The issues described above, whereby a spectra is produced with broad line widths is the result of something that can be categorically termed as 'solid effects' produced by using MRS to study anything other than liquids. The quintessential example of a solid effect, the one most often referred to in MRS texts, are orientation-dependent interactions, such as dipolar interactions. Dipolar interactions take place between nuclei when the nuclei are susceptible to the magnetic field generated by the surrounding nuclei. The magnitude of the dipole-dipole interaction effect of the interaction on spectral broadening is dependent on the distance between the nuclei, the angle between the nuclear vector, and the applied magnetic field, $B_{0;}$ and is proportional to $(3\cos^2 \theta - 1)$. This condition not only accounts for dipolar interactions, but also other solid effects. Andrew et al. (1959) addressed the dipolar situation when they showed that dipolar interactions could be overcome if the angle θ in the above equation was 54.74° away from the applied magnetic field. Hence, 54.74° is known as the magic angle, the angle at which dipolar interactions are greatly reduced. In order to achieve such manipulation, the sample is placed in a rotor and mechanically tipped to the magic angle.

When the sample is spinning, at rates anywhere up to ~35 k Hz (the current technical limit), the time average internuclear vector aligns at the magic angle and the spectra produced is extremely well resolved. The effective spinning rate is defined as the rate equal to or greater than the line width produced by solid effects. When it was observed by Lowe and Norberg (1967) that magic angle spinning (MAS) MR spectroscopy resulted in the Lorentzian shaped spectra preciously only observed in aqueous solutions, the technique was adopted for solid state MAS. **Figure 3** exemplifies the capability of the MAS technique. The spectra in 3a and 3b are produced from the same human prostate tissue sample, without and with spinning, respectively, without spinning, the spectra is little more than several broad peaks and noise; 3c is an expansion

of the 0.5 ppm to 3.0 ppm range of 3b, in which individual metabolites from human prostatic tissue are clear and quantifiable when the sample is spun at 600 Hz.

Although the MAS technique was well known to MRS physicists, it was not until many years later that it was adopted for studying biological tissues. During his postdoctoral work at the Massachusetts General Hospital and Harvard Medical School, one of the authors of this chapter discovered the MAS could be used on *unaltered* biological tissue specimens (Cheng et al., 1996). Proton (1H) MR spectroscopy of tissue samples, when mechanically rotated at the magic angle, produces spectra with resolution close to those measured in solution, which is sufficient for the detection and quantification of individual metabolites. For the purpose of measuring unaltered tissue specimens the procedure became known as high-resolution magic angle spinning (HRMAS).

The technique was further improved by D.C. Anthony's observation that at a restrained rotation tissue architecture was not damaged by the centrifugal force of HRMAS (Cheng et al., 2000). This property is critical as it allows histopathology to be performed on the same sample after spectroscopy is measured, allowing the methodology to address the aforementioned issue of human tumor hetereogenity. The ability to correlate spectroscopy with tissue pathology made HRMAS a premier modality for spectroscopic disease analysis. **Figure 4** displays an HRMAS 1HMRS spectra with metabolites of interest labeled, as well as an H&E slide of the unaltered prostate tissue that was analyzed and produced the pictured spectra. HRMAS 1HMRS has, since its advent in the mid 1990s, been adopted for a wide variety of research studies.

III. CURRENT TECHNIQUES

It is emphasized that histopathology from biopsy cores remains the gold standard for diagnosing and determining treatment of prostate cancer. However, although histopathology has served well in the past, it cannot meet the needs of the current oncology clinic in which evolving technologies have drastically increased the number of men diagnosed with early stage, moderately differentiated PC. MR spectroscopy may present one of many modalities being examined at present to meet the demands of 21st century diagnosis, prognosis, and treatment planning.

3.1 Current In Vivo Prostate Cancer Spectroscopy

The origins of modern *in vivo* MR spectroscopy for the human prostate date back to ~ 1980, like many applications of spectroscopy, MRS advanced with the rate of technological improvements in coils, field strength, pulse sequences, etc. Most commonly current *in vivo* MRS data are collected at the clinical field strength of 1.5T, with an increasing trend toward utilization of 3 T, using phased-array and endorectal coils. The advantage of the increase to 3 T is the doubling of the S/N, and theoretically a drastic improvement in spectral resolution. However, prostate spectroscopy and/or imaging at 3 T is still being evaluated and, in many ways, it is still in its infancy. Toward the same end of increased S/N, the endorectal coil produces spectra with ~10-fold increase in S/N versus a pelvic phased coil (Kurhanewicz et al., 2002). Normally, cancer is differentiated from healthy prostatic tissue by an increased ratio of choline (Cho) plus creatine (Cr) to citrate (Cit), as in [Cho + Cr]/Cit. Current *in vivo* MR spectroscopy has a reported sensitivity, specificity, and accuracy in detecting prostate cancer of up to 89%, 77%, and 83%, respectively (Squillaci et al., 2005). This means that MR spectroscopy is more sensitive than MR imaging, biopsy, and digital rectal exams. More crucially, when MRS was combined with magnetic resonance spectroscopic imaging (MRSI) it increased the latter's

specificity and accuracy in detecting cancer by 14% - 15% (Squillaci et al., 2005). These data clearly illustrate the additional benefit patients might have if they undergo MRS in conjunction with MRSI. However, *in vivo* MRS is often excluded at the time of diagnosis as it is considered time consuming and not cost effective as a screening tool.

In the last five years, as clinical interest in prostate *in vivo* MRSI increased, MR spectroscopic studies have become an adjunct to MRSI. Briefly, MRSI is a metabolic imaging modality that combines the imaging capability of MRI with a very limited amount of spectroscopic information provided by MRS. The metabolite distributions of a single metabolite (or the ratio of two metabolites) are recorded for the voxels of interest (in 3 dimensions) and surrounding tissue, then overlaid onto the MRI image to examine metabolites within the anatomy. Interpretation of MRSI is a complicated procedure for the prostate due to the potential of several histological tissue types being present in a single voxel. Thus, there can exist an inability to correlate the single metabolite (or ratio) with specific pathology. Despite the ability of MRS to indicate abnormal regions, it is normally used secondarily to MRI/MRSI to study the metabolism of areas that are already believed to be anomalous. Only time will reveal if the experimental research that supports the use of MRS will be enough to vault *in vivo* MR spectroscopy out of its current back-seat clinical role.

3.2 Ex Vivo Prostate Cancer Magnetic Resonance Spectroscopy

The history of *ex vivo* prostate spectroscopy is almost 20 years long, and has been improved drastically by the implementation of HRMAS techniques. The original aims of *ex vivo* PC spectroscopy were: to gain a better insight into the underlying tumor biology accompanying metabolic changes; to correlate tumor pathology with spectroscopic results; and to improve techniques for *in vivo* application. Unlike *in vivo* spectroscopy, *ex vivo* is rarely used in conjunction with imaging.

3.21 Ex Vivo Fluid Studies

Seminal fluid studies linking changes in citrate concentrations to prostate tumorogenesis started after citrate was discovered in human semen by Schersten in 1929 (Averna et al., 2005). Prostatic fluid makes up 50% of the volume of seminal fluid and it is, therefore, logical to assume that changes in prostate metabolism may be indicated in changes in seminal fluid metabolite concentrations.

In 1997, one of the first published studies linking seminal fluid to disease status using MRS focused on correlating several metabolites with one another and with the malignant condition (Lynch and Nicholson, 1997). In the words of the authors, "High resolution proton (1H) NMR spectroscopy is an ideal analytical probe where a range of structurally dissimilar metabolites are being measured in a complex matrix such as a biofluid. In addition to analytical information forthcoming from NMR measurements, dynamic molecular interactions of metabolites can also be studied in whole biofluids such as binding phenomena, metal complexation reactions, and enzymatic conversions" (Lynch et al., 1997). It was found in the study (with 38 subjects) that the concentration of citrate and spermine are linearly correlated ($p < 0.05 \times 10^{-10}$), and that there is a significant difference between the ratio of citrate to spermine in PC patients vs. normal controls ($p < 0.02$). It was also found that no significant differences existed between samples collected by prostatic massage and those from ejaculation. This study was followed by a more recent and more striking study into the relationship between citrate concentration in seminal fluid and the presence of prostate cancer.

Averna et al. (2005) indicated that 1H NMR measurement of citrate in seminal fluid could provide a new, rapid, noninvasive screening method. While this claim could be very relevant, the study could not report sensitivity or specificity, presumably due to a small sample pool (n = 7). Not only were the authors able to distinguish differences in citrate concentrations between PC patients, healthy controls, and men with BPH, they also developed spectral editing techniques to identify citrate in clinical *in vivo* MRS. The authors noted that seminal MRS could take as little as 5 min, rendering it more useful as a screening tool than currently lengthy and non cost-effective clinical MRS. Furthermore, they suggest that combining measurements of citrate and other metabolites could lead to the development of computer aided pattern recognition techniques. Studies by Lynch et. al. (1997) and Averna, et al. (2005) demonstrate the novelty, benefits, and deficits of using *ex vivo* MRS to study biofluids.

The most evident advantage of studying seminal fluid is its noninvasive nature. Collecting seminal fluid, either voluntarily or by prostate massage, is as straight forward as obtaining blood samples and less invasive than a core needle biopsy. Unfortunately, the published studies on MRS of seminal fluid are marred by meager participation ($n < 50$ from < 30 subjects in all studies). It is very plausible that most men have a conceptual issue with volunteering their seminal fluid, feeling that such specimen collection is embarrassing and crosses the boundary of personal space. While the seminal fluid studies presented here are promising, more conclusive evidence will likely be needed before such measures are clinically implemented. Moreover, advanced prostate cancer is known to mutate the acini, prohibiting the excretion of prostatic fluid. Thus, such fluid examination is only possible for a select group of patients. Finally, threshold values for what citrate concentration is conclusively indicative of each clinical status need to be established if seminal fluid MRS is to be of any utility. Nevertheless the results of the aforementioned studies are very encouraging and may help refine *in vivo* prostate MRS and establish more accurate screening methods.

3.22 Pre-Clinical Drug Studies

Studies discussed in this section are classified, for the purpose of this chapter, as ex vivo because they examine either cell lines or animal models. The authors acknowledge, however, that incorporation of MRS for drug studies clinically would most likely involve in vivo MRS. A very different, but equally intriguing, application of MRS is in toxicology studies, monitoring the metabolic effects of certain drugs on prostate cells and/or tumors. Presently, differentiating agents to treat prostate cancer are being explored in clinical trials. Such chemicals promote cell differentiation and apoptosis, often through poorly understood mechanisms of actions. Phenylacetate (PA) and phenylbutyrate (PB) are two such aromatic acids being investigated as differentiation inducers. Milkewitch et al. (2005) described the behavior of these compounds by treating DU145 human prostate carcinoma cells with PA and PB, then monitoring the metabolic changes induced with 1H and 31P diffusion-weighted MRS. DU145 cells (originally established from a metastasic brain lesion of prostate carcinoma) are a model of androgen-independent prostate cancer. In the study the cells were cultured then treated with 10 mM PA or PB while being continually monitored via MRS for 16 h. The single pulse, water suppressed spectra gathered on the 9.4 T spectrometer revealed significant metabolic changes in the signals from lactate, mobile lipids and neutral amino acids, fatty acids, total choline, and glycerophosphorylcholine (GPC). The results were compared with electron and light microscopy to associate metabolic changes with morphological variations. Further analysis of the spectroscopy and microscopy data indicates that PB treatment causes an arrest in the G1 phase of

the cell cycle leading to induction of apoptosis. Phenylacetate treatment, on the other hand, leads to an accumulation of G2/M cells and did not induce apoptosis (Milkevitch et al., 2005). Thus, the two differentiating agents, while structurally similar, affect different stages of the cell cycle. Not only did this study elucidate the cellular effects of PB and PA, it also demonstrates the feasibility of using MRS to monitor metabolic changes and analyze toxicological effects of potential chemotherapeutic agents.

The capacity of MRS to be used as a non-invasive monitor of drug efficacy is also supported by a study utilizing 1H and 31P spectroscopy to discriminate if genetic prodrug activation therapy (GPAT) could be used to treat hormone refractory prostate cancer (Eaton et al., 2001). Hormone refractory prostate cancer is an advanced disease with poor prognosis. Novel therapies being explored include gene therapy, often in combination with immunotherapy. Disease management of this type has demonstrated tumor-specific immune response, and GPAT functions by inserting 'suicide' genes (usually the herpes simplex virus thymadine kinase enzyme/ ganciclovir prodrug system) into tumor cells. Cells treated with GPAT not only die during the cell cycle, but also initiate an immune response important for the 'bystander effect' and, potentially, distant metastasis. Clinical trials, as of the early 2000s, produced limited clinical response, and MRS was proposed as a means to directly monitor cellular effects of the GPAT system. Serial monitoring similar to the previously described PA/PB study was undertaken. However, in the GPAT study MRS was done *in vivo* on animals from two mouse models. Significant changes were observed in tumor ATP/Pi and phosphomonester (PME)/phosphate ratios. In tumors of treated animals the ATP/Pi ratio increased, while the PME/phosphate ratio decreased; in contrast, contrarily, tumors of the control animals had a decrease in the ATP/Pi ratio and no change over time of the PME/phosphate ratio (Eaton et al., 2001). Changes to the PME/phosphate ratio are commonly observed in human prostate tumors, and are associated with an increased response to treatment. Further data from this study showed metabolic changes associated with GPAT system are similar to those produced by other, more widely used, chemotherapies. It was also reported that these metabolic effects, established by the MR spectra, were also present in cells undergoing subject to the "bystander effect." These data support the use of MRS to observe the effects of drugs *in vivo*.

The above-discussed studies expressly recommend the use of MRS for examining the toxicological effects of drugs ear marked as potential prostate cancer therapies. While we are encouraged by these studies, there remains a lack of clinical interest in utilizing this methodology. One explanation for this may be the slow pace at which clinical paradigms for treatment change. As previously mentioned, radical prostatectomy remains the gold-standard of treatment. Understandably, without reliable *in vivo* disease indicators that suggest the rate of tumor growth, many patients may not feel comfortable taking novel drugs to treat their disease when an alterative to remove the tumor entirely exists. One would hope that as early diagnosis and drug discovery increase, there may be more of a clinical demand to study new drug treatments, at which point *in vivo* MRS alone (or in conjunction with MRI) may be the best way to monitor treatment.

3.23 High Resolution Magic Angle Spinning Proton Magnetic Resonance Spectroscopy

Ex vivo prostate HRMAS 1HMRS has advanced rapidly and is currently being tested in our lab as a potential new diagnostic modality. In 2001 we first reported the use of the HRMAS 1HMRS methodology for investigating prostate cancer. The pivotal aspects of the study were the ability to successfully analyze delicate prostate tissues with HRMAS 1HMRS, and the capacity

to quantify the heterogeneous sample pathology following spectroscopic measurement. The demonstration that both MRS and pathology data could be collected from the same sample indicated the potential for HRMAS 1HMRS to become a critical tool in PC research. The study found that spermine concentration (measured by MRS) correlated with volume percentage (vol%) normal prostatic epithelial cells (Cheng et al., 2001). This study not only verified the capacity of HRMAS 1HMRS to probe the metabolic characteristics of prostate cancer, it also exemplified the importance of methodologies that preserve tissue architecture.

A report from Swanson et al. (2003) on the diagnostic ability of *ex vivo* prostate HRMAS 1HMRS examined the ability of MRI/3D-MRSI to target samples for *ex vivo* analysis, and the capacity of HRMAS 1HMRS to predict cancer. The authors found that HRMAS 1HMRS was able to significantly distinguish normal from malignant tissue on the basis of higher levels of citrate and the polyamines in normal gland, and increased choline compounds (choline, GPC, and phosphocholine) in cancer. The samples analyzed were chosen based on *in vivo* MRI/3D-MRSI analysis, and it was found the *in vivo* techniques targeted healthy tissue with 90% accuracy and cancerous gland with 71% accuracy. They were able to confirm that *ex vivo* analysis yields similar findings to *in vivo* analysis, mainly that choline is greatly increased in the malignant condition. They also studied several metabolites (including the polyamines) that were not quantifiable with *in vivo* methods.

The ability to analyze a wider array of metabolites could lead to the elucidation of the underlying biology of prostate tumorogensis, and the improvement of *in vivo* MRS/MRSI. While the study can be viewed as highly successful, the authors acknowledge the difficulties arising in their study from prostate heterogeneity. While generalizations could be made regarding "increased" or "decreased" metabolite levels, there was a large amount of variegation between metabolite profiles due to the heterogeneity of the samples. The spectral profiles were most reflective of the sample's disease status when 20% of the sample was cancer; unfortunately, this is a condition that could not be guaranteed as the 3D-MRSI had an accuracy of 71% when targeting tumor tissue. The authors acknowledged that a more comprehensive study needed to be undertaken, specifically one which overcomes issues of heterogeneity and find a way to classify metabolites so they reflect tissue pathology regardless of the percentage of each feature present.

Our group (Cheng et al., 2005) reported the first preclinical study of HRMAS 1HMRS on 199 *ex vivo* human prostate samples from prostatectomies of 82 PC cancer patients. Prior to this large-scale investigation of prostate cancer metabolic profiles, several technical developments have been necessary for prostate HRMAS to reach an optimal level. First, it must be acknowledged that prostatic tissues are fragile. While tissue architecture of breast samples may not be damaged at spinning rates up to 3.6 kHz, accurate prostate tissue histopathology is only possible if the tissue is spun at a rate < 1 kHz. For the purpose of most studies a speed of 600 or 700 Hz is sufficient. Unfortunately, at these relatively slow rates, spinning side bands (SSBs) appear in the spectra and overlap with regions of interest. Two SSB reduction schemes can be utilized to procure the entire prostate tissue spectra. First, a rotor-synchronized delays alternating with nutation for tailored excitation (DANTE) sequence is effective if the spectral SSBs are primarily from water and not from other metabolites (Taylor et al., 2003). If, however, the sample is contaminated by alcohol (a frequent occurrence in surgical samples) or SSBs are produced by metabolites, a editing procedure known as Min(A,B) is most useful (Burns et al., 2005). Min(A,B) is a mathematical model which edits two spectra (A,B) acquired at different spinning rates, such as 600 and 700 Hz, by the formula: $(A + B - |A - B|/2)$ (Burns et al., 2005).

Following the establishment of spectral editing protocols, we were able to test the efficacy of using prostate metabolic profiles (measured with HRMAS 1HMRS) to predict disease status (Cheng et al., 2005). The study found that tissue metabolite profiles can: 1) differentiate malignant from benign samples (colleted from the same patient); 2) correlate with patient PSA levels; 3) differentiate between aggressive and indolent tumors; and 4) predict tumor perineural invasion. All of these results were found to be significant with $P < 0.03$. Receiver operating characteristic curves (ROC) revealed the overall accuracy of using metabolic profiles to determine cancerous status was 98.2% based on evaluating paired metabolic profiles and histopathological analysis of samples from 13 patients.

Equally importantly, histopathology not only allows the correlation of the metabolic profile and tissue components, but also shows that no coincidental correlation exists between patient status information and percent volume of each cell type; this shows that the metabolic profiles are independent of cell volume, doubling time, etc. Additionally, though AJCC/TMN staging does not currently include tumor perineual invasion, the perineural invasion status does indicate prostate tumor aggressiveness and is thus incorporated into treatment planning. The ability of metabolic profiles generated by HRMAS 1HMRS to indicate cancer or benign status, identify tumor aggressiveness, and correlate with other clinical status features indicates the potential for said profiles to provide a "second opinion" for biopsy evaluation. More fascinatingly, the data supports the analysis of a biopsy core to predict tumor stage, even if the core itself contains no cancerous glands. Our findings indicate that HRMAS 1HMRS has the ability to generate profiles indicative of processes actively taking place, which has great implications in patient prognosis and treatment, but have not yet manifested in morphological changes identifiable histopathologically.

We value the potential impact this research may have on the prostate clinic, but we also acknowledge the unanswered questions that remain following our investigations. First, our data indicate the existence of a metabolic field effect, i.e., malignant metabolic profiles are delocalized from cancer cells. However, at present we do not know if these cancer metabolic profiles are only local near cancer containing glands or global throughout the organ. We do not have data regarding the proximity of the histo-benign tissue sample we analyzed to the cancer in the gland. Secondly, it is almost impossible to identify "normal" controls due to the possibility that many men over the age of 39 harbor a certain amount of PC in their prostate gland, which questions even the use of human autopsy if the entire prostate has not been thoroughly examined for complete pathological composition.

IV. FUTURE DIRECTIONS

Magnetic resonance spectroscopy, both *in vivo* and *ex vivo*, has advanced a remarkable way in a relatively short period of time. The biomedical uses for the modality, combined with the potential for further clinical integration, may present it as an extremely powerful tool for the management of human prostate cancer. The diversity of the studies presented here are an illustration of the wide scope of MRS and its implementation in the diagnosis, prognosis, and treatment planning for PC. We appreciate that histopathology remains the gold standard by which all techniques will be evaluated, but we also understand the limitations of this extremely subjective field. The objectivity of MRS combined with its ability to be non-invasive, sensitive, and specific will, we believe, continue to assert MRS as a premier technique of the 21st century.

In the coming months and years we look forward to further refinement of MRS, which will come in two major waves: first, the improvement of *in vivo* MRS and second, the clinical

acceptance of using *ex vivo* MRS. Regarding *in vivo* MRS, as technology improves (resulting in higher clinical field strength and better resolution of individual metabolites) the cost of MRS will decrease, which means that patients will have the benefit of utilizing MRS in conjunction with MRSI. This will be especially imperative if treatment moves away from radical prostatectomy and MRS becomes necessary to monitor tumor reaction to novel therapies. *Ex vivo* MRS, on the other hand, must bridge the gap between phenomenal research work and clinical inclusion. For this purpose we consider HRMAS 1HMRS to have the most relevance and potential.

As acceptance grows and we can move away from the "seeing is believing" method of diagnosis, new clinical paradigms will emerge in which MRS is an integral part. An essential part of improving MRS will come in the form of full automation, such that an entire metabolic profile can be constructed from a spectra, compared to literature values, and assigned a disease status. The ability of metabolic profiles to designate benign from malignant, and the aggressiveness of a tumor if present, would make spectroscopy a clinical necessity. One proposed combination of *in vivo* and *ex vivo* work would be to use *ex vivo* HRMAS 1HMRS to define the predictive metabolic signatures; these signatures could then be searched for *in vivo* to provide more accurate diagnosis or preventative screening. In this way spectroscopy will provide a truly 'systems biology' approach to PC management, one in which *in vivo* and *ex vivo* modalities are used in combination to provide the maximal benefit to the patient. In closing, we hope this chapter has provided an introductory account of the theory of MRS and the rationale behind applying MRS to prostate cancer, as well as the current and future prospects for spectroscopy in the field of medical oncology as it relates to prostate cancer.

ACKNOWLEDGEMENT: Authors acknowledge support from NIH grants CA211478, CA095624,and DOD grant W81XWH-04-1-0190.

REFERENCES

Ackerstaff, E., Pflug, B. R., Nelson, J. B., and Bhujwalla, Z. M. 2001. Detection of increased choline compounds with proton nuclear magnetic resonance spectroscopy subsequent to malignant transformation of human prostatic epithelial cells. Cancer Res. 61: 3599-3603.

Andrew, E.R., Bradbury, A., and Eades, R.G. 1959. Removal of dipolar broadening of nuclear magnetic resonance spectra of solids by specimen rotation. Nature 183: 1802-1803

Averna, T. A., Kline, E. E., Smith, A. Y., and Sillerud, L. O. 2005. A decrease in 1H nuclear magnetic resonance spectroscopically determined citrate in human seminal fluid accompanies the development of prostate adenocarcinoma. J. Urol. 173: 433-438.

Burns, M. A., Taylor, J. L., Wu, C. L., Zepeda, A. G., Bielecki, A., Cory, D., and Cheng, L. L. 2005. Reduction of spinning sidebands in proton NMR of human prostate tissue with slow high-resolution magic angle spinning. Magn. Reson. Med. 54: 34-42.

Carter, H. B., Walsh, P. C., Landis, P., and Epstein, J. I. 2002. Expectant management of nonpalpable prostate cancer with curative intent: preliminary results. J. Urol. 167: 1231-1234.

Cheng, L. L., Burns, M. A., Taylor, J. L., He, W., Halpern, E. F., McDougal, W. S., and Wu, C. L. 2005. Metabolic characterization of human prostate cancer with tissue magnetic resonance spectroscopy. Cancer Res. 65: 3030-3034.

Cheng, L.L., Lean, C.L., Bogdanova, A., Wright, S.D. Jr., Ackerman, J.L., Brady, T.J., and Garrido, L. 1996. Enhanced resolution of proton NMR spectra of malignant lymph nodes using magic-angle spinning. Magn Reson Med. 35: 653-658.

Cheng, L.L., Anthony, D.C., Comite, A.R., Black, P.M., Tzika, A.A., and Gonzalez, R.G. 2000 Quantification of microheterogeneity in glioblastoma multiforme with ex vivo high-resolution magic-angle spinning (HRMAS) proton magnetic resonance spectroscopy. Neuro-oncoly 2: 87-95.

Cheng, L. L., Wu, C., Smith, M. R., and Gonzalez, R. G. 2001. Non-destructive quantitation of spermine in human prostate tissue samples using HRMAS 1H NMR spectroscopy at 9.4 T. FEBS Lett. 494: 112-116.

Daviss, B. 2005. Growing pains for metabolomics. The Scientist 19: 25-28.

Eaton, J. D., Perry, M. J., Todryk, S. M., Mazucco, R. A., Kirby, R. S., Griffiths, J. R., and Dalgleish, A. G. 2001. Genetic prodrug activation therapy (GPAT) in two rat prostate models generates an immune bystander effect and can be monitored by magnetic resonance techniques. Gene Ther. 8: 557-567.

Farrar, T. C. 1997. Introduction to Pulse NMR Spectroscopy. Madison, Farragut Press.

Franklin, R. B., Milon, B., Feng, P., and Costello, L. C. 2005. Zinc and zinc transporters in normal prostate and the pathogenesis of prostate cancer. Front. Biosci. 10: 2230-2239.

Kurhanewicz, J., Swanson, M. G., Nelson, S. J., and Vigneron, D. B. 2002. Combined magnetic resonance imaging and spectroscopic imaging approach to molecular imaging of prostate cancer. J. Magn. Reson. Imag. 16: 451-463.

Lynch, M. J., and Nicholson, J. K. 1997. Proton MRS of human prostatic fluid: correlations between citrate, spermine, and myo-inositol levels and changes with disease. Prostate 30: 248-255.

Milkevitch, M., Shim, H., Pilatus, U., Pickup, S., Wehrle, J. P., Samid, D., Poptani, H., Glickson, J. D., and Delikatny, E. J. 2005. Increases in NMR-visible lipid and glycerophosphocholine during phenylbutyrate-induced apoptosis in human prostate cancer cells. Bioch. Biophys. Acta. 1734: 1-12.

Podo, F. 1999. Tumour phospholipid metabolism. NMR Biomed. 12: 413-439.

Ransohoff, D. F., McNaughton Collins, M., and Fowler, F. J. 2002. Why is prostate cancer screening so common when the evidence is so uncertain? A system without negative feedback. Am. J. Med. 113: 663-667.

Sohlman, M. E. 2003. Nobel Foundation directory 2003. Vastervik, Sweden, AB CO Ekblad.

Swanson, M. G., Vigneron, D. B., Tabatabai, Z. L., Males, R. G., Schmitt, L., Carroll, P. R., James, J. K., Hurd, R. E., and Kurhanewicz, J. 2003. Proton HR-MAS spectroscopy and quantitative pathologic analysis of MRI/3D-MRSI-targeted postsurgical prostate tissues. Magn. Reson. Med. 50: 944-954.

Taylor, J. L., Wu, C. L., Cory, D., Gonzalez, R. G., Bielecki, A., and Cheng, L. L. 2003. High-resolution magic angle spinning proton NMR analysis of human prostate tissue with slow spinning rates. Magn. Reson. Med. 50: 627-632.

Figure Legends:

Figure 1: When (a) a 90° B_1 pulse is applied to the nuclei in the magnetic field they (b) dephase from one another, (c) precess, and finally (d) the full macroscopic magnetization has returns the nuclei to the Z plane.

Figure 2 modified from (Farrar 1997): From L to R are the position of the nuclei in the rotating frame, the FID signal generated, and spectral signal after Fourier transformation for nuclei among the: (a) +x axis, (b) +y axis, (c) –x axis, and (d) –y azix.

Figure 3 modified from (Farrar 1997): (a) spectra produced by the same sample without MAS and (b) with MAS, clearly indicating the metabolites are distinguishable and quantifiable with MAS but not conventional MRS; (c) expansion for better detail is provided of the 3.0 to 0.5 ppm range of the MAS spectra in (b).

Figure 4: HRMAS 1HMRS spectra of an intact, surgical prostate sample. The sample was spun at 600 and 700 Hz, which was non-damaging to the tissue architecture, and histopathology on the slide shown was performed on the same sample following spectroscopic analysis.

Figure 1:

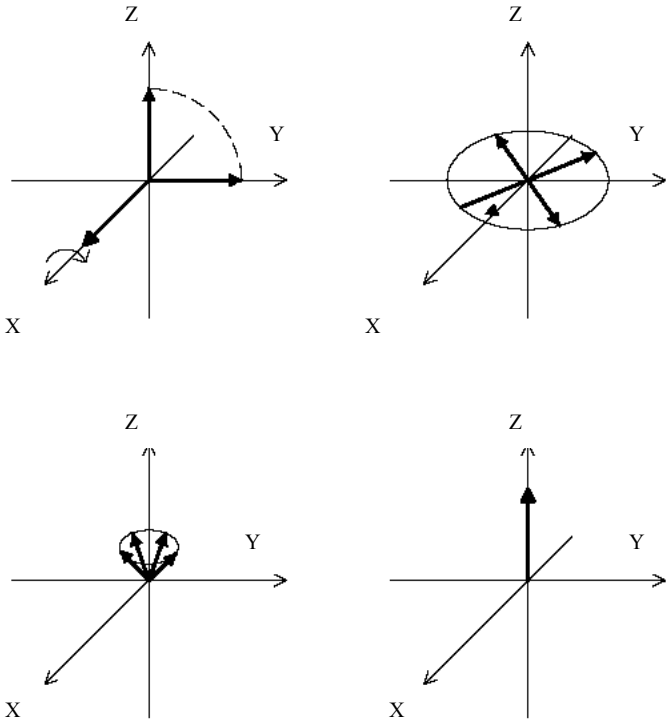

Figure 2:

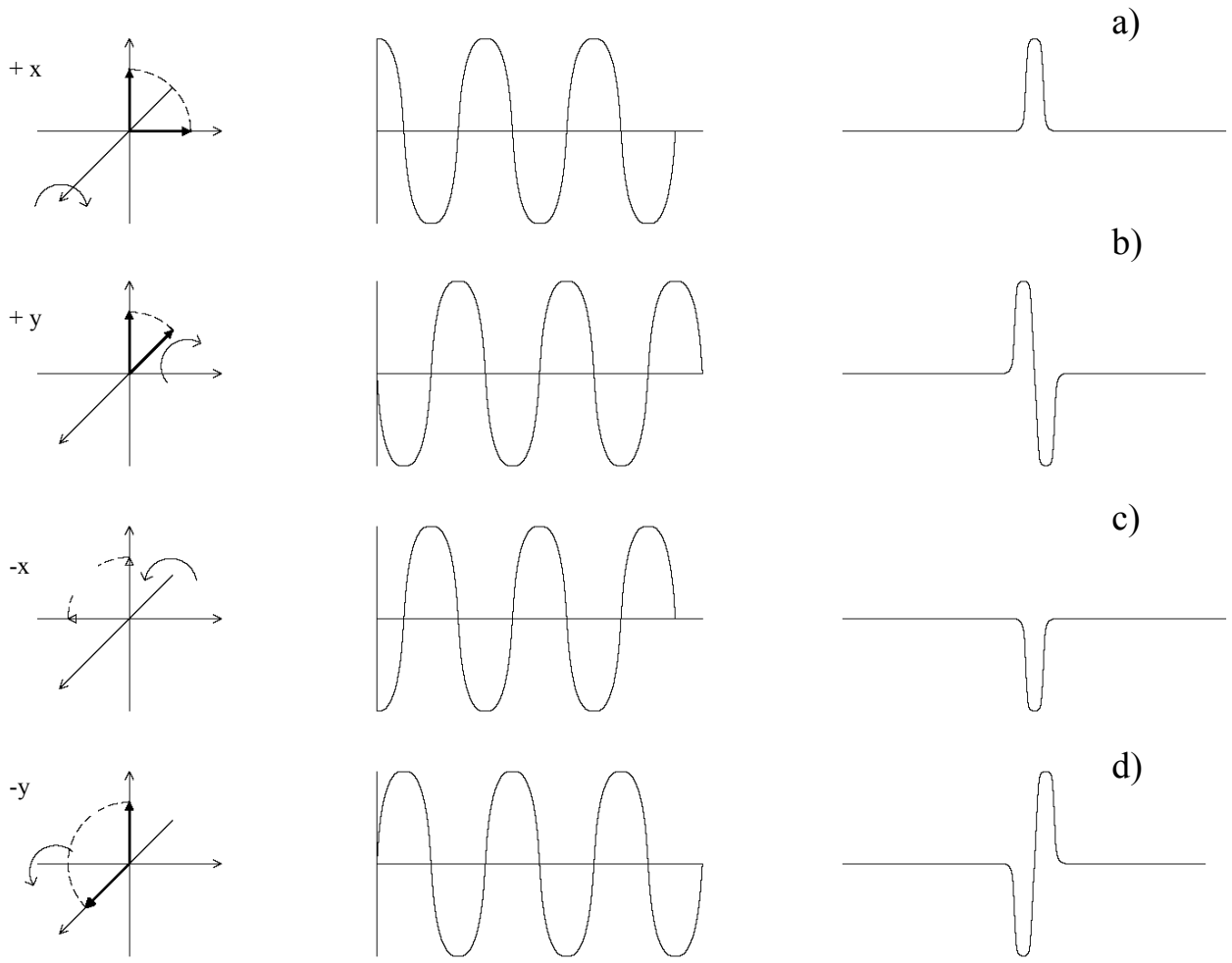

Figure 3:

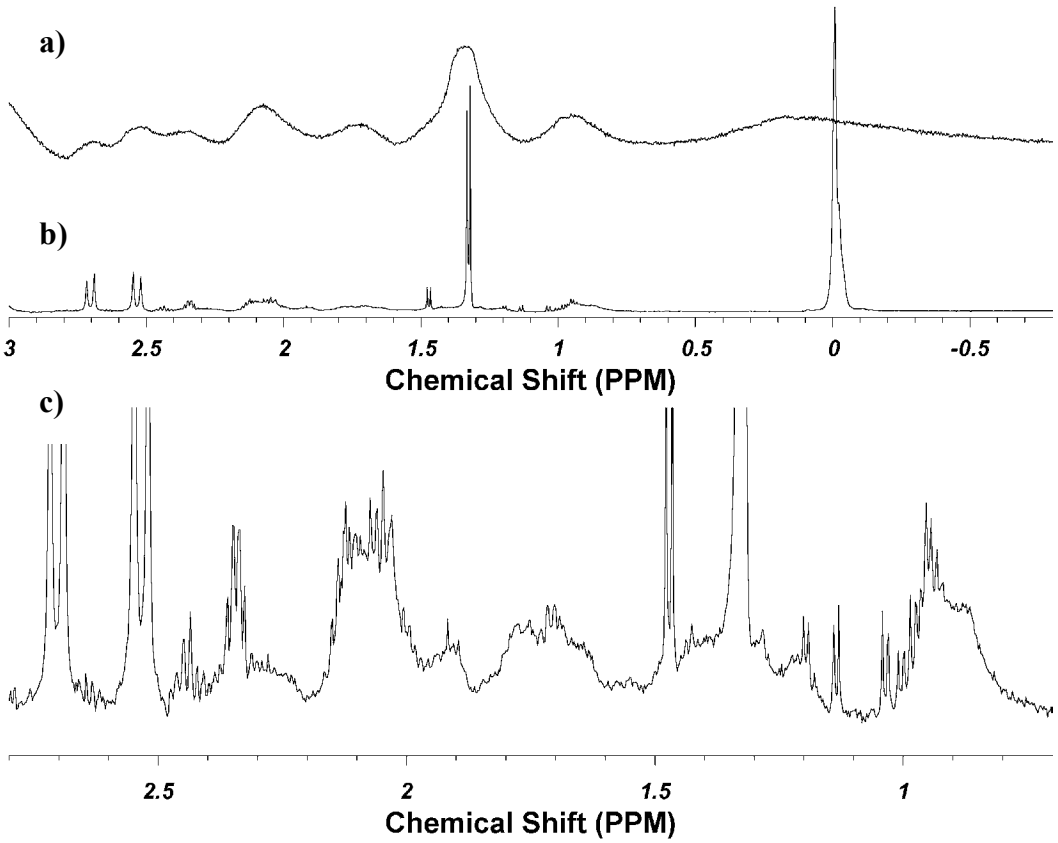
a)
b)
3
2.5
2
1.5
1
0.5
0
-0.5
Chemical Shift (PPM)
c)
2.5
2
1.5
1
Chemical Shift (PPM)

Figure 4:

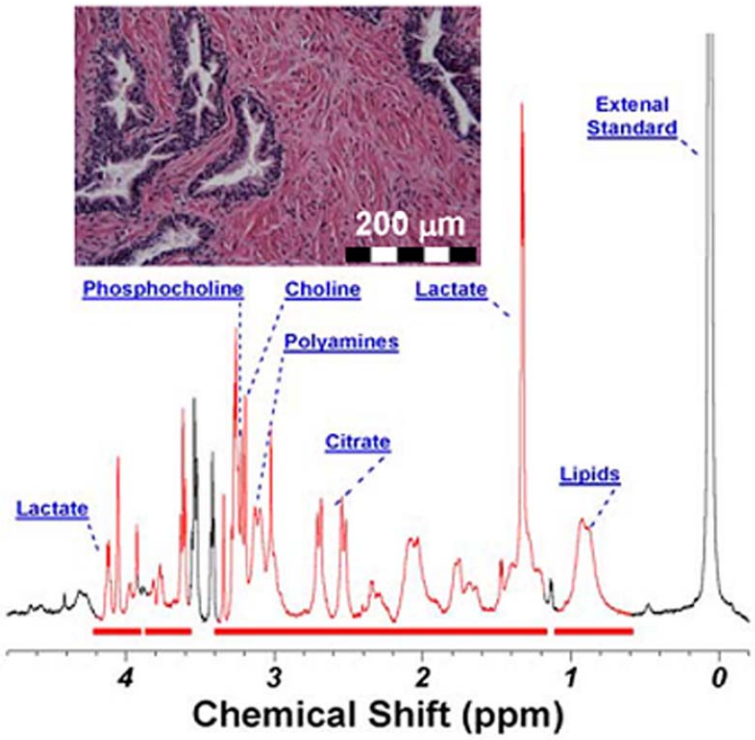
200 µm
Extenal Standard
Phosphocholine
Choline
Lactate
Polyamines
Citrate
Lipids
Lactate
4
3
2
1
0
Chemical Shift (ppm)

(12) INTERNATIONAL APPLICATION PUBLISHED UNDER THE PATENT COOPERATION TREATY (PCT)

(19) World Intellectual Property Organization
International Bureau

(43) International Publication Date
19 October 2006 (19.10.2006)

PCT

(10) International Publication Number
WO 2006/110768 A2

(51) International Patent Classification: Not classified

(21) International Application Number:
PCT/US2006/013517

(22) International Filing Date: 11 April 2006 (11.04.2006)

(25) Filing Language: English

(26) Publication Language: English

(30) Priority Data:
60/670,391 12 April 2005 (12.04.2005) US

(71) Applicant *(for all designated States except US)*: **THE GENERAL HOSPITAL CORPORATION** [US/US]; 55 Fruit Street, Boston, Massachusetts 02114 (US).

(72) Inventors; and

(75) Inventors/Applicants *(for US only)*: **CHENG, Leo, L.** [US/US]; 9 Ruggiero Way, Andover, Massachusetts 01810 (US). **JENKINS, Bruce** [US/US]; 76 Lorimer Road, Belmont, Massachusetts 02144 (US). **WU, Chin-Lee** [US/US]; 42 Parker Street, Newton, Massachusetts 02459 (US). **DAI, Guangping** [US/US]; 230 Parker Street, Action, Massachusetts 01720 (US). **HALPERN, Elkan, F.**; 169 Albemarle Road, Newton, Massachusetts 02460 (US).

(74) Agent: **ABELEV, Gary**; DORSEY & WHITNEY LLP, 250 Park Avenue, New York, New York 10177 (US).

(81) Designated States *(unless otherwise indicated, for every kind of national protection available)*: AE, AG, AL, AM, AT, AU, AZ, BA, BB, BG, BR, BW, BY, BZ, CA, CH, CN, CO, CR, CU, CZ, DE, DK, DM, DZ, EC, EE, EG, ES, FI, GB, GD, GE, GH, GM, HR, HU, ID, IL, IN, IS, JP, KE, KG, KM, KN, KP, KR, KZ, LC, LK, LR, LS, LT, LU, LV, LY, MA, MD, MG, MK, MN, MW, MX, MZ, NA, NG, NI, NO, NZ, OM, PG, PH, PL, PT, RO, RU, SC, SD, SE, SG, SK, SL, SM, SY, TJ, TM, TN, TR, TT, TZ, UA, UG, US, UZ, VC, VN, YU, ZA, ZM, ZW.

(84) Designated States *(unless otherwise indicated, for every kind of regional protection available)*: ARIPO (BW, GH, GM, KE, LS, MW, MZ, NA, SD, SL, SZ, TZ, UG, ZM, ZW), Eurasian (AM, AZ, BY, KG, KZ, MD, RU, TJ, TM), European (AT, BE, BG, CH, CY, CZ, DE, DK, EE, ES, FI, FR, GB, GR, HU, IE, IS, IT, LT, LU, LV, MC, NL, PL, PT,

[Continued on next page]

(54) Title: SYSTEM, METHOD AND SOFTWARE ARRANGEMENT FOR ANALYZING AND CORRELATING MOLECULAR PROFILES ASSOCIATED WITH ANATOMICAL STRUCTURES

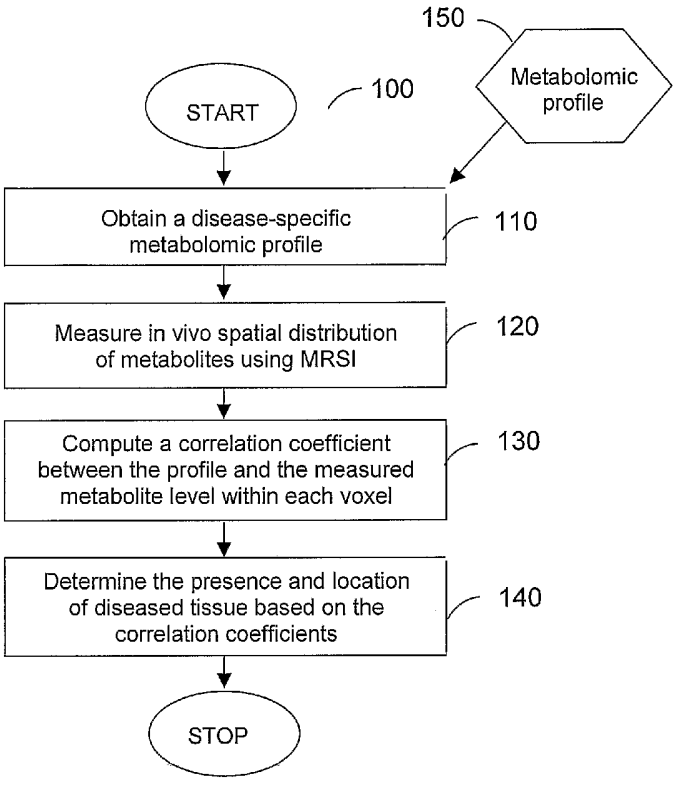

(57) Abstract: A system, method and software arrangement according to exemplary embodiments of the present invention are provided which can use molecular profiles obtained from unaltered human tissue specimens for clinical purposes including disease diagnoses and treatment evaluations. For example, spatial distributions of chemical species including metabolites within the tissue may be obtained using radiological techniques such as magnetic resonance spectroscopy imaging. Disease-specific profiles may be obtained by comparing the distributions of chemical species obtained in ex vivo tissues with pathological observations made on them using statistical analysis. The disease-specific profiles may then be correlated with in vivo or ex vivo molecular profiles to obtain spatial maps that can provide a more sensitive and accurate detection of diseased tissue. Thus, such exemplary systems, methods and software arrangements can include the ability to receive information relating to the distribution of at least three chemical species in the tissue of interest, compare this information statistically to a predetermined profile and, based on the statistical correlation between the information and the profile, determine certain characteristics of the tissue of interest such as, e.g., the presence or absence of diseased tissue.

WO 2006/110768 A2

RO, SE, SI, SK, TR), OAPI (BF, BJ, CF, CG, CI, CM, GA, GN, GQ, GW, ML, MR, NE, SN, TD, TG).

Published:

— *without international search report and to be republished upon receipt of that report*

For two-letter codes and other abbreviations, refer to the "Guidance Notes on Codes and Abbreviations" appearing at the beginning of each regular issue of the PCT Gazette.

SYSTEM, METHOD AND SOFTWARE ARRANGEMENT FOR ANALYZING AND CORRELATING MOLECULAR PROFILES ASSOCIATED WITH ANATOMICAL STRUCTURES

CROSS-REFERENCE TO RELATED APPLICATION(S)

This application claims priority from U.S. Patent Application Serial No. 60/670,391, filed April 12, 2005, the entire disclosure of which is incorporated herein by reference.

GOVERNMENTAL SUPPORT

The research leading to the present invention was supported, at least in part, by the United States National Institute of Health (NIH) under Grant number R01CA095624, and by the United States Department of Defense (DOD) under Grant number W81XWH-04-1-0190. Thus, the U.S. government may have certain rights in the invention.

FIELD OF THE INVENTION

The present invention relates to a system, method and software arrangement for analyzing and correlating molecular profiles associated with anatomical structures. More particularly, the profiles can be obtained using radiological methodologies and other in vivo analytical techniques for clinical uses, including but not limited to disease diagnoses and treatment evaluations.

BACKGROUND INFORMATION

Magnetic resonance spectroscopy (MRS) technologies can be used to detect the presence and concentration of various chemical species, such as metabolites, in a homogeneous magnetic field. These techniques may be utilized to determine a presence of chemical species in living tissues non-invasively, which can assist in evaluating physiological or pathological conditions present. Techniques for measuring metabolite concentrations in bodily tissues are described, e.g., in U.S. Patent No. 5,500,592.

Magnetic resonance imaging (MRI) techniques, which are widely used diagnostic radiology tools, are derived (in part) from MRS. MRI can be used to measure a single chemical, e.g., water, in an artificially-created inhomogeneous magnetic field. The inhomogeneity of the magnetic field generally allows for a detailed imaging of anatomical structures and tissues that can be presented as two-dimensional cross sections. Such cross sections may be combined to provide a three-dimensional mapping of tissue structures within the structures/tissues.

Combining the spectroscopy principles with the imaging capabilities developed over the past two decades for MRI technology presents the possibility of non-invasively measuring metabolic molecules in living tissue, and has led to the development of *in vivo* MRS and, more recently, to the generation of magnetic resonance spectroscopy imaging (MRSI) techniques for a diagnostic radiology. For diagnostic purposes, MRSI data (in the form of either single metabolite concentrations or simple ratios of the concentrations of two metabolites) have been mapped onto morphological MR images to determine the presence of metabolites within specific structures/tissues.

High-resolution magic-angle spinning (HRMAS) proton MRS is a technique that has been developed for an intact tissue analysis. Magic-angle spinning, generally used to reduce a resonance line-width in solid-state nuclear magnetic resonance (NMR) analyses, can subject sample structures/tissues to mechanical rotations in a kilohertz range at the "magic angle" of 54°44' from the direction of the spectrometer's static magnetic field while spectroscopy is recorded. When applied to intact tissues, HRMAS can produce highly-resolved spectra, allowing an identification of individual metabolites while preserving tissue pathological morphology. HRMAS techniques are described, e.g., in Cheng LL et al., "Enhanced resolution of proton NMR spectra of malignant lymph nodes using magic-angle spinning," Magn Reson Med, 1996; 36:653-8.

Prostate specific antigen (PSA) screening is a technique that can permit increased detection of prostate cancer at early stages. However, this histopathology technique alone generally may not reliably direct an appropriate treatment. The utility of PSA testing in detecting clinically significant prostate tumors has been clinically shown. However, there is a significant incidence of 'indolent' cancers in PSA

screening of certain populations. The inability of a PSA screening technique to distinguish 'indolent' from 'aggressive' carcinomas can result in adverse consequences of over-treatment.

The Gleason Score (GS) is a widely adopted histological grading system/technique for a prostate biopsy. This system/technique is described in, e.g., Gleason D., "Classification of prostatic carcinomas," Cancer Chemother Rep 1966; 50:125. For example, such a system/technique generally assigns the tumor two grades from 1 to 5, one to primary (dominant) and one to secondary (sub-dominant) tumor growth patterns. The sum of the two numbers (between 2 and 10) determines a tumor score. A value of 2 to 4 for the score is considered a "well-differentiated disease," whereas a value of 5 to 7 for the score indicates "moderately differentiated adenocarcinomas," and a value of 8 to 10 for the score denotes "poorly differentiated cancers." A higher score signifies greater probability of tumor extracapsular spread, nodal involvement, and metastases. However, more than 70% of cancers now diagnosed with PSA tests are GS 6 and 7 tumors, which generally may not be further sub-categorized without an additional surgical intervention (i.e., prostatectomy) to assess tumor virulence, and clinical outcomes for these patients have differed significantly.

Clinical and histopathological determinations from prostatectomy can be used to obtain or calculate another parameter, i.e., the stage of tumor, node, and metastasis (TNM) according to the American Joint Commission on Cancer (AJCC). This classification is described, e.g., in Carroll P, Lee K, Fuks Z, Kantoff P., "Cancer of the Prostate," in: DeVita V, Hellman S,Rosenberg S, editors, Cancer: Principle and Practice of Oncology, 6th ed., Philadelphia: Lippincott Williams & Wilkins; 2001.

Although prostate tumor grade and stage can be determined independently, they are often intrinsically related. However, it can be difficult to distinguish aggressive from indolent cancers, individually, even with the assistance of empirical nomograms. Therefore, the proper treatment course for the majority of patients (having a GS of 6-7) may be difficult to determine. Clinical evidence generally shows that the outcome for some patients of this group is satisfactory, while it is poor for other patients. Tumor aggressiveness, manifested in bioactivities, may be responsible for the variability of observed outcomes among individuals initially

diagnosed with GS 6 or 7 tumors. Therefore, modalities for quantifying the biological characteristics of tumor aggressiveness are needed.

The limited prognostic insight of such clinical measures such as PSA, GS, and digital rectal exams often leads to either unnecessarily aggressive or dangerously conservative treatment. For example, radical prostatectomies can result in impotence and/or incontinence of urine. Prostate tumor heterogeneity can further impair the usefulness of histopathology in comprehensive evaluations, as prostate cancer cells may elude biopsy analysis, producing false negative results.

Accordingly, more reliable and informative prognostic tools are needed.

SUMMARY OF EXEMPLARY EMBODIMENT OF THE INVENTION

According to the present invention, exemplary systems and methods are provided for improved diagnosis and treatment evaluations based on, e.g., in vivo analysis of bodily tissues based on magnetic resonance technology. For example, systems, methods and software arrangements are provided for accurately detecting and diagnosing diseases, including cancer, by comparing the detected levels of a plurality of molecules such as, e.g., metabolites, with disease- or condition-specific metabolomic profiles or maps.

Exemplary embodiments of the present invention relate to a concept that in a biological system, such as a human body, various metabolite processes or pathways are interconnected. Thus, alterations of the overall metabolite profiles (e.g., metabolomics) may be more sensitive and specific to a particular physiological and/or pathological condition than the change in any single metabolite or in the ratio of any two metabolites. This concept is similar to the correlation of genomic profiles that are based on thousands of genes on a microarray to identify the presence or propensity for a particular disease condition to manifest, rather than the disease or condition being based on the expression of only one or two genes.

Certain exemplary embodiments of the systems, methods and software arrangements in accordance with the present invention can utilize an objective modality capable of sensitively measuring unaltered human tissue specimens for

cancer-related changes in metabolic profiles, without destroying pathological structures.

In further exemplary embodiments of the present invention, in vivo disease detection may be achieved by comparing a plurality of measured metabolite parameters to specific profiles that may be indicative of the presence of the disease. Such profiles may be constructed or defined, for example, by ex vivo MRS measurements of a cancerous tissue, and a comparison of the observed metabolite profiles with those obtained from surrounding healthy tissue. Metabolomic profiles may then be constructed using statistical analysis to yield a strong correlation between combinations of individual metabolite profiles, and the presence or absence of a specific disease or condition.

For example, in vivo chemical shift imaging (CSI) or MRSI techniques may be used to obtain a MRS measurement for each voxel in the tissue region of interest. These measurements may then be compared to a particular metabolomic profile (e.g., a linear combination of certain measured metabolites established previously using ex vivo analysis) that corresponds to a specific condition. The voxel MRS data may be processed to produce a parameter indicating the correlation between the measured metabolite levels and the metabolomic profile. This parameter can be mapped onto a corresponding 2D or 3D morphological image. The voxels having metabolite concentrations that are highly correlated with the metabolomic profile can indicate regions of tissue having a heightened degree of disease involvement.

In still further exemplary embodiments of the present invention, other molecular measurements, including but not limited to genomic and proteomic measurements, may be compared to corresponding profiles in a manner similar to that described above for metabolomics. Such measurements can be made using modalities other than the magnetic resonance spectroscopy including, but not limited to, MRI, perfusion and diffusion MRI, genomic based molecular imaging, mass spectroscopy, optical spectroscopy, CT, or any other radiological or analytical technique that may be used in a clinical setting.

In yet further exemplary embodiments of the present invention, metabolite levels measured with magnetic resonance spectroscopy may be combined

with measurements of other molecular species, and the results can be compared to combined disease-specific metabolomic and molecular profiles. Thus, numerically measurable parameters other than those produced by metabolomics can also be included in the disease-specific molecular profiles, and used for an evaluation of measured tissue concentrations, if their inclusion improves the overall accuracy of disease identification.

In further exemplary embodiments of the present invention, an analysis of metabolites or other molecules measured ex vivo in a surgically removed organ may be compared to metabolomic or other profiles to assist pathologists in identifying, e.g., some or all of the cancerous or diseased regions within the removed tissue, and in predicting overall patient pathological status that cannot be achieved currently and clinical at a biopsy stage. An example can be an analysis of a prostate biopsy specimen, which may be performed to ensure a more accurate diagnosis.

These and other objects, features and advantages of the present invention will become apparent upon reading the following detailed description of embodiments of the invention, when taken in conjunction with the accompanying figures showing illustrative embodiments of the invention and the appended claims.

BRIEF DESCRIPTION OF THE DRAWINGS

FIG. 1 is a is a flow diagram of an exemplary embodiment of a method according to the present invention;

FIG. 2A is an illustration of an exemplary HRMAS spectrum obtained from a sample of intact prostate tissue;

FIG. 2B is a cross-sectional image of a prostate tissue sample used for a histopathology analysis;

FIG. 3 is an exemplary three-dimensional plot of detected chemical species correlated with pathological observations in prostate tissues in accordance with an exemplary embodiment of the present invention;

FIG. 4 is an exemplary canonical plot resulting from a discriminant analysis of the three variables shown in FIG. 3 in accordance with an exemplary embodiment of the present invention;

FIG. 5 is an exemplary graph of a receiver operating characteristic curve corresponding to the plot shown in FIG. 3;

FIG. 6A is an exemplary plot showing a correlation of the metabolite phosphocholine with pathological observations in prostate tissues;

FIG. 6B is an exemplary plot showing a correlation of the metabolite choline with pathological observations in the prostate tissues;

FIG. 7 is an exemplary plot showing a correlation of serum PSA levels with principal component 2 measured in histo-benign prostate tissues;

FIG. 8A is an exemplary plot showing a correlation of measured levels of principal component 2 with tumor stages in the prostate tissues;

FIG. 8B is an exemplary plot showing a correlation of measured levels of principal component 5 with tumor stages in the prostate tissues;

FIG. 8C is an exemplary plot showing a correlation of measured levels of principal component 2 with tumor stages in prostate tissues having a Gleason score of 6 or 7;

FIG. 8D is an exemplary plot showing a correlation of measured levels of principal component 5 with tumor stages in prostate tissues having a Gleason score of 6 or 7;

FIG. 9 is a high-resolution image of a removed cancerous human prostate that includes benign structures;

FIG. 10 is a block diagram of an system in accordance with exemplary embodiments of the present invention;

FIG. 11A is an exemplary matrix of spectral peak intensities;

FIG. 11B is an exemplary matrix of principal component (PC) coefficients determined from the peak intensities shown in FIG. 11A;

FIG. 11C illustrates an exemplary calculation that may be used to determine the PC coefficients; and

FIG. 12 illustrates the configuration of a phantom study of three metabolite solutions of varied concentrations together with the in vivo and ex vivo spectra obtained from these solutions.

DETAILED DESCRIPTION OF EXEMPLARY EMBODIMENTS

Systems, methods and software arrangements according to exemplary embodiments of the present invention may be used to analyze and evaluate molecular profiles measured in two- or three-dimensional radiological images for the purpose of clinical uses including, but not limited to, disease diagnoses and treatment evaluations. For example, using such exemplary embodiments, issue metabolomic or molecular profiles can be used to differentiate cancer or other conditions from histologically benign tissues. The use of profiles that include a plurality of detectable metabolites and/or molecules can be more accurate for detection of cancer or other diagnoses than conventional single-metabolite maps obtained using, e.g., MRSI, which may be based only on the presence or concentration of a single measurable metabolite or molecule.

For example, changes in tumor metabolism, downstream from genomic and proteomic transformations, may reflect disease-related biochemical reactivity, and can precede histologically observable changes in cell morphology. Detection and analysis of metabolite and molecular concentrations associated with such changes can offer an early way for predicting tumor behaviors.

With the assumption of the existence of disease specific metabolomic profiles, these exemplary embodiments of the present invention can be utilized. For instance, a conventional MRI scanner with CSI or MRSI capability can be used to convert the current CSI single spectrum for each voxel into metabolomic maps for different pathological interests with an addition of a converting subroutine.

FIG. 1 illustrates a flow diagram of an exemplary method 100 according to certain embodiments of the present invention. This exemplary flow diagram provides exemplary steps that may be used to obtained improved detection and diagnosis of diseased tissue within an anatomical structure. For example, a disease-specific metabolomic profile can first be obtained (step 110). This profile may include the local presence, absence, concentration, and/or concentration ratios of a plurality of detectable metabolites that may be characteristic of the diseased tissue. Disease-specific metabolomic and/or molecular profiles that may be used with exemplary embodiments of the present invention can be established using an ex vivo analysis of diseased and healthy tissue specimens. Other detectable chemical species may also be included in these profiles. Multiple profiles, each of which may be

associated with a different disease or condition, can be used in a single diagnostic analysis of a patient. Once a particular profile is obtained, it may be subsequently employed for detection of the corresponding disease or condition on any number of patients.

Metabolite distributions in the tissue being examined can then be determined using MRSI techniques (step 120). The distributions can be measured for each metabolite and/or other chemical species that are included in the profile being used. If more than one profile is being used to simultaneously detect the presence of more than one disease or condition, each metabolite or chemical species included in each profile used may be measured. The distributions may be determined using conventional analytical procedures. This can be achieved by detecting the concentration of a metabolite or species within each voxel, or volume element, targeted or scanned by the MRSI equipment or other detection apparatus. Other detection methods may be used instead of or in addition to MRSI techniques to obtain spatial distributions of metabolites and/or other species. Such detection methods can include, but are not limited to, perfusion and diffusion MRI, genomic-based molecular imaging, mass spectroscopy, optical spectroscopy, CT, or other radiological or analytical techniques.

A local correlation factor for the selected metabolomic profile may then be calculated or otherwise determined by a statistical comparison of the profile with the detected levels or concentrations of metabolites or other chemical species. This correlation factor may be determined for each voxel or other volume of tissue analyzed (step 130). The calculation can be performed using a modification of the routines that are used in some analytical equipment to calculate single-metabolite maps. The correlation factor can be determined as a statistical match to the selected metabolomic profile, which may be expressed as a linear combination of concentrations and/or concentration ratios of single-metabolites or other chemical species.

The correlation of the detected metabolite and/or chemical species concentrations with the selected profile can be displayed or presented as a spatial distribution of the local calculated correlation parameters. This distribution can be overlaid onto a morphological image of the tested tissue. Using such representation

of the correlation parameter, diseased regions of tissue may be identified as those exhibiting a high correlation with the selected profile (step 140). Tissue regions that exhibit concentrations of a plurality of metabolites and/or chemical species that are strongly correlated with profiles characteristic of the diseased tissue thus can provide an indicator that the tissue may be diseased. Such a correlation based on a plurality of metabolites and/or chemical species can be a more accurate and reliable indicator that the tissue is likely diseased or benign over the diagnostic methods that are based on the local concentration of a single metabolite or species.

A metabolomic profile 150 or other disease- or condition-specifc profile can be provided for use by the exemplary method 100 to allow for a detection of the disease or condition in the tissue being examined. Such profiles may be determined only once (or more than once) for each disease or condition, and may be used in subsequent analyses of many patients. Each profile can be determined using statistical analysis, such as the principal component analysis approach described hereinbelow. The analysis can be performed by correlating the concentrations or relative amounts of two or more detectable chemical species in a tissue sample with one or more characteristics of the tissue sample evaluated by other techniques, such as quantitative morphology of cross sections. The tissue sample can be in vivo when analyzed with localization techniques, or ex vivo, such as a biopsy sample or a removed bodily organ. Several profiles can be formulated for a single disease or condition. These profiles may be based on the same, distinct, or overlapping sets of chemical species such as metabolites.

Example

As an example, an investigation was performed to assess the sensitivity of local prostate metabolites in predicting prostate cancer status using the system, method and software arrangement according to exemplary embodiments of the present invention. 199 prostate tissue samples were obtained from 82 prostate cancer patients after prostatectomy. Prostate metabolite profiles were measured with intact tissue high-resolution magic angle spinning (HRMAS) proton MRS at 14.1T, and further analyzed with quantitative pathology.

Prostate metabolite profiles obtained from principle component analysis (PCA) of tissue spectra were correlated with pathology quantities and with patient serum PSA levels using a linear regression analysis. These correlations were evaluated against the pathological status of each patient using statistical analysis of variance (ANOVA).

Paired-t-tests indicated that tissue metabolite profiles can differentiate malignant from benign samples obtained from the same patient ($p<0.005$), and that these results correlate with patient serum prostate-specific antigen (PSA) levels ($p<0.006$). Metabolite profiles obtained from histologically benign tissue samples of GS 6-7 prostates can delineate a subset of less aggressive tumors ($p<0.008$) and predict tumor perineural invasion within the subset ($p<0.03$). These results indicate that MRS metabolite profiles of biopsy tissues may help to direct treatment plans by providing more accurate assessment of prostate cancer pathological stage and aggressiveness. Such assessment can be determined conventionally using histopathological methods only after a prostatectomy is performed.

A more detailed description of this application of diagnostic methods in accordance with certain exemplary embodiments of the present invention is provided below.

The patient population and individual prostate tissue samples were characterized by Gleason Score (GS) as: GS 5 [2 cases, 5 samples]; GS 6 [51 cases, 126 samples]; GS 7 [21 cases, 53 samples]; GS 8 [4cases, 9 samples]; and GS 9 [4 cases, 6 samples]. The patient population was also characterized by the American Joint Committee on Cancer/Tumor-Node-Metastasis (AJCC/TNM) stages (6^{th} ed.) as: T2ab [24 cases, 59 samples]; T2c [44 cases, 112 samples]; T3a [10 cases, 17 samples]; T3b [3 cases, 5 samples]; and T3ab [1 case, 6 samples]. The few T3a, T3b and T3ab cases identified were combined and collectively labeled in the study as T3. Surgical tissue samples were snap-frozen in liquid nitrogen and stored at -80°C until MRS analysis was performed. Patient clinical statuses were obtained from pathology reports.

A Bruker (Billerica, MA) AVANCE spectrometer operating at 600MHz (14.1T) was used for all MR experiments. Tissue samples were placed into a 4mm rotor with 10μl plastic inserts. 1.0μl of D_2O was added for field locking.

Spectra were recorded at 3°C with the spectrometer frequency set on the water resonance, and a rotor-synchronized DANTE experimental protocol was applied with spinning at 600 and 700Hz (±1.0Hz). 32 transients were averaged at a repetition time of 5s.

The resulting spectra were processed with AcornNMR-Nuts (Livermore, CA) using the following procedures: 0.5Hz apodization before Fourier transformation, baseline correction, and phase adjustment. Resonance intensities used were determined by calculating integrals of curve-fittings with Lorentzian-Gaussian line-shapes measured from either 600Hz or 700Hz HRMAS spectrum.

Following the spectroscopy analysis, samples were fixed in 10% formalin, embedded in paraffin, cut into 5μm sections at 100μm intervals throughout the entire sample, and stained with hematoxylin and eosin.

An Olympus BX41 Microscope Imaging System (Melville, NY), in conjunction with the image analyzer SoftImaging-MicroSuite™ (Lakewood, CO), was used to quantify sample cross-sections. The areal percentage of cancer cells, normal epithelial cells, and stroma were independently estimated for each cross-section to the nearest 5%. The volume percentage of these features was calculated from the sizes of the cross-sections and the corresponding areal percentage of each pathological feature within each cross section.

Analysis of the spectroscopy and cross-sectional results was performed to correlate spectral metabolite profiles with tissue pathologies and patient clinical statuses. Prior to investigating such correlations, the metabolite matrix was subjected to statistical data treatment in the form of a principal component analysis (PCA) to reduce the complexity of spectral data.

Because certain pathological processes can manifest simultaneous changes in several measurable metabolite levels, a change in concentration of a single metabolite may not accurately represent a specific underlying process. PCA attempts to identify principal components (PCs), which are combinations of the measured concentrations, that may indicate distinct pathological processes if they exist in the set of the samples. A positive contribution of a certain metabolite, for example, can indicate the elevation of the metabolite within the component (process), whereas a negative contribution can suggest a suppression of the metabolite.

The components can then be ordered by the extent to which they are associated with variability in the observed cases. If more metabolites are affected by a biological mechanism (i.e., a greater number of metabolites are associated with a particular PC), the association is greater. A stronger change in the metabolite level caused by a biological mechanism also yields a greater association. Additionally, the incidence of a process can be a factor in the associated variability. Extremely rare and extremely common biological mechanisms cause little variability, whereas biological mechanisms that are seen in approximately half of the cases have the greatest variability associated with them.

Principal components (PCs) may differ from the actual underlying biological mechanism in one important respect. PCs are independent, whereas actual biological mechanisms may affect some common metabolites. For example, one biological mechanism may elevate metabolites A, B, C, and D, while suppressing E and F. A second biological mechanism might elevate A and B, while suppressing C, D, E, and F. As both biological mechanisms affect metabolites A, B, E and F in the same way, it is likely that the PCA results may identify a strong component, expressing an elevation of A and B with the simultaneous suppression of E and F. Another possibly weaker component can express metabolites C and D, and may distinguish the first biological mechanism from the second.

Principle component (PC) analysis was performed on the spectra obtained from the prostate tissue samples as described above. Details of the PCA procedure are illustrated in FIGS. 11A-C. In this exemplary procedure, 199 biological tissue samples were obtained from 82 prostatectomy cases. The metabolites associated with the 36 strongest peaks were identified. FIG. 11A illustrates part of a peak intensity matrix of 199 (number of samples) x 36 (number of analyzed metabolites). Each matrix value px,y indicates the peak intensity for each identified peak x as measured in sample y. These values were then converted into a PC coefficient matrix of 36 (number of metabolites) x 36 (number of PCs). A portion of this PC coefficient matrix is shown in FIG. 11B. FIG. 11C illustrates an exemplary calculation used for determining the PC coefficients of FIG. 11B. This exemplary analysis resulted in the identification of 15 principal components (PC1 to PC15) having an eigenvalue greater than 0.5. Details of this study and identification of the

principal components are described, e.g., in Cheng LL, Burns MA, Taylor JL, He W, Halpern EF, McDougal WS, Wu CL, "Metabolic characterization of human prostate cancer with tissue magnetic resonance spectroscopy," Cancer Res 2005; 65(8):3030-3034.

Different metabolite profiles associated with different prostate pathological features (e.g., volume percent of epithelia, cancer cells or stroma) can thus be assessed using a linear regression analysis against these PCs. Paired Student t-tests were used to evaluate the ability of cancer-related PC13 and its major, contributing metabolites, phosphocholine (PChol) and choline (Chol) to differentiate cancerous tissue from histologically benign samples obtained from the same patient. Discriminant analyses were used to generate a canonical plot to achieve the maximum separation between the two groups, with accuracy being analyzed by receiver operating characteristic curves. These analyses are described, e.g., in McNeil BJ, Keller E, Adelstein SJ. "Primer on certain elements of medical decision making," N Engl J Med 1975; 293: 211-5. Student t-tests were used to investigate the relationship between cancer-related PC14 and tumor perineural invasion. The abilities of PC2 and PC5 to differentiate between pathological stages were tested using ANOVA. Statistical analyses were carried out using SAS-JMP (Cary, NC).

The HRMAS MRS technique permits the acquisition of high-resolution proton spectra from intact tissue while preserving tissue architectures for subsequent histopathological analysis. FIG. 2A shows an exemplary illustration of a High-Resolution Magic Angle Spinning (HRMAS) 1H MR spectrum. This spectrum was obtained from intact tissue from the removed prostate of a 61 y.o. patient with Gleason score 6, T2b tumors. A cross-section of this tissue is shown in FIG. 2B. Histopathology analysis of this tissue sample image after spectroscopy measurement indicated that the sample contained 40% histopathologically defined benign epithelium and 60% stromal structures, with no identifiable cancerous glands. The 36 most intense resonance peaks or metabolite groups above the horizontal bars 220 were selected for analyses, while the other regions were excluded from calculation, partly due to surgery-related alcohol contamination. Select cellular metabolites are labeled on the spectrum shown in FIG. 2A.

Conventional methods used prior to HRMAS techniques to achieve high-resolution metabolite profiles included analysis of metabolites after extraction from the samples by chemical solutions, so that the results were sensitive to the applied procedures including completeness of the extraction step. Tumor heterogeneity also limited the usefulness of such extraction methods.

Histomorphological evaluations can be important for an appropriate interpretation of spectroscopic data obtained from tissue samples. In the exemplary procedure described herein, 20 out of 199 analyzed samples from prostate cancer patients contained cancerous glands, while the remaining 179 samples represented histologically benign tissue obtained from cancerous prostates. These observations reflect the infiltrative, heterogeneous nature of prostate cancer. Thus no visible mass may be produced, and the morphology precludes cancer-selective removal of tissue. These factors help to account for the clinical complexity of prostate biopsy.

The PCA procedure was carried out on the concentrations of the 36 most intense resonance peaks or groups assigned to specific metabolites in order to generate PCs representing different variations of tissue metabolite profiles. Because pathological variations were observed among the samples, it is possible that certain PCs may be able to identify these variations. For example, PC2 (reflecting changes in polyamines, citrate, etc.) was found to differentiate epithelia from stroma with statistical significance (16.5% of variance; epithelia: $r=0.381$, $p<0.0001$; stroma: $r=-0.303$, $p<0.0001$). Moreover, both PC13 and PC14 were found to differentiate cancer from stroma (cf. PC14 represents 1.54% of variance; cancer: $r=-0.160$, $p=0.0243$; stroma: $r=0.217$, $p=0.0021$). The difference of variance representation (16.5% vs. 1.54% of the total variability of the standardized 36 metabolites for PC2 and PC14, respectively) is consistent with the observation that only 10% of the samples were identified as cancer-positive, while more than 90% of them were designated epithelium-positive. Not all PCs may be related with the evaluated pathologies. Many principal components may indicate intrinsic differences that are not evaluated, or they may indicate variables such as, e.g., spectrometer instabilities that are not relevant to the establishment of metabolomic profiles..

Histologically-defined cancer-absent (histo-benign) samples were analyzed from 13 out of 18 patients from whom histologically cancer-positive

samples were also analyzed. The three-dimensional plot shown in FIG. 3 of PC13 (300) versus PChol (310) and Chol (320) indicates a separation between the cancerous and histo-benign groups on a plane of observation. Both of these metabolites, PChol (310) and Chol (320), were found to be the major contributors to PC13 (300) and PC14. This observation is consistent with current descriptions in the literature associated witrh the MRS technique of their *in vivo* and *ex vivo* relationship with malignancy. See, e.g., Podo F. "Tumour phospholipid metabolism," NMR Biomed 1999; 12: 413-39. The paired Student's t-test (cancer vs. histo-benign from the same patients) results for PC13 (300), PChol (310) and Chol (320) were found to be 0.012, 0.004 and 0.001, respectively.

Additionally, both PC13 (300) and PC14 were found to be linearly correlated (p: 0.04, 0.02) with the observed volume percentage of cancer cells. Application of discriminant analysis to the three variables PC13 (300), PChol (310) and Chol (320) in FIG. 3 indicated a classification accuracy of about 92.3%. These results are shown in a plot of FIG. 4, which presents the maximum separation between the cancer and histo-benign groups of samples, which was obtained by this particular two-dimensional projection of a three-dimensional plot. An overall accuracy of about 98.2% for the identification of cancer samples was obtained from a receiver operating characteristic (ROC) curve generated from the three variables. This curve 500 is illustrated in FIG. 5. The curve 500 indicates the high degree of accuracy that can be achieved by using the three variables plotted in FIG. 3 to positively identify cancer samples.

FIGS. 6A and 6B show illustrations of the observed levels of the single metabolites PChol (310) and Chol (320), respectively, in benign and cancerous specimens. In contrast to the metabolomic correlations shown in FIGS. 3-5, the single-metabolite results indicate a much lesser correlation with the observed pathological condition. The illustrations provided in FIGS. 6A and 6B verify that pathological conditions can be determined more accurately using metabolite profiles than with single metabolite measurements.

Of the 82 prostatectomy cases studied, patient serum PSA levels prior to surgery were available for 59 of them. 111 histo-benign tissue samples were identified from different prostate zones (central, transitional, and peripheral) of these

59 cases. An evaluation of the relationship between PSA levels and tissue metabolite profiles indicated that PC2 was linearly correlated, with statistical significance, to PSA results. This correlation 700 is illustrated in FIG. 7. Because PC2 was observed to be linearly correlated with the volume percentage of histo-benign epithelial cells, any correlation observed between PSA levels and epithelial volume percentage among the measured samples is unlikely to be coincidental.

Correlations were also determined between PCs and tumor pathological stage. In each of the 199 samples examined, it was observed that PC2 differentiated T2c cancer (prostate-confined; both lobes) from T3 (invading extraprostatic tissue, $p < 0.03$) and T2ab (prostate-confined; one lobe, $p < 0.005$). PC5 was also observed to differentiate T2ab cancer from T2c ($p < 0.003$) and T3 ($p < 0.00005$). PC2 differentiation among tumor stages was again observed to be independent of epithelial content (e.g. T2ab: 21.88±2.59%; T2c: 20.21±1.91%).

The analysis of the 179 histo-benign samples indicated that similar differentiation between tumor stages could be identified for both PC2 and PC5. FIG. 8A shows a graph that indicates that PC2 can differentiate T2c stage tumors from T2ab and T3 tumors. Similarly, the results shown in the graph of FIG. 8B indicate that PC5 can differentiate T2ab from T2c and T3 stages, as defined by AJCC/TNM staging system (6^{th} ed.). Furthermore, when PC2 and PC5 were correlated with histo-benign samples of GS 6 and GS 7 tumors in 162 samples, both of them were capable of identifying the least aggressive tumor (i.e., GS 6 and T2ab tumors in 42 samples) from those in more aggressive groups (GS 6 T2c, GS 6 T3, and GS 7 tumors). These results for PC2 and PC5 are shown in FIGS. 8C and 8D, respectively.

Tumor perineural invasion status, although not yet incorporated in AJCC/TMN staging, can indicate prostate tumor aggressiveness and may aid treatment planning. However, a tumor heterogeneity can prevent a visualization of an invasion in the biopsy samples. A metabolomic profile analysis yielded a statistically significant correlation between PC14 levels and invasion status for all 199 samples studied (126 "+" and 73 "-", $p < 0.01$), the 179 histo-benign samples (103 "+" and 71 "-", $p < 0.035$), as well as the 42 histo-benign samples from GS 6/T2ab tumors (13 "+" and 29 "-", $p < 0.028$). This latter observation may have great clinical significance in identifying and managing the less aggressive tumor group within the

>70% newly diagnosed moderately differentiated tumors. Details of this analysis are provided, e.g., in Cheng et al., Cancer Res, referenced above.

The strong correlations presented above with respect to tumor pathological stages and perineural invasion represents an indication of the potential for the profile analysis method described herein to improve the current pathology in the diagnosis of prostate cancer. Despite its importance in treatment planning, a tumor pathological stage is presently assessed only by resected prostate tissue. The results described herein suggest that metabolite profiles can provide a "second opinion" for prostate biopsy evaluation. An additional biopsy core, obtained to generate metabolite profiles ex vivo, could also help predict tumor stage for cancer-positive patients, even if the core itself is histo-benign.

The phrase "histo-benign" is used in the description herein, e.g., to highlight that the non-cancer status of the tissue samples studied was determined by an exemplary histological examination. The metabolite results presented herein were analyzed using histopathology, which remains the "gold standard" for cancer diagnosis and treatment planning. The metabolite correlations presented herein and verified using these standard analytical techniques suggest that the metabolomic profile analysis may be performed in accordance with exemplary embodiments of the present invention may be a useful tool in providing improved diagnosis of diseased tissue.

Metabolites measured with tissue MRS can be correlated with histopathology findings, and that metabolite profiles can reveal overall tumor clinicopathological status and aggressiveness before either is visible via histopathology analysis. The results described herein demonstrate the diagnostic and prognostic usefulness of the metabolite protocol.

In further exemplary embodiments of the present invention, the system, method and software arrangement according to the present invention described herein may be used to assist pathologists to identify all of the cancerous regions in a surgically removed organ (such as a prostatectomy specimen) to ensure an accurate diagnosis (at least to a large extent). For example, FIG. 9 shows a high-resolution ex vivo image of a cancerous human prostate that is mingled with benign structures, where a morphological image alone may not differentiate cancerous glands

from those that are benign. If tissue chemical profiles are obtained using the a system, method and software arrangement in accordance with exemplary embodiments of the present invention, cancerous regions can be highlighted and differentiated from those regions containing benign structures. Such ex vivo analysis can provide valuable information that can be used by pathologist to target histopathological evaluations on the revealed cancerous regions and to ensure all the cancerous regions are histologically analyzed. This degree of analysis may not be achievable using conventional techniques.

The system, method and software arrangement according to exemplary embodiments of the present invention may be used to achieve in vivo diagnosis of disease. FIG. 12 illustrates a phantom study of three metabolite solutions of varied concentrations that were selected to mimic cancer-related metabolite changes. In this study, a phantom of three spheres 1210, 1220 and 1230 containing these three metabolite solutions (1, 2 and 3) was measured at 9.4T. The spectrum 1240 of solution 1 measured in vivo at 9.4T may be compared with the spectrum 1250 of solution 1 measured ex vivo using high-resolution magic angle spinning (HRMAS). Similarly, the spectra 1260, 1280 of solutions 2 and 3, respectively, measured in vivo at 9.4T may be compared with the spectra 1270, 1290 of these solutions measured ex vivo using high-resolution magic angle spinning (HRMAS). The similarity in the metabolite profiles observed for each in vivo/ex vivo pair suggests that metabolite profiles established with ex vivo analysis can be used to identify metabolites in vivo and to identify regional changes in these metabolites.

FIG. 10 is a block diagram of one exemplary embodiment of a system according to the present invention that can be configured to diagnose diseases or other bodily conditions based on molecular profiles. In this exemplary embodiment, the system 1000 includes an analytical arrangement 1010. This arrangement 1010 can be any analytical equipment capable of detecting chemical species or metabolites in one or more biological tissues using the techniques described herein such as, but not limited to, magnetic resonance imaging, magnetic resonance spectroscopy, magnetic resonance spectroscopy imaging, chemical shift imaging, genomic based molecular imaging, optical imaging, and/or other radiological or analytical techniques. The analytical arrangement 1010 can also be configured to perform a compositional

analysis on the biological tissue 1040. The analysis may be performed with varying degrees of spatial resolution, where the resolution can depend at least in part on the particular analytical technique being performed. The tissue 1040 may be a bodily organ or part or all of a patient's body that is being examined in vivo, and/or an ex vivo tissue such as a removed organ or a biopsy sample. The analytical arrangement 1010 may be configured to detect specific chemical species in the tissue 1040, and/or determine the presence or concentration of various chemical species based on some form of interaction between a generated signal and the biological tissue 1040.

The system 1000 can also include a processor 1020, which may be configured to accept data generated by the analytical arrangement 1010. The processor 1020 can be further configured to perform mathematical operations on this data, for example, to interpret the data or to provide visual representation of the compositions detected in the tissue 1040.

The processor 1020 may be further configured to accept data in the form of one or more metabolic profiles 1050 described above. The processor 1020 may also be configured to perform mathematical operations, such as statistical comparisons between the data received from the analytical device 1010 and the metabolic profile 1050 as described above (that can be stored in a storage arrangement , such as a memory disk, a hard drive, a CD-ROM, etc.). The output of these operations can include correlation coefficients that indicate the degree of matching between the chemical species detected by the analytical arrangement 1010 in the tissue 1040 and the combination of such species specified by the metabolic profile 1050. In certain exemplary embodiments of the present invention, the value of a correlation coefficient can indicate the present or absence of disease or other physiological conditions in the tissue region corresponding to the calculated coefficient. The processor 1020 may be configured to associate a set of such coefficients or similar parameters with specific regions of the biological tissue where data was obtained by the analytical device 1010 to produce the coefficient. The processor 1020 can be configured to perform such operations by executing a software program according to the exemplary embodiment of the present invention thereon.

The processor 1020 can be a separate component that is in communication with the analytical device 1010 or, optionally, it may be part of the

analytical device 1010 that can be located in the same housing. The processor 1020 may also include a plurality of individual processors, some or all of which may be associated with the analytical device 1010 and some or all of which may be present as a separate component such as a data analysis module that can be attached to the analytical device 1010.

The system 1000 may also include a display 1030, which can be in communication with the analytical device 1010 and/or the processor 1020. The display 1030 may be configured to accept data directly from the analytical device 1010 or data that has been processed by the processor 1020, and provide visual representations of the various measurements made by the analytical device 1010. These representations can include, e.g., two-dimensional or three-dimensional maps of the tissue 1040, as well as a spatial representation of any signals detected from the tissue 1040 by the analytical device 1010 such as, e.g., chemical species concentrations. The display 1030 can be capable of displaying maps that illustrate the values of correlation coefficients or other calculated parameters described above, overlayed onto corresponding image of the tissue region. Such maps can be displayed as colors in an image of the tissue structure on the display 1030, where certain colors can correspond to particular ranges of the correlation coefficients. Such displays can provide direct visual information revealing the characteristics of various tissue regions as determined by comparison of the local concentrations of various chemical species with one or more of the metabolic profiles 1050. The display 1030 may also provide information in the form of numerical data obtained from the analytical device 1010 and/or the processor 1020.

The foregoing merely illustrates the principles of the invention. Various modifications and alterations to the described embodiments will be apparent to those skilled in the art in view of the teachings herein. It will thus be appreciated that those skilled in the art will be able to devise numerous systems, arrangements and methods which, although not explicitly shown or described herein, embody the principles of the invention and are thus within the spirit and scope of the present invention. In addition, all publications, articles, patents and patent applications cited above are incorporated herein by reference in their entireties.

CLAIMS

1. A method for determining at least one characteristic in a biological structure, comprising:

receiving a first information relating to a distribution of at least three chemical species within the structure;

comparing the first information to at least one predetermined profile associated with the at least one characteristic to obtain a second information; and

determining at least one characteristic of the biological structure using the second information.

2. The method according to claim 1, wherein the first information is obtained in vivo from the biological structure.

3. The method according to claim 1, wherein the first information is obtained using a radiological analysis technique.

4. The method according to claim 3, wherein the radiological analysis is at least one of a magnetic resonance imaging technique, a magnetic resonance spectroscopy technique, a magnetic resonance spectroscopy imaging technique, a genomic based molecular imaging technique, an optical imaging technique, or a chemical shift imaging technique.

5. The method according to claim 1, wherein the first information comprises a two-dimensional radiological image.

6. The method according to claim 1, wherein the first information comprises a three-dimensional radiological image.

7. The method according to claim 3, wherein the radiological analysis technique comprises a magnetic resonance spectroscopy imaging technique.

8. The method according to claim 1, wherein at least one of the at least three chemical species comprises a metabolite.

9. The method according to claim 1, wherein the at least one predetermined profile comprises a concentration of at least one of the at least three chemical species.

10. The method according to claim 1, wherein the at least one predetermined profile comprises a linear combination of concentrations of the at least three chemical species.

11. The method according to claim 1, wherein the at least one predetermined profile comprises a ratio of concentrations of at least two of the at least three chemical species.

12. The method according to claim 1, further comprising obtaining ex vivo the predetermined profile via an analysis of at least one of the biological structure or a further biological tissue sample.

13. The method according to claim 12, wherein the analysis of the at least one of the biological structure or the further biological tissue sample comprises a pathological analysis.

14. The method according to claim 12, wherein the analysis of the at least one of the biological structure or the further biological tissue sample further comprises a compositional analysis.

15. The method according to claim 12, wherein the compositional analysis includes at least one of a chemical analysis technique, a magnetic resonance imaging technique, a magnetic resonance spectroscopy technique, a magnetic resonance spectroscopy imaging technique, a genomic based molecular imaging technique, or a chemical shift imaging technique.

16. The method according to claim 1, wherein the second information comprises a statistical correlation between the first information and the at least one predetermined profile.

17. The method according to claim 1, wherein the at least one characteristic includes least one of the presence of diseased biological tissue or the absence of diseased biological tissue.

18. The method according to claim 17, wherein the diseased biological tissue includes cancerous tissue.

19. The method according to claim 17, wherein the second information has the form of a two-dimensional distribution.

20. The method according to claim 17, wherein the second information has the form of a three-dimensional distribution.

21. An executable software arrangement for determining at least one characteristic in a biological structure, comprising:

(a) a first set of instructions which is capable of enabling a processing arrangement to receive first information which is associated with a distribution of at least three chemical species within the structure;

(b) a second set of instructions which is capable of enabling a processing arrangement to compare the first information to at least one predetermined profile associated with the at least one characteristic to obtain a second information; and

(c) a third set of instructions which is capable of enabling a processing arrangement to determine at least one characteristic of the biological structure using the second information.

22. The executable software arrangement according to claim 21, wherein the at least one characteristic includes at least one of the presence of diseased biological tissue or the absence of diseased biological tissue in the biological structure.

23. A system for determining at least one characteristic in a biological structure, comprising a processing arrangement configured to:

receive a first information relating to a distribution of at least three chemical species within the structure;

obtain at least one predetermined profile associated with the at least one characteristic;

compare the first information to the at least one predetermined profile associated with the at least one characteristic to obtain a second information; and

determine at least one characteristic of the biological structure using the second information.

24. The system according to claim 23, wherein the at least one characteristic includes at least one of the presence of diseased biological tissue or the absence of diseased biological tissue in the biological structure.

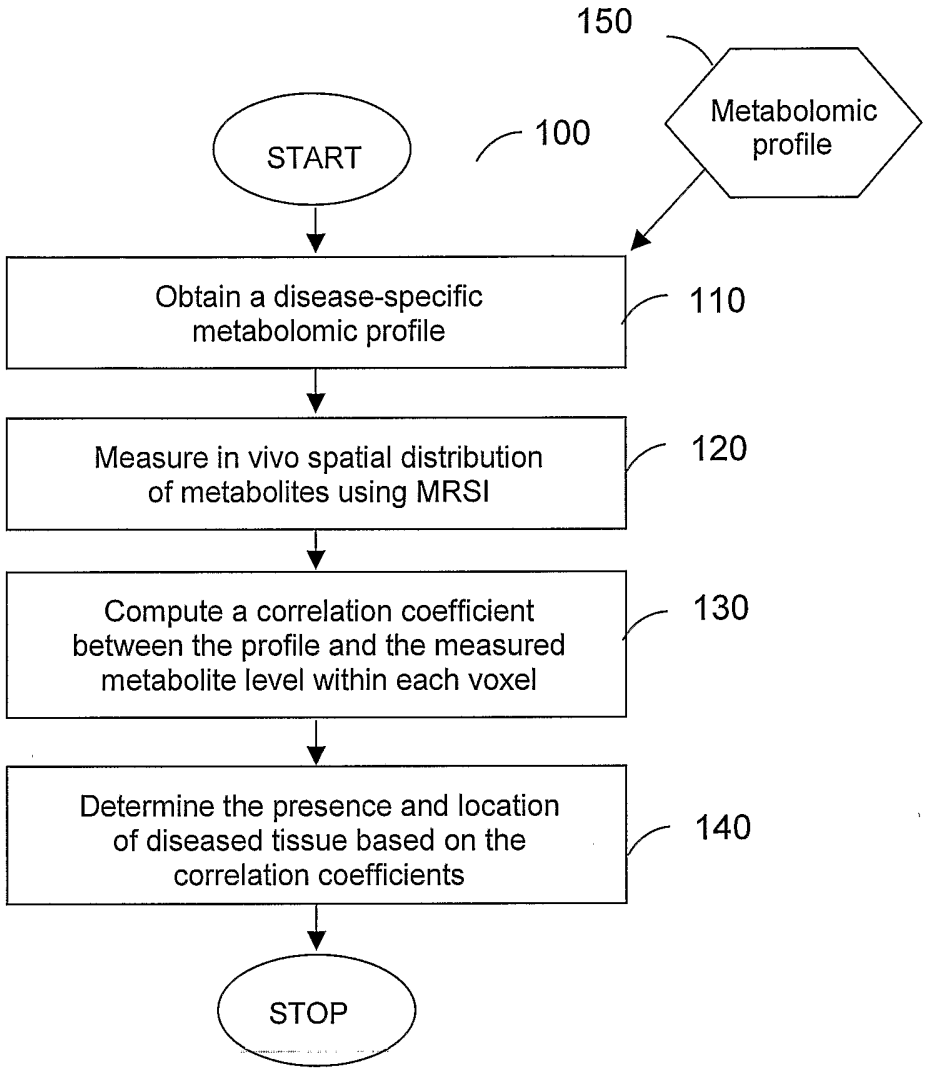
150
Metabolomic profile
START
100
Obtain a disease-specific metabolomic profile
110
Measure in vivo spatial distribution of metabolites using MRSI
120
Compute a correlation coefficient between the profile and the measured metabolite level within each voxel
130
Determine the presence and location of diseased tissue based on the correlation coefficients
140
STOP

FIG. 1

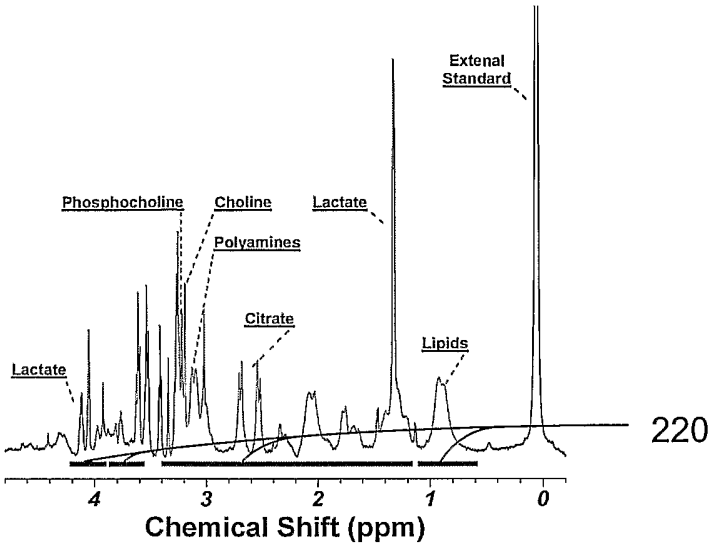

FIG. 2A

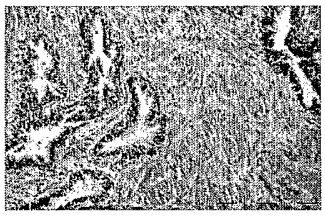

FIG. 2B

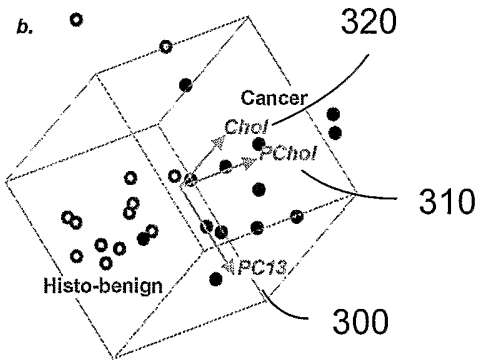

FIG. 3

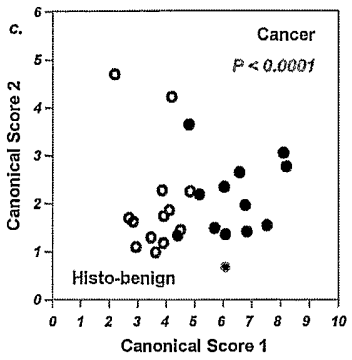
c.
Cancer
P < 0.0001
Histo-benign
Canonical Score 2
Canonical Score 1
0
1
2
3
4
5
6
7
8
9
10

FIG. 4

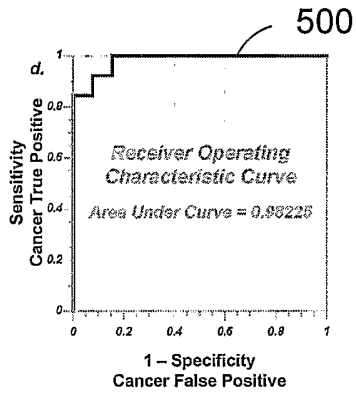
500
d.
Receiver Operating
Characteristic Curve
Area Under Curve = 0.98225
Sensitivity
Cancer True Positive
1 – Specificity
Cancer False Positive
0
0.2
0.4
0.6
0.8
1

FIG. 5

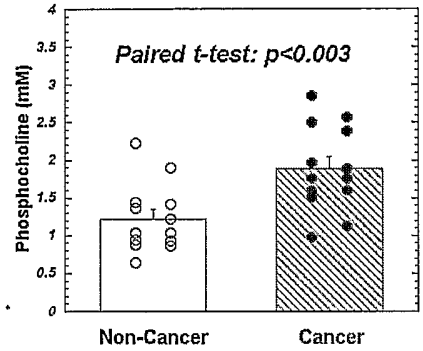
Paired t-test: p<0.003
Phosphocholine (mM)
4
3.5
3
2.5
2
1.5
1
0.5
0
Non-Cancer
Cancer

FIG. 6A

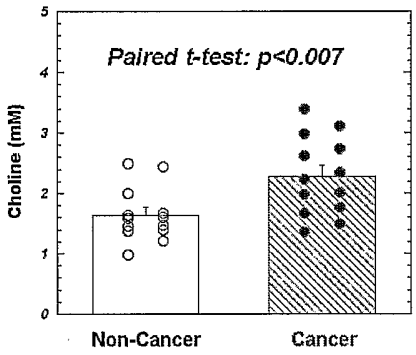
Paired t-test: p<0.007
Choline (mM)
5
4
3
2
1
0
Non-Cancer
Cancer

FIG. 6B

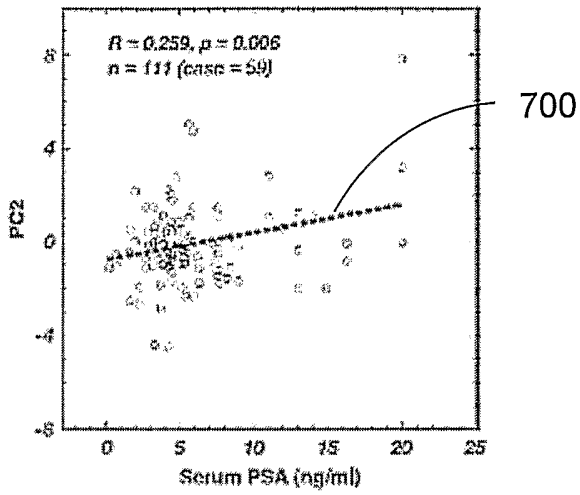
R = 0.259, p = 0.006
n = 111 (case = 59)
PC2
Serum PSA (ng/ml)
0
5
10
15
20
25
-4
0
4
700

FIG. 7

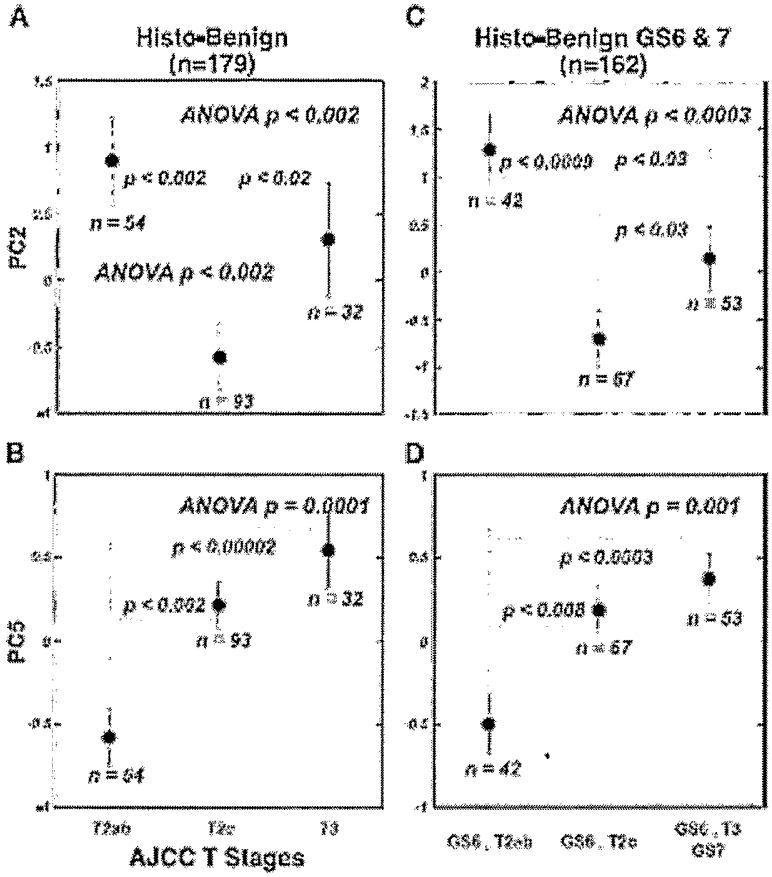
A
Histo-Benign
(n=179)
ANOVA p < 0.002
p < 0.002
p < 0.02
n = 54
n = 32
ANOVA p < 0.002
n = 93
PC2
C
Histo-Benign GS6 & 7
(n=162)
ANOVA p < 0.0003
p < 0.0009
p < 0.03
n = 42
p < 0.03
n = 53
n = 67
B
ANOVA p = 0.0001
p < 0.00002
p < 0.002
n = 32
n = 93
n = 64
PC5
T2ab
T2c
T3
AJCC T Stages
D
ANOVA p = 0.001
p < 0.0003
p < 0.008
n = 53
n = 67
n = 42
GS6 , T2ab
GS6 , T2c
GS6 , T3
GS7

FIG. 8

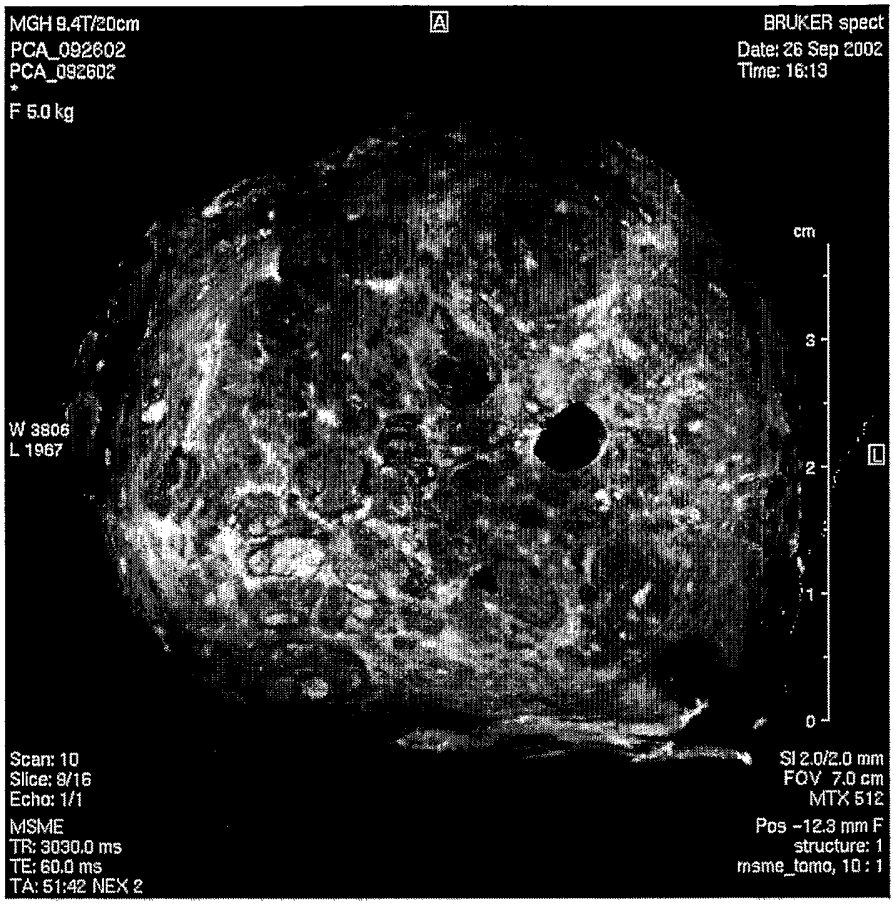
MGH 9.4T/20cm
PCA_092602
PCA_092602
*
F 5.0 kg
A
BRUKER spect
Date: 26 Sep 2002
Time: 16:13
cm
3
2
1
0
W 3806
L 1967
L
Scan: 10
Slice: 9/16
Echo: 1/1
MSME
TR: 3030.0 ms
TE: 60.0 ms
TA: 51:42 NEX 2
SI 2.0/2.0 mm
FOV 7.0 cm
MTX 512
Pos -12.3 mm F
structure: 1
msme_tomo, 10 : 1

FIG. 9

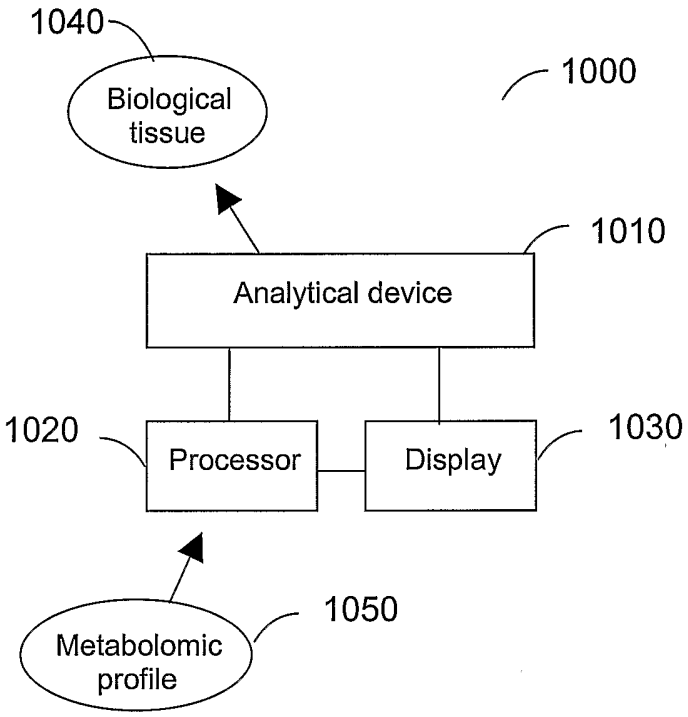
1040
Biological tissue
1000
1010
Analytical device
1020
Processor
Display
1030
Metabolomic profile
1050

FIG. 10

	P1	P2	P3	P35	P36
S1	p1,1	p2,1	p3,1	p35,1	p36,1
S2	p1,2	p2,2	p3,2	p35,2	p36,2
S3	p1,3	p2,3	p3,3	p35,3	p36,3
S198	p1,198	p2,198	p3,198	p35,19	p36,19
S199	p1,199	p2,199	p3,199	p35,19	p36,19

FIG. 11A

	PC1	*PC2*	*PC3*	*PC35*	*PC36*
P1	c1.1	c2.1	c3.1	c35.1	c36.1
P2	c1.2	c2.2	c3.2	c35.2	c36.2
P3	c1.3	c2.3	c3.3	c35.3	c36.3
P35	c1.35	c2.35	c3.35	c35.35	c36.35
P36	c1.36	c2.36	c3.36	c35.36	c36.36

FIG. 11B

Example:
PC3 for Sample 2
= A-(c3,1*p1,2
+c3,2*p2,2
+c3,3*p3,2+ ...
+c3,36*p36,2)

FIG. 11C

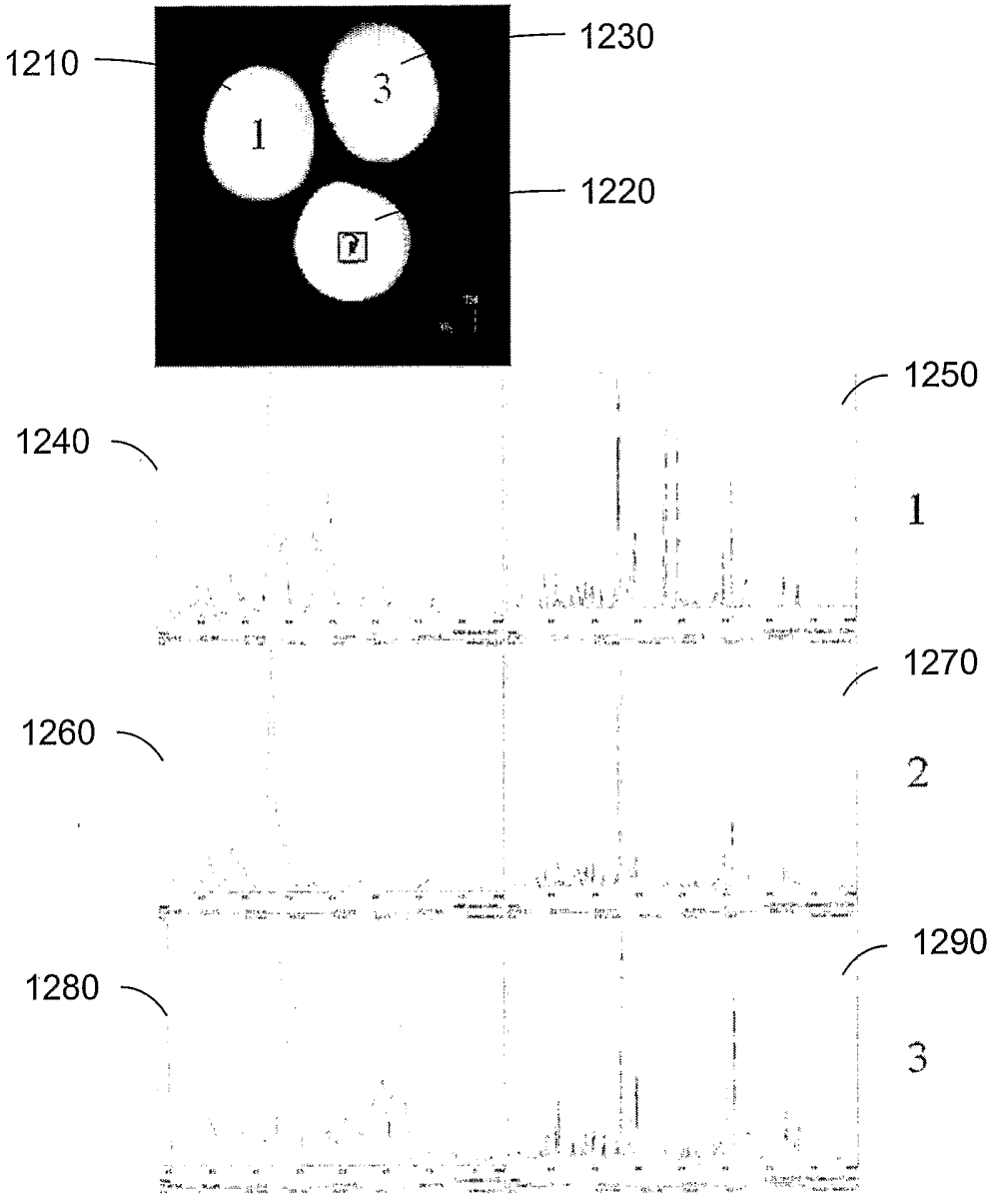

FIG. 12